Universidad Autónoma de Madrid

Departamento de Bioquímica

Deactive complex I triggers a superoxide signal through NCLX in acute hypoxia

Tesis doctoral

Pablo Hernansanz Agustín

Madrid, 2017

Departamento de Bioquímica

Facultad de Medicina

Universidad Autónoma de Madrid

Deactive complex I triggers a superoxide signal through NCLX in acute hypoxia

Memoria presentada por el licenciado en Biología:

Pablo Hernansanz Agustín

para optar al título de Doctor por la Universidad Autónoma de Madrid

Directores de la Tesis: Antonio Martínez Ruiz y Luis del Peso Ovalle

Este trabajo se realizó en el Servicio de Inmunología del Hospital de la Princesa y en el Instituto de Investigaciones Biomédicas "Alberto Sols"

Madrid, 2017

Antonio Martínez Ruiz, Doctor en Ciencias Químicas e Investigador del sistema nacional de salud,

y Luis del Peso Ovalle, Doctor en Ciencias Biológicas y Profesor titular de la Universidad Autónoma de Madrid.

CERTIFICAN:

Que Pablo Hernansanz Agustín, licenciado en Biología por la Universidad de Alcalá de Henares, ha realizado bajo nuestra dirección el trabajo de investigación correspondiente a su Tesis Doctoral con el título:

Deactive complex I triggers a superoxide signal through NCLX in acute hypoxia

Realizado este trabajo, los que suscriben consideran el trabajo realizado satisfactorio y autorizan su presentación para ser evaluado por el tribunal correspondiente.

Y para que así conste y a los efectos oportunos, firman el presente certificado en Madrid a 3 de marzo de 2017.

Fdo. Dr. Antonio Martínez Ruiz **Dr. Luis del Peso Ovalle**

Hay personas que quieren que algo ocurra,

algunas sueñan que pasará.

Otras hacen que suceda

Agradecimientos

Tras algo más de cinco años con esta tesis puedo decir que hay muchas cosas que he aprendido y otras que han cambiado, por suerte, todas a mejor. Aún recuerdo la primera vez que pisé el Servicio de Inmunología, y pregunté por Antonio Martínez Ruiz. Creo que fue la última vez que le llame así. Quiero agradeceros, Toño y Luis la oportunidad que me habéis dado de hacer este doctorado que de verdad, he disfrutado mucho y recordaré con cariño. Muchas gracias por la posibilidad que me has dado, Toño, de ir a tantos eventos científicos, congresos, charlas, etcétera. Espero que los próximos estudiantes tras de mí puedan disfrutar de oportunidades similares.

Desde mi llegada al laboratorio, ha cambiado mucho la cosa, lo que quiere decir que tengo mucha gente a la que agradecer este trabajo. Vaya momentazos he pasado en el laboratorio con las churris, además de todos los experimentos con los que me han ayudado. Momentazos que recuerdo con cariño, como el día que me escondisteis la mochila encima de la nevera. Además de esos 'switches' de la ISCU a escondidas en los que estuvisteis incubando el secundario que no era durante casi un mes. Muchas gracias Ali, por esos momentos de apoyo que fueron tan necesarios. Cuando estás empezando en esto hay ciertos momentos críticos en los que esa ayuda es vital. Y cómo no recordar las manos robóticas de Elena. Cuando recibía su ayuda era toda una tranquilidad saber que, saliera lo que saliera, iba a ser técnicamente impecable. Con estas compañeras, ¿cómo no iba a mejorar mi aprendizaje?

No puedo dejar atrás a compañeros que, aunque en menos tiempo, les estoy muy agradecido. Dani, Danielín, Juan Daniel o como quieras, eres un máquina. Qué buenos esos momentos en la cámara de hipoxia, microscopio y demás sitios del laboratorio en los que filosofábamos. Otra chica que vale un montón y a la que recuerdo muchas veces es a la futura profesora Villa Piña. Es la única vez en mi vida que he visto que algo que no le sale ni a un predoc, ni un posdoc, ni a un técnico, se lo des a una estudiante ¡y le salga como para paper!. Además, siempre pensando de forma muy razonada todo lo que ibas a hacer, de verdad que fuiste toda una sorpresa en el laboratorio.

Por supuesto a todos los compañeros hipóxicos, que nos hemos mantenido fuertes haciendo un gran trabajo durante estos años. No puedo dejar de hablar de gente que vale y ha significado mucho para mi doctorado sin dejar de hablar del Dr. Tello. Todas esas conversaciones que hemos tenido (sobre mitocondria, NUOMS, prohibitina…), las puestas a punto de técnicas y el trabajo siempre han sido muy enriquecedores, alentadores y divertidos, así da gusto hacer ciencia. Igualmente agradezco a David ese mano a mano que hemos tenido en el campo de la hipoxia, siempre tratando de mejorar su ciencia. Aunque llegué al laboratorio algo antes, casi hemos hecho nuestro doctorado en paralelo, espero que la fuerza te acompañe a partir de ahora. Lo mismo puedo decir de Flori, aunque la mudanza al Santa Cristina nos separó y no pudimos compartir tanto tiempo. Oscar, es una pena no haber podido trabajar más juntos, seguro que hubiéramos hecho un gran trabajo. Cómo no acordarme de Inés, Ainara, Ángel, Edu, Bárbara, y Esther, al igual que con

Flori fue una pena que se mudaran tan pronto. Elia y Andrea, muchas gracias por las mitocharlas. Y aunque menos tiempo, también son de agradecer esas conversaciones sobre la serranía de Cuenca y Molina con Tamara, y de todas las cosas de allí, que están tan mal.

Por supuesto, al grupo de los mayores y más grandes expertos en cosas de figuritas, películas y libros de ciencia ficción. Rafa, el gran compañero del nitrógeno, junto al que he capitaneado estos años el buen uso de ese infernal cuarto y con el que he pasado tan buenos ratos en las comidas navideñas del servicio. Eugenio, vaya currante. Además en la última temporada te dieron el marrón del nitrógeno (gracias a mi…s estancias). Imposible no agradecer ese sabor sevillano del laboratorio, Javi con ese salero nos hemos echado unas buenas risas. Al igual que con David y Flori, Alvarito, entre tu residencia y doctorado hemos coincidido desde mi máster hasta ahora. De verdad que te agradezco todos esos momentos de partirnos en la comida, charlas sobre política e historia, y momentos en el café. Llegaron a ser un arma muy efectiva contra el estrés. Por supuesto, muchísimas gracias por toda tu ayuda Noe. No sólo por las cosas de la tesis, si no por esos momentos de conversación, que también son necesarios en este 'mundillo'. Y cómo no, a Lola, muchas gracias por esa forma de pensar que creo es bastante parecida a la mía y me ha apoyado en ciertos momentos de bajonazo.

Raquelilla, muchas gracias por estos años en los que has conseguido hacer investigación en todos los laboratorios del servicio. Ánimo con la conquista del CBM. A quién también le tengo que mucho que agradecer es a la Dra. Amalia Lomana. Con ese punto irracional hemos pasado unos momentos muy divertidos de desvarío, en los que han flipado algunos compañeros pero que han merecido mucho la pena. La paciencia de Cris ha sido toda una lección para todos, tanto a tus lados como arriba y abajo. A Ali Vara, que siempre me ha ayudado con su experiencia y paciencia. De verdad que me ha sorprendido esa seguridad profesional y personal que constantemente demuestras, olé. A Ursa y Hortensia, por portarse tan bien conmigo, aunque el tiempo no acompañe. Sin olvidar a la máquina de café, de los mediodías que me has salvado.

A los jefes. María José, gracias por entenderme en ciertas situaciones que han sido muy estresantes. Te agradezco, Julián, esa parte de tratar de ir más allá en cada charla, escuchar atentamente y discutir cada resultado, por lejos que estuviera de tus proyectos. MOL, que aunque ya no está con nosotros te estaré siempre agradecido por apoyarme desde el principio, que es cuando más cuesta. A Miguel Vicente por su ayuda con el confocal y a Paco, por echarnos un cable siempre que podía.

Anna Bogdanova, I have enjoyed my time in Zurich thanks to your company in the lab. You always found the encouraging way to motivate me and that is why I am so thankful. I look forward to carry on with our work. Also, I should thank to the people in the StudentVinzenz. Honestly, I have never been in such a cool student residence: Next time I enroll to the SOLA race I will train to overcome my 42nd position. To Mike Murphy who led me know the exciting world of mitochondrial research in Cambridge. Also, to my Cambridge mates Andrew, Hiran and Marta, my

stay would not have been as easy as it was without you. Specially, Marta you were a great support in some moments.

Muchísimas gracias a mi familia. Cada día me siento más afortunado de teneros al lado y no puedo de dejar de agradeceros todo lo que me habéis aportado y ayudado de forma incondicional. Durante esta tesis ha habido muchos momentos duros en los que me habéis apoyado y habéis estado cuando lo necesitaba. No dejaré de daros las gracias.

Al campo, los tilos, las setas y esas horas de naturaleza. No tengo palabras para describir lo que me habéis ayudado para superar esta prueba, ha sido una terapia que no olvidaré jamás. E hilando con naturaleza, a l@s micorrizas. Con los que he visto que hay cosas más difíciles e imposibles que vivir de la ciencia.

A los pedazo de amigos del instituto, Fer, Fran, Luisete, Pablete, Juan Luis, Ángel, Javi, Jesús y Javier. Muchas gracias por esas cenas y cervezas desestresantes, aunque a veces, no lo fueran tanto. No puedo negar que pensar en qué tipo de hamburguesa me tocaba hacer o ibais a hacer, me despejaba de la rutina del laboratorio. Por esas visitas a tierras inglesas en las que perdíamos el listón y todas esas absurdeces que hacen tanta gracia.

Y cómo no, a los muchachitos de la comarca, que pedazo de amigos. Muchas gracias tio Divizz por darme hospedaje día si día también, por esos paseos camperos, por esas conversaciones y profesionalidad de la que he aprendido muchísimo. Tio Tobi, no sabes cuánto te agradezco todas las veces que me has ayudado y apoyado, hablando sobre esfuerzo y motivación, y todo lo que me ha ayudado eso en mi trabajo. Al tio Cachorro, por enseñarme lo importante que es la comunicación. Y como no a los momentos de aventura comarcal y transcomarcal con el tio Ossian. Sin olvidar a Rocío, de la que he aprendido muchas cosas que me ayudaron y ayudarán en mi carrera científica. A los senekitos, la mejor peña de Molina que siempre que lo he necesitado han estado ahí. A mi primo Jesús, el primo de zumosol que siempre se porta tan bien conmigo y desde siempre he tenido en un pedestal.

A alguno os dejo en el camino, a otros os seguiré disfrutando. Pero desde el primero hasta el último muchas gracias, porque sin vosotros este trabajo jamás hubiera sido imposible.

Summary

Summary

Oxygen is a key molecule for aerobic life. Eukaryotes have evolved towards an aerobic metabolism which has allowed them to adapt to a plethora of environments and to develop into multicellular systems. The proper distribution of oxygen inside the organism is vital for tissue function and its decreased availability, termed hypoxia, can compromise the survival of the organism. Cells, tissues and organs have developed a series of molecular responses in order to adapt to hypoxia.

Mitochondria are the main oxygen consumers in most eukaryotic cells and also a major source of production of reactive oxygen species (ROS) that can be used by the cells to trigger redox cell signaling processes. There has been a long debate on whether cells respond to hypoxia by increasing ROS production and their involvement in different responses to hypoxia. Since superoxide anion is the first ROS formed from oxygen reduction by the mitochondrial electron transport chain (ETC), we have focused on its specific detection in acute hypoxia. We have observed that superoxide anion production by the mitochondria is increased in the first minutes of hypoxia and that it decreases thereafter, reaching basal levels before one hour of hypoxia, what we have called a hypoxic superoxide 'burst'. In order to dissect the mechanism triggering this response, we have studied the role of different mitochondrial ETC complexes and ion transporters in the production of the hypoxic superoxide burst. We observe that complex I, complex III and the mitochondrial sodium/calcium exchanger (NCLX) are necessary for hypoxic ROS production, and that there could be a chain of events among them. Mitochondrial complex I (CI) undergoes 'deactivation' in acute hypoxia; this was inversely proportional to the oxygen concentration and could switch its activity to a sodium/proton antiporter. CI deactivation is necessary for the enhancement of mitochondrial sodium/calcium exchange through NCLX, which in turn promoted depolarization of the mitochondrial inner membrane. Mitochondrial sodium/calcium exchange is necessary for superoxide production in which complex III would be involved, although the exact source of superoxide has not been determined.

We have been able to observe the implication of NCLX in a variety of experimental settings, in which NCLX inhibition alter different responses to hypoxia, such as activation of the HIF pathway and hypoxic pulmonary vasoconstriction. We have assessed that this mechanism operates also in neurons and brain tissue and that treatment with a NCLX inhibitor diminishes cell death in a model of stroke, probably by reducing oxidative damage. These results open a new window in mitochondrial redox biology research due to the involvement of complex I deactivation and NCLX in superoxide production, which could also have therapeutic implications.

Resumen

Resumen

El oxígeno es una molécula clave para la vida aeróbica. Los organismos eucariotas han evolucionado hacia un metabolismo aeróbico que les ha permitido adaptarse a una plétora de ambientes y desarrollarse como sistemas multicelulares. La adecuada distribución del oxígeno dentro del organismo es vital para la función tisular y la disminución de sus disponibilidad, denominada hipoxia, puede comprometer la supervivencia del organismo. Las células, los tejidos y los órganos han desarrollado una serie de respuestas moleculares que permiten su adaptación a la hipoxia.

Las mitocondrias son los principales consumidores de oxígeno en muchas células eucariotas y son también una de las principales fuentes de producción de especies reactivas de oxígeno (ROS) que pueden usar las células para promover procesos de señalización celular redox. Se ha generado un prolongado debate sobre si las células responden a la hipoxia incrementando la producción de ROS y su implicación en las diferentes respuestas a la hipoxia. Dado que el anión superóxido es la primera ROS formada a partir de la reducción del oxígeno por la cadena de transporte electrónico (ETC) mitocondrial, nos hemos centrado en su detección específica en hipoxia aguda. Hemos observado que se incrementa la producción de anión superóxido en las mitocondrias en los primeros minutos de hipoxia, disminuyendo posteriormente hasta llegar a niveles basales antes de una hora de hipoxia, lo que hemos llamado un 'estallido' de superóxido en hipoxia. Para diseccionar el mecanismo que desencadena esta respuesta, hemos estudiado el papel de distintos complejos de la ETC y trasportadores mitocondriales de iones. Observamos que el complejo I, el complejo III y el intercambiador sodio/calcio mitocondrial (NCLX) son necesarios para la producción de ROS en hipoxia, y que puede haber una cadena de eventos entre ellos. El complejo I (CI) mitocondrial se desactiva en hipoxia aguda, de manera inversamente proporcional a la concentración de oxígeno, y puede cambiar su actividad a la de antiportador sodio/protón. La desactivación de CI es necesaria para activar el intercambio sodio/calcio a través de NCLX, lo que a su vez promueve la despolarización de la membrana mitocondrial interna. El intercambio sodio/calcio en la mitocondria es necesario para la producción de superóxido, en lo que está implicado el complejo III, si bien al fuente exacta de superóxido no se ha determinado.

Hemos podido observar la implicación de NCLX en una variedad de escenarios experimentales, en los que la inhibición de NCLX altera diferentes respuestas a la hipoxia, como la activación de la ruta de HIF y la vasoconstricción pulmonar hipóxica. Hemos comprobado que este mecanismo funciona también en neuronas y tejido cerebral, y que el tratamiento con un inhibidor de NCLX reduce la muerte celular en un modelo de ictus, probablemente disminuyendo el daño oxidativo. Estos resultados abren una nueva ventana en la biología redox mitocondrial debido a la implicación de la desactivación del complejo I y de NCLX en la producción de superóxido, l que puede tener también implicaciones terapéuticas.

Index

Index

List of abbreviations and symbols

List of abbreviations and symbols

BAEC: Bovine aortic endothelial cells
BNIP3: BCL2/adenovirus E1B 19 kDa protein-interacting protein 3
CDCFDA: 5(6)-carboxy-2',7'-dichlorofluorescein diacetate
DHE: Dihydroethidium
DMOG: dimethyloxalylglycine
DMS: Dimethyl succinate
ECAR: Extracellular acidification rate
ETC: Electron transport chain
FCCP: Carbonyl cyanide-p-trifluoromethoxyphenyl hydrazone
GLUT1: Glucose transporter 1
GM: Glutamine/malate
HIF: Hypoxia inducible factor
HPV: Hypoxic pulmonary vasoconstriction
HUVEC: Human umbilical endothelial cells
IMM: Inner mitochondrial membrane
IMS: Intermebrane space
Mito-HE: mitochondrial targeted hydroehtidium
MCU: Mitochondrial calcium uniporter
NCLX: Sodium/calcium exchanger
NDUFS2: NADH dehydrogenase-ubiquinone Fe-S protein 2
NDUFS4: NADH dehydrogenase-ubiquinone Fe-S protein 4
NHE: sodium/proton exchanger
OCR: Oxygen consumption rate
OMM: Outer mitochondrial membrane
OXPHOS: Oxidative phosphorylation
PA: Pulmonary artery
PDK: Pyruvate dehydrogenase
PHD: Prolyl hydroxylase
PINK1: PTEN-induced putative kinase 1
RET: Reverse electron transport
ROS: Reactive oxygen species
RISP: Rieske Fe-S protein
TCA: Tricarboxylic acid
TMRM: Tetramethylrhodamine methyl ester
$\Delta\mu_{mt}$: Mitochondrial proton-motive force
ΔpH_{mt}: Mitochondrial pH gradient
$\Delta\Psi_{mt}$: Mitochondrial membrane potential

Introduction

1 Introduction

1.1 Hypoxia

Oxygen is vital for eukaryotic life. In animals the correct respiratory system function is coupled to the precise delivery of oxygen by the circulatory system to organs, tissues and cells. However, occasionally oxygen supply is inefficient what can lead to cellular dysfunction and, eventually to cell death. Hypoxaemia is caused by abnormally low levels of oxygen in blood, frequently caused by respiratory disorders. This situation, as well as other localized factors, can lead to reduced local oxygen availability for cells within a tissue, which is known as hypoxia.

Hypoxia is present in many pathological situations. In cancer, the incorrect development of blood vessels into the solid body of the tumour creates hypoxic areas (Nagy et al., 2009). In ischemia an inappropriate blood flow through the vessels translates into lower oxygen supply (Reimer et al., 1977). Depending on the disorder and the tissue involved, the changes triggered by hypoxia in disease lead to cellular dysfunction or adaptation and, eventually to cell death or survival. However, there are physiological conditions where hypoxia is present and even necessary. In the course of embryo development there are situations where hypoxia is present and its role is crucial for the viability and correct maturation of tissues (Dunwoodie, 2009). Also, thymus is a hypoxic organ and thymocyte development and survival is linked to hypoxia (Hale et al., 2002). On the other hand, ventilatory response (i.e. due to increased physical activity) is modulated by sensing acute changes in oxygen concentration in blood by specialized organs such as the carotid body (Weir et al., 2005).

1.1.1 Adaptation to hypoxia

In response to hypoxia there are adaptations that can be exerted at the cellular, organ or organism level. This can be through long- or short-term mechanisms, depending on the cell type and the duration of hypoxia.

Long-term adaptation to hypoxia in mammals is mainly mediated by the activation of the hypoxia inducible factors (HIFs), heterodimeric transcription factors composed of a constitutively expressed subunit (HIF-β, also called aryl hydrocarbon receptor nuclear translocator, ARNT), and an oxygen -dependent HIF-α subunit (Semenza, 2007). There are three homologs of HIF-α (HIF-1 α, HIF-2α or EPAS-1, and HIF-3α), that are continuously degraded in normoxia through a mechanism mediated by a family of HIF prolyl hydroxylases (EGLNs or PHDs) which carry out an oxygen-dependent hydroxylation (Kaelin and Ratcliffe, 2008, Li et al., 2006, Schofield and Ratcliffe, 2004, Chowdhury et al., 2016). Hydroxylation in specific Pro residues of the α subunit (e.g. Pro 402 and 564 in HIF-1α) is necessary for its ubiquitination triggered by binding to the E3 ubiquitin ligase Von-Hippel Lindau protein (pVHL) and subsequent degradation by the 26S proteasome. EGLN activity becomes suppressed in hypoxia, inhibiting VHL-dependent ubiquitination and degradation,

in this way allowing HIF-α stabilization (Maxwell et al., 1999). This subunit then heterodimerizes with HIF-β and translocates into the nucleus, where it interacts with coactivators such as P300 and CBP which are required for binding to specific sequence features in the promoter region of the target genes, known as hypoxic response elements (HRE) (Freedman et al., 2002). Once the protein complex is bound to the HRE the hypoxic transcriptional programme starts, being able to induce more than 200 genes and to repress (by indirect mechanisms requiring other factors still under discovery) many other genes (Semenza, 2007, Kaelin and Ratcliffe, 2008). Hydroxylation of a specific Asn residue (e.g. Asn 803 in HIF-α) by the factor inhibiting HIF 1 (FIH-1), another oxygen-dependent reaction inhibited in hypoxia, impedes the interaction with P300 and transactivation of HIF transcriptional activity (Hewitson et al., 2002). The newly transcribed genes are related to metabolic adaptation to hypoxia which shift the metabolism from aerobic to anaerobic pathways (Tello et al., 2011, Fukuda et al., 2007, Soro-Arnaiz et al., 2016, Chen et al., 2001). Angiogenesis is also induced to develop blood vessel through the hypoxic area and irrigate them (Fraisl et al., 2009, Carmeliet, 2005). Also, it modulates the coordinated removal of unneeded structures such as mitochondria in order to provide of energy and anabolites during oxygen deprivation and finally determining cell fate (Zhang et al., 2008), among other processes.

Less known responses to long-term hypoxia involve the activity of iron response proteins (IRPs) in mammals. IRPs are RNA-binding proteins which bind to mRNA untranslated regions (UTRs) in which a specific sequence is present, the iron response element (IRE). The functional effect depends on the localization of the IRE (Rouault, 2006). In ferritin mRNA, IRP binding to the IRE in the 5'-UTR blocks its translation, while IRP binding to the IRE in the 3' UTR of TfR1 mRNA enhances its translation (Schneider and Leibold, 2003). IRP family is composed by two members, whose better known function is to regulate the transcription of a number of genes involved in the iron homeostasis. IRP1 is the cytosolic aconitase without enzymatic activity. In normoxia, IRP1 without the iron-sulphur cluster behaves as an mRNA-binding protein and in hypoxia its iron-sulphur cluster is recomposed, activating its aconitase activity by a yet unknown mechanism (Rouault, 2006). IRP2 is a structurally different protein that is ubiquitinated and degraded in normal conditions by the F-box/LRR-repeat protein 5 (FBXL5). FBXL5 is an hemerythrin-containing protein which senses oxygen and iron availability. Thus, in hypoxia or iron deprivation FBXL5 deactivates its IRP2-unbiquitinase function and ubiquitinates and targets itself to degradation, letting IRP2 to stabilize (Salahudeen et al., 2009, Vashisht et al., 2009).

On the other hand, acute oxygen sensing involves the rapid adaptation of tissues and organisms to sudden decreases in oxygen availability. Specialized organs or tissues such as the carotid body, pulmonary arteries, ductus arteriosus, adrenal medulla or neuroepithelial bodies in the lung drive specific adaptations to acute hypoxia that have been long studied. The carotid body is a cluster of chemoreceptor and supporting cells located near the bifurcation of the carotid artery which are involved in oxygen sensing and hypoxia-related whole-body response. The

chemoreceptor cells or glomus cells are the sensing units. Hypoxia promotes the depolarization of these cells through the blockage of potassium currents. This depolarization allows the opening of voltage-gated calcium channels what causes the exocytosis of vesicles filled with neurotransmitters to sensory nerve fibres that activate the respiratory centre in the brain, driving hyperventilation (Weir et al., 2005, López-Barneo et al., 2016, López-Barneo et al., 2009, Lahiri et al., 2006). It has been recently shown that mitochondrial complex I is involved in the inhibition of the potassium currents through NADH or reactive oxygen species (ROS) signalling (Fernandez-Agüera et al., 2015). Acute responses to hypoxia also occur in pulmonary arteries (PA), which contract upon hypoxia and let the blood to redistribute to more oxygenated areas of the lung. Smooth muscle cells are the cell type involved in oxygen sensing and contraction. Potassium channels are also blocked by hypoxia, causing depolarization and calcium entry via voltage-gated calcium channels, leading to vasoconstriction (Sweeney and Yuan, 2000, Weir and Olschewski, 2006). In this case, NADPH oxidases (NOXs) have been involved in the blockage of potassium currents (Frazziano et al., 2011), and NOXs activation is dominated by ceramide production through neutral sphingomyelinase (nSMase) (Cogolludo et al., 2009, Moreno et al., 2014a). Interestingly, mitochondria have been also involved in this pathway through the production of ROS which would activate nSMase in hypoxia, triggering the downstream signalling cascade (Moreno et al., 2014a).

1.2 Reactive oxygen species (ROS) in physiology and disease

1.2.1 ROS, definition and species

Reactive oxygen species (ROS) are oxygen products which are produced through the incomplete reduction of oxygen. Superoxide anion is the ROS formed by a one-electron reduction of oxygen; its half-life is as short as $2x10^5$ $M^{-1}s^{-1}$ (Kalyanaraman, 2013), what makes superoxide particularly difficult to detect (Kalyanaraman et al., 2017). It is not a powerful oxidant, and its effect on protein thiols is mainly limited to disruption of iron-sulfur clusters; in this regard, mitochondrial aconitase inactivation has been a classical hallmark of mitochondrial superoxide production (Fridovich, 1995, Gardner and Fridovich, 1991). Superoxide dismutates spontaneously or by the action of cytosolic or mitochondrial superoxide dismutases (Cu,Zn-SOD or Mn-SOD respectively) (Liochev and Fridovich, 2007), producing a reduced form, hydrogen peroxide, and an oxidized form, water. Hydrogen peroxide half-life is quite greater than that of its predecessor, 10^3-10^4 $M^{-1}s^{-1}$ (Kalyanaraman, 2013), it can cross biological membranes and reversibly oxidize thiols within Cys residues in proteins (Izquierdo-Álvarez and Martínez-Ruiz, 2011, Bindoli et al., 2008). The latter capacity has been a useful tool for nature to design molecular sensors of hydrogen peroxide such as peroxiredoxins; likewise several laboratories have developed different fluorescent proteins capable of detecting hydrogen peroxide through reversible oxidation of critical, sensitive thiols in their structure (Belousov et al., 2006, Ermakova et al., 2014, Hanson et al., 2004, Germond et al., 2016).

All together, these features make hydrogen peroxide the most easily detectable ROS and the best known. A one-electron reduction of hydrogen peroxide forms hydroxyl radical, a reaction that can be catalysed by the oxidation of Fe^{2+} into Fe^{3+} in the so-called Fenton reaction (Kalyanaraman, 2013). Hydroxyl radical is probably the most toxic ROS due to the initiation of radical chain reactions (Bokare and Choi, 2014). It is worth mentioning the very fast reaction of superoxide with nitric oxide to form peroxynitrite, with a rate comparable to that of diffusion, $4\text{-}6x10^{9}$ $M^{-1}s^{-1}$ (Kalyanaraman, 2013, Beckman and Koppenol, 1996). Although peroxynitrite is well known as an inducer of tyrosine nitration, it is a peroxide and as such it is a very effective two-electron oxidant of thiols and boronate-based probes. Also, it can modify iron-sulphur clusters (Keyer and Imlay, 1997).

1.2.2 Oxidative stress vs ROS signalling

ROS have been long considered harmful species from which cells had to make up defences and indeed, many pathological scenarios involve the massive production of ROS. In this situation, cell components such as proteins, lipids and nucleic acids become oxidized, worsening the cell fate. Lipid oxidation is normally linked to malfunction of membrane-associated enzymes and generation of toxic species potentially interfering in signalling events (Stark, 2005). Nucleic acid oxidation readily occurs in guanine residues in comparison to the other bases which is converted into 8-hydroxyguanine. This kind of stress is common in cancer disease since it can help transformation of the cell (Chao et al., 2013, Zheng et al., 2014). However, proteins under oxidative stress can be modified in several residues, such as Cys, Met or Tyr. Sulphonylation, methionine sulphoxidation and tyrosine nitration are the most common oxidative modifications in Cys, Met or Tyr residues when ROS production is exacerbated (Sies, 2015). These modifications can lead to malfunction of the protein, but in some cases they are involved in the development of cellular responses to oxidative stress. Oxidative stress has been involved in many diseases (Gorlach et al., 2015, Olmez and Ozyurt, 2012, Chandel and Tuveson, 2014, Surmeier et al., 2012, Chaturvedi and Flint Beal, 2013).

Lesser ROS amounts or time of production lead to signalling. The best known signalling ROS is hydrogen peroxide which has been related to many cellular pathways, such as laminar shear stress (Breton-Romero and Lamas, 2013, Breton-Romero and Lamas, 2014) or immune response (Lang et al., 2013, Hernansanz-Agustín et al., 2013). The capacity of this ROS to signal is performed by reversible thiol oxidation by which enzyme activity or protein function can be modulated (Martinez-Ruiz and Lamas, 2004, Izquierdo-Álvarez et al., 2012, Martinez-Ruiz et al., 2013).

Since ROS are constantly produced it is crucial for the cell to buffer them. In this way, there is a robust antioxidant system capable to quenching increases in ROS production. Redox homeostasis is based in the balance between production by ROS sources and buffering of ROS by

the antioxidant system. Indeed, variations in the level of antioxidant capacity can make a ROS signal harmful or ameliorate situations of oxidative stress which would normally be fateful (Nickel et al., 2015, Navarro et al., 2012).

1.2.3 ROS sources

There are many ROS sources in the cell, ranging from cytosolic to intermembrane enzymes or even captured into organelles. Its function and dysfunction is linked to physiological and pathological processes.

NADPH oxidases (NOXs) are membrane-associated protein complexes which catalyse the oxidation of NADPH to $NADP^+$ and produce ROS. There are seven members in its family (i.e. NOX1-5 and DuOX1-2) which produce superoxide with the exception of NOX4 which is a hydrogen peroxide generator (Breton-Romero and Lamas, 2013, Brown and Griendling, 2009, Lambeth, 2004, Nauseef, 2014). Phagosome-associated NOXs in macrophages and neutrophils activate in order to kill the phagocyted microorganisms, contributing to the immune response to infection (Lambeth, 2004). Plasma membrane NOXs are rather related to signalling, including among their targets protein kinase C (PKC) or every member of the mitogen activated protein kinases (MAPK) (Breton-Romero and Lamas, 2014, Brown and Griendling, 2009). NOX members such as NOX4 are linked to adaptive processes that are vital for endothelial function, such as the response to laminar shear stress (Sanchez-Gomez et al., 2015) and can also be found in the endoplasmic reticulum or the nucleus (Brown and Griendling, 2009).

Xanthine oxidase is a cytosolic enzyme which catalyses the oxygen-dependent oxidation of hypoxanthine and xanthine into xanthine and uric acid, respectively (Ardan et al., 2004). As by-product it produces hydrogen peroxide or superoxide (Galbusera et al., 2006), being the production of the latter associated with myocardial failure (Duncan et al., 2005, Stull et al., 2004, Kittleson and Hare, 2005). Xanthine and hypoxanthine are well known purine derivatives accumulating in ischemic conditions (Harmsen et al., 1981, Chouchani et al., 2014). Reappearance of oxygen in reperfusion promotes their rapid catalysis by xanthine oxidase what generates large amounts of ROS, contributing to cell death and tissue damage (Linas et al., 1990).

A large family of monooxygenases metabolize a wide range of substrates, including steroids, lipids and xenobiotics (Holmstrom and Finkel, 2014). These heme-containing proteins must tightly control the oxygen transfer to the substrate, otherwise ROS can be produced (Zangar et al., 2004, Hrycay and Bandiera, 2015). High amounts of substrates, instability or functional or transcriptional regulation balance the production of ROS by this enzyme (Zangar et al., 2004).

Cyclooxygenases (COX), lipoxygenases (LOX) and uncoupled nitric oxide synthases (NOS) are also ROS sources. COX is responsible for the conversion of free arachidonic acid into prostaglandin. However, it can also produce superoxide under stress, such as in brain injury (Kulkarni and Armstead, 2000). LOX catalyses the conversion of polyunsaturated fatty acids into

hydroperoxy fatty acids by the incorporation of an oxygen molecule (Glickman and Klinman, 1996). It was reported that LOX produced superoxide in the presence of NADPH (Roy et al., 1994) which was found a physiologically relevant source in skeletal muscle (Zuo et al., 2004). NOS catalyses the production of nitric oxide from L-arginine. Upon depletion of its cofactors or substrates, NOS can produce superoxide (Luo et al., 2014), although S-glutathionylation can also uncouple its activity and promote ROS production (Xia, 2007, Chen et al., 2010).

Mitochondria are a well-known source of ROS and are considered the largest ROS producers. There are at least eleven ROS sources in the organelle (Brand, 2016) which are located in the mitochondrial matrix and the inner mitochondrial membrane (IMM). In the mitochondrial matrix 2-oxoglutarate dehydrogenase and pyruvate dehydrogenase reversibly catalyse the decarboxylation of 2-oxoglutarate and pyruvate into succinyl-CoA and acetyl-CoA, respectively. Both enzymes reduce NAD^+ into NADH and produce carbon dioxide (CO_2). Superoxide and hydrogen peroxide is produced by both the forward and reverse reactions, being the latter the main contributor (Ambrus et al., 2015). However, the main sources of superoxide in the mitochondria are in the electron transport chain (ETC). The ETC is the principal consumer of oxygen in the cell and a constant current of electrons flow through its complexes could derive in large production of ROS (see below). Therefore a tight coupling in the electron transfer between cofactors and complexes prevents it, probably through the formation of supercomplexes (Maranzana et al., 2013, Wu et al., 2016, Gu et al., 2016, Letts et al., 2016).

1.2.4 ROS detection

ROS are generally difficult to measure due to their short half-life and low specificity of the probes available. There exist several approaches to measure the different ROS in cellular and whole body systems. Well-known examples of low-specificity probes are dichlorofluorescein (DCF) and CellROX fluorescent probes. DCF has been widely used to measure ROS production in cell culture given its easy manipulation and useful excitation/emission spectra. However, it reacts with many substrates in the cell, ranging from NAD^+ to nitric oxide or practically any ROS or RNS.

To measure superoxide a well-known tool is the aconitase activity assay since iron-sulphur clusters are labile upon superoxide treatment (Missirlis et al., 2003, Outten, 2007). It can also discern between superoxide released to the mitochondrial matrix or to the cytosol, since there exist a cytosolic and mitochondrial isoforms of aconitase. Also, it can be assayed from *in vivo* samples. However, this activity can also be inhibited by peroxynitrite (Keyer and Imlay, 1997, Castro et al., 1994), making this technique unspecific for superoxide detection. Currently, the most commonly used tool for its detection is the fluorescent probe dihidroethidium (DHE) which becomes fluorescent in a reaction with superoxide or by binding with nucleic acids. The specific product of DHE reaction with superoxide hidroxyethidium (2-OH-E) can be detected by fluorescent high performance liquid chromatography (HPLC), in which the 2-OH-E is separated from the DNA

oxidized form ehtidium (Eth), or by confocal microscopy since 2-OH-E has different spectral properties than 2-OH-E (Zielonka et al., 2009, Zhao et al., 2005). Although the exact chemistry of this reaction is not known, the specificity for superoxide detection is acknowledged. Furthermore, there exist mitochondrial targeted versions which allow the detection of superoxide in this organelle. The targeting of is performing by attaching the lipophilic cation triphenylphosphonium (TPP^+) to the DHE molecule, rendering the mitochondrial version of DHE, Mito-HE (Robinson et al., 2006). Importantly, since TPP^+ attraction to the mitochondria relies in its positive charge and its accumulation to the mitochondria in the mitochondrial membrane potential ($\Delta\Psi_{mt}$), changes in fluorescence could be due to differences in superoxide production or in $\Delta\Psi_{mt}$. Spin trap-based approaches have been also used to detect superoxide, however their specificity and low resolution early discarded this approach (Finkelstein et al., 1980).

Hydrogen peroxide is the most studied ROS given its role in cell signalling. However, there are a few reliable tools to measure it. Fluorescent proteins such as Hyper or RhoGFP are ratiometric probes which base their sensitivity in specific Cys residues (Guzman et al., 2010, Belousov et al., 2006). In the presence of hydrogen peroxide these Cys residues become oxidized and promote a conformational change in the protein. This, in turn, translates into a shift the absorption spectra of the proteins. These proteins can be expressed in live tissues allowing in situ ROS detection *in vivo* and can also be targeted to any cell compartment (Guzman et al., 2010). However, since its detection properties are based on thiol oxidation, nitrosylation or other peroxides such as peroxynitrite can modulate the spectral properties of the proteins. Boronate, a group of organic compounds react with hydrogen peroxide and peroxynitrite, and this feature has been exploited to detect it. Boronate has been linked to a fluorescent moiety which is converted from a weakly fluorescent to strongly fluorescent product upon oxidation (Miller et al., 2005, Zielonka et al., 2012). Furthermore, boronate probes have also been used to detect mitochondrial hydrogen peroxide *in vivo*. A linked TPP^+ moiety targets the arylboronate (i.e. MitoB) to the mitochondria. Accumulation of the probe and oxidation into its phenol product (i.e. MitoP) can be detected by mass spectrometry and then the ratio MitoB/MitoP be calculated (Cocheme et al., 2012). In this case, the calculation of MitoB/MitoP avoids the possible $\Delta\Psi_{mt}$-dependent artefact. Peroxyredoxin is a hydrogen peroxide scavenger which has oxidizable Cys residues. Upon oxidation peroxyredoxin dimerizes through a disulphur bridge and only after re-reduction of the critical thiols becomes a monomer again (Riquier et al., 2014, Knoops et al., 2011). This can be easily detected and given its specificity and reversibility is becoming increasingly used to measure hydrogen peroxide levels.

1.3 Mitochondrial signalling

1.3.1 Mitochondrial oxidative phosphorylation

Mitochondria are cellular organelles present in all eukaryotes. They are large ellipsoidal organelles which are connected to each other forming a network inside the cell. They are composed of an outer mitochondrial membrane (OMM) and an inner mitochondrial membrane (IMM), the space between both membranes is the intermembrane space (IMS) and the area inside the IMM is the mitochondrial matrix. The IMM is folded into the OMM forming crest-like structures called *crista* which are of vital importance for the correct function of the mitochondria (Cogliati et al., 2013). The OMM lipid composition is similar to the rest of the membranes, being closer to the endoplasmic reticulum membranes. In contrast, the IMM can be considered a special type of membrane in the cell due to its high protein/lipid ratio which confers special properties to the organelle, such as osmoresistance, high impermeability to ions or large capacity to regulate the transport of molecules (E.A., 2014, Nelson and Cox, 2012, Comte et al., 1976). Mitochondria perform many tasks, ranging from cellular signalling to the production of reducing equivalents for the antioxidant defence or contribution to anabolic pathways (Hernansanz-Agustín et al., 2014, Quijano et al., 2016, Soro-Arnaiz et al., 2016). However, the main function of mitochondria is the production stable energy molecules through the electron transport chain (ETC).

ETC use oxygen as the final electron acceptor, generating water and driving the production of the high-energy molecule ATP through oxidative phosphorylation (OXPHOS). The OXPHOS system is composed by mitochondrial complexes which couple the electron flow to the transport of proton ions across the mitochondrial inner membrane (complexes I-IV). The resulting proton gradient generates an electrical and pH difference (mitochondrial membrane potential ($\Delta\Psi_{mt}$) and mitochondrial proton gradient (ΔpH) respectively) between the mitochondrial matrix and the IMS, whose combination composes the so-called proton motive force ($\Delta\mu_{mt}$). The energy stored in $\Delta\mu_{mt}$ is used by the ATPase (complex V) to phosphorylate ADP in a gradient-favoured proton-translocation step, producing ATP. The electrons needed for this process come mainly from the tricarboxylic acid (TCA) cycle in which reducing equivalents such as NADH and $FADH_2$ are formed from substrates such as pyruvate, isocitrate, α-ketoglutarate or malate, and succinate, respectively. The OXPHOS is branched at the starting point since complex I or NADH-ubiquinone oxidoreductase exclusively oxidizes NADH and complex II or succinate dehydrogenase performs only succinate oxidation. Complex I catalyses the oxidation of NADH at its flavin-mononucleotide group (FMN) together with the reduction of ubiquinone to ubiquinol in its respective ubiquinone binding site (Q-site). The energy obtained in this reaction drives a series of conformational changes which translate into the translocation of four protons (Vinothkumar et al., 2014, Sazanov, 2015, Hirst and Roessler, 2016, Fiedorczuk et al., 2016, Zickermann et al., 2015). NADH-ubiquinone oxidoreduction reaction is reversible and can reduce NAD^+ through ubiquinol

oxidation and the pumping of four protons back into the mitochondrial matrix (Drose and Brandt, 2012). The electron transfer and proton pumping is performed by 14 'core' subunits of the complex which are conserved from bacteria to mammals (Vinothkumar et al., 2014, Letts et al., 2016). In mammals there are 30 'supernumerary' subunits which account for assembly and function of complex I (Stroud et al., 2016). Importantly, complex I can exist in two catalytic distinct forms, an active state in which it behaves as a reversible oxidoreductase, and a deactive form which is characterised for being catalytically inactive, exposing the Cys 39 of its ND3 subunit and behaving as a sodium/proton antiporter (Grivennikova et al., 2003, Drose et al., 2016, Babot et al., 2014, Grivennikova et al., 2001, Grivennikova et al., 1997, Galkin et al., 2008, Galkin et al., 2009, Roberts and Hirst, 2012).

Both complexes I and II reduce ubiquinone into ubiquinol which then transfers its two electrons to complex III or ubiquinol-cytochrome C oxidoreductase by means of the Q cycle. Complex III has two ubiquinone binding sites, Q_o (i.e. outer) and Q_i (i.e. inner). ubiquinol binds to the Q_o site and donates one electron to Rieske iron-sulphur protein (RISP) which then reduces cytochrome c1 and subsequently cytochrome c. The second electron is used to reduce another ubiquinone through hemes b_L and b_H to form a semiquinone radical at the Q_i site. A second cycle is needed to completely reduce the semiquinone to ubiquinol in the Q_i site (Zhang et al., 1998, Crofts et al., 1999). Complex III pumps two proton for every cycle performed, moving a total of four protons into the IMS (Iwata et al., 1998, Xia et al., 1997, Crofts et al., 2006). Cytochrome c reduces complex IV or cytochrome c oxidase which finally reduces oxygen into water in a reaction coupled to the pumping of four protons (Sazanov, 2015).

1.3.2 Mitochondrial cation gradients

One important consequence of the $\Delta\Psi_{mt}$ formation is the attraction of low molecular weight-positive charged ions. Therefore the IMM also contains channels and exchangers for ion management whose function is coupled to the OXPHOS engine (Nicholls, 2008). For example, the sodium/proton exchanger (NHE) extrudes sodium from the matrix into the intermembrane space, translocating proton back into the matrix (Donoso et al., 1992, Jung et al., 1992, Nicholls, 2010). This activity is exerted by the canonical mitochondrial NHE (mNHE), but also by the deactive form of mitochondrial complex I (Roberts and Hirst, 2012). This exchange is electroneutral, but decreases the ΔpH_{mt}. Uptake of sodium into mitochondria is largely mediated by the mitochondrial sodium/calcium exchanger (mNCX), also known as NCLX (sodium/calcium/lithium exchanger) due to its sensitivity to lithium (Palty et al., 2010, Poburko and Demaurex, 2012, Murphy and Eisner, 2009). NCLX imports three sodium ions into the mitochondrial matrix in exchange for one calcium ions, thus generating electrical charge movement across the membrane, i.e. exerting electrogenic activity, since there is a net gain of positive charges in the mitochondrial matrix (Baysal et al., 1994, Cortassa et al., 2003, Dash and Beard, 2008, Jung et al., 1992, Kim and Matsuoka,

2008). Of note, it has been shown that the extrusion of mitochondrial calcium is mainly performed by NCLX versus other antiporters, such as Letm1 (see below) (Jiang et al., 2009).

Calcium enters the mitochondria through the mitochondrial calcium uniporter (MCU) in a $\Delta\Psi_{mt}$-dependent manner (De Marchi et al., 2014, Baughman et al., 2011, Oxenoid et al., 2016). This has important implications since calcium is able increase the activity of several enzymes of the TCA cycle, such as 2-oxoglutarate dehydrogenase and its handling is coupled to OXPHOS function through $\Delta\Psi_{mt}$ axis (Pan et al., 2013, Cox and Matlib, 1993). Calcium can also enter the mitochondria by an electrogenic exchange (1 calcium: 1 proton) (Poburko and Demaurex, 2012). This reversible activity was proposed to be carried out by the leucine zipper and EF-hand containing transmembrane protein (Letm1) which was also reported to be ruthenium red-sensitive (Jiang et al., 2009). However, it is still to be proven whether this observation better fits with a potassium/proton antiporter (Nowikovsky et al., 2004).

Potassium movement across IMM is a rather slow process and has been shown to be performed by a potassium/proton exchanger (KHE) (Poburko and Demaurex, 2012, Bernardi, 1999). KHE is mainly related to the maintenance of mitochondrial volume and becomes activated upon organelle swelling and mitochondrial matrix alkalinisation (Beavis and Garlid, 1990, Garlid, 1980, Garlid and Paucek, 2003).

It is important to note that there is scarce data about regulation of these channels and exchangers. Only the molecular identity of MCU and Letm1 has been discovered (De Marchi et al., 2014, Baughman et al., 2011, Oxenoid et al., 2016). Only one essential protein of NCLX has been found so far and the identification of its complete composition remains obscure (Palty et al., 2010). There is no clue about what gene is encoding for NHE or KHE protein(s). In addition, the discovery of these is quite recent and there are not many studies relating their expression or regulation to physiological processes or pathophysiology. However, it is known that altered ion homeostasis occur in a bunch of disorders such as neurodegenerative diseases (Chan et al., 2007) ischemia (Tanonaka et al., 2012) or ischemia/reperfusion (Kalogeris et al., 2012).

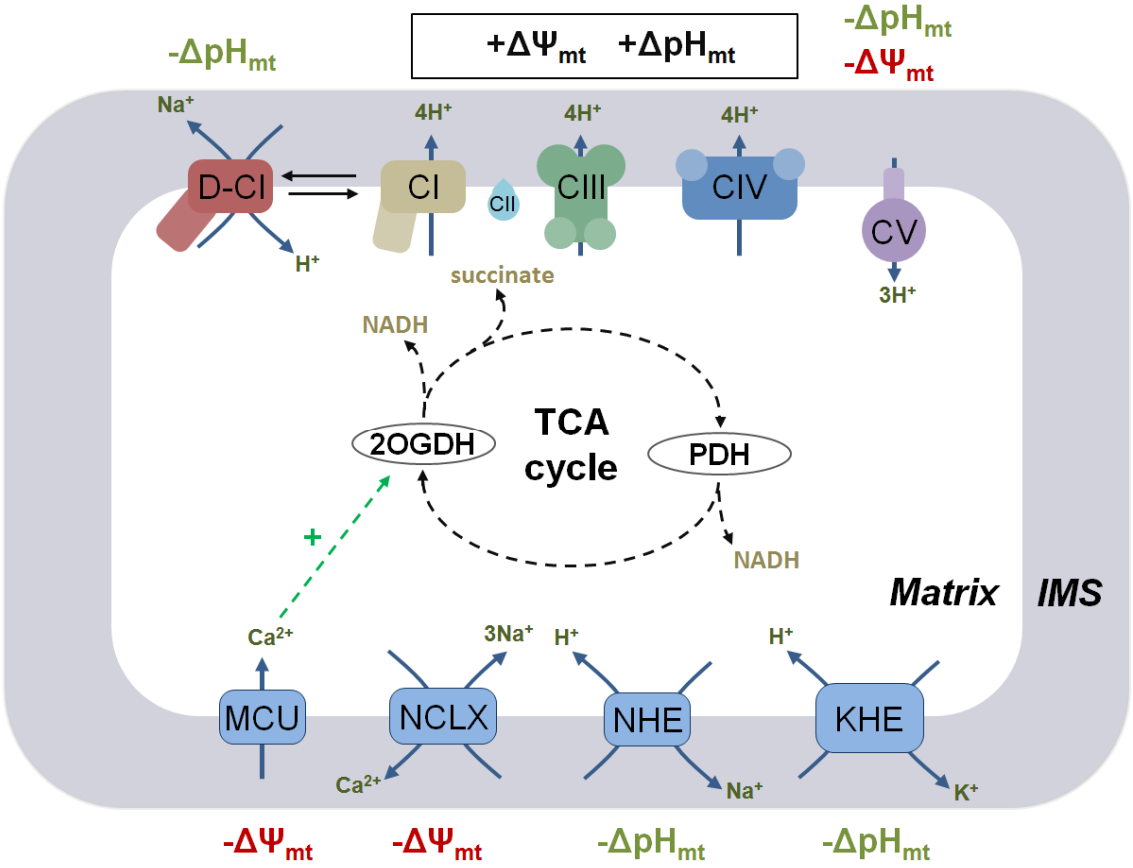

Figure 1.1 Cation transporters and OXPHOS complexes in the mitochondrial inner membrane and their effect on $\Delta\Psi_{mt}$ and ΔpH_{mt}. OXPHOS complexes I, III and IV pump protons across the IMM increasing $\Delta\mu_{mt}$. Cation transporters are grouped in blue. Mitochondrial calcium uniporter (MCU) allows calcium entry in the matrix, whereas it is extruded by NCLX in exchange of sodium in a ratio 1:3. Sodium/proton exchange by NHE can be performed by the canonical NHE (mNHE) or the deactive form of complex I. Potassium/proton antiporter (KHE) and NHE activities couple ion homeostasis to the activity of the ETC.

1.3.3 Mitochondrial cation homeostasis in health and disease

Mitochondrial cation regulation is important for cellular ion-dependent processes, such as regulation of action potentials or energy homeostasis. Cardiac pacemaker cells trigger their own action potential when a certain threshold is reached and do not need external stimulation, which is called automaticity. Cytosolic calcium, together with sodium and potassium oscillate which translates in membrane potential depolarization and repolarization cycles (Baruscotti et al., 2005). It was shown that HL-1 cardiomyocytes develop automaticity and that it could be modulated by NCLX, since inhibition of its expression translated in slower cycles (Takeuchi et al., 2013). In addition, TCA cycle enzymes activity such as 2-oxoglutarate dehydrogenase is enhanced by MCU-dependent calcium uptake (Wan et al., 1989, Tarasov et al., 2012)and this activation is abolished by NCLX-dependent sodium influx (Cox and Matlib, 1993). Activation of TCA cycle turnover could be a key event in episodes of high energy requirement, such as increases in heart workload. Therefore, raise in cytosolic sodium concentrations could affect TCA cycle activation in physiology and disease. Importantly, beyond certain threshold mitochondrial calcium can promote the opening

of the mitochondrial permeability transition pore (mPTP) (Wong et al., 2012, Bernardi and Di Lisa, 2015). This reversible augmentation of the IMM permeability has been linked to dimerization of the complex V which would form the actual pore, turning its function from an energy conserving to an energy dissipating device (Giorgio et al., 2013, Bernardi and Di Lisa, 2015). Therefore, mitochondrial calcium homeostasis must be tightly controlled since variations in its mitochondrial concentration can change the cell fate from cell survival to death.

Besides, the impact of sodium overload in mitochondrial-related dysfunctions has been widely studied in plants (Miller et al., 2010); however it is not the case of animals, despite it has been linked to several pathophysiological processes (Brocker et al., 2012). Cytosolic sodium burden can occur through environmental sodium overload or dysregulation of sodium channels. The best known hyperosmotic environment are inflammatory niches where osmotic stress has been linked to mitochondrial dysfunction and oxidative damage (Brocker et al., 2012). Of note, inflammatory areas become rapidly hypoxic and develop hypoxic adaptive response (Eltzschig and Carmeliet, 2011). Sodium overload is a hallmark of ischemic myocytes and it has been related to ischemic and ischemia/reperfusion injury (Tanonaka et al., 2012, Kohlhaas et al., 2010), in which mitochondria are directly involved (Chouchani et al., 2014, Chouchani et al., 2013). In addition, mutations in channels taking over sodium homeostasis are connected to neurological diseases whose pathology rely on mitochondrial function and its progression has been associated with hypoxic adaptation (Requejo-Aguilar et al., 2014). Therefore, sodium overload is a common signature of several diseases in which hypoxia is involved; however, how it alters mitochondrial function and hypoxic adaptation has not been studied, despite it has a potential big impact in diseases where sodium overload and hypoxia are present.

1.3.4 Mitochondrial ROS production by the ETC

As by-products of the incomplete reduction of oxygen a series of ROS are formed from during respiration (Turrens, 2003, Murphy, 2009). Superoxide can be produced by OXPHOS at the level of the first three complexes of the system. Complex III-dependent superoxide production relies on high $\Delta\Psi$mt and can be inhibited by Q_o blockers such as myxothiazol or stigmatellin, but not by Q_i blockers such as antimycin A (Drose and Brandt, 2012). This is most probably because superoxide production by complex III is based on semiquinone radical formation, since inhibition of Q_i would render a free semiquinone per every oxidized ubiquinol, whereas inhibition of Q_o would keep the ubiquinone fully reduced (Bleier and Drose, 2013, Lanciano et al., 2013). In the presence of the complex II substrate succinate and the inhibitors rotenone and myxothiazol (complex I and III respectively), superoxide formation by complex II can be detected (Drose, 2013). However, the major superoxide producer in the mitochondria is complex I and can produce superoxide both by forward or reverse reactions. The elder is only possible when Q-site inhibitors of complex I, such as rotenone, are applied in the presence of NADH (Drose and Brandt, 2012).

Whether superoxide is produced at the FMN or at the Q-site was a matter of debate, but later shown to occur at the FMN after full reduction of the iron-sulphur clusters in hydrophilic arm of complex I (Pryde and Hirst, 2011, Treberg et al., 2011, Drose and Brandt, 2012). The reverse electron transport (RET) occurs only in the exclusive presence of succinate which is necessary to create a high ubiquinol/ubiquinone ratio which overcomes catalytic turnover of complex III (Vinogradov and Grivennikova, 2005). Since ubiquinol, the enzymatic product of complex I is enormously increased, the law of mass action makes this complex to catalyse the reverse reaction pumping four protons back to the mitochondrial matrix and reducing NAD^+ into NADH. This is why RET requires mitochondrial hyperpolarisation (Drose and Brandt, 2012). In this mechanism superoxide is produced at the level of the FMN. Therefore, RET is inhibited by Q-site or FMN inhibitors of complex I (e.g. rotenone and diphenyleneiodonium (DPI), respectively) as well as by uncouplers (e.g. carbonyl cyanide-p-trifluoromethoxyphenylhydrazone; FCCP)(Drose and Brandt, 2012, Hirst et al., 2008)).

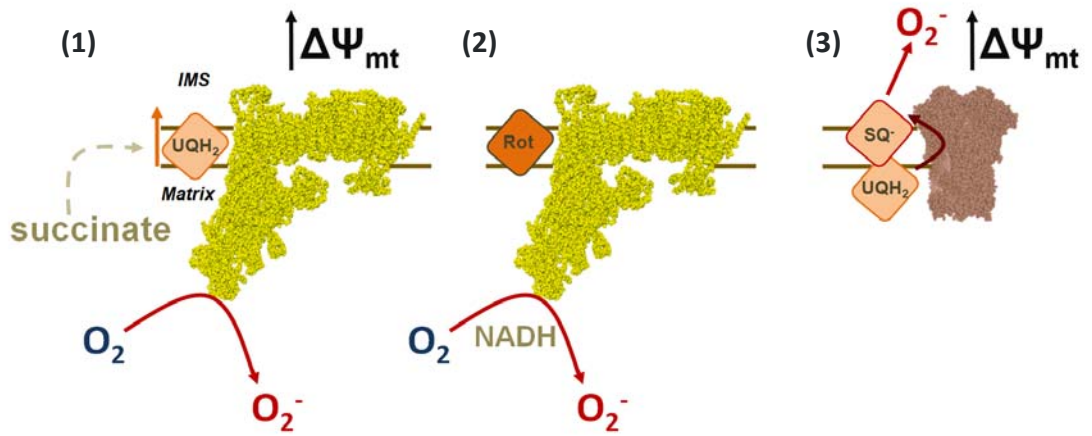

Figure 1.2 Mechanisms of superoxide production by the ETC. (1) RET requires the accumulation of large amounts of succinate which reduce the ubiquinone pool. Since complex I pumps protons back to the matrix it needs a highly hyperpolarized mitochondria. This reaction produces superoxide anion in the mitochondrial matrix. (2) In the forward reaction blockage of complex I by Q-site inhibitors such as rotenone do not allow transfer of electrons to ubiquinone. This translates into the reduction of oxygen at the FMN site of complex I. (3) Q-cycle through complex III drives the electron transfer through the complex. Inhibition of complex III or some physiological situations trigger the production of superoxide by means of uncomplete oxidation of ubiquinol and formation of semiquinone radicals.

Mitochondrial ROS are implied in many pathological scenarios (Gorlach et al., 2015) such as stroke (Olmez and Ozyurt, 2012), cancer (Chandel and Tuveson, 2014), Parkinson´s (Guzman et al., 2010), Alzheimer´s or cardiovascular diseases (Chaturvedi and Flint Beal, 2013), and its overproduction may contribute to the progression of the disease. However, it is acknowledged that mitochondrial ROS also act as second messengers in cell signalling processes in a variety of physiological conditions such as wound healing, thermogenesis or oxygen sensing (Nathan, 2003, Sena and Chandel, 2012, Hamanaka and Chandel, 2010, Muliyil and Narasimha, 2014, Chouchani et al., 2016, Moreno et al., 2014a), among others. Furthermore, some cell types such as endothelial

cells base their energy supply on glycolysis and not in OXPHOS, turning mitochondria into rather signalling organelles (Quintero et al., 2006).

1.3.5 The paradox of ROS in hypoxia

It has been proposed that ROS increase in hypoxia and that the main source is the mitochondria. However, since ROS are products of the oxygen reduction this is chemically difficult to explain and the fact that there grown discrepant results in the literature made these results to be hardly debated. The main controversy about mitochondrial ROS production in hypoxia arose from the unspecificity of the fluorescent probes used, that the protocols included reoxygenation of the samples and the application of antioxidants which also impact on other processes in redox biology and metabolism (Chandel et al., 1998, Chandel et al., 2000). Several reports have confirmed hypoxic ROS production in cells exposed to hypoxia while recording the fluorescent signal from HSP-FRET or roGFP (Robin et al., 2007, Guzy et al., 2005, Iwase et al., 2007, Waypa et al., 2010, Desireddi et al., 2010 (reviewed in {Guzy, 2006 #211, Schumacker, 2011, Guzy and Schumacker, 2006a). Both thiol-based protein sensors are oxidized by hydrogen peroxide, although oxidation by other intracellular such as peroxynitrite or nitric oxide cannot be ruled out. Furthermore, intracellular superoxide, which is the primary ROS produced from oxygen has been measured by different groups giving different results. Chua *et al* added the superoxide probe DHE after 3 hours of hypoxia, observing no change in fluorescence intensity and they concluded that there was not a change in ROS production in hypoxia (Chua et al., 2010). On the other hand, Quintero *et al* used the same probe but incubated it with the cells for the first 60 minutes of hypoxia and showed an increased superoxide production (Quintero et al., 2006). These studies are apparently discrepant, but the difference in the results may hide a differential production of superoxide over time, since the incubation times differed. Importantly, there is no study showing the dynamics of superoxide production upon lowering oxygen availability. Understanding the time course of superoxide production will help us to bring together the contradictory results in the literature.

As the role of mitochondria in ROS production in hypoxia has been suggested, several groups have also tried to measure it in isolated mitochondria, also with controversial results (Hoffman and Brookes, 2009, Hoffman et al., 2007, Korde et al., 2011). Whereas Hoffman *et al* showed that ROS production in hypoxia was proportional to oxygen concentration, Korde and colleagues observed the opposite. Interestingly, they both used Mannitol-sucrose based buffer as extraction and working solutions, being the main difference the presence or absence of 10 mM sodium chloride, respectively. As mentioned earlier, the principal effect of sodium on mitochondria is to activate NCLX, what depletes calcium from the mitochondrial compartment (Poburko and Demaurex, 2012, Hoffman et al., 2007). Thus, ion homeostasis and, specifically, NCLX function could be implied in the production of ROS during hypoxia.

1.3.6 Mitochondrial ROS in the hypoxic adaptation

Although it is clear since many years ago that ROS contribute to HIF-α stabilization (Gerald et al., 2004), it is not the case of hypoxic ROS production. ROS-related HIF-α stabilization has been linked to oxidative stress and disorders, such as Parkinson´s disease (Requejo-Aguilar et al., 2014), cancer (Galanis et al., 2008) or inflammation (Mittal et al., 2014). However, although it has been proposed that hypoxia-induced ROS production contributes to PHD inhibition and HIF-α stabilization (Moreno et al., 2014a, Chandel et al., 1998, Chandel et al., 2000, Guzy et al., 2005, Brunelle et al., 2005, Mansfield et al., 2005) (reviewed in (Guzy and Schumacker, 2006a, Hamanaka and Chandel, 2010)), most of the approaches made so far include the alteration of OXPHOS and potential artefacts in oxygen gradients (Hagen et al., 2003). Notably, the use of targeted antioxidant proteins to the mitochondria and the observation that ETC-derived ROS are necessary for hypoxic HIF-α stabilization *in vivo* have reinforced this hypothesis (Hamanaka et al., 2016, Sabharwal et al., 2013).

Acute oxygen sensing was elderly linked to oxygen sensors in the plasma membrane (López-Barneo and Castellano, 2005). Recently mitochondrial ROS have been implied in this response (Fernandez-Agüera et al., 2015). In the case of glomus cells of carotid body, it has been shown by genetic ablation of the complex I 'core' subunit NDUFS2 or pharmacological inhibition with rotenone, that complex I activity is essential for the acute response to hypoxia specifically. Whether it is complex I-derived NADH, ROS or both what triggers the stimulus is yet to be defined (Fernandez-Agüera et al., 2015). However, it is possible that small variations in oxygen availability translate tiny increases in ROS production which given the proximity of mitochondria with the plasma membrane, could affect potassium currents by reversibly oxidizing critical thiols and thus blocking the channels. HPV was also shown to be a mitochondrial ROS dependent acute-adaptation which could be abolished by rotenone or myxothiazol treatment (Moreno et al., 2014a). In this case, mitochondrial ROS serve as an initiator signal for the activation of another ROS source, the NADPH oxidases which modulate potassium current activity (Moreno et al., 2014a, Cogolludo et al., 2009). Now, given that mitochondria are not as close as in the carotid body it could be that this amplification system is necessary for thiol modification of the potassium currents.

From all the above examples, it is clear that mitochondrial ROS play a central role in long and short term hypoxic adaptation. However, although the molecular actors start to be discerned there is not a clear frame of the molecules involved. Since hypoxic adaptation is related to many physiological processes and diseases it is of vital importance to identify the actors and the pathways implicated on it.

Objectives

2 Objectives

- Ascertain whether there is increased superoxide production in acute hypoxia, studying the time course of production of superoxide and other ROS production in cells during the transition from normoxia to hypoxia.
- Investigate the possible mechanism of hypoxic ROS production and search for the molecular players involved, especially components of the mitochondrial electron transport chain and mitochondrial ion exchangers.
- Study the involvement of this hypoxic ROS production in adaptive response to hypoxia (hypoxic pulmonary vasoconstriction, activation of the HIF pathway).
- Evaluate the usefulness of molecular interventions that abolish the superoxide burst to mitigate ischemic damage in a murine model of stroke induced by photoactivated thrombus formation.

Materials and methods

3 Materials and methods

3.1 Antibodies

Table 1. Antibodies used showing the target protein, epitope, manufacturer, catalogue number, host species, clonality and working dilution from stock. Clonal: Clonality, Mono: monoclonal, Poly: polyclonal.

Protein	Epitope / attachment	Manufacturer	Catalog number	Host	Clonal	Dilution
Primary antibodies						
Prohibitin-1	C-term	Abgent	AJ1656a	Rabbit	Mono	IF: 1:1000
HIF-1α		R&D Systems	MAB1536	Mouse	Mono	WB: 1:500
NCLX		Aviva S.B.	ARP44042 _P050	Rabbit	Poly	WB: 1:1000
NDUFS4		Abcam	ab87399	Mouse	Mono	WB: 1:1000
NDUFS2		Abcam	ab110249	Mouse	Mono	WB: 1:4000
RISP		Abcam	ab14746	Mouse	Mono	WB: 1:1000
NDUFB6		Proteintech	16037-1-ap	Rabbit	Poly	WB: 1:2000
UQCRC1		Abcam	ab110252	Mouse	Mono	WB: 1:2000
α-tubulin		Sigma-Aldrich	T6199	Mouse	Mono	WB: 1:1000
PINK1		Santa Cruz	sc-33796	Rabbit	Poly	WB: 1:200
Secondary antibodies						
Rabbit IgG/HRP	HRP conjugated	GE Heathcare	NA934V	Donkey	Poly	WB: 1:1000
mouse Ig/HRP	HRP conjugated	Dako	p0260	Rabbit	Poly	WB: 1:1000
Rabbit IgG/Dylight 488	Dylight488 conjugated	Thermo	35552	Goat	Poly	IF: 1:50

3.2 Animals, cell culture and transfection

All animal experiments were performed following the Guide for the Care and Use of Laboratory Animals and were previously approved by the institutional ethics committee of the Universidad Autónoma de Madrid or the Universidad Complutense de Madrid, Spain, according to the European guidelines for the use and care of animals for research in accordance with the European Union Directive 2010/63/UE of 22 September 2010 and with the Spanish Real Decreto 53/2013 of 1 February 2013 . Animal management was performed by our collaborators (see below). All efforts were made to minimize the number of animals used and their suffering.

Bovine aortic endothelial cells (BAECs) were obtained from aortas donated by a local slaughterhouse and isolated as previously described (Navarro-Antolin et al., 2000). BAECs were cultured at 37 °C in RPMI 1640 (which contains 133 mM sodium and 5.3 mM potassium) supplemented with 15% heat-inactivated fetal bovine serum (FBS), 100 U/mL penicillin and 100

μg/mL streptomycin. . Human umbilical vein endothelial cells (HUVECs) were isolated as previously described (Muñoz et al., 1996) and cultured in Medium 199 supplemented with 20% heat-inactivated fetal bovine serum (FBS), 16 U/ml heparin, 100 mg/L ECGF (endothelial cell growth factor), 20 mM HEPES (4-(2-Hydroxyethyl)piperazine-1-ethanesulfonic acid),100 U/mL penicillin and 100 μg/mL streptomycin. For BAECs and HUVECs, dishes were treated with 0.02% gelatine for 30 min at 37ºC, which was removed before plating. BAECs were used between passages 3 to 9 and HUVECs between passages 3 to 7. Endothelial morphology was assessed by visual inspection and by Western blot for endothelial nitric oxide synthase.

EA.hy926 cells were provided by Dr. Cora-Jean S. Edgell (UNC, NC, USA) and were cultured at 37 °C in Dulbecco´s Modified Eagle Medium (DMEM; which contains 155 mM sodium and 5.4 mM potassium) supplemented with hypoxanthine, aminopterin and thymidine (HAT supplement 50x), 10% heat-inactivated FBS, 100 U/mL penicillin and 100 μg/mL streptomycin.

HeLa and human lilver cancer (HepG2) cells were cultured at 37 °C in DMEM supplemented with 10% heat-inactivated FBS, 100 U/mL penicillin and 100 μg/mL streptomycin.

ϱ^0L929 cells (mtDNA-less cells derived from L929 cells), and their control ϱ^+ transmitochondrial cybrids, TmC57BL/6J (herein called C57; generated by transferring functional mitochondria from platelets to ϱ^0L929 cells) were generated (Moreno-Loshuertos et al., 2006) and kindly provided by the group of Dr. José Antonio Enríquez (CNIC, Spain). They were cultured at 37 ºC in DMEM supplemented with 5% heat-inactivated FBS, 100 U/ml, penicillin and 100 μg/mL streptomycin. ϱ^0L929 cells were also supplemented with 50 μg/mL uridine.

HK-2 cells (kindly provided by Dr. María José Calzada, UAM & Instituto de Investigación Sanitaria Princesa, Madrid, Spain) were cultured at 37 °C in DMEM F-12-GlutaMAX supplemented with 10% heat-inactivated FBS, 100 U/mL penicillin and 100 μg/mL streptomycin, and 0.1% Insulin-Transferrin-Selenium-X solution.

Cardiomyocytes were isolated, in a collaboration with Dr. Anna Bogdanova´s group, from Wistar rat pups 2-3 days after birth as previously described (Rothen-Rutishauser et al., 1998). The cells were seeded on collagen-coated 6-well plates, supplemented with maintenance medium containing 1/5 part of M199 medium and 4/5 parts of the medium containing (mM): 116 NaCl, 32.1 $NaHCO_3$, 1 NaH_2PO_4 (pH 7.2), 0.8 $MgSO_4$, 5.5 Glucose, 1.8 $CaCl_2$, supplemented with 1% horse serum, penicillin, streptomycin and 2% glutamine. Cells were used within 5 days after the isolation.

Rat pulmonary artery smooth muscle cells (PASMCs) from Wistar rats were isolated as previously described (Moreno et al., 2014a) and cultured in DMEM supplemented with 10% FBS, 1.1 g/l pyruvate, 1% non-essential amino acids, 100 μg/ml streptomycin and 100 U/ml penicillin. Rat PASMCs were used within passages 2-3.

Immortalized mouse hippocampal cells (HT22 cell line) were cultured at 37 °C in DMEM supplemented with 10% heat-inactivated FBS, 20 mM HEPES, 100 U/mL penicillin and 100 μg/mL streptomycin.

Transfection of 30 nM siRNA or 0.25 μg C199S pHyPer-Myto (mitosypHer) vector DNA per 0.8 cm^2 well was carried out using Lipofectamine 2000 (Invitrogen) according to the manufacturer´s instructions. In PASMCs, 10 nM siRNA was transfected using Lipofectamine RNA iMAX (Invitrogen) according to the manufacturer's instructions; in parallel experiments, siRNA efficiency was measured by RT-PCR using commercially available primers (TaqMan Gene Expression Assay Rn01481405_m1, Applied Biosystems). Experiments were carried out 48 to 72 h after transfection.

3.3 siRNA preparation

Scramble siRNA (siSCR) was purchased from Santa Cruz Biotechnology, except for rat siNCLX for which specific siSCR was used (see below). Double-strand siRNA were purchased as follows:

Table 2. siRNA sense chain used showing the target mRNA and species, manufacturer and sequence.

Target	Manufacturer	Sequence/Catalogue number
Bovine NCLX	Dharmacon	AGCGGCCACUCAACUGCCU
Bovine NDUFS4	Integrated DNA Technologies	GCUGCCGUUUCCGUUUCCAAGGUUUTT
Bovine NDUFS2	Integrated DNA Technologies	TCGGACAGTCGACATTGGGATT
Bovine RISP	Integrated DNA Technologies	CCAAGAAUGUCGUCUCUCAGUUUTT
Bovine PINK1	Integrated DNA Technologies	GGCUGCUAAUGUGCUUCAUUU
Human NCLX	Dharmacon	AACGGCCACUCAACUGUCU
Rat NCLX	OriGene	SR504963
siSCR (rat NCLX)	OriGene	SR30004

3.4 Fluorescence microscopy in fixed cells and quantification

Cells were seeded a day before experimentation on glass coverslips. For treatments in hypoxia, all the solutions were pre-equilibrated to hypoxic conditions before use; in some experiments, 1 mM Tiron (4,5-dihydroxy-1,3-benzene disulfonic acid), 1 μM carbonyl cyanide-p-trifluoromethoxyphenylhydrazone (FCCP), 100 mM sodium chloride, 30 mM lithium chloride, 5 mM potassium chloride, 25 mM glucose, 5 mM G/M (2.5 mM glutamine, plus 2.5 mM dimethylmalate), 5 mM dimethylsuccinate (DMS), 120 mM D-sorbitol, 120 mM N-methyl-D-glucamine (NMDG), 1 μM rotenone´, 1 μM antimycin A, 1 μM myxothiazol or 10 μM 7-chloro-5-(2-chlorophenyl)-1,5-dihydro-4,1-benzothiazepin-2(3H)-one (CGP-37157) was added 30 min before experimentation and maintained during the experiment. Plated cells were introduced in an Invivo2 400 or Invivo2 200 workstation (Ruskinn) set at 1% oxygen (2% oxygen when stated), 5% CO_2, 37 ºC, and incubated for the indicated times (0, 15, 30, 45 and 60 min) in new medium,

washed three times with Hank´s Balanced Salt Solution with calcium /Mg^{2+} (HBSS+Ca/Mg) and incubated with 5 μM mito-hydroethidine (Mito-HE; 3.33 or 10 μM when stated) or 5 μM dihydroethidium (DHE) for 10 min, or with 10 μM 5(6)-carboxy-2',7'-dichlorofluorescein diacetate (CDCFDA) for 15 min (all probes in HBSS+Ca/Mg), in darkness. After incubation, excess of probe was washed three times with HBSS+Ca/Mg, the cells were fixed by adding 4% paraformaldehyde (PFA), and incubated in darkness at 4 ºC for 15 min. After fixation, wells were again washed three times with HBSS+Ca/Mg and coverslips placed on slides. In normoxic cells, medium was also changed for new normoxic medium, and treated as hypoxic cells, but in a standard cell incubator. When normoxia was set at 7% oxygen, the cells were placed in an Invivo2 200 workstation (Ruskinn) at 7% oxygen, 5% CO_2, 37 ºC, incubated overnight and treated in the same chamber or transferred to the Invivo2 400 chamber for 1% oxygen hypoxia as above. Antimycin A was added to a final concentration of 10 μM onto normoxic cells 30 min before and during incubation with the probe.

Three images per coverslip were taken in a Leica DMR fluorescence microscope with a 63x objective, using the following excitation/emission filter pairs: 546-12/560 for DHE and Mito-HE, 480-40/505 for CDCFDA. The images (three images per each coverslip; the number of independent experiments is described in the figure legends) were quantified using Image J software. The quantification consisted on setting the same threshold for all the images and obtaining the mean value from the histogram of each image. This mean value of the three images from the same coverslip was then averaged and the obtained number was treated as one replicate.

Significance of the hypoxia-induced changes was analysed by ANOVA (analysis of variance) for normoxic and all the hypoxic time groups, and intergroup comparison was done by the multiple comparison test (Dunnett posteriori test with respect to the normoxia group). The change of fluorescence with the time in hypoxia was evaluated by linear trend test of all the hypoxia groups (Armitage, 2012). Homoscedasticity was tested with Levene´s test and normality with Shapiro-Wilk test. Appropriate transformation was done to perform the analysis in case of no normal distribution. When no transformation gave normal distribution (as in Figure 4.1d), non-parametric tests were used: differences among normoxic and all the hypoxic time groups were analysed with the Kruskal-Wallis test and intergroup comparison was done with the Mann-Whitney test with respect to the normoxia group; the change of fluorescence with the time in hypoxia was evaluated by non-linear trend test of all the hypoxia groups. These analyses were performed using Stata version 11 software and R version 2.15.2, by the Methodology Unit of the Instituto de Investigación Sanitaria Princesa (Madrid, Spain).

3.5 Detection of intracellular calcium, sodium, ROS and mitochondrial membrane potential by live imaging fluorescence microscopy

These experiments were carried out at the Department of Physiology of the University of Zürich, using a Leica DM 16000B fluorescence microscope equipped with a Leica DFC360FX camera, an automated stage for live imaging and a thermostated hypoxic cabinet.

Cells were seeded in 6-well plates one day before experimentation. Plated cells were washed three times with HBSS+Ca/Mg and incubated with 30 nM tetramethylrhodamine methyl ester (TMRM), 1 μM Fluo-4AM, 10 μM CoroNa Green AM, Mito-HE, DHE or 10 μM 6-carboxy-2',7'-dichlorodihydrofluorescein diacetate (CDCFDA) for 20 min at 37 ºC in the dark. In some experiments 1 μM FCCP, 100 mM sodium chloride, 30 mM lithium chloride, 5 mM potassium chloride or 10 μM CGP-37157 were also added and maintained during the experiment. CDCFDA, CoroNa Green AM and Fluo-4AM were then washed out and new HBSS+Ca/Mg was added. For Fluo-4AM imaging, cells were further incubated for 30 min at 37ºC in the dark to allow complete de-esterification of the probe. After this time, the plate was placed into the microscope. The planes were focused for image capture, and images were taken with a 20x objective every 2 min during 40 min. Normoxia experiments started and ended at 20% oxygen and 5% CO_2, whereas hypoxia experiments started at 20% oxygen and 5% CO_2 and then were switched to 2% oxygen and 5% CO_2 after 2 min. The gas mixture stably equilibrated at 2% oxygen after 1 min. The excitation/emission filter pairs used were as follows: 546-12/560 for Mito-HE and DHE and TMRM, and 480-40/505 for CDCFDA, Fluo-4AM and CoroNa Green AM. Three independent experiments were performed for each condition.

For mitochondrial membrane potential controls, 12.5 μM oligomycin or 1 μM FCCP were added prior to focusing the planes.

Images were quantified with Leica Las-AF software or Image J. Two different routines were used to quantify the fluorescence. The "line method" was applied with the Leica Las-AF software and was based on the creation of a linear region of interest (ROI) crossing an individual cell. Four ROIs were created in each experiment and condition, and the mean fluorescence of each ROI for the cycles 0, 5, 10, 15 and 20 was collected. The "circular method" was applied with image J. For each experiment and condition, four ROIs surrounding individual cells were created and the maximum peak value of all the cycles was collected for each ROI. Three independent experiments were performed for each condition. In DHE or Mito-HE experiments, the linear method was applied but the lines were created on non-nuclear regions of different cells (to avoid measuring nuclear binding of Mito-HE and DHE).

The rate of fluorescence for each replicate was estimated by linear regression of the data for all the ROI and time points. Differences of the mean of the rates of fluorescence were analysed by the Student t test. Homoscedasticity was tested with Levene´s test and normality with Shapiro-

Wilk test. Appropriate transformation was done to perform the analysis in case of no homoscedasticity or no normal distribution. These statistical analyses were performed using G-stat version 2.0.1 software.

Treatment effect was analysed with GEE (generalized estimating equations method) with gaussian family and identity link function (Hardin and Hilbe, 2012). Variability of statistics derived from time observations was analysed with independent and autoregressive of order one -AR(1)- correlation structures (Hardin and Hilbe, 2012). However, only the independent correlation structure is showed for the within-subject correlation, because it was the most parsimonious model (p-value and coefficient were similar between the two structures, therefore the statistical independence of observations could be assumed). This independent correlation structure is equal to simple regression models. When the response variables were not normally distributed appropriate transformations were used. These analyses were performed using Stata version 12 software by the Methodology Unit of the Instituto de Investigación Sanitaria Princesa (Madrid, Spain).

3.6 Detection of intracellular calcium, sodium, hydrogen peroxide and intramitochondrial hydrogen peroxide, calcium, pH and colocalization by live imaging confocal microscopy

These experiments were carried out in the Hospital de La Princesa, using a Leica SP-5 confocal microscope, with an automated stage for live imaging and a thermostated hypoxic cabinet

To detect intracellular calcium and sodium, cells were seeded one day before experimentation, washed three times with HBSS+Ca/Mg and incubated with 1 μM Fluo-4AM or 5 μM CoroNa Green AM for 30 min at 37 ºC in the dark. In some experiments, 10 μM CGP-37157, 1 μM rotenone, 1 μM antimycin A, 1 μM myxothiazol, 10 μM KCN or 10 μM ethyl-isopropyl amiloride (EIPA) were also added and maintained during the rest of the experiment. CoroNa Green AM and Fluo-4AM were then washed out and new HBSS+Ca/Mg plus 25 mM glucose was added. For Fluo-4AM imaging, cells were further incubated for 30 min at 37ºC in the dark to allow complete de-esterification of the probe. After this time, the plate was placed into the microscope. The planes were focused for each sample and images were taken with a 20x objective every 2 min during 40 min. Normoxia experiments started and ended at 20% oxygen and 5% CO_2, whereas hypoxia experiments started at 20% oxygen and 5% CO_2 and then were switched to 1% oxygen and 5% CO_2 after 2 min. The gas mixture stably equilibrated at 1% oxygen after 1 min. Loaded cells were excited with a Ar/Kr laser using the 496 nm line. Fluorescence emission of Fluo-4AM and CoroNa Green was detected in 500-575 nm range.

To detect intramitochondrial pH, cells were transfected with the ratiometric probe mitosypHer in 8-well plates two days before the experiment. The same protocol as above was used, except that the objective was 63x and imaging time was 30 min, with 7 cycles of 5 min. Excitation was performed with a 405 diode laser for 405 nm line and Ar/Kr for 488 nm line and fluorescent

emission was recorded at 515-535 nm range. To assess mitochondrial colocalization of the probe transfected cells were incubated with 25 nM MitoTracker CMTMRos for 20 minutes at 37 ºC in HBSS+Ca/Mg in the dark, washed again three times with HBSS+Ca/Mg and fixed with 4% PFA; samples were excited with an Ar/Kr laser using the 488 nm line mitosypHer and a He/Ne laser using the 543 nm line for MitoTracker. Fluorescence emission of mitosypHer was detected in 515-535 nm range and MitoTracker in 575-590 nm range. 30 μM NaOH and 8 mM of HCl were used as controls of basification and acidification, respectively.

For hydrogen peroxide detection, BAECs were transfected with the non-targeted or mitochondrial targeted version of HyPer following the same procedure for live imaging as with mitosypHer. 2 mM DTT and 30 μM of antimycin A were used as controls for thiol reduction and oxidation, respectively.

For intramitochondrial calcium detection a mitochondrial targeted version of the Pericam-based probe GEM-GECO, kindly provided by Prof. Jorgina Satrústegui (CBMSO, UAM, Madrid), was used. Samples were excited with an Ar laser using the 405 nm line. Fluorescence emission of the fluorescent protein was detected in 475-495 nm range for the cyan fluorescent protein (CFP) and 515-555 nm range for the yellow fluorescence protein (YFP), and then the ratio CFP/YFP was calculated. Histamine 10 μM was used as a control for mitochondrial calcium overload.

Images were quantified with ImageJ software using the circular method of quantification. Three or four independent experiments were performed for each condition.

The rate of variation for each replicate was estimated by linear regression of the data for all the ROI and time points. The differences of mean of the replicate rates were analyzed by the Student t test (as indicated in figure legends).

3.7 Mitochondrial localization of Mito-HE by confocal microscopy

Cells were seeded a day before experimentation on glass coverslips. Plated cells were washed three times with HBSS+Ca/Mg and incubated with 5 μM mito-hydroethidine (Mito-HE, also called MitoSOX) for 10 min in darkness. After incubation, excess of probe was washed three times with HBSS+Ca/Mg, the cells were fixed by adding 4% PFA, and incubated in darkness at RT for 10 min. After fixation, wells were again washed with HBSS+Ca/Mg and cells permeabilized with 0.5 % Triton X-100 in PBS for 10 min at RT. Blocking solution, consisting in Tris-NaCl blocking buffer (TNB; 11096176001; Roche Diagnosis) in PBS, was added for 20 min at 37 ºC and antibody against prohibitin-1 C-term was incubated for 1 h at 37 ºC. Coverslips were washed three times with 0.1 % Tween-20 in PBS (PBS-T) and incubated with DyLightTM-488-labeled goat anti-rabbit secondary antibody for 30 min at 37ºC. Cells were washed three times with PBS-T and one with distilled water, and coverslips mounted in slides. Tri-color Z stacks were generated using Leica SP-5 confocal microscope. Samples were excited with Ar/Kr laser using the 488 nm line and a second diode laser fitted with 561 nm line. Fluorescence emission was taken using the spectral

capability of the SP-5 according to manufacturer's instrucions. For 3-dimensional analysis, stacks were projected using the 3D project tool of Image J software.

3.8 Measurement of superoxide formation with high performance liquid chromatography (HPLC) analysis

These experiments were part of a collaboration with Dr. Santiago Lamas´ group at the Centro de Biología Molecular Severo Ochoa (CBM-SO) and the HPLC analysys was performed by Dr. Francisco Javier Sánchez Gómez. This method separates 2-hydroxyethidium (2-OH-E), the specific product of the reaction of DHE with superoxide, from other by-products such as ethidium (Eth).

Cells were seeded a day before experimentation in 60 mm diameter plates. For hypoxia treatments, plated cells were introduced in an Invivo2 400 workstation (Ruskinn) set at 1% oxygen, 5% CO_2, 37 ºC, and incubated for the indicated times (0, 15, 30, 45 and 60 min) in pre-hypoxic medium, washed three times with pre-hypoxic HBSS+Ca/Mg and incubated with 5 μM dihydroethidium (DHE) for 10 min (in pre-hypoxic HBSS+Ca/Mg solution), in the darkness. After incubation, excess of probe was washed once with pre-hypoxic PBS and cells lysed with 0.1% of Triton X-100, and frozen overnight at -80 ºC. Homogenates were thawed on ice and 100 μl transferred into a new tube. 1-butanol (250 μl) was added to the lysate, vortexed for 1 minute, centrifuged during 3 minutes at maximum speed and the upper alcoholic phase was recovered and dried. The desiccated fraction was resuspended in 100 μl HPLC-grade water and vortexed. An HPLC 2695 separation module from Waters was used to load and separate 50 μl of the samples in a "Mediterranean Sea" C18 column using acetonitrile 10 %-TFA 0.1 % and acetonitrile 100 %-TFA 0.1 % as mobile phases. Fluorescence of the samples was detected by a W474 module at 490 nm excitation wavelength and 560 nm emission wavelengths. The peak area corresponding to 2-OH-E formation was quantified and corrected with the protein concentration of the sample (determined by the BCA assay).

Significance of the hypoxia-induced changes was analysed by ANOVA (analysis of variance) for normoxic and all the hypoxic time groups, and intergroup comparison was done by the multiple comparison test (Dunnett posteriori test with respect to the normoxia group). The change of fluorescence with the time in hypoxia was evaluated by linear trend test of all the hypoxia groups (Armitage, 2012). Homoscedasticity was tested with Levene´s test and normality with Shapiro-Wilk test. All analyses were performed using Stata version 11 software and R version 2.15.2, by the Methodology Unit of the Instituto de Investigación Sanitaria Princesa (Madrid, Spain). Three or four independent experiments were performed for each condition.

3.9 Extraction method for evaluating HIF-1α stabilization and target gene expression

For hypoxic stabilization of HIF-1α resolved by western blot or quantitative real time PCR of mRNA extracted from hypoxic samples , cells or hippocampal slices were placed into an Invivo2 400 workstation or an Invivo2 200 workstation (Ruskinn) set at 1% oxygen, 5% CO_2, 37 ºC and incubated for 4 (western blot) or 6 (PCR) hours in normoxia, hypoxia or dimethyloxalylglycine (DMOG). Cells or hippocampal slices were taken out of the hypoxia chamber on ice, washed in ice-cold PBS and lysed in Laemmli buffer or Trizol Reagent.

3.10 Western blot analysis

Protein samples were extracted with non-reducing Laemmli buffer without bromophenol blue and quantified by the BCA assay. Laemmli buffer composition was 50 mM Tris-HCl pH 7.6, 2 mM ethylenediaminetetraacetic acid (EDTA), 1% sodium dodecyl sulphate (SDS) and 10% glycerol. After addition of 0.02% bromophenol blue and 5% 2-mercaptoethanol, extracts were then loaded and separated in 10% standard polyacrylamide gel electrophoresis, and transferred to nitrocellulose membranes. In the case of BN-PAGE gels (see below), they were transferred to polyvinylidene difluoride (PVDF) membranes. Membranes were blocked for 30 min with blocking buffer (5% non-fat milk powder in PBS + 1% Tween). All antibodies where diluted in washing buffer (PBS + 1% Tween; 4 ºC), with the exception of anti-HIF-1α which was diluted in blocking buffer. After overnight incubation for primary antibodies, membranes were washed with washing buffer for 30 min several times and further incubated with species-specific secondary antibodies labeled with horseradish peroxidase (HRP) in washing buffer for 1 hour. Subsequently, membranes were washed for further 30 min in washing buffer. HRP substrate and enhancer (Thermo Scientific SuperSignal West Femto; Catalogue number 34095) were added and chemiluminiscence visualized on a digital luminescent image analyzer (Fujifilm LAS-4000).

Images were quantified using ImageQuant TL7.0 software, applying a rolling ball method for subtracting the background and with supervised band detection and quantitation. Each band was quantified and relativized by its corresponding loading control (i.e. tubulin) and the ratio was then plotted in histograms.

3.11 Quantitative real time PCR

Total RNA was extracted from HUVECs or HeLa using Trizol reagent (Vitro) following the manufacturer´s instructions. The amount of RNA was quantified on Nanodrop ND-1000 spectrophotometer (Thermo) and a control quality performed in a 2100 Bioanalyzer (Agilent Technologies) and 0.5 μg was reverse-transcribed (Gene Amp Gold RNA PCR Core Kit; Applied Biosystems) following manufacturer´s instructions. The PCR was performed with Gotaq qPCR

Master Mix (Promega) or Power SYBR Green PCR Master Mix (Applied Biosystems) with 1 μL of cDNA and specific primer pairs (Table S1). β-actin mRNA was measured as an internal sample control. Hypoxanthine-guanine phosphoribosyltransferase (HRPT) and 28S ribosome subunit were used as internal controls. Two reactions were performed for each condition and gene tested in each independent experiment.

The threshold cycle value (C_T) is the number of the cycle in which the fluorescence produced in the reaction overcomes the fluorescence threshold. The fluorescence threshold was automatically set by the software as ten standard deviations above the mean fluorescence generated during the baseline cycles. C_T for the two duplicates was averaged only if the difference between them was not greater than 0.5, otherwise the experiment were discarded. The resulting value was expressed as fold change vs normoxia, relativized to β-actin and plotted as mean ± s.e.m of at least three replicates.

Table 3. Specific primers pairs used showing the target forward and reverse sequences.

	Forward	Reverse
HIF1-α	5´-AGCCGAGGAAGAACTATGAACATAA-3´	5´-GTGGCCTGTGCAGTGCAA-3´
HIF2-α	5´-CAATCAGCTTCCTGCGAACA-3´	5´-TTCGGCTTCGGACTCGTTT-3´
PDK1	5´-GTGGTTTATGTACCATCCCATCTCT-3´	5´-TCCATAGTGGCTCTCATTGCAT-3´
GLUT1	5´-TCAACCGCAACGAGGAGAA-3´	5´-CTGTCCCGCGCAGCTT-3´
BNIP3	5´-TCAAGTCGGCCGGAAAATAT-3´	5´-GCGCTTCGGGTGTTTAAAGA-3´
B-actin	5´-GGCACCCAGCACAATGAAG-3´	5´-CCGATCCACACGGAGTACTTG-3´

3.12 Measurement of cellular oxygen consumption

Oxygen consumption rate (OCR) in cell culture was measured using an XF24 Extracellular Flux Analyzer (Seahorse Bioscience). BAECs, $6x10^4$ per well (6-7 wells per treatment for each independent experiment) were plated one day before the experiment. Cells were preincubated with unbuffered DMEM (155.462 mM sodium and 5.366 mM potassium) supplemented with 25 mM glucose, 1 mM pyruvate, and 2 mM glutamine for 1 h at 37 °C in an incubator without CO_2 regulation. OCR measurements were programmed with successive injections of unbuffered DMEM, 5 μg/mL oligomycin, 300 nM FCCP, and 1 μM rotenone plus 1 μM antimycin A. DMSO or 10 μM CGP-37157 were added before starting the measurements. In experiments using silenced cells, as proliferation and cell growth may vary after plating, protein concentration from each condition (i.e. all the wells from the same condition in the same plate were mixed) was quantified by the BCA assay to normalise the OCR. Calculations of OCR and associated parameters were performed following the manufacturer´s instructions. After measuring basal respiration, oligomycin was added to inhibit respiration (by blocking complex V), therefore, the amount of oxygen used to produce ATP by OXPHOS is estimated from the difference with basal oxygen consumption (i.e. coupling efficiency). FCCP uncouples OXPHOS by translocating proton from intermembrane space to matrix, thus maximizing electron flux through the ETC, giving the maximal respiration

rate. This treatment provides information about the stored energy in mitochondria that a cell could use in an energetic crisis (i.e. reserve capacity). Antimycin A and rotenone block complexes III and I, respectively, consequently inhibiting electron flux through the ETC and eliminating any proton translocation, therefore, the leftover value is non-mitochondrial respiration, i.e. the oxygen consumed by other enzymes in the cell. Ultimately, proton leak is calculated from the remaining respiration after oligomycin addition less the non-mitochondrial respiration, giving the respiration due to the proton translocation due to other molecules than complex V.

3.13 Simultaneous measurement of oxygen consumption and hydrogen peroxide in isolated mitochondria

OCR in intact isolated mitochondria was performed in the Mitochondrial Biology Unit (Cambridge, United Kingdom) and measured using an Oxygraph-2k (O2k, OROBOROS Instruments, Innsbruck, Austria) and combined with the Fluorescence-Sensor Green of the O2k-Fluo LED2-Module for hydrogen peroxide measurement. Experiments were carried out in potassium chloride medium (120 mM potassium plus 1 mM EGTA) in two parallel chambers. Before experiment 500 μg of rat heart mitochondria, 10 μM amplex red, 1mg/ml SOD, 1 mg/ml HRP, 10 mg/ml bovine serum albumin (BSA) were added. 5mM glutamate and 5 mM malate (GM) addition at the beginning of the experiment acted as a mitochondrial-NADH generating system (state 2), 2.5 mM ADP was added to couple respiration (state 3) followed by the addition of 10 mM succinate to study complex II contribution to the total oxygen consumption or hydrogen peroxide production.

3.14 Submitochondrial particles (SMPs) isolation and blue native polyacrylamide gel electrophoresis (BN-PAGE)

This procedure was performed before BN-PAGE or detection of ND3 by fluorescent labelling. BAECs or HepG2 cells were plated in one 100 mm-diameter dish for each condition. Each plate washed twice in ice-cold PBS, scraped off the plate and centrifuged for 5 min 600 g at 4ºC. Hippocampal slices were washed and disaggregated in ice-cold PBS and centrifuged for 5 min at 600 g at 4ºC. To obtain SMPs, cells were resuspended in 200 μL of PBS, mixed with 200 μL of 8 mg/mL of pure digitonin and incubated for 10 min in ice. After this, 1 mL PBS was added and the samples were centrifuged 5 min at 10,000 g, 4ºC. The resulting pellet of SMPs was washed and resuspended in 100 μL of 1.5 M aminocaproic acid, 50 mM Bis-Tris/HCl pH 7.0. Protein concentration was quantified by BCA assay. SMPs were centrifuged 2 min at 13,500 g at 4ºC and the pellet was resuspended at 10 μg/μL with 1.5 M aminocaproic acid, 50 mM Bis-Tris/HCl pH 7.0. SMPs were solubilized with 4 g/g digitonin, incubated 5 min in ice and centrifuged 30 min 16,000 g at 4ºC.

For BN-PAGE analysis supernatants were collected and mixed with sample buffer (Coommassie brilliant blue G-250 5% in 1 M aminocaproic acid solution). For each sample, 100-150 μg was loaded and run on a 3-20% gradient BN-PAGE gel as described elsewhere (Schagger, 1995, Schagger and von Jagow, 1991). Gel transfer was performed onto PVDF membranes, which were then washed with methanol for 3 min before western blotting.

3.15 Fluorescent labelling of ND3 Cys-39 from isolated mitochondrial membranes

For cell extracts and *ex vivo* samples, the same procedure previously described for SMP preparation was used. For *in vivo* samples, brain mitochondria isolation was performed using the Mitochondrial Isolation Kit for tissue (ab110168; Abcam) according to the manufacturer's protocol. Briefly, brain tissue was washed and minced in Isolation Buffer and cells were disrupted using a Dounce tissue grinder pestle (Sigma). Then, homogenized tissue was centrifuged at 1,000 g for 10 minutes at 4 °C and the supernatant was centrifuged at 12,000 g for 15 minutes at 4 °C, giving the enriched mitochondria and cytosol fractions in the pellet and the supernatant, respectively.

SMP or mitochondrial protein amount was determined by the BCA assay and then proteins were solubilized with 4 g/g digitonin, incubated 5 min in ice and centrifuged 30 min at 16,000 g, 4ºC. Samples from cell cultures were split into two parts, one part was incubated at 37 ºC for 60 min to fully deactivate complex I and the other part was kept on ice. Samples were then incubated with Bodipy-TMR C5-maleimide (Invitrogen) for 20 min at 15 ºC in the dark; then, 1 mM cysteine was added and the samples were further incubated for 5 min. After this time, the samples were precipitated twice with acetone, centrifuged at 9,500 g for 10 min at 4 ºC in the dark, and the resulting pellet was resuspended in non-reducing Laemmli loading buffer. For each sample, 100 μg was loaded onto 10% Tricine-SDS-PAGE gels as previously described (Schagger and von Jagow, 1991). Total protein staining was performed with Sypro Ruby (Invitrogen) following the manufacturers' instructions. The images corresponding to Bodipy-TMR C5-maleimide fluorescence were obtained with Cy3 settings (excitation with green LED, emission filter 575DF20) and the total protein by Sypro with a UV transiluminator and 605DF40 filter, using a digital fluorescent image analyzer (Fujifilm LAS-4000). The signal of the ND3 band was quantified using ImageQuant TL7.0 software in the two images from the same gel (Bodipy-TMR and Sypro Ruby) and the ratio of signals, Bodipy-TMR/Sypro Ruby, quantified for each band.

Data were analysed one-way ANOVA followed by a Tukey's test (when comparing multiple groups), as indicated in the figure legends. Values of $p < 0.05$ were considered to be statistically significant.

3.16 Protein mass spectrometry analysis

These experiments were performed in collaboration with Dr. Anabel Marina´s group at the CBM-SO (Proteomics Unit of the CBM-SO and the IIS-IP, a member of ProteoRed-ISCIII / PRB2) by Nuria Sánchez-López and Laura Peláez-Aguado, in order to confirm the identity of the protein bands corresponding to ND3. After drying, the electrophoretic bands that migrated at the position expected for ND3 were cut in pieces, destained in acetonitrile:water 1:1, reduced with 10 mM DTT for 1 h at 56 ºC, alkylated with 50 mM iodoacetamide for 1 h at room temperature (RT) in the dark and digested *in situ* with sequencing grade trypsin (Promega, Madison, WI) as described by Shevchenko *et al*(Shevchenko et al., 1996) with minor modifications. The gel pieces were shrunk by removing all liquid using sufficient ACN. Acetonitrile was pipetted out and the gel pieces were dried in a speedvac. The dried gel pieces were re-swollen in 50 mM ammonium bicarbonate pH 8.8 (AB) with 12.5 ng/μL trypsin for 1 h in an ice-bath. The digestion buffer was removed and gels were covered again with AB and incubated at 37 °C for 12 h. Digestion was stopped by the addition of 1% TFA. Whole supernatants were dried down and then desalted onto ZipTip C18 Pipette tips (Millipore).

The desalted protein digest was dried, resuspended in 10 μl of 0.1% formic acid and analyzed by RP-LC-MS/MS in an Easy-nLC II system coupled to an ion trap LTQ-Orbitrap-Velos-Pro mass spectrometer (Thermo Scientific), as previously described (Moreno et al., 2014a) with minor modifications. The peptides were concentrated (on-line) by reverse phase chromatography using a 0.1 mm × 20 mm C18 RP precolumn (Proxeon), and then separated using a 0.075 mm x 250 mm C18 RP column (Proxeon) operating at 0.3 μl/min. Peptides were eluted using a 240-min dual gradient from 5 to 25% solvent B in 180 min followed by gradient from 25 to 40% solvent B over 240 min (Solvent A: 0.1% formic acid in water, solvent B: 0.1% formic acid, 80% acetonitrile in water). ESI ionization was carried out using a Nano-bore emitters Stainless Steel ID 30 μm (Proxeon) interface.

The mass spectrometer was operated in the selected MS/MS ion monitoring mode (SMIM mode (Jorge et al., 2007). In this mode, the LTQ-Orbitrap-Velos-Pro detector was programmed to perform, along the same entire gradient, a continuous sequential operation in the MS/MS mode on the doubly or triply charged ions corresponding to the peptide selected previously from the theoretical prediction.

Peptides were detected in survey scans from 400 to 1600 amu (1 μscan), followed by ten data-dependent MS/MS scans (Top 10), using an isolation width of 2 u (in mass-to-charge ratio units), normalized collision energy of 35%, and dynamic exclusion applied during 30 sec periods. The Orbitrap resolution was set at 30,000. Peptide identification from raw data was carried out using the SEQUEST algorithm (Proteome Discoverer 1.4, Thermo Scientific). Database search was performed against handmade database and search against decoy database (integrated decoy approach) using false discovery rate (FDR) < 0.01. The following constraints were used for the

searches: tryptic cleavage after Arg and Lys, up to two missed cleavage sites, and tolerances of 20 ppm for precursor ions and 0.8 Da for MS/MS fragment ions, and the searches were performed allowing optional Met oxidation, Cys carbamidomethylation and Cys N-ethylmaleimide modification.

3.17 Measurement of pulmonary artery contraction

These experiments were carried out by Dr. Laura Moreno, in Dr. Angel Cogolludo´s lab at Universidad Complutense de Madrid (UCM). Third division branches of the pulmonary arteries (PA) were isolated from male Wistar rats and mounted in a wire myograph. Contractile responses were recorded as previously reported (Moreno et al., 2014a). The chambers were filled with Krebs buffer containing (in mM) NaCl 118, KCl 4.75, $NaHCO_3$ 25, $MgSO_4$ 1.2, $CaCl_2$ 2.0, KH_2PO_4 1.2 and glucose 11, maintained at 37 °C and aerated with 21% oxygen -5% CO_2-74% N_2 gas (pO_2 17-19 kPa). After an equilibration period of 30 min, PA (internal diameter 300-400 μm) were distended to a resting tension corresponding to a transmural pressure of 2.66 kPa. Preparations were initially stimulated by raising the potassium concentration of the buffer (to 80 mM) in exchange for sodium. Vessels were washed three times and allowed to recover. Then, each vessel was exposed to two hypoxic challenges (95% N_2-5% CO_2; pO_2 = 2.6-3.3 kPa), the second one after 40 min incubation with vehicle (control) or CGP-37157 (30 μM). The steady state contraction is the force of contraction 10 min after peak contraction. Both were measured and relativized to the first hypoxic challenge.

Data were analysed using one-way ANOVA followed by a Bonferroni's test. Values of $p < 0.05$ were considered to be statistically significant

3.18 Preparation of mouse hippocampal slices

These experiments were part of a collaboration with Dr. Manuela G. López´s group and were performed by Dr. Elisa Navarro. Three-month-old C57BL/6 mice were anesthetized with 1.5% isoflurane in oxygen under spontaneous respiration, then decapitated and forebrains were rapidly removed from the skull and placed into ice-cold Krebs bicarbonate dissection buffer (pH 7.4), containing (in mM): NaCl 120, KCl 2, $CaCl_2$ 0.5, $NaHCO_3$ 26, $MgSO_4$ 10, KH_2PO_4 1.18, glucose 11 and sucrose 200. The hippocampi were dissected, and slices (250-μm thick) were prepared using a McIlwain Tissue Chopper. Then, the slices were transferred to vials containing sucrose-free dissection buffer to allow tissue recovery from slicing trauma before experimentation (equilibration period). Both solutions were gassed with 5% CO_2 at least 30 minutes before use to ensure pH 7.4.

3.19 Detection of superoxide in hippocampal slices by confocal microscopy

For treatments in hypoxia, all solutions were pre-equilibrated to hypoxic conditions before use; when necessary, 10 μM CGP-37157 or 10 μM antimycin A was added 30 min before the experiment and maintained during the rest of the procedure. Hippocampal slices were placed into an Invivo2 400 workstation (Ruskinn) set at 1% oxygen, 5% CO_2, 37 ºC, and incubated for 30 min in fresh sucrose-free dissection buffer, washed three times with HBSS+Ca/Mg and incubated with 5 μM DHE for 10 min in the dark. After incubation, excess probe was removed by three washes in HBSS+Ca/Mg, slices were fixed with 4% PFA, and incubated in the dark at 4 ºC for 15 min. After fixation, wells were again washed three times with HBSS+Ca/Mg and the slices placed on slides with coverslips on top. For normoxic treatments, medium was changed for fresh normoxic medium, and treated as above, but in a standard cell incubator. Images of CA1 region of hippocampal slices were taken with a Leica SP-5 confocal microscope with a 40x objective. Samples were excited with an Ar/Kr laser using the 488 nm line for OHE and 496 nm line for E. Fluorescence emission of 2-OH-E was detected at 560-570 nm and Eth at 570-600 nm following previously-reported methods (Zhao et al., 2005). Three-dimensional image stacks were processed using ImageJ software. For each stack, the mean fluorescence from the CA1 region of each condition was obtained and the background substracted,. The value from of two hippocampal slices in every condition was promediated in each independent experiment.

Data were analysed using one-way ANOVA followed by a Bonferroni's test (when comparing multiple groups). Values of $p < 0.05$ were considered to be statistically significant.

3.20 In vivo photothrombotic stroke

These experiments were part of a collaboration with Dr. Manuela G. López´s group and were performed by Dr. Javier Egea and Dr. Esther Parada. Three-month-old male C57BL/6 mice (30-35 g) were anesthetized with 1.5% isoflurane in oxygen under spontaneous respiration. Mice were then placed in a stereotaxic frame (David Kopf Instruments, Tujunga, CA, USA) and physiological temperature (37 ± 0.5 ºC) was maintained by a servo-controlled rectal probe heating pad (Cibertec, Madrid, Spain). A small incision in the midline was made and, after removal of the periosteum, bregma and lambda points were identified. A cold light (Zeiss KL 1500 LCD, Jena, Germany) was centred using a micromanipulator at 0.2 mm posterior and 1.5 mm lateral to bregma on the right side using a fibre optic bundle of 2 mm in diameter. One milligram of the photosensitive dye Rose Bengal (Sigma Aldrich, St. Louis, MO, USA) dissolved in sterile saline (0.1 mL) was injected intraperitoneally (i.p.). and 5 min later the brains were illuminated during 20 min. After completion of the surgical procedures, the incision was sutured and the mice were allowed to recover for 24 h. Animals were randomly distributed into 2 groups (Jahan and Vinuela, 2009):

control (treated with vehicle) and CGP-37157 30 mg/kg. CGP-37157 was dissolved in Tween 80 and diluted with 5x volume of NaCl 0.9% and was administered i.p. 5 min after photothrombotic stroke induction.

Twenty-four hours after stroke induction, mice were anesthetized and sacrificed by decapitation and brains were quickly removed. Then, coronal sections of 1-mm-thickness were cut and slices were incubated in a 2% solution of triphenyltetrazolium chloride and then fixed in a buffered formalin solution. Infarcted tissue was defined by the unstained area and the morphometric determination of cortical infarct volume was calculated by the use of an unbiased stereological estimator of volume based on Cavalieri's principle (Avendano et al., 1995). Data were analysed using Student's unpaired t test. Values of $p < 0.05$ were considered to be statistically significant.

3.21 Statistics

In addition to specific statistical analyses described in each method, other data were analysed using Student's unpaired t test (when comparing two groups) or by one-way ANOVA followed by a Bonferroni's test (when comparing multiple groups), as indicated in the figure legends. Values of $p < 0.05$ were considered to be statistically significant.

Results

4 Results

4.1 Hypoxia produces a superoxide burst in cells

4.1.1 Hypoxia induces a superoxide burst in the first minutes of hypoxia in endothelial cells

So far, the level of ROS production in hypoxia has been debated, mostly because of discrepancies in the results obtained by several groups (Chua et al., 2010, Chandel et al., 1998). Such differences could result from the use of non-specific probes for ROS detection, reoxygenation of the samples and times of hypoxia studied. We aimed to determine whether reduction in oxygen concentration was able to induce the production of superoxide at different times of short hypoxia in endothelial cells. Since endothelial cells are the first cells in the vessel lumina, they could be important in sensing oxygen variations. In addition, since it is a rather gycolityc cell type mitochondria would serve as a rather signalling organelle and approaches altering mitochondrial homeostasis would affect drastically to their bioenergetics.

Dihydroethidium (DHE) reacts specifically with superoxide to produce 2-hydroxyethidium (2-OH-E) which can be detected by fluorescence microscopy. We have developed a method for measuring superoxide production analysing the 2-OH-E signal in fixed cells. As a positive control we used antimycin A which inhibits complex III of the OXPHOS system, increasing superoxide production (Turrens, 2003). Primary bovine aortic endothelial cells (BAEC) were subjected to hypoxia for different times, ranging from 10 to 70 min. DHE was added over the last 10 min of hypoxic exposure, and after that, cells were fixed in the hypoxia chamber, avoiding reoxygenation. The amount of 2-OH-E produced was assessed in a fluorescence microscope (Figure 4.1a-b). Antimycin A gave a clear signal, (not compared in the statistical test, as it was just a positive control). A significant increase in superoxide amount was observed within the first minutes of hypoxia, compared to the value in normoxia. An additional analysis of the linear trend (p trend(Armitage, 2012)) among the measures at different times in hypoxia showed that superoxide production was progressively diminished over the following hour. Similar results were obtained with a cell line derived from human endothelial cells, EA.hy926 (Edgell et al., 1983)(Figure 4.1c-d).

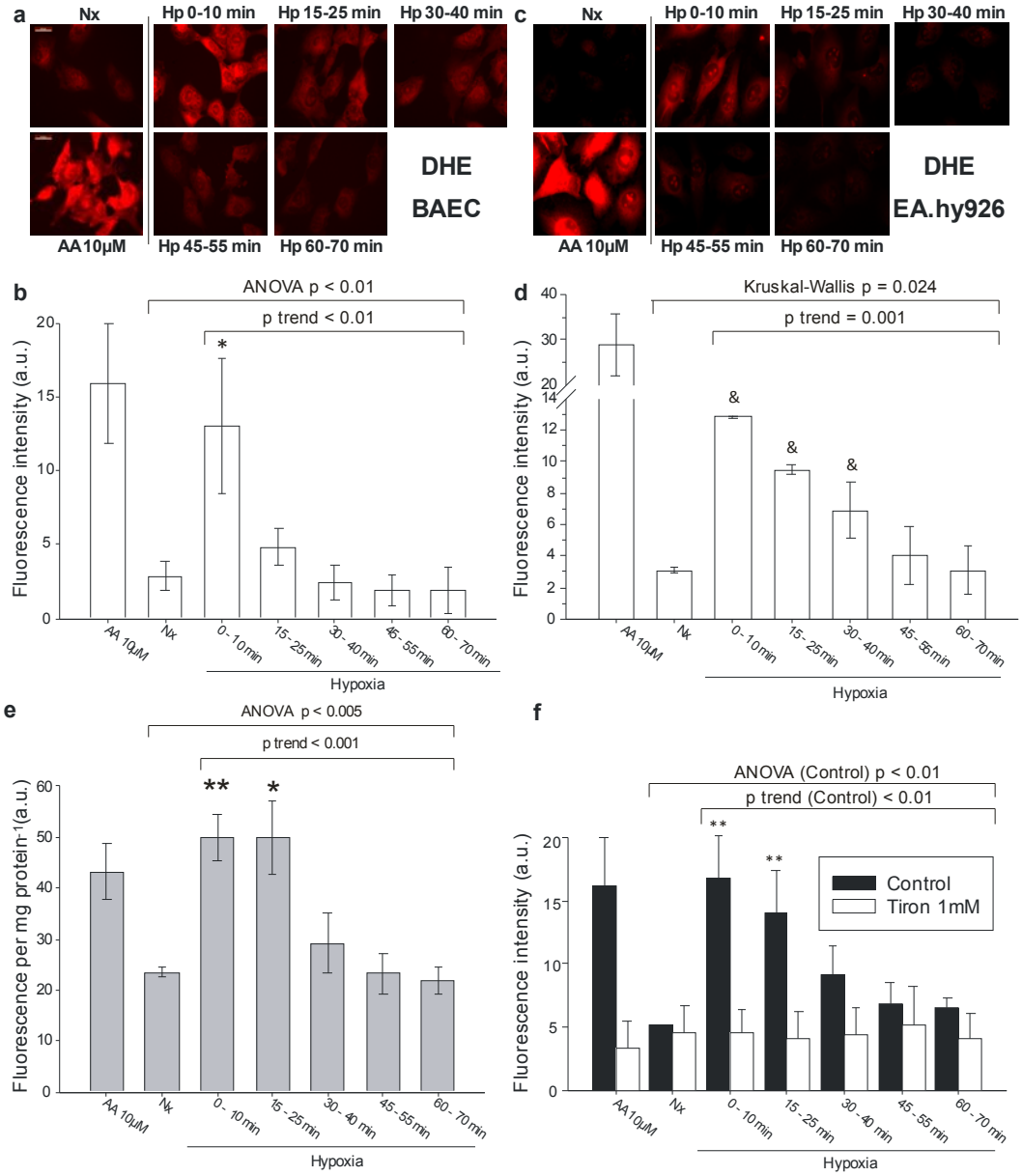

Figure 4.1. Superoxide detection by DHE in endothelial cells. BAECs **(a, b)** and EA.hy926 cells **(c, d)** were incubated for 60 min in normoxia (Nx), in normoxia with antimyicin A (AA, 10 µM for 30 min) or incubated in a hypoxia chamber at 1% oxygen with medium pre-equilibrated in the hypoxic condition (Hp) for 0, 15, 30, 45 or 60 min. 5 µM DHE was added for 10 min more, and cells were fixed in the hypoxia chamber. **(a, c)** Representative images showing DHE fluorescence. **(b, d)** Quantification of images from four **(b)** or three **(d)** independent experiments. **(e)** BAECs were treated as in **(a)**; after DHE incubation cells were lysed in the hypoxia chamber, frozen and 2-OH-E amount was analyzed by HPLC with fluorescent detection. Data are presented as mean ± s.e.m. of four independent experiments. **(f)** Quantification of three independent experiments of control BAECs (black bars) and BAECs incubated with 1 mM Tiron (white bars), treated as in **(a)**. Data are presented as mean ± s.e.m. * $p < 0.05$, ** $p < 0.01$, & $p = 0.0495$ versus Nx (one-way ANOVA or Kruskal-Wallis). Linearity of fluoresncence intensity among hypoxic samples was analyzed by linear trend test. Linearity significant p trend < 0.05. a.u., arbitrary units.

DHE oxidation measurement by fluorescence microscopy is not completely specific for superoxide detection, as there are other reactions that can also give fluorescent products, but 2-

OH-E can be differentiated from ethidium and other products by HPLC analysis with fluorescent detection (Zhao et al., 2005). In order to confirm the results from microscopy and to unambiguously detect the production of superoxide, we performed HPLC analysis of cell lysates from BAECs subjected to hypoxia, incubated with DHE and extracted in the hypoxia chamber. The peak of 2-OH-E is clearly separated from the peak of ethidium (Eth), both in control experiments with cyclosporine A treatment (Redondo-Horcajo et al., 2010) and in hypoxia treatments (Figure 4.2a-b). With this methodology we also observed a transient burst of superoxide production during the first minutes of hypoxia (Figure 4.1e). Superoxide signal thereafter decreased, and did not differ from normoxic values after 45-60 min in hypoxia. These findings correlated with the results obtained by fluorescence microscopy (Figure 4.1a-d), confirming the specific detection of superoxide in our setting. In order to further confirm the superoxide burst, we aimed to inhibit it with specific reagents, so we treated BAECs with 1 mM Tiron before and during the hypoxic incubation in microscopy experiments. Tiron reacts with superoxide, and clearly abolished the signal from the superoxide burst in hypoxia (Figure 4.1f).

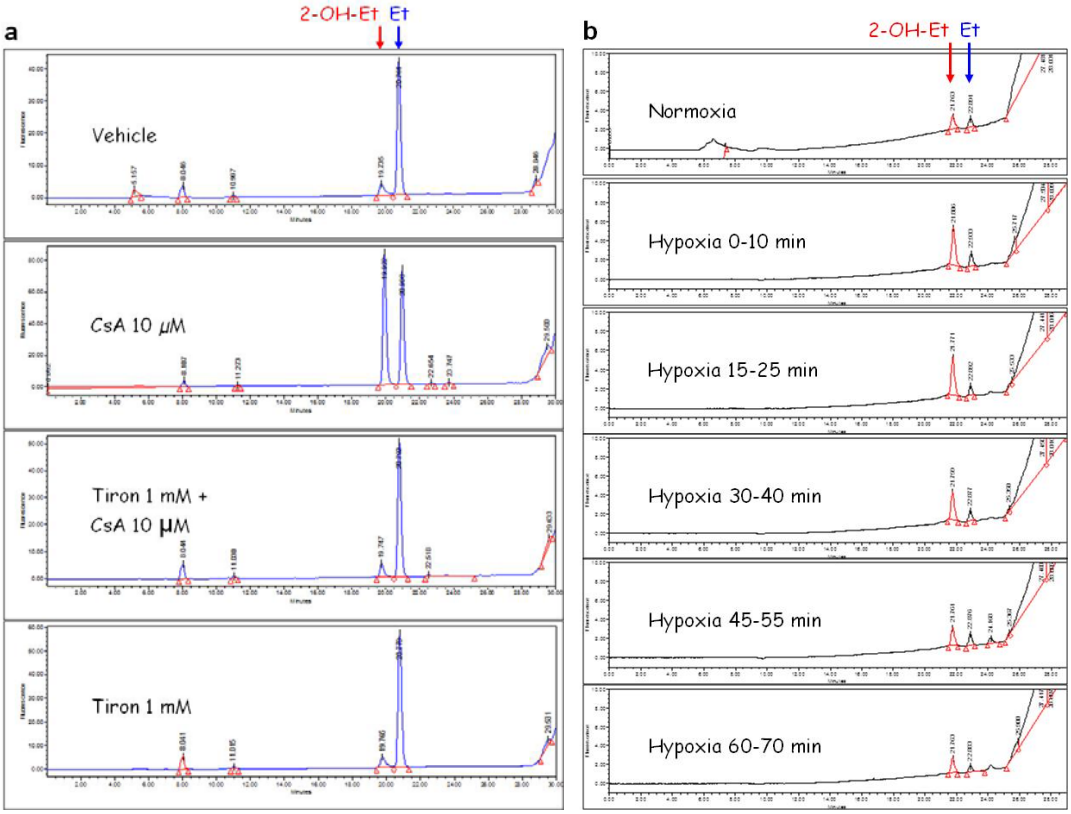

Figure 4.2. **Chromatograms from control experiments showing the separation of the peaks corresponding to 2-hyroxyethidium (2-OH-E) and ethidium (Eth). (a)** Treatment of BAECs with cyclosporin A (CsA) induced superoxide anion production (Redondo-Horcajo et al., 2010), which was abolished by treatment with 1 mM Tiron. **(b)** Chromatograms from a representative experiment included in Figure 4.1e. Exposure of BAECs to hypoxia increased the area of 2-OH-Et peak in the first minutes, decreasing to normoxic values thereafter (quantified in Figure 4.1e), independently of the Eth peak.

Next, we wanted to assess if this superoxide burst is specific of the change in oxygen concentrations we have used in the experimental setting, so we performed similar experiments with different initial and final oxygen concentrations. First, we used a lower initial "normoxic" reference concentration, 7% oxygen, which could be more physiologically relevant for endothelial cells, maintaining the hypoxia at 1% oxygen. We observed a similar superoxide burst (Figure 4.3a). Similar increase in superoxide production was observed when 2% oxygen was used as hypoxia while ambient air was used as normoxia. In fact the amplitude of superoxide burst at 2% oxygen exceeded that observed at 1% oxygen (Figure 4.3b).

In order to determine the production of other ROS (Kalyanaraman et al., 2012) that could be derived from the superoxide burst we used 5(6)-carboxy-2',7'-dichlorofluorescein diacetate (CDCFDA). BAECs incubated in hypoxia showed a burst in CDCFDA oxidation, which peaks at 15-30 min (Figure 4.3c-d), suggesting that the superoxide burst is translated into a burst of other ROS such as hydrogen peroxide with a slight delay.

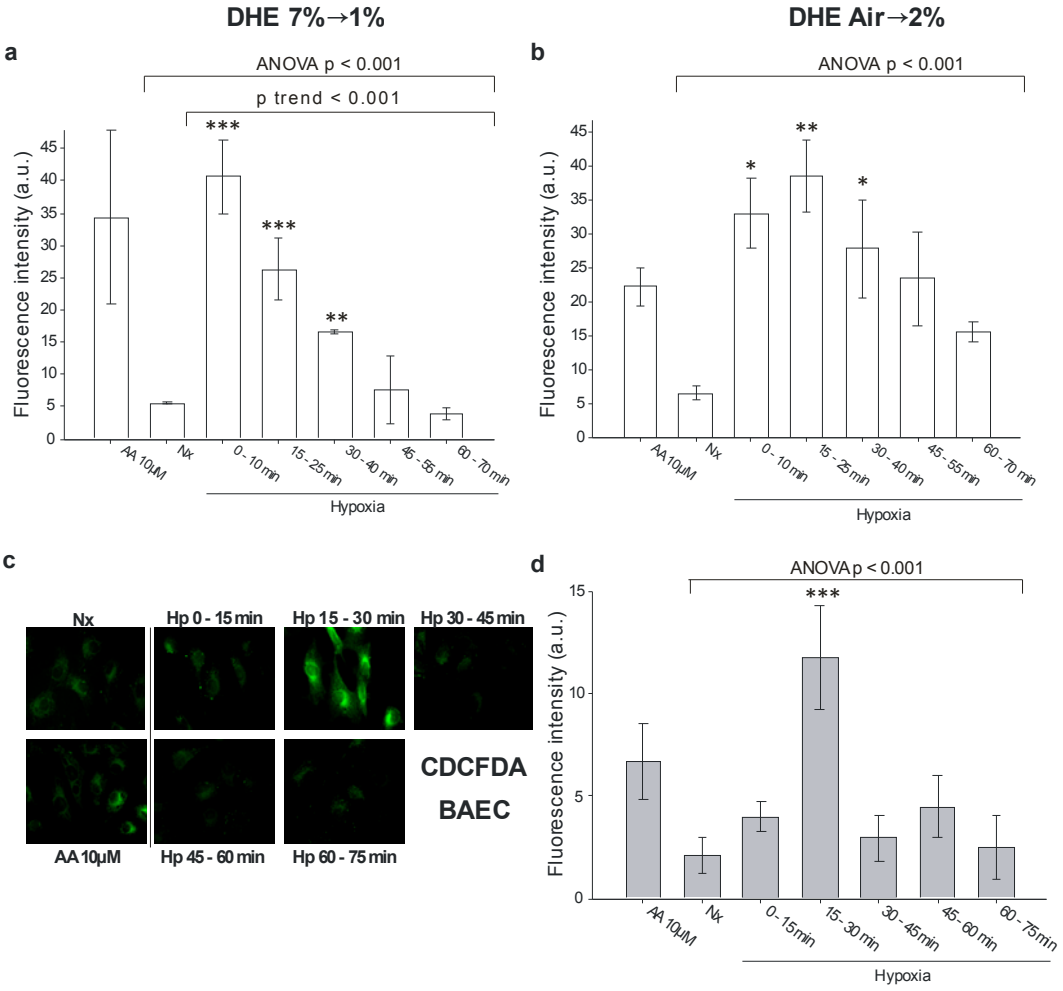

Figure 4.3. The time course of ROS production varies slightly with different concentrations of oxygen in normoxia and hypoxia, and the probe used. (a) BAECs were treated as in Figure 1, but normoxia was set at 7% oxygen. **(b)** BAECs were treated as in Figure 1, but the hypoxia chamber was set at 2% oxygen and normoxia performed at atmospheric oxygen concentration. **(a and b)** Quantification of

images from three independent experiments. **(c and d)** BAECs were treated as in Figure 1. CDCFDA 10 μM was added for 15 min more, and cells were fixed in the hypoxia chamber. **(c)** Representative images showing CDCFDA fluorescence. **(d)** Quantification of images from four independent experiments. Data are presented as mean ± s.e.m. *** $p < 0.001$ versus Nx, ** $p < 0.01$ versus Nx, * $p < 0.05$ versus Nx.

4.1.2 Superoxide is produced in mitochondria

We next wanted to explore the role of mitochondria in the superoxide production induced in acute hypoxia. To this end, we used the mitochondria-targeted probe Mito-HE, in which a triphenylphosphonium (TPP^+) group is linked to DHE. Mito-HE accumulates within active mitochondria since positively charged TPP^+ drives the compound to the negatively charged mitochondrial matrix (Robinson et al., 2006). EA.hy926 incubated with Mito-HE during the last 10 min of exposure to 1% oxygen showed a similar acute transient rise of superoxide production in response to hypoxia (Figure 4.4a-b), suggesting mitochondrial localization of superoxide production. Again, similar results were obtained in BAECs, where superoxide production in hypoxia could be even higher (Figure 4.4c-d).

We confirmed mitochondrial targeting of Mito-HE by assessing colocalization with prohibitin-1, a mitochondrial protein (Nijtmans et al., 2000) (Figure 4.4e). In order to additionally control that Mito-HE signal was actually related with increases in superoxide production and there was no saturation effect in the signal, we tested different concentrations of Mito-HE, observing that there is a clear increase with the Mito-HE concentration (Figure 4.4f).

A complementary approach to analyse the mitochondrial origin of the superoxide production came from the study of the hypoxia response in ϱ^0 cells, which do not have a functional OXPHOS due to mitochondrial DNA damage. ϱ^0 cells are cells treated with small amounts of ethidium bromide which depletes mitochondria from its DNA, leaving nuclear DNA undamaged (Perales-Clemente et al., 2008). Nuclear DNA expression is maintained, although there could be some variations dude to the long ethidium bromide exposure. Thus. ϱ^0 cells (ϱ^0L929) had their control cybrids with non-damaged mitochondria (TmC57BL/6J, from now on called C57)(Moreno-Loshuertos et al., 2006). ϱ^0 cells and C57 were subjected to hypoxia and DHE fluorescence was measured in the same conditions as with endothelial cells. C57 cells also showed a superoxide burst in the first minutes of hypoxia (Figure 4.4g, black bars). However, ϱ^0L929 cells showed much lower DHE signal, which does not increase with antimycin A treatment (due to the lack of OXPHOS); hypoxic exposure of ϱ^0L929 cells did not significantly affected the DHE signal (Figure 4.4g, white boxes). In line with the previous data these findings point to the mitochondrial origin of the superoxide burst that we observe in the first minutes of hypoxia.

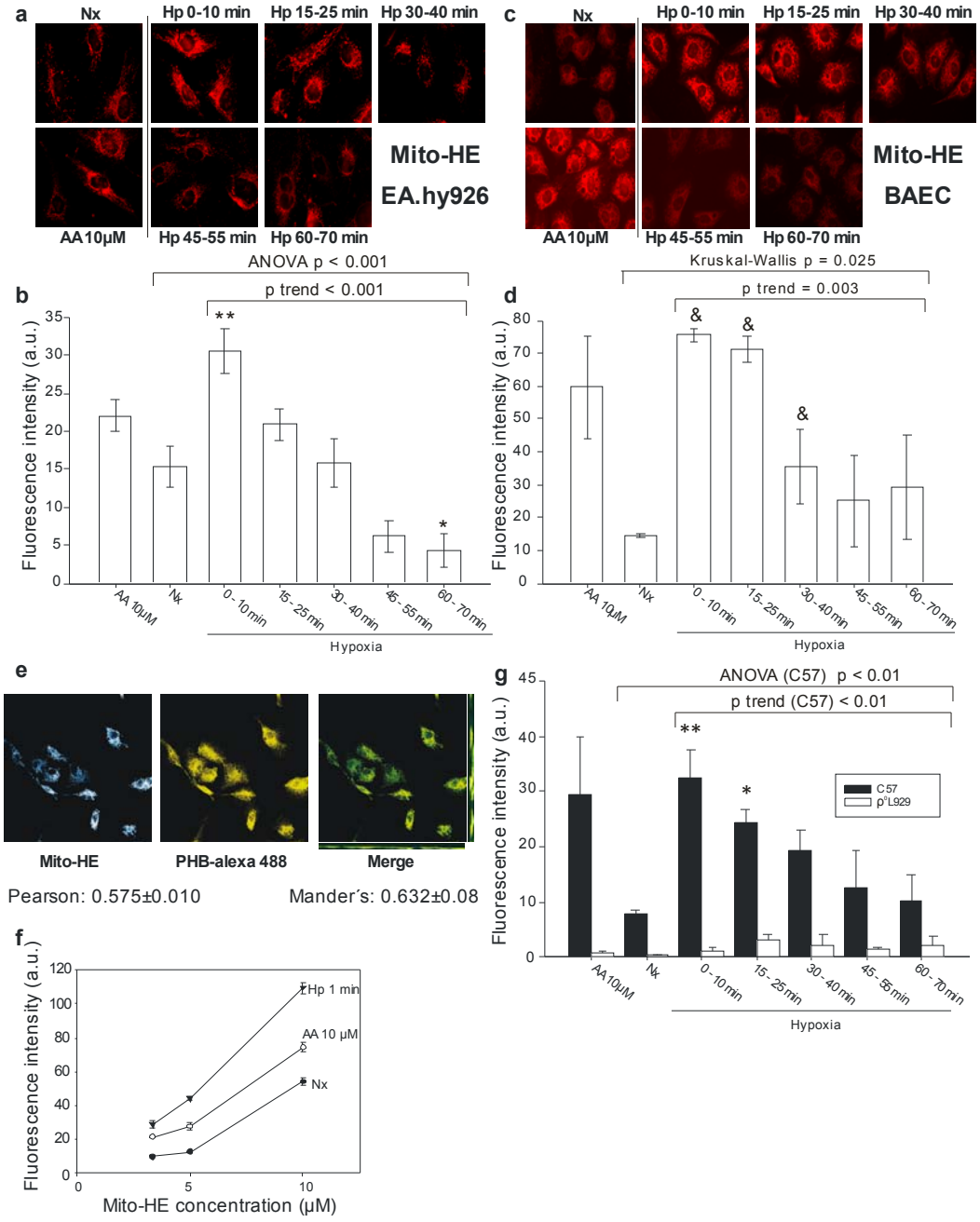

Figure 4.4. Hypoxic superoxide production is produced by mitochondria. EA.hy926 cells **(a, b)** and BAECs **(c, d)** were treated as in Figure 1. Mito-HE 5 μM was added for 10 min more, and cells were fixed in the hypoxia chamber. **(a, c)** Representative images showing Mito-HE fluorescence. **(b, d)** Quantification of images from three independent experiments. **(e)** BAECs were incubated with 5 μM Mito-HE for 10 min, fixed and immunostained with anti-prohibitin (PHB) antibody. Representative images show mitochondrial localization of Mito-HE. Pearson and Mander's correlation coefficients for colocalization of both signals were estimated. **(f)** BAECs were treated as in **(a)**, but incubated with different Mito-HE concentrations. Quantification of images from three independent experiments. **(g)** C57 (black bars) and ρ^0L929 cells (white bars) were treated as in Figure 1 and quantification shows three independent experiments. Data are presented as mean ± s.e.m. ** $p < 0.05$, * $p < 0.01$ versus Nx.

4.1.3 Early hypoxic superoxide production is confirmed in living cells

In the previous experiments the accumulation of ROS was detected for 10 (DHE) or 15 (CDCFDA) min following 0-60 min of incubation at hypoxic or normoxic conditions. In other words, the cells were incubated with the probe for the same period of time in all conditions, but this incubation time window was opened after different times of hypoxic treatment. In order to get a complementary measure of ROS production in hypoxia, we monitored the rates of oxidation of the ROS-sensitive probes using live imaging under normoxic or hypoxic conditions. In these conditions, the probe is added before the beginning of the measurement, and remains throughout all the experiment, so the incubation time with the probe increases progressively; thus, we expect the fluorescent signal to accumulate over time due to the irreversible oxidative modification of the probes.

Under normoxic conditions a gradual sustained increase in the oxidation signal was detected in BAECs using DHE, Mito-HE and CDCFDA (Figure 4.5a-c, black circles). This increase corresponds to the normoxic ROS production that oxidizes the probes. For assessing acute hypoxia, the oxygen concentration in the gas chamber around the cells in the microscope was changed to 2% oxygen after the first measurement at time 0. The oxidation signal of the probes increased more than in the cells under normoxia (Figure 4.5a-c, white circles). We calculated the rates of oxidation of the probes for the whole time of the experiment, which are clearly increased in hypoxia (Figure 4.5a-c, insets).

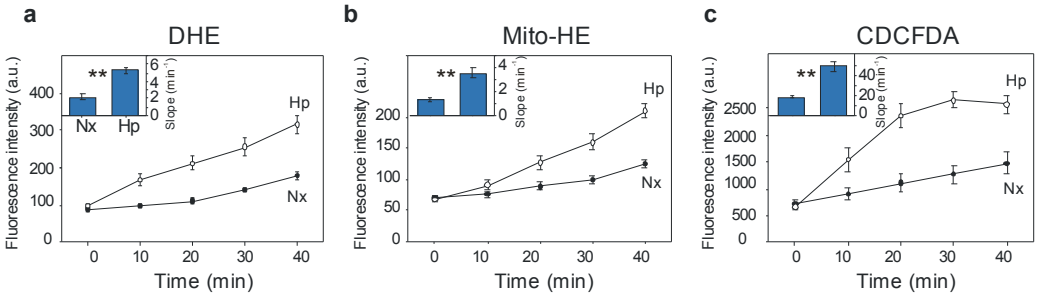

Figure 4.5. Superoxide and ROS production in acute hypoxia measured by fluorescence microscopy in living endothelial cells. BAEC were treated with 10 µM DHE **(a)**, 5 µM Mito-HE **(b) or** 15 µM CDCFDA **(c)** for 20 min and subsequently incubated in a chamber with atmospheric and temperature control in a fluorescence microscope, where they were maintained in normoxia for 40 min or placed in normoxia and switched to hypoxia (2% oxygen) for the rest of the experiment. Black circles: normoxia (Nx); white circles: hypoxia (Hp). Quantification of four regions for three independent experiments is plotted for each time as mean ± s.e.m. **(Insets)** Oxidation rates considering all time points of each replicate (n=3) are plotted as mean ± s.e.m. **p<0.01 versus Nx.

Using live imaging we have also explored the hypoxia-dependent changes in the mitochondrial membrane potential ($\Delta\Psi_{mt}$). Mitochondrial targeting of Mito-HE is driven by $\Delta\Psi_{mt}$. Thus, hyperpolarization is associated with greater accumulation of Mito-HE within mitochondria and a concomitant increase in fluorescence which is not caused by increased superoxide formation.

We have measured $\Delta\Psi_{mt}$ in BAECs using tetramethylrhodamine (TMRM) in non-quenching mode. TMRM-based probes are positive charged fluorescent molecules which are easily attracted by $\Delta\Psi_{mt}$. Thus, less accumulation inside the mitochondria due to depolarization would mean less fluorescent signal, this is so called the non-quenching mode. However, above certain concentrations (~ 50 nM) the accumulation of the probe drives its aggregation and quenching of the fluorescence. This translates into less signal upon hyperpolarization due to further aggregation of the probe and more fluorescence after depolarization because of its liberation from the aggregates (Perry et al., 2011). We confirmed non quenching mode measurement by the clear and immediate decrease in the signal when FCCP (which depolarizes by uncoupling OXPHOS) was added (Figure 4.6a). We also observed a signal increase after addition of oligomycin (which inhibits ATPase causing mitochondrial hyperpolarization) (Figure 4.6a). Hypoxic treatment of BAECs was associated with mitochondrial depolarization, while the potential was maintained or slightly increased in BAECs in normoxia (Figure 4.6b). Thus, oxygen production in the mitochondria of hypoxic BAECs could be underestimated using Mito-HE as the dye levels in depolarized hypoxic mitochondria would be lower than in the mitochondria of normoxic cells.

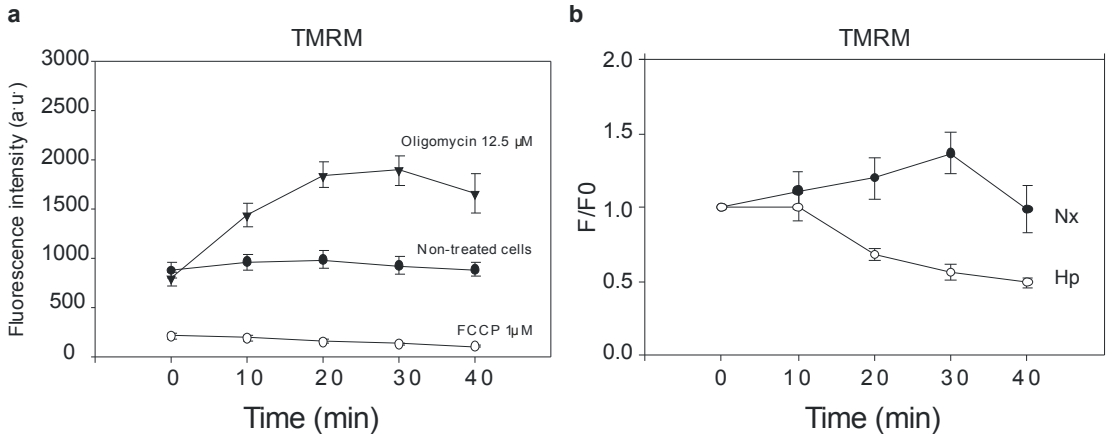

Figure 4.6. Mitochondrial membrane potential measurement by fluorescence microscopy in live untreated endothelial cells and treated with oligomycin or FCCP. (a) BAECs were treated with 30 nM TMRM as in Figure 4.5 but only in normoxia. Oligomycin or FCCP were added prior to image acquisition. Quantification of four regions for three replicates is plotted for each time as mean ± s.e.m. Black circles: non-treated cells; white circles: FCCP treatment; black inverted triangles: oligomycin treatment. **(b)** BAECs were treated as in Figure 4.5. Black circles: normoxia (Nx); white circles: hypoxia (Hp). Fluorescence quantification was plotted as F/F0 in order to make clearer the comparison of Nx vs Hp in-time variations.

We also used a model of cells in which OXPHOS is inactive to confirm the mitochondrial implication in the increased superoxide production in hypoxia. While C57 cells exhibit a clear increase in the DHE and CDCFDA signals when they are subjected to hypoxia, ϱ^0L929 cells do not have these changes when subjected to hypoxia (Figure 4.7).

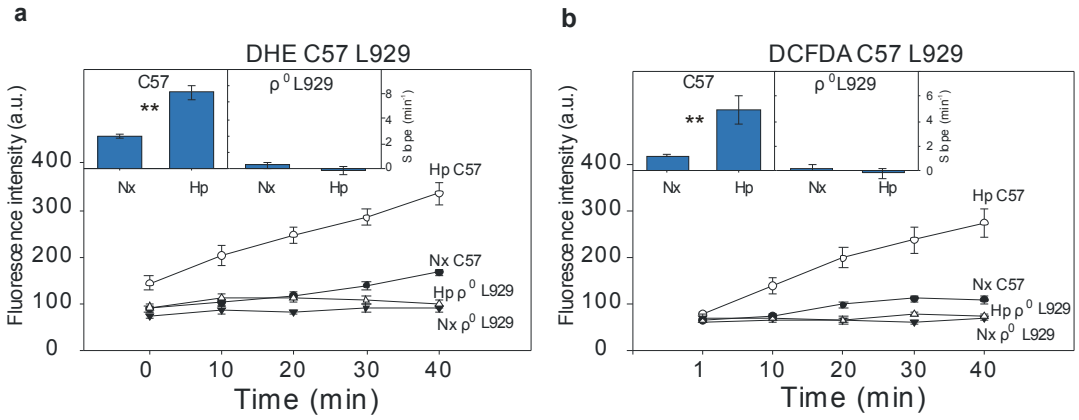

Figure 4.7. Superoxide and ROS production in acute hypoxia measured by fluorescence microscopy in living ρ0 cells. C57 and ρ^0L929 cells were incubated with 10 µM DHE **(a)** and 15 µM CDCFDA **(b)** and treated as in Figure 4.5. Black circles: C57 in normoxia (Nx C57); white circles: C57 in hypoxia (Hp C57); black inverted triangles: ρ^0L929 in normoxia (Nx ρ^0L929); white triangles: ρ^0L929 in hypoxia (Hp ρ^0L929). Quantification of four regions for three independent experiments is plotted for each time as mean ± s.e.m. **(Insets)** Oxidation rates considering all time points of each replicate (n=3) are plotted as mean ± s.e.m. **p<0.01 versus Nx.

4.1.4 Superoxide burst and ROS formation in hypoxia is not specific of endothelial cells

We wondered whether the hypoxia-induced superoxide burst and the increase in ROS production was specific to endothelial cells or a common feature for several cell types, so we studied it in different cell types.

First, we carried out live imaging experiments with cultured neonatal rat cardiomyocytes. In line with the results obtained in endothelial cells, hypoxia triggered a significant increase in the rate of oxidation of DHE, Mito-HE and CDCFDA, indicating an increased production of ROS (Figure 4.8a-c). Furthermore, depolarization of mitochondrial membrane in hypoxic cardiomyocytes was confirmed when monitoring the TMRM signal (Figure 4.8d), suggesting that superoxide production within mitochondria could be underestimated.

We also assessed whether tumour cells could exhibit a similar response to hypoxia. HeLa and HK2 cells were exposed to acute hypoxia and incubated with Mito-HE at different times, and. the response was similar to that of endothelial cells (Figure 4.8e-f). We also confirmed by HPLC with fluorescent detection that the DHE probe was specifically detecting the superoxide burst in HeLa cells (Figure 4.8g).

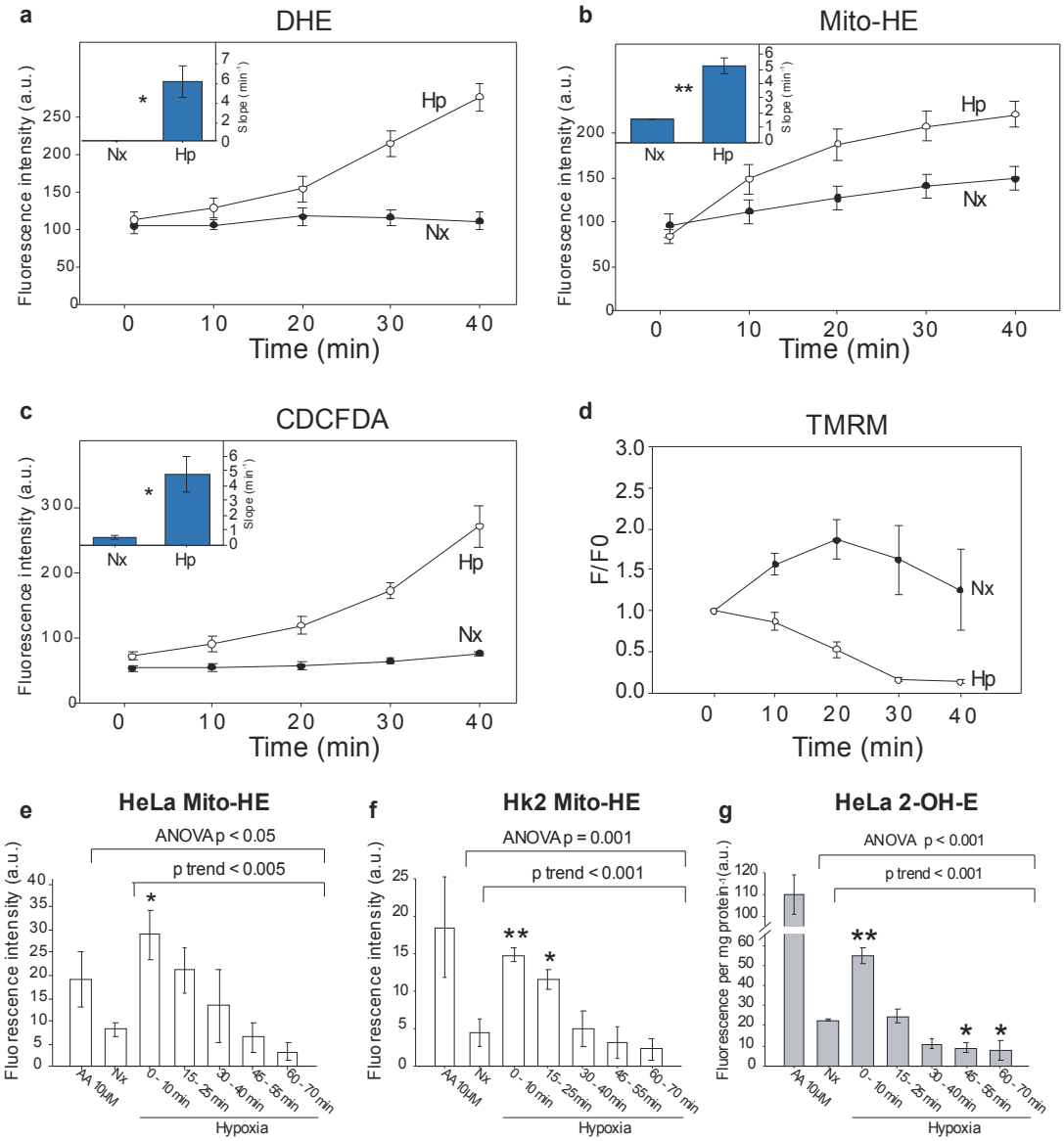

Figure 4.8. Hypoxia produces a superoxide burst and mitochondrial depolarization in different cell types. (a) Primary neonatal cardiomyocytes were treated and data obtained and plotted as in Figure 4. HeLa **(e)** and HK2 cells **(f)** were treated as in Figure 3a. 5 µM Mito-HE was added for 10 min more, and cells were fixed in the hypoxia chamber. **(g)** HeLa cells were treated as in Figure 1e. After DHE incubation (5 µM DHE, 10 min) cells were lysed in the hypoxia chamber, frozen and 2-OH-E amount was analyzed by HPLC with fluorescent detection. Data are presented as mean ± s.e.m. of three independent experiments. ** $p < 0.01$ versus Nx, * $p < 0.05$ versus Nx.

These results reinforce the involvement of mitochondria in hypoxic superoxide burst, and suggest that this could represent a general mechanism for different cell types.

4.2 Complex I deactivation and mitochondrial sodium/calcium exchange through NCLX are necessary for hypoxic ROS production

4.2.1 Hypoxia triggers sodium/calcium exchange via mitochondrial NCLX

We questioned whether sodium or calcium movements between cellular compartments were altered during acute hypoxia. To measure cytosolic calcium (Ca^{2+}_i) and sodium (Na^{+}_i) levels, BAECs were loaded with Fluo-4AM or CoroNa GreenAM fluorescent probes (they become fluorescent after calcium or sodium binding, respectively; acetoxymethyl ester –AM– makes these probes cell permeant and is removed with cellular esterases) for live cell imaging and exposed to normoxia or hypoxia for 40 min. A clear increase in Ca^{2+}_i and a decrease in Na^{+}_i was detected in cells acutely exposed to hypoxia, whereas the signals in normoxic cells remained constant (Figure 4.9a-b). We then treated BAECs with 10 μM CGP-37157 (CGP), a specific NCLX inhibitor, which abolished both the release of calcium into the cytosol (Figure 4.9c) and the concomitant depletion of cytosolic sodium (Figure 4.9d) in hypoxia-exposed cells.

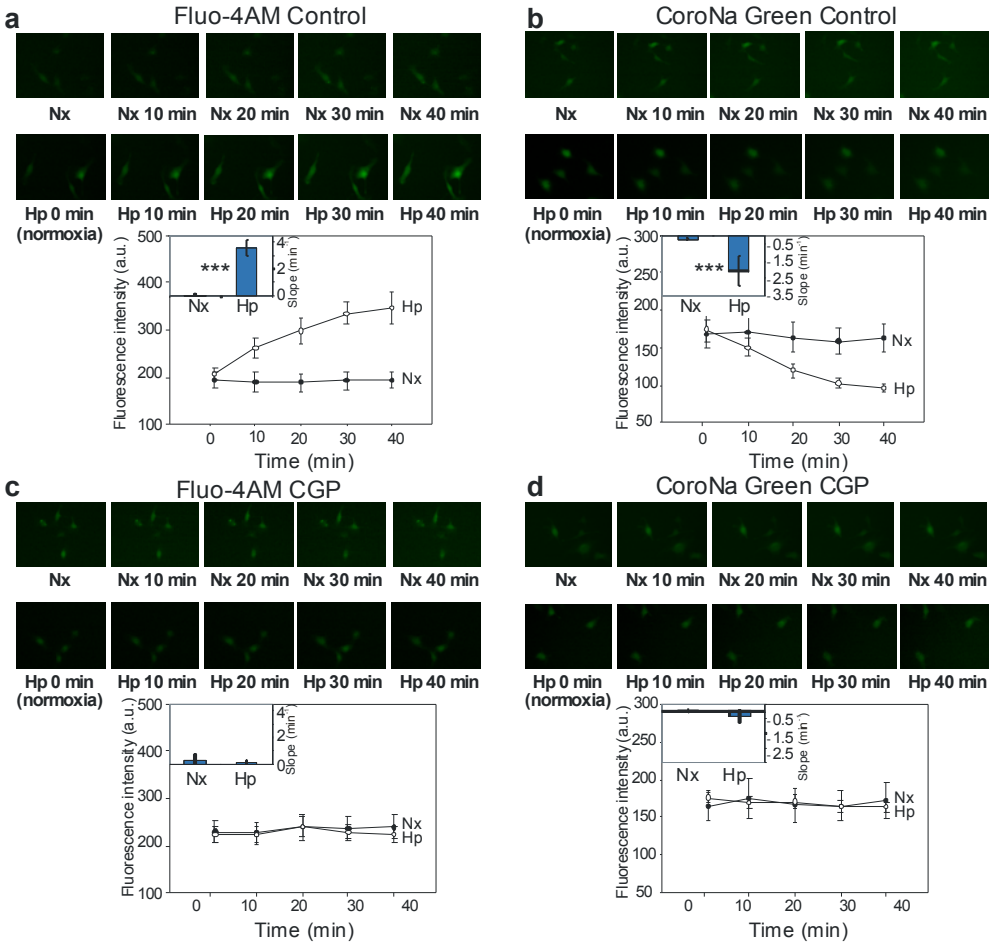

Figure 4.9. Acute hypoxia produces variations in cytosolic calcium and sodium inhibited by CGP-37157. Cytosolic calcium measured with the Fluo-4AM probe **(a and c)** or cytosolic sodium measured with the CoroNa Green probe **(b and d)** in normoxic (Nx, ●) and hypoxic (2% oxygen; Hp, ○)

conditions in BAECs by live cell imaging fluorescence microscopy. **(a, b)** Control treatment. **(c, d)** Addition of 10 μM CGP-37157 (NCLX inhibitor). Data are represented as mean ± s.e.m. of three independent experiments. **(Photographs)** Representative images of Nx and Hp times 0, 10, 20, 30 and 40 min. **(Insets in a-d)** Slopes considering all the ROI and time points of each replicate (n = 3) were estimated by linear regression and plotted as mean ± s.e.m. *** p<0.001 (Student's t-test).

Hypoxia-induced sodium/calcium exchange was not affected transfection with a scramble siRNA (siSCR), while it was abolished when we silenced NCLX by transfecting a siRNA specific for this gene (siNLCX; Figure 4.10).

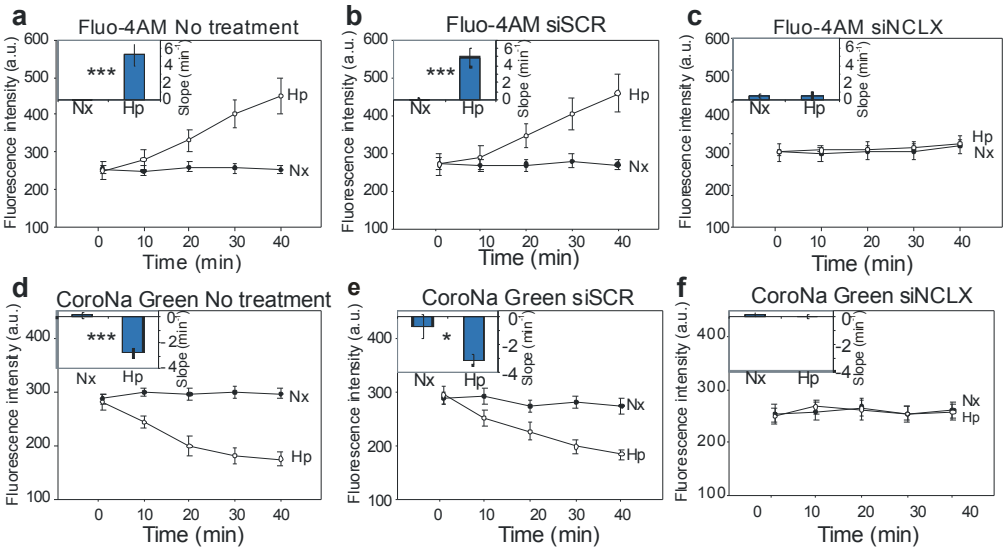

Figure 4.10. Acute hypoxia triggers calcium and sodium exchange via NCLX. Cytosolic calcium **(a-c)** or cytosolic sodium **(d-f)** in normoxic (Nx, ●) and hypoxic (2% oxygen; Hp, ○) conditions were measured as in Figure 4.9 in BAECs by live cell imaging fluorescence microscopy. **(a and d)** Non-treated controls. **(b and e)** Cells transfected with scramble siRNA (siSCR). **(c and f)** Cells transfected with siRNA for NCLX (siNCLX). Data are represented as mean ± s.e.m. of three independent experiments. **(Insets in a-f)** Slopes considering all the ROI and time points of each replicate (n = 3) were estimated by linear regression and plotted as mean ± s.e.m. *** p<0.001, * p < 0.05 (Student's t-test).

NCLX mediates the extrusion of one calcium in exchange for three sodium ions (Poburko and Demaurex, 2012) triggering an electrogenic process that is capable of modifying the mitochondrial membrane potential (Kim and Matsuoka, 2008). Thus, we questioned whether NCLX activity could take part in the mitochondrial depolarization that we have seen in acute hypoxia (Figure 4.6). Treatment of BAECs with CGP (Figure 4.11a-b) or NCLX gene knockdown (Figure 4.11c-e) inhibited mitochondrial depolarization in acute hypoxia as shown by live cell imaging. These findings were corroborated in primary rat cardiomyocytes (Figure 4.11f-g).

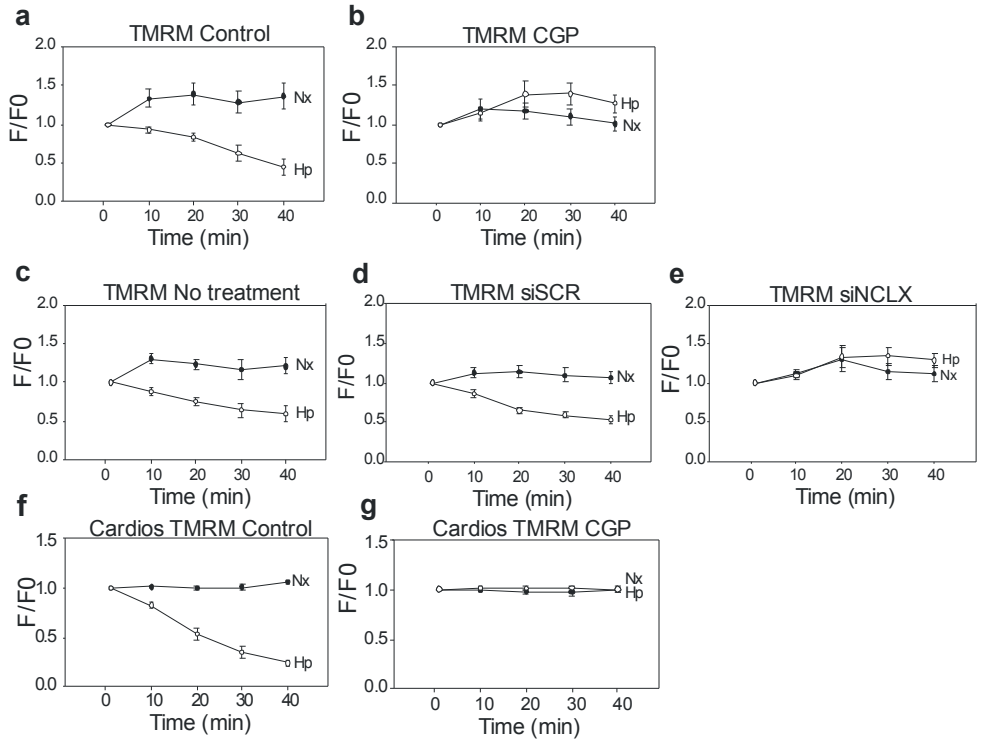

Figure 4.11. Inhibition of NCLX prevents hypoxic mitochondrial depolarization. BAECs **(a-b)** or rat primary cardiomyocytes **(f-g)** untreated **(a, f)** or treated with 10 μM CGP-37157 **(b, g)** were subjected to normoxia (Nx, ●) or hypoxia (2% oxygen; Hp, ○) and mitochondrial membrane potential detected with the TMRM probe. **(f-h)** Same as a-b in untreated **(c)**, siSCR-treated **(d)** or siNCLX-treated **(e)** BAECs. Data are represented as mean ± s.e.m. of the actual fluorescence divided by the fluorescence at time 0 (F/F_0) of three independent experiments.

Overall, these results show that in acute hypoxia NCLX alters the calcium and sodium concentrations in the cytosol, and is involved in the hypoxia-induced mitochondrial depolarization.

4.2.2 NCLX activity is needed for ROS production in acute hypoxia

We next explored whether NCLX participates in superoxide production in hypoxia. To do this, we exposed BAECs to different periods of hypoxia after which we added DHE for 10 min. Pre-incubation of BAECs with CGP inhibited the hypoxic burst (Figure 4.12a-b). Similar results were obtained in human umbilical vein endothelial cells (HUVECs) treated with CGP (Figure 4.12c) and in BAECs after NCLX knockdown (Figure 4.12d).

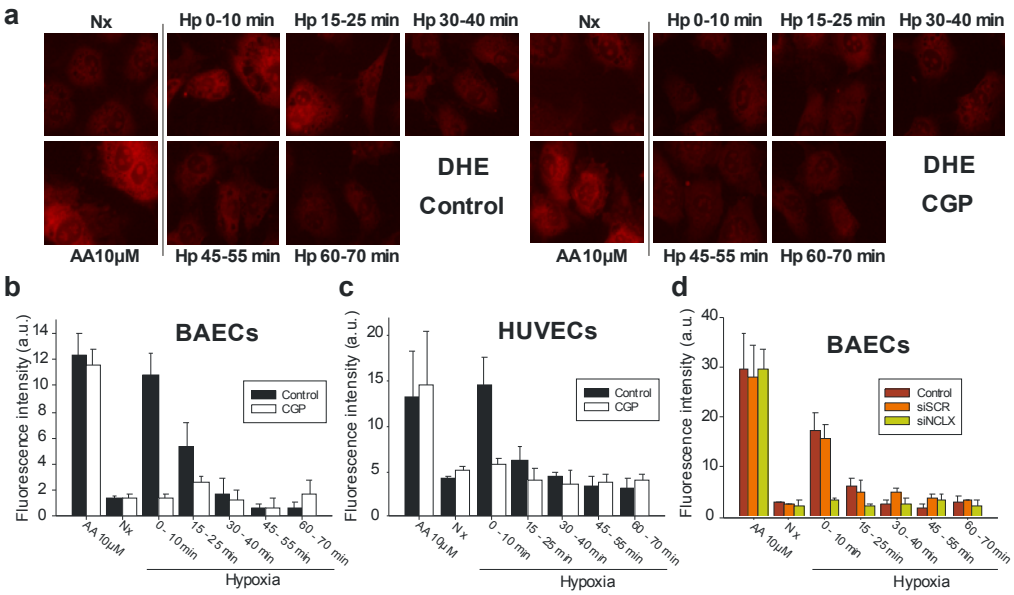

Figure 4.12. Inhibition of NCLX prevents the superoxide burst triggered by hypoxia. (a-d) Detection of superoxide production by fluorescence microscopy in fixed cells. Cells were incubated for 60 min in normoxia (Nx), for 30 min in normoxia with antimycin A (AA 10 μM) or incubated with pre-hypoxic medium in a hypoxia chamber at 1% oxygen (Hp) for 0, 15, 30, 45 or 60 min. DHE (5 μM) was added for 10 min more and cells were fixed in the hypoxia chamber. BAECs **(a, b)** or HUVECs **(c)** without (Control) or with 10 μM CGP-37157. **(d)** BAECs untreated (Control), or treated with scramble siRNA (siSCR) or siRNA against NCLX (siNCLX). **(a)** Representative images showing DHE fluorescence in BAECs. **(b-d)** Data are presented as mean ± s.e.m. of three independent experiments.

We also performed live imaging to measure general ROS production using CDCFDA. BAECs treated with CGP did not show an increased DCFDA fluorescence intensity during hypoxia (Figure 4.13a-b).

In addition, we used the ratiometric fluorescent protein HyPer, which is reversibly oxidized in cysteine residues by hydrogen peroxide or other peroxides; this oxidation alters the fluorescence signal, allowing it to detect changes in the redox state of the cell compartments (Belousov et al., 2006). When we transfected BAECs with a cytosolic version of the protein, CytoHyPer, the oxidation signal decreased upon treatment with dithiothreitol (a thiol-reduding agent) and increased after mitochondrial ROS production induced by antimycin A (Figure 4.13c); this shows that the protein is sensing redox changes in these cells. Hypoxia induced the increase in the HyPer signal during the first 20 minutes of hypoxia, which decreased thereafter (Figure 4.13d), confirming the burst in ROS production which is reverted in longer hypoxia times. This peak in ROS production was abolished upon treatment with CGP (Figure 4.13e) or 1 μM rotenone (Figure 4.13f). We also used mitoHyPer, a HyPer version targeted to the mitochondrial matrix, obtaining similar results (Figure 4.13g-h).

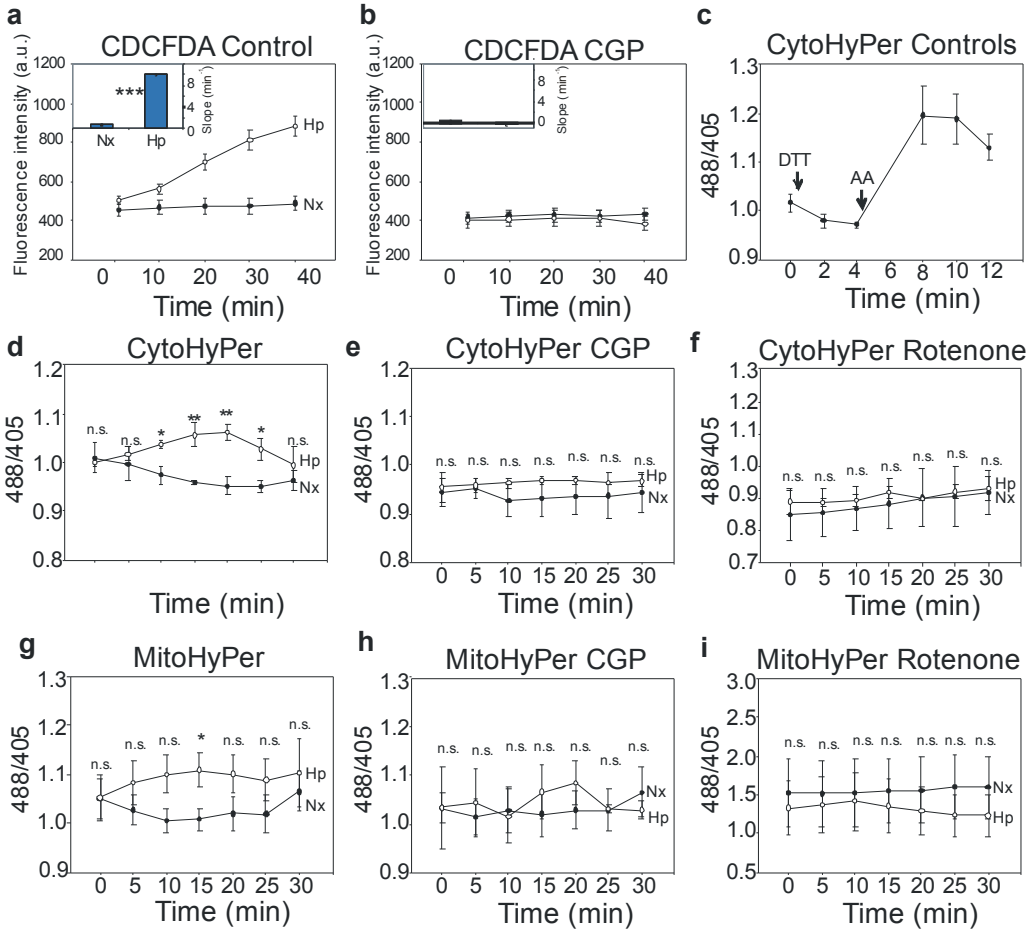

Figure 4.13. Inhibition of NCLX prevents the increase in mitochondrial ROS production triggered by hypoxia. (a and b) Detection of ROS production by live fluorescence microscopy with CDCFDA. BAECs untreated **(a)** or treated with 10 µM CGP-37157 **(b)** were subjected to normoxia (Nx, ●) or hypoxia (2% oxygen; Hp, ○). Data are presented as the mean ±s.e.m. of three independent experiments. **(Insets in a and b)** Slopes considering all time points of each replicate (n = 3) are plotted as mean ±s.e.m. The slope for each replicate was estimated by linear regression of the data for all the ROI and time points. * $p<0.05$ (Student's t-test). **(g-j)** Detection of hydrogen peroxide by the ratiometric fluorescent probe CytoHyPer. **(c)** BAECs were transfected with CytoHyPer, treated with 2 mM of the thiol reducing agent DTT and with 30 µM of antimycin A (AA). **(d-f)** CytoHyPer transfected BAECs either untreated **(d)**, treated with 10 µM CGP-37157 **(e)** or with 1 µM rotenone **(f)** were subjected to normoxia (Nx, ●) or hypoxia (1% oxygen; Hp, ○). **(a-c)** Detection of mitochondrial hydrogen peroxide by the ratiometric fluorescent probe Mito-HyPer. BAECs transfected with Mito-HyPer were either untreated **(g)**, treated with 10 µM CGP-37157 **(h)** or with 1 µM rotenone **(i)** and subjected to normoxia (Nx, ●) or hypoxia (1% oxygen; Hp, ○). Data are presented as the mean ±s.e.m. of four independent experiments. n.s. non-significant difference, * $p < 0.05$, ** $p < 0.01$ (Student's t-test).

4.2.3 NCLX inhibition has no effect on respiration

We next sought to determine whether NCLX inhibition impacted cellular respiration. A widely used approach to analyse the bioenergetic footprint in cells is the measurement of oxygen consumption with subsequent injections of oligomycin, FCCP and antimycin A/rotenone (BOFA assay; Figure 4.14a). Once basal respiration is measured, oligomycin is added to inhibit complex V,

blocking respiration. Therefore, the amount of oxygen used to produce ATP by OXPHOS is estimated from the difference with basal oxygen consumption (i.e. coupling efficiency). FCCP uncouples OXPHOS by making the IMM permeable to protons, thus maximizing electron flux through the ETC what translates into the cellular maximal respiration. This treatment provides information about the stored energy in mitochondria that a cell could use in an energetic crisis (i.e. reserve capacity). Antimycin A and rotenone block complexes III and I, respectively, and inhibit electron flux through the ETC. This eliminates any proton translocation through this complexes. Therefore, the leftover value is the non-mitochondrial respiration, i.e. the oxygen consumed by other enzymes in the cell. Ultimately, proton leak is the respiration due to the proton translocation due to other molecules than complex V, which is calculated from the remaining respiration after oligomycin addition less the non-mitochondrial respiration.

We performed BOFA analysis to evaluate the effect of CGP on oxygen consumption rate (OCR) and several other respiratory parameters (Figure 4.14a). CGP treatment had no effect on any of measured parameters (Figure 4.14a-f) and NCLX knockdown did not affect respiration in comparison with control (Figure 4.14g-l), except for an increase in maximal respiration, indicating a higher reserve capacity (Figure 4.14j).

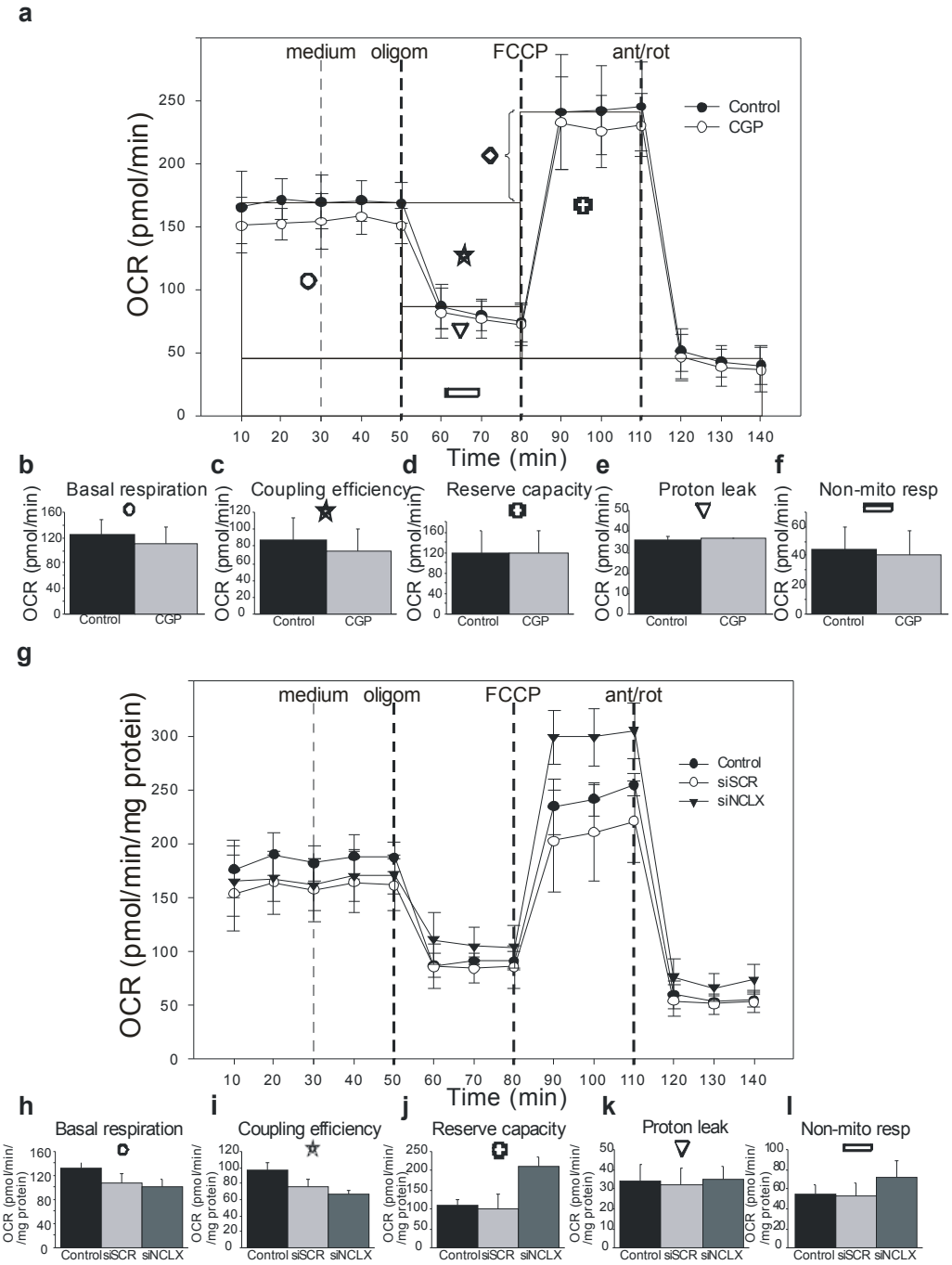

Figure 4.14. Inhibition of NCLX has no effect on oxygen consumption rate (OCR). (a-f Oxygen consumption was measured in a Seahorse XF24 Analyzer in untreated BAECs (Control, ●) or BAECs treated with 10 µM CGP-37157 (CGP, ○). (g-l) Oxygen consumption in untreated BAECs (Control, ●), BAECs treated with scramble siRNA (siSCR, ○) or with siRNA against NCLX (siNCLX, ▼) was measured in a Seahorse XF24 Analyzer. (a and g) OCR plots indicating the sequential addition of drugs: medium, 5 µg/ml oligomycin (oligom), 300 nM FCCP, 1 µM rotenone and 1 µM antimycin A (ant/rot). Boxes (exemplified for the control measurements) represent the calculations shown in b-f and h-l: (⬯) Basal respiration (b, h), (★) coupling efficiency (c, i), (✪) maximal respiration, (◇) reserve capacity (d, j), (▽) proton leak (e, k) and (▭) non-mitochondrial respiration (f, l). Data are presented as mean ± s.e.m. of three (a-f) or four (g-l) independent experiments.

4.2.4 NCLX-dependent sodium/calcium exchange is dependent on mitochondrial complex I, but not on complex III

We next wanted to analyse the relationship between the induction of NCLX activity in acute hypoxia and the function of mitochondrial complexes. Previous reports have shown that mitochondrial complex III Rieske iron-sulphur protein (RISP) is necessary for ROS production in hypoxia (Guzy and Schumacker, 2006a, Hamanaka and Chandel, 2010, Hamanaka et al., 2016) and that rotenone, a well-established complex I inhibitor, can abolish it (Archer et al., 1993, Chandel et al., 1998). We therefore silenced the expression of key genes in complex I and complex III in BAECs to determine whether they were implicated in hypoxic ROS production. NDUFS2 gene encodes for the bovine 49 kDa core subunit of complex I whose function is related to the binding of ubiquinone. NDUFS4 gene encodes for the bovine 18 kDa accessory subunit of complex I, and is related to the stability of the complex (Stroud et al., 2016). UQCRFS1 encodes for RISP protein in complex III and is vital for electron transfer from ubiquinol to the rest of complex (Iwata et al., 1998). Interference with siNUFS4, siNDUFS2 and siRISP reduced clearly the amount of each protein interfered (Figure 4.15a-c). We also analysed by blue native electrophoresis (BN-PAGE) the organization of mitochondrial complexes and supercomplexes after the interferences. NDUFS4 knockdown destabilized most of complex I and its corresponding supercomplexes, leaving a subcomplex which could be complex I less the N-module as recently reported (Stroud et al., 2016); in contrast, the assembly of complex III and the lighter complex III containing supercomplexes was not affected (Figure 4.15d-e). RISP knockdown destabilized complex III-containing supercomplexes, while preserving a band corresponding to complex III; Western blot of complex I in siRISP confirmed the loss of complex III-containing supercomplexes, while the band for complex I was maintained assembly was not affectedtogether with the lightest complex I containing supercomplex (Figure 4.15d-e).

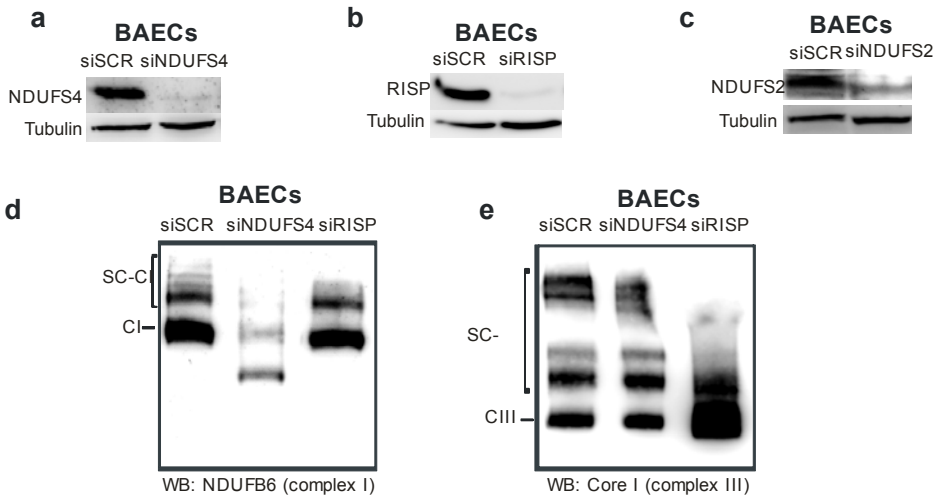

Figure 4.15. Complex I and complex III subunits interference. (a-c) Protein extracts from BAECs treated with siSCR, siNDUFS4, siRISP or siNDUFS2 were immunoblotted for NDUFS4, RISP or NDUFS2 proteins with tubulin as a loading control. **(d and e)** BN-PAGE of siSCR-treated, siNDUFS4-treated or siRISP-treated BAECs, revealed by western blotting with antibodies against NDUFB6 (complex I; d) or Core I (complex III; e).

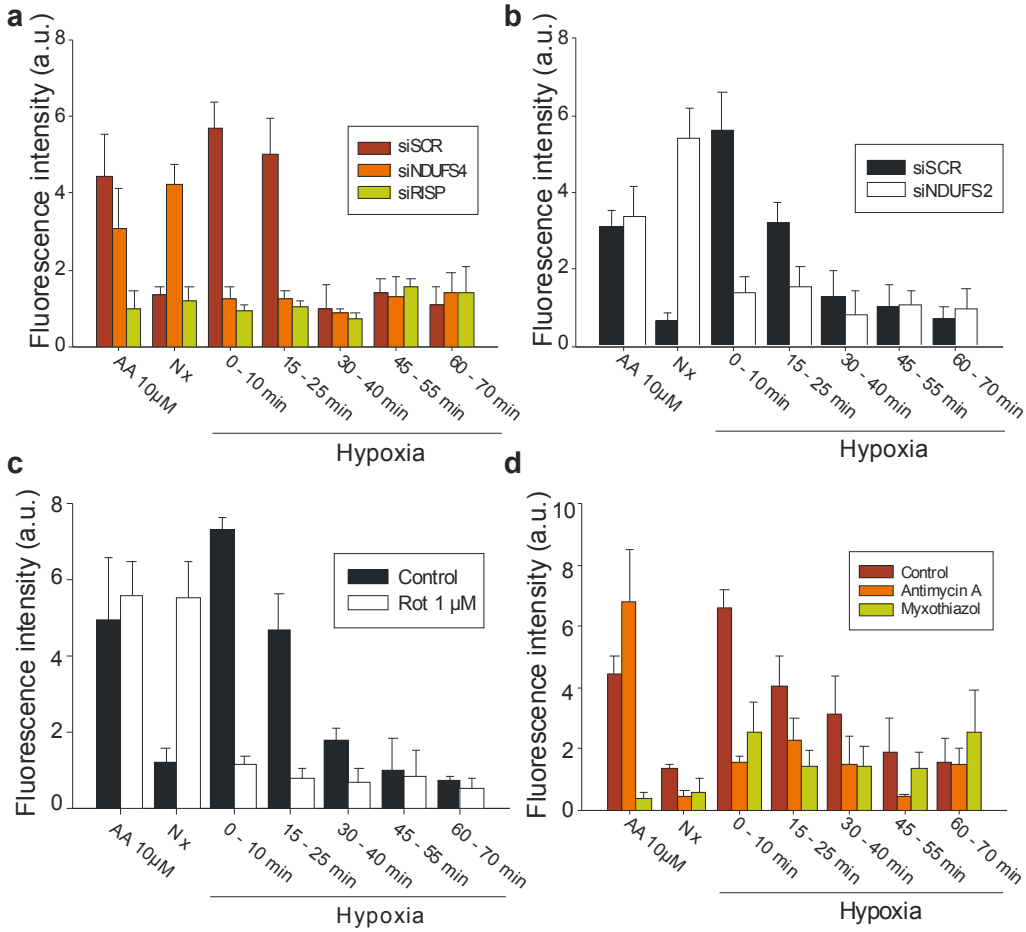

Figure 4.16. Complex I or complex III deficiency or inhibition prevents hypoxic ROS production. (a and b) Superoxide detection by fluorescence microscopy with DHE after fixation in BAECs treated with siSCR (red or black), siNDUFS4 (orange), siRISP (yellow) or siNDUFS2 (white) and subjected to the same protocol as in Figure 1. **(c)** Untreated (black) or BAECs treated with 1 µM

rotenone (white) were subjected to the same protocol as in Figure 1. **(d)** Untreated (red) or BAECs treated with 1 μM myxothiazol (orange) or 1 μM antimycin A (yellow) were subjected to the same protocol as in Figure 4.1. Of note, 1 μM was added to inhibit complex III and 10 μM as the positive control.

All these interventions inhibited the superoxide burst in hypoxia (Figure 4.16a-b); however, whereas RISP knockdown resulted in the maintenance of a low superoxide level both in normoxia and hypoxia, NDUFS4 and NDUFS2 knockdown increased superoxide levels in normoxia whilst reducing them in hypoxia (Figure 4.16a-b). In order to assess the specificity of these interventions, we also used rotenone, an inhibitor of complex I (Figure 4.16c), and 1 μM antimycin A or myxothiazol, inhibitors of different sites of complex III (Figure 4.16d), obtaining similar results.

We performed live imaging to evaluate whether hypoxia-induced sodium/calcium exchange was also perturbed in cells after knockdown of complex I and complex III subunits. Whereas NDUFS4 knockdown abrogated the activation of sodium/calcium exchange in hypoxia, RISP knockdown had no effect (Figure 4.17). In addition, the complex I inhibitor piericidin A abolished the sodium/calcium hypoxic exchange, in contrast to the complex III inhibitor antimycin A or the complex IV inhibitor potassium cyanide (KCN; Figure 4.18).

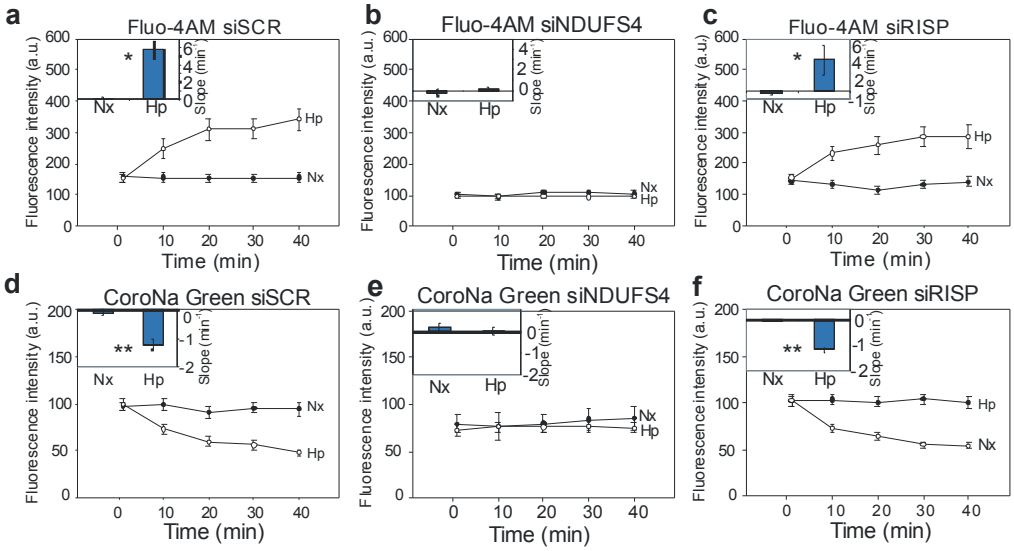

Figure 4.17. Complex I, but not complex III deficiency prevents hypoxic sodium/ calcium exchange. (a-f) Live cell imaging by confocal microscopy measuring cytosolic calcium with the Fluo-4AM probe **(a-c)** or cytosolic sodium with the CoroNa Green probe **(d-f)** in BAECs treated with siSCR **(a, d)**, siNDUFS4 **(b, e)** or siRISP **(c, f)** subjected to normoxia (Nx, ●) or hypoxia (1% oxygen; Hp, ○). Data are represented as mean ± s.e.m. of three (d-f) or four (a-c) independent experiments. **(Insets in e-j)** Slopes considering all the ROI and time points of each replicate (n = 4 in a-c; n=3 in d-f) were estimated by linear regression and plotted as mean ± s.e.m. * $p < 0.05$, ** $p < 0.01$ (Student's t-test).

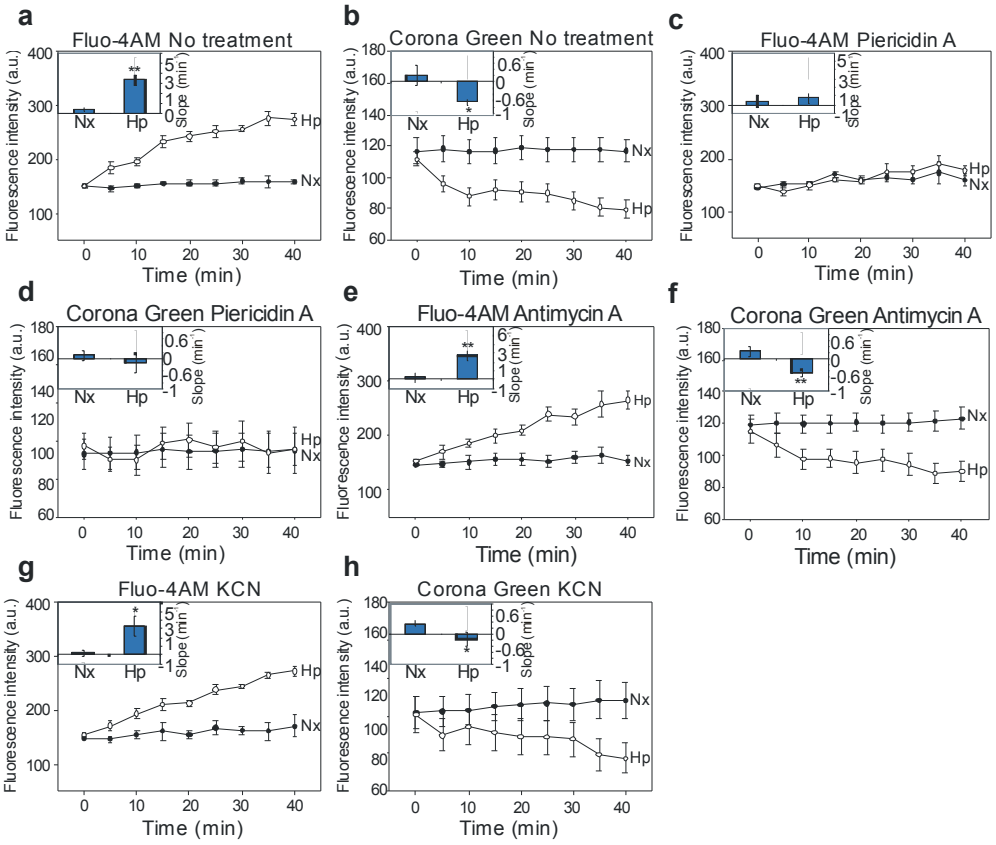

Figure 4.18. Complex I, but not complex III or complex IV inhibition prevents hypoxic sodium/ calcium exchange. Live cell imaging by confocal microscopy measuring cytosolic calcium with the Fluo-4AM probe (a, c, e and g) or cytosolic sodium with the CoroNa Green probe (b, d, f and h) in BAECs non treated (a and b) or treated with piericidin A (c and d), antimycin A (e and f) or KCN (g and h) subjected to normoxia (Nx, ●) or hypoxia (1% oxygen; Hp, ○). Data are represented as mean ± s.e.m. of three or four independent experiments. **(Insets)** Slopes considering all the ROI and time points of each replicate (n = 3 in a, c, e and g; n=4 in b, d, f and h) were estimated by linear regression and plotted as mean ± s.e.m. * $p<0.05$, ** $p<0.01$ (Student's t-test).

These results demonstrate the essential role of complex I, but not other mitochondrial complexes, in triggering the sodium/calcium exchange in acute hypoxia. In addition, both complex I and complex III are necessary for hypoxic superoxide burst

4.2.5 PTEN-induced putative kinase 1 (PINK1) is not involved in the hypoxic superoxide burst

Since PINK1 mutation has been associated with inhibition of NCLX activity (Gandhi et al., 2009), we silenced PINK1 (Figure 4.19a). We observed that superoxide increased in normoxia but hypoxia still triggered the superoxide burst (Figure 4.19b). Interestingly, both raised superoxide levels and hypoxic burst could be abolished by treatment with CGP (Figure 4.19b).

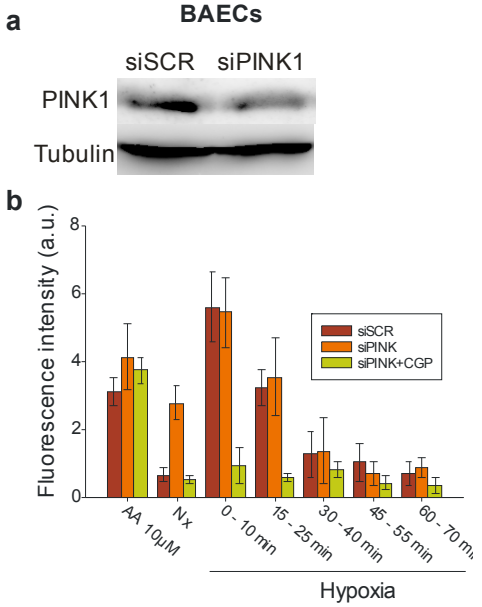

Figure 4.19. PINK1 deificiency doea not affect the hypoxic superoxide burst. (a) Protein extracts from BAECs treated with siSCR or siPINK1 were immunoblotted for PINK1 protein with tubulin as a loading control. **(b)** Superoxide detection by fluorescence microscopy with DHE after fixation in BAECs treated with siSCR (black), siPINK1 (red) or siPINK1 plus 10 μM CGP-37157(green) and subjected to the same protocol as in Figure 4.1.

4.2.6 Hypoxia increases the deactive state of mitochondrial complex I

Activation of NCLX in acute hypoxia could be mediated by the active to deactive transition (A/D transition) of complex I and enhancement of its NHE activity. A/D transition involves a conformational rearrangement of compelx I resulting in the exposure of Cys-39 within the bovine mitochondrial subunit ND3, among other subunits (Babot et al., 2014, Zickermann et al., 2015). Labelling of this thiol group with thiol-specific reagents thus constitutes a suitable marker for deactivation of complex I (Babot et al., 2014, Galkin et al., 2008, Roberts and Hirst, 2012). Our research group is expert in labelling Cys residues with fluorescent residues for their detection in electrophoresis techniques (Tello et al., 2009, Izquierdo-Alvarez et al., 2012, Moreno et al., 2014b), so we have developed a specific methodology for detecting the exposed Cys-39 residue of ND3 using a fluorescent maleimide reagent under non-denaturing conditions.

Using this technique, exposed cysteines in mitochondrial membrane preparations from cells subjected to normoxia or hypoxia were labelled with a fluorescent maleimide. The detection of the exposed Cys labelling was performed by running the samples in a SDS-PAGE with tricine buffer (Schagger, 2006) and total protein signal was stained by Sypro Ruby (Figure 4.20a-b). The exposed Cys signal of a protein species of approximately 10 kDa was clearly increased after thermal deactivation (Babot et al., 2014, Galkin et al., 2008) (Figure 4.20b, left) and, more interestingly, in

samples from hypoxia-treated BAECs (Figure 4.20b, bottom). Total protein amounts, detected with Sypro Ruby, were similar in all gel lanes (Figure 4.20b, right). In order to confirm the identity of this band, we digested it with trypsin and performed tandem mass spectrometry analysis (LC-MS/MS), obtaining a fragmentation spectrum corresponding to a peptide of ND3 containing Cys-39 (Figure 4.20e-f); according to the sequence of the protein, this is the only tryptic peptide that can be detected in the usual procedure with this technique.

Quantification of the ratio of TMR/Sypro signals (exposed Cys vs total protein) for this band in several replicates clearly showed that Cys-39 (the only Cys of this protein) was more exposed after 5 min of hypoxia and was unaffected by CGP treatment in BAECs (Figure 4.20c) or in the hepatocyte cell line HepG2 (Figure 4.20g). Furthermore, exposure of ND3 Cys-39 was maintained from 5 to 30 min of hypoxia (Figure 4.20h) and increased gradually with decreasing oxygen tension (Figure 4.20d).

Taken together, these results show that acute hypoxia induces the transition of complex I to its deactive state, exposing ND3 Cys-39, and that this occurs proportionally to the level of hypoxia. Furthermore, it is maintained during hypoxia and it is a conserved mechanism in other cell types.

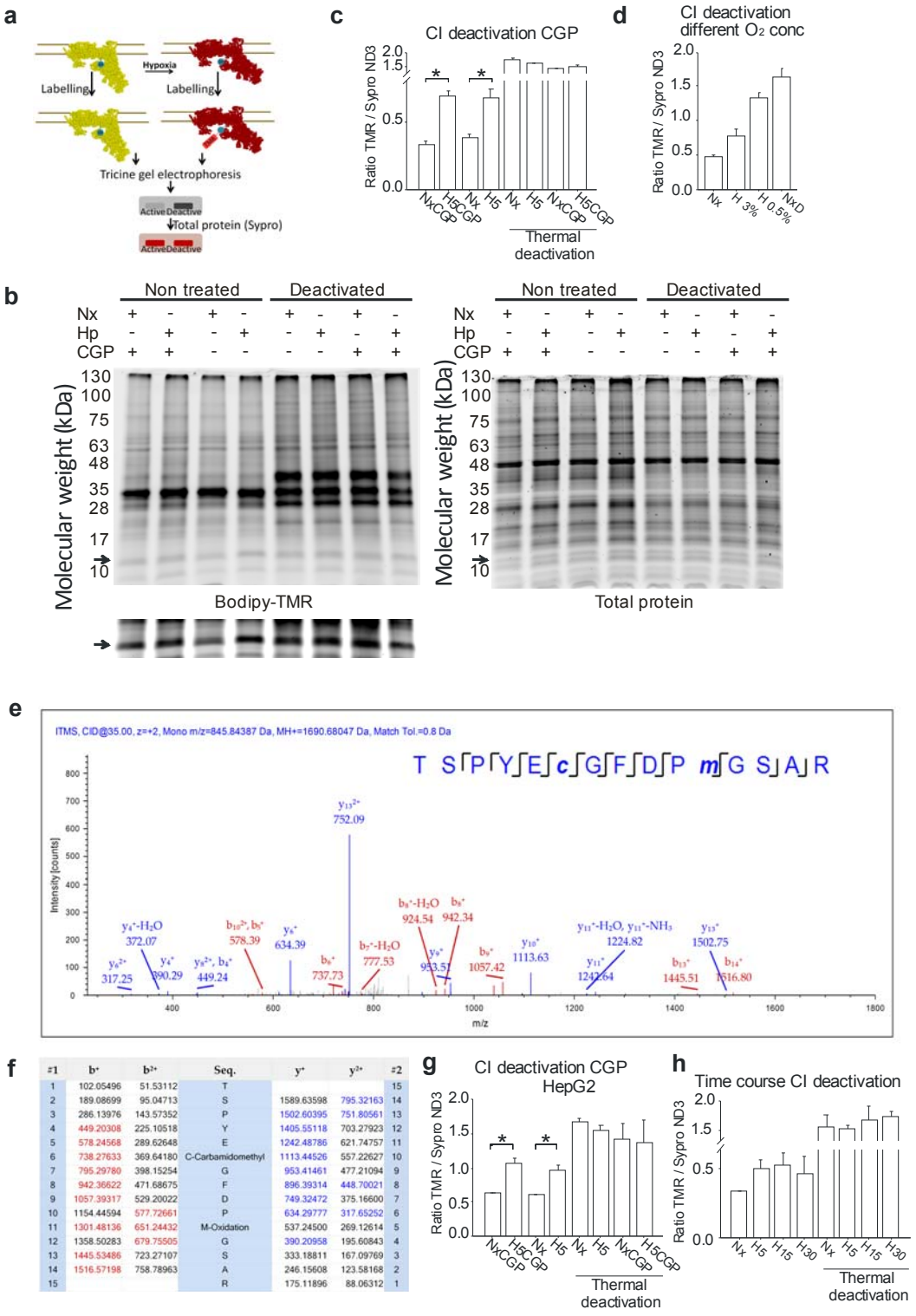

Figure 4.20. Acute hypoxia deactivates complex I. (a-d) Fluorescent labelling of exposed Cys in ND3, reflecting complex I deactivation. **(a)** Cys-39 of ND3 remains buried in active complex I (yellow), while it is exposed in deactive complex I (red). Mal-Bodipy-TMR was used to label exposed Cys before electrophoretic protein separation. TMR fluorescence signal for the ND3 band was higher when complex I was deactive (grey picture). Protein amount for the same band is detected with Sypro Ruby staining (red picture). **(b, c)** Mitochondrial membranes from BAECs treated for 5 min in normoxia (Nx), hypoxia (1% oxygen, Hp or H5), normoxia with 10 µM CGP-37157 (NxCGP) or hypoxia with 10 µM CGP-37157 (H5CGP) were split in two equal parts; one part was incubated for 1 hour at 37 ºC to

fully deactivate complex I (Deactivated), whereas the other was kept on ice (Non treated). **(b)** Bodipy-TMR signal reflects exposed Cys (left) and Sypro Ruby signal detects total protein (right). Arrows (➙) mark the band corresponding to ND3 identified by LC-MS/MS; the lower image on the left is a more exposed photograph of the Bodipy-TMR signal. **(c)** Band corresponding to TMR-labeled ND3 was quantified and relativized to total ND3. **(d)** Same as (c) for BAECs subjected to normoxia or different hypoxia conditions (3% or 0.5% oxygen) for 5 min; NxD: thermal deactivation of normoxic sample. Data are presented as the mean ± s.e.m. of six (c) or three (d) independent experiments. **(e-f)** MS/MS identification of a peptide of bovine ND3 containing Cys-39, obtained from tryptic digestion of the band of a gel from experiment in figure 11b. CID fragmentation MS/MS spectrum **(e)** and table **(f)** indicating the assigned fragments from the b and y series. **(g)** ND3 Cys exposure in HepG2 cells subjected to the same protocol as in figure 11b-c. **(h)** ND3 Cys exposure in BAECs treated for 5, 15 or 30 minutes under hypoxia (H5, H15 and H30) or 5 min of normoxia as in figure 11b-c. Data in (c-d) are represented as mean ± s.e.m. of three independent experiments. * $p<0.05$ (Student's t-test).

4.2.7 Hypoxia enhances complex I sodium/proton exchanger (NHE) activity

It has been reported that deactive complex I can function as a NHE antiporter (Roberts and Hirst, 2012), so NCLX and complex I function can be coupled by this NHE. However, the NHE activity in the inner mitochondrial membrane is usually attributed to the canonical mNHE. Thus, we questioned whether mNHE or deactive complex I were involved in this response. Since the molecular identity of the mNHE is not known, we treated BAECs with an inhibitor of this antiporter 5-(N-ethyl-N-isopropyl)amiloride (EIPA) (Arias et al., 2008), or with rotenone, an inhibitor of complex I that inhibits also its NHE activity (Roberts and Hirst, 2012), and observed that sodium/calcium exchange was inhibited by rotenone, but not by EIPA (Figure 4.21), suggesting that canonical mNHE is not involved in the activation of NCLX.

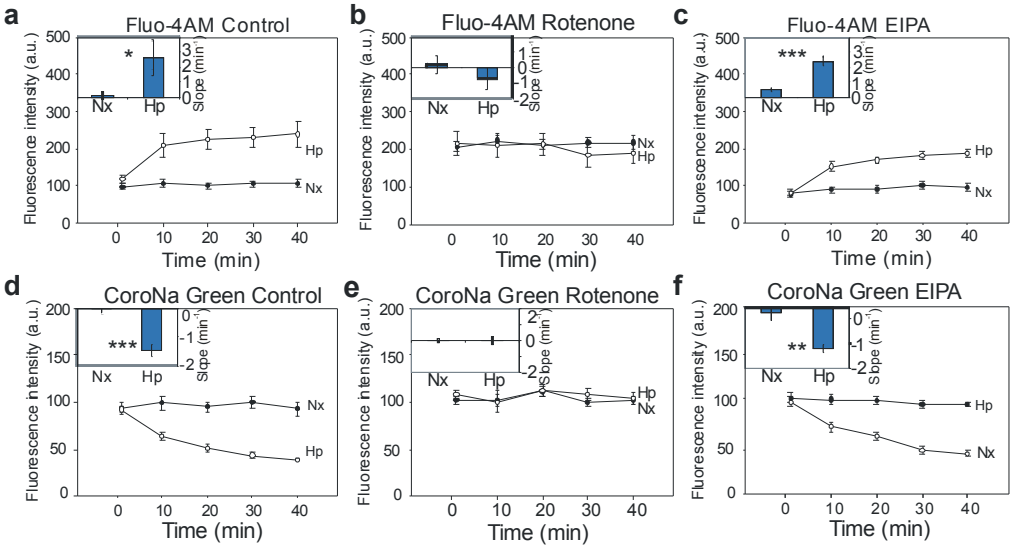

Figure 4.21. Complex I inhibition, but not mNHE inhibition, abolished sodium/calcium exchange in acute hypoxia. Cytosolic calcium **(a-c)** or cytosolic sodium **(d-f)** measured by live confocal microscopy in normoxic (Nx, ●) and hypoxic (1% oxygen; Hp, ○) conditions in control (a, d), rotenone-treated (b, e) or EIPA-treated (c-f) BAECs. **(Insets)** Slopes considering all the ROI and time points of

each replicate (n=4) were estimated by linear regression and plotted as mean ± s.e.m. * $p < 0.05$, ** $p < 0.01$, *** $p < 0.001$ (Student's t-test).

We measured mitochondrial matrix pH as a readout of NHE activity in BAECs transfected with the FRET-based mitochondrial pH indicator mitosypHer (Poburko et al., 2011). We validated the ability of the cytosolic version of this fluorescent protein, CytosypHer, to respond to pH changes (Figure 4.22a), the subcellular localization of its mitochondria-targeted version (Figure 4.22b) and its ability to measure mitochondrial matrix acidification after incubation of cells with FCCP or oligomycin (Figure 4.22c). Acute hypoxia acidified the mitochondrial matrix (Figure 4.22d) independently of CGP treatment (Figure 4.22e). Rotenone treatment abolished hypoxia-induced acidification (Figure 4.22f). Although this approach does not exclude other mechanisms that could also contribute to matrix acidification, the results are compatible with the hypothesis of an increase in the NHE activity of complex I.

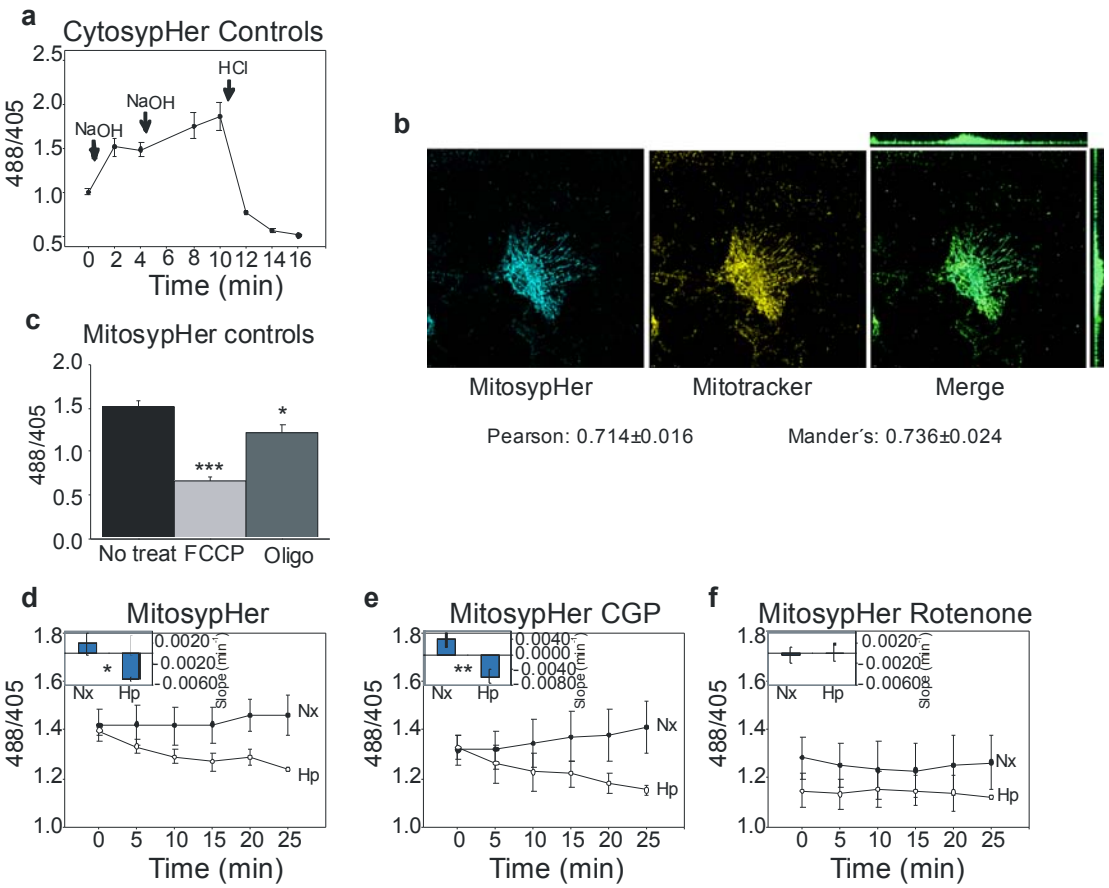

Figure 4.22. Mitochondrial matrix is acidifed in acute hypoxia. (a) A non-targeted version of sypHer was used in BAECs in order to perform an experimental control of pH change. BAECs were treated with two subsequent additions of 30 µM NaOH and one of 8 mM HCl. Data are represented as mean ± s.e.m. of eight different ROIs. **(b)** BAECs transfected with mitosypHer were incubated with 25 nM MitoTracker CMTMRos for 20 min and fixed. Representative images show mitochondrial localization of mitosypHer by confocal microscopy. Pearson and Mander's correlation coefficients for colocalization of both signals were estimated. **(c-f)** Intramitochondrial pH measured with mitosypHer. **(c)**

488/405 signals ratio reflecting intramitochondrial pH in BAECs transfected with mitosypHer either untreated (No treat), or treated with 1 μM FCCP (FCCP) or with 12.5 μM oligomycin (Oligo). Data are represented as mean ± s.e.m. of four independent experiments. * $p < 0.05$, *** $p < 0.001$ (one-way ANOVA). Transfected BAECs either untreated (c), treated with 10 μM CGP-37157 (d) or with 1 μM rotenone (e) were subjected to normoxia (Nx, ●) or hypoxia (1% oxygen; Hp, ○). Data are represented as mean ± s.e.m. of the ratio between the fluorescence signals with excitation at 488 nm and 405 nm of four independent experiments. **(Insets in d-f)** Slopes considering all time points of each replicate (n = 4) are plotted as mean ±s.e.m. * $p < 0.05$, ** $p < 0.01$ (Student's t-test).

These results indicate that NCLX ion exchange is not mediated by the canonical NHE and that acidification of the mitochondrial matrix is probably due to deactive complex I NHE activity.

As a proof of principle, if sodium/proton exchange triggers sodium/calcium exchange and superoxide production in hypoxia, normoxic induction of sodium/proton exchange should imitate the mentioned events. Accordingly, treatment with the sodium/proton exchanger monensin increased intracellular calcium (Figure 4.23a) and superoxide production in normoxia (Figure 4.23b).

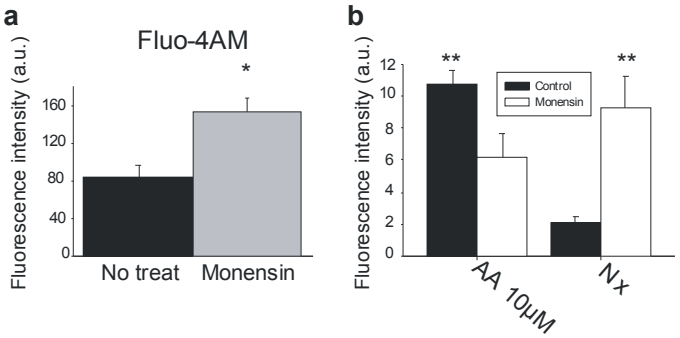

Figure 4.23. Induced sodium/proton exchange mimics hypoxic response. (a) Live cell imaging by fluorescence microscopy measuring cytosolic calcium with the Fluo 4-AM probe after treating BAECs with 10 μM monensin for 20 min. * $p<0.05$ (Student's t-test). **(b)** Non treated BAECs or treated with 10 μM monensin for 30 min were subjected to the same procedure as in Figure 4.1. Mean ± s.e.m. of at least three independent experiments. ** $p < 0.01$ (one-way ANOVA).

4.2.8 The superoxide burst is not caused by complex I reverse electron transport (RET)

Since we have observed that complex I is involved in the hypoxic production of ROS by mitochondria, we wondered whether RET was involved. Complex I is a reversible enzyme which can perform the reduction of NAD^+ into NADH by oxidizing ubiquinone into ubiquinol (Drose, 2013) and translocating protons into the mitochondrial matrix. This process requires large amounts of ubiquinol which are normally generated from succinate, and hyperpolarized mitochondria, so that the electron flux through complex III is inhibited. In this process the flavin group of complex I can reduce large amounts of oxygen into superoxide and has been related to pathophysiological processes, such as ischemia/reperfusion injury (Chouchani et al., 2014).

Thus, given that succinate is necessary for this process, incubation of cells in media adding only the permeable form of succinate, dimethylsucciante (DMS), would maintain the superoxide burst in the transition to hypoxia. In the contrary, facilitating the forward complex I reaction by NADH-generating substrates such as permeable derivates of glutamate and malate (i.e. glutamine and dimethylmalate; GM), would inhibit it. However, in the presence of GM the superoxide burst resembled to the control, whereas DMS fed cells did not produce superoxide in hypoxia (Figure 4.24a). On the other hand, since RET requires hyperpolarized mitochondria, depolarization by ionophores should abolish ROS production. We treated BAECs with FCCP and observed that there was no difference between non-treated and FCCP-treated cells by differenct approaches (Figure 4.24b-d).

These results indicate that RET is not involved in hypoxic ROS production. Of note, hypoxic stabilization of HIF-1α was not affected by mitochondrial depolarization, which supports the results discarding RET as the mechanism producing ROS in hypoxia (Figure 4.24e-f).

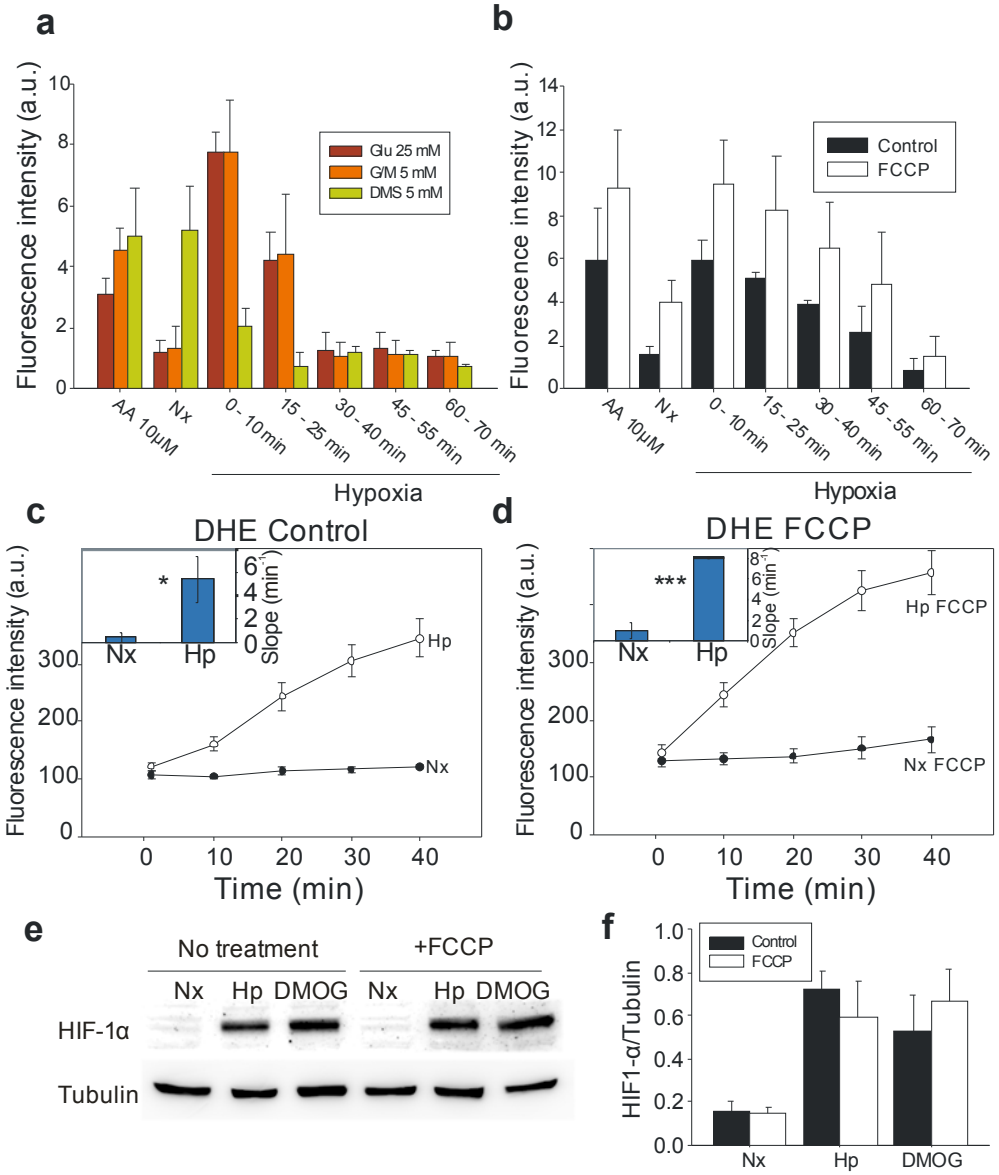

Figure 4.24. Hypoxic ROS production is not due to RET. (a-b) Non treated BAECs (red or black) or treated with 5 mM GM (orange), 5 mM DMS (yellow) or 1 µM FCCP (white) were subjected to the same procedure as in Figure 4.1. **(c)** BAECs either non treated or treated with 1 µM FCCP were subjected to the same protocol as in Figure 4.5a. **(e-f)** BAECs untreated or treated 1µM FCCP were exposed for 4 hours to normoxia (Nx), normoxia with 1 mM dimethyloxalylglycine (DMOG, a positive control for PHD inhibition and HIF-1α stabilization) or to hypoxia (1% oxygen, Hp), proteins extracted and blotted against HIF-1α protein. Representative image is shown in **(e)** and densitometry of three independent experiments in **(f)**.

4.2.9 Mitochondrial calcium does not vary in hypoxia

We don't know any commercially available probe to measure mitochondrial sodium concentration. However, new Förster resonance energy transfer (FRET)-based fluorescent proteins such as GEM-GECO have been developed in the recent years which allow a reliable quantitative measurement of cellular calcium concentration (Zhao et al, 2010). Also, these proteins can be

targeted to specific cell compartments, such as mitochondria. We transfected BAECs with a version of the GEM-GECO protein targeted to the mitochondrial matrix (MitoGEM-GECO) and added 10 μM histamine in order to release endoplasmic reticulum calcium stores. Histamine increases cytosolic calcium which then translates into an augmentation in mitochondrial calcium through the MCU (Jou et al., 1996). We observed an increase of mitochondrial calcium after 10 μM histamine addition (Figure 4.25a). We also incubated transfected BAECs with 10 μM CGP-37157, 1 μM of the MCU blocker ruthenium red or 1 μM rotenone and subjected the cells to normoxia or hypoxia. CGP-treated cells showed increased mitochondrial calcium, compatible with the inhibition of NCLX. Strikingly, we observed no change upon hypoxia in any of the conditions tested (Figure 4.25b-e), indicating that calcium extrusion from mitochondria was probably being compensated by calcium refilling by a MCU-independent pathway.

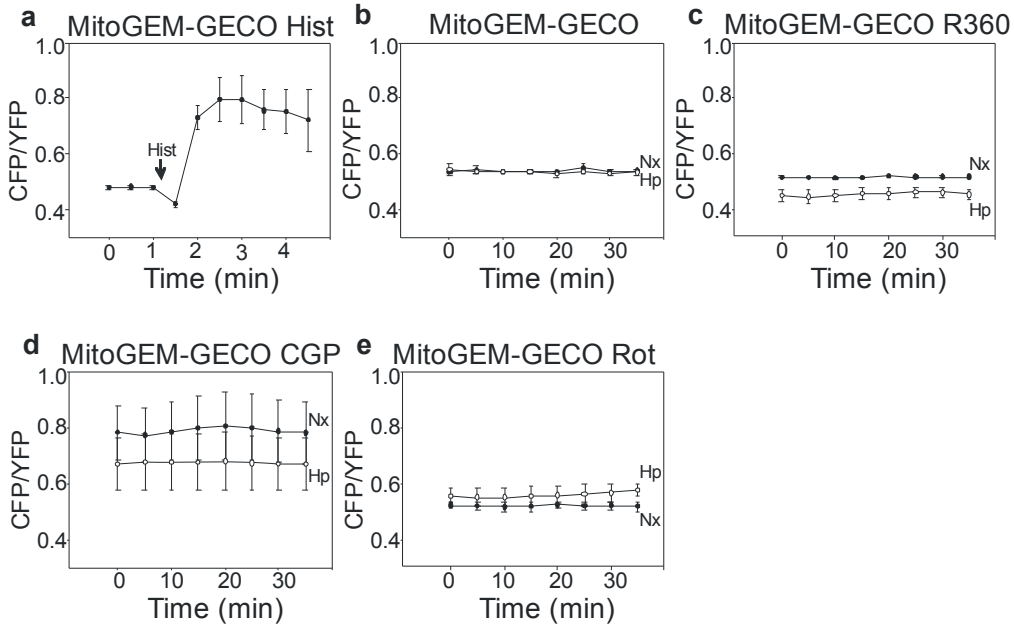

Figure 4.25. Mitochondrial calcium does not change during hypoxia. (a) BAECs were transfected with MitoGEM-GECO and treated with 10 μM histamine. (b). Transfected BAECs were either untreated or treated with 1 μM ruthenium red 360 (a specific inhibitor of the MCU), 10 μM CGP-37157 or 1 μM rotenone for 20 min and subsequently incubated in a chamber with atmospheric and temperature control in a confocal microscope, where they were maintained in normoxia for 30 min or placed in normoxia and switched to hypoxia (1% oxygen) for the rest of the experiment. Black circles: normoxia (Nx); white circles: hypoxia (Hp). Quantification of four independent experiments is plotted for each time as mean ± s.e.m

4.2.10 Isolated mitochondria produce a burst of ROS triggered by successive additions of sodium chloride and calcium chloride

As mentioned previously, two different groups which have tried to detect ROS in isolated mitochondria under hypoxia and obtained opposite results (Hoffman et al., 2007, Korde et al.,

2011). In both cases, the buffers used to isolate mitochondria do not contain sodium and deplete calcium by the addition of a chelating agent (EDTA); the main difference was the addition or not of 10 mM sodium chloride in the working solutions. Hoffman *et al* included sodium chloride into the isolation buffer and to the working solutions, and detected that ROS production decreased with hypoxia. We reasoned that sodium addition would deplete mitochondrial calcium stores by activating NCLX prior to the measurements.

As a proof of concept, if NCLX activity was necessary for ROS production by mitochondria, sodium addition could activate NCLX, triggering calcium extrusion and producing ROS in isolated mitochondria in normoxia.

We first tested whether the addition of sodium chloride or calcium chloride was able to induce any change in ROS production or respiration in isolated adult rat heart mitochondria. There are several states in which isolated mitochondria can be maintained. Mitochondrial solutions with no energy source are in the so called state 1, thus oxygen is not consumed. Addition of substrates such as glutamate/malate (GM; donate electrons through complex I) or succinate (through complex II) triggers the state 2 and oxygen consumption increases. Coupling respiration with ADP stimulates respiratory state 3, leading to maximal respiration. State 4 is reached after all the ADP is converted to ATP what translates into a decrease in oxygen consumption. Finally, anoxia stops respiration and mitochondria fall into state 5 (Chance and Williams, 1955, Babcock and Wikstrom, 1992).

We performed experiments in which mitochondrial respiratory state 2 was induced by addition of GM. Successive additions of the specified salts or diluent (water) were performed and ADP added thereafter; finally, complex II-based respiration was induced by succinate add-on (Figure 4.26a; black circles). Successive additions of calcium chloride produced a biphasic effect om respiration, which increased after the two additions, and then decreased after reaching 1 mM of total calcium chloride concentration addition (Figure 4.26a; white bars). Notably, after addition of the highest calcium chloride amount, neither ADP nor succinate were able to fully couple respiration. Hydrogen peroxide production slightly decreased after several additions of water, probably due to dilution of the sample, and increased only with succinate (Figure 4.26b; black bars). Mitochondria treated with calcium chloride rose hydrogen peroxide levels only after reaching 1 mM concentration, coinciding with the decrease shown in respiration (Figure 4.26b; white bars). In contrast, progressive increase in sodium chloride concentration up to 15.6 mM had no effect on oxygen consumption or ROS (Figure 4.26c-d), indicating that sodium had no effect on any of them and that chloride was not responsible for the effects seen in Figure 4.26a-b.

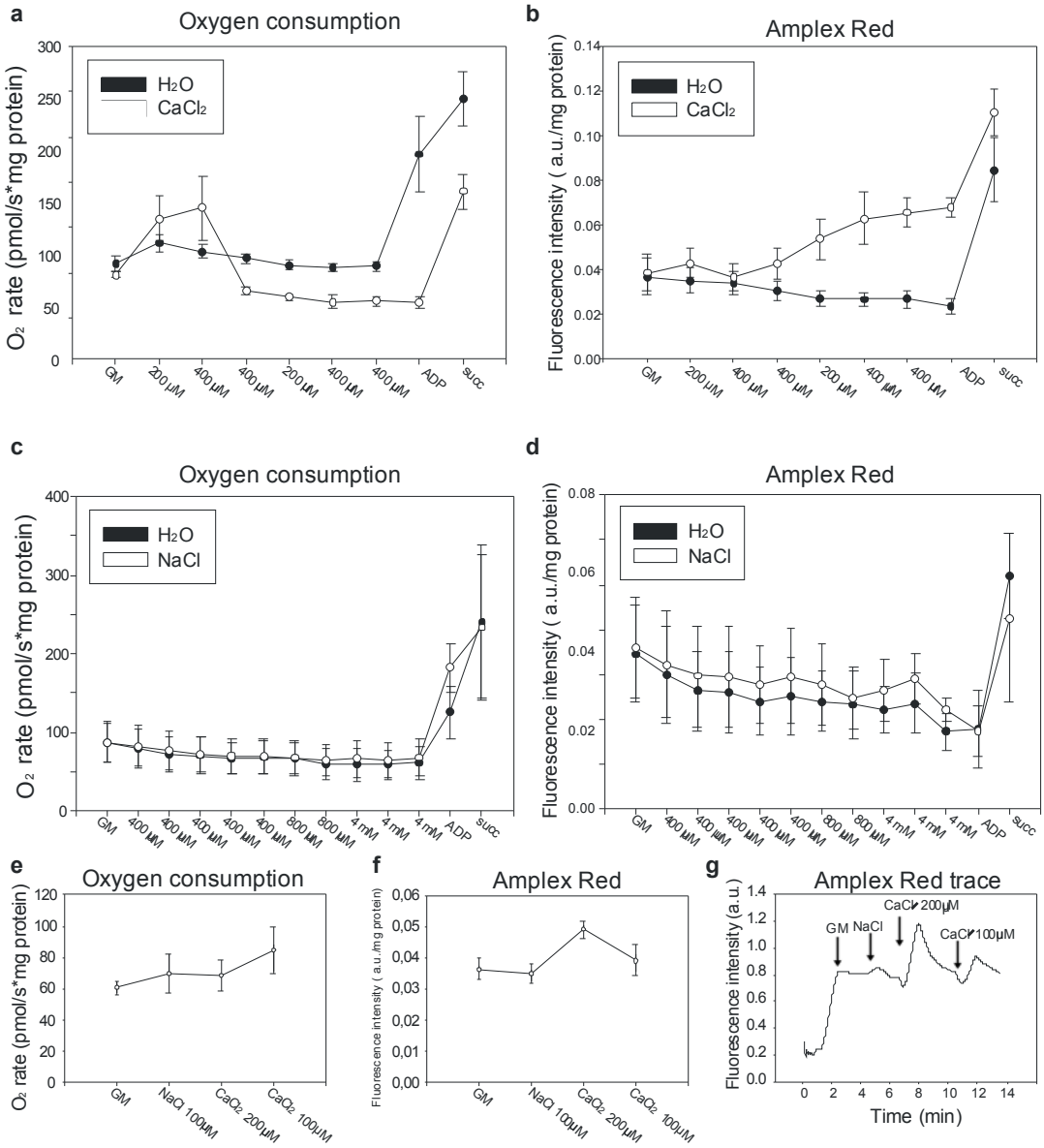

Figure 4.26. Different effects of calcium and sodium additions in energized isolated mitochondria. (a and c) Variations in oxygen consumption induced by successive additions of calcium chloride **(a)** or sodium chloride **(c)** after glutamate and malate based state 2 measured by Oxygraph-2k . State 3 was induced by addition of ADP and contribution of complex II by succinate. **(b and d)** ROS production in calcium chloride **(b)** or sodium chloride **(d)** treated mitochondria was measured by Amplex Red in parallel to respiration. **(e and f)** Successive addition of small amounts of sodium chloride and calcium chloride were aded in order to activate NCLX and the effects on respiration **(e)** and ROS production **(f)** were measured. **(g)** Representative trace of ROS production with successive addition of small amounts of sodium chloride and calcium chloride.

It has been reported that mixtures of sodium chloride and calcium chloride could activate NCLX in isolated energized mitochondria (Carafoli et al., 1974). 100 µM of sodium chloride ddi not had any effect in neither oxygen consumption nor ROS production (Figure 4.26e-f). However, subsequent addition of 200 µM calcium choride moderately increased respiration hydrogen peroxide levels (Figure 4.26e-f). Interestingly, 100 µM calcium chloride further increased

respiration and produced a new burst of ROS, although less pronounced (Figure 4.26e-f).The production of ROS by mixtures of sodium chloride and calcium chloride generate a reversible induction of ROS. This is represented in Figure 4.26g which is the trace of one experimental replicate. Therefore, activation of NCLX by small amounts of sodium and calcium are sufficient to produce a burst of ROS in rat heart isolated mitochondria.

4.3 NCLX activity is involved in hypoxic adaptation and injury

4.3.1 Hypoxic adaptation through HIF-1 α stabilization correlates with the hypoxic superoxide burst, but superoxide is not the key species in this pathway

As previously stated, hypoxic ROS production has been implicated in triggering hypoxia adaptation signals through the HIF pathway, mediated by HIF-α subunits stabilization (Guzy and Schumacker, 2006b, Hamanaka and Chandel, 2009, Guzy and Schumacker, 2006a, Hamanaka and Chandel, 2010). Additionally, we have recently showed that in endothelial cells there is a reversible oxidation in certain proteins after two hours of hypoxia, that could be implied in acute responses to hypoxia (Izquierdo-Álvarez et al., 2012). Indeed, it has been recently shown that PHD proteins respond to Cys oxidation (Briggs et al., 2016). Thus, the superoxide burst we observe could take part in hypoxic signals at longer times, related with the different kinetics of accumulation of different oxidized species.

In order to test this, we studied HIF-1α stabilization in the systems in which we have been able to abolish the superoxide burst in hypoxia. First, we used ϱ^0 cells, as it has been published elsewhere for other ϱ^0 cells that they are not able to stabilize HIF-1α (Guzy et al., 2005, Mansfield et al., 2005, Chandel et al., 1998). ϱ^0L929 cells subjected to 4 hours of hypoxia did not stabilize HIF-1α as happened in the control C57 cells (Figure 4.27). However, treatment with 1 mM dimethyloxalylglycine (DMOG, a PHD inhibitor) stabilized the α subunit in both cell lines, indicating that PHDs activity was similar (Figure 4.27).

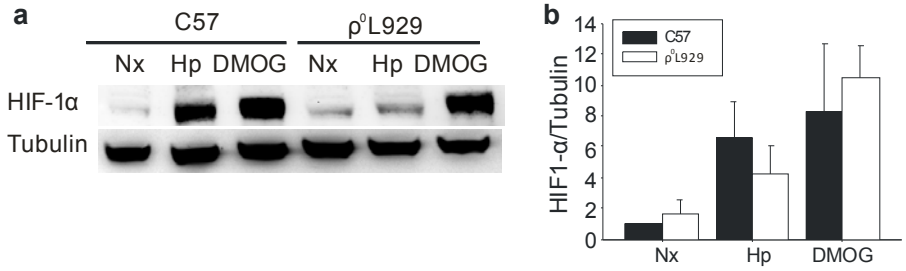

Figure 4.27. Hypoxic HIF-1α stabilization relies on functional mitochondria. C57 and ρ^0L929 cells were exposed for 6 hours to normoxia (Nx), normoxia with 1 mM DMOG, a positive control for PHD) or to hypoxia (1% oxygen, Hp), proteins extracted and blotted against HIF-1α protein. Representative image is shown in **(a)** and densitometry of three independent experiments in **(b)**.

Second, we assayed HIF-1α stabilization after NCLX inhibition. Inhibition of NCLX activity with CGP abolished hypoxic HIF-1α stabilization in BAECs (Figure 4.28a-b) and in HUVECs (Figure 4.28c-d), and a comparable effect was detected after silencing NCLX expression (Figure 4.28e-f). Importantly, induction of sodium/proton exchange with monensin stabilized HIF-1α in normoxia in BAECs (Figure 4.28g-h).

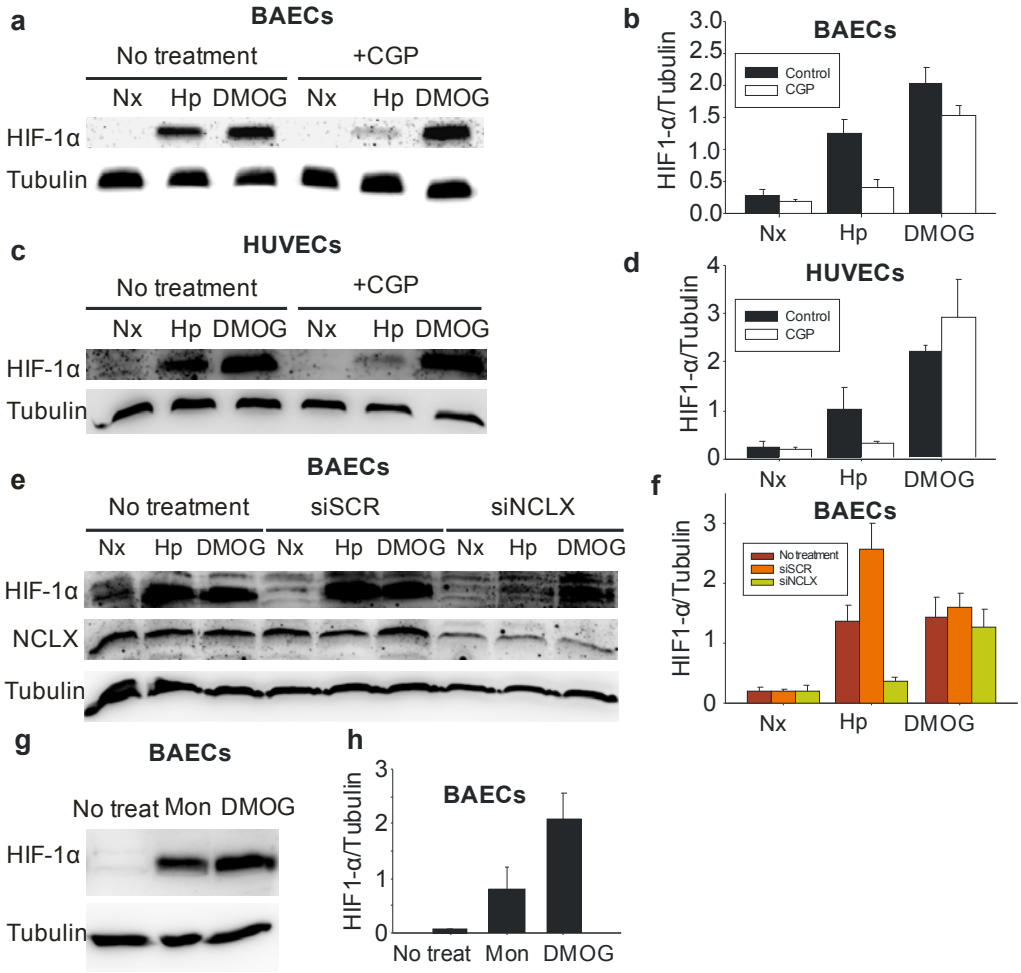

Figure 4.28. Inhibition of NCLX inhibits HIF-1α stabilization. HIF-1α stabilization measured by western blotting in BAECs **(a and b)** or HUVECs **(c and d)** treated or not with 10 μM CGP-37157 (CGP), or BAECs untreated or treated with siSCR or siNCLX **(e and f)**, and exposed for 4 h to normoxia (Nx), normoxia with 1 mM DMOG or to hypoxia (1% oxygen, Hp). Tubulin was used as a loading control. Representative images of at least four independent experiments are shown. Densitometries of a, c and e are shown in b, d and f. **(g and h)** HIF-1α stabilization measured by western blotting in BAECs either untreated, treated with 10 μM monensin (Mon) or with 1 mM DMOG for 4 h in normoxia. Representative image is shown in (g) and densitometry of three independent experiments in (l).

We also measured expression levels of HIF target genes, such as PDK1, Glut1 and BNIP3 by RT-PCR in HUVECs. Treatment with CGP diminished the hypoxic induction of all genes in comparison with non-treated cells (Figure 4.29a-c), whereas HIF-1α and HIF-2α mRNAs amounts did not change after treatment with CGP (Figure 4.29d-e).

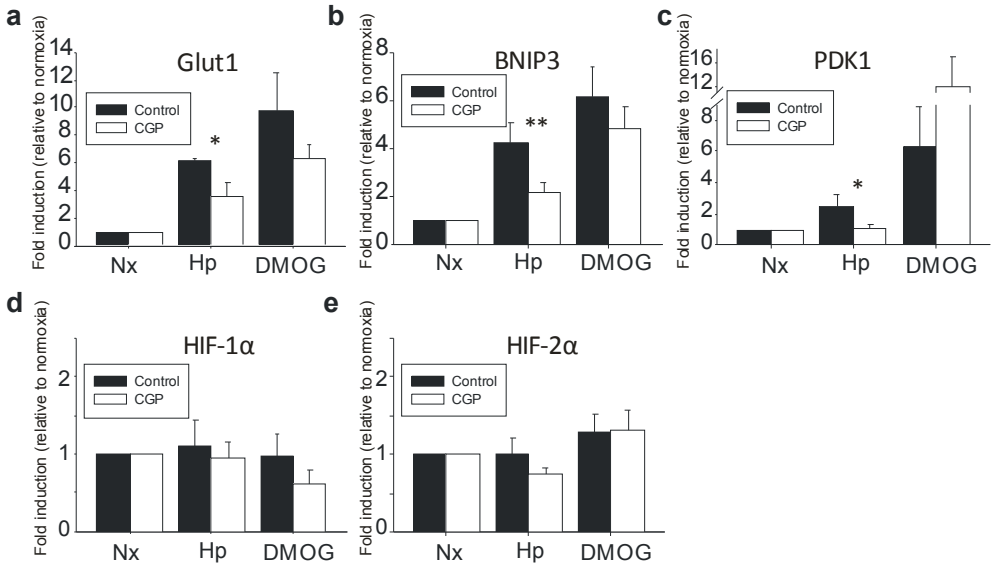

Figure 4.29. Activation of the HIF pathway is prevented by NCLX inhibition. (a-e) Quantitative RT-PCR analysis of Glut1 **(b)**, BNIP3 **(c)**, PDK1 **(d)**, HIF-1α **(e)** and HIF-2α **(f)** mRNAs in untreated (black) or 10 μM CGP-37157-treated (white) HUVECs subjected to 6 hours of normoxia (Nx), hypoxia (1% oxygen, Hp) or normoxia with 1 mM DMOG. Data are represented as mean ±s.e.m. of the β-actin ratio relative to normoxia for four independent experiments. * $p < 0.05$, ** $p < 0.01$ Control Hp versus CGP Hp of each condition (Student's t-test).

Third, we used Tiron, which abolishes the superoxide burst (Figure 4.1f). However, Tiron treatment in BAECs did not abolish HIF-1α stabilization in hypoxia and even increased it, both in normoxia and in hypoxia (Figure 4.30a-b). Measurement of CDCFDA oxidation showed that cells with Tiron produced equal or slightly higher signals than cells without treatment (Figure 4.30c; this can be related to the oxidation of superoxide due to the reaction with Tiron, producing mainly hydrogen peroxide, Thus, we can discard superoxide as the species directly involved in HIF-1α stabilization, while the increase in hydrogen peroxide could be implied in it. which can explain increased HIF-1 α stabilization.

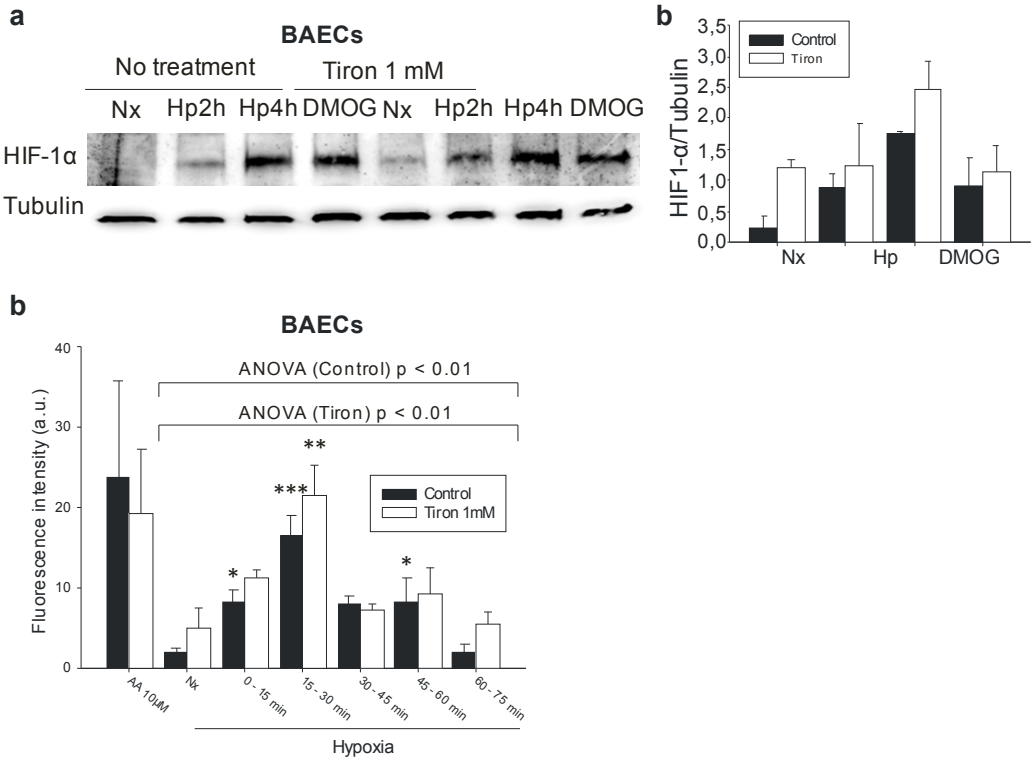

Figure 4.30. Hypoxic HIF-1α stabilization does not depend on superoxide anion. (a and b) BAECs were exposed for 4 hours to normoxia (Nx), normoxia with 1 mM DMOG or to hypoxia for 2 (Hp2H) or 4 hours (Hp4H), proteins extracted and blotted against HIF-1α protein. Representative image is shown in **(a)** and densitometry of three independent experiments in **(b)**. **(c)** Control BAECs (black bars) and BAECs incubated with 1 mM Tiron (white bars) were treated as in Figure 2c and d. 10 μM CDCFDA was added for 15 min more, and cells were fixed in the hypoxia chamber. Plot shows the quantification of images from three independent experiments. Data are presented as mean ± s.e.m. *** $p < 0.001$ versus Nx, ** $p < 0.01$ versus Nx, * $p < 0.05$ versus Nx of each condition (Dunnet post-hoc test; n = 3).

4.3.2 Inhibition of NCLX inhibits the redox component of hypoxic pulmonary vasoconstriction (HPV)

We wondered whether inhibition of the mechanism we have revealed, in which NCLX is implied in the hypoxic superoxide burst, played a role in physiological or pathological scenarios where hypoxia has been described to produce reactive oxygen species.

Among the acute responses to hypoxia, HPV helps to match lung ventilation with perfusion by inducing a contractile response in pulmonary arteries (PA) which has been shown to depend on increased mitochondrial ROS (Connolly et al., 2013, Frazziano et al., 2011, Sylvester et al., 2012). Smooth muscle cells are the key cells implied in HPV, so we subjected rat pulmonary artery smooth muscle cells (PASMCs) to acute hypoxia, observing the superoxide$^-$ burst in the first minutes of hypoxia, which was abolished upon silencing of NCLX (Figure 4.31a-b); this confirms the presence of the same NCLX-dependent hypoxic response in these cells. In rat PA, exposure to hypoxia in the absence of pretone (precontraction) induced a rapid contractile response within 2-4

min (peak contraction), which then decayed and reached a plateau after 10-12 minutes (steady state contraction). This response resembled physiological HPV and was reproducible in successive treatments of the same artery (Figure 4.31c). A second challenge with hypoxia was performed in the absence or in the presence of CGP. In arteries treated with vehicle, the peak and steady state contractions of HPV were similar to those obtained during the first hypoxic challenge (Figure 4.31c-d). By contrast, CGP treatment had no effect on the peak contraction but markedly reduced the steady-state component of the HPV contraction (Figure 4.31d-e). A similar inhibition was shown upon treatment with ROS scavengers and ETC inhibitos (Moreno et al., 2014a). Thus, NCLX inhibition blocks part of the HPV in PA which could be related to the abolition of the superoxide burst in smooth muscle cells in hypoxia.

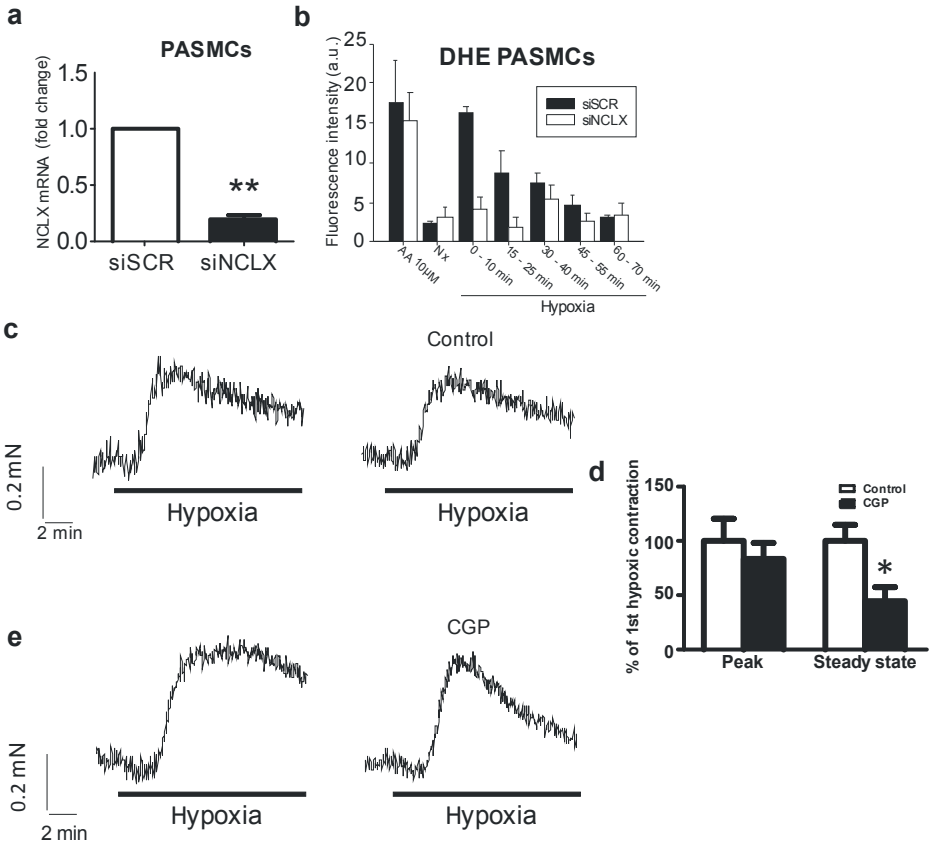

Figure 4.31. Inhibition of NCLX blunts hypoxic pulmonary vasoconstriction (HPV). (a) Quantitative RT-PCR analysis of NCLX mRNA in PASMCs treated with siSCR or siNCLX. Data are presented as mean ±s.e.m. of the GAPDH ratio relative to siSCR-treated cells for three independent experiments. ** $p<0.01$ (Student's t-test vs. 1). **(b)** PASMCs were treated with siSCR or siNCLX and subjected to the same procedure as in Figure 1a. Mean ± s.e.m. of four independent experiments. **(c-e)** Representative traces (c and e) and average values (d) of HPV measured in rat PA. Each artery was exposed twice to hypoxia. The second hypoxic challenge was performed in the absence (control, c) or the presence of 30 µM CGP-37157 (CGP; e). Data are expressed as a percentage of the first hypoxic contractile response, represented as mean ± s.e.m. * $p < 0.05$ vs control (ANOVA and Bonferroni's test; n = 7-9).

4.3.3 Inhibition of NCLX abolishes the hypoxic response in neuronal cells and brain tissue, and reduces brain ischemic damage

Since most of the preceding experiments were carried out in non-excitable cells (mainly primary endothelial cells), we questioned whether inhibition of NCLX activity could also be observed in excitable cells, such as neurons. Both the hypoxic superoxide burst and HIF-1α stabilization was abolished in HT22 immortalized mouse hippocampal neuronal cells treated with CGP (Figure 4.32a, c). To check for the specificity of the treatment, NCLX expression was silenced in HT22 cells, which also abolished the superoxide burst in acute hypoxia (Figure 4.32b).

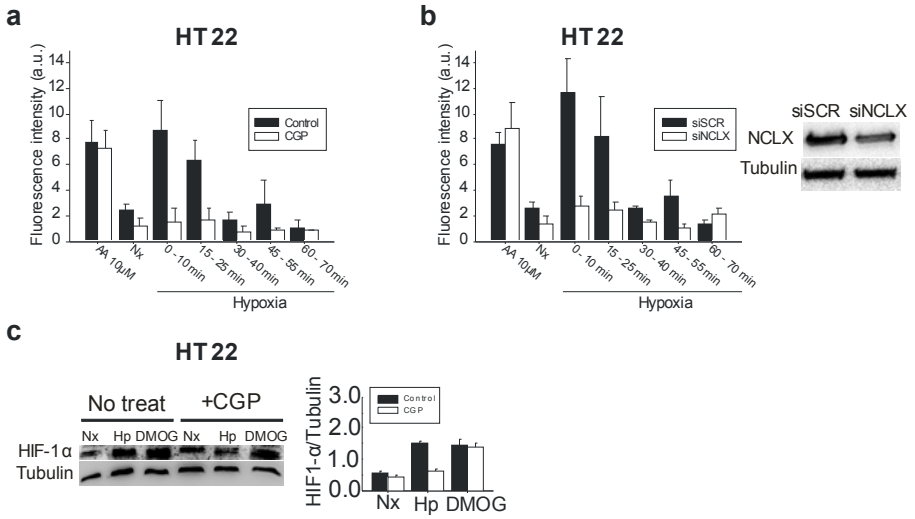

Figure 4.32. NCLX inhibition abolishes hypoxic ROS production and HIF-1α stabilization in neurons. (a) Control untreated (black) and 10 µM CGP-37157-treated (CGP; white), **(b)** or treated with siSCR or siNCLX HT22 cells were subjected to the same procedure as in Figure 4.1a. Mean ± s.e.m. of three independent experiments. On the right, protein extracts from BAECs treated with siSCR or siNCLX immunoblotted for NCLX protein with tubulin as a loading control. **(c)** HT22 cells were subjected to the same procedure as in Figure 4.27. Representative images and densitometry of three independent experiments.

To further study this effect in brain tissue, we exposed isolated mouse hippocampal slices to acute hypoxia. After 30 min of hypoxia, complex I was deactivated, independently of the treatment with CGP (Figure 4.33a). However, the hypoxia-dependent increase in superoxide production (Figure 4.33b-c) and HIF-1α stabilization (Figure 4.33d) were selectively abolished with CGP. Overall, these results strongly suggest that the same mechanism operates in excitable cells such as neurons and in the hippocampus.

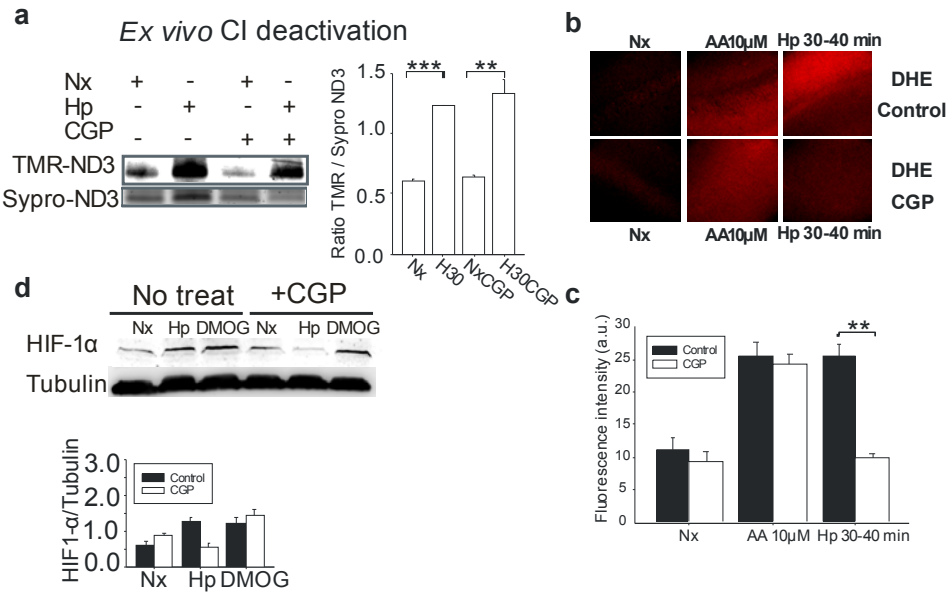

Figure 4.33. NCLX inhibition abolishes hypoxic ROS production and HIF-1α stabilization, but not complex I deactivation, in brain tissue. (a) Hippocampal slices were subjected to 30 min of normoxia (Nx), hypoxia (1% oxygen; H30), normoxia with 30 μM CGP-37157 (NxCGP) or hypoxia with 30 μM CGP-37157 (H30CGP) and treated as in Figure 4.20b-c. Mean ± s.e.m. of three independent experiments. **(b and c)** Hippocampal slices untreated (Control) or treated with 30 μM CGP-37157 (CGP) were incubated for 30 min in normoxia (Nx), in normoxia with antimycin A (AA 10 μM) or in hypoxia at 1% oxygen (Hp 30-40 min). DHE (5 μM) was added for 10 min more, and slices were fixed in the hypoxia chamber. (b) Representative images showing DHE fluorescence. (c) Data are presented as mean ± s.e.m. of four independent experiments. **(d)** Untreated or 30 μM CGP-37157-treated hippocampal slices were exposed for 4 hours to normoxia (Nx), normoxia with 1 mM DMOG or to hypoxia (1% oxygen, Hp), proteins extracted and blotted against HIF-1α protein and tubulin. Representative image and densitometry of four independent experiments. ** $p<0.01$, *** $p<0.001$ (Student's t-test).

Finally, we addressed whether the pharmacological inhibition of NCLX could be protective in an *in vivo* model of photothrombotic ischemic injury. The ischemic insult is caused by the reaction of the photosensitive dye Rose Bengal with a cold light, which induces thrombi formation in the brain vessels. At the end of the experiment, the infarcted area is differentiated by triphenyltetrazolium chloride staining. We have analysed separately the infarcterd area, the ipsilateral area including the penumbra region around the infarct (where there is a partial ischemia) and the contralateral area (the symmetric half of the brain, which remains in normoxia). Complex I deactivation was clearly observed in the infarcted area of mice, independently of CGP treatment which was less obvious but also seen in the ipsilateral area (Figure 4.34a). In contrast, CGP-treated mice had a significantly smaller infarct size compared with non-treated littermates (Figure 4.34b-c).

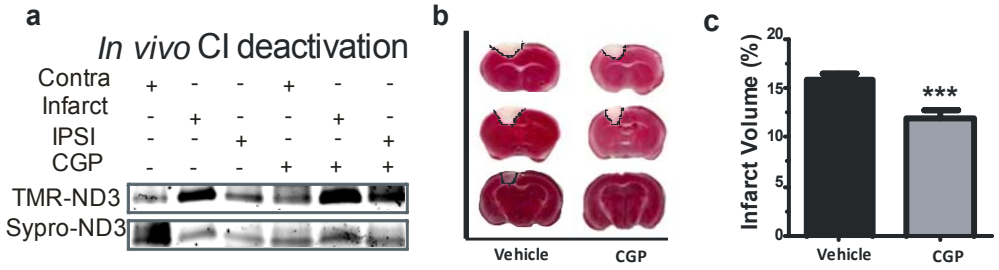

Figure 4.34. NCLX inhibition protects brain from ischemic damage without affecting complex I deactivation. Mice were subjected to photothrombotic stroke induction and treated either with vehicle or with 30 mg/kg of CGP-37157 5 min after illumination. **(a)** ND3 Cys exposure (as in Figure 4.20b) from samples of different regions of the brain: infarct, ipsilateral (IPSI) and contralateral (Contra). **(b and c)** Brain tissue was stained with triphenyltetrazolium chloride and the infarct volume quantified. Data represents mean ± s.e.m. of the quantification of the infarct volume. *** $p < 0.001$ vs vehicle (Student's t-test; n = 7).

In summary, NCLX inhibition prevents the superoxide burst in hypoxia in neurons and neuronal tissue, independently of Complex I deactivation and lowers the infarct size in an ischemic injury mice model.

4.4. Sodium overload alters NCLX activity and ROS production

4.4.1 Sodium overload alters the sodium/calcium exchange in acute hypoxia

As mentioned in the introduction, sodium overload is a common feature in diseases where hypoxia is present. Therefore, we wondered whether sodium overload could affect the Complex I-NCLX-ROS pathway in the transition from normoxia to hypoxia. Since we have described most of this pathway in non-excitable primary endothelial cells and the measurement of $Ca^{2+}{}_i$ and $Na^{+}{}_i$ is not reliable in excitable cells due to the action potential variations (personal observation), we decided to study sodium overload by adding 100 mM of sodium chloride salt in BAECs culture medium of BAECs (i.e. doubling the normal sodium chloride concentration in RPMI, which is 120 mM).

First, we analysed sodium and calcium cytosolic concentrations in the transition from normoxia to hypoxia by live fluorescence imaging. Increased extracellular sodium concentration augmented basal intracellular $Na^{+}{}_i$; (Figure 4.35a). Incubation of BAECs in hypoxia decreased $Na^{+}{}_i$, while in normoxia treatment it remained constant throughout all the experiment (Figure 4.35a-b). Sodium overload altered the hypoxic $Na^{+}{}_i$ decrease (Figure 4.35a-b). Indeed, hypoxia triggered a $Ca^{2+}{}_i$ rise which was abolished by sodium overload (Figure 4.35c-d). Of note, basal $Ca^{2+}{}_i$ levels were higher in BAECs under sodium overload than in non-treated controls (Figure 4.35c) which suggests NCLX activation upon sodium overload.

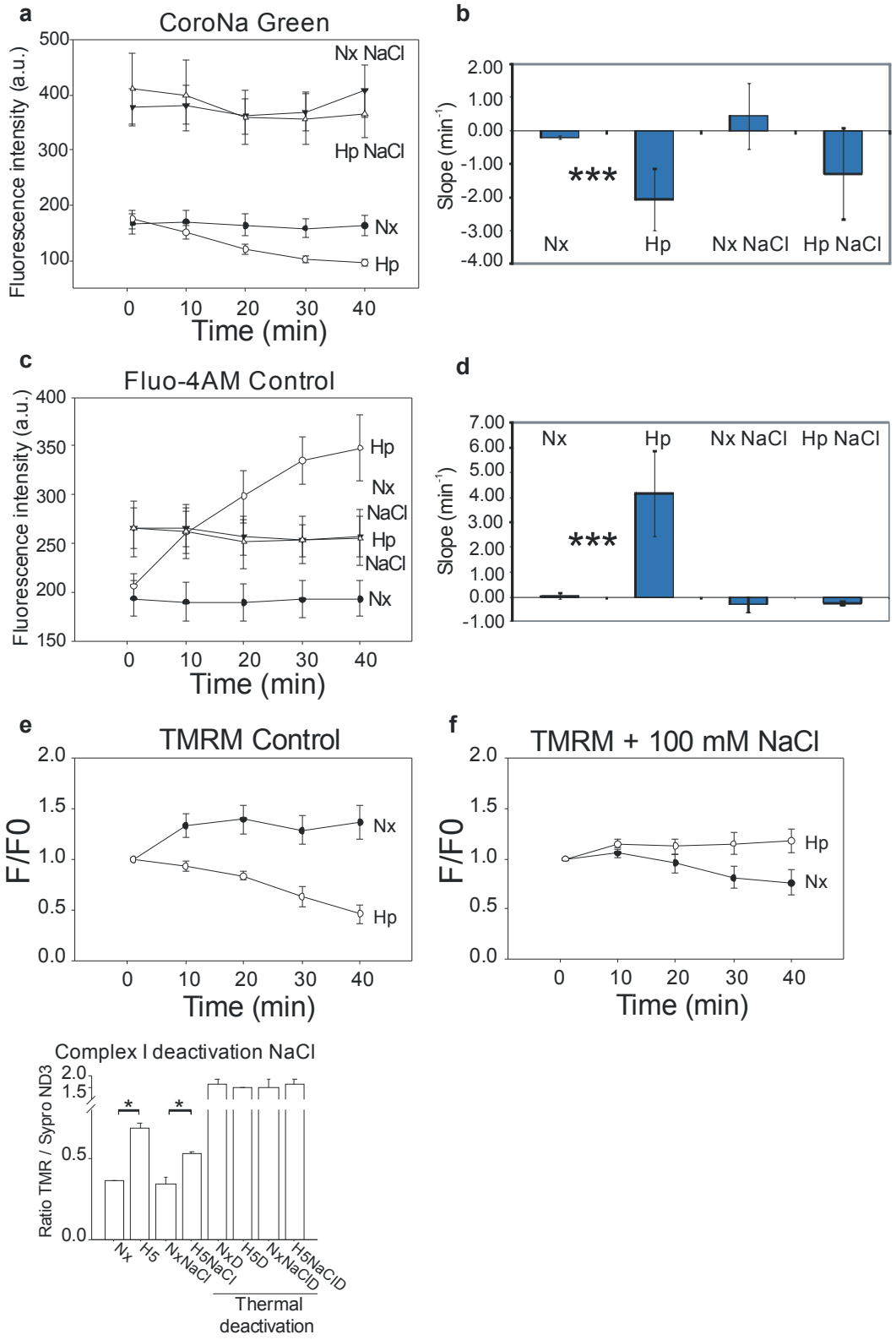

Figure 4.35. Sodium overload alters hypoxic sodium/ calcium exchange, but not complex I deactivation. (a) Cytosolic sodium measured with the CoroNa Green probe or cytosolic calcium measured with Fluo-4AM **(C)** in normoxia (Nx, ●), hypoxia (2% oxygen; Hp, ○), normoxia plus 100 mM sodium chloride (Nx NaCl,) or hypoxia plus 100 mM sodium chloride (Hp NaCl,) in BAECs by live cell imaging fluorescence microscopy. **(b and d)** Slopes considering all the ROI and time points of each replicate (n = 3) were estimated by linear regression and plotted as mean ± s.e.m. A and C are plotted in B

and D respectively. Untreated BAECs **(e)** or treated with extra 100 mM sodium chloride **(f)** were subjected to normoxia (Nx, ●) or hypoxia (2% oxygen; Hp, ○) and mitochondrial membrane potential detected with the TMRM probe. Data are represented as mean ± s.e.m. of the actual fluorescence divided by the fluorescence at time 0 (F/F0) of three independent experiments. **(g)** Fluorescent thiol labelling and quantification of ND3 residue Cys39. BAECs were subjected to hypoxia or normoxia for 5 min in the presence or absence of further 100 mM sodium chloride. Maximal exposure of the residue was measured by treating the same samples at 37ºC for 60 min. Quantification shows the mean ± s.e.m. of three independent experiments. *** $p < 0.001$ (Student's t-test; $n = 3$).

As NCLX-mediated exchange is an electrogenic process, we also measured mitochondrial depolarization in acute hypoxia. Non-treated BAECs showed hypoxic mitochondrial depolarization (Figure 4.35e) which was inhibited by sodium overload (Figure 4.35f). Interestingly, increased sodium depolarized mitochondria in normoxic conditions (Figure 4.35f). This correlates well with overactivation of NCLX which performs an electrogenic exchange and mitochondrial repolarization (Kim and Matsuoka, 2008).

We also questioned whether the dysregulation of sodium/calcium exchange by sodium overload was due to alteration of hypoxic complex I deactivation. Sodium overload was induced in BAECs before and during acute hypoxia and complex I deactivation detected through ND3 Cys39 fluorescent labelling. We observed an increased deactivation of complex I in acute hypoxia, which was maintained by sodium overload (Figure 4.35g).

NCLX is the only member in its family insensitive to potassium and blocked by lithium (Palty et al., 2010), thus if any other member of the sodium/calcium exchanger family was involved the response, it should be inhibited by increased potassium and not by lithium. We treated BAECs with doubled media potassium concentration (i.e. addition of 5 mM potassium chloride in the media over the already 5 mM present) or added 30 mM lithium chloride. Increased potassium diminished the raise in cytosolic calcium and had no effect on sodium decrease (Figure 4.36b,e), in contrast to, lithium chloride treatment which clearly abolished both (Figure 4.36c,f). Thus, sodium/calcium exchange is specifically inhibited by lithium chloride, reinforcing the hypothesis of the involvement of NCLX. Besides, the effect seen in the hypoxic cytosolic calcium by potassium may arise from alteration of plasma membrane potassium currents.

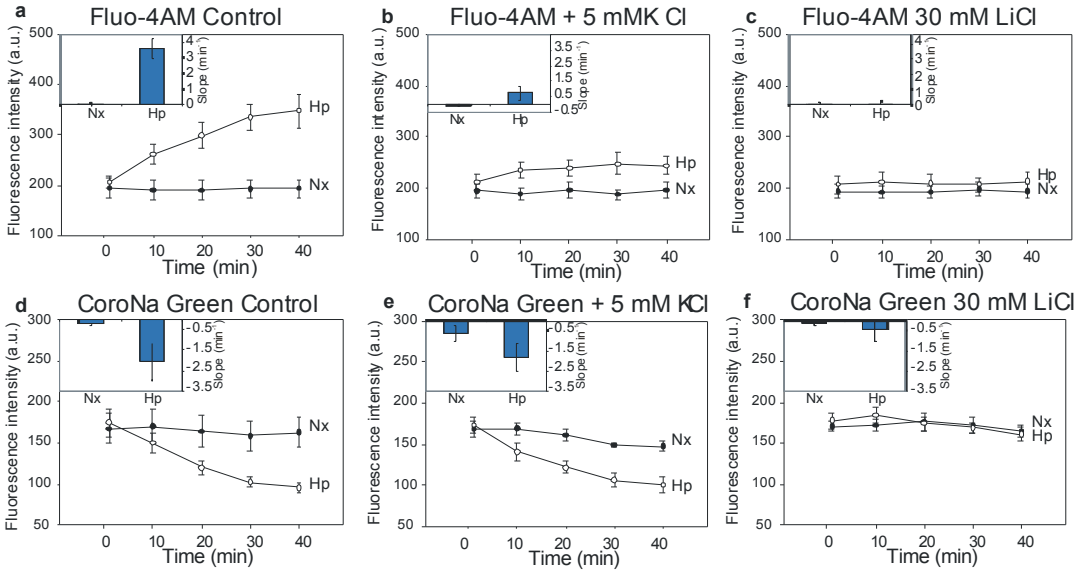

Figure 4.36. Alteration of NCLX activity modifies hypoxic mitochondrial sodium/ calcium exchange. (a-c) Cytosolic calcium measured with the Fluo-4AM probe or cytosolic sodium measured with Corona Green **(d-f)** in BAECs non treated or treated with extra 5 mM potassium chloride or 30 mM lithium chloride subjected to normoxia (Nx, ●) or hypoxia (2% oxygen; Hp, ○) by live cell imaging fluorescence microscopy. **(Insets in a-f)** Slopes considering all the ROI and time points of each replicate (n = 3) were estimated by linear regression and plotted as mean ± s.e.m.

We measured the variation in mitochondrial membrane potential in BAECs and observed that increased potassium had no effect in any of the conditions and lithium chloride inhibited hypoxic mitochondrial depolarization (Figure 4.37). In neonatal rat primary cardiomyocytes addition of 100 mM sodium chloride or 30 mM lithium chloride clearly abolished hypoxic mitochondrial depolarization, while addition of 5 mM potassium chloride did not affect it (Figure 4.38).

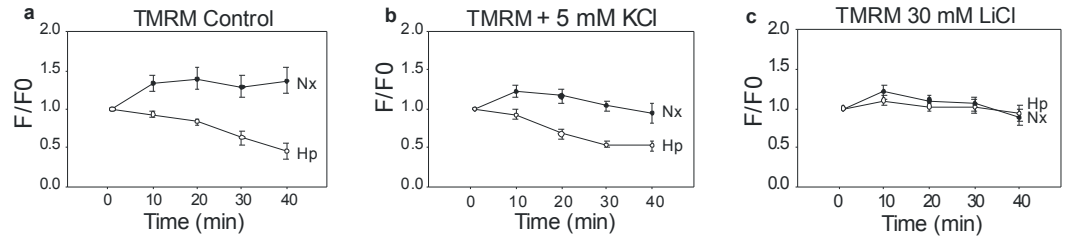

Figure 4.37. Alteration of NCLX activity modifies hypoxic mitochondrial depolarization. Untreated BAECs **(a)** or BAECs treated with extra 5 mM potassium chloride **(b)** or 30 mM lithium chloride **(c)** were subjected to the same protocol as in Figure 4.11. Data for TMRM fluorescence are represented as mean ± s.e.m. of the actual fluorescence divided by the fluorescence at time 0 (F/F0) of three independent experiments.

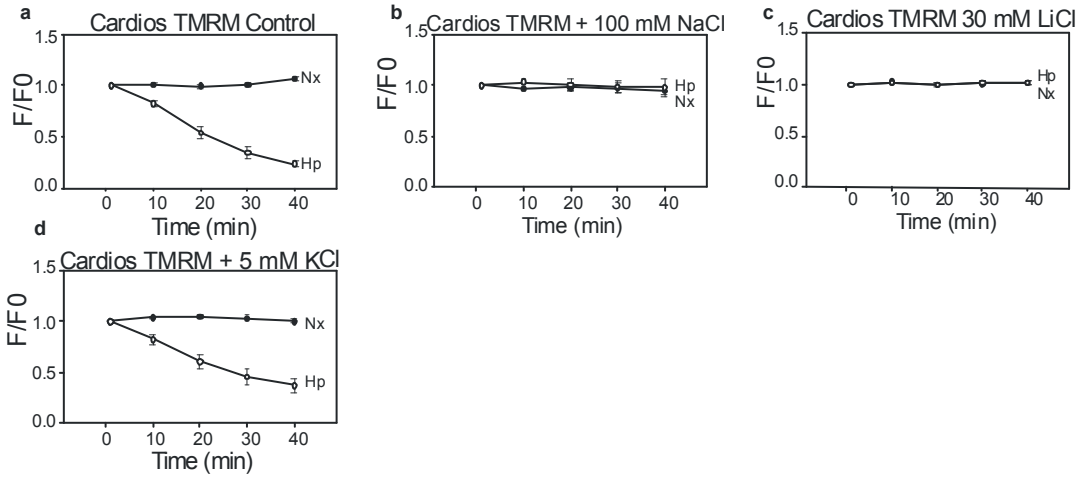

Figure 4.38. Alteration of NCLX activity modifies hypoxic mitochondrial depolarization in cardiomyocytes. Untreated primary rat cardiomyocytes untreated **(j)** or treated with extra 100 mM sodium chloride **(k)**, 30 mM lithium chloride **(l)** or extra 5 mM potassium chloride **(m)** were subjected to the same protocol as in Figure 4.11. Data for TMRM fluorescence are represented as mean ± s.e.m. of the actual fluorescence divided by the fluorescence at time 0 (F/F0) of three independent experiments.

All together, these results show that sodium overload abolishes hypoxic mitochondrial sodium/calcium exchange and depolarization, independently of complex I deactivation. Of note, excess of sodium probably pulls calcium out of mitochondria via NCLX anticipating the hypoxic sodium/calcium exchange.

4.4.2 Sodium overload alters cellular respiration

Since we observed that sodium overload depolarizes mitochondria we reasoned that it could have an effect on mitochondrial bioenergetics. Thus, we examined whether oxygen consumption was altered in a BOFA experiment. Basal respiration and coupling efficiency (i.e. the amount of oxygen used for the OXPHOS to produce ATP) were affected (Figure 4.39a-c), which was expected since both are directly dependent on $\Delta\Psi_{mt}$. The reserve capacity (oxygen consumed from the mitochondrial energy stores) of sodium-overloaded BAECs was abolished (Figure 4.39d); this suggests that the excess of sodium reduces TCA cycle dehydrogenases turnover, probably due to depletion of mitochondrial calcium through NCLX activation. Interestingly, proton leak was not affected by this treatment, indicating that it did not permeabilize the IMM or trigger uncoupling due to activation of uncoupling proteins (UCPs), mitochondrial permeability transition pore (mPTP) or by other means (Figure 4.39e). Intriguingly, non-mitochondrial respiration also decreased, suggesting that other systems using oxygen as a substrate were affected as well (Figure 4.39f).

The extracellular acidification rate (ECAR) is proportional to the glycolysis rate in cells. ECAR was higher in sodium-overloaded BAECs in comparison to control, indicating that the reduction in OXPHOS was compensated with an increased glycolysis (Figure 4.39g). Accordingly,

the glycolytic reserve (i.e. maximal glycolysis), which is obtained after oligomycin addition, was lower in sodium overloaded cells, suggesting that they already reached the highest glycolysis rate (Figure 4.39h). Strikingly, this value was negative in sodium overloaded BAECs. Sodium-dependent inhibition of respiration would translate in matrix acidification since sodium entry into the mitochondria would activate the canonical NHE. This would extrude sodium in exchange of protons which acidifies the matrix. Now, in response to matrix acidification and in order to maintain certain level of $\Delta\Psi_{mt}$, complex V could work pumping protons to the IMS. Thus, inhibition by oligomycin woul stop proton pumping by complex V, decreasing extramitochondrial and, in turn, extracellular proton content,, lowering ECAR.

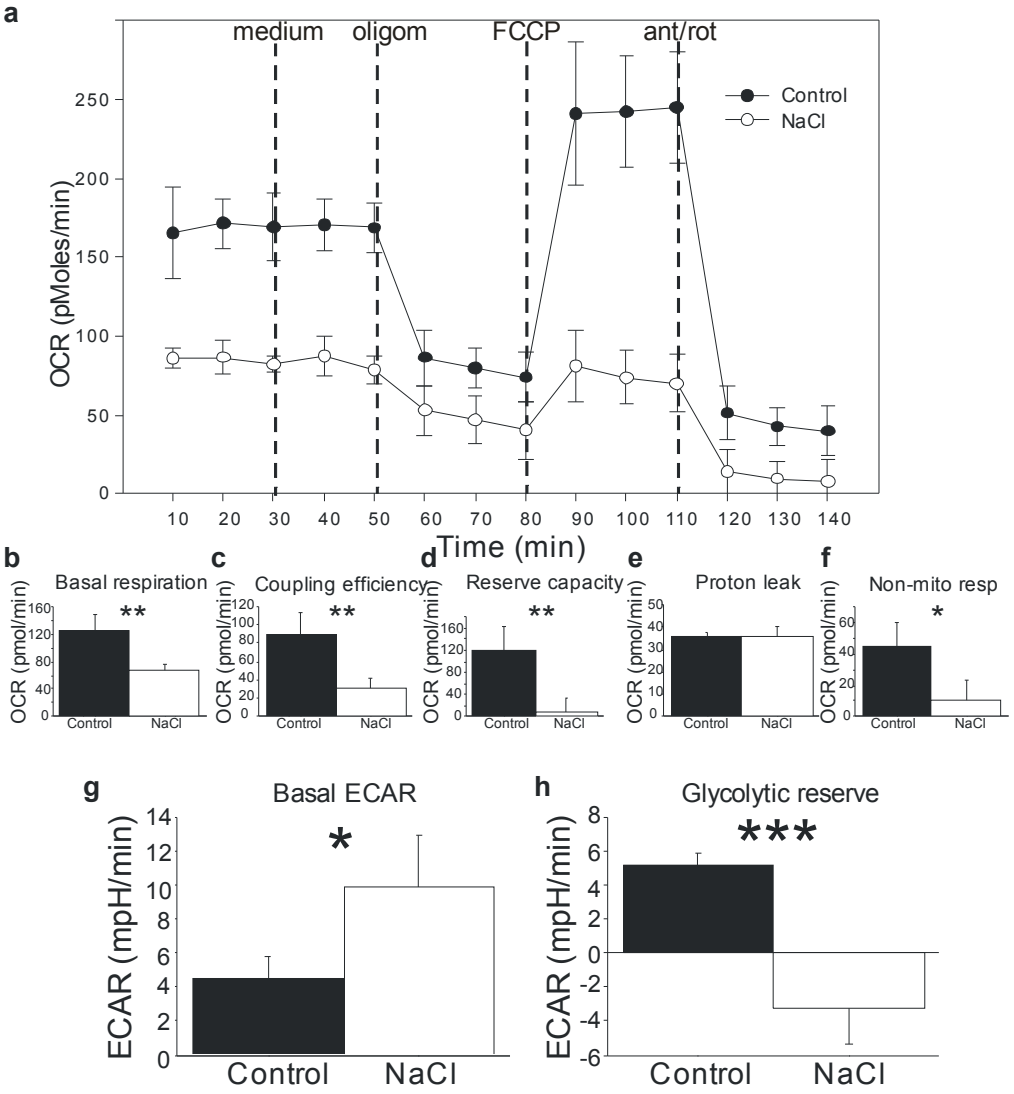

Figure 4.39. Sodium overload switches aerobic to anaerobic metabolism. (a-f) Oxygen consumption was measured in a Seahorse XF24 Analyzer in untreated BAECs (Control, ●) or BAECs treated with 100 mM sodium chloride added to the media (NaCl, ○). **(a)** OCR plots indicating the sequential addition of drugs: medium, 5 µg/ml oligomycin (oligom), 300 nM FCCP, 1 µM rotenone and 1 µM antimycinA (ant/rot). Basal respiration **(b)**, coupling efficiency **(c)**, maximal respiration **(d)**, reserve capacity, proton leak **(e)** and non-mitochondrial respiration **(f)**. **(g)** Extracellular acidification rate

(ECAR) measured in untreated or BAECs treated with extra 100 mM sodium chloride. **(h)** ECAR measured after oligomycin addition, indicating the glycolytic reserve of the cells. Data are presented as mean ± s.e.m. of three independent experiments. * $p < 0.05$, ** $p < 0.01$, *** $p < 0.001$ (Student's t-test; $n = 4$).

In summary, sodium overload switches the metabolism, probably through NCLX, towards a rather glycolytic profile without increasing mitochondrial permeability.

4.4.3 Hypoxic superoxide burst is altered by sodium overload

Since mitochondrial hypoxic sodium/calcium exchange was altered by sodium overload we wondered whether superoxide production in hypoxia was also affected when we added extra 100 mM sodium chloride to the cells. Non-treated BAECs generated superoxide in the first minutes of hypoxia, which declined to basal levels within an hour (Figure 4.40a,c). However, sodium overload increased superoxide production in normoxia which then diminished in hypoxia, thus rendering superoxide levels proportional to oxygen concentration (Figure 4.40b,d). Importantly, normoxic sodium overload-derived increase in superoxide was abolished by CGP-37157 (Figure 4.40b), indicating that NCLX is specifically required for the effect of sodium overload in normoxic ROS production, and suggesting again that sodium chloride addition may drive a normoxic sodium/calcium exchange in the mitochondria through NCLX, which affects superoxide production.

In addition, we performed live imaging experiments using the fluorescent probe CDCFDA. Sodium overload inhibited ROS increase in hypoxia, but it raised the basal levels of ROS (Figure 4.40e-f). Of note, sodium-overloaded BAECs did not show a decline in ROS production with CDCFDA in hypoxia in comparison to normoxia, probably due to irreversibility of the probe oxidation.

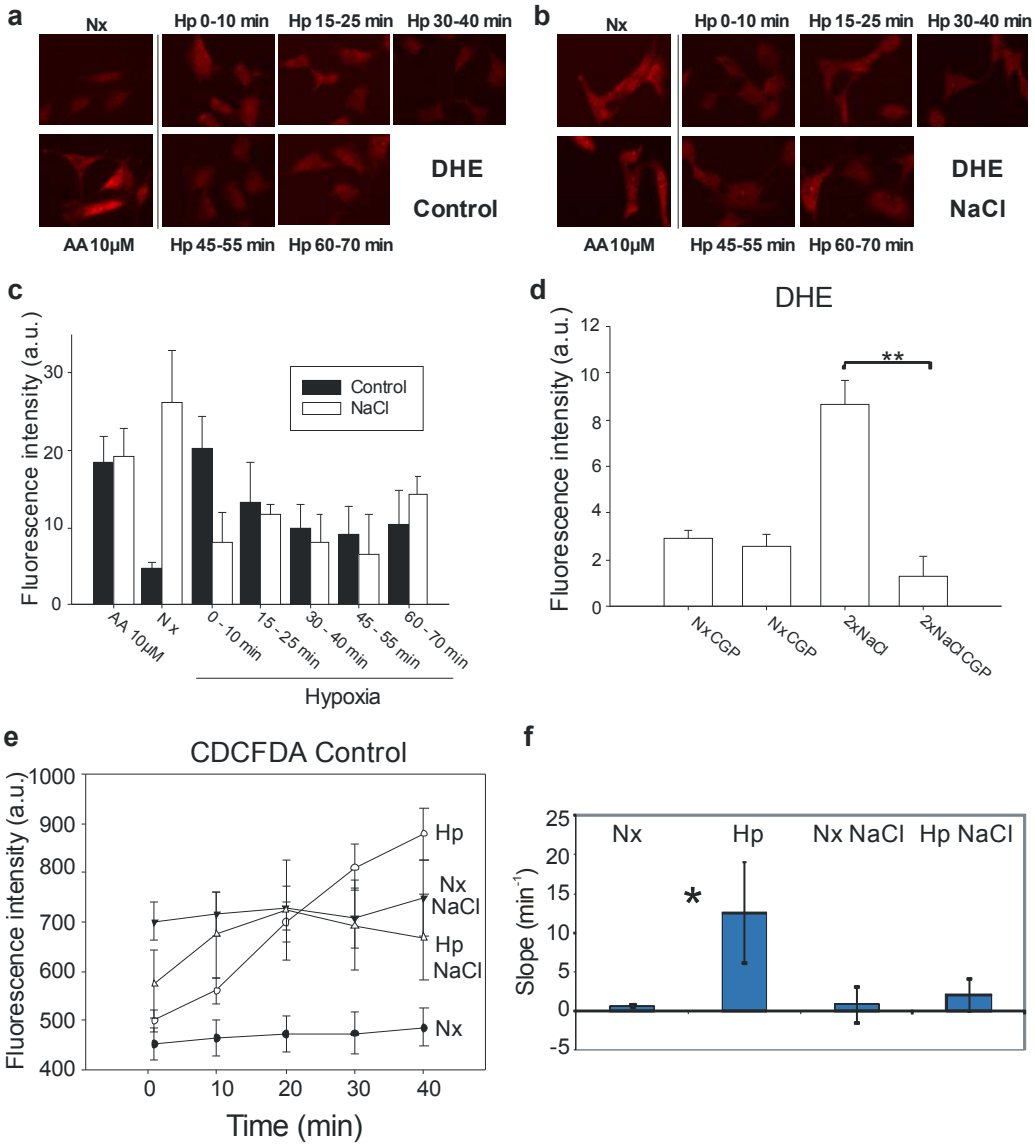

Figure 4.40. Sodium overload and not high osmolarity increases normoxic superoxide levels and abolishes the hypoxic superoxide burst. (a-d) Detection of superoxide production by fluorescence microscopy in fixed cells. Cells were incubated as in Figure 4.1. **(a and b)** Representative images showing DHE fluorescence in BAECs. Superoxide levels were measured in non-treated BAECs (Control) or with extra 100 mM sodium chloride (NaCl) **(a-c)**, CGP-37157 or 100 mM sodium chloride plus 10 µM CGP-37157 **(d)**. Data are presented as mean ± s.e.m. of three independent experiments. ** $p < 0.01$ (one-way ANOVA). **(e and f)** Detection of ROS production by live fluorescence microscopy with CDCFDA. **(e)** Untreated BAECs in normoxia (Nx, ●) or hypoxia (2% oxygen; Hp, ○), or treated with extra 100 mM sodium chloride in normoxia (Nx NaCl, ▼) or hypoxia (2% oxygen; NaCl Hp, △). **(f)** Slopes considering all time points of each replicate (n = 3) are plotted as mean ±s.e.m. The slope for each replicate was estimated by linear regression of the data for all the ROI and time points. * $p<0.05$ of Nx versus Hp (Student's t-test).

Furthermore, in order to check whether the superoxide burst was being altered via NCLX we treated BAECs with doubled potassium or 30 mM lithium chloride. Expectedly, whereas potassium addition had no effect on the superoxide burst, lithium abolished it (Figure 4.41a-b). The same results were obtained with the probe CDCFDA (Figure 4.41c-e).

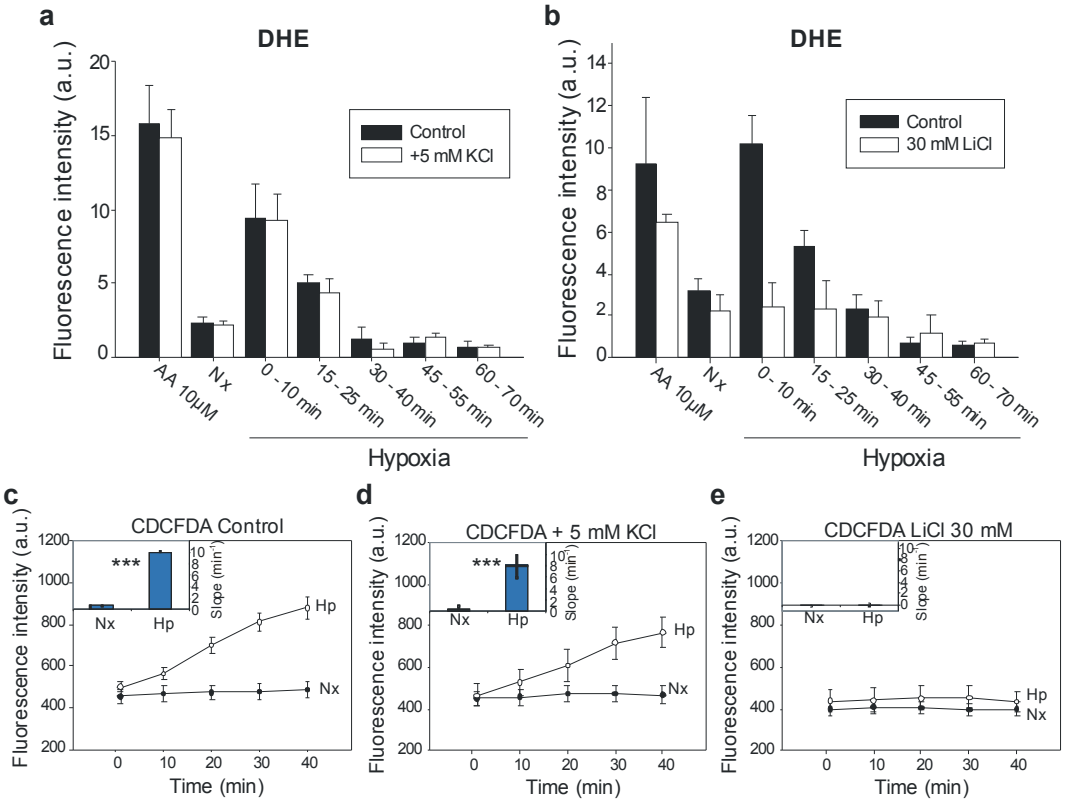

Figure 4.41. Modification of NCLX activity influences hypoxic superoxide and ROS production. (a and b) Detection of superoxide production by fluorescence microscopy in fixed cells. Non-treated BAECs (Control) or treated with extra 5 mM potassium chloride (KCl) **(a)** or 30 mM lithium chloride **(b)** were subjected to the same protocol as in Fig. 3A. **(c-e)** Detection of ROS production by live fluorescence microscopy with DCFDA. **(c)** Untreated BAECs in normoxia (Nx, ●) or hypoxia (2% oxygen; Hp, ○), or treated with extra 5 mM potassium chloride **(d)** or 30 mM lithium chloride **(e)**. **(Instets in c-e)** Slopes considering all time points of each replicate (n = 3) are plotted as mean ±s.e.m. The slope for each replicate was estimated by linear regression of the data for all the ROI and time points. Data are presented as the mean ±s.e.m. of three independent experiments.

Altogether, these results show that sodium overload inverts NCLX-dependent ROS production in the transition from normoxia to hypoxia. Importantly, activating NCLX-dependent sodium/calcium exchange by sodium overload in normoxia promotes mitochondrial depolarization and ROS production. This supports the hypothesis of NCLX activation as a key player in superoxide generation by mitochondria.

4.4.4 HIF-1 pathway activation in hypoxia is inhibited by sodium overload

Since hypoxic HIF-1α stabilization has been linked to ROS production in hypoxia (Guzy et al., 2005, Chandel et al., 1998, Brunelle et al., 2005, Mansfield et al., 2005) and since sodium overload altered ROS levels both in normoxia and hypoxia, we wondered whether sodium increase affected HIF-1α presence in hypoxia. We observed an increase in HIF-1α stabilization in hypoxia and DMOG, while sodium-overloaded BAECs showed a reduced stabilization of HIF-1 α in

hypoxia, in contrast to DMOG-treated cells (Figure 4.42a-b). This was replicable in human umbilical vein endothelial cells (HUVECs) and HeLa cells (Figure 4.42c-d).

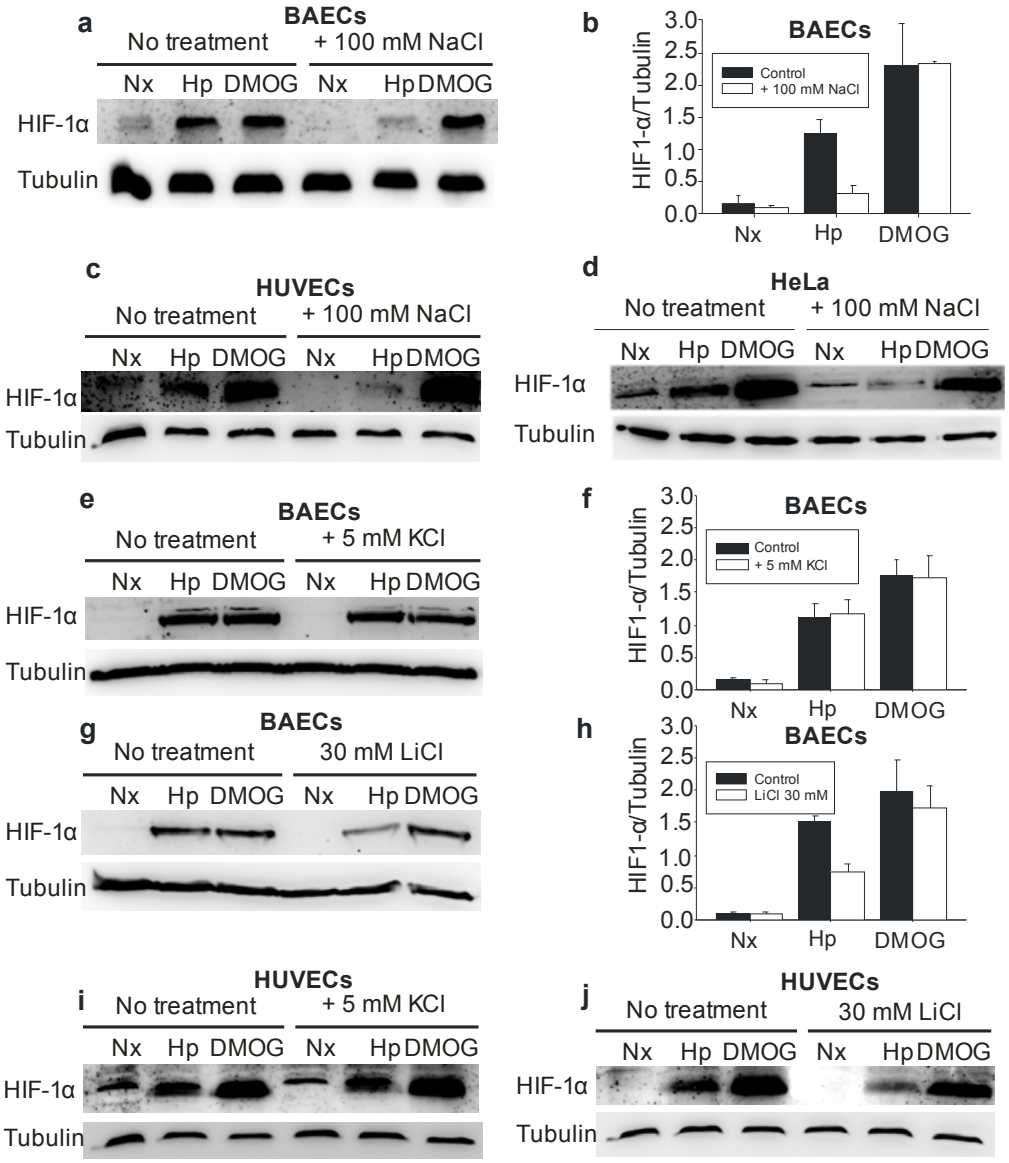

Figure 4.42. Sodium overload abolishes HIF-1α stabilization through NCLX inactivation in several cell types. HIF-1α stabilization measured by western blotting in BAECs **(a, b and e-h)**, HUVECs **(c, i and j)** and HeLa **(d)** treated or not with extra 100 mM sodium chloride (a-d), extra 5 mM potassium chloride (e, f and i) or 30 mM lithium chloride (g and j) and exposed for 4 h to normoxia (Nx), normoxia with 1 mM DMOG or to hypoxia (1% oxygen, Hp). Tubulin was used as a loading control. **(a, c, d, e, g, i and j)** Representative images of at least three independent experiments are shown. Densitometry of a, e and h is shown in b, f and h, respectively.

Previous results showed that doubled potassium did not affect NCLX activity and ROS production, in contrast to addition of 30 mM lithium chloride. In accordance to this, hypoxic stabilization of HIF-1α was not affected by the former but it was in the presence of latter (Figure 4.43a-f).

The amount of HIF-1α or HIF-2α mRNAs varied slighyly but not significantly between different conditions (Figure 4.43g-h). However, gene expression of HIF-1 targets such as PDK1, BNIP3 or PHD3 was induced in hypoxia, which was abolished or diminished by sodium overload (Figure 4.43i-k). Of note, increased sodium tended to inhibit DMOG-dependent expression of these genes (Figure 4.43i-k).

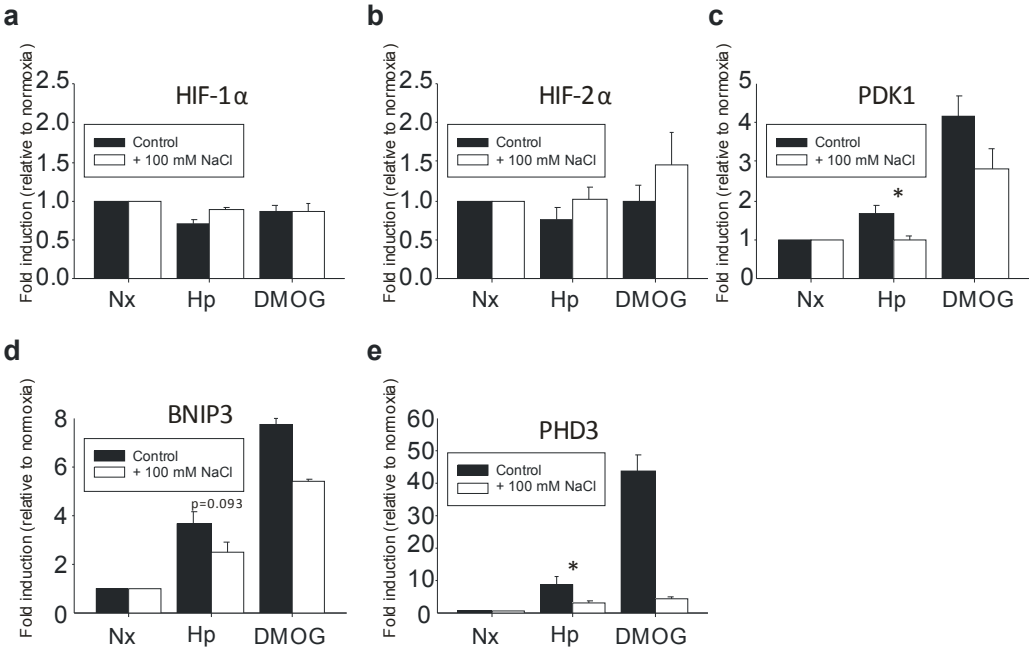

Figure 4.43. Sodium overload inhibits HIF-1α stabilization and function through NCLX in different cells. Quantitative RT-PCR analysis of HIF-1α **(a)**, HIF-2α **(b)**, PDK1 **(c)**, BNIP3 **(d)** and PHD3 **(ke** mRNAs in untreated (black) or treated with extra 100 mM sodium chloride (white) HUVECs subjected to 6 hours of normoxia (Nx), hypoxia (1% oxygen, Hp) or normoxia with 1 mM DMOG. Data are represented as mean ±s.e.m. of the β-actin ratio relative to normoxia for four independent experiments. * $p < 0.05$ Control Hp versus +NaCl 100 mM Hp of each condition (Student's t-test).

In summary, sodium overload decreases HIF-1α stabilization in hypoxia, which could be related to its effect on hypoxic ROS production through NCLX. Furthermore, HIF-1 pathway activity was decreased both in hypoxia and DMOG-treated cells, suggesting that sodium chloride addition is also altering the mechanisms of HIF-1α stabilization.

4.4.5 The effects of sodium chloride addition are not due to osmotic stress

The addition of extra 100 mM sodium chloride could produce an osmotic stress or change in ionic strength that could be the cause of the effects observed. The effects of high salinity due to increased sodium chloride have been widely studied in plants, where osmotic stress can also affect mitochondrial ROS production (Miller et al., 2010). In order to study the effects of osmolarity an inert osmolyte such as D-sorbitol is added. Apart from the osmolarity, the fact of introducing a positive charge and not the specific effect of a particular ion (e.g. Na^+) can alter ion homeostasis in the cell and mitochondria. Therefore, an inert organic monovalent cation such as N-Methyl-D-

glucamine (NMDG) is added to test it. Thus, we measured the superoxide burst in the presence of 100 mM D-sorbitol or NMDG, observing that they had no effect on the superoxide burst (Figure 4.44a-b). Indeed, we confirmed these results by checking HIF-1α stabilization upon treatment with 100 mM D-sorbitol and observed no change in comparison to non-treated cells (Figure 4.44c-d).

We also checked whether the effects on HIF-1α stabilization of doubling potassium chloride concentration (i.e. addition of 5 mM potassium gives a total of 10 mM potassium in the medium) or of addition of 30 mM lithium chloride were due to differences in osmolarity or specifically to potassium, chloride or lithium ions, by switching the concentrations. Thus, we increased total potassium up to 30 mM and decreased lithium chloride addition to 10 mM. Even with this change in the concentrations, we could still observe that potassium chloride addition had no effect while lithium chloride inhibited HIF-1α stabilization (Figure 4.44e-h).

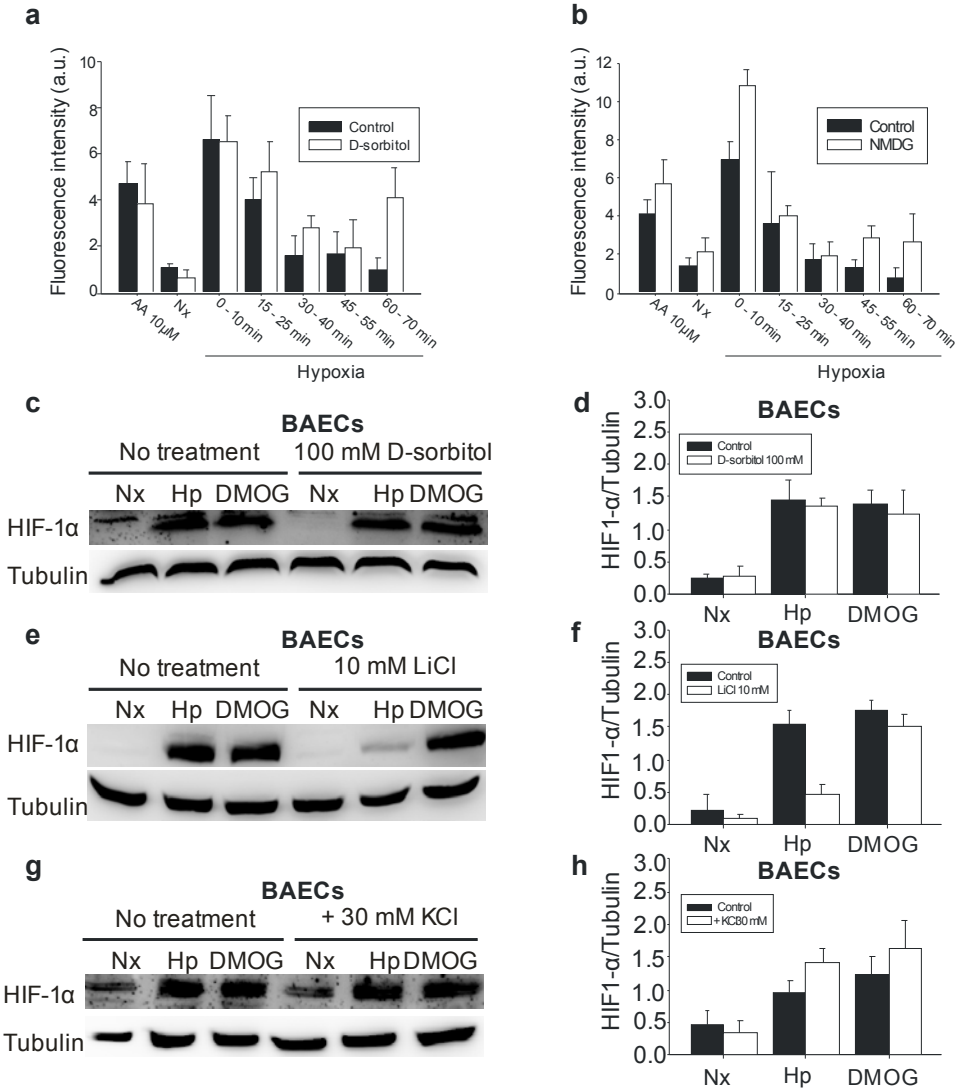

Figure 4.44. ROS production and HIF-1α stabilization inhibition by sodium overload is not due to high osmolarity or high potassium concentration. Non-treated BAECs (Control) or with extra 100 mM D-sorbitol **(a)** or 100 mM N-methyl D-glucamine (NMDG) **(b)** were treated as in Figure 4.1. Data are presented as mean ± s.e.m. of three independent experiments. **(c-h)** HIF-1α stabilization measured by western blotting in BAECs treated or not with 100 mM D-sorbitol **(c and d)**, 10 mM lithium

chloride **(e and f)** or 30 mM potassium chloride **(g and h)** and exposed for 4 h to normoxia (Nx), normoxia with 1 mM DMOG or to hypoxia (1% oxygen, Hp). Tubulin was used as a loading control. **(c, e and g)** Representative images of at least three independent experiments are shown and its densitometries are shown in b, d and f.

In summary, the effects observed with sodium overload are specifically due to this ion and not to osmotic stress or changes in ionic strength. Furthermore, the effects of potassium chloride or lithium addition are not due to differences in concentrations, but rather probably to their specific effects on NCLX function.

Discussion

5 Discussion

We have focused our research on the detection of superoxide anion in acute hypoxia and in the characterization of the molecular players involved in triggering its production in the mitochondria. We have detected superoxide anion production specifically and observed that in behaved as a burst in the first minutes of hypoxia. We observed that it was related to hypoxic HIF-1α stabilization.

Our results indicated that complex I deactivates proportionally to the level of hypoxia and in an acute manner. Such deactivation would preclude its activity switch to a sodium/proton antiporter. Complex I is needed for mitochondrial sodium/calcium exchange via NCLX and both are required for the superoxide burst. Hypoxic superoxide burst relies also on complex III, although we have not assessed its specific role. Inhibition of NCLX correlated with inhibition of hypoxic HIF-1α stabilization in cell culture and hippocampal slices, and with loss of steady-state contraction of PA. Blockage of NCLX diminished infarct size in phototrombotic ischemic injury in mice.

Finally, we have also studied the influence of sodium overload in the hypoxic response and observed that the response is altered at the level of NCLX.

5.1 Hypoxia produces a mitochondrial superoxide anion burst

Using several converging methodologies that avoid re-oxygenation we have demonstrated that exposure of cells to acute mild hypoxia (1-2% oxygen in our culture conditions) was associated with a burst in superoxide production within the first minutes. Thereafter the levels of superoxide production in hypoxic cells reduced gradually over time. In one hour no difference in superoxide production could be detected between hypoxic (1% oxygen) and normoxic cells (Figure 5.1). We made special efforts in detecting specifically the first product of one-electron reduction of oxygen, superoxide anion. This allowed us to rule out other ROS sources or mechanisms producing other species, such as hydrogen peroxide or peroxynitrite. Our results comparing different hypoxic oxygen concentrations in the same experimental setting (Figures 4.1a and 4.3 b) show that at 2% oxygen the superoxide burst can be more intense and sustained than at 1% oxygen. This allows speculating that the decrease in superoxide production after some time of hypoxia could be related to a decrease in the oxygen availability near the mitochondria. Although most of our experiments have been done setting hypoxic conditions at 1% oxygen (except for Figure 4.3b and live imaging experiments performed in the fluorescence microscope at the University of Zürich), it will be very interesting to study the magnitude of the superoxide burst and downstream responses in moderate hypoxia. In these conditions, increased superoxide production can be a cellular signal anticipating the reduction in oxygen availability, triggering adaptive responses before oxygen concentration decreases below the threshold for inactivating key enzymes such as cytochrome *c* oxidase.

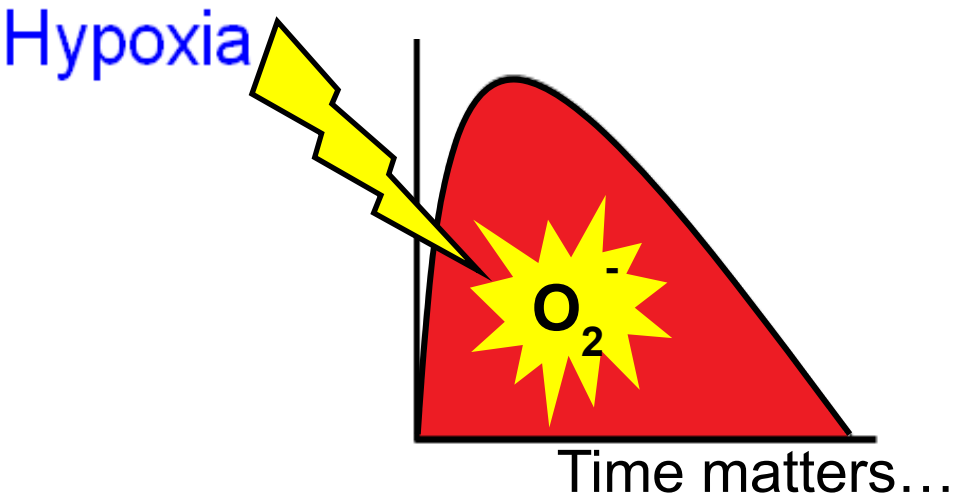

Figure 5.1 Hypoxia produces a superoxide burst in cells. Mitochondria generate superoxide in the first minutes of hypoxia which decreases up to an hour. Since discrepant literature has emerged due to measurements in different times, this scheme highlights the importance of time in ROS detection.

Our observation of the temporal dynamics of superoxide levels in acute hypoxia resolve the seeming contradictory findings reported earlier, in which some groups reported increased ROS levels in hypoxia and others showed no increase (Mehta et al., 2008). For example, Quintero *et al.* analysed superoxide production by incubating endothelial cells with DHE for the first 60 min of hypoxia (3% oxygen), showing a clear increase in the fluorescence signal (Quintero et al., 2006); in these conditions, DHE would be oxidized by the superoxide burst that we have seen in our experiments. On the other hand, Chua *et al.* have seen no increase in DHE fluorescence when HEK293 cells were exposed to 1% hypoxia; however, in this case DHE was added for 30 min after 3 h of incubation of the cells in hypoxia (Chua et al., 2010), which would not allow to detect the initial superoxide burst. This illustrates the importance of time in ROS measurements (Figure 5.1). Other studies have also shown an increase in DHE oxidation in cardiomyocytes in a model of acute ischemia during up to 60 min, where in addition to hypoxia nutrients were removed from the cell culture medium (Becker et al., 1999).

The fact that DCFDA oxidation was maximal after 15 min of hypoxic exposure suggests that the superoxide burst during the first minutes of hypoxia translates into an increase in hydrogen peroxide or other ROS with a certain delay in time. This could be related with the different kinetics of accumulation of the diverse ROS, although it can be also an effect of the different probes used or even that the superoxide burst could trigger peroxide generation by other pathways. In line with this, we had performed a proteomic characterization of protein cysteine residues that were reversibly oxidised in endothelial cells after two hours of hypoxia (Izquierdo-Álvarez et al., 2012), and we have seen a peak in protein cysteine oxidation between 30 and 120 min of hypoxia (unpublished results). This suggests that the increase in each ROS or in their downstream effects may have different kinetics that could fit in a signal transduction scheme in the cell.

We have seen a similar superoxide burst and ROS production in different cell types exposed to hypoxia, and using either probes distributed throughout the cell, cytosolic or mitochondria-targeted probes. When using ϱ^0 cells lacking a functional OXPHOS the superoxide burst was abolished; this strongly suggests that the superoxide burst in the first minutes of hypoxia comes from the mitochondrial OXPHOS system (Chandel et al., 1998).

5.2 Complex I deactivation is required for ROS production in acute hypoxia

We have also studied in more detail the molecular aspects triggering the hypoxic superoxide burst, showing that both complex I and NCLX are required. Our results highlight the role of complex I responding proportionally to different levels of acute hypoxia and triggering hypoxic adaptation through a superoxide signal. Complex I deactivation produces a conformational change (Babot et al., 2014, Galkin et al., 2008, Zickermann et al., 2015) that exposes several of its subunits, including Cys-39 of ND3 (Galkin et al., 2008, Babot et al., 2014), and switches its activity to a sodium/proton exchanger, NHE (Roberts and Hirst, 2012). We show that ND3 Cys-39 becomes more exposed in acute hypoxia in different experimental models, strongly suggesting that complex I deactivation is a key event in response to oxygen deprivation. We also show that the mitochondrial matrix is acidified in hypoxia in a complex I-dependent manner, which is compatible with its increased NHE activity. Increased NHE activity induces matrix acidification which is known to solubilize mitochondrial calcium-phosphate precipitates which would increase calcium concentration in the matrix, turnover of TCA cycle dehydrogenases and NADH production which is necessary for other processes in the cell, such as cell signalling or maintenance of the antioxidant defence through NADPH generation (Fernandez-Agüera et al., 2015, Nickel et al., 2015). However, further experimental confirmation of the complex I NHE activity would be needed. Besides, the specific mechanism(s) by which oxygen levels influence the conformation and activity of complex I, as well as other aspects such as possible oxygen binding sites or hypoxia sensing by complex-I partner proteins remain to be elucidated.

It has recently been described that complex I and ROS signals are essential components of acute oxygen sensing by the carotid body (Fernandez-Agüera et al., 2015). In this study, the response to hypoxia of carotid body glomus cells lacking the 'core' subunit NDUFS2 was selectively abolished, while higher level of ROS were generated in normoxia (Fernandez-Agüera et al., 2015). We show here that different interventions that reduce the activity of complex I abolished the superoxide burst in hypoxia while increasing superoxide levels in normoxia. This underlines the role of complex I in mitochondrial ROS production, either in response to acute hypoxia (which can be used by the cell as a signal) or in chronic situations (where it can be more related to oxidative stress).

5.3 NCLX links hypoxic complex I deactivation to ROS production

We have found that NCLX is a key element linking the primary oxygen sensing event and superoxide production through sodium/calcium exchange. It is well known that NCLX activity is linked to OXPHOS through NHE (Murphy and Eisner, 2009, Poburko and Demaurex, 2012), therefore activation of NHE would increase mitochondrial sodium/calcium exchange through NCLX. We expected that increased mitochondrial calcium extrusion by NCLX would decrease matrix calcium concentration, which could translate in decreased TCA cycle dehydrogenases turnover and NADH production (Cox and Matlib, 1993); however we observed that mitochondrial calcium concentration was maintained in hypoxia even in the presence of the MCU blocker ruthenium red (Figure 4.25). This paradox could be explained with the involvement of other mechanisms that could increase matrix calcium concentration, such as matrix acidification and solubilisation of calcium-phosphate precipitates of the mitochondrial matrix (see above).

NCLX activity is electrogenic as it extrudes one calcium ion (Ca^{2+}) while it imports three sodium cations (Na^{+}). We have shown that hypoxia depolarizes mitochondria in an NCLX-dependent manner, suggesting that this exchanger can regulate respiration in hypoxia, a situation where mitochondrial oxygen consumption and energy conversion would become inefficient. In accordance, enhancing NCLX activity by sodium overload decreased basal respiration. In this regard, studying the regulation of NCLX and its relationship with physiology and disease would be interesting.

We have also correlated the activity of NCLX to the production of ROS in hypoxia. Up to our knowledge, this is the first description of the implication of this ion transporter in ROS production. This poses a new window of research since directly links mitochondrial ion homeostasis and redox biology. There are several tissues were this may have special importance in pathogenesis. This is the case of heart or brain diseases, where the correct regulation of action potentials govern the main function of the organ and ROS production are involved in many of their pathologies, such as ischemia/reperfusion injury, Parkinson´s or Alzheimer´s disease (Chouchani et al., 2014, Guzman et al., 2010). Therefore, dysregulation of ion homeostasis could impact NCLX function and ROS production by mitochondria. On the other hand, enhancement of NCLX function (e.g. by complex I deactivation) would translate into ROS production which could modify the activity of ion channels involved in brain or heart homeostasis, contributing to the development of the diseases.

We cannot attribute ROS production after NCLX activation to a precise ROS source in the mitochondria. Our results measuring mitochondrial calcium allow to discard the modulation by calcium of TCA cycle dehydrogenases activity (Cox and Matlib, 1993). The intrusion of sodium into the mitochondrial matrix or the extrusion of calcium could have many unknown effects on different enzymes. We have performed experiments with ρ^0 cells and uncouplers which suggested

that a functional OXPHOS was required for the hypoxic superoxide burst. Given that complex I becomes deactive in acute hypoxia and since the second major producer of superoxide in the ETC is complex III, it could be that this complex is involved. We have shown that lack of functional complex III is required for hypoxic ROS production, despite the presence of complex I. In addition, complex III inhibition at the Qi site promotes the production of semiquinone radical which is a well-known superoxide producer. Semiquinone is normally formed from ubiquinol oxidation. Indeed, in preliminary experiments we observed that acute hypoxia oxidized ubiquinol pool which was prevented by NCLX inhibition (unpublished results). These results would support previous findings involving complex III as superoxide producer in hypoxia (Chandel et al., 2000, Brunelle et al., 2005, Guzy et al., 2005). However, how NCLX activity influences complex III ROS production is still to be elucidated.

We propose a model in which we connect our findings regarding the role of complex I deactivation and NCLX activation in response to acute hypoxia (Figure 5.2), Our results indicate that acute hypoxia deactivates complex I which switches to its NHE activity. We hypothesize that sodium extrusion through complex I mediates NCLX activation. This results in an increase in cytosolic calcium, a decrease in cytosolic sodium, and mitochondrial depolarization due to electrogenic exchange. In parallel, mitochondrial sodium/calcium exchange activation is required for induction of superoxide burst in hypoxic cells. Further work will be needed to pinpoint the precise source of superoxide production in acute hypoxia. Complex III activity is required for superoxide production but not for the activation of the sodium/calcium exchange. Importantly, activation of NCLX in energized isolated mitochondria by complex I substrates through mixtures of low amounts of sodium and calcium triggers ROS production, highlighting that isolated mitochondria are sufficient to produce ROS upon sodium/calcium exchange.

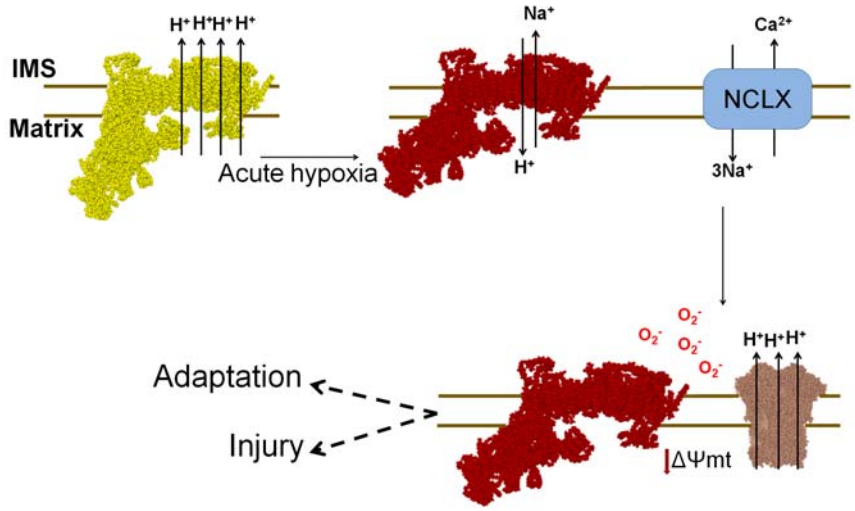

Figure 5.2. Scheme of the role of complex I and NCLX in acute hypoxia. Active complex I (yellow) switches to its deactive conformation (red) in acute hypoxia, which enhances its sodium/proton antiporter activity and sodium/calcium exchange through NCLX, promoting mitochondrial depolarization as well as

ROS production by OXPHOS complexes, which can be a signal for hypoxic adaptation or can lead to ischemic injury.

5.4 NCLX is required for ROS-dependent hypoxic adaptation and injury

By exploiting the fact that NCLX inhibition abolishes the hypoxic superoxide burst without increasing normoxic levels, we show that this mechanism participates in different ROS-dependent adaptations to hypoxia. First, activation of the HIF pathway is impaired when NCLX is inhibited, both in cultured cells and in brain tissue *ex vivo*; these results suggest a tight relationship between acute and chronic responses to hypoxia. Second, activation of the complex I-NCLX-ROS pathway could be a primary event in acute oxygen sensing in different cell types, which would be translated into specific responses in those specialized cells that have the adequate machinery to transduce this ROS signal into effective acute adaptations. PA could be such an example, and we have shown that NCLX inhibition impairs the redox-dependent component of their contraction in acute hypoxia, which is relevant for HPV. In this setting, the mitochondrial superoxide signal would be amplified and transduced to the activation of specific plasma membrane ion channels (Frazziano et al., 2011, Rathore et al., 2008). The carotid body can be another example, as the observed complex I-dependent ROS production (Fernandez-Agüera et al., 2015) could affect redox-dependent activity of specialized potassium channels, which could also be mediated by Cys oxidation of specific enzymes that transduce and/or amplify the primary signal (Yuan et al., 2015).

The mechanism we present here may also be engaged in pathological scenarios where ROS production is exacerbated by hypoxia. In an *in vivo* model of stroke, treatment with CGP clearly reduced infarct volume, suggesting that it may reduce ROS production and oxidative damage, although a ROS-independent role of NCLX cannot be discarded.

5.5 Sodium overload alters hypoxic response

Finally, we have uncovered the effects of sodium overload on the complex I-NCLX-ROS pathway. Alterations in cytosolic sodium content could contribute to the development of diseases or trigger responses related to NCLX. We have observed that sodium overload increased cytosolic calcium, probably from mitochondria since it also caused drop in respiration which correlates well with lower TCA cycle dehydrogenase turnover. ROS production was also increased in normoxia in a NCLX-dependent manner (Figure 4.40), suggesting that enhancement of NCLX activity promotes mitochondrial ROS production.

Mutations or environmental alterations in membrane sodium channels or exchangers can cause cytosolic sodium overload which could primarily cause an energetic crisis due to decreased respiration and increased ROS production (Kunzelmann et al., 2007, Brocker et al., 2012). Indeed, application of the sodium/potassium ATPase inhibitor ouabain leads to busted mitochondrial ATP

production and higher ROS levels in pancreatic islets (Kajikawa et al., 2002). Thus, mutations inhibiting this enzyme could also cause this phenotype. In addition, given our results with cellular respiration sodium overload could also explain respiratory alterations derived from phenotypic modifications in plasma membrane sodium channels, since accumulation of cytosolic sodium could trigger the extrusion of mitochondrial calcium (Kunzelmann et al., 2007, Alsuwaidi et al., 2014, Babsky et al., 2001). Importantly, we have observed that sodium overloaded cells cannot stabilize HIF-1α in hypoxia. This could have important implications since the hypoxic response in these mutants could vary from canonical adaptations.

Sodium overload is present in pathological situations such as heart ischemia or ischemia/reperfusion and inflammation (Brocker et al., 2012, Murphy and Eisner, 2009). Since sodium increase in ischemia is well known to occur in cardiomyocytes (Murphy and Eisner, 2009) but we could not detect it in endothelial cells (see Figure 4.9 for example) we reasoned that it could be a cell type-specific event, suggesting possible NCLX-independent pathways controlling sodium content in ischemia. However, given that sodium measurement in cardiomyocytes is technically difficult due to the interference of the action potential (personal observation) and that we have performed most of our studies in endothelial cells, we decided to study the effect of sodium overload in endothelial cells. The divergence on cytosolic sodium variations between cardiomyocytes and endothelial cells could highlight differences seen in hypoxic ΔΨmt and ROS production (Figures 4.5 and 4.8a-d). Furthermore, given that inflammatory areas become normally hypoxic, whether or not there is sodium overload could lead to very different scenarios and be crucial for the outcome of the disease.

Conclusions

6 Conclusions

- Different cell types increase their superoxide levels in the first minutes after being exposed to hypoxia, which declines during an hour approximately. This effect can be called a 'superoxide burst'.
- The hypoxic superoxide burst is produced by functional mitochondria.
- The mitochondrial sodium/calcium exchanger, NCLX, is necessary for the hypoxic superoxide burst.
- Acute hypoxia triggers a sodium/calcium exchange in endothelial cells through NCLX, and mitochondrial complex I is necessary for this process.
- We have developed a novel method to measure mitochondrial complex I deactivation, showing that complex I is deactivated in acute hypoxia in cell culture, hippocampal slices and in a stroke model.
- We propose a model for explaining how complex I deactivation and NCLX activation are implied in the hypoxic superoxide burst. According to this model, acute hypoxia deactivates complex I and enhances its sodium/proton antiporter function. This activates sodium/calcium exchange through NCLX, which depolarizes the mitochondrial inner membrane. These events lead to increased superoxide production in the mitochondria, probably by the electron transport chain, although the exact source still has to be determined.
- NCLX inhibition can abolish several adaptations to hypoxia such as HIF-1α stabilization and the 'steady-state' component of hypoxic pulmonary vasoconstriction.
- NCLX inhibition ameliorates brain ischemic injury *in vivo* in a mouse model of photothrombotic stroke.
- Addition of sodium to endothelial cell cultures alters the response to hypoxia through modification of NCLX function.

Conclusiones

7 Conclusiones

- Diferentes tipos celulares aumentan los niveles de superóxido en los primeros minutos tras la exposición a hipoxia y disminuyen antes de la primera hora. A este efecto le podemos llamar un 'estallido' de superóxido.
- El estallido hipóxico de superóxido lo producen mitocondrias funcionales.
- El intercambiador de sodio/calcio mitochondrial (NCLX) es necesario para el estallido hipóxico de superóxido.
- La hipoxia aguda dispara un intercambio de sodio/calcio en células endoteliales a través de NCLX, proceso en el que el complejo I mitocondrial es necesario.
- Hemos desarrollado un nuevo método para medir la desactivación de complejo I, mostrando que el complejo I se desactiva en hipoxia aguda en cultivo celular, rodajas de hipocampo y en un modelo de ictus.
- Proponemos un modelo que explica cómo la desactivación de complejo I y la activación de NCLX están implicadas en el estallido hipóxico de superóxido. De acuerdo con este modelo, la hipoxia aguda desactiva el complejo I e incrementa su función antiportadora sodio/protón. Esto activa el intercambio sodio/calcio a través de NCLX, el cual despolariza la membrane mitocondria interna. Estos eventos promueven un incremento en la producción de superóxido por parte de la mitocondria, probablemente a través de la cadena de transporte de electrones, aunque la fuente exacta está todavía por determinar.
- La inhibición de NCLX puede abolir varias adaptaciones a hipoxia, tales como la estabilización de HIF-1α y el componente de 'estado estable' de la vasoconstricción hipóxica pulmonar.
- La inhibición de NCLX disminuye el daño isquémico in vivo en modelos de isquemia cerebral fototrombótica en ratón.
- La adición de sodio en cultivos de células endoteliales altera la respuesta a hipoxia a través de la modificación de la función de NCLX.

References

8 References

Alsuwaidi, A. R., Albawardi, A., Almarzooqi, S., Benedict, S., Othman, A. R., Hartwig, S. M., Varga, S. M. & Souid, A. K. 2014. Respiratory syncytial virus increases lung cellular bioenergetics in neonatal C57BL/6 mice. *Virology,* 454-455**,** 263-9.

Ambrus, A., Nemeria, N. S., Torocsik, B., Tretter, L., Nilsson, M., Jordan, F. & Adam-Vizi, V. 2015. Formation of reactive oxygen species by human and bacterial pyruvate and 2-oxoglutarate dehydrogenase multienzyme complexes reconstituted from recombinant components. *Free Radic Biol Med,* 89**,** 642-50.

Archer, S. L., Huang, J., Henry, T., Peterson, D. & Weir, E. K. 1993. A redox-based O2 sensor in rat pulmonary vasculature. *Circ Res,* 73**,** 1100-12.

Ardan, T., Kovaceva, J. & Cejkova, J. 2004. Comparative histochemical and immunohistochemical study on xanthine oxidoreductase/xanthine oxidase in mammalian corneal epithelium. *Acta Histochem,* 106**,** 69-75.

Arias, R. L., Sung, M. L., Vasylyev, D., Zhang, M. Y., Albinson, K., Kubek, K., Kagan, N., Beyer, C., Lin, Q., Dwyer, J. M., Zaleska, M. M., Bowlby, M. R., Dunlop, J. & Monaghan, M. 2008. Amiloride is neuroprotective in an MPTP model of Parkinson's disease. *Neurobiol Dis,* 31**,** 334-41.

Armitage, P. B., G (Geoffrey). 2012. *Statistical methods in medical research.*

Avendano, C., Roda, J. M., Carceller, F. & Diez-Tejedor, E. 1995. Morphometric study of focal cerebral ischemia in rats: a stereological evaluation. *Brain Res,* 673**,** 83-92.

Babcock, G. T. & Wikstrom, M. 1992. Oxygen activation and the conservation of energy in cell respiration. *Nature,* 356**,** 301-9.

Babot, M., Birch, A., Labarbuta, P. & Galkin, A. 2014. Characterisation of the active/de-active transition of mitochondrial complex I. *Biochim Biophys Acta,* 1837**,** 1083-92.

Babsky, A., Doliba, N., Doliba, N., Savchenko, A., Wehrli, S. & Osbakken, M. 2001. Na+ effects on mitochondrial respiration and oxidative phosphorylation in diabetic hearts. *Exp Biol Med (Maywood),* 226**,** 543-51.

Baruscotti, M., Bucchi, A. & Difrancesco, D. 2005. Physiology and pharmacology of the cardiac pacemaker ("funny") current. *Pharmacol Ther,* 107**,** 59-79.

Baughman, J. M., Perocchi, F., Girgis, H. S., Plovanich, M., Belcher-Timme, C. A., Sancak, Y., Bao, X. R., Strittmatter, L., Goldberger, O., Bogorad, R. L., Koteliansky, V. & Mootha, V. K. 2011. Integrative genomics identifies MCU as an essential component of the mitochondrial calcium uniporter. *Nature,* 476**,** 341-5.

Baysal, K., Jung, D. W., Gunter, K. K., Gunter, T. E. & Brierley, G. P. 1994. Na(+)-dependent Ca2+ efflux mechanism of heart mitochondria is not a passive Ca2+/2Na+ exchanger. *Am J Physiol,* 266**,** C800-8.

Beavis, A. D. & Garlid, K. D. 1990. Evidence for the allosteric regulation of the mitochondrial K+/H+ antiporter by matrix protons. *J Biol Chem,* 265**,** 2538-45.

Becker, L. B., Vanden Hoek, T. L., Shao, Z. H., Li, C. Q. & Schumacker, P. T. 1999. Generation of superoxide in cardiomyocytes during ischemia before reperfusion. *Am J Physiol,* 277**,** H2240-6.

Beckman, J. S. & Koppenol, W. H. 1996. Nitric oxide, superoxide, and peroxynitrite: the good, the bad, and ugly. *Am J Physiol,* 271**,** C1424-37.

Belousov, V. V., Fradkov, A. F., Lukyanov, K. A., Staroverov, D. B., Shakhbazov, K. S., Terskikh, A. V. & Lukyanov, S. 2006. Genetically encoded fluorescent indicator for intracellular hydrogen peroxide. *Nat Methods,* 3**,** 281-6.

Bernardi, P. 1999. Mitochondrial transport of cations: channels, exchangers, and permeability transition. *Physiol Rev,* 79**,** 1127-55.

Bernardi, P. & Di Lisa, F. 2015. The mitochondrial permeability transition pore: molecular nature and role as a target in cardioprotection. *J Mol Cell Cardiol,* 78**,** 100-6.

Bindoli, A., Fukuto, J. M. & Forman, H. J. 2008. Thiol chemistry in peroxidase catalysis and redox signaling. *Antioxid Redox Signal,* 10**,** 1549-64.

Bleier, L. & Drose, S. 2013. Superoxide generation by complex III: from mechanistic rationales to functional consequences. *Biochim Biophys Acta,* 1827**,** 1320-31.
Bokare, A. D. & Choi, W. 2014. Review of iron-free Fenton-like systems for activating H2O2 in advanced oxidation processes. *J Hazard Mater,* 275**,** 121-35.
Brand, M. D. 2016. Mitochondrial generation of superoxide and hydrogen peroxide as the source of mitochondrial redox signaling. *Free Radic Biol Med,* 100**,** 14-31.
Breton-Romero, R. & Lamas, S. 2013. Hydrogen peroxide signaling mediator in the activation of p38 MAPK in vascular endothelial cells. *Methods Enzymol,* 528**,** 49-59.
Breton-Romero, R. & Lamas, S. 2014. Hydrogen peroxide signaling in vascular endothelial cells. *Redox Biol,* 2**,** 529-34.
Briggs, K. J., Koivunen, P., Cao, S., Backus, K. M., Olenchock, B. A., Patel, H., Zhang, Q., Signoretti, S., Gerfen, G. J., Richardson, A. L., Witkiewicz, A. K., Cravatt, B. F., Clardy, J. & Kaelin, W. G., Jr. 2016. Paracrine Induction of HIF by Glutamate in Breast Cancer: EglN1 Senses Cysteine. *Cell,* 166**,** 126-39.
Brocker, C., Thompson, D. C. & Vasiliou, V. 2012. The role of hyperosmotic stress in inflammation and disease. *Biomol Concepts,* 3**,** 345-364.
Brown, D. I. & Griendling, K. K. 2009. Nox proteins in signal transduction. *Free Radic Biol Med,* 47**,** 1239-53.
Brunelle, J. K., Bell, E. L., Quesada, N. M., Vercauteren, K., Tiranti, V., Zeviani, M., Scarpulla, R. C. & Chandel, N. S. 2005. Oxygen sensing requires mitochondrial ROS but not oxidative phosphorylation. *Cell Metab,* 1**,** 409-14.
Carafoli, E., Tiozzo, R., Lugli, G., Crovetti, F. & Kratzing, C. 1974. The release of calcium from heart mitochondria by sodium. *J Mol Cell Cardiol,* 6**,** 361-71.
Carmeliet, P. 2005. VEGF as a key mediator of angiogenesis in cancer. *Oncology,* 69 Suppl 3**,** 4-10.
Castro, L., Rodriguez, M. & Radi, R. 1994. Aconitase is readily inactivated by peroxynitrite, but not by its precursor, nitric oxide. *J Biol Chem,* 269**,** 29409-15.
Cocheme, H. M., Logan, A., Prime, T. A., Abakumova, I., Quin, C., Mcquaker, S. J., Patel, J. V., Fearnley, I. M., James, A. M., Porteous, C. M., Smith, R. A., Hartley, R. C., Partridge, L. & Murphy, M. P. 2012. Using the mitochondria-targeted ratiometric mass spectrometry probe MitoB to measure H2O2 in living Drosophila. *Nat Protoc,* 7**,** 946-58.
Cogliati, S., Frezza, C., Soriano, M. E., Varanita, T., Quintana-Cabrera, R., Corrado, M., Cipolat, S., Costa, V., Casarin, A., Gomes, L. C., Perales-Clemente, E., Salviati, L., Fernandez-Silva, P., Enriquez, J. A. & Scorrano, L. 2013. Mitochondrial cristae shape determines respiratory chain supercomplexes assembly and respiratory efficiency. *Cell,* 155**,** 160-71.
Cogolludo, A., Moreno, L., Frazziano, G., Moral-Sanz, J., Menendez, C., Castaneda, J., Gonzalez, C., Villamor, E. & Perez-Vizcaino, F. 2009. Activation of neutral sphingomyelinase is involved in acute hypoxic pulmonary vasoconstriction. *Cardiovasc Res,* 82**,** 296-302.
Comte, J., Maisterrena, B. & Gautheron, D. C. 1976. Lipid composition and protein profiles of outer and inner membranes from pig heart mitochondria. Comparison with microsomes. *Biochim Biophys Acta,* 419**,** 271-84.
Connolly, M. J., Prieto-Lloret, J., Becker, S., Ward, J. P. & Aaronson, P. I. 2013. Hypoxic pulmonary vasoconstriction in the absence of pretone: essential role for intracellular Ca2+ release. *J Physiol,* 591**,** 4473-98.
Cortassa, S., Aon, M. A., Marban, E., Winslow, R. L. & O'rourke, B. 2003. An integrated model of cardiac mitochondrial energy metabolism and calcium dynamics. *Biophys J,* 84**,** 2734-55.
Cox, D. A. & Matlib, M. A. 1993. A role for the mitochondrial Na(+)-Ca2+ exchanger in the regulation of oxidative phosphorylation in isolated heart mitochondria. *J Biol Chem,* 268**,** 938-47.
Crofts, A. R., Hong, S., Ugulava, N., Barquera, B., Gennis, R., Guergova-Kuras, M. & Berry, E. A. 1999. Pathways for proton release during ubihydroquinone oxidation by the bc(1) complex. *Proc Natl Acad Sci U S A,* 96**,** 10021-6.
Crofts, A. R., Lhee, S., Crofts, S. B., Cheng, J. & Rose, S. 2006. Proton pumping in the bc1 complex: a new gating mechanism that prevents short circuits. *Biochim Biophys Acta,* 1757**,** 1019-34.

Chan, C. S., Guzman, J. N., Ilijic, E., Mercer, J. N., Rick, C., Tkatch, T., Meredith, G. E. & Surmeier, D. J. 2007. 'Rejuvenation' protects neurons in mouse models of Parkinson's disease. *Nature,* 447**,** 1081-6.

Chance, B. & Williams, G. R. 1955. Respiratory enzymes in oxidative phosphorylation. I. Kinetics of oxygen utilization. *J Biol Chem,* 217**,** 383-93.

Chandel, N. S., Maltepe, E., Goldwasser, E., Mathieu, C. E., Simon, M. C. & Schumacker, P. T. 1998. Mitochondrial reactive oxygen species trigger hypoxia-induced transcription. *Proc Natl Acad Sci U S A,* 95**,** 11715-20.

Chandel, N. S., Mcclintock, D. S., Feliciano, C. E., Wood, T. M., Melendez, J. A., Rodriguez, A. M. & Schumacker, P. T. 2000. Reactive oxygen species generated at mitochondrial complex III stabilize hypoxia-inducible factor-1alpha during hypoxia: a mechanism of O2 sensing. *J Biol Chem,* 275**,** 25130-8.

Chandel, N. S. & Tuveson, D. A. 2014. The promise and perils of antioxidants for cancer patients. *N Engl J Med,* 371**,** 177-8.

Chao, M. R., Rossner, P., Jr., Haghdoost, S., Jeng, H. A. & Hu, C. W. 2013. Nucleic acid oxidation in human health and disease. *Oxid Med Cell Longev,* 2013**,** 368651.

Chaturvedi, R. K. & Flint Beal, M. 2013. Mitochondrial diseases of the brain. *Free Radic Biol Med,* 63**,** 1-29.

Chen, C., Pore, N., Behrooz, A., Ismail-Beigi, F. & Maity, A. 2001. Regulation of glut1 mRNA by hypoxia-inducible factor-1. Interaction between H-ras and hypoxia. *J Biol Chem,* 276**,** 9519-25.

Chen, C. A., Wang, T. Y., Varadharaj, S., Reyes, L. A., Hemann, C., Talukder, M. A., Chen, Y. R., Druhan, L. J. & Zweier, J. L. 2010. S-glutathionylation uncouples eNOS and regulates its cellular and vascular function. *Nature,* 468**,** 1115-8.

Chouchani, E. T., Kazak, L., Jedrychowski, M. P., Lu, G. Z., Erickson, B. K., Szpyt, J., Pierce, K. A., Laznik-Bogoslavski, D., Vetrivelan, R., Clish, C. B., Robinson, A. J., Gygi, S. P. & Spiegelman, B. M. 2016. Mitochondrial ROS regulate thermogenic energy expenditure and sulfenylation of UCP1. *Nature,* 532**,** 112-6.

Chouchani, E. T., Methner, C., Nadtochiy, S. M., Logan, A., Pell, V. R., Ding, S., James, A. M., Cocheme, H. M., Reinhold, J., Lilley, K. S., Partridge, L., Fearnley, I. M., Robinson, A. J., Hartley, R. C., Smith, R. A., Krieg, T., Brookes, P. S. & Murphy, M. P. 2013. Cardioprotection by S-nitrosation of a cysteine switch on mitochondrial complex I. *Nat Med,* 19**,** 753-9.

Chouchani, E. T., Pell, V. R., Gaude, E., Aksentijevic, D., Sundier, S. Y., Robb, E. L., Logan, A., Nadtochiy, S. M., Ord, E. N., Smith, A. C., Eyassu, F., Shirley, R., Hu, C. H., Dare, A. J., James, A. M., Rogatti, S., Hartley, R. C., Eaton, S., Costa, A. S., Brookes, P. S., Davidson, S. M., Duchen, M. R., Saeb-Parsy, K., Shattock, M. J., Robinson, A. J., Work, L. M., Frezza, C., Krieg, T. & Murphy, M. P. 2014. Ischaemic accumulation of succinate controls reperfusion injury through mitochondrial ROS. *Nature,* 515**,** 431-5.

Chowdhury, R., Leung, I. K., Tian, Y. M., Abboud, M. I., Ge, W., Domene, C., Cantrelle, F. X., Landrieu, I., Hardy, A. P., Pugh, C. W., Ratcliffe, P. J., Claridge, T. D. & Schofield, C. J. 2016. Structural basis for oxygen degradation domain selectivity of the HIF prolyl hydroxylases. *Nat Commun,* 7**,** 12673.

Chua, Y. L., Dufour, E., Dassa, E. P., Rustin, P., Jacobs, H. T., Taylor, C. T. & Hagen, T. 2010. Stabilization of hypoxia-inducible factor-1alpha protein in hypoxia occurs independently of mitochondrial reactive oxygen species production. *J Biol Chem,* 285**,** 31277-84.

Dash, R. K. & Beard, D. A. 2008. Analysis of cardiac mitochondrial Na+-Ca2+ exchanger kinetics with a biophysical model of mitochondrial Ca2+ handling suggests a 3:1 stoichiometry. *J Physiol,* 586**,** 3267-85.

De Marchi, U., Santo-Domingo, J., Castelbou, C., Sekler, I., Wiederkehr, A. & Demaurex, N. 2014. NCLX protein, but not LETM1, mediates mitochondrial Ca2+ extrusion, thereby limiting Ca2+-induced NAD(P)H production and modulating matrix redox state. *J Biol Chem,* 289**,** 20377-85.

Desireddi, J. R., Farrow, K. N., Marks, J. D., Waypa, G. B. & Schumacker, P. T. 2010. Hypoxia increases ROS signaling and cytosolic Ca(2+) in pulmonary artery smooth muscle cells of mouse lungs slices. *Antioxid Redox Signal,* 12**,** 595-602.

Donoso, P., Mill, J. G., O'neill, S. C. & Eisner, D. A. 1992. Fluorescence measurements of cytoplasmic and mitochondrial sodium concentration in rat ventricular myocytes. *J Physiol,* 448**,** 493-509.

Drose, S. 2013. Differential effects of complex II on mitochondrial ROS production and their relation to cardioprotective pre- and postconditioning. *Biochim Biophys Acta,* 1827**,** 578-87.

Drose, S. & Brandt, U. 2012. Molecular mechanisms of superoxide production by the mitochondrial respiratory chain. *Adv Exp Med Biol,* 748**,** 145-69.

Drose, S., Stepanova, A. & Galkin, A. 2016. Ischemic A/D transition of mitochondrial complex I and its role in ROS generation. *Biochim Biophys Acta,* 1857**,** 946-57.

Duncan, J. G., Ravi, R., Stull, L. B. & Murphy, A. M. 2005. Chronic xanthine oxidase inhibition prevents myofibrillar protein oxidation and preserves cardiac function in a transgenic mouse model of cardiomyopathy. *Am J Physiol Heart Circ Physiol,* 289**,** H1512-8.

Dunwoodie, S. L. 2009. The role of hypoxia in development of the Mammalian embryo. *Dev Cell,* 17**,** 755-73.

E.A., M. 2014. *The structure of mitochondria.*

Edgell, C. J., Mcdonald, C. C. & Graham, J. B. 1983. Permanent cell line expressing human factor VIII-related antigen established by hybridization. *Proc Natl Acad Sci U S A,* 80**,** 3734-7.

Eltzschig, H. K. & Carmeliet, P. 2011. Hypoxia and inflammation. *N Engl J Med,* 364**,** 656-65.

Ermakova, Y. G., Bilan, D. S., Matlashov, M. E., Mishina, N. M., Markvicheva, K. N., Subach, O. M., Subach, F. V., Bogeski, I., Hoth, M., Enikolopov, G. & Belousov, V. V. 2014. Red fluorescent genetically encoded indicator for intracellular hydrogen peroxide. *Nat Commun,* 5**,** 5222.

Fernandez-Agüera, M. C., Gao, L., Gonzalez-Rodríguez, P., Pintado, C. O., Arias-Mayenco, I., García-Flores, P., García-Perganeda, A., Pascual, A., Ortega-Saenz, P. & López-Barneo, J. 2015. Oxygen Sensing by Arterial Chemoreceptors Depends on Mitochondrial Complex I Signaling. *Cell Metab,* 22**,** 825-37.

Fiedorczuk, K., Letts, J. A., Degliesposti, G., Kaszuba, K., Skehel, M. & Sazanov, L. A. 2016. Atomic structure of the entire mammalian mitochondrial complex I. *Nature,* 538**,** 406-410.

Finkelstein, E., Rosen, G. M. & Rauckman, E. J. 1980. Spin trapping of superoxide and hydroxyl radical: practical aspects. *Arch Biochem Biophys,* 200**,** 1-16.

Fraisl, P., Mazzone, M., Schmidt, T. & Carmeliet, P. 2009. Regulation of angiogenesis by oxygen and metabolism. *Dev Cell,* 16**,** 167-79.

Frazziano, G., Moreno, L., Moral-Sanz, J., Menendez, C., Escolano, L., Gonzalez, C., Villamor, E., Alvarez-Sala, J. L., Cogolludo, A. L. & Perez-Vizcaino, F. 2011. Neutral sphingomyelinase, NADPH oxidase and reactive oxygen species. Role in acute hypoxic pulmonary vasoconstriction. *J Cell Physiol,* 226**,** 2633-40.

Freedman, S. J., Sun, Z. Y., Poy, F., Kung, A. L., Livingston, D. M., Wagner, G. & Eck, M. J. 2002. Structural basis for recruitment of CBP/p300 by hypoxia-inducible factor-1 alpha. *Proc Natl Acad Sci U S A,* 99**,** 5367-72.

Fridovich, I. 1995. Superoxide radical and superoxide dismutases. *Annu Rev Biochem,* 64**,** 97-112.

Fukuda, R., Zhang, H., Kim, J. W., Shimoda, L., Dang, C. V. & Semenza, G. L. 2007. HIF-1 regulates cytochrome oxidase subunits to optimize efficiency of respiration in hypoxic cells. *Cell,* 129**,** 111-22.

Galanis, A., Pappa, A., Giannakakis, A., Lanitis, E., Dangaj, D. & Sandaltzopoulos, R. 2008. Reactive oxygen species and HIF-1 signalling in cancer. *Cancer Lett,* 266**,** 12-20.

Galbusera, C., Orth, P., Fedida, D. & Spector, T. 2006. Superoxide radical production by allopurinol and xanthine oxidase. *Biochem Pharmacol,* 71**,** 1747-52.

Galkin, A., Abramov, A. Y., Frakich, N., Duchen, M. R. & Moncada, S. 2009. Lack of oxygen deactivates mitochondrial complex I: implications for ischemic injury? *J Biol Chem,* 284**,** 36055-61.

Galkin, A., Meyer, B., Wittig, I., Karas, M., Schagger, H., Vinogradov, A. & Brandt, U. 2008. Identification of the mitochondrial ND3 subunit as a structural component involved in the active/deactive enzyme transition of respiratory complex I. *J Biol Chem,* 283**,** 20907-13.

Gandhi, S., Wood-Kaczmar, A., Yao, Z., Plun-Favreau, H., Deas, E., Klupsch, K., Downward, J., Latchman, D. S., Tabrizi, S. J., Wood, N. W., Duchen, M. R. & Abramov, A. Y. 2009. PINK1-associated Parkinson's disease is caused by neuronal vulnerability to calcium-induced cell death. *Mol Cell,* 33**,** 627-38.

Gardner, P. R. & Fridovich, I. 1991. Superoxide sensitivity of the Escherichia coli aconitase. *J Biol Chem,* 266**,** 19328-33.

Garlid, K. D. 1980. On the mechanism of regulation of the mitochondrial K+/H+ exchanger. *J Biol Chem,* 255**,** 11273-9.

Garlid, K. D. & Paucek, P. 2003. Mitochondrial potassium transport: the K(+) cycle. *Biochim Biophys Acta,* 1606**,** 23-41.

Gerald, D., Berra, E., Frapart, Y. M., Chan, D. A., Giaccia, A. J., Mansuy, D., Pouyssegur, J., Yaniv, M. & Mechta-Grigoriou, F. 2004. JunD reduces tumor angiogenesis by protecting cells from oxidative stress. *Cell,* 118**,** 781-94.

Germond, A., Fujita, H., Ichimura, T. & Watanabe, T. M. 2016. Design and development of genetically encoded fluorescent sensors to monitor intracellular chemical and physical parameters. *Biophys Rev,* 8**,** 121-138.

Giorgio, V., Von Stockum, S., Antoniel, M., Fabbro, A., Fogolari, F., Forte, M., Glick, G. D., Petronilli, V., Zoratti, M., Szabo, I., Lippe, G. & Bernardi, P. 2013. Dimers of mitochondrial ATP synthase form the permeability transition pore. *Proc Natl Acad Sci U S A,* 110**,** 5887-92.

Glickman, M. H. & Klinman, J. P. 1996. Lipoxygenase reaction mechanism: demonstration that hydrogen abstraction from substrate precedes dioxygen binding during catalytic turnover. *Biochemistry,* 35**,** 12882-92.

Gorlach, A., Dimova, E. Y., Petry, A., Martinez-Ruiz, A., Hernansanz-Agustin, P., Rolo, A. P., Palmeira, C. M. & Kietzmann, T. 2015. Reactive oxygen species, nutrition, hypoxia and diseases: Problems solved? *Redox Biol,* 6**,** 372-85.

Grivennikova, V. G., Kapustin, A. N. & Vinogradov, A. D. 2001. Catalytic activity of NADH-ubiquinone oxidoreductase (complex I) in intact mitochondria. evidence for the slow active/inactive transition. *J Biol Chem,* 276**,** 9038-44.

Grivennikova, V. G., Maklashina, E. O., Gavrikova, E. V. & Vinogradov, A. D. 1997. Interaction of the mitochondrial NADH-ubiquinone reductase with rotenone as related to the enzyme active/inactive transition. *Biochim Biophys Acta,* 1319**,** 223-32.

Grivennikova, V. G., Serebryanaya, D. V., Isakova, E. P., Belozerskaya, T. A. & Vinogradov, A. D. 2003. The transition between active and de-activated forms of NADH:ubiquinone oxidoreductase (Complex I) in the mitochondrial membrane of Neurospora crassa. *Biochem J,* 369**,** 619-26.

Gu, J., Wu, M., Guo, R., Yan, K., Lei, J., Gao, N. & Yang, M. 2016. The architecture of the mammalian respirasome. *Nature,* 537**,** 639-43.

Guzman, J. N., Sanchez-Padilla, J., Wokosin, D., Kondapalli, J., Ilijic, E., Schumacker, P. T. & Surmeier, D. J. 2010. Oxidant stress evoked by pacemaking in dopaminergic neurons is attenuated by DJ-1. *Nature,* 468**,** 696-700.

Guzy, R. D., Hoyos, B., Robin, E., Chen, H., Liu, L., Mansfield, K. D., Simon, M. C., Hammerling, U. & Schumacker, P. T. 2005. Mitochondrial complex III is required for hypoxia-induced ROS production and cellular oxygen sensing. *Cell Metab,* 1**,** 401-8.

Guzy, R. D. & Schumacker, P. T. 2006a. Oxygen sensing by mitochondria at complex III: the paradox of increased reactive oxygen species during hypoxia. *Exp Physiol,* 91**,** 807-19.

Guzy, R. D. & Schumacker, P. T. 2006b. Oxygen sensing by mitochondria at complex III: the paradox of increased reactive oxygen species during hypoxia. *Exp Physiol,* 91**,** 807-819.

Hagen, T., Taylor, C. T., Lam, F. & Moncada, S. 2003. Redistribution of intracellular oxygen in hypoxia by nitric oxide: effect on HIF1alpha. *Science,* 302**,** 1975-8.

Hale, L. P., Braun, R. D., Gwinn, W. M., Greer, P. K. & Dewhirst, M. W. 2002. Hypoxia in the thymus: role of oxygen tension in thymocyte survival. *Am J Physiol Heart Circ Physiol,* 282**,** H1467-77.

Hamanaka, R. B. & Chandel, N. S. 2009. Mitochondrial reactive oxygen species regulate hypoxic signaling. *Curr Opin Cell Biol,* 21**,** 894-9.

Hamanaka, R. B. & Chandel, N. S. 2010. Mitochondrial reactive oxygen species regulate cellular signaling and dictate biological outcomes. *Trends Biochem Sci,* 35**,** 505-13.

Hamanaka, R. B., Weinberg, S. E., Reczek, C. R. & Chandel, N. S. 2016. The Mitochondrial Respiratory Chain Is Required for Organismal Adaptation to Hypoxia. *Cell Rep,* 15**,** 451-9.

Hanson, G. T., Aggeler, R., Oglesbee, D., Cannon, M., Capaldi, R. A., Tsien, R. Y. & Remington, S. J. 2004. Investigating mitochondrial redox potential with redox-sensitive green fluorescent protein indicators. *J Biol Chem,* 279**,** 13044-53.

Hardin, J. W. & Hilbe, J. M. 2012. *Generalized Estimating Equations.*

Harmsen, E., De Jong, J. W. & Serruys, P. W. 1981. Hypoxanthine production by ischemic heart demonstrated by high pressure liquid chromatography of blood purine nucleosides and oxypurines. *Clin Chim Acta,* 115**,** 73-84.

Hernansanz-Agustín, P., Izquierdo-Álvarez, A., García-Ortiz, A., Ibiza, S., Serrador, J. M. & Martínez-Ruiz, A. 2013. Nitrosothiols in the immune system: signaling and protection. *Antioxid Redox Signal,* 18**,** 288-308.

Hernansanz-Agustín, P., Izquierdo-Álvarez, A., Sánchez-Gómez, F. J., Ramos, E., Villa-Piña, T., Lamas, S., Bogdanova, A. & Martínez-Ruiz, A. 2014. Acute hypoxia produces a superoxide burst in cells. *Free Radic Biol Med,* 71**,** 146-56.

Hewitson, K. S., Mcneill, L. A., Riordan, M. V., Tian, Y. M., Bullock, A. N., Welford, R. W., Elkins, J. M., Oldham, N. J., Bhattacharya, S., Gleadle, J. M., Ratcliffe, P. J., Pugh, C. W. & Schofield, C. J. 2002. Hypoxia-inducible factor (HIF) asparagine hydroxylase is identical to factor inhibiting HIF (FIH) and is related to the cupin structural family. *J Biol Chem,* 277**,** 26351-5.

Hirst, J., King, M. S. & Pryde, K. R. 2008. The production of reactive oxygen species by complex I. *Biochem Soc Trans,* 36**,** 976-80.

Hirst, J. & Roessler, M. M. 2016. Energy conversion, redox catalysis and generation of reactive oxygen species by respiratory complex I. *Biochim Biophys Acta,* 1857**,** 872-83.

Hoffman, D. L. & Brookes, P. S. 2009. Oxygen sensitivity of mitochondrial reactive oxygen species generation depends on metabolic conditions. *J Biol Chem,* 284**,** 16236-45.

Hoffman, D. L., Salter, J. D. & Brookes, P. S. 2007. Response of mitochondrial reactive oxygen species generation to steady-state oxygen tension: implications for hypoxic cell signaling. *Am J Physiol Heart Circ Physiol,* 292**,** H101-8.

Holmstrom, K. M. & Finkel, T. 2014. Cellular mechanisms and physiological consequences of redox-dependent signalling. *Nat Rev Mol Cell Biol,* 15**,** 411-21.

Hrycay, E. G. & Bandiera, S. M. 2015. Involvement of Cytochrome P450 in Reactive Oxygen Species Formation and Cancer. *Adv Pharmacol,* 74**,** 35-84.

Iwase, H., Robin, E., Guzy, R. D., Mungai, P. T., Vanden Hoek, T. L., Chandel, N. S., Levraut, J. & Schumacker, P. T. 2007. Nitric oxide during ischemia attenuates oxidant stress and cell death during ischemia and reperfusion in cardiomyocytes. *Free Radic Biol Med,* 43**,** 590-9.

Iwata, S., Lee, J. W., Okada, K., Lee, J. K., Iwata, M., Rasmussen, B., Link, T. A., Ramaswamy, S. & Jap, B. K. 1998. Complete structure of the 11-subunit bovine mitochondrial cytochrome bc1 complex. *Science,* 281**,** 64-71.

Izquierdo-Álvarez, A. & Martínez-Ruiz, A. 2011. Thiol redox proteomics seen with fluorescent eyes: the detection of cysteine oxidative modifications by fluorescence derivatization and 2-DE. *J Proteomics,* 75**,** 329-38.

Izquierdo-Alvarez, A., Ramos, E., Villanueva, J., Hernansanz-Agustin, P., Fernandez-Rodriguez, R., Tello, D., Carrascal, M. & Martinez-Ruiz, A. 2012. Differential redox proteomics allows identification of proteins reversibly oxidized at cysteine residues in endothelial cells in response to acute hypoxia. *J Proteomics,* 75**,** 5449-62.

Izquierdo-Álvarez, A., Ramos, E., Villanueva, J., Hernansanz-Agustín, P., Fernandez-Rodríguez, R., Tello, D., Carrascal, M. & Martínez-Ruiz, A. 2012. Differential redox proteomics allows

identification of proteins reversibly oxidized at cysteine residues in endothelial cells in response to acute hypoxia. *J Proteomics,* 75**,** 5449-62.
Jahan, R. & Vinuela, F. 2009. Treatment of acute ischemic stroke: intravenous and endovascular therapies. *Expert Rev Cardiovasc Ther,* 7**,** 375-87.
Jiang, D., Zhao, L. & Clapham, D. E. 2009. Genome-wide RNAi screen identifies Letm1 as a mitochondrial Ca2+/H+ antiporter. *Science,* 326**,** 144-7.
Jorge, I., Casas, E. M., Villar, M., Ortega-Perez, I., Lopez-Ferrer, D., Martinez-Ruiz, A., Carrera, M., Marina, A., Martinez, P., Serrano, H., Canas, B., Were, F., Gallardo, J. M., Lamas, S., Redondo, J. M., Garcia-Dorado, D. & Vazquez, J. 2007. High-sensitivity analysis of specific peptides in complex samples by selected MS/MS ion monitoring and linear ion trap mass spectrometry: application to biological studies. *J Mass Spectrom,* 42**,** 1391-403.
Jou, M. J., Peng, T. I. & Sheu, S. S. 1996. Histamine induces oscillations of mitochondrial free Ca2+ concentration in single cultured rat brain astrocytes. *J Physiol,* 497 (Pt 2)**,** 299-308.
Jung, D. W., Apel, L. M. & Brierley, G. P. 1992. Transmembrane gradients of free Na+ in isolated heart mitochondria estimated using a fluorescent probe. *Am J Physiol,* 262**,** C1047-55.
Kaelin, W. G., Jr. & Ratcliffe, P. J. 2008. Oxygen sensing by metazoans: the central role of the HIF hydroxylase pathway. *Mol Cell,* 30**,** 393-402.
Kajikawa, M., Fujimoto, S., Tsuura, Y., Mukai, E., Takeda, T., Hamamoto, Y., Takehiro, M., Fujita, J., Yamada, Y. & Seino, Y. 2002. Ouabain suppresses glucose-induced mitochondrial ATP production and insulin release by generating reactive oxygen species in pancreatic islets. *Diabetes,* 51**,** 2522-9.
Kalogeris, T., Baines, C. P., Krenz, M. & Korthuis, R. J. 2012. Cell biology of ischemia/reperfusion injury. *Int Rev Cell Mol Biol,* 298**,** 229-317.
Kalyanaraman, B. 2013. Teaching the basics of redox biology to medical and graduate students: Oxidants, antioxidants and disease mechanisms. *Redox Biol,* 1**,** 244-57.
Kalyanaraman, B., Darley-Usmar, V., Davies, K. J., Dennery, P. A., Forman, H. J., Grisham, M. B., Mann, G. E., Moore, K., Roberts, L. J., 2nd & Ischiropoulos, H. 2012. Measuring reactive oxygen and nitrogen species with fluorescent probes: challenges and limitations. *Free Radic Biol Med,* 52**,** 1-6.
Kalyanaraman, B., Hardy, M., Podsiadly, R., Cheng, G. & Zielonka, J. 2017. Recent developments in detection of superoxide radical anion and hydrogen peroxide: Opportunities, challenges, and implications in redox signaling. *Arch Biochem Biophys,* 617**,** 38-47.
Keyer, K. & Imlay, J. A. 1997. Inactivation of dehydratase [4Fe-4S] clusters and disruption of iron homeostasis upon cell exposure to peroxynitrite. *J Biol Chem,* 272**,** 27652-9.
Kim, B. & Matsuoka, S. 2008. Cytoplasmic Na+-dependent modulation of mitochondrial Ca2+ via electrogenic mitochondrial Na+-Ca2+ exchange. *J Physiol,* 586**,** 1683-97.
Kittleson, M. M. & Hare, J. M. 2005. Xanthine oxidase inhibitors: an emerging class of drugs for heart failure. *Eur Heart J,* 26**,** 1458-60.
Knoops, B., Goemaere, J., Van Der Eecken, V. & Declercq, J. P. 2011. Peroxiredoxin 5: structure, mechanism, and function of the mammalian atypical 2-Cys peroxiredoxin. *Antioxid Redox Signal,* 15**,** 817-29.
Kohlhaas, M., Liu, T., Knopp, A., Zeller, T., Ong, M. F., Bohm, M., O'rourke, B. & Maack, C. 2010. Elevated cytosolic Na+ increases mitochondrial formation of reactive oxygen species in failing cardiac myocytes. *Circulation,* 121**,** 1606-13.
Korde, A. S., Yadav, V. R., Zheng, Y. M. & Wang, Y. X. 2011. Primary role of mitochondrial Rieske iron-sulfur protein in hypoxic ROS production in pulmonary artery myocytes. *Free Radic Biol Med,* 50**,** 945-52.
Kulkarni, M. & Armstead, W. M. 2000. Superoxide generation links nociceptin/orphanin FQ (NOC/oFQ) release to impaired N-methyl-D-aspartate cerebrovasodilation after brain injury. *Stroke,* 31**,** 1990-6.
Kunzelmann, K., Sun, J., Meanger, J., King, N. J. & Cook, D. I. 2007. Inhibition of airway Na+ transport by respiratory syncytial virus. *J Virol,* 81**,** 3714-20.
Lahiri, S., Roy, A., Baby, S. M., Hoshi, T., Semenza, G. L. & Prabhakar, N. R. 2006. Oxygen sensing in the body. *Prog Biophys Mol Biol,* 91**,** 249-86.
Lambeth, J. D. 2004. NOX enzymes and the biology of reactive oxygen. *Nat Rev Immunol,* 4**,** 181-9.

Lanciano, P., Khalfaoui-Hassani, B., Selamoglu, N., Ghelli, A., Rugolo, M. & Daldal, F. 2013. Molecular mechanisms of superoxide production by complex III: a bacterial versus human mitochondrial comparative case study. *Biochim Biophys Acta,* 1827**,** 1332-9.

Lang, P. A., Xu, H. C., Grusdat, M., Mcilwain, D. R., Pandyra, A. A., Harris, I. S., Shaabani, N., Honke, N., Maney, S. K., Lang, E., Pozdeev, V. I., Recher, M., Odermatt, B., Brenner, D., Haussinger, D., Ohashi, P. S., Hengartner, H., Zinkernagel, R. M., Mak, T. W. & Lang, K. S. 2013. Reactive oxygen species delay control of lymphocytic choriomeningitis virus. *Cell Death Differ,* 20**,** 649-58.

Letts, J. A., Fiedorczuk, K. & Sazanov, L. A. 2016. The architecture of respiratory supercomplexes. *Nature,* 537**,** 644-648.

Li, Q. F., Wang, X. R., Yang, Y. W. & Lin, H. 2006. Hypoxia upregulates hypoxia inducible factor (HIF)-3alpha expression in lung epithelial cells: characterization and comparison with HIF-1alpha. *Cell Res,* 16**,** 548-58.

Linas, S. L., Whittenburg, D. & Repine, J. E. 1990. Role of xanthine oxidase in ischemia/reperfusion injury. *Am J Physiol,* 258**,** F711-6.

Liochev, S. I. & Fridovich, I. 2007. The effects of superoxide dismutase on H2O2 formation. *Free Radic Biol Med,* 42**,** 1465-9.

López-Barneo, J. & Castellano, A. 2005. Multiple facets of maxi-k+ channels: the heme connection. *J Gen Physiol,* 126**,** 1-5.

López-Barneo, J., Macias, D., Platero-Luengo, A., Ortega-Saenz, P. & Pardal, R. 2016. Carotid body oxygen sensing and adaptation to hypoxia. *Pflugers Arch,* 468**,** 59-70.

López-Barneo, J., Ortega-Saenz, P., Pardal, R., Pascual, A., Piruat, J. I., Duran, R. & Gómez-Diaz, R. 2009. Oxygen sensing in the carotid body. *Ann N Y Acad Sci,* 1177**,** 119-31.

Luo, S., Lei, H., Qin, H. & Xia, Y. 2014. Molecular mechanisms of endothelial NO synthase uncoupling. *Curr Pharm Des,* 20**,** 3548-53.

Mansfield, K. D., Guzy, R. D., Pan, Y., Young, R. M., Cash, T. P., Schumacker, P. T. & Simon, M. C. 2005. Mitochondrial dysfunction resulting from loss of cytochrome c impairs cellular oxygen sensing and hypoxic HIF-alpha activation. *Cell Metab,* 1**,** 393-9.

Maranzana, E., Barbero, G., Falasca, A. I., Lenaz, G. & Genova, M. L. 2013. Mitochondrial respiratory supercomplex association limits production of reactive oxygen species from complex I. *Antioxid Redox Signal,* 19**,** 1469-80.

Martinez-Ruiz, A., Araujo, I. M., Izquierdo-Alvarez, A., Hernansanz-Agustin, P., Lamas, S. & Serrador, J. M. 2013. Specificity in S-nitrosylation: a short-range mechanism for NO signaling? *Antioxid Redox Signal,* 19**,** 1220-35.

Martinez-Ruiz, A. & Lamas, S. 2004. S-nitrosylation: a potential new paradigm in signal transduction. *Cardiovasc Res,* 62**,** 43-52.

Maxwell, P. H., Wiesener, M. S., Chang, G. W., Clifford, S. C., Vaux, E. C., Cockman, M. E., Wykoff, C. C., Pugh, C. W., Maher, E. R. & Ratcliffe, P. J. 1999. The tumour suppressor protein VHL targets hypoxia-inducible factors for oxygen-dependent proteolysis. *Nature,* 399**,** 271-5.

Mehta, J. P., Campian, J. L., Guardiola, J., Cabrera, J. A., Weir, E. K. & Eaton, J. W. 2008. Generation of oxidants by hypoxic human pulmonary and coronary smooth-muscle cells. *Chest,* 133**,** 1410-4.

Miller, E. W., Albers, A. E., Pralle, A., Isacoff, E. Y. & Chang, C. J. 2005. Boronate-based fluorescent probes for imaging cellular hydrogen peroxide. *J Am Chem Soc,* 127**,** 16652-9.

Miller, G., Suzuki, N., Ciftci-Yilmaz, S. & Mittler, R. 2010. Reactive oxygen species homeostasis and signalling during drought and salinity stresses. *Plant Cell Environ,* 33**,** 453-67.

Missirlis, F., Hu, J., Kirby, K., Hilliker, A. J., Rouault, T. A. & Phillips, J. P. 2003. Compartment-specific protection of iron-sulfur proteins by superoxide dismutase. *J Biol Chem,* 278**,** 47365-9.

Mittal, M., Siddiqui, M. R., Tran, K., Reddy, S. P. & Malik, A. B. 2014. Reactive oxygen species in inflammation and tissue injury. *Antioxid Redox Signal,* 20**,** 1126-67.

Moreno-Loshuertos, R., Acin-Perez, R., Fernandez-Silva, P., Movilla, N., Perez-Martos, A., Rodriguez De Cordoba, S., Gallardo, M. E. & Enriquez, J. A. 2006. Differences in reactive

oxygen species production explain the phenotypes associated with common mouse mitochondrial DNA variants. *Nat Genet,* 38**,** 1261-8.

Moreno, L., Moral-Sanz, J., Morales-Cano, D., Barreira, B., Moreno, E., Ferrarini, A., Pandolfi, R., Ruperez, F. J., Cortijo, J., Sanchez-Luna, M., Villamor, E., Perez-Vizcaino, F. & Cogolludo, A. 2014a. Ceramide mediates acute oxygen sensing in vascular tissues. *Antioxid Redox Signal,* 20**,** 1-14.

Moreno, M. L., Escobar, J., Izquierdo-Alvarez, A., Gil, A., Perez, S., Pereda, J., Zapico, I., Vento, M., Sabater, L., Marina, A., Martinez-Ruiz, A. & Sastre, J. 2014b. Disulfide stress: a novel type of oxidative stress in acute pancreatitis. *Free Radic Biol Med,* 70**,** 265-77.

Muliyil, S. & Narasimha, M. 2014. Mitochondrial ROS regulates cytoskeletal and mitochondrial remodeling to tune cell and tissue dynamics in a model for wound healing. *Dev Cell,* 28**,** 239-52.

Muñoz, C., Castellanos, M. C., Alfranca, A., Vara, A., Esteban, M. A., Redondo, J. M. & De Landázuri, M. O. 1996. Transcriptional up-regulation of intracellular adhesion molecule-1 in human endothelial cells by the antioxidant pyrrolidine dithiocarbamate involves the activation of activating protein-1. *J Immunol,* 157**,** 3587-97.

Murphy, E. & Eisner, D. A. 2009. Regulation of intracellular and mitochondrial sodium in health and disease. *Circ Res,* 104**,** 292-303.

Murphy, M. P. 2009. How mitochondria produce reactive oxygen species. *Biochem J,* 417**,** 1-13.

Nagy, J. A., Chang, S. H., Dvorak, A. M. & Dvorak, H. F. 2009. Why are tumour blood vessels abnormal and why is it important to know? *Br J Cancer,* 100**,** 865-9.

Nathan, C. 2003. Specificity of a third kind: reactive oxygen and nitrogen intermediates in cell signaling. *J Clin Invest,* 111**,** 769-78.

Nauseef, W. M. 2014. Detection of superoxide anion and hydrogen peroxide production by cellular NADPH oxidases. *Biochim Biophys Acta,* 1840**,** 757-67.

Navarro-Antolin, J., Rey-Campos, J. & Lamas, S. 2000. Transcriptional induction of endothelial nitric oxide gene by cyclosporine A. A role for activator protein-1. *J Biol Chem,* 275**,** 3075-80.

Navarro, S. J., Trinh, T., Lucas, C. A., Ross, A. J., Waymire, K. G. & Macgregor, G. R. 2012. The C57BL/6J Mouse Strain Background Modifies the Effect of a Mutation in Bcl2l2. *G3 (Bethesda),* 2**,** 99-102.

Nelson, D. L. & Cox, M. M. 2012. *Lehninger Principles of Biochemistry.*

Nickel, A. G., Von Hardenberg, A., Hohl, M., Loffler, J. R., Kohlhaas, M., Becker, J., Reil, J. C., Kazakov, A., Bonnekoh, J., Stadelmaier, M., Puhl, S. L., Wagner, M., Bogeski, I., Cortassa, S., Kappl, R., Pasieka, B., Lafontaine, M., Lancaster, C. R., Blacker, T. S., Hall, A. R., Duchen, M. R., Kastner, L., Lipp, P., Zeller, T., Muller, C., Knopp, A., Laufs, U., Bohm, M., Hoth, M. & Maack, C. 2015. Reversal of Mitochondrial Transhydrogenase Causes Oxidative Stress in Heart Failure. *Cell Metab,* 22**,** 472-84.

Nicholls, D. G. 2008. Forty years of Mitchell's proton circuit: From little grey books to little grey cells. *Biochim Biophys Acta,* 1777**,** 550-6.

Nicholls, D. G. 2010. Mitochondrial ion circuits. *Essays Biochem,* 47**,** 25-35.

Nijtmans, L. G., De Jong, L., Artal Sanz, M., Coates, P. J., Berden, J. A., Back, J. W., Muijsers, A. O., Van Der Spek, H. & Grivell, L. A. 2000. Prohibitins act as a membrane-bound chaperone for the stabilization of mitochondrial proteins. *EMBO J,* 19**,** 2444-51.

Nowikovsky, K., Froschauer, E. M., Zsurka, G., Samaj, J., Reipert, S., Kolisek, M., Wiesenberger, G. & Schweyen, R. J. 2004. The LETM1/YOL027 gene family encodes a factor of the mitochondrial K+ homeostasis with a potential role in the Wolf-Hirschhorn syndrome. *J Biol Chem,* 279**,** 30307-15.

Olmez, I. & Ozyurt, H. 2012. Reactive oxygen species and ischemic cerebrovascular disease. *Neurochem Int,* 60**,** 208-12.

Outten, F. W. 2007. Iron-sulfur clusters as oxygen-responsive molecular switches. *Nat Chem Biol,* 3**,** 206-7.

Oxenoid, K., Dong, Y., Cao, C., Cui, T., Sancak, Y., Markhard, A. L., Grabarek, Z., Kong, L., Liu, Z., Ouyang, B., Cong, Y., Mootha, V. K. & Chou, J. J. 2016. Architecture of the mitochondrial calcium uniporter. *Nature,* 533**,** 269-73.

Palty, R., Silverman, W. F., Hershfinkel, M., Caporale, T., Sensi, S. L., Parnis, J., Nolte, C., Fishman, D., Shoshan-Barmatz, V., Herrmann, S., Khananshvili, D. & Sekler, I. 2010. NCLX is an essential component of mitochondrial Na+/Ca2+ exchange. *Proc Natl Acad Sci U S A,* 107**,** 436-41.

Pan, X., Liu, J., Nguyen, T., Liu, C., Sun, J., Teng, Y., Fergusson, M. M., Rovira, Ii, Allen, M., Springer, D. A., Aponte, A. M., Gucek, M., Balaban, R. S., Murphy, E. & Finkel, T. 2013. The physiological role of mitochondrial calcium revealed by mice lacking the mitochondrial calcium uniporter. *Nat Cell Biol,* 15**,** 1464-72.

Perales-Clemente, E., Bayona-Bafaluy, M. P., Perez-Martos, A., Barrientos, A., Fernandez-Silva, P. & Enriquez, J. A. 2008. Restoration of electron transport without proton pumping in mammalian mitochondria. *Proc Natl Acad Sci U S A,* 105**,** 18735-9.

Perry, S. W., Norman, J. P., Barbieri, J., Brown, E. B. & Gelbard, H. A. 2011. Mitochondrial membrane potential probes and the proton gradient: a practical usage guide. *Biotechniques,* 50**,** 98-115.

Poburko, D. & Demaurex, N. 2012. Regulation of the mitochondrial proton gradient by cytosolic Ca(2)(+) signals. *Pflugers Arch,* 464**,** 19-26.

Poburko, D., Santo-Domingo, J. & Demaurex, N. 2011. Dynamic regulation of the mitochondrial proton gradient during cytosolic calcium elevations. *J Biol Chem,* 286**,** 11672-84.

Pryde, K. R. & Hirst, J. 2011. Superoxide is produced by the reduced flavin in mitochondrial complex I: a single, unified mechanism that applies during both forward and reverse electron transfer. *J Biol Chem,* 286**,** 18056-65.

Quijano, C., Trujillo, M., Castro, L. & Trostchansky, A. 2016. Interplay between oxidant species and energy metabolism. *Redox Biol,* 8**,** 28-42.

Quintero, M., Colombo, S. L., Godfrey, A. & Moncada, S. 2006. Mitochondria as signaling organelles in the vascular endothelium. *Proc Natl Acad Sci U S A,* 103**,** 5379-84.

Rathore, R., Zheng, Y. M., Niu, C. F., Liu, Q. H., Korde, A., Ho, Y. S. & Wang, Y. X. 2008. Hypoxia activates NADPH oxidase to increase [ROS]i and [Ca2+]i through the mitochondrial ROS-PKCepsilon signaling axis in pulmonary artery smooth muscle cells. *Free Radic Biol Med,* 45**,** 1223-31.

Redondo-Horcajo, M., Romero, N., Martinez-Acedo, P., Martinez-Ruiz, A., Quijano, C., Lourenco, C. F., Movilla, N., Enriquez, J. A., Rodriguez-Pascual, F., Rial, E., Radi, R., Vazquez, J. & Lamas, S. 2010. Cyclosporine A-induced nitration of tyrosine 34 MnSOD in endothelial cells: role of mitochondrial superoxide. *Cardiovasc Res,* 87**,** 356-65.

Reimer, K. A., Lowe, J. E., Rasmussen, M. M. & Jennings, R. B. 1977. The wavefront phenomenon of ischemic cell death. 1. Myocardial infarct size vs duration of coronary occlusion in dogs. *Circulation,* 56**,** 786-94.

Requejo-Aguilar, R., Lopez-Fabuel, I., Fernandez, E., Martins, L. M., Almeida, A. & Bolanos, J. P. 2014. PINK1 deficiency sustains cell proliferation by reprogramming glucose metabolism through HIF1. *Nat Commun,* 5**,** 4514.

Riquier, S., Breton, J., Abbas, K., Cornu, D., Bouton, C. & Drapier, J. C. 2014. Peroxiredoxin post-translational modifications by redox messengers. *Redox Biol,* 2**,** 777-85.

Roberts, P. G. & Hirst, J. 2012. The deactive form of respiratory complex I from mammalian mitochondria is a Na+/H+ antiporter. *J Biol Chem,* 287**,** 34743-51.

Robin, E., Guzy, R. D., Loor, G., Iwase, H., Waypa, G. B., Marks, J. D., Hoek, T. L. & Schumacker, P. T. 2007. Oxidant stress during simulated ischemia primes cardiomyocytes for cell death during reperfusion. *J Biol Chem,* 282**,** 19133-43.

Robinson, K. M., Janes, M. S., Pehar, M., Monette, J. S., Ross, M. F., Hagen, T. M., Murphy, M. P. & Beckman, J. S. 2006. Selective fluorescent imaging of superoxide in vivo using ethidium-based probes. *Proc Natl Acad Sci U S A,* 103**,** 15038-43.

Rothen-Rutishauser, B. M., Ehler, E., Perriard, E., Messerli, J. M. & Perriard, J. C. 1998. Different behaviour of the non-sarcomeric cytoskeleton in neonatal and adult rat cardiomyocytes. *J Mol Cell Cardiol,* 30**,** 19-31.

Rouault, T. A. 2006. The role of iron regulatory proteins in mammalian iron homeostasis and disease. *Nat Chem Biol,* 2**,** 406-14.

Roy, P., Roy, S. K., Mitra, A. & Kulkarni, A. P. 1994. Superoxide generation by lipoxygenase in the presence of NADH and NADPH. *Biochim Biophys Acta,* 1214**,** 171-9.

Sabharwal, S. S., Waypa, G. B., Marks, J. D. & Schumacker, P. T. 2013. Peroxiredoxin-5 targeted to the mitochondrial intermembrane space attenuates hypoxia-induced reactive oxygen species signalling. *Biochem J,* 456**,** 337-46.

Salahudeen, A. A., Thompson, J. W., Ruiz, J. C., Ma, H. W., Kinch, L. N., Li, Q., Grishin, N. V. & Bruick, R. K. 2009. An E3 ligase possessing an iron-responsive hemerythrin domain is a regulator of iron homeostasis. *Science,* 326**,** 722-6.

Sanchez-Gomez, F. J., Calvo, E., Breton-Romero, R., Fierro-Fernandez, M., Anilkumar, N., Shah, A. M., Schroder, K., Brandes, R. P., Vazquez, J. & Lamas, S. 2015. NOX4-dependent Hydrogen peroxide promotes shear stress-induced SHP2 sulfenylation and eNOS activation. *Free Radic Biol Med,* 89**,** 419-30.

Sazanov, L. A. 2015. A giant molecular proton pump: structure and mechanism of respiratory complex I. *Nat Rev Mol Cell Biol,* 16**,** 375-88.

Schagger, H. 1995. Native electrophoresis for isolation of mitochondrial oxidative phosphorylation protein complexes. *Methods Enzymol,* 260**,** 190-202.

Schagger, H. 2006. Tricine-SDS-PAGE. *Nat Protoc,* 1**,** 16-22.

Schagger, H. & Von Jagow, G. 1991. Blue native electrophoresis for isolation of membrane protein complexes in enzymatically active form. *Anal Biochem,* 199**,** 223-31.

Schneider, B. D. & Leibold, E. A. 2003. Effects of iron regulatory protein regulation on iron homeostasis during hypoxia. *Blood,* 102**,** 3404-11.

Schofield, C. J. & Ratcliffe, P. J. 2004. Oxygen sensing by HIF hydroxylases. *Nat Rev Mol Cell Biol,* 5**,** 343-54.

Schumacker, P. T. 2011. Lung cell hypoxia: role of mitochondrial reactive oxygen species signaling in triggering responses. *Proc Am Thorac Soc,* 8**,** 477-84.

Semenza, G. L. 2007. Life with oxygen. *Science,* 318**,** 62-4.

Sena, L. A. & Chandel, N. S. 2012. Physiological roles of mitochondrial reactive oxygen species. *Mol Cell,* 48**,** 158-67.

Shevchenko, A., Wilm, M., Vorm, O. & Mann, M. 1996. Mass spectrometric sequencing of proteins silver-stained polyacrylamide gels. *Anal Chem,* 68**,** 850-8.

Sies, H. 2015. Oxidative stress: a concept in redox biology and medicine. *Redox Biol,* 4**,** 180-3.

Soro-Arnaiz, I., Li, Q. O., Torres-Capelli, M., Melendez-Rodriguez, F., Veiga, S., Veys, K., Sebastian, D., Elorza, A., Tello, D., Hernansanz-Agustin, P., Cogliati, S., Moreno-Navarrete, J. M., Balsa, E., Fuertes, E., Romanos, E., Martinez-Ruiz, A., Enriquez, J. A., Fernandez-Real, J. M., Zorzano, A., De Bock, K. & Aragones, J. 2016. Role of Mitochondrial Complex IV in Age-Dependent Obesity. *Cell Rep,* 16**,** 2991-3002.

Stark, G. 2005. Functional consequences of oxidative membrane damage. *J Membr Biol,* 205**,** 1-16.

Stroud, D. A., Surgenor, E. E., Formosa, L. E., Reljic, B., Frazier, A. E., Dibley, M. G., Osellame, L. D., Stait, T., Beilharz, T. H., Thorburn, D. R., Salim, A. & Ryan, M. T. 2016. Accessory subunits are integral for assembly and function of human mitochondrial complex I. *Nature,* 538**,** 123-126.

Stull, L. B., Leppo, M. K., Szweda, L., Gao, W. D. & Marban, E. 2004. Chronic treatment with allopurinol boosts survival and cardiac contractility in murine postischemic cardiomyopathy. *Circ Res,* 95**,** 1005-11.

Surmeier, D. J., Guzman, J. N., Sanchez, J. & Schumacker, P. T. 2012. Physiological phenotype and vulnerability in Parkinson's disease. *Cold Spring Harb Perspect Med,* 2**,** a009290.

Sweeney, M. & Yuan, J. X. 2000. Hypoxic pulmonary vasoconstriction: role of voltage-gated potassium channels. *Respir Res,* 1**,** 40-8.

Sylvester, J. T., Shimoda, L. A., Aaronson, P. I. & Ward, J. P. 2012. Hypoxic pulmonary vasoconstriction. *Physiol Rev,* 92**,** 367-520.

Takeuchi, A., Kim, B. & Matsuoka, S. 2013. The mitochondrial Na+-Ca2+ exchanger, NCLX, regulates automaticity of HL-1 cardiomyocytes. *Sci Rep,* 3**,** 2766.

Tanonaka, K., Motegi, K., Arino, T., Marunouchi, T., Takagi, N. & Takeo, S. 2012. Possible pathway of Na(+) flux into mitochondria in ischemic heart. *Biol Pharm Bull,* 35**,** 1661-8.

Tarasov, A. I., Griffiths, E. J. & Rutter, G. A. 2012. Regulation of ATP production by mitochondrial Ca(2+). *Cell Calcium,* 52**,** 28-35.

Tello, D., Balsa, E., Acosta-Iborra, B., Fuertes-Yebra, E., Elorza, A., Ordóñez, A., Corral-Escariz, M., Soro, I., López-Bernardo, E., Perales-Clemente, E., Martínez-Ruiz, A., Enríquez, J. A., Aragonés, J., Cadenas, S. & Landázuri, M. O. 2011. Induction of the mitochondrial NDUFA4L2 protein by HIF-1alpha decreases oxygen consumption by inhibiting Complex I activity. *Cell Metab,* 14**,** 768-79.

Tello, D., Tarín, C., Ahicart, P., Bretón-Romero, R., Lamas, S. & Martínez-Ruiz, A. 2009. A "fluorescence switch" technique increases the sensitivity of proteomic detection and identification of S-nitrosylated proteins. *Proteomics,* 9**,** 5359-70.

Treberg, J. R., Quinlan, C. L. & Brand, M. D. 2011. Evidence for two sites of superoxide production by mitochondrial NADH-ubiquinone oxidoreductase (complex I). *J Biol Chem,* 286**,** 27103-10.

Turrens, J. F. 2003. Mitochondrial formation of reactive oxygen species. *J Physiol,* 552**,** 335-44.

Vashisht, A. A., Zumbrennen, K. B., Huang, X., Powers, D. N., Durazo, A., Sun, D., Bhaskaran, N., Persson, A., Uhlen, M., Sangfelt, O., Spruck, C., Leibold, E. A. & Wohlschlegel, J. A. 2009. Control of iron homeostasis by an iron-regulated ubiquitin ligase. *Science,* 326**,** 718-21.

Vinogradov, A. D. & Grivennikova, V. G. 2005. Generation of superoxide-radical by the NADH:ubiquinone oxidoreductase of heart mitochondria. *Biochemistry (Mosc),* 70**,** 120-7.

Vinothkumar, K. R., Zhu, J. & Hirst, J. 2014. Architecture of mammalian respiratory complex I. *Nature,* 515**,** 80-4.

Wan, B., Lanoue, K. F., Cheung, J. Y. & Scaduto, R. C., Jr. 1989. Regulation of citric acid cycle by calcium. *J Biol Chem,* 264**,** 13430-9.

Waypa, G. B., Marks, J. D., Guzy, R., Mungai, P. T., Schriewer, J., Dokic, D. & Schumacker, P. T. 2010. Hypoxia triggers subcellular compartmental redox signaling in vascular smooth muscle cells. *Circ Res,* 106**,** 526-35.

Weir, E. K., Lopez-Barneo, J., Buckler, K. J. & Archer, S. L. 2005. Acute oxygen-sensing mechanisms. *N Engl J Med,* 353**,** 2042-55.

Weir, E. K. & Olschewski, A. 2006. Role of ion channels in acute and chronic responses of the pulmonary vasculature to hypoxia. *Cardiovasc Res,* 71**,** 630-41.

Wong, R., Steenbergen, C. & Murphy, E. 2012. Mitochondrial permeability transition pore and calcium handling. *Methods Mol Biol,* 810**,** 235-42.

Wu, M., Gu, J., Guo, R., Huang, Y. & Yang, M. 2016. Structure of Mammalian Respiratory Supercomplex I1III2IV1. *Cell,* 167**,** 1598-1609 e10.

Xia, D., Yu, C. A., Kim, H., Xia, J. Z., Kachurin, A. M., Zhang, L., Yu, L. & Deisenhofer, J. 1997. Crystal structure of the cytochrome bc1 complex from bovine heart mitochondria. *Science,* 277**,** 60-6.

Xia, Y. 2007. Superoxide generation from nitric oxide synthases. *Antioxid Redox Signal,* 9**,** 1773-8.

Yuan, G., Vasavda, C., Peng, Y. J., Makarenko, V. V., Raghuraman, G., Nanduri, J., Gadalla, M. M., Semenza, G. L., Kumar, G. K., Snyder, S. H. & Prabhakar, N. R. 2015. Protein kinase G-regulated production of H2S governs oxygen sensing. *Sci Signal,* 8**,** ra37.

Zangar, R. C., Davydov, D. R. & Verma, S. 2004. Mechanisms that regulate production of reactive oxygen species by cytochrome P450. *Toxicol Appl Pharmacol,* 199**,** 316-31.

Zhang, H., Bosch-Marce, M., Shimoda, L. A., Tan, Y. S., Baek, J. H., Wesley, J. B., Gonzalez, F. J. & Semenza, G. L. 2008. Mitochondrial autophagy is an HIF-1-dependent adaptive metabolic response to hypoxia. *J Biol Chem,* 283**,** 10892-903.

Zhang, Z., Huang, L., Shulmeister, V. M., Chi, Y. I., Kim, K. K., Hung, L. W., Crofts, A. R., Berry, E. A. & Kim, S. H. 1998. Electron transfer by domain movement in cytochrome bc1. *Nature,* 392**,** 677-84.

Zhao, H., Joseph, J., Fales, H. M., Sokoloski, E. A., Levine, R. L., Vasquez-Vivar, J. & Kalyanaraman, B. 2005. Detection and characterization of the product of hydroethidine and intracellular superoxide by HPLC and limitations of fluorescence. *Proc Natl Acad Sci U S A,* 102**,** 5727-32.

Zhao, Y., Araki, S., Wu, J., Teramoto, T., Chang, Y. F., Nakano, M., Abdelfattah, A. S., Fujiwara, M., Ishihara, T., Nagai, T., Campbell, R. E. 2011. An expanded palette of genetically encoded Ca2+ indicators. Science. 333, 6051. 1888-91.

Zheng, G., Fu, Y. & He, C. 2014. Nucleic acid oxidation in DNA damage repair and epigenetics. *Chem Rev,* 114**,** 4602-20.

Zickermann, V., Wirth, C., Nasiri, H., Siegmund, K., Schwalbe, H., Hunte, C. & Brandt, U. 2015. Structural biology. Mechanistic insight from the crystal structure of mitochondrial complex I. *Science,* 347**,** 44-9.

Zielonka, J., Hardy, M. & Kalyanaraman, B. 2009. HPLC study of oxidation products of hydroethidine in chemical and biological systems: ramifications in superoxide measurements. *Free Radic Biol Med,* 46**,** 329-38.

Zielonka, J., Sikora, A., Hardy, M., Joseph, J., Dranka, B. P. & Kalyanaraman, B. 2012. Boronate probes as diagnostic tools for real time monitoring of peroxynitrite and hydroperoxides. *Chem Res Toxicol,* 25**,** 1793-9.

Zuo, L., Christofi, F. L., Wright, V. P., Bao, S. & Clanton, T. L. 2004. Lipoxygenase-dependent superoxide release in skeletal muscle. *J Appl Physiol (1985),* 97**,** 661-8.

Annexes

List of publicactions

The following publications are directly derived from the results included in this thesis:

Acute hypoxia produces a superoxide burst in cells.
Hernansanz-Agustín P, Izquierdo-Álvarez A, Sánchez-Gómez FJ, Ramos E, Villa-Piña T, Lamas S, Bogdanova A, Martínez-Ruiz A.
Free Radic Biol Med. 2014 Jun;71:146-56.
doi: 10.1016/j.freeradbiomed.2014.03.011.

- *Mitochondrial complex I deactivation is related to superoxide production in acute hipoxia.* **Hernansanz-Agustín P**, Ramos E, Navarro E, Parada E, Sánchez-López, Peláez-Aguado L, Cabrera-García JD, Tello D, Buendía I, Marina A, Egea J, López MG, Bogdanova A, Martínez-Ruiz A. Redox Biol. *Under review*

- *The mitochondrial sodium/calcium exchanger links complex I deactivation to superoxide production in acute hypoxia.* **Hernansanz-Agustín P**, Ramos E, Navarro E, Parada E, Moreno L, Sánchez-López, Peláez-Aguado L, Cabrera-García JD, Izquierdo-Álvarez A, Villa-Piña T, Tello D, Buendía I, Marina A, Egea J, Cogolludo A, López MG, Bogdanova A, Martínez-Ruiz A. *In preparation*

- *Sodium overload inhibits hypoxic superoxide production and hypoxic HIF-1α stabilization through NCLX function alteration.* **Hernansanz-Agustín P**, *et al. In preparation*

- New players in mitochondrial ROS production in acute hypoxia. **Hernansanz-Agustín P**, Martínez-Ruiz A. In preparation.

I have participated in the following publications during the research period of my thesis:

- *Differential redox proteomics allows identification of proteins reversibly oxidized at cysteine residues in endothelial cells in response to acute hypoxia*. Izquierdo-Álvarez A, Ramos E, Villanueva J, **Hernansanz-Agustín P**, Fernández-Rodríguez R, Tello D, Carrascal M, Martínez-Ruiz A. J Proteomics. 2012 Sep 18;75(17):5449-62. doi: 10.1016/j.jprot.2012.06.035.

- *Reactive oxygen species, nutrition, hypoxia and diseases: Problems solved?* Görlach A, Dimova EY, Petry A, Martínez-Ruiz A, **Hernansanz-Agustín P**, Rolo AP, Palmeira CM, Kietzmann T. Redox Biol. 2015 Dec;6:372-85. doi: 10.1016/j.redox.2015.08.016.

- *"Oxygen Sensing" by Na,K-ATPase: These Miraculous Thiols*. Bogdanova A, Petrushanko IY, **Hernansanz-Agustín P**, Martínez-Ruiz A. Front Physiol. 2016 Aug 2;7:314. doi: 10.3389/fphys.2016.00314.

- *Role of Mitochondrial Complex IV in Age-Dependent Obesity*. Soro-Arnaiz I, Li QO, Torres-Capelli M, Meléndez-Rodríguez F, Veiga S, Veys K, Sebastian D, Elorza A, Tello D, **Hernansanz-Agustín P**, Cogliati S, Moreno-Navarrete JM, Balsa E, Fuertes E, Romanos E, Martínez-Ruiz A, Enriquez JA, Fernandez-Real JM, Zorzano A, De Bock K, Aragonés J. Cell Rep. 2016 Sep 13;16(11):2991-3002. doi: 10.1016/j.celrep.2016.08.041.

- *Nitrosothiols in the immune system: signaling and protection*. **Hernansanz-Agustín P**, Izquierdo-Álvarez A, García-Ortiz A, Ibiza S, Serrador JM, Martínez-Ruiz A. Antioxid Redox Signal. 2013 Jan 20;18(3):288-308. doi: 10.1089/ars.2012.4765.

- *Specificity in S-nitrosylation: a short-range mechanism for NO signaling?* Martínez-Ruiz A, Araújo IM, Izquierdo-Álvarez A, **Hernansanz-Agustín P**, Lamas S, Serrador JM. Antioxid Redox Signal. 2013 Oct 10;19(11):1220-35. doi: 10.1089/ars.2012.5066.

Free Radical Biology and Medicine 71 (2014) 146–156

Contents lists available at ScienceDirect

Free Radical Biology and Medicine

journal homepage: www.elsevier.com/locate/freeradbiomed

Original Contribution

Acute hypoxia produces a superoxide burst in cells

Pablo Hernansanz-Agustín [a,b], Alicia Izquierdo-Álvarez [a], Francisco J. Sánchez-Gómez [c,d,1], Elena Ramos [a], Tamara Villa-Piña [a], Santiago Lamas [c,d], Anna Bogdanova [e], Antonio Martínez-Ruiz [a,*]

[a] Servicio de Inmunología, Hospital Universitario de La Princesa, Instituto de Investigación Sanitaria Princesa, E-28006 Madrid, Spain
[b] Departamento de Bioquímica, Facultad de Medicina, Universidad Autónoma de Madrid and Instituto de Investigaciones Biomédicas Alberto Sols, E-28029 Madrid, Spain
[c] Laboratorio Mixto, Consejo Superior de Investigaciones Científicas/Fundación Renal "Iñigo Alvarez de Toledo," E-28049 Madrid, Spain
[d] Departamento de Biología Celular e Inmunología, Centro de Biología Molecular "Severo Ochoa," Consejo Superior de Investigaciones Científicas–Universidad Autónoma de Madrid, E-28049 Madrid, Spain
[e] Institute of Veterinary Physiology, Vetsuisse Faculty, and Zurich Center for Integrative Human Physiology, University of Zurich, CH-8057 Zurich, Switzerland

ARTICLE INFO

Article history:
Received 28 January 2014
Received in revised form
7 March 2014
Accepted 8 March 2014
Available online 15 March 2014

Keywords:
Hypoxia
Ischemia
Cell signaling
Superoxide
Reactive oxygen species
Oxidative phosphorylation
Free radicals

ABSTRACT

Oxygen is a key molecule for cell metabolism. Eukaryotic cells sense the reduction in oxygen availability (hypoxia) and trigger a series of cellular and systemic responses to adapt to hypoxia, including the optimization of oxygen consumption. Many of these responses are mediated by a genetic program induced by the hypoxia-inducible transcription factors (HIFs), regulated by a family of prolyl hydroxylases (PHD or EGLN) that use oxygen as a substrate producing HIF hydroxylation. In parallel to these oxygen sensors modulating gene expression within hours, acute modulation of protein function in response to hypoxia is known to occur within minutes. Free radicals acting as second messengers, and oxidative posttranslational modifications, have been implied in both groups of responses. Localization and speciation of the paradoxical increase in reactive oxygen species production in hypoxia remain debatable. We have observed that several cell types respond to acute hypoxia with a transient increase in superoxide production for about 10 min, probably originating in the mitochondria. This may explain in part the apparently divergent results found by various groups that have not taken into account the time frame of hypoxic ROS production. We propose that this acute and transient hypoxia-induced superoxide burst may be translated into oxidative signals contributing to hypoxic adaptation and preconditioning.

In most metazoans, oxygen has to be distributed through the organism to be used by cells within various organs. In several physiological and pathophysiological scenarios, cells undergo a decrease in the amount of available oxygen, known as hypoxia, which induces acute and long-term cellular, local, and systemic responses [1]. Most of the long-term responses are mediated by the induction of over 100 genes by the hypoxia-inducible factors (HIFs), heterodimeric transcription factors composed of a constitutively expressed subunit (HIF-β) and an O_2-dependent HIF-α subunit. In normoxia the latter subunit is continuously degraded through a mechanism mediated by a family of HIF prolyl hydroxylases (EGLNs or PHDs), which carry out an O_2-dependent hydroxylation that is suppressed when oxygen concentration decreases, allowing HIF-α stabilization [2]. Some studies revealed that HIF-α stabilization was associated with an acute increase in reactive oxygen species (ROS) production in hypoxia [3,4].

It has been shown that acute responses to hypoxia involve local temporal changes in redox state due to the alterations in production of short-lived reactive oxygen species [5–8]. However, the nature of oxygen-sensing free radical generators, the targets of these radicals, and the resulting changes in enzyme activity and, finally, whether hypoxia causes a decrease or an increase in ROS production remain a matter of debate. Hypoxia-induced ROS production has been attributed mainly to the mitochondrial oxidative phosphorylation system (OXPHOS) and has been proposed to contribute to PHD inhibition and HIF-α stabilization [9–12] (reviewed in [13,14]).

Abbreviations: 2-OH-E, 2-hydroxyethidium; BAEC, bovine aortic endothelial cell; CDCFDA, 5(6)-carboxy-2′,7′-dichlorofluorescein diacetate; DCF, dichlorofluorescein; DHE, dihydroethidium; HIF, hypoxia-inducible factor; Mito-HE, mito-hydroethidine; OXPHOS, mitochondrial oxidative phosphorylation system; ROS, reactive oxygen species; TMRM, tetramethylrhodamine methyl ester

* Corresponding author. Fax: +34 915202374.
E-mail address: amartinezruiz@salud.madrid.org (A. Martínez-Ruiz).
[1] *Present address:* Departamento de Biología Físico-Química, Centro de Investigaciones Biológicas, CSIC, E-28040 Madrid, Spain.

http://dx.doi.org/10.1016/j.freeradbiomed.2014.03.011
0891-5849/

This posed a paradox, as superoxide is directly produced from oxygen so its production rate should decrease with a decrease in oxygen availability [13,15]. Indeed, some of these findings and methodological approaches have been questioned [16,17] (reviewed in [18]). However, detailed investigations confirmed that increased ROS production occurred under conditions of mild hypoxia (1–3% O_2), but not during severe hypoxia or anoxia [13,19,20].

ROS production in hypoxia has often been measured with fluorescent probes that are oxidized by different species. The main limitation of some (if not most) of these studies is that the fluorescence measurements were performed outside the hypoxia chamber with reoxygenation occurring during the measurements. Several recent reports have confirmed hypoxic ROS production in cells exposed to hypoxia while recording the fluorescent signal from HSP-FRET or roGFP [5,9,21–23] (reviewed in [13,24]). Both thiol-based protein sensors are oxidized by H_2O_2, although oxidation by other intracellular oxidants cannot be ruled out. Superoxide anion is the primary ROS produced by the OXPHOS. However, there are few reports using a specific probe for direct measurement of this species in hypoxic cells [17,20,25] and we are not aware of any study showing the dynamics of superoxide production upon deoxygenation. Understanding the time course of superoxide production will help us approach the mechanisms underlying that response.

By using a novel proteomic method for detecting reversible thiol oxidation (redox fluorescence switch), we have recently shown a specific pattern of proteins in which cysteine thiol residues are reversibly oxidized when endothelial cells are subjected to acute hypoxia for 2 h [8]. This suggests a role for hypoxia-induced ROS production in cell signaling: the increased ROS levels can produce specific oxidative posttranslational modifications that may regulate the HIF pathway or promote other acute responses [8]. We herein present the data on superoxide production directly assessed in the cytosol and in the mitochondria of cells exposed to acute hypoxic challenge, combining different techniques to avoid potential artifacts.

Materials and methods

Cell culture

Bovine aortic endothelial cells (BAECs) were obtained from aortas donated by a local slaughterhouse and isolated as previously described [26]. BAECs were cultured at 37 °C in RPMI 1640 supplemented with 15% heat-inactivated fetal bovine serum (FBS), 100 U/ml penicillin, and 100 μg/ml streptomycin. They were used between passages 3 and 9; endothelial morphology was assessed by visual inspection and by Western blot for endothelial nitric oxide synthase.

EA.hy926 cells (kindly provided by Dr. Cora-Jean S. Edgell, University of North Carolina, NC, USA) were cultured at 37 °C in Dulbecco's modified Eagle medium (DMEM) supplemented with HAT, 10% heat-inactivated FBS, 100 U/ml penicillin, and 100 μg/ml streptomycin

HeLa cells were cultured at 37 °C in DMEM supplemented with 10% heat-inactivated FBS, 100 U/ml penicillin, and 100 μg/ml streptomycin.

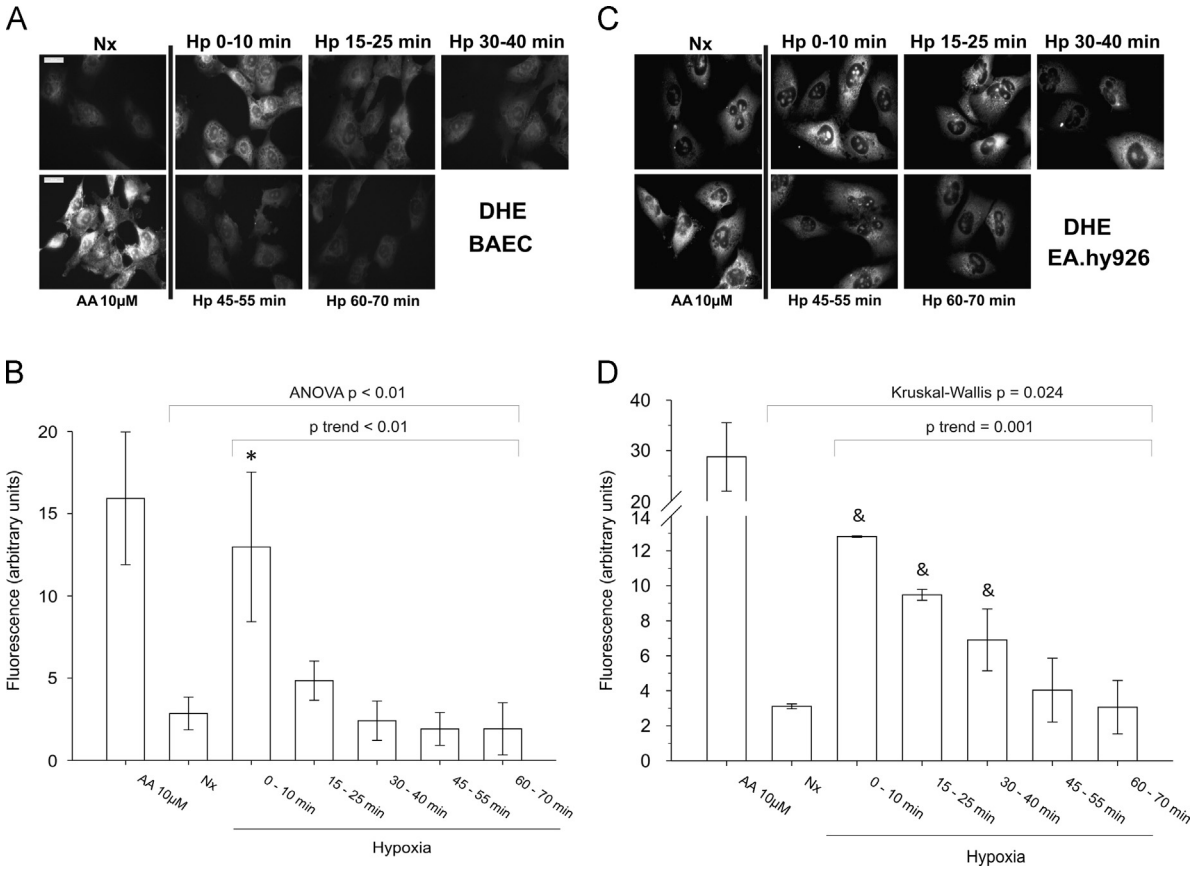

Fig. 1. Superoxide detection by DHE and fluorescence microscopy in fixed endothelial cells. (A, B) BAECs and (C, D) EA.hy926 cells were incubated for 60 min in normoxia (Nx) or in normoxia with antimycin A (AA, 10 μM for 30 min) or incubated in a hypoxia chamber at 1% O_2 with medium preequilibrated in the hypoxic condition (Hp) for 0, 15, 30, 45, or 60 min. 5 μM DHE was added for 10 min more, and the cells were fixed in the hypoxia chamber. (A, C) Representative images showing DHE fluorescence. (B, D) Quantification of images from four (B) or three (D) independent experiments. Data are presented as the mean ± SEM. $^*p < 0.05$, &$p = 0.0495$ versus Nx.

ρ^0L929 cells (mitochondrial DNA-less cells derived from L929 cells) and their control ρ^+ transmitochondrial cybrids, TmC57BL/6J (generated by transferring functional mitochondria from platelets to ρ^0L929 cells), were generated [27] and kindly provided by the group of Dr. José Antonio Enríquez (CNIC, Spain). They were cultured at 37 °C in DMEM supplemented with 5% heat-inactivated FBS, 100 U/ml penicillin, and 100 μg/ml streptomycin. ρ^0L929 cells were also supplemented with 50 μg/ml uridine.

HK-2 cells (kindly provided by Dr. María José Calzada, UAM and Instituto de Investigación Sanitaria Princesa, Madrid, Spain) were cultured at 37 °C in DMEM F-12–GlutaMAX supplemented with 10% heat-inactivated FBS, 100 U/ml penicillin and 100 μg/ml streptomycin, and 0.1% insulin–transferrin–selenium-X solution.

Cardiomyocytes were isolated from rat pups 2–3 days after birth as previously described [28]. The cells were seeded on collagen-coated six-well plates, supplemented with maintenance medium containing 1 part M199 medium and 4 parts medium containing (in mM) 116 NaCl, 32.1 $NaHCO_3$, 1 NaH_2PO_4 (pH 7.2), 0.8 $MgSO_4$, 5.5 glucose, 1.8 $CaCl_2$, supplemented with 1% horse serum, penicillin, streptomycin, and 2% glutamine. Cells were maintained in cell culture incubators (95% air, 5% CO_2 in gas phase, 37 °C) and used within 5 days of isolation.

Fluorescence microscopy in fixed cells and quantification

Cells were seeded a day before experimentation on glass coverslips. For treatments in hypoxia, all the solutions were preequilibrated to hypoxic conditions before use; in some experiments, 1 mM Tiron (4,5-dihydroxy-1,3-benzene disulfonic acid) was added 30 min before experimentation and maintained during the rest of the experiment. Plated cells were introduced in an Invivo2 400 workstation (Ruskinn) set at 1% O_2 (2% O_2 when stated), 5% CO_2, 37 °C, and incubated for the indicated times (0, 15, 30, 45, and 60 min) in new medium, washed three times with Hanks' balanced salt solution with Ca^{2+}/Mg^{2+} (HBSS + Ca/Mg) and incubated with 5 μM mito-hydroethidine (Mito-HE; 3.33 or 10 μM when stated) or 5 μM dihydroethidium (DHE) for 10 min, or with 10 μM 5(6)-carboxy-2′,7′-dichlorofluorescein diacetate (CDCFDA) for 15 min (all probes in HBSS + Ca/Mg), in darkness. After incubation, excess probe was washed away three times with HBSS + Ca/Mg, and the cells were fixed by adding 4% paraformaldehyde and incubated in darkness at 4 °C for 15 min. After fixation, wells were again washed three times with HBSS + Ca/Mg and coverslips placed on slides. In normoxic cells, medium was also changed for new normoxic medium and treated as hypoxic cells, but in a standard cell incubator. When normoxia was set at 7% O_2, the cells were placed in an Invivo2 200 workstation (Ruskinn) at 7% O_2, 5%

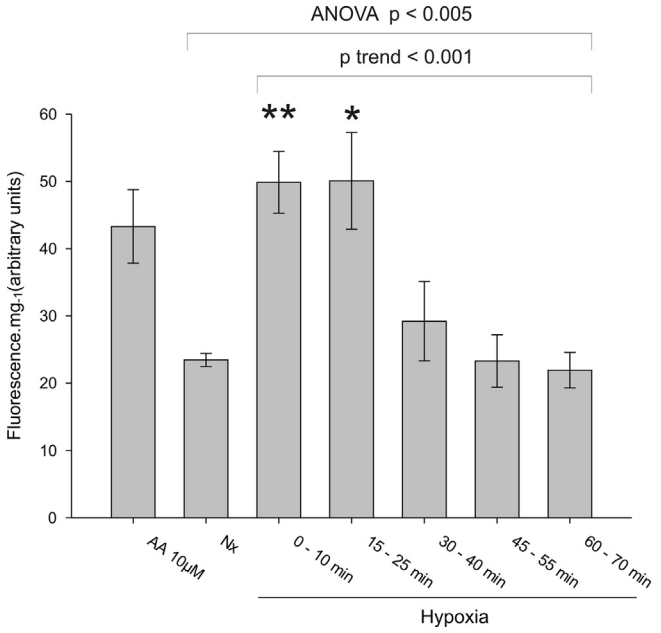

Fig. 2. Superoxide detection by DHE and HPLC in endothelial cells. BAECs were treated as in Fig. 1. After DHE incubation (5 μM DHE, 10 min) cells were lysed in the hypoxia chamber and frozen, and 2-OH-E amount was analyzed by HPLC with fluorescence detection. Data are presented as the mean ± SEM of four independent experiments. $^*p < 0.05$, $^{**}p < 0.01$ versus Nx.

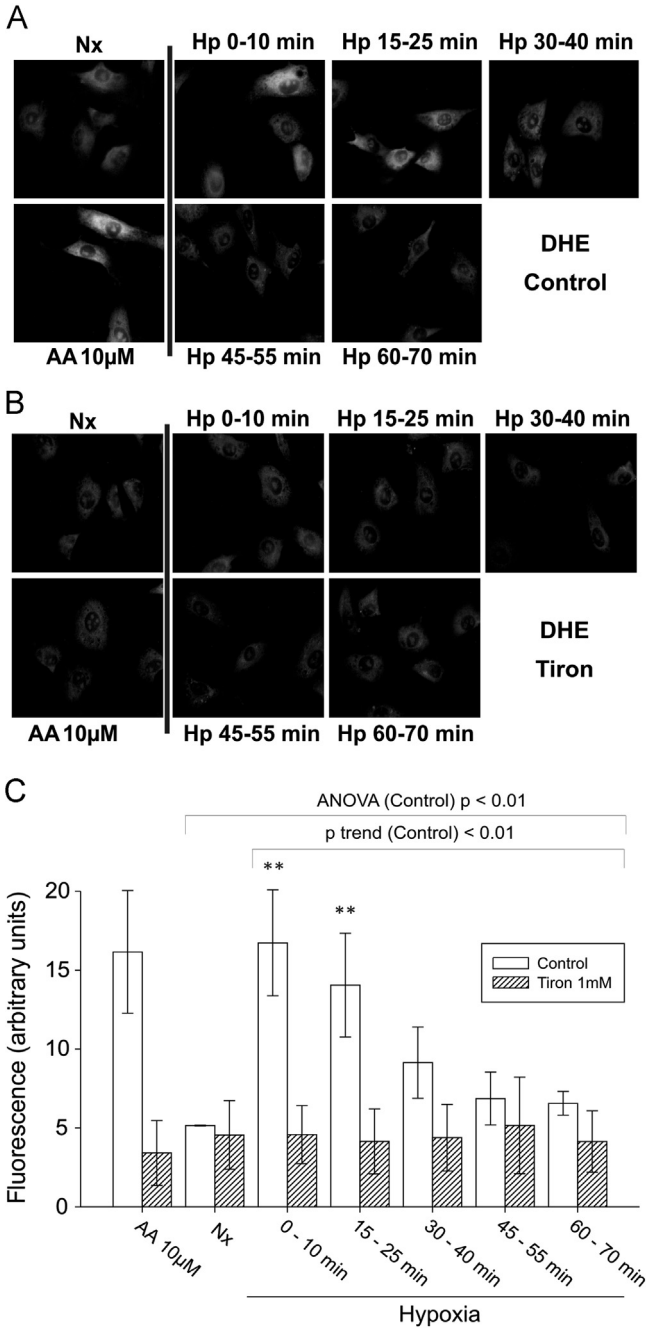

Fig. 3. Superoxide detection by DHE and fluorescence microscopy in fixed endothelial cells treated with 1 mM Tiron. (A) Control BAECs and (B) BAECs incubated with 1 mM Tiron were treated as in Fig. 1. (A, B) Representative images showing DHE fluorescence. (C) Quantification of images from three independent experiments. Data are presented as the mean ± SEM. $^{**}p < 0.01$ versus Nx.

CO_2, 37 °C, incubated overnight, and treated in the same chamber or transferred to the Invivo2 400 chamber for 1% O_2 hypoxia as above. Antimycin A was added to a final concentration of 10 μM onto normoxic cells 30 min before and during incubation with the probe. Three images per coverslip were taken in a Leica DMR fluorescence microscope with a 63× objective, using the following excitation/emission filter pairs: 546-12/560 for DHE and Mito-HE, 480-40/505 for CDCFDA. The images (three images per coverslip; the number of independent experiments is described in the figure legends) were quantified using ImageJ software. The same threshold was set for all the images and the mean value from the histogram was averaged for the three images of each coverslip.

Significance of the hypoxia-induced changes was analyzed using analysis of variance (ANOVA) for normoxic and all the hypoxic time groups, and intergroup comparison was done by the multiple comparison test (Dunnett posteriori test with respect to the normoxia group). The change in fluorescence with the time in hypoxia was evaluated by linear trend test of all the hypoxia groups [29]. Homoscedasticity was tested with Levene's test and normality with the Shapiro–Wilk test. Appropriate transformation was done to perform the analysis in the case of no normal distribution. When no transformation gave normal distribution (Figs. 1D and 6D), nonparametric tests were used: differences among normoxic and all the hypoxic time groups were analyzed with the Kruskal–Wallis test and intergroup comparison was done with the Mann–Whitney test with respect to the normoxia group; the change in fluorescence with the time in hypoxia was evaluated by nonlinear trend test of all the hypoxia groups. All analyses were performed using Stata version 11 software and R version 2.15.2, with the help of the Methodology Unit of the Instituto de Investigación Sanitaria Princesa (Madrid, Spain).

Colocalization analysis of Mito-HE by confocal microscopy

Cells were seeded a day before experimentation on glass coverslips. Plated cells were washed three times with HBSS + Ca/Mg and incubated with 5 μM Mito-HE for 10 min in darkness. After incubation, excess probe was washed away three times with HBSS + Ca/Mg, and the cells were fixed by adding 4% paraformaldehyde and incubated in darkness at room temperature (RT) for 10 min. After fixation, wells were again washed with HBSS + Ca/Mg and cells permeabilized with 0.5% Triton in phosphate-buffered saline (PBS) for 10 min at RT. Blocking solution, consisting in 5-thio-2-nitrobenzoic acid in PBS, was added for 20 min at 37 °C, and antibody against prohibitin-1 C-term (AJ1656a; Abgent) was incubated for 1 h at 37 °C. Coverslips were washed three times with 0.1% Tween 20 in PBS (PBS-T) and incubated with DyLight-488-labeled goat anti-rabbit secondary antibody for 30 min at 37 °C. Cells were washed three times with PBS-T and once with distilled water and coverslips mounted in slides. Tri-color Z stacks were generated using a Leica SP-5 confocal microscope. Samples were excited with an Ar/Kr laser using the 488 nm line and a second diode laser fitted with a 561 nm line. Fluorescence

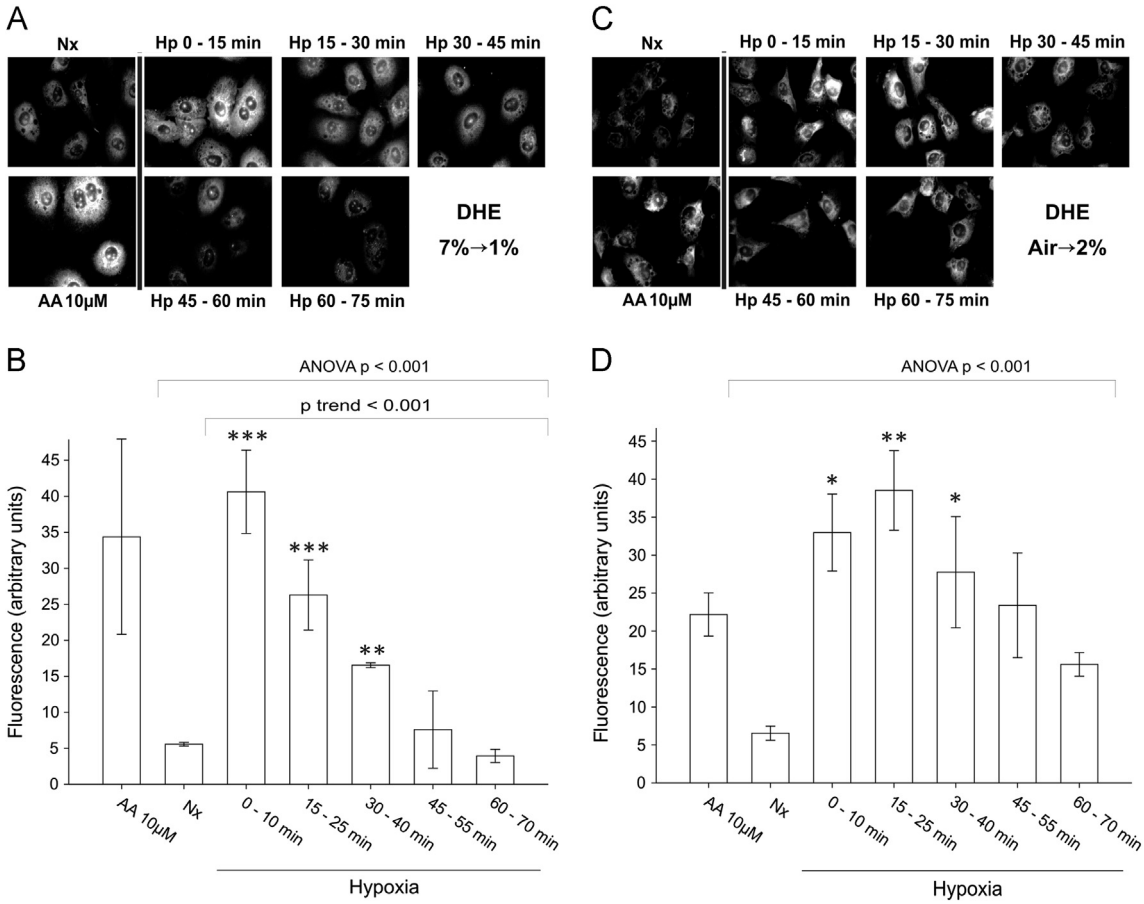

Fig. 4. Superoxide detection by DHE in endothelial cells at different concentrations of O_2 in normoxia and hypoxia. (A, B) BAECs were treated as in Fig. 1, but normoxia was set at 7% O_2. (C, D) BAECs were treated as in Fig. 1, but the hypoxia chamber was set at 2% O_2 and normoxia performed at atmospheric O_2 concentration. (A, C) Representative images showing DHE fluorescence. (B, D) Quantification of images from three independent experiments. Data are presented as the mean ± SEM. $^{***}p < 0.001$ versus Nx, $^{**}p < 0.01$ versus Nx, $^{*}p < 0.05$ versus Nx.

emission was taken using the spectral capability of the SP-5 according to the manufacturer's instructions. For three-dimensional analysis, stacks were processed using ImageJ software.

High-performance liquid chromatography (HPLC) analysis

Cells were seeded a day before experimentation in 60-mm-diameter plates. For hypoxia treatments, plated cells were introduced into an Invivo2 400 workstation (Ruskinn) set at 1% O_2, 5% CO_2, 37 °C, and incubated for the indicated times (0, 15, 30, 45, and 60 min) in prehypoxic medium, washed three times with prehypoxic HBSS + Ca/Mg and incubated with 5 μM DHE for 10 min (in prehypoxic HBSS + Ca/Mg solution), in the darkness. After incubation, excess probe was washed away once with prehypoxic PBS and cells were lysed with 0.1% Triton X-100 and frozen overnight at −80 °C. Homogenates were thawed on ice and 100 μl was transferred into a new tube. 1-butanol (250 μl) was added to the lysate, vortexed for 1 min, and centrifuged for 3 min at maximum speed and the upper alcoholic phase was recovered and dried. The desiccated fraction was resuspended in 100 μl HPLC-grade water and vortexed. An HPLC 2695 separation module from Waters was used to load and separate 50 μl of the samples in a Mediterranean Sea C18 column using acetonitrile 10%–trifluoroacetic acid (TFA) 0.1% and acetonitrile 100%–TFA 0.1% as mobile phases. Fluorescence of the samples was detected by a W474 module at 490 nm excitation wavelength and 560 nm emission wavelength. The peak area corresponding to hydroxyethidium formation was quantified and corrected with the protein concentration of the sample (determined by the BCA assay). Statistical analysis was performed as for fluorescence microscopy in fixed cells (see above).

Live imaging fluorescence microscopy and quantification

Cells were seeded in six-well plates a day before experimentation. Plated cells were washed three times with HBSS + Ca/Mg and incubated with 5 μM Mito-HE, 10 μM DHE, 30 nM tetramethylrhodamine methyl ester (TMRM), or 10 μM CDCFDA for 20 min at 37 °C in darkness. After that the plate was placed in a Leica DM 16000B fluorescence microscope equipped with a Leica DFC360FX camera, an automated stage for live imaging, and a thermostated hypoxic cabinet. The planes were focused for image capture, and images were taken with a 20× objective every 2 min for 40 min, providing a total of 20 cycles. Normoxia experiments started and ended at 20% O_2 and 5% CO_2, whereas hypoxia experiments started at 20% O_2 and 5% CO_2 and were switched to 2% O_2 and 5% CO_2 in cycle 2. The excitation/emission filter pairs used were 546-12/560 for DHE, Mito-HE, and TMRM, 480-40/505 for CDCFDA.

For mitochondrial membrane potential controls, 12.5 μM oligomycin or 1 μM carbonyl cyanide-4-(trifluoromethoxy)phenylhydrazone (FCCP) were added before focusing the planes.

Images were quantified with Leica Las-AF software. Three independent experiments were performed for each condition. For each experiment and condition, four identical linear regions of interest (ROIs) were created on nonnuclear regions of different cells (to avoid measuring nuclear binding of Mito-HE and DHE). The maximum peak value of cycles 0, 5, 10, 15, and 20 was collected for each ROI. The oxidation rate for each replicate was estimated by linear regression of the data for all the ROIs and time points. The differences in the means of the replicate oxidation rates were analyzed by the Student *t* test. Homoscedasticity was tested with Levene's test and normality with the Shapiro–Wilk test. Appropriate transformation was done to perform the analysis in the case of no homoscedasticity or no normal distribution. These statistical analyses were performed using G-Stat version 2.0.1 software.

Treatment effect was analyzed with GEE (generalized estimating equations method) with Gaussian family and identity link function [30]. Variability of statistics derived from time observations was analyzed with independent and autoregressive of order 1 (AR1)—correlation structures [30]. However, only the independent correlation structure is shown for the within-subject correlation, because it was the most parsimonious model (*p* value and coefficient were similar between the two structures, therefore the statistical independence of observations could be assumed). This independent correlation structure is equal to simple regression models. When the response variables were not normally distributed appropriate transformations were used. These analyses were performed using Stata version 12 software with the help of the Methodology Unit of the Instituto de Investigación Sanitaria Princesa (Madrid, Spain).

Western blot analysis

Protein extracts were run on 10% standard polyacrylamide gel electrophoresis and transferred to nitrocellulose membranes. Monoclonal anti-HIF-1α antibody (MAB1536; R&D Systems) and monoclonal anti-α-tubulin antibody (T6199; Sigma) were used. Antibody binding was detected by chemiluminescence with species-specific secondary antibodies labeled with horseradish peroxidase and visualized on a digital luminescence image analyzer (Fujifilm LAS-4000).

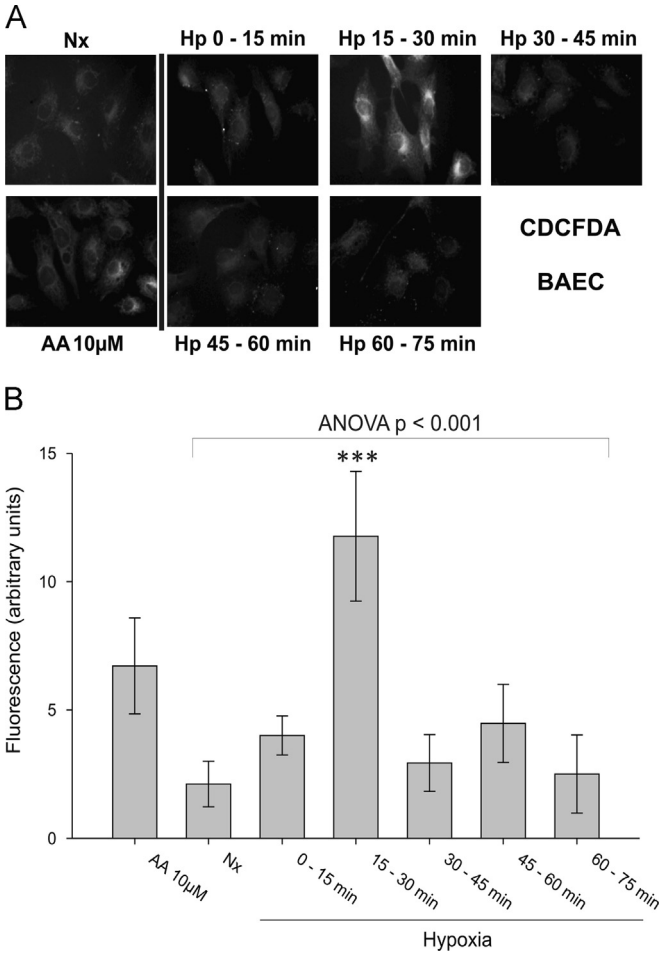

Fig. 5. ROS detection by CDCFDA and fluorescence microscopy in fixed endothelial cells. BAECs were treated as in Fig. 1. CDCFDA 10 μM was added for 15 min more, and cells were fixed in the hypoxia chamber. (A) Representative images showing CDCFDA fluorescence. (B) Quantification of images from four independent experiments. Data are presented as the mean ± SEM. $^{***}p < 0.001$ versus Nx.

Results and discussion

Hypoxia induces a superoxide burst in the first minutes of hypoxia in endothelial cells

We aimed to determine whether reduction in oxygen concentration was able to induce the production of superoxide ($O_2^{\bullet-}$) at different times. DHE reacts with superoxide to produce 2-hydroxyethidium (2-OH-E), which can be detected by fluorescence microscopy. As a positive control we used antimycin A, which inhibits complex III of the OXPHOS system, increasing superoxide production [31]. Primary BAECs were subjected to hypoxia for various times, ranging from 10 to 70 min. DHE was added over the last 10 min of hypoxic exposure, and after that, the cells were fixed in the hypoxia chamber. The amount of 2-OH-E produced was assessed in a fluorescence microscope (Fig. 1A and B). Compared to the measure in normoxia, a significant increase in superoxide production was observed within the first minutes of hypoxia. An additional analysis of the linear trend (*p* trend [29]) among the measures at various times in hypoxia showed that superoxide production was progressively diminished over the following hour. Similar results were obtained with a cell line derived from human endothelial cells, EA.hy926 [32] (Fig. 1C and D).

DHE oxidation measurement by fluorescence microscopy is not completely specific for superoxide detection, as there are other reactions that can also give fluorescent products, but 2-OH-E can be differentiated from ethidium and other products by HPLC analysis with fluorescence detection [33]. To confirm the results from microscopy and to unambiguously detect the production of superoxide, we performed HPLC analysis of cell lysates from BAECs subjected to hypoxia, incubated with DHE, and extracted in the hypoxia chamber. The peak of 2-OH-E was clearly separated from the peak of ethidium, both in control experiments with cyclosporin A treatment [34] and in hypoxia treatments (Supplementary Fig. 1). With this methodology we also observed a transient burst of superoxide production during the first minutes of hypoxia (Fig. 2). Superoxide signal thereafter decreased and did not differ from normoxic values after 45–60 min in hypoxia. These findings correlated with the results obtained by fluorescence microscopy (Fig. 1), confirming the specific detection of superoxide in our setting.

To further confirm the superoxide burst, we aimed to inhibit it with specific reagents, so we treated BAECs with Tiron before and during the hypoxic incubation in microscopy experiments. Tiron reacts with superoxide, and clearly abolished the signal from the superoxide burst in hypoxia (Fig. 3).

To assess if this superoxide burst is specific for the change in oxygen concentrations we have used in the experimental setting, we performed similar experiments with different initial and final oxygen concentrations. First, we used a lower initial "normoxic" reference concentration, 7% O_2, which could be more physiologically relevant for endothelial cells, maintaining the hypoxia at 1% O_2. We observed a similar superoxide burst (Fig. 4A and B). A similar increase in superoxide production was observed when 2% O_2 was used as hypoxia and ambient air was used as normoxia. In fact the amplitude of the superoxide burst at 2% O_2 exceeded that observed at 1% O_2 (Fig. 4C and D).

To determine the production of H_2O_2 (along with $ONOO^-$ and other ROS [35]) that could be derived from the superoxide burst we used CDCFDA. BAECs incubated in hypoxia showed a burst in

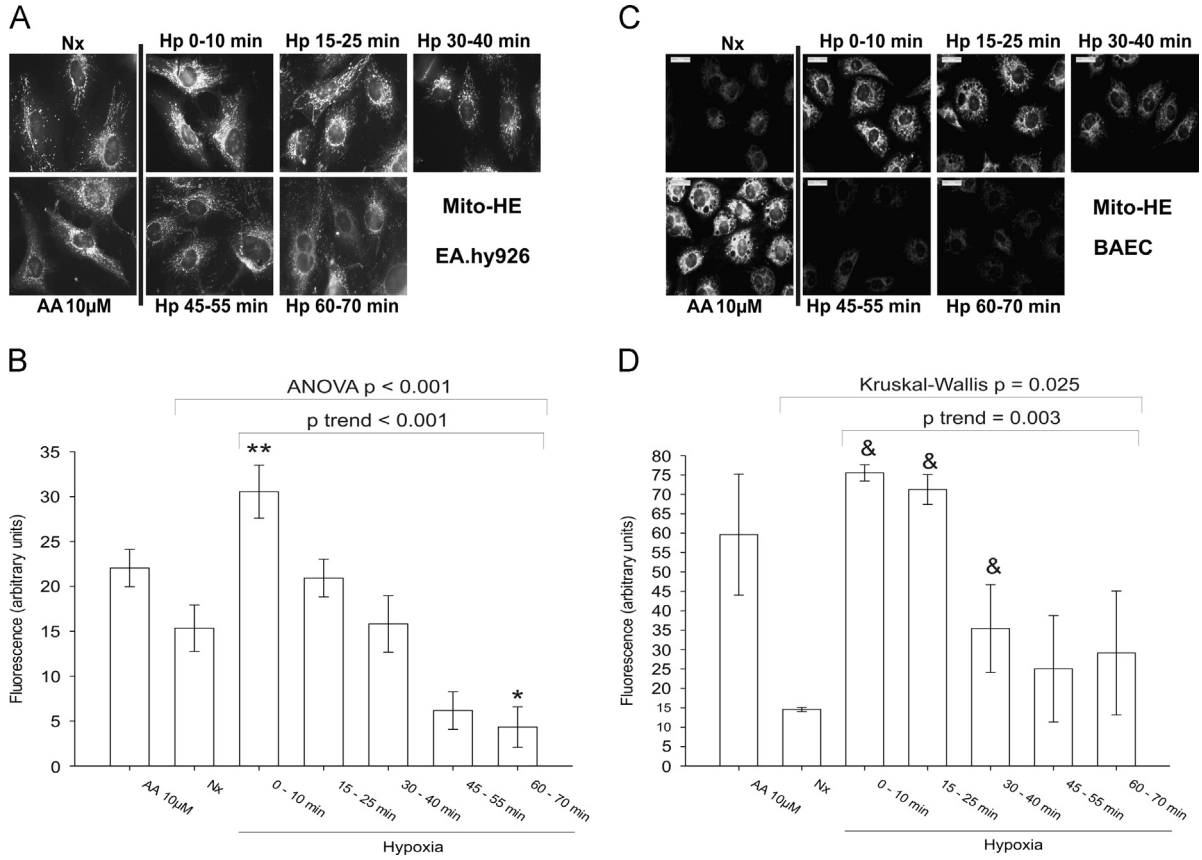

Fig. 6. Mitochondrial superoxide detection by Mito-HE and fluorescence microscopy in fixed endothelial cells. (A, B) EA.hy926 cells and (C, D) BAECs were treated as in Fig. 1. Mito-HE 5 μM was added for 10 min more, and the cells were fixed in the hypoxia chamber. (A, C) Representative images showing Mito-HE fluorescence. (B, D) Quantification of images from three independent experiments. Data are presented as the mean ± SEM. $^*p < 0.05$, $^{**}p < 0.01$, &$p = 0.0495$ versus Nx.

CDCFDA oxidation, which peaks at 15–30 min (Fig. 5), suggesting that the superoxide burst is translated into a burst of other ROS such as H_2O_2 with a slight delay. A similar kinetics has been described for CDCFDA oxidation after VEGF addition, increased under hypoxic conditions [36].

Superoxide is produced in mitochondria

We next wanted to explore the role of mitochondria in hypoxia-induced superoxide production. To this end, we used the mitochondria-targeted probe Mito-HE, in which a triphenylphosphonium (TPP^+) group is linked to DHE. Mito-HE accumulates within active mitochondria because positively charged TPP^+ drives the compound to the negatively charged mitochondrial matrix. EA.hy926 cells incubated with Mito-HE during the last 10 min of exposure to 1% O_2 showed a similar acute transient rise in superoxide production in response to hypoxia (Fig. 6A and B), suggesting mitochondrial localization of superoxide production. Again, similar results were obtained in BAECs, in which superoxide production in hypoxia could be even higher (Fig. 6C and D).

We confirmed mitochondrial targeting of Mito-HE by assessing colocalization with prohibitin-1, a mitochondrial protein (Supplementary Fig. 2A) [37]. To additionally control that the Mito-HE signal was actually related to increases in superoxide production and there was no saturation effect in the signal, we tested different concentrations of Mito-HE, observing that there is a clear increase with the Mito-HE concentration (Supplementary Fig. 2B).

A complementary approach to analyzing the mitochondrial origin of the superoxide production came from the study of the hypoxia response in ρ^0 cells, which do not have a functional OXPHOS owing to mitochondrial DNA damage. ρ^0 cells (ρ^0L929) and their control cybrids with undamaged mitochondria (TmC57BL/6J, from now on called C57) [27] were subjected to hypoxia and DHE fluorescence was measured under the same conditions as with endothelial cells. C57 cells also showed a superoxide burst in the first minutes of hypoxia (Fig. 7). However, ρ^0L929 cells showed much lower DHE signal, which did not increase with antimycin A treatment (owing to the lack of OXPHOS); hypoxic exposure of ρ^0L929 cells also did not significantly affect the DHE (Fig. 7). In line with the previous data these findings point also to the mitochondrial origin of the superoxide burst that we observe in the first minutes of hypoxia.

Early hypoxic superoxide production is confirmed in living cells

In the previous experiments the accumulation of ROS was detected over the 10 or 15 min after 0–60 min of incubation under hypoxic or normoxic conditions. To get a complementary measure of ROS production in hypoxia, we monitored the rates of oxidation of the ROS-sensitive probes using live imaging under normoxic or hypoxic conditions. Under normoxic conditions a gradual sustained increase in the oxidation signal was detected in BAECs using DHE, Mito-HE, and CDCFDA (Fig. 8A–C). In these experiments, the fluorescent signal accumulated over time because of the irreversible oxidative modification of the probes. Thus, this method allowed assessing only the change in the rate of oxidation, which reflects the relative changes in differences in ROS production, and not the differences between the time points. We confirmed a significant increase in the rate of ROS production in BAECs for all the three probes when cells were subjected to hypoxia (Fig. 8A–C).

Using live imaging we also explored the oxygen-dependent changes in the mitochondrial membrane potential. Mitochondrial targeting of Mito-HE is driven by mitochondrial membrane potential. Thus, hyperpolarization is associated with greater accumulation of Mito-HE within mitochondria and a concomitant increase in fluorescence, which is not caused by increased superoxide formation. We measured the mitochondrial membrane potential in BAECs using TMRM in nonquenching mode [38], confirmed by the clear and immediate decrease in the signal when FCCP (which depolarizes the membrane by uncoupling OXPHOS) was added and the increase after addition of oligomycin (which inhibits ATPase, increasing the potential) (Supplementary Fig. 3). Hypoxic treatment of BAECs was associated with mitochondrial depolarization, whereas the potential was maintained in BAECs in normoxia (Fig. 8D). Thus, superoxide production in the mitochondria of hypoxic BAECs could be underestimated using

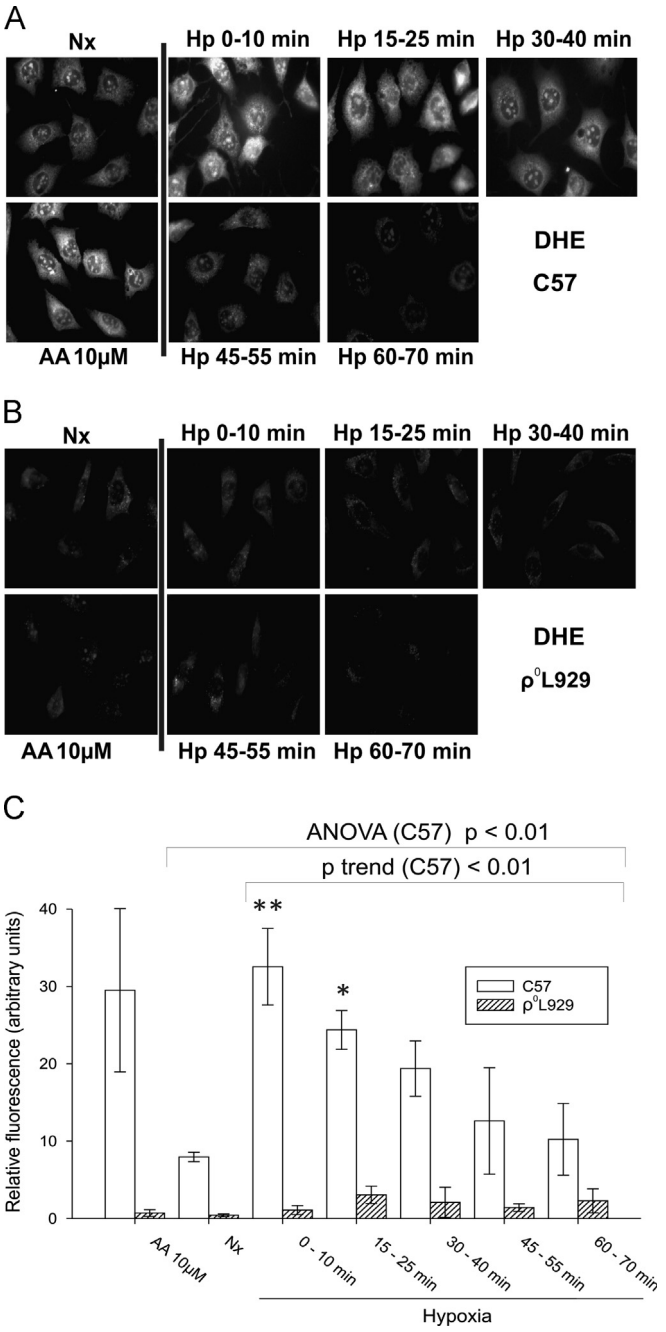

Fig. 7. Superoxide detection by DHE and fluorescence microscopy in fixed C57 and ρ^0L929 cells. (A) C57 and (B) ρ^0L929 cells were treated as in Fig. 1. (A, B) Representative images showing DHE fluorescence. (C) Quantification of images from three independent experiments. Data are presented as the mean ± SEM. $^{**}p < 0.05$, $^{*}p < 0.01$ versus Nx.

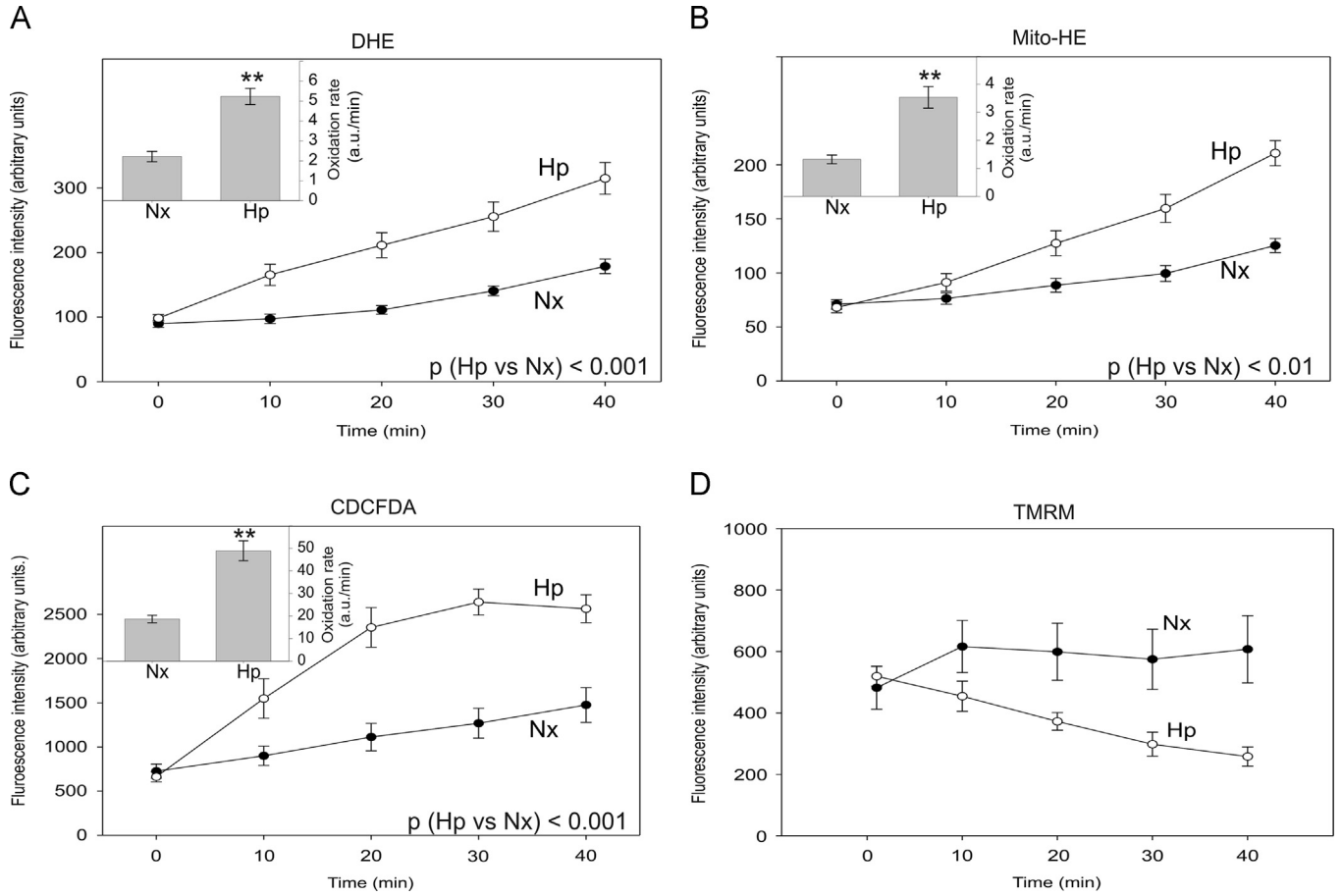

Fig. 8. Superoxide, ROS, and mitochondrial membrane potential measurement by fluorescence microscopy in live endothelial cells. BAECs were incubated with (A) 10 μM DHE, (B) 5 μM Mito-HE, (C) 15 μM CDCFDA, or (C) 30 nM TMRM for 20 min and subsequently incubated in a chamber with atmospheric and temperature control in a fluorescence microscope, where they were maintained in normoxia or subjected to 2% O_2 for 40 min. Quantification of four regions for three independent experiments is plotted for each time as the mean ± SEM. Black circles, normoxia (Nx); white circles, hypoxia (Hp). The *p* value shown corresponds to the evaluation of the treatment effect evaluated with the GEE method with independent correlation structure. (Insets in A–C) Oxidation rates considering all time points of each replicate ($n = 3$) are plotted as the mean ± SEM. $^{**}p < 0.01$ versus Nx.

Mito-HE, as the dye levels in depolarized hypoxic mitochondria would be lower than in the mitochondria of normoxic cells.

Live imaging also confirmed the mitochondrial implication in the increased superoxide production in hypoxia. Whereas C57 cells exhibit a clear increase in the DHE and CDCFDA signals when they are subjected to hypoxia, ρ^0L929 cells do not show these changes when subjected to hypoxia (Fig. 9).

Superoxide burst and ROS formation in hypoxia are not specific solely to endothelial cells

We wondered whether the hypoxia-induced superoxide burst and the increase in ROS production were specific to endothelial cells or a common feature for several cell types, in addition to the fibroblasts previously shown (Figs. 7 and 9). We carried out live imaging experiments with cultured neonatal rat cardiomyocytes. In line with the results obtained in endothelial cells, hypoxia triggered a significant increase in the rate of oxidation of DHE, Mito-HE, and CDCFDA, indicating an increased production of ROS (Fig. 10A–C). Furthermore, depolarization of the mitochondrial membrane in hypoxic cardiomyocytes was confirmed when monitoring signal intensity of TMRM (Fig. 10D), suggesting that superoxide production within mitochondria could be underestimated.

We also assessed whether tumor cells could exhibit a similar response to hypoxia. HeLa and HK2 cells were exposed to acute hypoxia and incubated with Mito-HE at different times (Supplementary Figs. 4 and 5). The response was similar to that of endothelial cells, thus reinforcing the involvement of mitochondria in hypoxic superoxide production and suggesting that this could represent a general mechanism for various cell types.

Superoxide burst as a regulator of HIF-1α stability

As previously stated, hypoxic ROS production has been implicated in triggering hypoxia adaptation signals through the HIF pathway, mediated by HIF-α subunit stabilization [13,14]. Additionally, we have recently shown that in endothelial cells there is a reversible oxidation in certain proteins after 2 h of hypoxia, which could be implied in acute responses to hypoxia [8]. Thus, the superoxide burst we observe could take part in hypoxic signals at longer times, related to the different kinetics of accumulation of different oxidized species.

To test this, we studied HIF-1α stabilization in the systems in which we have been able to abolish the superoxide burst in hypoxia, namely ρ^0 cells and treatment with Tiron. In accordance with results published elsewhere for other ρ^0 cells [3,9,10], ρ^0L929 cells did not stabilize HIF-1α in hypoxia as happened in the control C57 cells (Fig. 11A). Contrary to our hypothesis, Tiron treatment in BAECs did not abolish HIF-1α stabilization in hypoxia and even increased it, both in normoxia and in hypoxia (Fig. 11B). Measurement of CDCFDA oxidation showed that cells with Tiron produced equal or slightly higher signals than cells

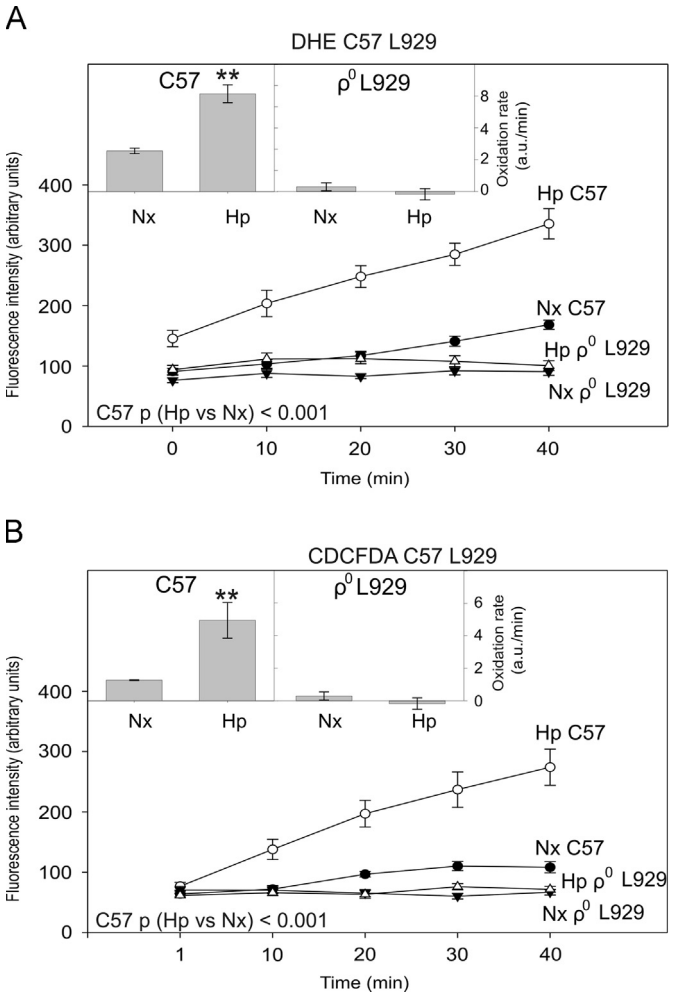

Fig. 9. Superoxide and ROS measurement by fluorescence microscopy in live C57 and ρ^0L929 cells. C57 and ρ^0L929 cells were incubated with (A) 10 μM DHE and (B) 15 μM CDCFDA and treated as in Fig. 8. Quantification of four regions for three independent experiments is plotted for each time as the mean ± SEM. Black circles, C57 in normoxia (Nx C57); white circles, C57 in hypoxia (Hp C57); black inverted triangles, ρ^0L929 in normoxia (Nx ρ^0L929); white triangles, ρ^0L929 in hypoxia (Hp ρ^0L929). The *p* value shown corresponds to the evaluation of the treatment effect evaluated with the GEE method with independent correlation structure. (Insets) Oxidation rates considering all time points of each replicate ($n = 3$) are plotted as the mean ± SEM. $^{**}p < 0.01$ versus Nx.

without treatment (Supplementary Fig. 6); this can be related to the reduction of superoxide due to the reaction with Tiron, producing mainly H_2O_2, which can explain increased HIF-1α stabilization.

Conclusions and future directions

Using several converging methodologies that avoid reoxygenation we have demonstrated that exposure of cells to acute mild hypoxia (1–2% O_2 under our culture conditions) was associated with a burst in superoxide production within the first minutes. Thereafter the levels of superoxide production in hypoxic cells reduced gradually over time. In 1 h no difference in superoxide production could be detected between hypoxic (1% O_2) and normoxic cells. Our results comparing different hypoxic O_2 concentrations in the same experimental setting (Figs. 1, 4C, and 4D) show that at 2% O_2 the superoxide burst can be slower and more sustained than at 1% O_2. These observations resolve the seeming contradiction in the findings reported earlier. For example, Quintero et al. [20] analyzed superoxide production by incubating endothelial cells with DHE for the first 60 min of hypoxia (3% O_2), showing a clear increase in the fluorescence signal; under these conditions, DHE would be oxidized by the superoxide burst that we have seen in our experiments. On the other hand, Chua et al. [17] saw no increase in DHE fluorescence when HEK293 cells were exposed to 1% hypoxia; but in this case DHE was added for 30 min after 3 h of incubation of the cells in hypoxia, which would not allow the detection of the initial superoxide burst.

Other studies have also shown an increase in DHE oxidation in cardiomyocytes in a model of acute ischemia for up to 60 min, in which, in addition to hypoxia, nutrients were removed from the cell culture medium [39]. Further studies would be interesting to evaluate the relative role of oxygen and nutrient depletion, as well as the putative significance of this mechanism in ischemic preconditioning.

We have seen a similar superoxide burst in different types of cells exposed to hypoxia and using either a probe distributed throughout the cell or a mitochondria-targeted probe. When we used ρ^0 cells, lacking a functional OXPHOS, the superoxide burst was abolished. Although we cannot rule out that other mechanisms of superoxide production could be implicated, this strongly suggests that the superoxide burst in the first minutes of hypoxia comes from the mitochondrial OXPHOS system, and it could be related to an early rearrangement of oxygen distribution and the electron transport chain throughout the system. The fact that at 2% O_2 the superoxide production seems to be more intense and prolonged than at 1% O_2 allows speculation that the decrease in superoxide production after some time of hypoxia could be related to a decrease in the O_2 availability inside the mitochondria, which could be delayed with respect to the O_2 reduction outside the cells.

The fact that DCF oxidation was maximal after 15 min of hypoxic exposure suggests that the superoxide burst during the first minutes of hypoxia translates into an increase in H_2O_2 or other ROS with a certain delay in time. This could be related to the different kinetics of accumulation of the diverse ROS, although it can be also an effect of the different probes used or even that the superoxide burst could trigger peroxide generation by other pathways; a more detailed evaluation of this relationship would deserve further investigation. The increase in protein modification by thiol oxidation occurs later on and was observed after 2 h of hypoxia in endothelial cells [8]; in further experiments, we have observed protein thiol oxidation initiating after 30 min of hypoxia in the same setting (unpublished results). If this signal takes part in the stabilization of a transcription factor such as HIF-α, and accumulation of target mRNAs, this could happen at even longer times. Our experiments studying the functional consequences of ablating the superoxide burst on HIF-1α stabilization (Fig. 11) are not fully conclusive. On one hand, although both the superoxide burst and the HIF-1α stabilization were ablated in ρ^0 cells, there could be many other effects related to OXPHOS impairment that could be taking part. On the other hand, Tiron was effective in scavenging superoxide, but probably increased H_2O_2 levels, which correlated with equal or increased HIF-1α stabilization. Thus, further experiments would be needed to assess this, probably with more specific interventions to inhibit the superoxide burst.

We propose that a superoxide production burst in the first minutes, which is translated into cell signals mediated by redox posttranslational modifications, may result in complex responses of the cells to hypoxia (and maybe ischemia) such as adaptation and preconditioning. This may include the activation of the HIF pathway and the concomitant modification of gene expression, although other HIF-independent responses could be triggered by such redox-based signal. Further research in this area should take into account not only the intensity of the hypoxic stimulus and the cell type and context, but also the time frame of the stimuli and of ROS production and signaling.

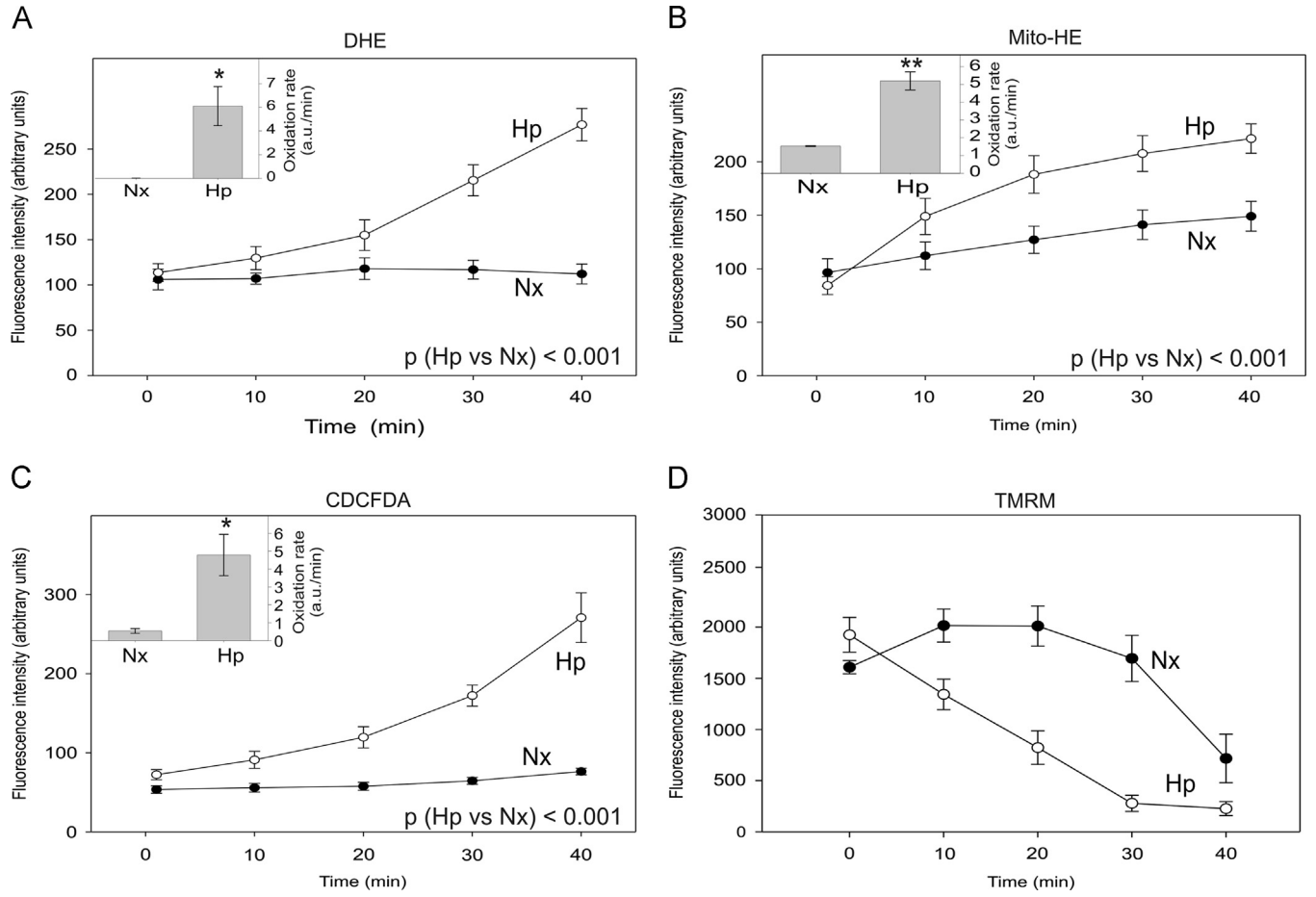

Fig. 10. Superoxide, ROS, and mitochondrial membrane potential measurement by fluorescence microscopy in live cardiomyocytes. Primary cardiomyocytes were treated and data obtained and plotted as in Fig. 8.

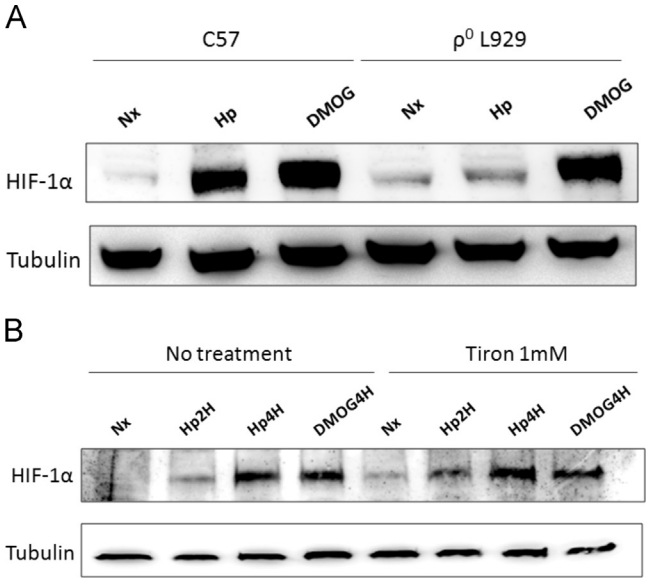

Fig. 11. Immunoblot analysis of HIF-1α in C57 and ρ^0L929 cells and endothelial cells untreated or treated with 1 mM Tiron. (A) C57 and ρ^0L929 cells were exposed for 6 h to normoxia (Nx), normoxia with 1 mM dimethyloxalylglycine (DMOG; a positive control for PHD inhibition and HIF-1α stabilization), or hypoxia (1% O_2, Hp). Proteins were extracted and blotted against HIF-1α protein. Representative image of five independent experiments. (B) BAECs were exposed for 4 h to normoxia (Nx), normoxia with 1 mM DMOG, or hypoxia for 2 (Hp2H) or 4 h (Hp4H). Proteins were extracted and blotted against HIF-1α protein. Representative image of three independent experiments.

Acknowledgments

We thank Lorena Vega Piris and Francisco Rodriguez Salvanés, from the Methodology Unit of the Instituto de Investigación Sanitaria Princesa (IP), for help with statistical analysis and helpful discussions and advice regarding statistics. We thank Dr. Mariusz Kowalewski (Institute of Veterinary Anatomy, UZH) for offering us the microscope to use in our live imaging studies. We thank Dr. José Antonio Enríquez (CNIC, Madrid, Spain), for kindly providing ρ^0 cells and their controls, and Dr. Luis del Peso (UAM, Madrid, Spain) and Dr. Francisco Sánchez-Madrid (IP) for their support. This research has been financed by the Spanish government Grants CSD2007-00020 (RosasNet, Consolider-Ingenio 2010 program; to S.L. and A.M.-R.), CP07/00143 (Miguel Servet program), PS09/00101 and PI12/00875 (to A.M.-R), and SAF2009-7520, SAF 2012-31338, and the "New Indigo" Partnership Program "Nitroxdiab" (PIM2010ENI-00631) (to S.L.); by Swiss National Science Foundation Grant 310030_124970/1 to A.B., by a travel grant from the Instituto de Investigación Sanitaria Princesa (to P.H.-A.); and by the COST actions TD0901 (HypoxiaNet) BM1005 (ENOG–European Network on Gasotransmitters) and BM1203 (EU-ROS). P.H.-A. is the recipient of an FPU fellowship from the Spanish government, and A. M.-R. is supported by the I3SNS program (ISCIII, Spanish government).

Appendix A. Supplementary material

Supplementary data associated with this article can be found in the online version at http://dx.doi.org/10.1016/j.freeradbiomed.2014.03.011.

References

[1] Semenza, G. L. Life with oxygen. *Science* **318:**62–64; 2007.
[2] Kaelin Jr W. G.; Ratcliffe, P. J. Oxygen sensing by metazoans: the central role of the HIF hydroxylase pathway. *Mol. Cell* **30:**393–402; 2008.
[3] Chandel, N. S.; Maltepe, E.; Goldwasser, E.; Mathieu, C. E.; Simon, M. C.; Schumacker, P. T. Mitochondrial reactive oxygen species trigger hypoxia-induced transcription. *Proc. Natl. Acad. Sci. USA* **95:**11715–11720; 1998.
[4] Archer, S. L.; Huang, J.; Henry, T.; Peterson, D.; Weir, E. K. A redox-based O_2 sensor in rat pulmonary vasculature. *Circ. Res.* **73:**1100–1112; 1993.
[5] Desireddi, J. R.; Farrow, K. N.; Marks, J. D.; Waypa, G. B.; Schumacker, P. T. Hypoxia increases ROS signaling and cytosolic $Ca(2+)$ in pulmonary artery smooth muscle cells of mouse lungs slices. *Antioxid. Redox Signaling* **12:**595–602; 2010.
[6] Yakushev, S.; Band, M.; Tissot van Patot, M. C.; Gassmann, M.; Avivi, A.; Bogdanova, A. Cross talk between S-nitrosylation and S-glutathionylation in control of the Na,K-ATPase regulation in hypoxic heart. *Am. J. Physiol. Heart Circ. Physiol.* **303:**H1332–H1343; 2012.
[7] Petrushanko, I. Y.; Yakushev, S.; Mitkevich, V. A.; Kamanina, Y. V.; Ziganshin, R. H.; Meng, X.; Anashkina, A. A.; Makhro, A.; Lopina, O. D.; Gassmann, M.; Makarov, A. A.; Bogdanova, A. S-glutathionylation of the Na,K-ATPase catalytic alpha subunit is a determinant of the enzyme redox sensitivity. *J. Biol. Chem.* **287:**32195–32205; 2012.
[8] Izquierdo-Álvarez, A.; Ramos, E.; Villanueva, J.; Hernansanz-Agustín, P.; Fernández-Rodríguez, R.; Tello, D.; Carrascal, M.; Martínez-Ruiz, A. Differential redox proteomics allows identification of proteins reversibly oxidized at cysteine residues in endothelial cells in response to acute hypoxia. *J. Proteomics* **75:**5449–5462; 2012.
[9] Guzy, R. D.; Hoyos, B.; Robin, E.; Chen, H.; Liu, L.; Mansfield, K. D.; Simon, M. C.; Hammerling, U.; Schumacker, P. T. Mitochondrial complex III is required for hypoxia-induced ROS production and cellular oxygen sensing. *Cell Metab.* **1:**401–408; 2005.
[10] Mansfield, K. D.; Guzy, R. D.; Pan, Y.; Young, R. M.; Cash, T. P.; Schumacker, P. T.; Simon, M. C. Mitochondrial dysfunction resulting from loss of cytochrome c impairs cellular oxygen sensing and hypoxic HIF-[alpha] activation. *Cell Metab.* **1:**393–399; 2005.
[11] Brunelle, J. K.; Bell, E. L.; Quesada, N. M.; Vercauteren, K.; Tiranti, V.; Zeviani, M.; Scarpulla, R. C.; Chandel, N. S. Oxygen sensing requires mitochondrial ROS but not oxidative phosphorylation. *Cell Metab.* **1:**409–414; 2005.
[12] Bell, E. L.; Emerling, B. M.; Ricoult, S. J.; Guarente, L. SirT3 suppresses hypoxia inducible factor 1alpha and tumor growth by inhibiting mitochondrial ROS production. *Oncogene* **30:**2986–2996; 2011.
[13] Guzy, R. D.; Schumacker, P. T. Oxygen sensing by mitochondria at complex III: the paradox of increased reactive oxygen species during hypoxia. *Exp. Physiol.* **91:**807–819; 2006.
[14] Hamanaka, R. B.; Chandel, N. S. Mitochondrial reactive oxygen species regulate hypoxic signaling. *Curr. Opin. Cell Biol.* **21:**894–899; 2009.
[15] Murphy, M. P. How mitochondria produce reactive oxygen species. *Biochem. J.* **417:**1–13; 2009.
[16] Vaux, E. C.; Metzen, E.; Yeates, K. M.; Ratcliffe, P. J. Regulation of hypoxia-inducible factor is preserved in the absence of a functioning mitochondrial respiratory chain. *Blood* **98:**296–302; 2001.
[17] Chua, Y. L.; Dufour, E.; Dassa, E. P.; Rustin, P.; Jacobs, H. T.; Taylor, C. T.; Hagen, T. Stabilization of hypoxia-inducible factor-1alpha protein in hypoxia occurs independently of mitochondrial reactive oxygen species production. *J. Biol. Chem.* **285:**31277–31284; 2010.
[18] Hagen, T. Oxygen versus reactive oxygen in the regulation of HIF-1alpha: the balance tips. *Biochem. Res. Int.* **2012:**436981; 2012.
[19] Schroedl, C.; McClintock, D. S.; Budinger, G. R. S.; Chandel, N. S. Hypoxic but not anoxic stabilization of HIF-1alpha requires mitochondrial reactive oxygen species. *Am. J. Physiol. Lung Cell. Mol. Physiol.* **283:**L922–L931; 2002.
[20] Quintero, M.; Colombo, S. L.; Godfrey, A.; Moncada, S. Mitochondria as signaling organelles in the vascular endothelium. *Proc. Natl. Acad. Sci. USA* **103:**5379–5384; 2006.
[21] Robin, E.; Guzy, R. D.; Loor, G.; Iwase, H.; Waypa, G. B.; Marks, J. D.; Hoek, T. L. V.; Schumacker, P. T. Oxidant stress during simulated ischemia primes cardiomyocytes for cell death during reperfusion. *J. Biol. Chem.* **282:**19133–-19143; 2007.
[22] Iwase, H.; Robin, E.; Guzy, R. D.; Mungai, P. T.; Vanden Hoek, T. L.; Chandel, N. S.; Levraut, J.; Schumacker, P. T. Nitric oxide during ischemia attenuates oxidant stress and cell death during ischemia and reperfusion in cardiomyocytes. *Free Radic. Biol. Med.* **43:**590–599; 2007.
[23] Waypa, G. B.; Marks, J. D.; Guzy, R.; Mungai, P. T.; Schriewer, J.; Dokic, D.; Schumacker, P. T. Hypoxia triggers subcellular compartmental redox signaling in vascular smooth muscle cells. *Circ. Res.* **106:**526–535; 2010.
[24] Schumacker, P. T. Lung cell hypoxia: role of mitochondrial reactive oxygen species signaling in triggering responses. *Proc. Am. Thorac. Soc.* **8:**477–484; 2011.
[25] Yang, W.; Block, E. R. Effect of hypoxia and reoxygenation on the formation and release of reactive oxygen species by porcine pulmonary artery endothelial cells. *J. Cell. Physiol.* **164:**414–423; 1995.
[26] Navarro-Antolín, J.; Rey-Campos, J.; Lamas, S. Transcriptional induction of endothelial nitric oxide gene by cyclosporine A: a role for activator protein-1. *J. Biol. Chem.* **275:**3075–3080; 2000.
[27] Moreno-Loshuertos, R.; Acín-Pérez, R.; Fernández-Silva, P.; Movilla, N.; Pérez-Martos, A.; Rodríguez de Córdoba, S.; Gallardo, M. E.; Enríquez, J. A. Differences in reactive oxygen species production explain the phenotypes associated with common mouse mitochondrial DNA variants. *Nat. Genet.* **38:**1261–1268; 2006.
[28] Rothen-Rutishauser, B. M.; Ehler, E.; Perriard, E.; Messerli, J. M.; Perriard, J. C. Different behaviour of the non-sarcomeric cytoskeleton in neonatal and adult rat cardiomyocytes. *J. Mol. Cell. Cardiol.* **30:**19–31; 1998.
[29] Armitage, P.; Berry, G.; Matthews, J. *Statistical Methods in Medical Research*. Oxford: Blackwell Sci.; 2002.
[30] Hardin, J. W.; Hilbe, J. M. *Generalized Estimating Equations*. Boca Raton, FL: Chapman & Hall/CRC Press; 2002.
[31] Turrens, J. F. Mitochondrial formation of reactive oxygen species. *J. Physiol.* **552:**335–344; 2003.
[32] Edgell, C. J.; McDonald, C. C.; Graham, J. B. Permanent cell line expressing human factor VIII-related antigen established by hybridization. *Proc. Natl. Acad. Sci. USA* **80:**3734–3737; 1983.
[33] Zhao, H.; Joseph, J.; Fales, H. M.; Sokoloski, E. A.; Levine, R. L.; Vasquez-Vivar, J.; Kalyanaraman, B. Detection and characterization of the product of hydroethidine and intracellular superoxide by HPLC and limitations of fluorescence. *Proc. Natl. Acad. Sci. USA* **102:**5727–5732; 2005.
[34] Redondo-Horcajo, M.; Romero, N.; Martínez-Acedo, P.; Martínez-Ruiz, A.; Quijano, C.; Lourenço, C. F.; Movilla, N.; Enríquez, J. A.; Rodríguez-Pascual, F.; Rial, E.; Radi, R.; Vázquez, J.; Lamas, S. Cyclosporine A-induced nitration of tyrosine 34 MnSOD in endothelial cells: role of mitochondrial superoxide. *Cardiovasc. Res.* **87:**356–365; 2010.
[35] Kalyanaraman, B.; Darley-Usmar, V.; Davies, K. J.; Dennery, P. A.; Forman, H. J.; Grisham, M. B.; Mann, G. E.; Moore, K.; Roberts 2nd L. J.; Ischiropoulos, H. Measuring reactive oxygen and nitrogen species with fluorescent probes: challenges and limitations. *Free Radic. Biol. Med.* **52:**1–6; 2012.
[36] Calvani, M.; Comito, G.; Giannoni, E.; Chiarugi, P. Time-dependent stabilization of hypoxia inducible factor-1alpha by different intracellular sources of reactive oxygen species. *PLoS One* **7:**e38388; 2012.
[37] Nijtmans, L. G.; de Jong, L.; Artal Sanz, M.; Coates, P. J.; Berden, J. A.; Back, J. W.; Muijsers, A. O.; van der Spek, H.; Grivell, L. A. Prohibitins act as a membrane-bound chaperone for the stabilization of mitochondrial proteins. *EMBO J.* **19:**2444–2451; 2000.
[38] Perry, S. W.; Norman, J. P.; Barbieri, J.; Brown, E. B.; Gelbard, H. A. Mitochondrial membrane potential probes and the proton gradient: a practical usage guide. *Biotechniques* **50:**98–115; 2011.
[39] Becker, L. B.; vanden Hoek, T. L.; Shao, Z. H.; Li, C. Q.; Schumacker, P. T. Generation of superoxide in cardiomyocytes during ischemia before reperfusion. *Am. J. Physiol.* **277:**H2240–H2246; 1999.

JOURNAL OF PROTEOMICS 75 (2012) 5449–5462

Available online at www.sciencedirect.com

SciVerse ScienceDirect

www.elsevier.com/locate/jprot

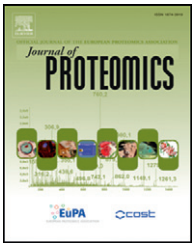

Differential redox proteomics allows identification of proteins reversibly oxidized at cysteine residues in endothelial cells in response to acute hypoxia

Alicia Izquierdo-Álvarez[a], *Elena Ramos*[a], *Joan Villanueva*[b], *Pablo Hernansanz-Agustín*[a], *Rubén Fernández-Rodríguez*[a,1], *Daniel Tello*[a], *Montserrat Carrascal*[b], *Antonio Martínez-Ruiz*[a,*]

[a]*Servicio de Inmunología, Hospital Universitario de La Princesa, Instituto de Investigación Sanitaria Princesa (IP), C/Diego de León 62, E-28006 Madrid, Spain*

[b]*Laboratorio de Proteómica-CSIC/UAB, IIBB-CSIC, IDIBAPS, C/Rosellón 161, 6a planta, E-08036 Barcelona, Spain*

ARTICLE INFO

Article history:
Received 10 January 2012
Accepted 26 June 2012
Available online 16 July 2012

Keywords:
Post-translational modifications
Cysteine oxidation
Thiol redox proteomics
Redox fluorescence switch (RFS)
Two-dimensional electrophoresis (2-DE)
Cell signaling

ABSTRACT

Adaptation to decreased oxygen availability (hypoxia) is crucial for proper cell function and survival. In metazoans, this is partly achieved through gene transcriptional responses mediated by hypoxia-inducible factors (HIFs). There is abundant evidence that production of reactive oxygen species (ROS) increases during hypoxia, which contributes to the activation of the HIF pathway. In addition to altering the cellular redox balance, leading to oxidative stress, ROS can transduce signals by reversibly modifying the redox state of cysteine residues in certain proteins. Using the "redox fluorescence switch" (RFS), a thiol redox proteomic technique that fluorescently labels reversibly oxidized cysteines, we analyzed endothelial cells subjected to acute hypoxia and subsequent reoxygenation. We observed a general increase in cysteine oxidation during hypoxia, which was reversed by reoxygenation, and two-dimensional electrophoresis revealed the differential oxidation of specific proteins. Using complementary derivatization techniques, we confirmed the modification of individual target proteins and identified specific cysteine residues that were oxidized in hypoxic conditions, thereby overcoming several limitations associated with fluorescence derivatization. These findings provide an important basis for future studies of the role of these modifications in HIF activation and in other acute adaptive responses to hypoxia.

Abbreviations: CAM, carboxyamidomethylation; FDR, false discovery rate; Grp78, 78 kDa glucose-regulated protein; HIF, hypoxia-inducible factor; Hsc70, Heat shock cognate 71 kDa protein; Hsp, heat shock protein; HUVEC, human umbilical vein endothelial cells; LDH, lactate dehydrogenase; NEM, N-ethylmaleimide; OPTM, oxidative post-translational modifications; PHD, HIF prolyl hydroxylase; RFS, redox fluorescence switch; RT, room temperature.

* *Corresponding author at:* Servicio de Inmunología, Hospital Universitario de La Princesa, C/Diego de León 62, E-28006 Madrid, Spain. Tel.: +34 915202371; fax: +34 915202374.
E-mail address: amartinezr.hlpr@salud.madrid.org (A. Martínez-Ruiz).
[1] Present address: Centro Pfizer-Universidad de Granada-Junta de Andalucía de Genómica e Investigación Oncológica (GENYO), Av. Ilustración 114, E-18,007 Granada, Spain.

1874-3919/$ – see front matter © 2012 Elsevier B.V. All rights reserved.
doi:10.1016/j.jprot.2012.06.035

1. Introduction

Reactive oxygen species (ROS) are produced as a consequence of cellular activity and they can induce modifications that damage DNA, lipids and proteins. These alterations are usually associated with oxidative stress, whereby ROS production exceeds the reduction capacity of the cell's antioxidant systems [1]. However, ROS are also involved in physiological cell signaling processes in which adequate antioxidant activities are sustained [2,3].

Due to their reactivity, cysteine residues are key targets of a variety of oxidative post-translational modifications (OPTM). Irreversible modifications such as sulfonic acid (–SO_3H) formation are associated with oxidative stress, while reversible oxidative modifications are thought to act as redox sensors in molecular cell signaling pathways [2,4–8]. These reversible OPTMs include sulfenic acid (–SOH) formation, S-nitrosylation (formation of a nitrosothiol, R-SNO) and the formation of disulfide bonds between protein cysteines (intra- or interchain disulfides) or between protein cysteines and low molecular mass thiols, such as glutathione (S-glutathionylation) [9,10].

There are several methods to identify proteins that are reversibly oxidized at cysteine residues, collectively known as the "thiol redox proteome". These approaches are mainly based on derivatization techniques coupled to either gel-based separation of labeled proteins or LC-based peptide separation (for recent reviews, see [11–15]). Recently developed fluorescent derivatization methods can be used in conjunction with gel separation, and they represent relatively accessible and affordable techniques to process a large number of samples, which have proved effective in analyzing these modifications. However, to date this technique has mainly been used to identify proteins that are oxidized in models of oxidative stress (provoked by adding reagents such as diamide or H_2O_2), and not in physiological conditions in which OPTM may participate in cell signaling [15]. Moreover, this approach suffers from several technical limitations, including difficulties in identifying the residues modified [15].

Cells and living organisms have developed several systems to sense oxygen (O_2) availability, allowing them to activate specific adaptive responses in hypoxic conditions. Examples include the activation of the angiogenic response through VEGF overexpression, and the induction of metabolic rearrangements to activate glycolysis and reduce oxidative phosphorylation, thereby limiting oxygen consumption [16,17]. In metazoans, many of these responses are mediated by transcriptional programs activated by a set of hypoxia-inducible factors (HIFs), transcription factors that modulate the expression of a large number of genes and whose stability is controlled mainly by a family of specific HIF prolyl hydroxylases (PHDs) that behave as monooxygenases, using O_2 as substrate [18,19].

Despite much debate in recent years, there is abundant evidence that ROS production augments in hypoxic cells and that mitochondria are the main source of these ROS. Indeed, this increase in ROS production has been implicated in the activation of the HIF pathway (reviewed in [20–22]). Increased protein cysteine oxidation has been linked with the production of ROS in hypoxia, as shown with distinct fluorescent sensors in different cell types [23–25], including pulmonary artery endothelial cells [26]. As the identity of the proteins directly oxidized in hypoxia remains unknown, the use of thiol redox proteomics methods with sufficient sensitivity to detect differential oxidation may help identify them.

Here, we describe the use of a "redox fluorescence switch" (RFS) to reversibly label oxidized cysteines with a fluorophore that can subsequently be detected after two-dimensional electrophoresis (2-DE) separation. We used this differential thiol redox proteomics technique to evaluate cysteine oxidation in endothelial cells during the acute response to hypoxia. This is a physiological state in which ROS production does not induce oxidative stress but contributes to cell signaling. We identified a number of reversibly oxidized proteins that may mediate physiological responses to hypoxia, either by signaling via the HIF-induced response pathway or by promoting acute adaptive responses to oxygen deprivation. The use of complementary "switch" techniques allowed us to confirm the modification of individual proteins and to overcome some of the limitations of current methods in identifying the residues that are specifically modified in hypoxia.

2. Experimental procedures

2.1. Cell culture, treatment and extraction

EA.hy926 cells (kindly provided by Dr Cora-Jean S. Edgell, UNC, NC, USA) were cultured at 37 °C in DMEM supplemented with HAT, 10% heat-inactivated fetal calf serum, 100 U/mL penicillin and 100 μg/mL streptomycin, in an atmosphere of 5% CO_2.

Human umbilical vein endothelial cells (HUVEC) were isolated as described previously [27] and cultured on gelatin-coated plates at 37 °C in medium 199 supplemented with 20% heat-inactivated fetal calf serum, 100 U/mL penicillin, 100 μg/mL streptomycin and 0.5 mg/ml ECGF, in an atmosphere of 5% CO_2.

Hypoxia was induced for 2 h in an Invivo2 200 workstation (Ruskinn) set at 0.5% O_2, 5% CO_2 and 37 °C. Cells were introduced into the workstation, washed with pre-hypoxic physiological serum, and pre-hypoxic medium was added prior to treatment. After induction of hypoxia, some cells were reoxygenated for 30 min.

After treatment, the cells were washed twice with physiological serum and protein extracts were obtained by incubating at room temperature (RT) for 10 min in TENT buffer (50 mM Tris pH 7.5, 1 mM EDTA, 100 μM neocuproine, 1% Triton X-100) with protease inhibitors and 50 mM iodoacetamide. The cell debris was removed by centrifugation and 2% SDS was added to the supernatant, which was incubated for an additional 30 min at 37 °C to block free thiols. Samples were aliquoted and frozen at −80 °C, and the protein concentration was estimated by the BCA assay (Pierce). Hypoxic samples were obtained inside the workstation.

2.2. Redox fluorescence switch

Protein extracts (400 μg) were precipitated with acetone, resuspended in 800 μl of TENS buffer (50 mM Tris pH 7.5, 1 mM EDTA, 100 μM neocuproine, 1% SDS) with 2.5 mM DTT and incubated for 10 min at RT. Samples were again precipitated with acetone, resuspended in 800 μl of TENS buffer with 40 μM BODIPY FL N-(2-aminoethyl)maleimide (Invitrogen) and

incubated for 30 min at 37 °C. The fluorophore reaction was stopped by adding 2.5 mM DTT. After precipitating again with acetone, the samples were resuspended in the corresponding buffer. For analytical experiments (SDS-PAGE) the quantities were downscaled to 25 or 50 μg of protein.

2.3. Protein electrophoresis and fluorescence detection

For SDS-PAGE the samples were resuspended in non-reducing SDS loading buffer and they were then separated on 10% acrylamide gels using standard protocols.

For 2-DE, samples were resuspended in 300 μl of rehydration buffer (7 M urea, 2 M thiourea, 4% CHAPS, bromophenol blue) with 1% of the corresponding ampholytes, 2% DTT and Destreak, and they were applied to dry IPG 17 cm strips pH 4–7 L for overnight reswelling. Isoelectric focusing was performed at a maximum of 50 mA per IPG strip in the Protein IEF cell (Bio-Rad), starting at 250 V and progressively increasing the voltage to 10,000 V. After focusing the strips for at least 60,000 Vh, they were incubated for 10 min with equilibration buffer (50 mM Tris–HCl pH 8.8, 6 M urea, 30% glycerol and 2% SDS) plus 2% DTT, and with 2.5% iodoacetamide for a further 10 min. The second dimension was run on 10% SDS-PAGE gels. After imaging the BODIPY-FL fluorescence (see below), total protein staining was performed with SYPRO Ruby (Invitrogen), following the manufacturers' instructions. The images of the different fluorophores were obtained using a Kodak Image Station 4000MM with excitation/emission filters set at 470/535 nm for BODIPY-FL and 430/600 nm for SYPRO Ruby.

2.4. Gel analysis

Images were analyzed with PDQuest 2-D gel analysis software. An initial analysis was performed using RFS images. Four biological replicates for each condition (normoxia, hypoxia, hypoxia with reoxygenation) were matched in a single gel set and quantified, and spots were selected when the fluorescence signal was at least two-fold higher in hypoxic versus normoxic conditions in at least two replicates. For several spots, no signal was detected in the normoxic conditions, or it was much lower than in hypoxia. A quantitative analysis was performed on the remaining spots, calculating the mean hypoxia:normoxia ratio in each experiment, and significant differences were determined using a repeated measures ANOVA test.

Images of the total protein signal for each gel were matched in a separate gel set and quantified. The spots selected from the RFS analysis were manually matched to their corresponding total protein signal spots, and only those where the amount of total protein remained constant were finally selected for identification.

2.5. In-gel protein digestion and sample preparation

Spots of interest were excised manually from SYPRO Ruby-stained gels, deposited in 96-well plates and processed automatically in a Proteineer DP (Bruker Daltonics, Bremen, Germany). A digestion protocol described previously was used [28], with minor variations. The gel plugs were first washed with 50 mM ammonium bicarbonate and then with acetonitrile (ACN), prior to reduction with 10 mM DTT in 25 mM ammonium bicarbonate solution. Alkylation was carried out with 55 mM iodoacetamide in 50 mM ammonium bicarbonate solution, after which the gel pieces were rinsed with 50 mM ammonium bicarbonate and then ACN, before they were dried under a stream of nitrogen. Modified porcine trypsin (sequencing grade; Promega, Madison WI) was added at a final concentration of 16 ng/μl in a 50 mM ammonium bicarbonate solution with 25% ACN and the protein was digested at 37 °C for 6 h. The reaction was stopped by adding 0.5% TFA to extract the peptides. The tryptic peptides eluted were dried by speed-vacuum centrifugation and resuspended in 4 μl of MALDI solution (33% 2-propanol, 16.7% ACN and 0.5% TFA). A 0.8 μl aliquot of each peptide mixture was deposited onto a 386 well OptiTOF™ Plate (Applied Biosystems, Framingham, MA, USA) and dried at RT. A 0.8 μl aliquot of the matrix solution (3 mg/mL CHCA in MALDI solution) was then deposited onto the dried digest and the mixture was again dried at RT.

2.6. MALDI peptide mass fingerprinting, MS/MS analysis and database searching

For MALDI-TOF/TOF analysis, samples were acquired automatically in an ABi 4800 MALDI TOF/TOF mass spectrometer (Applied Biosystems, Framingham, MA, USA) in positive ion reflector mode (the ion acceleration voltage was 25 kV to MS acquisition and 1 kV to MS/MS) and the spectra obtained were stored in the ABi 4000 Series Explorer Spot Set Manager. Peptide mass fingerprinting (PMF) and MS/MS fragment ion spectra were smoothed and corrected to the zero baseline using routines embedded in the ABi 4000 Series Explorer Software v3.6. Each PMF spectrum was internally calibrated using the mass signals of the trypsin autolysis ions in order to achieve a typical mass measurement accuracy of <25 ppm. Known trypsin and keratin mass signals were removed from the peak list, as were potential sodium and potassium adducts (+21 Da and +39 Da). GPS Explorer v4.9 was used to enter the combined PMF and MS/MS data into MASCOT software v.2.2.04 (Matrix Science, London, UK) to search the non-redundant Uniprot/SwissProt protein database (Uniprot/Swiss-Prot, release 57.15, 02-Mar-2010: 515,203 sequences, 181,334,896 residues), restricting the search to human proteins. The following search parameters were used: enzyme, trypsin; 1 allowed missed cleavage; carbamidomethyl cysteine as a fixed modification; oxidation of methionine as a variable modification; mass tolerance set to ±25 ppm for precursors and to ±0.3 Da for MS/MS fragment ions. The confidence interval for protein identification was set to ≥95% ($p<0.05$) and only peptides with an individual ion score above the identity threshold were considered to be correctly identified.

2.7. Redox biotin switch

For each sample, 250 μg of protein extracts blocked with IAM was precipitated with acetone, resuspended in 500 μl of TENS buffer with 2.5 mM DTT, and incubated for 10 min at RT. Samples were then precipitated with acetone, resuspended

in TENS buffer with 1 mM N-[6-(biotinamido)hexyl]-3′-(2′-pyridyldithio)propionamide (Biotin-HPDP, Pierce) and incubated for 1 h at RT. After further precipitation with acetone, the samples were resuspended in 500 μl neutralization buffer (20 mM HEPES pH 7.7, 100 mM NaCl, 1 mM EDTA, 0.5% Triton X-100). At this point an aliquot (50 μl) of each sample was separated as the input fraction, while the remaining sample was mixed with NeutrAvidin Plus UltraLink Resin (Pierce) pre-equilibrated with equilibration buffer (20 mM HEPES pH 7.7, 100 mM NaCl, 1 mM EDTA) and incubated for 1 h at RT. The resin was then washed three times with wash buffer (20 mM HEPES pH 7.7, 600 mM NaCl, 1 mM EDTA, 0.5% Triton X-100) and the retained proteins were incubated for 20 min at 37 °C with elution buffer (20 mM HEPES pH 7.7, 100 mM NaCl, 1 mM EDTA, 100 mM 2-mercaptoethanol). Eluted samples and 15 μl of the input fraction were analyzed in Western blots probed with antibodies against the following proteins: LDH-B (ProteinTech), Hsp90 (Santa Cruz Biotechnology), Hsc70,

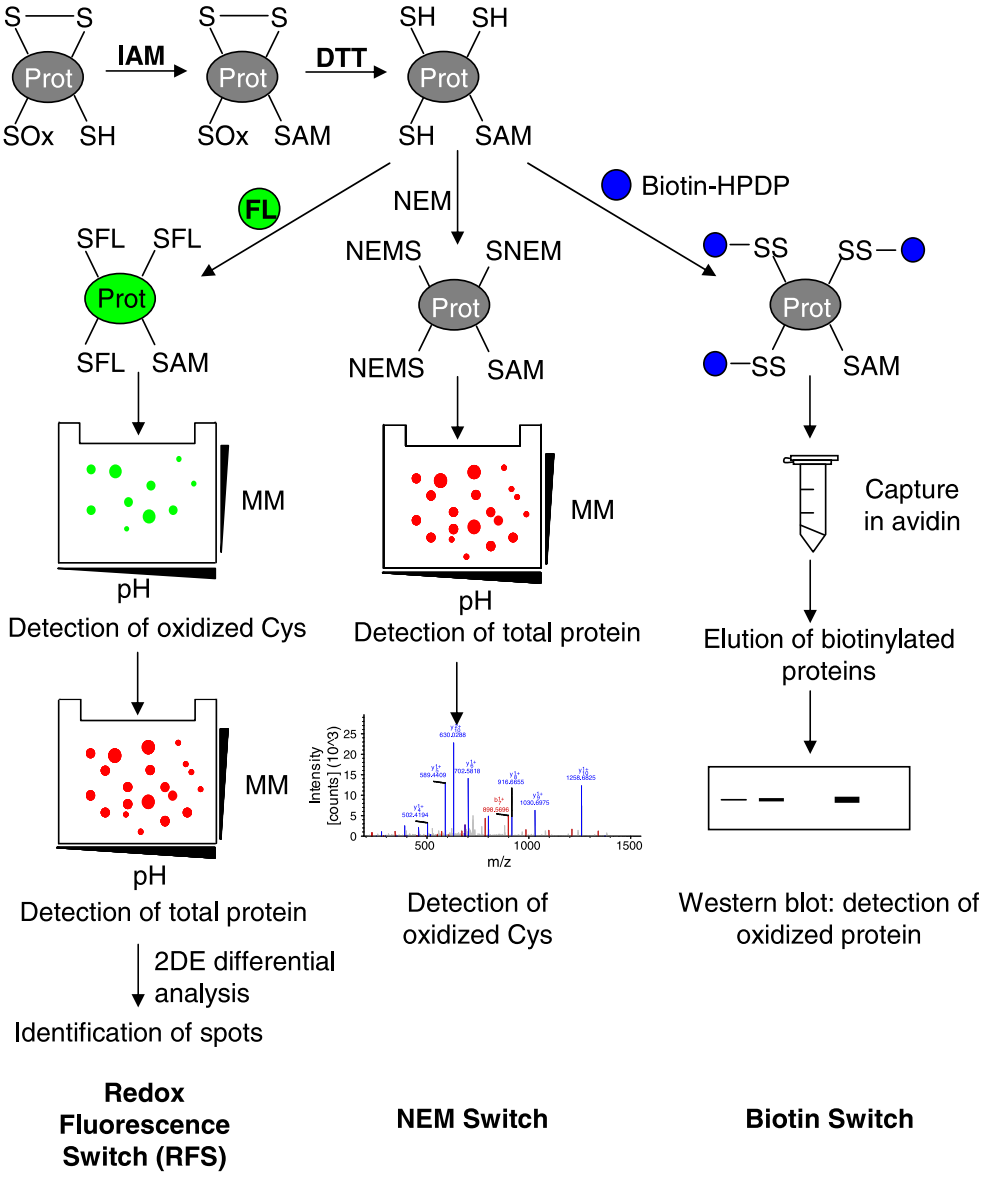

Fig. 1 – Schematic outline of the methodologies used. In all cases, reversibly oxidized protein thiols are switched for a labeled thiol. Two steps are common to all methods: reduced thiols are blocked by reaction with IAM and oxidized thiols are reduced with DTT. In RFS, fluorophore labeling was performed and oxidized cysteine residues were detected by 2-DE analysis. Total protein was detected by Sypro Ruby staining of the gel and differentially oxidized spots were selected by 2-DE differential analysis. In the NEM switch, newly reduced cysteine residues were labeled with NEM, the sample was separated by 2-DE and total protein was detected by Sypro Ruby staining. Previously selected spots were excised from the gel and NEM-derivatized cysteines were detected by LC–MS/MS. In the biotin switch, newly reduced cysteines were labeled with biotin-HPDP and captured with an avidin-conjugated resin. After elution, individual oxidized proteins were detected with specific antibodies.

(Abcam), CAPNS1 (Sigma-Aldrich), Tgm2 (Thermo Scientific) and PHD2 (Bethyl).

2.8. *Identification of oxidized cysteine residues (NEM switch)*

Samples from cells subjected to normoxia and hypoxia were processed in parallel to those subjected to RFS, employing a similar procedure but using 400 μM NEM instead of the fluorophore. After precipitation with acetone, the samples were separated by 2-DE. Images of the RFS samples were used as controls of oxidation and all gels were stained with SYPRO Ruby to detect total protein. The spots of interest were excised manually from the hypoxic sample and digested as described above.

LC–MS/MS analysis was performed with a linear LTQ-Velos linear ion trap apparatus equipped with a microESI ion source (ThermoFisher, San Jose, CA). Each extract was diluted to a final volume of 40 μL with 1% formic acid and the samples were loaded onto a chromatography system equipped with a C18 preconcentration cartridge (Agilent Technologies, Barcelona, Spain) connected to a 10 cm long, 150 μm i.d. Vydac C18 column (Vydac, IL, USA). Separation was performed at 1 μL/min in a 30 min acetonitrile gradient from 0 to 40% (solvent A: 0.1% formic acid, solvent B: acetonitrile plus 0.1% formic acid). The HPLC system consisted of an Agilent 1200 capillary pump, a binary pump and a thermostated microinjector.

The LTQ-Velos apparatus was operated in the positive ion mode with a spray voltage of 2 kV. The scan range of each full MS was m/z 400–2000, and the maximum ion times set for the MS and MS/MS experiments were 10 and 100 ms, respectively. Spectrometry was performed in a targeted mode, acquiring a full scan followed by a list of MS/MS experiments. Precursor ions for the MS/MS experiments were selected after in silico tryptic digestion of the target protein, using NEM and IAM as variable modifications for cysteine, and oxidation as a variable modification for methionine. The number of targeted MS/MS experiments per cycle was reduced to less than 25 transitions by excluding non-cysteine-containing peptides. In some cases peptides with missed cleavages or oxidized methionine were excluded.

The MS/MS fragmentation spectra were searched using Proteome Discoverer v1.3 (ThermoFisher, San Jose, CA) to identify NEM- and IAM-derived peptides. The following parameters were used in the database search: peptide mass tolerance, 2 Da; fragment tolerance, 0.8 Da; enzyme, trypsin; up to one missed cleavage permitted; dynamic modifications were CAM (+57 Da) and NEM (+125 Da) for cysteines and methionine oxidation (+16 Da). The database search used was limited to include only the targeted proteins identified in this study. The spectra were filtered using 1% FDR and all identifications were validated manually. NEM derivatives were confirmed by manual comparison of their MS/MS spectra with the corresponding CAM derivatives.

3. Results

We sought to determine whether exposure of endothelial cells to acute hypoxia and subsequent reoxygenation induced a global change in the oxidation state of protein cysteines. We used a "redox fluorescent switch" (RFS) method that tags reversibly oxidized cysteines with a fluorescent label, similar to the fluorescence switch approach that we previously used to study protein S-nitrosothiols [29]. This RFS method is based on three successive chemical steps (Fig. 1): i) blocking of free thiols; ii) reduction of oxidized cysteines with dithiothreitol (DTT); and iii) labeling of the newly-formed free thiols with a

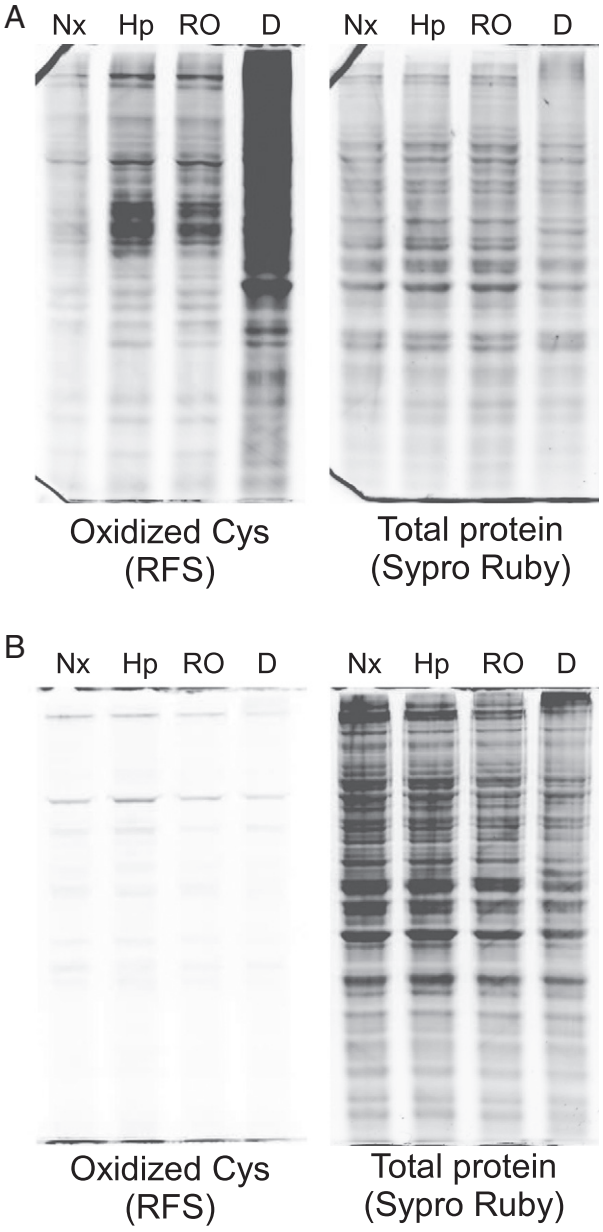

Fig. 2 – SDS-PAGE analysis of the general pattern of protein cysteine oxidation determined using the Redox Fluorescence Switch method. A) Endothelial cells were treated with 0.5% O_2 for 2 h (Hp), 0.5% O_2 for 2 h followed by 30 min of reoxygenation (RO), or 2 mM diamide for 10 min (D). Normoxic samples (Nx) were used as controls. B) Cells were treated as above and RFS was performed without DTT. The images are representative of at least four biological replicates.

fluorescent reagent [30–32]. As a positive control for this method we employed diamide, a general non-specific oxidant. We subjected EA.hy926 cells (an established model human endothelial cell line [33]) to acute hypoxia (2 h at 0.5% O_2), or to acute hypoxia followed by 30 min reoxygenation. HIFα subunits began to accumulate after 2 h in hypoxic conditions, although to a lesser degree than after longer treatments, indicating that the HIF-induced transcription program is not fully operative following such acute oxygen deprivation (Supplementary Fig. 1).

When the samples were resolved by SDS-PAGE (Fig. 2A), a moderate increase in cysteine oxidation was evident in response to hypoxia, which was more pronounced in specific bands and that differed from the general oxidation pattern produced by diamide. Moreover, this effect was partially reversed when cells were reoxygenated. Indeed, the fluorescence signal corresponding to oxidized cysteines was lost when DTT was omitted (Fig. 2B), showing the specificity of the technique.

To determine which proteins exhibit differential cysteine oxidation during acute hypoxia, we separated protein extracts subjected to RFS by two-dimensional electrophoresis. The strength of the signal from the derivatizing probe used in the RFS method, BODIPY-FL (green, upper panels in Fig. 3), provides a measure of the extent of cysteine oxidation. The RFS signal from cells subjected to hypoxia revealed an overall pattern similar to that seen in normoxic cells, although differences in a number of spots were observed. Most of these differences reflected an increase in oxidation during hypoxia, which was reversed upon reoxygenation (Fig. 4). Diamide treatment increased the number of spots and the intensity of many of these, consistent with the general cysteine oxidation induced by this reagent.

The Sypro Ruby signal (red, middle panels in Fig. 3) corresponds to the total protein in each spot and indicates that there were no significant differences between treatments. Merging of both signals (lower panels in Fig. 3) demonstrated a significant overlap of the signals corresponding to the same spots, which was due to the use of a neutral and relatively small probe for RFS, rather than a charged probe that displaces the spots of derivatized proteins [29]. As expected, the pattern for each signal differed given that only proteins bearing oxidized cysteines are derivatized, and these represent only a small fraction of the proteins in the cell extracts. A stronger similarity was observed between signal patterns after diamide treatment due to the relatively non-specific oxidation of protein cysteines induced by this agent.

Spots displaying differential cysteine oxidation were further analyzed with 2-DE-analysis software, comparing RFS signals in gels from four experimental replicates of the cell extracts maintained in normoxic and hypoxic conditions, or subjected to hypoxia–reoxygenation. Spots were selected when the signal in hypoxic conditions was at least 2-fold

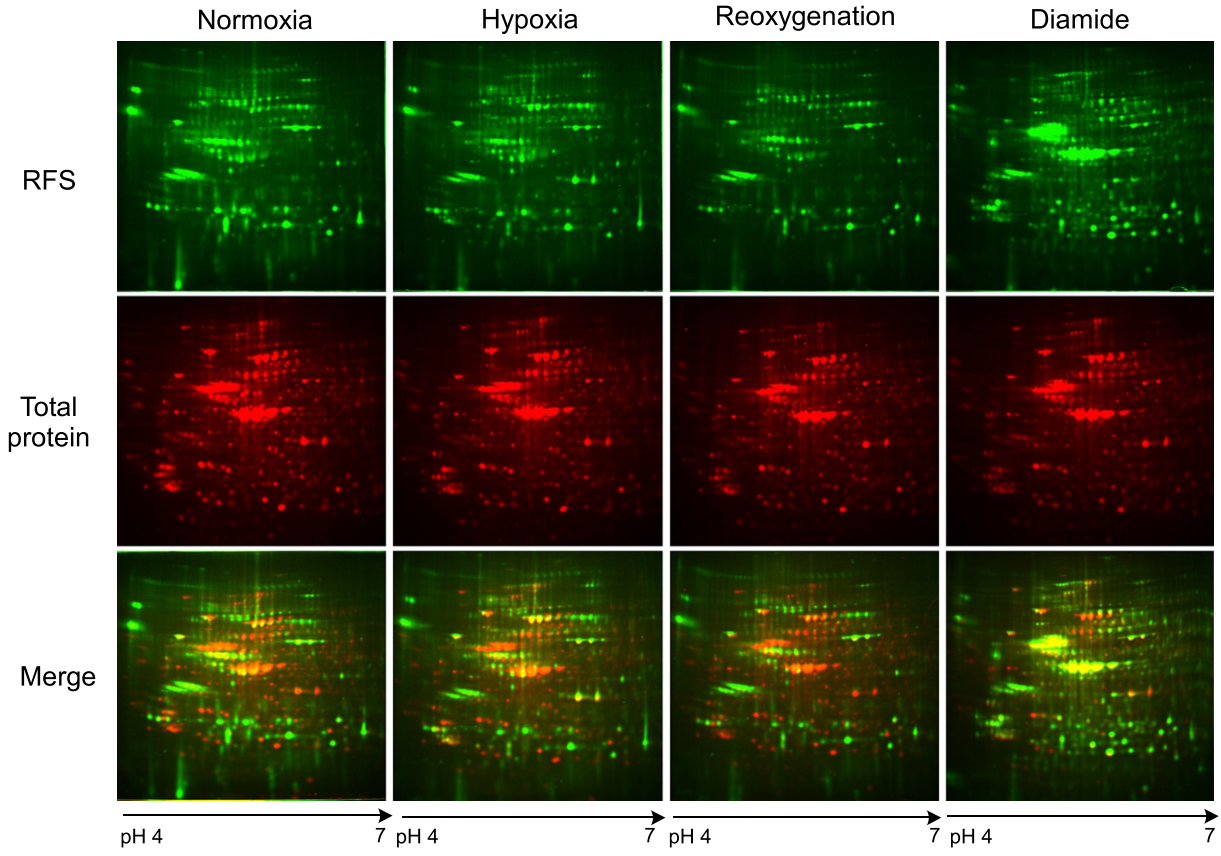

Fig. 3 – 2-DE analysis of oxidized cysteines labeled using the Redox Fluorescence Switch method. Endothelial cells were treated as in Fig. 2, loaded onto 17 cm IPG strips (pH 4–7L) and separated by 2-DE. Green signal corresponds to RFS, showing oxidized cysteines. Red signal corresponds to Sypro Ruby staining for total protein.

higher than in normoxia in at least two replicates. For some spots, qualitative difference was clear, as there was no RFS signal in the normoxia gel for some of the replicates or, when present, it was more than 7-fold smaller (Table 1). For other spots, the RFS spot was clear in most of the replicate gels of hypoxia samples, and a statistical analysis was performed (see Experimental procedures), selecting those spots with a p value of less than 0.05 (Table 1). The selected RFS spots were matched to the corresponding total protein spots in the same gels, ensuring that they displayed a constant total protein signal (Fig. 4). These spots were manually excised from the gels and digested, and the peptides obtained were analyzed by MALDI-TOF/TOF (Supplementary Fig. 2). Twelve different proteins were identified from these spots (Table 1) and although Hsp90α and Hsp90β were detected in the same spot, the remaining proteins were identified as single or multiple spots (Supplementary Fig. 2). In addition, 78 kDa glucose-regulate protein (Grp78), was identified from a RFS spot localized in three replicates of normoxia and hypoxia gels, with a mean ratio of 15.5±1.05, but with a p value of 0.08, thus considered to be non significant.

The oxidation of individual proteins was confirmed using a "redox biotin switch", in which oxidized cysteines were derivatized with a biotin moiety. Biotinylated proteins were then captured with an avidin resin, allowing individual proteins to be analyzed in Western blots (Fig. 1). Using extracts from endothelial cells subjected to the same treatments, this technique was employed to analyze cysteine oxidation in some of the proteins identified: lactate dehydrogenase B (LDH-B), heat shock protein 90 (Hsp90:), transglutaminase 2 (Tgm2) and Hsc70 (Fig. 5). These results confirmed the specific oxidation of these proteins in hypoxia, which was reversed after reoxygenation. Interestingly, the proteins behaved differently when the cells were challenged with diamide, and while oxidation of most of them increased, LDH-B remained in a reduced state. This observation supports the view that hypoxia promotes the oxidation of specific proteins that are not oxidized in other circumstances. Additionally, we included analysis of PHD2 oxydation, as it is the main protein controlling HIF-1α stability and its activity is inhibited by H_2O_2 [34,35]. However, we found that there is no differential oxidation between normoxia and hypoxia, further supporting that oxidation in hypoxia is limited to a particular set of proteins.

In order to confirm the results in primary endothelial cells, we subjected HUVEC cultures to the same treatments we had performed on EA.hy926 cells, obtaining similar results. RFS with SDS-PAGE showed that there is an increase in cysteine oxidation after acute hypoxia, reverted with reoxygenation (Fig. 6A). Redox biotin switch with Western blots against LDH B, Hsp90 and calpain small subunit 1 (CPNS1) showed also increased oxidation of these proteins in hypoxia (Fig. 6B). PHD2 oxidation was not affected in hypoxia and LDH B was not oxidized with diamide, confirming the results obtained with the cell line.

Tests with standards were performed and showed that peptides derivatized with BODIPY FL N-(2-aminoethyl)maleimide

Table 1 – Proteins differentially oxidized in endothelial cells subjected to hypoxia.

Uniprot ID	Protein definition	# of spots [a]				Mascot Score	Mascot expect.	MM (Da) theoretical	Theoretical pI	Matched peptides	% coverage
		Nx	Hp								
Qualitative analysis				**Minimal ratio [b]**							
CPNS1_HUMAN	Calpain small subunit 1	0	4			581	1.60E–54	28,469	5.05	12	45
SPSY_HUMAN	Spermine synthase	1	4	7.4		420	2.00E–38	41,698	4.87	9	24
HS105_HUMAN	Heat shock protein 105 kDa	0	3			596	5.10E–56	97,716	5.28	25	27
LDHB_HUMAN	L-lactate dehydrogenase B chain	0	4			567	4.00E–53	36,900	5.71	20	42
1433Z_HUMAN	14-3-3 protein zeta/delta	2	4	63		862	1.30E–82	27,899	4.73	24	70
1433T_HUMAN	14-3-3 protein theta	2	4	7.9		509	2.60E–47	28,032	4.68	18	42
1433B_HUMAN	14-3-3 protein beta/alpha	2	3	61		837	4.00E–80	28,179	4.76	26	74
Quantitative analysis				**Mean ratio [c]**	**p**						
HS90A_HUMAN [d]	Heat shock protein HSP 90-alpha	2	2	2.5±0.4	0.03	641	1.60E–60	85,006	4.94	28	36
HS90B_HUMAN [d]	Heat shock protein HSP 90-beta					433	1.00E–39	83,554	4.97	25	17
TGM2_HUMAN	Protein-glutamine gammaglutamyltransferase 2	2	3	7.2±2.4	0.04	907	4.00E–87	78,420	5.11	31	51
HSP7C_HUMAN	Heat shock cognate 71 kDa protein	4	4	3.1±1.3	0.04	1110	2.00E–107	71,082	5.37	35	49
ACTN4_HUMAN	Alpha-actinin-4	3	4	3.5±2.0	0.01	1010	2.00E–97	105,245	5.27	45	49

[a] Number of replicates in which the spot is detected. Nx, normoxia; Hp, hypoxia.
[b] Minimal value obtained for the ratio (RFS signal in Hp/RFS signal in Nx) of replicate(s) in which a spot was found in normoxia.
[c] Mean±standard deviation of the ratios (RFS signal in Hp/RFS signal in Nx) in individual experiments.
[d] Both proteins were identified in the same spot.

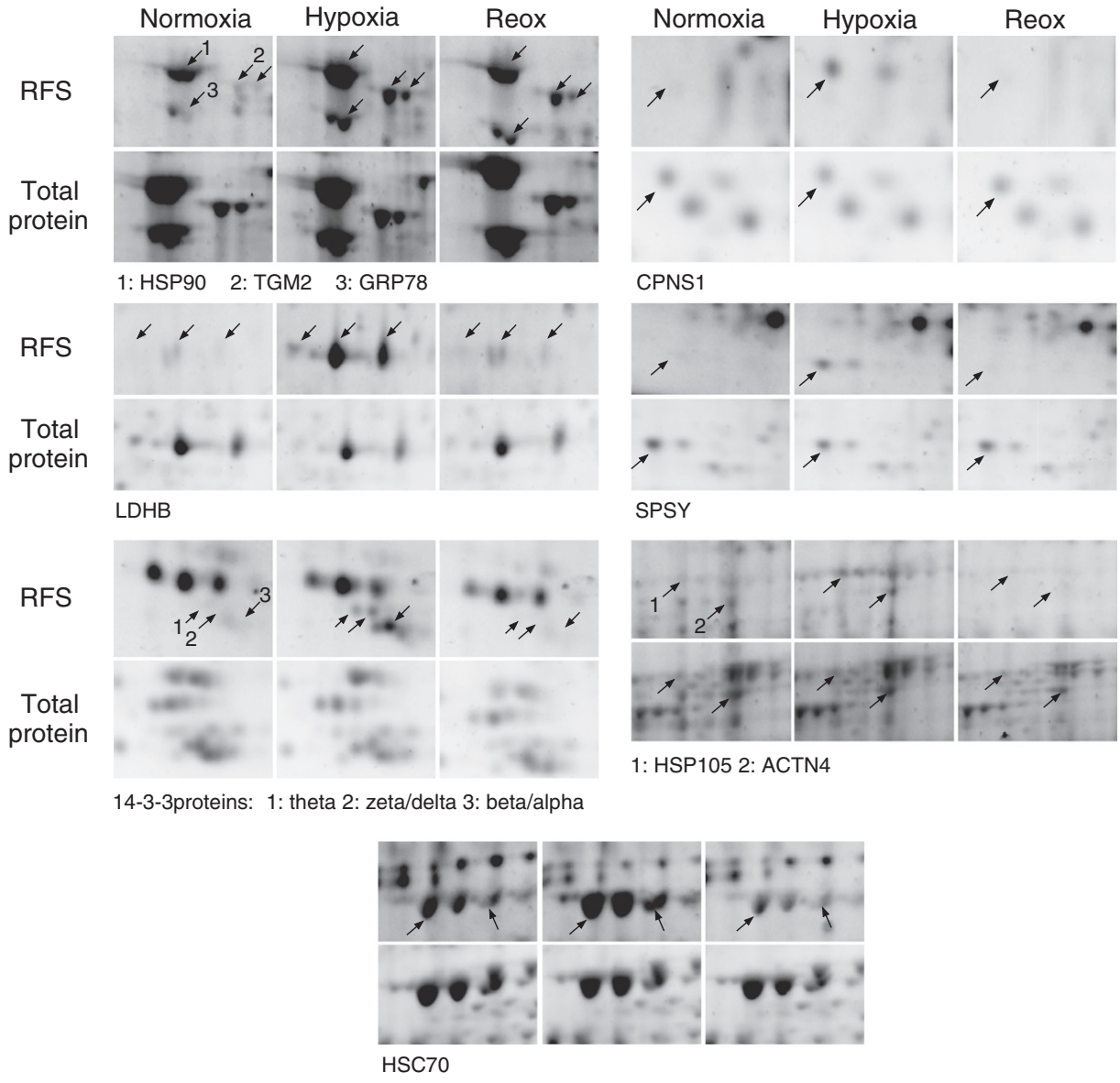

Fig. 4 – Detailed 2-DE images showing spots that were differentially oxidized in hypoxic conditions (labeled with arrows). Endothelial cells were treated as in Fig. 2, loaded onto 17 cm IPG strips (pH 4–7L) and separated by 2-DE. RFS detect oxidized cysteines, and total protein was stained with Sypro Ruby. Names of proteins are as in Table 1.

do not exhibit the same MS/MS fragmentation pattern as underivatized peptides (data not shown). The LC–IT-MS/MS spectra of BODIPY derivatives did not display the classic pattern of sequential b and y fragments, and they were largely dominated by a neutral loss of one or two HF (hydrogen fluoride) units [36]. As a result, the LC–IT-MS/MS spectra of peptides derivatized with BODIPY FL N-(2-aminoethyl)maleimide contained little structural information regarding the peptide. Therefore, RFS derivatized proteins could not be analyzed in LC–IT-MS/MS experiments to identify the cysteine residues modified.

To overcome this problem, we used a different "redox switch" procedure designed to more accurately identify cysteine residues after peptide fragmentation analysis by MS/MS, a procedure similar to that previously used to analyze individual reversibly oxidized proteins [37]. Accordingly, oxidized cysteines were labeled with N-ethylmaleimide (NEM), a reagent compatible with peptide sequencing by MS/MS (Fig. 1). As NEM derivatives cannot be monitored by fluorescence, the same samples were also subjected to RFS, and both derivatized extracts were analyzed in parallel 2-DE gels. We excised the spots that were differentially oxidized in the RFS samples from the hypoxic NEM gels. The identity of the proteins was confirmed by MALDI-TOF/TOF, and the tryptic extracts were subjected to targeted LC–MS/MS to detect and sequence NEM-derivatized peptides. A total of eight peptides were positively identified as NEM derivatives and from these, five oxidized cysteines were identified in five distinct proteins (Table 2). The peptides with NEM-derivatized cysteines were further validated by a more detailed comparison of the mass spectra with the CAM-derivatized homologue (Fig. 7 and Supplementary Fig. 3). Remarkably, all five cysteines detected as NEM derivatives were also detected as CAM derivatives

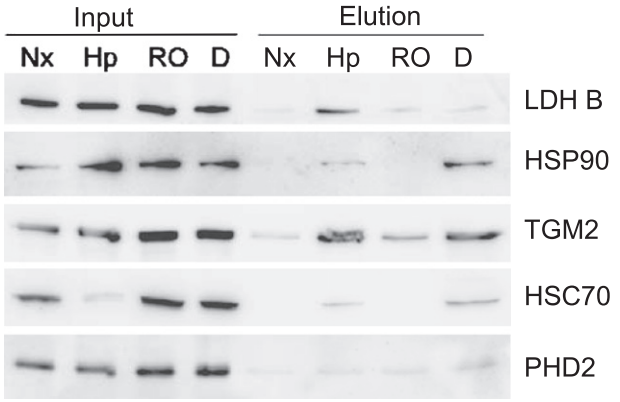

Fig. 5 – Redox biotin switch showing oxidation of individual proteins. Endothelial cells were treated with 0.5% O_2 for 2 h (Hp), 0.5% O_2 for 2 h followed by 30 min of reoxygenation (RO), or 2 mM diamide for 10 min (D). Normoxic samples (Nx) were used as controls. After the redox biotin switch, an aliquot was separated (input) and after avidin purification, the eluted samples and the input samples were analyzed in Western blots with antibodies for the indicated proteins. The images are representative of at least three biological replicates.

(Table 2), indicating the coexistence of oxidized and reduced forms of these five proteins, consistent with the potential role of reversible cysteine oxidation in signal transduction.

4. Discussion

We have developed a proteomic method using fluorescence derivatization and electrophoresis to analyze reversible oxidative cysteine modifications, which we have named "redox fluorescence switch" (RFS). Negative and positive controls demonstrated the validity of this method in detecting such modifications: a low background signal was detected when DTT was omitted from the reaction, while the signal was clearly enhanced in cells treated with diamide, a powerful cysteine oxidant.

When coupled with SDS-PAGE, the RFS technique allowed us to compare protein thiol oxidation in several samples, demonstrating its utility to screen the global protein thiol status in different physiological or cell conditions. We used this approach to evaluate the global oxidation in endothelial cells subjected to acute hypoxia (2 h at 0.5% O_2). In these conditions, we observed an increase in protein cysteine oxidation, which was partially lost when the cells were reoxygenated with ambient air. This result is consistent with recent studies using novel protein fluorescent sensors that respond specifically to cysteine oxidation, such as HSP-FRET and RoGFP, in which acute hypoxia (either hypoxia alone or hypoxic ischemia) increased cysteine oxidation in cultured cells, an effect that was reversed by reoxygenation [24,38,39]. However, our method is a global detection method to study endogenous protein cysteine oxidation rather than one using specific proteins that act as specialized probes, as in these earlier studies.

By coupling RFS to 2-DE, we analyzed differential cysteine oxidation in individual protein spots, identifying the proteins that were further oxidized in hypoxic conditions. This approach offers two novel advantages over a previously described method used to detect S-nitrosylated proteins [29]: i) the use of BODIPY-FL as the labeling fluorophore increases the accuracy with which cysteine oxidation and the total protein signals from individual protein spots are matched; ii) the use of iodoacetamide as a blocking reagent, rather than maleimide, enhances IEF resolution and reduces horizontal streaking [15]. In expression proteomics, DIGE technology reduces gel-to-gel variation by running samples and standards labeled with different fluorophores in the same gel. However, when analyzing post-translational modifications, such as cysteine oxidation, differences in the oxidation signal of a spot may reflect a difference in the ratio of oxidized protein in that spot or alternatively, a difference in the amount protein. Thus, running each sample in a different gel allowed us to control for the

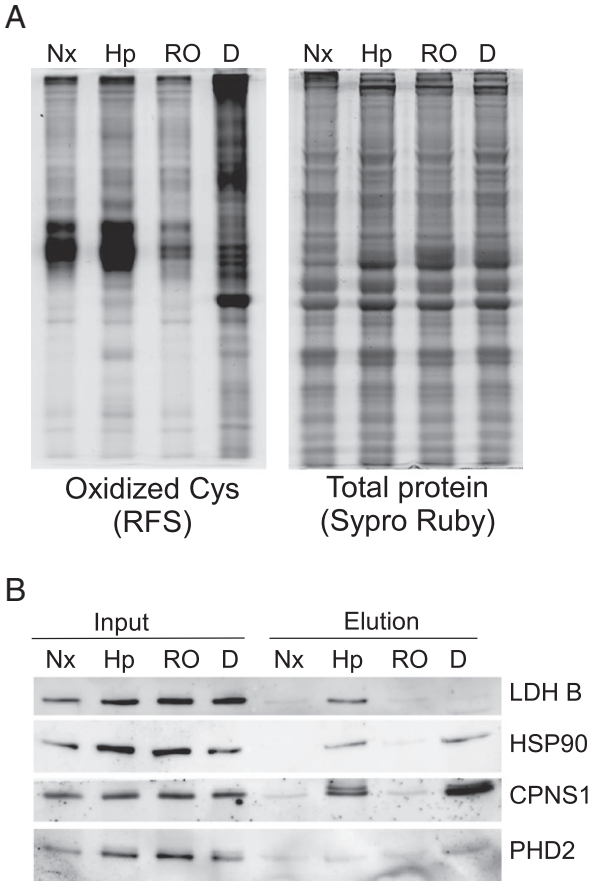

Fig. 6 – RFS and biotin switch analysis in primary endothelial cells. HUVEC were treated with 0.5% O_2 for 2 h (Hp), 0.5% O_2 for 2 h followed by 30 min of reoxygenation (RO), or 2 mM diamide for 10 min (D). Normoxic samples (Nx) were used as controls. A) SDS-PAGE showing RFS (oxidized cysteines) and Sypro Ruby (total protein) signals. B) Oxidation of individual proteins, showed by redox biotin switch and Western blot with antibodies for the indicated proteins, performed as in Fig. 5. The images are representative of at least three biological replicates.

Table 2 – List of NEM-derivatized peptides identified by targeted LC–MS/MS of spots corresponding to oxidized proteins. These NEM derivatives indicate the position of oxidized cysteines in the protein. In all cases we identified both the IAM and NEM derivatives of the same peptides, indicating the coexistence of both the reduced and oxidized forms of the protein.

Uniprot accession number	Uniprot ID	Protein length	Peptide identified	Cys residue number	Peptide modification	Charge	Precursor $[M+H]^+$	Number of spectra	Max. XCorr
P08238	HS90B_HUMAN	724	C*LELFSELAEDKENYK	412	NEM	2	2057.1	7	4.99
					IAM	2	1989.4	3	3.41
			C*LELFSELAEDK	412	NEM	2	1522.7	3	3.83
					IAM	2	1454.8	2	3.86
P63104	1433Z_HUMAN	245	DIC*NDVLSLLEK	94	NEM	2	743.5	4	3.84
P27348	1433T_HUMAN	245	SIC*TTVLELLDK	94	NEM	2	1458.3	2	2.26
					IAM	2	1390.7	11	3.82
P04632	CPNS1_HUMAN	268	YSDESGNmDFDNFISC*LVR	232	NEM	2	2352.1	2	3.29
					IAM	2	2283.9	14	5.04
			YSDESGNmDFDNFISC*LVRLDA MFRAFK	232	NEM	3	3416.4	1	2.48
P11142	HSP7C_HUMAN	646	ILDKC*NEIINWLDK	574	NEM	3	1840.2	2	3.59
					IAM	3	1771.9	2	2.76
			C*NEIINWLDK	574	NEM	2	1371.4	10	3.26
					IAM	2	1303.9	9	3.62

C* — cysteine derivatized with either NEM or IAM.
m — oxidized methionine.

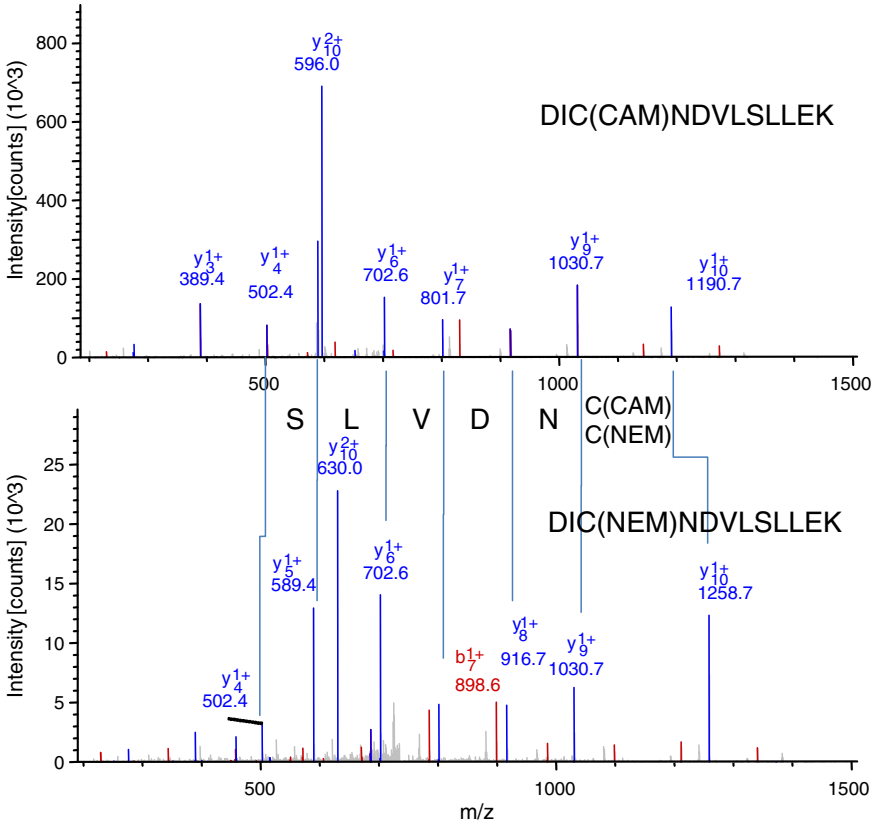

Fig. 7 – Comparison of MS/MS spectra from the CAM (top) and NEM (bottom) derivatized peptide sequence DIC*NDVLSLLEK (1433Z_HUMAN). Signals corresponding to the y sequence dominated both spectra. The m/z values interpreted as the fragments from y_3 to y_9 coincided in both spectra. However, the intense fragments corresponding to the derivatized cysteine (y^{1+}_{10} and y^{2+}_{10}) were shifted by 68 Da, a value that coincided with the expected mass difference between NEM (125 Da) and CAM (57 Da).

amount of protein (both RFS-labeled and unlabeled protein) in each protein spot.

Several studies seeking to establish a catalog of putative targets for cysteine oxidation have described proteins that are differentially oxidized after treating cells with strong oxidizing reagents such as diamide [30,32]. We used diamide as a positive control, while focusing on changes induced in more physiological contexts in which oxidative stress is not induced and where differential protein oxidation may modulate signal transduction pathways or produce specific adaptations. We identified several proteins that were oxidized in response to acute hypoxia (Table 1), demonstrating the validity of the RFS method for this type of analysis. Indeed, we observed LDH-B oxidation in response to hypoxia but not after diamide treatment, indicating that hypoxia may indeed induce a specific pattern of protein oxidation.

Using complementary derivatization techniques, we confirmed the validity of the RFS method and circumvented some of its limitations. The "redox biotin switch" allowed us to label oxidized cysteines with a biotin moiety and to subsequently purify the oxidized proteins. Using this approach, we confirmed the oxidation in hypoxia of several of the identified proteins, corroborating the results of the RFS approach. Interestingly, this finding demonstrates the specificity of thiol oxidation of LDH-B in hypoxia when compared with oxidation by diamide, consistent with a previous study that reported no alterations in LDH catalytic activity following diamide treatment [40].

Attempts to detect fluorophore-labeled peptides from spots on RFS 2-DE gels using either MALDI-TOF/TOF or ESI-MS/MS were unsuccessful, probably due to the chemical characteristics of the BODIPY-FL moiety. This problem was successfully resolved using an alternative methodology, whereby oxidized cysteines were labeled with NEM, which is a smaller reagent that does not interfere with MS detection. As proteins migrated to the same position in parallel 2-DE gels after both the RFS and the "NEM switch", we used this approach to identify oxidized Cys residues in the spots detected by RFS (Table 2). Our findings further confirm the utility of RFS, and provide important information regarding the oxidative modifications of these proteins and their putative functional relevance.

In the Supplementary Table 1 we have compiled structural and functional information on the proteins identified as oxidation targets in hypoxia. At least four of these proteins were previously shown to be functionally regulated by different thiol oxidative modifications (see Supplementary Table 1): Hsp90 [41,42], transglutaminase-2 [43–46], Hsc70 [47] and LDH-B [48,49]. As some of these proteins have been previously implicated in the hypoxia response, their functional modulation by oxidation may constitute an acute response mechanism contributing to HIF activation, or to early events independent of the HIF pathway.

PHD2 has a direct role in the response to hypoxia by promoting HIF-α degradation. It has been reported that H_2O_2 addition to cells stabilizes HIF-1α [34], and purified PHD2 treated with H_2O_2 has a decreased activity, an effect dependent on the presence of two cysteine residues [35]. Thus, ROS produced in hypoxia could oxidize these cysteine residues, which would contribute to PHD2 inhibition and HIF activation. However, we have not found differential oxidation under hypoxia conditions, arguing against a direct effect, at least in endothelial cells.

Hypoxia enhances the oxidation of three heat shock proteins. Hsp90 binds to and stabilizes HIF-α subunits, protecting them from degradation via the pVHL-independent RACK1-dependent pathway [50–52]. We previously reported that S-nitrosylation of Cys 597 inhibits Hsp90 activity [41] and here we observed a moderate increase in Hsp90 cysteine oxidation, although a different Cys residue was identified as the site of modification. Thus, the functional relevance of Hsp90 cysteine oxidation in HIF-α stabilization remains unclear. As the effects of Hsp90 on other proteins are inhibited in a ROS-dependent manner in hypoxic conditions, such as in the case of the hERG K^+ channel [53], the oxidation observed may be functionally related to specialized proteins not involved in the HIF pathway. Hsc70 is a member of the Hsp70 family, a type of chaperones for which a selective role in degrading HIF-1α but not HIF-2α has been described [54]. Since both HIFα subunits are expressed in endothelial cells, oxidation of this chaperone may be an influential event. In addition, Hsp105 has been reported to inhibit some activities of the Hsp70 family. More detailed studies of the relative oxidation of the individual Hsp proteins will be necessary to fully determine its functional consequences.

Calpain protease activity participates in the proteasome-independent cleavage of HIF-α subunits and increased calpain activity has been described following acute hypoxia [55,56]. We observed increased oxidation of a calpain regulatory subunit in acute hypoxia. Although this finding suggests that oxidation may regulate this pathway, the functional consequences of the modification of this specific subunit remain unknown.

Cell adaptation to hypoxia involves the inhibition of protein synthesis via mTOR inactivation. This process is mediated by activating the mTOR inhibitor, TSC1/2, which is normally inhibited by the binding of 14-3-3 proteins. Hypoxia induces REDD1 expression via HIF, and as REDD1 binds to and sequesters 14-3-3 from complexes with TSC2, TSC2 can inactivate mTOR [57–59]. Moreover, oxidation of 14-3-3 inhibits its interaction with other proteins [60]. It is therefore tempting to speculate that the acute oxidation of a conserved Cys residue in several 14-3-3 isoforms inhibits its binding to TSC2, anticipating the effect of a HIF-induced gene and advancing the inhibition of mTOR.

Similar acute effects may be hypothesized for lactate dehydrogenase B (LDH-B) oxidation in terms of the metabolic adaptation to hypoxia. LDH isoforms catalyze the conversion between pyruvate and lactate, linked with the NADH/NAD^+ redox pair. In hypoxia, activation of glycolysis and inhibition of NADH consumption via mitochondrial oxidative phosphorylation require an increased rate of pyruvate to lactate conversion and NAD^+ regeneration. This is achieved by the HIF-dependent induction of LDH-A [61,62], the gene encoding the LDH M chain (named after its strong expression in skeletal muscle), which favors the conversion of pyruvate to lactate [63]. By contrast, the H chain (highly expressed in heart) is better adapted to aerobic metabolism and favors the conversion of lactate to pyruvate [63]. While the catalytic centers are very similar, the amino acid composition of both chains produces variations in the pK_a of the catalytic histidine, which accounts for the differential activity [64]. Cys 164 of the H chain (LDH-B) has been historically described as a reactive cysteine. While enzyme inactivation

has been reported when this residue is modified (reviewed in [65]), more detailed studies using a small modifier, methyl methanethiosulfonate, demonstrated that such modification alters its catalytic activity, making it more similar to the M chain [48,49]. Reversible oxidation by small modifiers may thus provide a mechanism for acute regulation of LDH activity in hypoxia, before gene responses mediated by the HIF pathway are established, promoting the conversion of pyruvate to lactate.

5. Conclusions

We show here that RFS is a useful proteomic approach to detect reversible oxidation of cysteine residues in cells subjected to a physiological treatment that promotes ROS-induced cell signaling. Using complementary switch protocols, oxidation of individual proteins can be studied in greater detail, and oxidized cysteine residues can be identified. Cysteine oxidation of several proteins is enhanced in endothelial cells subjected to acute hypoxia, although these proteins do not necessarily coincide with those that are altered in response to a non-specific oxidant stimulus. The identification of some of these proteins provides an important basis for further studies into the functional impact of these modifications on the acute cell responses to hypoxia.

Supplementary data to this article can be found online at http://dx.doi.org/10.1016/j.jprot.2012.06.035.

Conflict of interest statement

The authors have no conflicts of interest to declare.

Acknowledgments

This study was supported by the following grants from the Spanish Government to A.M.-R.: CP07/00143 (Miguel Servet program), CSD2007-00020 (RosasNet, Consolider-Ingenio 2010 program) and PS09/00101. We thank Silvia Juárez and Sergio Ciordia from the Proteomics Facility (CNB-CSIC) and "ProteoRed-ISCIII" platform for their helpful technical support with the protein identification. We thank Lorena Vega Piris and Francisco Rodriguez Salvanés, from the Methodology Unit of the Instituto de Investigación Sanitaria Princesa, for help with statistical analysis. We also thank Drs Jesús Vázquez, Santiago Lamas, María José Calzada and Manuel O. Landázuri for helpful discussions of the results and the manuscript, and Mark Sefton (BiomedRed) for careful revision of the manuscript.

REFERENCES

[1] Sies H, Jones D. Oxidative stress. In: Fink G, editor. Encyclopedia of stress. New York: Academic Press; 2007. p. 45-8.
[2] D'Autreaux B, Toledano MB. ROS as signalling molecules: mechanisms that generate specificity in ROS homeostasis. Nat Rev Mol Cell Biol 2007;8:813-24.
[3] Hamanaka RB, Chandel NS. Mitochondrial reactive oxygen species regulate cellular signaling and dictate biological outcomes. Trends Biochem Sci 2010;35:505-13.
[4] Ying J, Clavreul N, Sethuraman M, Adachi T, Cohen RA. Thiol oxidation in signaling and response to stress: detection and quantification of physiological and pathophysiological thiol modifications. Free Radic Biol Med 2007;43:1099-108.
[5] Charles RL, Schroder E, May G, Free P, Gaffney PR, Wait R, et al. Protein sulfenation as a redox sensor: proteomics studies using a novel biotinylated dimedone analogue. Mol Cell Proteomics 2007;6:1473-84.
[6] Poole LB, Nelson KJ. Discovering mechanisms of signaling-mediated cysteine oxidation. Curr Opin Chem Biol 2008;12:18-24.
[7] Spadaro D, Yun BW, Spoel SH, Chu C, Wang YQ, Loake GJ. The redox switch: dynamic regulation of protein function by cysteine modifications. Physiol Plant 2010;138:360-71.
[8] Finkel T. Signal transduction by reactive oxygen species. J Cell Biol 2011;194:7–15.
[9] Martínez-Ruiz A, Lamas S. S-nitrosylation: a potential new paradigm in signal transduction. Cardiovasc Res 2004;62:43-52.
[10] Martínez-Ruiz A, Lamas S. Signalling by NO-induced protein S-nitrosylation and S-glutathionylation: convergences and divergences. Cardiovasc Res 2007;75:220-8.
[11] Leonard SE, Carroll KS. Chemical 'omics' approaches for understanding protein cysteine oxidation in biology. Curr Opin Chem Biol 2011;15:88–102.
[12] Chouchani ET, James AM, Fearnley IM, Lilley KS, Murphy MP. Proteomic approaches to the characterization of protein thiol modification. Curr Opin Chem Biol 2011;15:120-8.
[13] Lindahl M, Mata-Cabana A, Kieselbach T. The disulfide proteome and other reactive cysteine proteomes: analysis and functional significance. Antioxid Redox Signal 2011;14:2581-642.
[14] Burgoyne JR, Eaton P. Contemporary techniques for detecting and identifying proteins susceptible to reversible thiol oxidation. Biochem Soc Trans 2011;39:1260-7.
[15] Izquierdo-Álvarez A, Martínez-Ruiz A. Thiol redox proteomics seen with fluorescent eyes: the detection of cysteine oxidative modifications by fluorescence derivatization and 2-DE. J Proteomics 2011;75:329-38.
[16] Semenza GL. Regulation of tissue perfusion in mammals by hypoxia-inducible factor 1. Exp Physiol 2007;92:988-91.
[17] Aragonés J, Fraisl P, Baes M, Carmeliet P. Oxygen sensors at the crossroad of metabolism. Cell Metab 2009;9:11-22.
[18] Semenza GL. Life with oxygen. Science 2007;318:62-4.
[19] Kaelin Jr WG, Ratcliffe PJ. Oxygen sensing by metazoans: the central role of the HIF hydroxylase pathway. Mol Cell 2008;30:393-402.
[20] Guzy RD, Schumacker PT. Oxygen sensing by mitochondria at complex III: the paradox of increased reactive oxygen species during hypoxia. Exp Physiol 2006;91:807-19.
[21] Cash TP, Pan Y, Simon MC. Reactive oxygen species and cellular oxygen sensing. Free Radic Biol Med 2007;43:1219-25.
[22] Hamanaka RB, Chandel NS. Mitochondrial reactive oxygen species regulate hypoxic signaling. Curr Opin Cell Biol 2009;21:894-9.
[23] Guzy RD, Hoyos B, Robin E, Chen H, Liu L, Mansfield KD, et al. Mitochondrial complex III is required for hypoxia-induced ROS production and cellular oxygen sensing. Cell Metab 2005;1:401-8.
[24] Waypa GB, Marks JD, Guzy R, Mungai PT, Schriewer J, Dokic D, et al. Hypoxia triggers subcellular compartmental redox signaling in vascular smooth muscle cells. Circ Res 2010;106:526-35.

[25] Desireddi JR, Farrow KN, Marks JD, Waypa GB, Schumacker PT. Hypoxia increases ROS signaling and cytosolic Ca(2+) in pulmonary artery smooth muscle cells of mouse lungs slices. Antioxid Redox Signal 2010;12:595-602.
[26] Chi AY, Waypa GB, Mungai PT, Schumacker PT. Prolonged hypoxia increases ROS signaling and RhoA activation in pulmonary artery smooth muscle and endothelial cells. Antioxid Redox Signal 2010;12:603-10.
[27] Muñoz C, Castellanos MC, Alfranca A, Vara A, Esteban MA, Redondo JM, et al. Transcriptional up-regulation of intracellular adhesion molecule-1 in human endothelial cells by the antioxidant pyrrolidine dithiocarbamate involves the activation of activating protein-1. J Immunol 1996;157:3587-97.
[28] Shevchenko A, Wilm M, Vorm O, Mann M. Mass spectrometric sequencing of proteins silver-stained polyacrylamide gels. Anal Chem 1996;68:850-8.
[29] Tello D, Tarín C, Ahicart P, Bretón-Romero R, Lamas S, Martínez-Ruiz A. A "fluorescence switch" technique increases the sensitivity of proteomic detection and identification of S-nitrosylated proteins. Proteomics 2009;53:59-70.
[30] Baty JW, Hampton MB, Winterbourn CC. Detection of oxidant sensitive thiol proteins by fluorescence labeling and two-dimensional electrophoresis. Proteomics 2002;2:1261-6.
[31] Alvarez S, Wilson GH, Chen S. Determination of in vivo disulfide-bonded proteins in Arabidopsis. J Chromatogr B Analyt Technol Biomed Life Sci 2009;877:101-4.
[32] Hochgräfe F, Mostertz J, Albrecht D, Hecker M. Fluorescence thiol modification assay: oxidatively modified proteins in *Bacillus subtilis*. Mol Microbiol 2005;58:409-25.
[33] Edgell CJ, McDonald CC, Graham JB. Permanent cell line expressing human factor VIII-related antigen established by hybridization. Proc Natl Acad Sci U S A 1983;80:3734-7.
[34] Pan Y, Mansfield KD, Bertozzi CC, Rudenko V, Chan DA, Giaccia AJ, et al. Multiple factors affecting cellular redox status and energy metabolism modulate hypoxia-inducible factor prolyl hydroxylase activity in vivo and in vitro. Mol Cell Biol 2007;27:912-25.
[35] Nytko KJ, Maeda N, Schlafli P, Spielmann P, Wenger RH, Stiehl DP. Vitamin C is dispensable for oxygen sensing in vivo. Blood 2011;117:5485-93.
[36] Drummen GP, Gadella BM, Post JA, Brouwers JF. Mass spectrometric characterization of the oxidation of the fluorescent lipid peroxidation reporter molecule C11-BODIPY(581/591). Free Radic Biol Med 2004;36:1635-44.
[37] Zee RS, Yoo CB, Pimentel DR, Perlman DH, Burgoyne JR, Hou X, et al. Redox regulation of sirtuin-1 by S-glutathiolation. Antioxid Redox Signal 2010;13:1023-32.
[38] Iwase H, Robin E, Guzy RD, Mungai PT, Vanden Hoek TL, Chandel NS, et al. Nitric oxide during ischemia attenuates oxidant stress and cell death during ischemia and reperfusion in cardiomyocytes. Free Radic Biol Med 2007;43:590-9.
[39] Robin E, Guzy RD, Loor G, Iwase H, Waypa GB, Marks JD, et al. Oxidant stress during simulated ischemia primes cardiomyocytes for cell death during reperfusion. J Biol Chem 2007;282:19133-43.
[40] Blázquez M, Fominaya JM, Hofsteenge J. Oxidation of sulfhydryl groups of ribonuclease inhibitor in epithelial cells is sufficient for its intracellular degradation. J Biol Chem 1996;271:18638-42.
[41] Martínez-Ruiz A, Villanueva L, de Orduña CG, López-Ferrer D, Higueras MÁ, Tarín C, et al. S-nitrosylation of Hsp90 promotes the inhibition of its ATPase and endothelial nitric oxide synthase regulatory activities. Proc Natl Acad Sci U S A 2005;102:8525-30.
[42] Mollapour M, Neckers L. Post-translational modifications of Hsp90 and their contributions to chaperone regulation. Biochim Biophys Acta 2012;1823:648-55.
[43] Chung SI, Folk JE. Mechanism of the inactivation of guinea pig liver transglutaminase by tetrathionate. J Biol Chem 1970;245:681-9.
[44] Connellan JM, Folk JE. Mechanism of the inactivation of guinea pig liver transglutaminase by 5,5′-dithiobis-(2-nitrobenzoic acid). J Biol Chem 1969;244:3173-81.
[45] Lai TS, Hausladen A, Slaughter TF, Eu JP, Stamler JS, Greenberg CS. Calcium regulates S-nitrosylation, denitrosylation, and activity of tissue transglutaminase. Biochemistry 2001;40:4904-10.
[46] Lai TS, Liu Y, Tucker T, Daniel KR, Sane DC, Toone E, et al. Identification of chemical inhibitors to human tissue transglutaminase by screening existing drug libraries. Chem Biol 2008;15:969-78.
[47] Hoppe G, Chai YC, Crabb JW, Sears J. Protein S-glutathionylation in retinal pigment epithelium converts heat shock protein 70 to an active chaperone. Exp Eye Res 2004;78:1085-92.
[48] Bloxham DP, Sharma RP, Wilton DC. A detailed investigation of the properties of lactate dehydrogenase in which the 'essential' cysteine-165 is modified by thioalkylation. Biochem J 1979;177:769-80.
[49] Bloxham DP, Wilton DC. Modification of pig heart lactate dehydrogenase with methyl methanethiosulphonate to produce an enzyme with altered catalytic activity. Biochem J 1977;161:643-51.
[50] Isaacs JS, Jung YJ, Mimnaugh EG, Martinez A, Cuttitta F, Neckers LM. Hsp90 regulates a von Hippel–Lindau-independent hypoxia-inducible factor-1 alpha-degradative pathway. J Biol Chem 2002;277:29936-44.
[51] Katschinski DM, Le L, Schindler SG, Thomas T, Voss AK, Wenger RH. Interaction of the PAS B domain with HSP90 accelerates hypoxia-inducible factor-1alpha stabilization. Cell Physiol Biochem 2004;14:351-60.
[52] Liu YV, Baek JH, Zhang H, Diez R, Cole RN, Semenza GL. RACK1 competes with HSP90 for binding to HIF-1alpha and is required for O(2)-independent and HSP90 inhibitor-induced degradation of HIF-1alpha. Mol Cell 2007;25:207-17.
[53] Nanduri J, Bergson P, Wang N, Ficker E, Prabhakar NR. Hypoxia inhibits maturation and trafficking of hERG K(+) channel protein: role of Hsp90 and ROS. Biochem Biophys Res Commun 2009;388:212-6.
[54] Luo W, Zhong J, Chang R, Hu H, Pandey A, Semenza GL. Hsp70 and CHIP selectively mediate ubiquitination and degradation of hypoxia-inducible factor (HIF)-1alpha but not HIF-2alpha. J Biol Chem 2010;285:3651-63.
[55] Zhang J, Patel JM, Block ER. Hypoxia-specific upregulation of calpain activity and gene expression in pulmonary artery endothelial cells. Am J Physiol 1998;275:L461-8.
[56] Zhou J, Kohl R, Herr B, Frank R, Brüne B. Calpain mediates a von Hippel–Lindau protein-independent destruction of hypoxia-inducible factor-1alpha. Mol Biol Cell 2006;17:1549-58.
[57] Brugarolas J, Lei K, Hurley RL, Manning BD, Reiling JH, Hafen E, et al. Regulation of mTOR function in response to hypoxia by REDD1 and the TSC1/TSC2 tumor suppressor complex. Genes Dev 2004;18:2893-904.
[58] DeYoung MP, Horak P, Sofer A, Sgroi D, Ellisen LW. Hypoxia regulates TSC1/2-mTOR signaling and tumor suppression through REDD1-mediated 14-3-3 shuttling. Genes Dev 2008;22:239-51.
[59] Horak P, Crawford AR, Vadysirisack DD, Nash ZM, DeYoung MP, Sgroi D, et al. Negative feedback control of HIF-1 through REDD1-regulated ROS suppresses tumorigenesis. Proc Natl Acad Sci U S A 2010;107:4675-80.
[60] Kim JS, Huang TY, Bokoch GM. Reactive oxygen species regulate a slingshot-cofilin activation pathway. Mol Biol Cell 2009;20:2650-60.
[61] Firth JD, Ebert BL, Ratcliffe PJ. Hypoxic regulation of lactate dehydrogenase A. Interaction between hypoxia-inducible

factor 1 and cAMP response elements. J Biol Chem 1995;270: 21021-7.
[62] Semenza GL, Jiang BH, Leung SW, Passantino R, Concordet J-P, Maire P, et al. Hypoxia response elements in the aldolase A, enolase 1, and lactate dehydrogenase A gene promoters contain essential binding sites for hypoxia-inducible factor 1. J Biol Chem 1996;271:32529-37.
[63] Dawson DM, Goodfriend TL, Kaplan NO. Lactic dehydrogenases: functions of the two types. Rates of synthesis of the two major forms can be correlated with metabolic differentiation. Science 1964;143:929-33.
[64] Read JA, Winter VJ, Eszes CM, Sessions RB, Brady RL. Structural basis for altered activity of M- and H-isozyme forms of human lactate dehydrogenase. Proteins 2001;43: 175-85.
[65] Holbrook JJ, Gutfreund H. Approaches to the study of enzyme mechanisms lactate dehydrogenase. FEBS Lett 1973;31: 157-69.

Redox Biology 6 (2015) 372–385

Contents lists available at ScienceDirect

Redox Biology

journal homepage: www.elsevier.com/locate/redox

Review Article

Reactive oxygen species, nutrition, hypoxia and diseases: Problems solved?

Agnes Görlach [a,b], Elitsa Y. Dimova [c], Andreas Petry [a,b], Antonio Martínez-Ruiz [d], Pablo Hernansanz-Agustín [d,e], Anabela P. Rolo [f], Carlos M. Palmeira [f], Thomas Kietzmann [c,*]

[a] Experimental and Molecular Pediatric Cardiology, German Heart Center Munich, Technical University Munich, Germany
[b] DZHK (German Centre for Cardiovascular Research), partner site Munich Heart Alliance, Munich, Germany
[c] Faculty of Biochemistry and Molecular Medicine, Biocenter Oulu, University of Oulu, Oulu, Finland
[d] Servicio de Immunología, Hospital Universitario de La Princesa, Instituto de Investigación Sanitaria Princesa, Madrid, Spain
[e] Departamento de Bioquímica, Facultad de Medicina, Universidad Autónoma de Madrid, Madrid, Spain
[f] Department of Life Sciences, University of Coimbra and Center for Neurosciences and Cell Biology, University of Coimbra, Portugal

ARTICLE INFO

Article history:
Received 10 July 2015
Received in revised form
21 August 2015
Accepted 25 August 2015
Available online 28 August 2015

Keywords:
Free radicals
Diets
Oxygen
Metabolism
Diseases
Mitochondria
Hypoxia
Diabetes
Obesity

ABSTRACT

Within the last twenty years the view on reactive oxygen species (ROS) has changed; they are no longer only considered to be harmful but also necessary for cellular communication and homeostasis in different organisms ranging from bacteria to mammals. In the latter, ROS were shown to modulate diverse physiological processes including the regulation of growth factor signaling, the hypoxic response, inflammation and the immune response. During the last 60–100 years the life style, at least in the Western world, has changed enormously. This became obvious with an increase in caloric intake, decreased energy expenditure as well as the appearance of alcoholism and smoking; These changes were shown to contribute to generation of ROS which are, at least in part, associated with the occurrence of several chronic diseases like adiposity, atherosclerosis, type II diabetes, and cancer. In this review we discuss aspects and problems on the role of intracellular ROS formation and nutrition with the link to diseases and their problematic therapeutical issues.

Contents

* Correspondence to: Faculty of Biochemistry and Molecular Medicine, Biocenter Oulu, University of Oulu, Aapistie 7, FI-90220 Oulu, Finland.
E-mail address: tkietzm@gwdg.de (T. Kietzmann).

http://dx.doi.org/10.1016/j.redox.2015.08.016
2213-2317/

1. Introduction

The research within the last twenty years on chemically reactive molecules containing oxygen, commonly called reactive oxygen species (ROS), has shown that these molecules are important for cellular communication and homeostasis in different organisms ranging from bacteria to mammals. Thereby, ROS were shown to modulate diverse physiological processes including the regulation of growth factor signaling, the hypoxic response, inflammation and the immune response in mammalian cells. ROS are often simply called "free radicals" because their majority is characterized by at least one unpaired electron in their outer orbitals; however, peroxides like hydrogen peroxide may also give rise to the formation of oxygen radicals and are therefore also considered as ROS. Frequently the incomplete reduction of oxygen by one electron producing superoxide anion ($O_2^{\cdot-}$) is the first step for the formation of most other ROS [1,2].

The action of ROS is usually balanced by the antioxidative capacity of a cell or organism and a disturbance of this balance in favor of a prooxidant state is commonly referred to as oxidative stress. Oxidative stress is usually coupled to harmful effects due to the primary chemical reactions of ROS with lipids and proteins. In this respect, diseases frequently associated with a Western lifestyle and nutritional regime like type II diabetes, cardiovascular diseases or cancer were found to be associated with a deregulated ROS formation [3–7]. Hence, it appears to be of special interest that production of ROS due to nutrition may affect signaling pathways and the pathogenesis of these diseases. In the current review we aim to summarize some aspects on the role of ROS, nutrition, intracellular ROS formation, and the link to diseases.

2. Cellular sources of ROS

A number of studies within the last decade indicated that overnutrition-induced ROS formation and oxidative stress contribute to the development of metabolic disorders, in particular to insulin resistance, as well as to cardiovascular diseases, and cancer [8–12].

In mammalian cells ROS can be generated in different cellular compartments such as membranes, cytoplasm, mitochondria, endoplasmic reticulum (ER), lysosomes, and peroxisomes (Fig.1). In the following we will give only a short summary because the role of each compartment in ROS formation has been discussed elsewhere in excellent detail [13].

2.1. Plasma membranes and ROS production

The prototypic NADPH oxidase was found in phagocytes localized in the plasma membrane and phagosomes [14]. It is composed of gp91phox and the smaller subunit p22phox forming the flavocytochrome b558 [15,16] which is the catalytic core of the NADPH oxidase generating $O_2^{\cdot-}$. Several homologs of gp91phox – now termed NOX2-named NOX1-5, and the more distantly related DUOX1/2 (dual oxidases) were found [17–19]. NOX2 is mainly expressed in polymorphonuclear cells, macrophages and endothelial cells, but its expression was also verified in other cell types including cells from the CNS, smooth muscle cells, fibroblasts, cardiomyocytes, skeletal muscle, hepatocytes, and hematopoietic stem cells [20] (Table 1).

NOX1 is highly expressed in the colon epithelia [21] and was also detected in lower abundance in smooth muscle cells, endothelial cells, uterus, placenta, pancreatic islet beta cells and other cell types [22,23]; it is mainly localized in the plasma membrane of caveolae, but also in early endosomes or nucleus [24,25].

NOX3 has long been considered to be expressed in fetal tissues, but is it now also found in the inner ear, HepG2 cells, the mouse macrophage cell line RAW264.7, and in murine lung endothelium [26] (Table 1).

NOX4 is widely expressed in many tissues, especially in the kidney [27], but also in most other tissues and cells including endothelial cells, smooth muscle cells, fibroblasts and hepatocytes [25,28–30]. In contrast to most other NOXes, NOX4 is mainly localized in the endoplasmic reticulum as well as in the outer membrane of the nucleus [31,32]. Finally, NOX5 expression has been detected in testis, prostate, spleen, lymph nodes, but also in endothelial and smooth muscle cells [26] and its mainly localized in the endoplasmic reticulum of the cell [33] (Table 1).

The two DUOX1/2 proteins are highly expressed in the thyroid, but also in lung epithelium and gastrointestinal tract [34–36]; mainly in the endoplasmic reticulum and plasma membrane [32].

Most NOXes as well as the two DUOX members require cytosolic subunits for full activation. In the case of NOX2 these are the cytosolic subunits p40phox, p47phox, p67phox as well as the small monomeric GTPase Rac [16]. NOX1 and NOX3 can be regulated by NOXO1 (p67phox homolog) and NOXA1 (p47phox

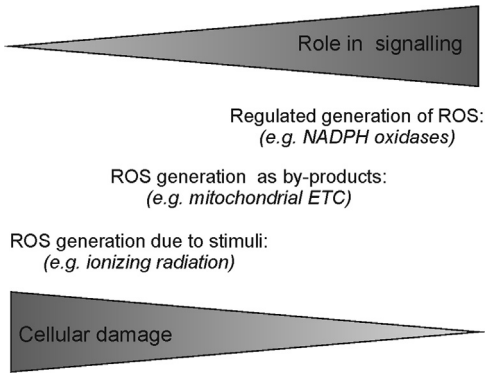

Fig. 1. ROS generation in cells. ROS can be generated in response to various stimuli among them diets or radiation which is supported by the action(s) of enzyme (s) located in different intracellular compartments. ETC, electron transport chain;

Table 1
Overview of the NOX family members (see text for details and references)

Name	Subcellular localization	Expression[#]	Cofactors
NOX1	Caveolae membrane	Colon epithelia	p22phox
		Smooth muscle cells	NOXO1
	Endosomes	Endothelial cells	
		Uterus	NOXA1
	Nucleus	Placenta	p47phox(?)
		Pancreatic islet beta cells	RAC 1
NOX2	Plasma membrane	Neutrophils	p22phox
		Macrophages	
		Endothelial cells	p40phox
		Central nervous system	
		Smooth muscle cells	p47phox
		Fibroblasts	
	Phagosomes	Cardiomyocytes	p67phox
		Skeletal muscle	
		Hepatocytes	RAC 1/2
		Hematopoietic stem cells	
NOX3		Fetal tissues	p22phox
		Inner ear	NOXO1
		Hepatoblastoma cell line HepG2	NOXA1
		Murine Macrophage cell line RAW264.7	P47phox(?)
		Murine lung endothelium	RAC 1
NOX4	Endoplasmic reticulum	Kidney	p22phox
		Endothelial cells	
	Outer nucleus membrane	Smooth muscle cells	RAC 1(?)
		Fibroblasts	
		Hepatocytes	
NOX5[a]	Endoplasmic reticulum	Testis	Ca^{2+}
		Prostate	
		Spleen	Calmodulin
		Lymph nodes	
		Endothelial cells	
		Smooth muscle cells	
DUOX1/2	Endoplasmic reticulum	Thyroid	Ca^{2+}
	Plasma membrane	Lung epithelium	DUOX1/2
		Gastrointestinal tract	

[a] NOX5 is not present in rodents.
[#] Most relevant expression listed with no claim to completeness.

homolog) while DUOX1 and -2 require their regulators DUOXA1 and DUOXA2, respectively [26,32]. NOX4 activity seems to be independent of regulatory subunits, though a role for Rac is discussed [26] and it is mainly regulated at the expression level. In addition to regulatory proteins, activation of NOX5 and DUOX1/2 requires calcium [17,33] and in case with NOX5 also calmodulin [37] (Table 1). Most generated ROS in non-phagocytic cells are mainly considered to act as second messenger molecules in several processes including responses to nutrition [26].

2.2. Mitochondria and ROS production

Mitochondria are well known to be major ROS producers [38] and the fraction of oxygen that is used for ROS production varies and ranges from 0.15% to 4% [39]. Interestingly, in females mitochondria produce less ROS than in males; a difference which can be seen also in the induced levels of antioxidant enzymes in females which is largely due to the action of estrogens [40]. The electron transport chain (ETC) within mitochondria constitutes an important source of $O_2^{\cdot-}$ formation primarily due to leaking electrons from complex I (NADH-CoQ reductase) and complex III (cytochrome c reductase). Thereby complex I generates $O_2^{\cdot-}$ only within the matrix, while complex III can contribute to $O_2^{\cdot-}$ formation also in the intermembrane space [41]. In addition to the ETC, also the acetyl-CoA generating enzyme pyruvate dehydrogenase (PDH) and the Krebs cycle enzyme α-ketoglutarate dehydrogenase (KGDH) can be sources of $O_2^{\cdot-}$ [42–46]. Moreover, it was shown that the redox enzyme p66Shc is involved in the direct reduction of oxygen to H_2O_2 in the intermembrane space by using reducing equivalents through the oxidation of cytochrome C [47].

2.3. The endoplasmic reticulum (ER) and ROS production

The endoplasmic reticulum is a place with a high rate of ROS generation. On the one hand ER-localized ROS can be a byproduct of ER-localized oxygenases and oxidases during oxidative protein folding-among them endoplasmic oxidoreductin 1 (ERO1) as the most prominent one [13,48]. On the other hand there are also ER localized NADPH oxidases such as NOX4, NOX5, and DUOX1/2 which can contribute to ROS generation in the ER [31,33]. In addition, there is a crosstalk between enzymes of the protein folding machinery and NADPH oxidases due to a described interaction between PDI and NOX1/NOX4 as well as an interaction between calmodulin and NOX5 [37,49]. Further, ER localized iron deposits may also contribute to the pool of ROS by the formation of $\cdot OH$ via a Fenton reaction [50].

2.4. Lysosomes and ROS production

Lysosomes are important organelles involved in degradation of intracellular and extracellular materials which interlinks them with phagocytosis, endocytosis and autophagy. To operate the degradative acidic hydrolases require a pH of about 4.8. To generate this pH, lysosomes appear to contain a redox chain which similar to the mitochondrial ETC contributes to proton distribution. As a byproduct ROS are generated. Thereby, reduction of O_2 in three steps can give rise to $\cdot OH$ generation [51]. Since lysosomes are degrading iron- and copper containing macromolecules they accumulate iron and copper. Due to the acidic and reducing lysosomal environment iron is mainly in the divalent, thus redox active, state whereas lysosomal copper is usually complexed with various thiols and is thus likely not redox-active [52]. Hence, the presence of divalent iron further fosters generation of $\cdot OH$ by Fenton reactions which may affect lysosomal membrane integrity [52].

2.5. Peroxisomes and ROS production

Peroxisomes participate in several metabolic processes, including long-chain fatty acid β-oxidation, the oxidative part of the pentose phosphate pathway, phospholipid biosynthesis, purine, and polyamine metabolism as well as amino acid and polyamine oxidation [53]. Many of the enzymes operating in these pathways are flavin-dependent oxidases [53] which produce H_2O_2 as a result of their activity [54]. The major process forming H_2O_2 is β–oxidation of fatty acids whereas a peroxisomal xanthine oxidase appears to provide not only H_2O_2 but also $O_2^{\cdot-}$ [54]. Since H_2O_2 can give rise to formation of other ROS which could damage the cells, it needs to be degraded into per se non-reactive substances. This is done by the enzyme catalase which converts H_2O_2 into O_2 and H_2O [55].

2.6. Detrimental action of ROS

The harmful action of ROS is primarily due to their ability to

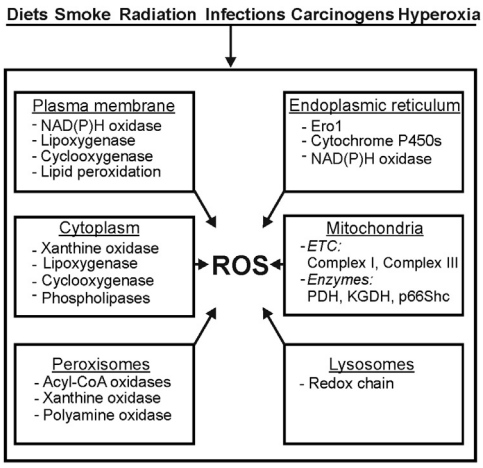

Fig. 2. Interrelation between ROS in signaling and cell damage. ROS generated in cells by specific action of various enzymes appear to have a more critical role in signaling than ROS generated as by-products of intracellular processes or due to external toxic stimuli. ETC, electron transport chain. PDH, pyruvate dehydrogenase; KGDH, α-ketoglutarate dehydrogenase.

oxidize and subsequently damage DNA, proteins and (membrane) lipids (Fig. 2). Among the ROS, ·OH are known to mainly damage DNA by reacting with all four bases whereas $^1O_2$ selectively attacks guanine [56]; O_2^- and H_2O_2 contribute indirectly to DNA damage by forming ·OH and lipid peroxides which contribute to formation of DNA adducts [57]. Again, most protein damage is exerted due to the action of ·OH at the protein polypeptide backbone [58]; as a consequence, further radicals such as peroxyl, alkylperoxide, or alkoxyl radicals are formed [59].

It appears that mitochondrial DNA is more susceptible to DNA damage than nuclear DNA since it lacks histones, has only a limited repair capacity, and is ultimately exposed to mitochondrial ROS [60]. In particular the displacement loop (D-loop) in mitochondrial DNA is known as mutational hotspot and associated with hepatocellular carcinoma [61], ovarian cancer [62], breast cancer [63], colorectal cancer [64] and melanoma [65].

Moreover, ROS can also influence epigenetic modifications (for review see [66]). For example, ROS can affect DNA methylation [67] by downregulating the expression of O-6-methylguanine-DNA methyltransferase and MLH1 (mutL homolog 1) [5]. In addition, it has been speculated that oxidative stress may also be involved in the oxidation of 5-methylcytosines to 5-hydroxy-methylcytosine [68]. Moreover, ROS-mediated formation of 8-oxodG adjacent to a cytosine may prevent methylation of the latter [69].

3. ROS-dependent regulation of signaling pathways

3.1. Kinase signaling and ROS

The action of ROS in various signaling networks is connected to their physiological role but also to diseases [70–73]. Various stimuli, among them nutrients like fatty acids, growth factors, hormones, coagulation factors, cytokines, and hypoxia were shown to act at least partially via regulated ROS generation (Fig. 2). Thus, aberrant generation or even degradation of ROS may limit the signaling function of these stimuli often affecting the mitogen-activated protein kinases (MAPK) and/or phosphatidylinositol 3-kinases (PI3K)/Akt cascades. ROS also affect pathways like protein kinase C (PKC), Wnt/β-catenin, Hedgehog, Notch [71, 74–76] in several ways [77], and many excellent reviews have covered the details [78,79]. We will thus concentrate only on some principles

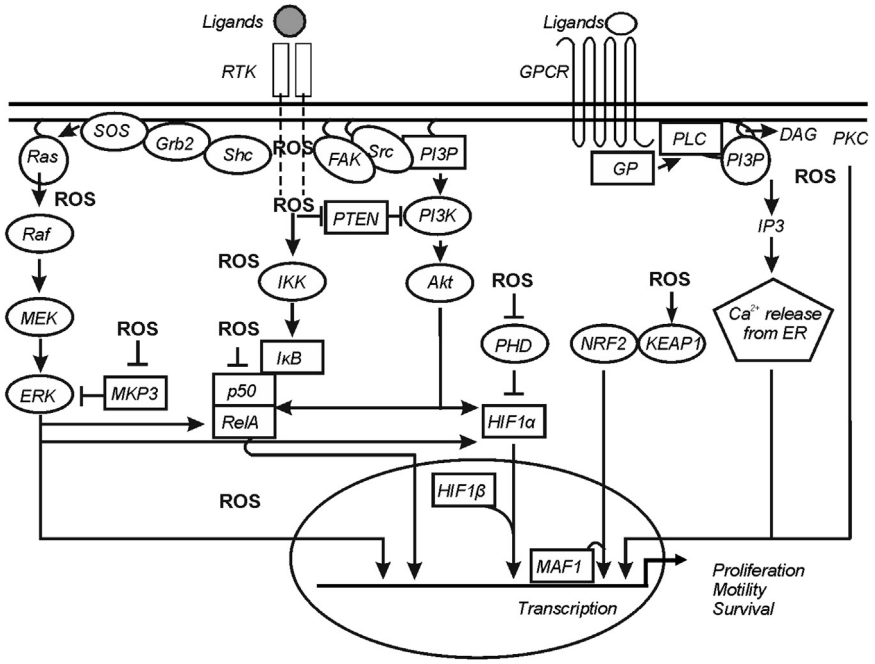

Fig. 3. ROS-regulated signaling pathways. Simplified diagram representing major ROS regulated signaling pathways. ROS can influence the pathways either positively or negatively; see text for further explanations. ROS necessary for regulation of signaling pathways are mostly generated through specific enzymatic reactions as well as due to the changes in cellular metabolic activity leading to altered ROS production.
DAG, diacylglycerol; ERK, extracellular signal-regulated kinase; FAK, focal adhesion kinase; GP, G-protein; GPCR, G-protein coupled receptor; Grb2, growth factor receptor-bound protein 2; HIF-1α, hypoxia-inducible factor-1α; IκB, inhibitor of NF-κB; IKK, IκB kinase; MEK, MAPK/ERK kinase; MKP3, mitogen-activated protein (MAP) kinase phosphatase/dual specificity protein phosphatase-6; PHD, prolyl hydroxylase; PI3K, phosphatidylinositol 3-kinases; PI3P, phosphatidylinositol 3-phosphate; PKB/Akt, protein kinase B; PKC, protein kinase C; PTEN, phosphatase and tensin homolog deleted on chromosome 10; Raf, ras attachement factor; Ras, Rat sarcoma; RTK, receptor tyrosine kinase; SOS, son of sevenless; Shc, SHC-transforming protein; Src, sarcoma.
ETC, electron transport chain; NF-κB, nuclear factor kappa B; NOX, NADPH oxidase subunit; PKC, protein kinase C; PPAR, peroxisome proliferator-activated receptor; SOD, superoxide dismutase; TCA, tricarboxylic acid.

of the best studied so far.

3.2. MAPK signaling

ROS are known to be able to activate the ERK (extracellular signal-regulated kinase) and JNK (c-Jun NH2-terminal kinase) MAPK cascades. Thereby they are supposed to cause autophosphorylation of the epidermal growth factor receptor (EGFR) or PDGFR in a ligand-dependent manner [80]. In addition, oxidative modification of Ras, a major component of the ERK1/2 cascade, at Cys118 [81] inhibits GDP/GTP exchange, and activates Ras and the whole cascade. Since MEK1/2 (MAPK/ERK kinase 1/2) inhibitors can suppress ROS-mediated ERK1/2 activation [82] ROS might act indirectly at the level of MEK1/2 or by antagonizing phosphatases (see below) like mitogen-activated protein kinase phosphatase (MKP3) [83] (Fig. 3).

3.3. PI3K/Akt signaling

In addition to MAPK pathway activation, growth factor protein tyrosine kinase receptors including EGFR or PDGFR are also known to stimulate the protein kinase B (PKB/Akt) pathway [84]; ROS, especially H_2O_2 were found to activate PKB/Akt. In addition, the tumor suppressor PTEN (phosphatase and tensin homolog deleted on chromosome 10), a counter regulator of PKB/Akt activation was found to be inactivated by ROS-dependent oxidation of Cys124 [85] thus enhancing PKB/Akt activation. Moreover, loss of PTEN also causes depletion of antioxidant enzymes [86] (Fig. 3).

3.4. PKC signaling

Three major PKC subfamilies are distinguished; (i) conventional PKC isoforms (cPKCs; α, with alternatively spliced βI/βII isoforms, and γ); (ii) the so called novel PKCs (nPKCs, with isoforms δ, θ, ε, and η), and (iii) atypical PKCs (aPKC; with isoforms Mζ, and ι/λ). The cPKCs require diacylglycerol and calcium for their activity while nPKCs can be activated by diacylglycerol independent of calcium; aPKCs do neither require calcium nor diacylglycerol. All are potentially susceptible to redox modifications due to their content in cysteine residues. Indeed, some proteinkinase C (PKC) isoforms like α, βI, and γ of cPKC, δ and ε of nPKC, and Mζ of aPKC, were activated upon treatment of cells with H_2O_2 [87] and further evidence points to ROS-dependent changes in a conserved cysteine-rich region in PKCα binding diacylglycerol [88]. However, it appeared that the redox-dependent activation of PKC can also be communicated in an indirect manner. In fact, the activation of PKCδ by H_2O_2 was not mediated by cysteine modification. Interestingly, the H_2O_2-dependent increase in PKCδ activity was caused by the tyrosine kinase Lck (a member of the Src family) which phosphorylated a tyrosine residue between the regulatory and catalytic domain [89]. Overall, the existence of various PKC isoforms with the option of a direct or indirect redox-dependent regulation adds another layer of complexity to the understanding of PKC regulation. This may in particular be important for those PKCs involved in metabolic regulation; in particular isoform θ in skeletal muscle and δ in liver can be activated by fatty acid metabolites such as fatty acyl CoA and diacylglycerol. As a consequence this can lead to inhibitory serine phosphorylation of insulin receptor substrates and an attenuation of insulin signaling [90] (Fig. 3).

3.5. Protein tyrosine phosphatases

Oxidation of catalytic cysteine residues and inactivation of protein tyrosine phosphatases (PTP) is another ROS-dependent regulatory mechanism of action [91]. Extracellular ligand-stimulated ROS and signal-independent ROS production can cause PTP oxidation. In addition to classical PTPs dephosphorylating phosphotyrosine, also dual-specificity phosphatases like MAPK phosphatases can be inactivated by ROS-dependent oxidation [91] (Fig. 3).

4. Transcription factors and ROS

Transcription factors are among the ROS targets which can positively or negatively respond to nutrients by changing gene expression. Thereby the transcription factors nuclear factor kappa B (NF-κB), nuclear factor erythroid-2-related factor-2 (Nrf2), as well as hypoxia-inducible factor-1α (HIF-1α) and hypoxia-inducible factor-2α (HIF-2α) appear to integrate the responses to different primary stimuli at the level of ROS signaling. [92,93] (Fig. 3). Activation/inhibition of these transcription factors can be crucial for adaptation, survival and progression of diseases like inflammation, type II diabetes, or cancer.

4.1. NF-κB signaling

The activation of NF-κB is closely linked with ROS generation during inflammation and obesity [94]. ROS were found to mediate inhibitor of NF-κBα (IκBα) kinase (IKKα and IKKβ) phosphorylation and release of free NF-κB dimers [95]. Tumor necrosis factor α (TNFα), a bona fide NF-κB activator, was shown to mediate a redox-dependent activation of protein kinase A [96] which subsequently phosphorylated Ser276 on RelA (v-rel avian reticuloendotheliosis viral oncogene homolog A). By contrast, the NF-κB member p50 was found to have reduced DNA binding activity when oxidized at Cys62 [97,98].

4.2. Nrf2 signaling

The Nrf2 and its partner Keap1 (Kelch-like ECH-associated protein (1) are considered as the major transcriptional regulators in the response and defense against oxidative stress [99,100]. The regulation of this dimer is primarily achieved by the sulfhydryl groups within Keap1 which act as sensors for electrophiles and oxidants [101]. In the absence of ROS binding of Keap1 promotes proteasomal degradation of Nrf2. In the presence of ROS, cysteine residues in Keap1, with Cys151 being the most critical, become oxidized leading to a conformational change of Keap1, which prevents its binding to Nrf2. In addition to oxidation, ROS can contribute to dephosphorylation of Keap1 at Tyr141 which contributes to Keap1 degradation [102]. As an overall consequence, Nrf2 is no longer degraded and can be transported to the nucleus. Moreover, oxidation of Cys183 in Nrf2 inhibits binding of the nuclear export protein CRM1 and thus promotes nuclear presence. In the nucleus, Nrf2 heterodimerizes with a small Maf protein to activate genes of the antioxidant response such as NAD(P)H:quinone oxidoreductase 1, glutathione *S*-transferases, cysteine-glutamate exchange transporter, and multidrug resistance-associated protein.

Interestingly, Nrf2 activating substances like quercetin, genistein, curcumin and sulforaphane are often components of plants, fruits and vegetables; therapeutics such as oltipraz, auranofin and acetaminophen; environmental agents like paraquat, and metals as well as endogenous substances like hydrogen peroxide, NO, or 4-hydroxynonenal also activate Nrf2 signaling [103]. This somehow may imply that an activation of the Nrf2 pathway may be of therapeutical benefit. However, Keap1 knockout mice die shortly after birth. This finding and the rescue of this lethal phenotype in Keap1/Nrf2 double knockout mice [104] suggests that excessive Nrf2 activity may be detrimental for normal life. Indeed, this was

supported by a study showing that constitutive activation of the Nrf2 pathway was beneficial for tumor survival [105].

4.3. HIFα signaling

ROS play an important role in HIF signaling (for review see [106]). Both HIF-1α and HIF-2α can be modified by ROS in a direct and indirect manner. Direct regulation requires presence of redox factor-1 (Ref-1) and affects transactivation of HIF-1α at Cys800 and of HIF-2α at Cys848 [107] as well as recruitment of coactivators such as steroid receptor coactivator-1 and transcription intermediary factor 2. Another direct redox effect is oxidation of the Cys present in the DNA-binding domain of HIF-2α, but not HIF-1α [108]. The indirect effects of ROS are mediated via regulation of prolyl hydroxylases (PHD), asparagine hydroxylases, redox-sensitive kinases, and phosphatases (for review see [3,109]). The PHDs hydroxylate HIF-1α and HIF-2α at critical proline residues thereby inducing HIF degradation under normoxia. The PHDs belong to a family of oxygen, Fe^{2+}, 2-oxoglutarate, and ascorbate dependent dioxygenases (reviewed by [110]) which need a radical cycling system to regenerate the iron after each catalytic cycle [111]. Even though ascorbate is a key agent in the regeneration of iron, glutathione could substitute it in mice deficient in vitamin C synthesis, pointing to the importance of thiol oxidation/reduction cycles. In line, a pair of cysteine residues in one of the PHDs was described to modulate its redox sensitivity [112], again highlighting the possible involvement of thiol oxidation in regulating PHD activity, though in endothelial cells subjected to hypoxia, no variation in PHD cysteine oxidation was observed [113].

Both, HIF-1α and HIF-2α could be prevented from hydroxylation and degradation by increasing ROS generation from ER-localized NOX4 or addition of hydrogen peroxide to cells [114]. Moreover, ROS generated at the Qo site of the mitochondrial complex III affected HIF-1α and HIF-2α regulation [115,116]. Thereby mitochondrial ROS seemed to act upstream of prolyl hydroxylases in regulating HIF-1α and HIF-2α [117]. From the ROS formed, hydrogen peroxide seems to be of major importance for HIF regulation since overexpression of glutathione peroxidase or catalase, but not superoxide dismutase 1 or 2, prevented the hypoxic stabilization of HIF-1α [115,116,118]. Together, ROS appear to constitute an important link for HIF regulation especially under certain metabolic regimes or diseases like cancer which are associated with altered mitochondrial activity [119].

In addition, HIFα signaling is known to undergo a crosstalk with both PI3K/Akt and MAPK cascades where ROS and NOX enzymes act as activators (reviewed by [120]). In line, antioxidants or NOX inhibitors blocked signaling via PI3K/Akt to HIF-1α [121]. In addition, a number of ROS inducing substances like angiotensin-II [122], prostaglandin E2 [123], shock waves [124], thrombin [121] or chromium (VI) [125] contribute to HIF-1α induction via ERK1/2 which also can phosphorylate HIF-1α [120]. Further, p38 MAPKs and the p38 upstream kinases MKK3 and MKK6 [126] were shown to be involved in the induction of HIF-1α by thrombin [121] and chromium (VI) [125]. In addition, these NADPH oxidases activating substances can also induce HIF-1α mRNA levels in several cell types [127–130]. In line, HIF-1α is a direct target gene of NFκB [131–135], and ROS derived from NOXes or direct application of H_2O_2 regulates NFκB–dependent HIF-1α transcription [132,136,137].

Taken together, ROS are important regulators of the HIF system and the crosstalk between ROS and HIF is an important pathophysiological link for a wide variety of disorders.

5. Hypoxia and ROS, a paradoxical and complex relationship

Paradoxically an increased availability of lipids and carbohydrates which is typical for a Western diet will also increase the demand on energy synthesis in form of ATP; i.e provision of these substances will activate usage of the mitochondrial electron transport chain and oxygen [138]. As a result of an acute hypoxic event a superoxide burst can occur [139]; however, hypoxia per se seems to affect ROS production with subsequent consequences for metabolic activity. In addition to mitochondria [119], several other sources have been proposed to be involved in the modulation of ROS levels under hypoxia, such as NADPH oxidases [140], or xanthine oxidase [141].

The variability of ROS production in response to changes in the ambient oxygen partial pressure has been linked with the activation of the HIF α-subunits. Although controversial data exist, there is evidence for a feedback regulation between ROS production and the HIF pathway. However, it appears that the molecular links between ROS, the complexes involved in oxidative phosphorylation (OXPHOS), and responses to hypoxia through the HIF pathway are complex, less direct and may involve cell specific factors [142,143]. This is indicated by the fact that most of the interventions (if not all) on OXPHOS complexes alter not only ROS production but also other activities, especially oxygen consumption, oxygen redistribution [144], or metabolites taking part in the HIF-α degrading PHD reaction such as 2-oxoglutarate or succinate (see above). In addition to this, several molecular approaches including overexpression of antioxidant enzymes showed a link between HIF activation and ROS formation which was independent of the cellular oxygen consumption [115–118].

Vice versa, adaptation to hypoxia through the HIF pathway has also an effect on ROS production. Both, NOX2 and NOX4 NADPH oxidases are HIF1 target genes [114,145] and are involved in maintaining angiogenesis, cellular proliferation, and hypoxia-induced pulmonary hypertension [114], as well as in metabolic diseases [146,147]. In mitochondria, several HIF-dependent mechanisms have been described that actively contribute to reduce OXPHOS activity under hypoxia and which have been shown (in more or less detail) to reduce mitochondrial ROS production: reduction of pyruvate entry into the TCA cycle through enhanced expression of PDK1 [148,149], PDK3 [150] or PDK4 [151,152], reduction of complex I activity through upregulation of NDUFA4L2 expression [153], and reduction of the activity of iron-sulfur clusters-containing proteins (among them OXPHOS complexes) by enhanced expression of miR-210, which represses the iron-sulfur cluster assembly proteins ISCU1/2 [154].

In addition, HIF-1α and HIF-2α are able to affect mitochondrial ROS production also in a negative manner. Thereby HIF-1 regulates the hypoxic switch from COX4-1 to COX4-2 in cytochrome c oxidase at complex IV, and the mitochondrial protease LON which degrades COX4-1 [155]. In line, HIF-1α-dependent upregulation of the tumor suppressor REDD1 decreases ROS production while loss of REDD1 increases mitochondrial ROS [156]. HIF-2α was found to be involved in the regulation of the SOD2 gene [157]. Together, these mechanisms are part of a negative feedback loop for regulation of HIF-1α and HIF-2α.

Another mechanism by which hypoxic responses can be mediated through ROS production is reversible protein cysteine oxidation. Indeed, the recent use of a redox proteomic method, by which reversibly oxidized protein cysteines are specifically labeled [158], has helped to identify a number of proteins specifically oxidized in cardiac mitochondria from mice subjected to ischemia/reperfusion or from endothelial cells subjected to acute hypoxia [113,159]. Thus, the identification of reversibly oxidized proteins by a fluorescent labeling and LC-MS/MS-based approach provides the option to explore more closely the links between acute or chronic adaptations to hypoxia and ROS generation.

Together, it is obvious that an intricate interplay between hypoxia and ROS production exists and that this involves feed-

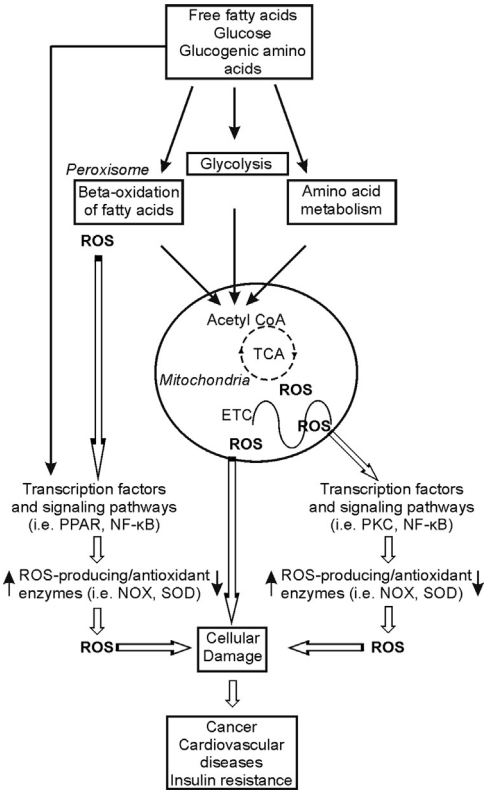

Fig. 4. Nutrients modulate ROS generation. Nutrients (free fatty acids, glucose, amino acids) stimulate ROS production by increasing the postprandial metabolic rate, especially in mitochondria. Further, nutrients affect ROS via signal cascades and transcription factors that regulate expression of antioxidant/ROS-generating enzymes.

forward and feed-back mechanisms involving HIFs function. However, the detailed mechanisms, the timing of the responses as well as the cell-type specific factors involved in these regulations need still further investigations before they are completely understood.

6. Dietary fashion, ROS, and diseases

In Western societies, a significant part of the day is spent in the postprandial state. Postprandial oxidative stress is characterized by an increased susceptibility of the organism towards oxidative damage after consumption of a meal rich in lipids, proteins and/or carbohydrates (Fig.4). Evolution of dietary patterns and lifestyle in most developed countries support the evidence that there is a direct relationship between diet, lifestyle and risk of certain diseases including cancer; up to 35% of risk is estimated to be associated with diet [160]. The postprandial state is characterized by persistent substrate abundance in the circulation. Increased substrate availability (like glucose), leads to an increased insulin release and also to an increment in oxidative stress as, for example, a higher production of reactive oxygen species (ROS) [161]. The permanent availability of oxidizable substrates at rest leads to an enhanced mitochondrial membrane potential which, in turn, leads to a diminished velocity in oxidative phosphorylation and, thus, a higher possibility for electrons to "leak" from the respiratory chain directly to molecular oxygen, resulting in ROS generation [162] (Fig. 4). In turn, the diminished substrate utilization is accompanied by an increment in NADH, in both the cytosol and in mitochondria. NAD+ and NADH values are kept relatively constant within a cell, and the ratio between them is considered to be a marker of the metabolic status [163]. As such, high levels of cellular nutrient metabolites result in ROS production and oxidative stress as well as the development and progression of diseases like obesity, non-alcoholic fatty liver diseases (NAFLD), type II diabetes, atherosclerosis or cancer which are increasing, rapidly reaching epidemic proportions.

In addition to the direct effect on ROS production, mainly via the ETC, although data on NADPH oxidases also exist, nutrients have long-term indirect effects on ROS levels via regulation of gene expression. Thereby peroxisome proliferator-activated receptors (PPAR), liver X receptors, and sterol response element-binding proteins, contribute to fatty acid-induced transcription [164]. In particular PPARγ was found to promote elimination of ROS; in a murine model of type 2 diabetes, PPARγ activation exerted an antioxidant effect in vivo [165] and decreased expression of PPARγ in morbidly obese persons was associated with the decrease of Cu/ZnSOD and glutaredoxin activities and an increase in the concentration of free fatty acids after a fat meal [166]. These features as well as the link between PPARγ, HIF-1α and activated fatty acid uptake and glycerolipid synthesis seem to be important for cardiac contractile dysfunction. Indeed, deletion of HIF-1α in the heart of mice prevented hypertrophy-induced PPARγ activation, metabolic reprogramming, and contractile dysfunction [167]. In addition, fatty acids and glucose may modify the activity of transcription factors like NF-κB, and HIF-1α [74,164] which have antioxidant as well as ROS-generating enzyme coding genes as targets. Therefore, transcription factors like NF-κB or HIF-1 can respond to a macronutrient-dependent burst in ROS as well as to the macronutrient-mediated regulation of intracellular signaling pathways like PKC or PKB. Overall, the short-term action of macronutrients may increase ROS, but they may also cause increased ROS scavenging via their long-term action on transcription factors.

6.1. Diets and oxidative stress

High-fat diets (HFDs) typically contain about 32–60% of calories from fat and are commonly used to induce obesity in rodents [168,169]. A HFD is associated with body weight increase, fat deposition throughout various organs, a marked insulin resistance and development of a hypoxic status in the fat depositing organs. Before a significant peripheral fat deposition occurs, HFDs typically increase liver fat levels as well as hepatic insulin resistance, elevation of ROS and oxidative stress [170]. In addition, the hypoxic status becomes evident already after three days of feeding a HFD in white adipocytes. Subsequently, HIF-1α induction contributes to an off-set of the chronic adipose tissue inflammatory response [171]. Importantly, the source of dietary fat can modify the "phenotype"; e.g. in comparison to fat from butter, polyunsaturated fats present in olive and fish oil increase liver fat oxidation, reduce liver triglyceride accumulation and liver cholesterol levels, respectively [172] as well as induce expression of pro-inflammatory genes [173].

An excess intake of refined carbohydrates is associated with increased weight gain, hypertriglyceridemia, ROS production and insulin resistance in humans and animal models [174,175]. Usually, rodent chow diets contain only 4% sucrose and less than 0.5% of free fructose with most carbohydrates as both digestible starch and non-digestible fiber from grain sources. In contrast, low-fat purified diets can contain higher levels of sucrose and this will depend heavily on the formula being used. It is possible to modify purified diets by manipulating only the carbohydrates while the essential nutrients remain at recommended levels to promote a metabolic syndrome and to have different oxidative stress levels.

A methionine and choline-deficient (MCD) diet rapidly induces hepatic macrovesicular steatosis in rodents and leads to inflammation, fibrosis and cancer [176,177]. The MCD diet also contains sucrose, which induces de novo lipogenesis and

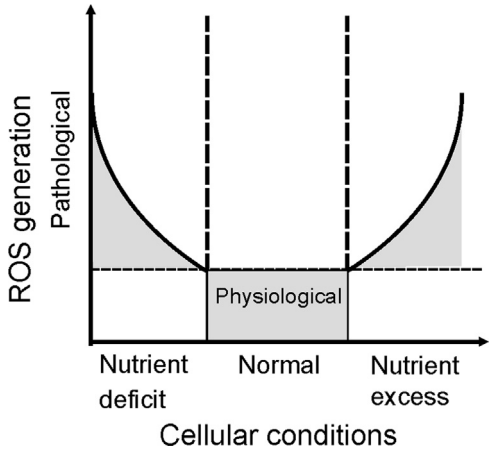

Fig. 5. ROS generation and nutrient availability. Under nutrient-deficient conditions, as well as in the presence of nutrient excess ROS formation is above the physiological threshold. As such, these conditions may be considered as pathological situations, with abnormally high ROS generation.

triglyceride synthesis. Despite inducing the same overall level of hepatic fat accumulation, fructose was more effective than glucose in inducing hepatocellular injury in mice fed MCD diets for 21 days [178]. A choline-deficient diet alone induces only steatosis, inflammation and fibrosis within 10 weeks [179,180], but not a marked hepatitis, cirrhosis or hepatocellular carcinoma. A choline-deficient L-amino acid-defined diet leads to the development of typical non-alcoholic steatohepatitis (NASH), with lobular inflammation and fibrosis, a basis on which further hepatocarcinoma develops [181].

6.2. Metabolic reprogramming and ROS generation

Several studies are consistent with the idea that an increased caloric intake and/or obesity are associated with a pro-oxidant environment and increased oxidative damage [8–12] (Fig. 5). In line, both protein carbonylation and lipid peroxidation were increased in white adipose tissue and liver of animals with high-nutrient feeding induced obesity [182]. Increased ROS production was shown in mitochondria isolated from skeletal muscle, kidney, liver and adipose tissue from obese HFD fed animals [183–186]. In addition, NADPH oxidases have also been described to contribute to elevated ROS levels and to be upregulated in the liver in several animal models of nonalcoholic fatty liver disease and nonalcoholic steatohepatitis [187,188] where animals were treated with an "high-fat" or "hypercholesterolemic" diet. Interestingly, female mice lacking the NADPH oxidase subunit p47phox are protected against high fat diet induced obesity [189]. Similar results have been obtained in NOX2-deficient mice [190] while NOX4 deficient mice were reported to be more obese and to have hepatic steatosis and whole body insulin resistance [191]. The role of NOX2 in insulin resistance was also corroborated in skeletal muscle. Here, a long-term HFD increased NOX2 expression, superoxide production, and impaired insulin signaling in skeletal muscle of wild-type mice; these effects were not occurring in NOX2-deficient mice. Cell culture experiments with C2C12 myotubes revealed a key role for H_2O_2 in mediating insulin resistance since down-regulation of NOX2 by shRNA prevented insulin resistance induced by high glucose or palmitate [192].

Further, increased mitochondrial ROS were found to be involved in short-term HFD-induced insulin resistance in white adipose tissue. Consuming a high-fat diet for one week impaired insulin signaling, increased c-Jun NH2-terminal kinase phosphorylation and mitochondrial ROS formation. Overexpression of human catalase in the mitochondria of these mice attenuated mitochondrial ROS formation, inflammation, and maintained insulin signaling. Thus, elevated mitochondrial ROS formation can contribute to HFD-induced insulin resistance in white adipose tissue [193]. Moreover, HIF transcription factors were shown to be induced by NOX4-derived ROS [132,194] and lipid load [106,195]. Thus, HIFs and NOXes appear to be involved in insulin resistance, metabolic dysfunction and inflammation [171,196,197] and thus might play an important role in the concert of redox related processes promoting the development of steatohepatitis, obesity and type II diabetes, and aging-related diseases. Aging tissues exhibit higher rates of ROS generation, genetic instability, and inflammation and in some cases telomere shortening which is accelerated during diabetes [198,199].

Conditions of reduced glucose supply activate metabolic reprogramming that switches cells to metabolize fatty acids and amino acids through the TCA cycle and OXPHOS; this elevates the risk of mitochondrial oxidative damage, when compared only to the metabolization of glucose via glycolysis (Fig. 5). Exposure of cells in culture to free fatty acids increases ROS, suggesting that an elevated concentration of fatty acids in the circulation may provide an additional source of excess OXPHOS substrates through increased fatty acid oxidation [200]. However, studies performed with obese animals that develop diabetes, have shown a state of metabolic inefficiency where an increase in cardiac fatty acid utilization is associated with enhanced mitochondrial oxygen consumption but a lower cardiac contractile capacity [201–203]. Moreover, these hearts exhibit limited ATP generation associated with fatty acid-induced mitochondrial uncoupling and are unable to modulate their substrate utilization in response to insulin and fatty acid supply [201,204]. These findings suggest that mitochondrial dysfunction in response to diets may arise from lipotoxicity or oxidative stress [205,206] rather than from changes in glucose concentrations [204,206]. This view is supported by a study indicating that ROS are also involved in obesity-induced autophagy. Interestingly HFD fed transgenic mice with cardiac overexpression of catalase did not display ROS production and showed suppressed autophagy in the heart. In addition, the HFD compromised myocardial geometry and function like hypertrophy, enlarged left ventricular end systolic and diastolic diameters, fractional shortening, cardiomyocyte contractile capacity and intracellular Ca^{2+} were attenuated by catalase. On the molecular level these HFD-mediated effects in the heart seemed to be transmitted by an IKKβ-AMPK-dependent pathway which could be inhibited by catalase [207].

By contrast, the metabolism in cancer cells is a strong example how glucose deprivation and altered mitochondrial function contribute to massive ROS production [208]. Energy production in cancer cells is abnormally dependent on glycolysis classically best known the "Warburg effect". Moreover, the rapid proliferating status dictates an increased biosynthesis which is dependent on the availability of building blocks and reducing equivalents [209]. Therefore, cancer cells may be considered to be in a perpetually "hungry" state. NOX1 seems to be involved in regulation of the Warburg effect and metabolic remodeling of hepatic tumor cells towards a sustained production of building blocks required to maintain a high proliferative rate [210].

Moreover, cancer cells often proliferate in a hypoxic milieu, where the adaptation is largely dependent on HIF transcription factors regulated by NOX, and the transcriptional activation of genes involved in various metabolic pathways, among them carbohydrate and fatty acid metabolism. Thereby, the role of hypoxia and HIFs, especially HIF-1 as regulator of carbohydrate metabolism is well established. In this respect, HIFs respond to enhanced levels of insulin [211–213] and regulate almost every gene which is involved in glucose uptake, glycogen synthesis, and glycolysis [142,214]. Reciprocally, gluconeogenesis in liver is reduced under

hypoxia as indicated by the decreased expression of the key gluconeogenic enzyme PCK1 [215]. Moreover, lipid metabolism, in particular in liver, appears to be more regulated by HIF-2 [216]. In addition to the direct involvement of the HIF proteins as powerful regulators of metabolism, recent findings indicated a cross-talk between the insulin signaling pathway and hypoxia signaling at the level of the HIF-regulating proline hydroxylases in liver. In particular PHD3 was found to have a key role since its acute deletion improved insulin sensitivity and ameliorated diabetes by specifically stabilizing HIF-2α [217].

Moreover, a vast majority of endogenously derived fatty acids are synthesized in the cytosol from acetyl-CoA through a large polyfunctional fatty acid synthetase encoded by the FASN gene. Both the cytosolic form of acetyl-CoA synthase and FASN itself can be induced by hypoxia [218]. However, hypoxic induction of FASN appears to be an indirect HIF effect involving first HIF-dependent up-regulation of SREBP1 and an action of SREBP1 on the promoter of FASN [218]. Further, hypoxia and the Ras regulated MAPK pathway were also shown to regulate elongation and desaturation of fatty acids for lipogenesis [219]. In addition to the role of hypoxia/HIF-1-dependent regulation of lipid metabolism, there exist also a number of hypoxia mediated, but HIF1α-independent alterations of lipid metabolites and associated enzymes. For example, a recent metabolomics approach showed that enzymatic steps in fatty acid synthesis and the de novo synthesis of phosphatidylethanolamine and phosphatidylcholine were modified in a HIF1α-dependent fashion whereas palmitate, stearate, phospholipase D3 and platelet activating factor 16 were regulated in a HIF-independent manner [220]. Overall, these findings help to understand why an increased lipid content is a common feature of hypoxic cancer cells [142]

Although stabilization of HIF-1α contributes to a decrease in oxidative phosphorylation, and an initial increase in ROS production, likely via NOX4, it also initiates a later counteracting adaptive response e.g. by switching complex IV subunits or by increasing the mitochondrial manganese superoxide dismutase content [143]. These features may be important for the survival of metastatic cancer cells since it was described that colonization of lungs with cancer cells is dependent on reduced ROS due to HIF-1-mediated metabolic reprogramming [221].

In line, the up-regulation of the antioxidant capacity in some subsets of cancer stem cells appears to be associated with resistance to therapy [222]. This makes exogenous agents, which are able to modulate the susceptibility of cancer cells to oxidative insults, interesting for anticancer strategies [223] and may, at least in part, explain why antioxidant supplementation in cancer patients is not necessarily beneficial (see below).

Recent findings from experiments where the mitochondria targeted redox cycler mitoquinone was able to induce an autophagic growth arrest in breast cancer cells associated with enhanced ROS levels and the initiation of an antioxidant response underline this. Interestingly, a further knockdown of Nrf2 in these cells potentiated the autophagy [224]. In line, more recent data indicate that high ROS can cause autophagy, but that autophagy is able to trigger an antioxidant feedback response by linking autophagy related gene 7 (Atg7) with Keap1 and Nrf2 [225]. Overall, this is in line with findings that a forced activation of Nrf2 has a pro-carcinogenic function (see above) and why antioxidants are not simply protective against cancer (see below).

Moreover, inactivating mutations in genes that promote autophagy have been described in several human cancers, as well as activation of genes that block autophagy [226]. Hyperactivation of the Ser/Thr kinase mammalian target of rapamycin complex 1 (mTORC1) has been shown to promote breast cancer progression through increasing autophagy [227] and aberrant mTORC1 signaling has been frequently detected among common human cancers [228]. Thereby mTORC1 integrates the activation of kinase complexes like receptor tyrosine kinases (RTKs), the PI3K, and the mitogen activated protein kinase (MAPK) pathways which are ROS sensitive and dictates the balance between the energetic and anabolic demands of rapidly proliferating cancer cells [229]; hence linking autophagy with ROS, cancer and nutrition.

6.3. *Antioxidative therapeutic strategies: rather harmful than beneficial?*

The association of ROS with various diseases like atherosclerosis, type II diabetes or cancer is known for more than three decades [5,6,71,230] and accordingly this led to the believe that an antioxidant supplementation would have beneficial therapeutic effects. Indeed, the first observations were promising and an 'antioxidant hype' emerged throughout the world. As a result, high doses of antioxidants were examined in hundreds of studies among them about a dozen of large randomized trials where various combinations of the best known antioxidants except polyphenols (so called 'traditional antioxidants') were included [231]. More than 10 large-scale trials have been completed (for review see [232]). The outcome was enigmatic. There was no corroboration of the data derived from non-human models as well as from observational epidemiologic studies. In particular, meta-analyses of randomized controlled trials including tens of thousands subjects found no overall association between the consumption of antioxidant supplements and cancer risk [233] (for detailed review see [232]). This 'antioxidant paradox' [234] is not only limited to cancer but also reported for type II diabetes and cardiovascular diseases [235,236].

So far it is not known why the antioxidants did not exert the expected protective effects. The wrong type, dose, combination, and/or duration of exposure may explain some but not all. Indeed, in almost all large-scale trials high doses of each antioxidant were used either alone or in limited combinations. In addition, mechanisms of actions have been neglected; some antioxidants including vitamin E, vitamin C, and quercetin, can act as prooxidants at high concentrations. Indeed, meta-analyses of the vitamin E dose and total mortality indicated that vitamin E at high doses $\geq$ 400 IU/day) may be associated with increased mortality due to the prooxidant effects of vitamin E at these concentrations [237]. Moreover, β–carotene can act as prooxidant when given to smokers [238,239]. In line, quercetin at concentrations in the range of 1–40 μM reacts with ROS and chelates metal ions whereas at concentrations higher than 40 μM it increases oxidative stress [240]. Thus, antioxidant therapy may be improved if patients would be tested for subclinical deficiencies of antioxidants before such a therapy is initiated. In addition, the large clinical trials did not test for compliance like the EPIC Norfolk clinical trial in which certain antioxidant levels were measured in plasma and where significant improvement of various parameters could be reported. For example, parental administration of vitamin C was highly beneficial in many different disease conditions [241].

However, the beneficial effects of antioxidant-rich food at least with respect to cancer are widely reported [242–244]; but these benefits are achieved by the diet itself and not by supplementation [245]. Moreover, the dietary intake involves low doses of various antioxidants and not high doses of a single antioxidant. In line, while high doses of single antioxidants were shown to be harmful in smokers, two antioxidant-rich diets were found to be safe in a randomised controlled trial in male smokers [246]. Overall, this suggests that antioxidant therapies are not hopeless but to find an optimal way more research on ROS, antioxidants and nutrition in line with large multicenter trials are necessary.

7. Conclusion

ROS have likely evolved together with the appearance of oxygen on earth and the evolution of aerobic living cells. At the same time aerobic living cells developed systems allowing to use ROS in signaling and to protect themselves from their harmful effects. Within these systems components need to be maintained and provision of certain substances through the diet is a prerequisite. Although the human genome seems to be quite stable for the last ten thousand years (spontaneous mutation rate is appr. 0.5% per million years [247]), dietary fashion, food amount and composition has changed within the last 60–100 years; at least in the Western world. In addition to the increase in the caloric intake, also the decreased energy expenditure as well as alcoholism and smoking contribute to generation of more ROS than needed. As a consequence the antioxidant capability is confronted with various problems and not always able to maintain redox homeostasis, which is, at least in part, associated with the occurrence of several chronic diseases like adiposity, atherosclerosis, type II diabetes, and cancer. In addition, the little or no benefit evidence from the large scale studies with antioxidant supplementation demands to further improve the knowledge about the interconnection of ROS with nutrition and diseases indicating that the associated health problems are not yet solved.

Conflict of interest statement

The authors declare no conflict of interest.

Acknowledgments

The authors are grateful and apologize to all researchers who contributed to the field and whose work could not be cited due to space limitations. This work was supported by grants from German Research Foundation (DFG-GO709/4-5), DZHK (German Centre for Cardiovascular Research), German Federal Ministry of Education and Research (Acidox, Epiros), to AG. Work in the AMR lab was supported by grants from the Spanish Government (PI12/00875) and from the Fundación Domingo Martínez; AMR and PHA are supported by the I3SNS and FPU programs of the Spanish Government, respectively. Work in the TK lab was supported by grants from the Finnish Academy of Sciences, the Sigrid Juselius Foundation, CIMO, and Biocenter Oulu. Some of the authors were supported by the European Cooperation in Science and Technology (COST Action BM1203/EU-ROS).

References

[1] P.M. Wood, The potential diagram for oxygen at pH 7, Biochem. J. 253 (1988) 287–289.
[2] C.C. Winterbourn, Reconciling the chemistry and biology of reactive oxygen species, Nat. Chem. Biol. 4 (2008) 278–286.
[3] T. Kietzmann, A. Gorlach, Reactive oxygen species in the control of hypoxia-inducible factor-mediated gene expression, Semin. Cell. Dev. Biol. 16 (2005) 474–486.
[4] A. Ceriello, E. Motz, Is oxidative stress the pathogenic mechanism underlying insulin resistance, diabetes, and cardiovascular disease? The common soil hypothesis revisited, Arterioscler. Thromb. Vasc. Biol. 24 (2004) 816–823.
[5] D. Ziech, R. Franco, A. Pappa, M.I. Panayiotidis, Reactive oxygen species (ROS)—induced genetic and epigenetic alterations in human carcinogenesis, Mutat. Res. 711 (2011) 167–173.
[6] S.C. Gupta, D. Hevia, S. Patchva, B. Park, W. Koh, et al., Upsides and downsides of reactive oxygen species for cancer: the roles of reactive oxygen species in tumorigenesis, prevention, and therapy, Antioxid. Redox Signal. 16 (2012) 1295–1322.
[7] E.Y. Dimova, A. Samoylenko, T. Kietzmann, Oxidative stress and hypoxia: implications for plasminogen activator inhibitor-1 expression, Antioxid. Redox Signal. 6 (2004) 777–791.
[8] M. Sankhla, T.K. Sharma, K. Mathur, J.S. Rathor, V. Butolia, et al., Relationship of oxidative stress with obesity and its role in obesity induced metabolic syndrome, Clin. Lab. 58 (2012) 385–392.
[9] C. Chrysohoou, D.B. Panagiotakos, C. Pitsavos, J. Skoumas, X. Krinos, et al., Long-term fish consumption is associated with protection against arrhythmia in healthy persons in a Mediterranean region–the ATTICA study, Am. J. Clin. Nutr. 85 (2007) 1385–1391.
[10] N. Houstis, E.D. Rosen, E.S. Lander, Reactive oxygen species have a causal role in multiple forms of insulin resistance, Nature 440 (2006) 944–948.
[11] S. Furukawa, T. Fujita, M. Shimabukuro, M. Iwaki, Y. Yamada, et al., Increased oxidative stress in obesity and its impact on metabolic syndrome, J. Clin. Invest. 114 (2004) 1752–1761.
[12] C.K. Roberts, K.K. Sindhu, Oxidative stress and metabolic syndrome, Life Sci. 84 (2009) 705–712.
[13] N. Kaludercic, S. Deshwal, F. Di Lisa, Reactive oxygen species and redox compartmentalization, Front. Physiol. 5 (2014) 285.
[14] M. Ushio-Fukai, Localizing NADPH oxidase-derived ROS, Sci. STKE 2006 (2006) re8.
[15] M. Geiszt, T.L. Leto, The Nox family of NAD(P)H oxidases: host defense and beyond, J. Biol. Chem. 279 (2004) 51715–51718.
[16] B.M. Babior, J.D. Lambeth, W. Nauseef, The neutrophil NADPH oxidase, Arch. Biochem. Biophys. 397 (2002) 342–344.
[17] X. De Deken, D. Wang, M.C. Many, S. Costagliola, F. Libert, et al., Cloning of two human thyroid cDNAs encoding new members of the NADPH oxidase family, J. Biol. Chem. 275 (2000) 23227–23233.
[18] Y.A. Suh, R.S. Arnold, B. Lassegue, J. Shi, X. Xu, et al., Cell transformation by the superoxide-generating oxidase Mox1, Nature 401 (1999) 79–82.
[19] G. Cheng, Z. Cao, X. Xu, E.G. van Meir, J.D. Lambeth, Homologs of gp91phox: cloning and tissue expression of Nox3, Nox4, and Nox5, Gene 269 (2001) 131–140.
[20] K. Bedard, K.H. Krause, The NOX family of ROS-generating NADPH oxidases: physiology and pathophysiology, Physiol. Rev. 87 (2007) 245–313.
[21] K. Rokutan, T. Kawahara, Y. Kuwano, K. Tominaga, K. Nishida, et al., Nox enzymes and oxidative stress in the immunopathology of the gastrointestinal tract, Semin. Immunopathol. 30 (2008) 315–327.
[22] X.L. Cui, D. Brockman, B. Campos, L. Myatt, Expression of NADPH oxidase isoform 1 (Nox1) in human placenta: involvement in preeclampsia, Placenta 27 (2006) 422–431.
[23] Y. Uchizono, R. Takeya, M. Iwase, N. Sasaki, M. Oku, et al., Expression of isoforms of NADPH oxidase components in rat pancreatic islets, Life Sci. 80 (2006) 133–139.
[24] F.J. Miller Jr., M. Filali, G.J. Huss, B. Stanic, A. Chamseddine, et al., Cytokine activation of nuclear factor kappa B in vascular smooth muscle cells requires signaling endosomes containing Nox1 and ClC-3, Circ. Res. 101 (2007) 663–671.
[25] L.L. Hilenski, R.E. Clempus, M.T. Quinn, J.D. Lambeth, K.K. Griendling, Distinct subcellular localizations of Nox1 and Nox4 in vascular smooth muscle cells, Arterioscler. Thromb. Vasc. Biol. 24 (2004) 677–683.
[26] A. Petry, M. Weitnauer, A. Gorlach, Receptor activation of NADPH oxidases, Antioxid. Redox Signal. 13 (2010) 467–487.
[27] M. Geiszt, J.B. Kopp, P. Varnai, T.L. Leto, Identification of renox, an NAD(P)H oxidase in kidney, Proc. Natl. Acad. Sci. USA 97 (2000) 8010–8014.
[28] I. Carmona-Cuenca, B. Herrera, J.J. Ventura, C. Roncero, M. Fernandez, et al., EGF blocks NADPH oxidase activation by TGF-beta in fetal rat hepatocytes, impairing oxidative stress, and cell death, J. Cell. Physiol. 207 (2006) 322–330.
[29] T. Ago, T. Kitazono, H. Ooboshi, T. Iyama, Y.H. Han, et al., Nox4 as the major catalytic component of an endothelial NAD(P)H oxidase, Circulation 109 (2004) 227–233.
[30] I. Cucoranu, R. Clempus, A. Dikalova, P.J. Phelan, S. Ariyan, et al., NAD(P)H oxidase 4 mediates transforming growth factor-beta1-induced differentiation of cardiac fibroblasts into myofibroblasts, Circ. Res. 97 (2005) 900–907.
[31] A. Petry, T. Djordjevic, M. Weitnauer, T. Kietzmann, J. Hess, et al., NOX2 and NOX4 mediate proliferative response in endothelial cells, Antioxid. Redox Signal. 8 (2006) 1473–1484.
[32] D.I. Brown, K.K. Griendling, Nox proteins in signal transduction, Free Radic. Biol. Med. 47 (2009) 1239–1253.
[33] R.S. BelAiba, T. Djordjevic, A. Petry, K. Diemer, S. Bonello, et al., NOX5 variants are functionally active in endothelial cells, Free Radic. Biol. Med. 42 (2007) 446–459.
[34] X. De Deken, D. Wang, J.E. Dumont, F. Miot, Characterization of ThOX proteins as components of the thyroid H(2)O(2)-generating system, Exp. Cell Res. 273 (2002) 187–196.
[35] H. Fischer, Mechanisms and function of DUOX in epithelia of the lung, Antioxid. Redox Signal. 11 (2009) 2453–2465.
[36] E.M. Ha, C.T. Oh, Y.S. Bae, W.J. Lee, A direct role for dual oxidase in Drosophila gut immunity, Science 310 (2005) 847–850.
[37] F. Tirone, J.A. Cox, NADPH oxidase 5 (NOX5) interacts with and is regulated by calmodulin, FEBS Lett. 581 (2007) 1202–1208.
[38] M.P. Murphy, How mitochondria produce reactive oxygen species, Biochem. J. 417 (2009) 1–13.
[39] M.D. Brand, The sites and topology of mitochondrial superoxide production, Exp. Gerontol. 45 (2010) 466–472.
[40] J. Vina, J. Gambini, R. Lopez-Grueso, K.M. Abdelaziz, M. Jove, et al., Females live longer than males: role of oxidative stress, Curr. Pharm. Des. 17 (2011)

3959–3965.
[41] T. Nishikawa, D. Edelstein, X.L. Du, S. Yamagishi, T. Matsumura, et al., Normalizing mitochondrial superoxide production blocks three pathways of hyperglycaemic damage, Nature 404 (2000) 787–790.
[42] A.R. Cardoso, B. Chausse, F.M. da Cunha, L.A. Luevano-Martinez, T.B. Marazzi, et al., Mitochondrial compartmentalization of redox processes, Free Radic. Biol. Med. 52 (2012) 2201–2208.
[43] C.L. Quinlan, R.L. Goncalves, M. Hey-Mogensen, N. Yadava, V.I. Bunik, et al., The 2-oxoacid dehydrogenase complexes in mitochondria can produce superoxide/hydrogen peroxide at much higher rates than complex I, J. Biol. Chem. 289 (2014) 8312–8325.
[44] K.H. Fisher-Wellman, L.A. Gilliam, C.T. Lin, B.L. Cathey, D.S. Lark, et al., Mitochondrial glutathione depletion reveals a novel role for the pyruvate dehydrogenase complex as a key H2O2-emitting source under conditions of nutrient overload, Free Radic. Biol. Med. 65 (2013) 1201–1208.
[45] L. Tretter, V. Adam-Vizi, Generation of reactive oxygen species in the reaction catalyzed by alpha-ketoglutarate dehydrogenase, J. Neurosci. 24 (2004) 7771–7778.
[46] A.A. Starkov, G. Fiskum, C. Chinopoulos, B.J. Lorenzo, S.E. Browne, et al., Mitochondrial alpha-ketoglutarate dehydrogenase complex generates reactive oxygen species, J. Neurosci. 24 (2004) 7779–7788.
[47] M. Giorgio, E. Migliaccio, F. Orsini, D. Paolucci, M. Moroni, et al., Electron transfer between cytochrome c and p66Shc generates reactive oxygen species that trigger mitochondrial apoptosis, Cell 122 (2005) 221–233.
[48] A. Gorlach, P. Klappa, T. Kietzmann, The endoplasmic reticulum: folding, calcium homeostasis, signaling, and redox control, Antioxid. Redox Signal. 8 (2006) 1391–1418.
[49] M. Janiszewski, L.R. Lopes, A.O. Carmo, M.A. Pedro, R.P. Brandes, et al., Regulation of NAD(P)H oxidase by associated protein disulfide isomerase in vascular smooth muscle cells, J. Biol. Chem. 280 (2005) 40813–40819.
[50] Q. Liu, U. Berchner-Pfannschmidt, U. Moller, M. Brecht, C. Wotzlaw, et al., A Fenton reaction at the endoplasmic reticulum is involved in the redox control of hypoxia-inducible gene expression, Proc. Natl. Acad. Sci. USA 101 (2004) 4302–4307.
[51] H. Nohl, L. Gille, The bifunctional activity of ubiquinone in lysosomal membranes, Biogerontology 3 (2002) 125–131.
[52] T. Kurz, J.W. Eaton, U.T. Brunk, Redox activity within the lysosomal compartment: implications for aging and apoptosis, Antioxid. Redox Signal. 13 (2010) 511–523.
[53] V.D. Antonenkov, S. Grunau, S. Ohlmeier, J.K. Hiltunen, Peroxisomes are oxidative organelles, Antioxid. Redox Signal. 13 (2010) 525–537.
[54] M. Schrader, H.D. Fahimi, Peroxisomes and oxidative stress, Biochim. Biophys. Acta 1763 (2006) 1755–1766.
[55] A.C. Maehly, B. Chance, The assay of catalases and peroxidases, Methods Biochem. Anal. 1 (1954) 357–424.
[56] H. Wiseman, B. Halliwell, Damage to DNA by reactive oxygen and nitrogen species: role in inflammatory disease and progression to cancer, Biochem. J. 313 (Pt 1) (1996) 17–29.
[57] L.J. Marnett, Oxy radicals, lipid peroxidation and DNA damage, Toxicology 181–182 (2002) 219–222.
[58] M. Valko, C.J. Rhodes, J. Moncol, M. Izakovic, M. Mazur, Free radicals, metals and antioxidants in oxidative stress-induced cancer, Chem.-Biol. Interact. 160 (2006) 1–40.
[59] E.R. Stadtman, Role of oxidant species in aging, Curr. Med. Chem. 11 (2004) 1105–1112.
[60] J.S. Carew, P. Huang, Mitochondrial defects in cancer, Mol. Cancer 1 (2002) 9.
[61] A. Tamori, S. Nishiguchi, M. Nishikawa, S. Kubo, N. Koh, et al., Correlation between clinical characteristics and mitochondrial D-loop DNA mutations in hepatocellular carcinoma, J. Gastroenterol. 39 (2004) 1063–1068.
[62] V.W. Liu, H.H. Shi, A.N. Cheung, P.M. Chiu, T.W. Leung, et al., High incidence of somatic mitochondrial DNA mutations in human ovarian carcinomas, Cancer Res. 61 (2001) 5998–6001.
[63] D.J. Tan, R.K. Bai, L.J. Wong, Comprehensive scanning of somatic mitochondrial DNA mutations in breast cancer, Cancer Res. 62 (2002) 972–976.
[64] A. Lievre, C. Chapusot, A.M. Bouvier, F. Zinzindohoue, F. Piard, et al., Clinical value of mitochondrial mutations in colorectal cancer, J. Clin. Oncol. 23 (2005) 3517–3525.
[65] H. Takeuchi, A. Fujimoto, D.S. Hoon, Detection of mitochondrial DNA alterations in plasma of malignant melanoma patients, Ann. N. Y. Acad. Sci. 1022 (2004) 50–54.
[66] Y. Mikhed, A. Gorlach, U.G. Knaus, A. Daiber, Redox regulation of genome stability by effects on gene expression, epigenetic pathways and DNA damage/repair, Redox Biol. 5 (2015) 275–289.
[67] R. Franco, O. Schoneveld, A.G. Georgakilas, M.I. Panayiotidis, Oxidative stress, DNA methylation and carcinogenesis, Cancer Lett. 266 (2008) 6–11.
[68] N. Chia, L. Wang, X. Lu, M.C. Senut, C. Brenner, et al., Hypothesis: environmental regulation of 5-hydroxymethylcytosine by oxidative stress, Epigenetics 6 (2011) 853–856.
[69] P.W. Turk, A. Laayoun, S.S. Smith, S.A. Weitzman, DNA adduct 8-hydroxyl-2'-deoxyguanosine (8-hydroxyguanine) affects function of human DNA methyltransferase, Carcinogenesis 16 (1995) 1253–1255.
[70] P. Kapahi, M.E. Boulton, T.B. Kirkwood, Positive correlation between mammalian life span and cellular resistance to stress, Free Radic. Biol. Med. 26 (1999) 495–500.
[71] B. Vurusaner, G. Poli, H. Basaga, Tumor suppressor genes and ROS: complex networks of interactions, Free Radic. Biol. Med. 52 (2012) 7–18.
[72] M.J. Morgan, Z.G. Liu, Crosstalk of reactive oxygen species and NF-kappaB signaling, Cell Res. 21 (2011) 103–115.
[73] A.R. Kristal, K.B. Arnold, M.L. Neuhouser, P. Goodman, E.A. Platz, et al., Diet, supplement use, and prostate cancer risk: results from the prostate cancer prevention trial, Am. J. Epidemiol. 172 (2010) 566–577.
[74] A. Comba, Y.H. Lin, A.R. Eynard, M.A. Valentich, M.E. Fernandez-Zapico, et al., Basic aspects of tumor cell fatty acid-regulated signaling and transcription factors, Cancer Metastasis Rev. 30 (2011) 325–342.
[75] H. Yao, E. Ashihara, T. Maekawa, Targeting the Wnt/beta-catenin signaling pathway in human cancers, Expert Opin. Ther. Targets 15 (2011) 873–887.
[76] M. Lauth, RAS and Hedgehog—partners in crime, Front. Biosci. (Landmark edition) 16 (2011) 2259–2270.
[77] P.D. Ray, B.W. Huang, Y. Tsuji, Reactive oxygen species (ROS) homeostasis and redox regulation in cellular signaling, Cell. Signal. 24 (2012) 981–990.
[78] N. Badid, F.Z. Ahmed, H. Merzouk, S. Belbraouet, N. Mokhtari, et al., Oxidant/antioxidant status, lipids and hormonal profile in overweight women with breast cancer, Pathol. Oncol. Res. 16 (2010) 159–167.
[79] P. Basnet, N. Skalko-Basnet, Curcumin: an anti-inflammatory molecule from a curry spice on the path to cancer treatment, Molecules 16 (2011) 4567–4598.
[80] A. Knebel, H.J. Rahmsdorf, A. Ullrich, P. Herrlich, Dephosphorylation of receptor tyrosine kinases as target of regulation by radiation, oxidants or alkylating agents, EMBO J. 15 (1996) 5314–5325.
[81] H.M. Lander, D.P. Hajjar, B.L. Hempstead, U.A. Mirza, B.T. Chait, et al., A molecular redox switch on p21(ras). Structural basis for the nitric oxide-p21(ras) interaction, J. Biol. Chem. 272 (1997) 4323–4326.
[82] J.A. McCubrey, L.S. Steelman, W.H. Chappell, S.L. Abrams, E.W. Wong, et al., Roles of the Raf/MEK/ERK pathway in cell growth, malignant transformation and drug resistance, Biochim. Biophys. Acta 1773 (2007) 1263–1284.
[83] D.W. Chan, V.W. Liu, G.S. Tsao, K.M. Yao, T. Furukawa, et al., Loss of MKP3 mediated by oxidative stress enhances tumorigenicity and chemoresistance of ovarian cancer cells, Carcinogenesis 29 (2008) 1742–1750.
[84] M.Z. Mehdi, Z.M. Azar, A.K. Srivastava, Role of receptor and nonreceptor protein tyrosine kinases in H2O2-induced PKB and ERK1/2 signaling, Cell Biochem. Biophys. 47 (2007) 1–10.
[85] J. Lee, S. Giordano, J. Zhang, Autophagy, mitochondria and oxidative stress: cross-talk and redox signalling, Biochem. J. 441 (2012) 523–540.
[86] Y.Y. Huo, G. Li, R.F. Duan, Q. Gou, C.L. Fu, et al., PTEN deletion leads to deregulation of antioxidants and increased oxidative damage in mouse embryonic fibroblasts, Free Radical Biol. Med. 44 (2008) 1578–1591.
[87] H. Konishi, M. Tanaka, Y. Takemura, H. Matsuzaki, Y. Ono, et al., Activation of protein kinase C by tyrosine phosphorylation in response to H_2O_2, Proc. Natl. Acad. Sci. USA 94 (1997) 11233–11237.
[88] M.G. Kazanietz, Targeting protein kinase C and "non-kinase" phorbol ester receptors: emerging concepts and therapeutic implications, Biochim. Biophys. Acta 1754 (2005) 296–304.
[89] H. Konishi, E. Yamauchi, H. Taniguchi, T. Yamamoto, H. Matsuzaki, et al., Phosphorylation sites of protein kinase C delta in H2O2-treated cells and its activation by tyrosine kinase in vitro, Proc. Natl. Acad. Sci. USA 98 (2001) 6587–6592.
[90] M. Qatanani, M.A. Lazar, Mechanisms of obesity-associated insulin resistance: many choices on the menu, Genes Dev. 21 (2007) 1443–1455.
[91] A. Ostman, J. Frijhoff, A. Sandin, F.D. Bohmer, Regulation of protein tyrosine phosphatases by reversible oxidation, J. Biochem. 150 (2011) 345–356.
[92] Y. Lavrovsky, B. Chatterjee, R.A. Clark, A.K. Roy, Role of redox-regulated transcription factors in inflammation, aging and age-related diseases, Exp. Gerontol. 35 (2000) 521–532.
[93] A. Speciale, J. Chirafisi, A. Saija, F. Cimino, Nutritional antioxidants and adaptive cell responses: an update, Curr. Mol. Med. 11 (2011) 770–789.
[94] L. Tornatore, A.K. Thotakura, J. Bennett, M. Moretti, G. Franzoso, The nuclear factor kappa B signaling pathway: integrating metabolism with inflammation, Trends Cell Biol. 22 (2012) 557–566.
[95] H. Kamata, T. Manabe, S. Oka, K. Kamata, H. Hirata, Hydrogen peroxide activates IkappaB kinases through phosphorylation of serine residues in the activation loops, FEBS Lett. 519 (2002) 231–237.
[96] M. Jamaluddin, S. Wang, I. Boldogh, B. Tian, A.R. Brasier, TNF-alpha-induced NF-kappaB/RelA Ser(276) phosphorylation and enhanceosome formation is mediated by an ROS-dependent PKAc pathway, Cell. Signal. 19 (2007) 1419–1433.
[97] J.R. Matthews, W. Kaszubska, G. Turcatti, T.N. Wells, R.T. Hay, Role of cysteine62 in DNA recognition by the P50 subunit of NF-kappa B, Nucl. Acids Res. 21 (1993) 1727–1734.
[98] E. Pineda-Molina, P. Klatt, J. Vazquez, A. Marina, M. Garcia de Lacoba, et al., Glutathionylation of the p50 subunit of NF-kappaB: a mechanism for redox-induced inhibition of DNA binding, Biochemistry 40 (2001) 14134–14142.
[99] H. Motohashi, M. Yamamoto, Nrf2-Keap1 defines a physiologically important stress response mechanism, Trends Mol. Med. 10 (2004) 549–557.
[100] L. Baird, A.T. Dinkova-Kostova, The cytoprotective role of the Keap1-Nrf2 pathway, Arch. Toxicol. 85 (2011) 241–272.
[101] A.T. Dinkova-Kostova, W.D. Holtzclaw, R.N. Cole, K. Itoh, N. Wakabayashi, et al., Direct evidence that sulfhydryl groups of Keap1 are the sensors regulating induction of phase 2 enzymes that protect against carcinogens and oxidants, Proc. Natl. Acad. Sci. USA 99 (2002) 11908–11913.
[102] A.K. Jain, S. Mahajan, A.K. Jaiswal, Phosphorylation and dephosphorylation of tyrosine 141 regulate stability and degradation of INrf2: a novel mechanism in Nrf2 activation, J. Biol. Chem. 283 (2008) 17712–17720.

[103] Q. Ma, X. He, Molecular basis of electrophilic and oxidative defense: promises and perils of Nrf2, Pharmacol. Rev. 64 (2012) 1055–1081.
[104] N. Wakabayashi, K. Itoh, J. Wakabayashi, H. Motohashi, S. Noda, et al., Keap1-null mutation leads to postnatal lethality due to constitutive Nrf2 activation, Nat. Genet. 35 (2003) 238–245.
[105] T. Jiang, N. Chen, F. Zhao, X.J. Wang, B. Kong, et al., High levels of Nrf2 determine chemoresistance in type II endometrial cancer, Cancer Res. 70 (2010) 5486–5496.
[106] A. Gorlach, T. Kietzmann, Superoxide and derived reactive oxygen species in the regulation of hypoxia-inducible factors, Methods Enzymol. 435 (2007) 421–446.
[107] P. Carrero, K. Okamoto, P. Coumailleau, S. O'Brien, H. Tanaka, et al., Redox-regulated recruitment of the transcriptional coactivators CREB-binding protein and SRC-1 to hypoxia-inducible factor 1alpha, Mol. Cell. Biol. 20 (2000) 402–415.
[108] D. Lando, I. Pongratz, L. Poellinger, M.L. Whitelaw, A redox mechanism controls differential DNA binding activities of hypoxia-inducible factor (HIF) 1alpha and the HIF-like factor, J. Biol. Chem. 275 (2000) 4618–4627.
[109] T. Hagen, Oxygen versus reactive oxygen in the regulation of HIF-1alpha: the balance tips, Biochem. Res. Int. 2012 (2012) 436981.
[110] T. Jokilehto, P.M. Jaakkola, The role of HIF prolyl hydroxylases in tumour growth, J. Cell. Mol. Med. 14 (2010) 758–770.
[111] V.A. Kobliakov, Mechanisms of tumor promotion by reactive oxygen species, BiochemistryBiokhimiia 75 (2010) 675–685.
[112] K.J. Nytko, N. Maeda, P. Schlafli, P. Spielmann, R.H. Wenger, et al., Vitamin C is dispensable for oxygen sensing in vivo, Blood 117 (2011) 5485–5493.
[113] A. Izquierdo-Alvarez, E. Ramos, J. Villanueva, P. Hernansanz-Agustin, R. Fernandez-Rodriguez, et al., Differential redox proteomics allows identification of proteins reversibly oxidized at cysteine residues in endothelial cells in response to acute hypoxia, J. Proteom. 75 (2012) 5449–5462.
[114] I. Diebold, A. Petry, J. Hess, A. Gorlach, The NADPH oxidase subunit NOX4 is a new target gene of the hypoxia-inducible factor-1, Mol. Biol. Cell 21 (2010) 2087–2096.
[115] J.K. Brunelle, E.L. Bell, N.M. Quesada, K. Vercauteren, V. Tiranti, et al., Oxygen sensing requires mitochondrial ROS but not oxidative phosphorylation, Cell Metab. 1 (2005) 409–414.
[116] E.L. Bell, T.A. Klimova, J. Eisenbart, C.T. Moraes, M.P. Murphy, et al., The Qo site of the mitochondrial complex III is required for the transduction of hypoxic signaling via reactive oxygen species production, J. Cell Biol. 177 (2007) 1029–1036.
[117] K.D. Mansfield, R.D. Guzy, Y. Pan, R.M. Young, T.P. Cash, et al., Mitochondrial dysfunction resulting from loss of cytochrome c impairs cellular oxygen sensing and hypoxic HIF-alpha activation, Cell Metab. 1 (2005) 393–399.
[118] R.D. Guzy, B. Hoyos, E. Robin, H. Chen, L. Liu, et al., Mitochondrial complex III is required for hypoxia-induced ROS production and cellular oxygen sensing, Cell Metab. 1 (2005) 401–408.
[119] R.B. Hamanaka, N.S. Chandel, Mitochondrial reactive oxygen species regulate hypoxic signaling, Curr. Opin. Cell Biol. 21 (2009) 894–899.
[120] E.Y. Dimova, C. Michiels, T. Kietzmann, Kinases as upstream regulators of the HIF system: their emerging potential as anti-cancer drug targets, Curr. Pharm. Des. 15 (2009) 3867–3877.
[121] A. Gorlach, I. Diebold, V.B. Schini-Kerth, U. Berchner-Pfannschmidt, U. Roth, et al., Thrombin activates the hypoxia-inducible factor-1 signaling pathway in vascular smooth muscle cells: Role of the p22(phox)-containing NADPH oxidase, Circ. Res. 89 (2001) 47–54.
[122] D.E. Richard, E. Berra, J. Pouyssegur, Nonhypoxic pathway mediates the induction of hypoxia-inducible factor 1alpha in vascular smooth muscle cells, J. Biol. Chem. 275 (2000) 26765–26771.
[123] R. Fukuda, B. Kelly, G.L. Semenza, Vascular endothelial growth factor gene expression in colon cancer cells exposed to prostaglandin E2 is mediated by hypoxia-inducible factor 1, Cancer Res. 63 (2003) 2330–2334.
[124] F.S. Wang, C.J. Wang, Y.J. Chen, P.R. Chang, Y.T. Huang, et al., Ras induction of superoxide activates ERK-dependent angiogenic transcription factor HIF-1alpha and VEGF-A expression in shock wave-stimulated osteoblasts, J. Biol. Chem. 279 (2004) 10331–10337.
[125] N. Gao, B.H. Jiang, S.S. Leonard, L. Corum, Z. Zhang, et al., p38 Signaling-mediated hypoxia-inducible factor 1alpha and vascular endothelial growth factor induction by Cr(VI) in DU145 human prostate carcinoma cells, J. Biol. Chem. 277 (2002) 45041–45048.
[126] T. Kietzmann, K. Jungermann, A. Gorlach, Regulation of the hypoxia-dependent plasminogen activator inhibitor 1 expression by MAP kinases, Thromb. Haemost. 89 (2003) 666–673.
[127] S. Frede, C. Stockmann, P. Freitag, J. Fandrey, Bacterial lipopolysaccharide induces HIF-1 activation in human monocytes via p44/42 MAPK and NF-kappaB, Biochem. J. 396 (2006) 517–527.
[128] L. Tacchini, C. De Ponti, E. Matteucci, R. Follis, M.A. Desiderio, Hepatocyte growth factor-activated NF-kappaB regulates HIF-1 activity and ODC expression, implicated in survival, differently in different carcinoma cell lines, Carcinogenesis 25 (2004) 2089–2100.
[129] E.L. Page, G.A. Robitaille, J. Pouyssegur, D.E. Richard, Induction of hypoxia-inducible factor-1alpha by transcriptional and translational mechanisms, J. Biol. Chem. 277 (2002) 48403–48409.
[130] I. Diebold, T. Djordjevic, J. Hess, A. Gorlach, Rac-1 promotes pulmonary artery smooth muscle cell proliferation by upregulation of plasminogen activator inhibitor-1: role of NFkappaB-dependent hypoxia-inducible factor-1alpha transcription, Thromb. Haemost. 100 (2008) 1021–1028.
[131] J. Rius, M. Guma, C. Schachtrup, K. Akassoglou, A.S. Zinkernagel, et al., NF-kappaB links innate immunity to the hypoxic response through transcriptional regulation of HIF-1alpha, Nature 453 (2008) 807–811.
[132] S. Bonello, C. Zahringer, R.S. BelAiba, T. Djordjevic, J. Hess, et al., Reactive oxygen species activate the HIF-1alpha promoter via a functional NFkappaB site, Arterioscler. Thromb. Vasc. Biol. 27 (2007) 755–761.
[133] P. van Uden, N.S. Kenneth, S. Rocha, Regulation of hypoxia-inducible factor-1alpha by NF-kappaB, Biochem. J. 412 (2008) 477–484.
[134] A. Gorlach, S. Bonello, The cross-talk between NF-kappaB and HIF-1: further evidence for a significant liaison, Biochem. J. 412 (2008) e17–e19.
[135] R.S. Belaiba, S. Bonello, C. Zahringer, S. Schmidt, J. Hess, et al., Hypoxia up-regulates hypoxia-inducible factor-1alpha transcription by involving phosphatidylinositol 3-kinase and nuclear factor kappaB in pulmonary artery smooth muscle cells, Mol. Biol. Cell. 18 (2007) 4691–4697.
[136] I. Diebold, A. Petry, T. Djordjevic, R.S. Belaiba, J. Fineman, et al., Reciprocal regulation of Rac1 and PAK-1 by HIF-1alpha: a positive-feedback loop promoting pulmonary vascular remodeling, Antioxid. Redox Signal. 13 (2010) 399–412.
[137] A. Petry, R.S. BelAiba, M. Weitnauer, A. Gorlach, Inhibition of endothelial nitric oxyde synthase increases capillary formation via Rac1-dependent induction of hypoxia-inducible factor-1alpha and plasminogen activator inhibitor-1, Thromb. Haemost. 108 (2012) 849–862.
[138] A. Rudich, H. Kanety, N. Bashan, Adipose stress-sensing kinases: linking obesity to malfunction, Trends Endocrinol. Metab. 18 (2007) 291–299.
[139] P. Hernansanz-Agustin, A. Izquierdo-Alvarez, F.J. Sanchez-Gomez, E. Ramos, T. Villa-Pina, et al., Acute hypoxia produces a superoxide burst in cells, Free Radic. Biol. Med. 71 (2014) 146–156.
[140] C. Marshall, A.J. Mamary, A.J. Verhoeven, B.E. Marshall, Pulmonary artery NADPH-oxidase is activated in hypoxic pulmonary vasoconstriction, Am. J. Respir. Cell Mol. Biol. 15 (1996) 633–644.
[141] A.Y. Abramov, A. Scorziello, M.R. Duchen, Three distinct mechanisms generate oxygen free radicals in neurons and contribute to cell death during anoxia and reoxygenation, J. Neurosci. 27 (2007) 1129–1138.
[142] G.L. Semenza, HIF-1: upstream and downstream of cancer metabolism, Curr. Opin. Genet. Dev. 20 (2010) 51–56.
[143] E. Hervouet, A. Cizkova, J. Demont, A. Vojtiskova, P. Pecina, et al., HIF and reactive oxygen species regulate oxidative phosphorylation in cancer, Carcinogenesis 29 (2008) 1528–1537.
[144] T. Hagen, C.T. Taylor, F. Lam, S. Moncada, Redistribution of intracellular oxygen in hypoxia by nitric oxide: effect on HIF1alpha, Science 302 (2003) 1975–1978.
[145] I. Diebold, A. Petry, K. Sabrane, T. Djordjevic, J. Hess, et al., The HIF1 target gene NOX2 promotes angiogenesis through urotensin-II, J. Cell Sci. 125 (2012) 956–964.
[146] A. Whaley-Connell, J.R. Sowers, Oxidative stress in the cardiorenal metabolic syndrome, Curr. Hypertens. Rep. 14 (2012) 360–365.
[147] S.R. Costford, J. Castro-Alves, K.L. Chan, L.J. Bailey, M. Woo, et al., Mice lacking NOX2 are hyperphagic and store fat preferentially in the liver, Am. J. Physiol. Endocrinol. Metab. 306 (2014) E1341–E1353.
[148] J.W. Kim, I. Tchernyshyov, G.L. Semenza, C.V. Dang, HIF-1-mediated expression of pyruvate dehydrogenase kinase: a metabolic switch required for cellular adaptation to hypoxia, Cell Metab. 3 (2006) 177–185.
[149] I. Papandreou, R.A. Cairns, L. Fontana, A.L. Lim, N.C. Denko, HIF-1 mediates adaptation to hypoxia by actively downregulating mitochondrial oxygen consumption, Cell Metab. 3 (2006) 187–197.
[150] C.W. Lu, S.C. Lin, K.F. Chen, Y.Y. Lai, S.J. Tsai, Induction of pyruvate dehydrogenase kinase-3 by hypoxia-inducible factor-1 promotes metabolic switch and drug resistance, J. Biol. Chem. 283 (2008) 28106–28114.
[151] J.H. Lee, E.J. Kim, D.K. Kim, J.M. Lee, S.B. Park, et al., Hypoxia induces PDK4 gene expression through induction of the orphan nuclear receptor ERR-gamma, PLoS One 7 (2012) e46324.
[152] L. Zhong, A. D'Urso, D. Toiber, C. Sebastian, R.E. Henry, et al., The histone deacetylase Sirt6 regulates glucose homeostasis via Hif1alpha, Cell 140 (2010) 280–293.
[153] D. Tello, E. Balsa, B. Acosta-Iborra, E. Fuertes-Yebra, A. Elorza, et al., Induction of the mitochondrial NDUFA4L2 protein by HIF-1alpha decreases oxygen consumption by inhibiting Complex I activity, Cell Metab. 14 (2011) 768–779.
[154] S.Y. Chan, Y.Y. Zhang, C. Hemann, C.E. Mahoney, J.L. Zweier, et al., MicroRNA-210 controls mitochondrial metabolism during hypoxia by repressing the iron-sulfur cluster assembly proteins ISCU1/2, Cell Metab. 10 (2009) 273–284.
[155] R. Fukuda, H. Zhang, J.W. Kim, L. Shimoda, C.V. Dang, et al., HIF-1 regulates cytochrome oxidase subunits to optimize efficiency of respiration in hypoxic cells, Cell 129 (2007) 111–122.
[156] P. Horak, A.R. Crawford, D.D. Vadysirisack, Z.M. Nash, M.P. DeYoung, et al., Negative feedback control of HIF-1 through REDD1-regulated ROS suppresses tumorigenesis, Proc. Natl. Acad. Sci. USA 107 (2010) 4675–4680.
[157] M. Scortegagna, K. Ding, Y. Oktay, A. Gaur, F. Thurmond, et al., Multiple organ pathology, metabolic abnormalities and impaired homeostasis of reactive oxygen species in Epas1-/- mice, Nat. Genet. 35 (2003) 331–340.
[158] A. Izquierdo-Alvarez, A. Martinez-Ruiz, Thiol redox proteomics seen with fluorescent eyes: the detection of cysteine oxidative modifications by fluorescence derivatization and 2-DE, J. Proteom. 75 (2011) 329–338.
[159] P. Martinez-Acedo, E. Nunez, F.J. Gomez, M. Moreno, E. Ramos, et al., A novel strategy for global analysis of the dynamic thiol redox proteome, Mol. Cell. Proteom. 11 (2012) 800–813.

[160] R. Baena Ruiz, P. Salinas Hernandez, Diet and cancer: risk factors and epidemiological evidence, Maturitas 77 (2014) 202–208.
[161] H.P. Hammes, X. Du, D. Edelstein, T. Taguchi, T. Matsumura, et al., Benfotiamine blocks three major pathways of hyperglycemic damage and prevents experimental diabetic retinopathy, Nat. Med. 9 (2003) 294–299.
[162] A.P. Rolo, C.M. Palmeira, Diabetes and mitochondrial function: role of hyperglycemia and oxidative stress, Toxicol. Appl. Pharmacol. 212 (2006) 167–178.
[163] J.S. Teodoro, A.P. Gomes, A.T. Varela, F.V. Duarte, A.P. Rolo, et al., Uncovering the beginning of diabetes: the cellular redox status and oxidative stress as starting players in hyperglycemic damage, Mol. Cell. Biochem. 376 (2013) 103–110.
[164] T. Vallim, A.M. Salter, Regulation of hepatic gene expression by saturated fatty acids, Prostaglandins Leukot. Essent. Fatty Acids 82 (2010) 211–218.
[165] Z. Bagi, A. Koller, G. Kaley, PPARgamma activation, by reducing oxidative stress, increases NO bioavailability in coronary arterioles of mice with Type 2 diabetes, Am. J. Physiol. Heart Circ. Physiol. 286 (2004) H742–H748.
[166] E. Garcia-Fuentes, M. Murri, L. Garrido-Sanchez, S. Garcia-Serrano, J. M. Garcia-Almeida, et al., PPARgamma expression after a high-fat meal is associated with plasma superoxide dismutase activity in morbidly obese persons, Obesity (Silver Spring, Md) 18 (2010) 952–958.
[167] J. Krishnan, M. Suter, R. Windak, T. Krebs, A. Felley, et al., Activation of a HIF1alpha-PPARgamma axis underlies the integration of glycolytic and lipid anabolic pathways in pathologic cardiac hypertrophy, Cell Metab. 9 (2009) 512–524.
[168] L. Ghibaudi, J. Cook, C. Farley, M. van Heek, J.J. Hwa, Fat intake affects adiposity, comorbidity factors, and energy metabolism of sprague-dawley rats, Obes. Res. 10 (2002) 956–963.
[169] S.L. Johnston, D.M. Souter, B.J. Tolkamp, I.J. Gordon, A.W. Illius, et al., Intake compensates for resting metabolic rate variation in female C57BL/6J mice fed high-fat diets, Obesity (Silver Spring) 15 (2007) 600–606.
[170] V.T. Samuel, Z.X. Liu, X. Qu, B.D. Elder, S. Bilz, et al., Mechanism of hepatic insulin resistance in non-alcoholic fatty liver disease, J. Biol. Chem. 279 (2004) 32345–32353.
[171] Y.S. Lee, J.W. Kim, O. Osborne, Y. Oh da, R. Sasik, et al., Increased adipocyte O_2 consumption triggers HIF-1alpha, causing inflammation and insulin resistance in obesity, Cell 157 (2014) 1339–1352.
[172] O. Hussein, M. Grosovski, E. Lasri, S. Svalb, U. Ravid, et al., Monounsaturated fat decreases hepatic lipid content in non-alcoholic fatty liver disease in rats, World J. Gastroenterol. 13 (2007) 361–368.
[173] G.S. Lee, J.S. Yan, R.K. Ng, S. Kakar, J.J. Maher, Polyunsaturated fat in the methionine-choline-deficient diet influences hepatic inflammation but not hepatocellular injury, J. Lipid Res. 48 (2007) 1885–1896.
[174] M.E. Daly, C. Vale, M. Walker, K.G. Alberti, J.C. Mathers, Dietary carbohydrates and insulin sensitivity: a review of the evidence and clinical implications, Am. J. Clin. Nutr. 66 (1997) 1072–1085.
[175] H. Basciano, L. Federico, K. Adeli, Fructose, insulin resistance, and metabolic dyslipidemia, Nutr. Metab. (Lond.) 2 (2005) 5.
[176] A. Sahai, P. Malladi, H. Melin-Aldana, R.M. Green, P.F. Whitington, Upregulation of osteopontin expression is involved in the development of non-alcoholic steatohepatitis in a dietary murine model, Am. J. Physiol. Gastrointest. Liver Physiol. 287 (2004) G264–G273.
[177] M.D. Weltman, G.C. Farrell, C. Liddle, Increased hepatocyte CYP2E1 expression in a rat nutritional model of hepatic steatosis with inflammation, Gastroenterology 111 (1996) 1645–1653.
[178] M.K. Pickens, H. Ogata, R.K. Soon, J.P. Grenert, J.J. Maher, Dietary fructose exacerbates hepatocellular injury when incorporated into a methionine-choline-deficient diet, Liver Int. 30 (2010) 1229–1239.
[179] J.S. Teodoro, A.P. Rolo, F.V. Duarte, A.M. Simoes, C.M. Palmeira, Differential alterations in mitochondrial function induced by a choline-deficient diet: understanding fatty liver disease progression, Mitochondrion 8 (2008) 367–376.
[180] K. Fujita, Y. Nozaki, M. Yoneda, K. Wada, H. Takahashi, et al., Nitric oxide plays a crucial role in the development/progression of nonalcoholic steatohepatitis in the choline-deficient, L-amino acid-defined diet-fed rat model, Alcohol Clin. Exp. Res. 34 (Suppl 1) (2010) S18–S24.
[181] A. Takeuchi-Yorimoto, T. Noto, A. Yamada, Y. Miyamae, Y. Oishi, et al., Persistent fibrosis in the liver of choline-deficient and iron-supplemented L-amino acid-defined diet-induced nonalcoholic steatohepatitis rat due to continuing oxidative stress after choline supplementation, Toxicol. Appl. Pharmacol. 268 (2013) 264–277.
[182] J.M. Curtis, W.S. Hahn, E.K. Long, J.S. Burrill, E.A. Arriaga, et al., Protein carbonylation and metabolic control systems, Trends Endocrinol. Metab. 23 (2012) 399–406.
[183] E.J. Anderson, M.E. Lustig, K.E. Boyle, T.L. Woodlief, D.A. Kane, et al., Mitochondrial H2O2 emission and cellular redox state link excess fat intake to insulin resistance in both rodents and humans, J. Clin. Invest. 119 (2009) 573–581.
[184] C. Ruggiero, M. Ehrenshaft, E. Cleland, K. Stadler, High-fat diet induces an initial adaptation of mitochondrial bioenergetics in the kidney despite evident oxidative stress and mitochondrial ROS production, Am. J. Physiol. Endocrinol. Metab. 300 (2011) E1047–E1058.
[185] C. Raffaella, B. Francesca, F. Italia, P. Marina, L. Giovanna, et al., Alterations in hepatic mitochondrial compartment in a model of obesity and insulin resistance, Obesity (Silver Spring) 16 (2008) 958–964.
[186] J.M. Curtis, P.A. Grimsrud, W.S. Wright, X. Xu, R.E. Foncea, et al., Downregulation of adipose glutathione S-transferase A4 leads to increased protein carbonylation, oxidative stress, and mitochondrial dysfunction, Diabetes 59 (2010) 1132–1142.
[187] L.K. Sarna, N. Wu, P. Wang, S.Y. Hwang, Y.L. Siow, et al., Folic acid supplementation attenuates high fat diet induced hepatic oxidative stress via regulation of NADPH oxidase, Can. J. Physiol. Pharmacol. 90 (2012) 155–165.
[188] I.C. Abreu, J.F. Guerra, R.R. Pereira, M. Silva, W.G. Lima, et al., Hypercholesterolemic diet induces hepatic steatosis and alterations in mRNA expression of NADPH oxidase in rat livers, Arq. Bras. Endocrinol. Metabol. 58 (2014) 251–259.
[189] M.J. Ronis, N. Sharma, J. Vantrease, S.J. Borengasser, M. Ferguson, et al., Female mice lacking p47phox have altered adipose tissue gene expression and are protected against high fat-induced obesity, Physiol. Genom. 45 (2013) 351–366.
[190] J.K. Pepping, L.R. Freeman, S. Gupta, J.N. Keller, A.J. Bruce-Keller, NOX2 deficiency attenuates markers of adiposopathy and brain injury induced by high-fat diet, Am. J. Physiol. Endocrinol. Metab. 304 (2013) E392–E404.
[191] N. Li, B. Li, T. Brun, C. Deffert-Delbouille, Z. Mahiout, et al., NADPH oxidase NOX2 defines a new antagonistic role for reactive oxygen species and cAMP/PKA in the regulation of insulin secretion, Diabetes 61 (2012) 2842–2850.
[192] A. Souto Padron de Figueiredo, A.B. Salmon, F. Bruno, F. Jimenez, H. G. Martinez, et al., Nox2 mediates skeletal muscle insulin resistance induced by a high fat diet, J. Biol. Chem. 290 (2015) 13427–13439.
[193] S. Paglialunga, A. Ludzki, J. Root-McCaig, G.P. Holloway, In adipose tissue, increased mitochondrial emission of reactive oxygen species is important for short-term high-fat diet-induced insulin resistance in mice, Diabetologia 58 (2015) 1071–1080.
[194] I. Diebold, D. Flugel, S. Becht, R.S. Belaiba, S. Bonello, et al., The hypoxia-inducible factor-2alpha is stabilized by oxidative stress involving NOX4, Antioxid. Redox Signal. 13 (2010) 425–436.
[195] S. Anavi, M. Hahn-Obercyger, Z. Madar, O. Tirosh, Mechanism for HIF-1 activation by cholesterol under normoxia: A redox signaling pathway for liver damage, Free Radic. Biol. Med. 71 (2014) 61–69.
[196] C.M. Girgis, K. Cheng, C.H. Scott, J.E. Gunton, Novel links between HIFs, type 2 diabetes, and metabolic syndrome, Trends Endocrinol. Metab. 23 (2012) 372–380.
[197] A. Qu, M. Taylor, X. Xue, T. Matsubara, D. Metzger, et al., Hypoxia-inducible transcription factor 2alpha promotes steatohepatitis through augmenting lipid accumulation, inflammation, and fibrosis, Hepatology 54 (2011) 472–483.
[198] G.S. Hotamisligil, Inflammation and metabolic disorders, Nature 444 (2006) 860–867.
[199] S.J. Russell, C.R. Kahn, Endocrine regulation of ageing, Nat. Rev. Mol. Cell Biol. 8 (2007) 681–691.
[200] B.B. Kahn, J.S. Flier, Obesity and insulin resistance, J. Clin. Invest. 106 (2000) 473–481.
[201] P.K. Mazumder, B.T. O'Neill, M.W. Roberts, J. Buchanan, U.J. Yun, et al., Impaired cardiac efficiency and increased fatty acid oxidation in insulin-resistant ob/ob mouse hearts, Diabetes 53 (2004) 2366–2374.
[202] J. Buchanan, P.K. Mazumder, P. Hu, G. Chakrabarti, M.W. Roberts, et al., Reduced cardiac efficiency and altered substrate metabolism precedes the onset of hyperglycemia and contractile dysfunction in two mouse models of insulin resistance and obesity, Endocrinology 146 (2005) 5341–5349.
[203] O.J. How, E. Aasum, D.L. Severson, W.Y. Chan, M.F. Essop, et al., Increased myocardial oxygen consumption reduces cardiac efficiency in diabetic mice, Diabetes 55 (2006) 466–473.
[204] S. Boudina, S. Sena, B.T. O'Neill, P. Tathireddy, M.E. Young, et al., Reduced mitochondrial oxidative capacity and increased mitochondrial uncoupling impair myocardial energetics in obesity, Circulation 112 (2005) 2686–2695.
[205] B. Niemann, Y. Chen, M. Teschner, L. Li, R.E. Silber, et al., Obesity induces signs of premature cardiac aging in younger patients: the role of mitochondria, J. Am. Coll. Cardiol. 57 (2011) 577–585.
[206] C. Sloan, J. Tuinei, K. Nemetz, J. Frandsen, J. Soto, et al., Central leptin signaling is required to normalize myocardial fatty acid oxidation rates in caloric-restricted ob/ob mice, Diabetes 60 (2011) 1424–1434.
[207] L. Liang, X.L. Shou, H.K. Zhao, G.Q. Ren, J.B. Wang, et al., Antioxidant catalase rescues against high fat diet-induced cardiac dysfunction via an IKKbeta-AMPK-dependent regulation of autophagy, Biochim. Biophys. Acta 1852 (2015) 343–352.
[208] M. Dodson, V. Darley-Usmar, J. Zhang, Cellular metabolic and autophagic pathways: traffic control by redox signaling, Free Radic. Biol. Med. 63 (2013) 207–221.
[209] I.A. Barbosa, N.G. Machado, A.J. Skildum, P.M. Scott, P.J. Oliveira, Mitochondrial remodeling in cancer metabolism and survival: potential for new therapies, Biochim. Biophys. Acta 1826 (2012) 238–254.
[210] K. Bertram, C.M. Valcu, M. Weitnauer, U. Linne, A. Gorlach, NOX1 supports the metabolic remodeling of HepG2 cells, PLoS One 10 (2015) e0122002.
[211] D.P. Stiehl, W. Jelkmann, R.H. Wenger, T. Hellwig-Burgel, Normoxic induction of the hypoxia-inducible factor 1alpha by insulin and interleukin-1beta involves the phosphatidylinositol 3-kinase pathway, FEBS Lett. 512 (2002) 157–162.
[212] C. Treins, S. Giorgetti-Peraldi, J. Murdaca, G.L. Semenza, E. Van Obberghen, Insulin stimulates hypoxia-inducible factor 1 through a phosphatidylinositol 3-kinase/target of rapamycin-dependent signaling pathway, J. Biol. Chem. 277 (2002) 27975–27981.
[213] T. Kietzmann, A. Samoylenko, U. Roth, K. Jungermann, Hypoxia-inducible

factor-1 and hypoxia response elements mediate the induction of plasminogen activator inhibitor-1 gene expression by insulin in primary rat hepatocytes, Blood 101 (2003) 907–914.
[214] G.L. Semenza, HIF-1 mediates metabolic responses to intratumoral hypoxia and oncogenic mutations, J. Clin. Invest. 123 (2013) 3664–3671.
[215] K. Jungermann, T. Kietzmann, Oxygen: modulator of metabolic zonation and disease of the liver, Hepatology 31 (2000) 255–260.
[216] E.B. Rankin, J. Rha, M.A. Selak, T.L. Unger, B. Keith, et al., Hypoxia-inducible factor 2 regulates hepatic lipid metabolism, Mol. Cell. Biol. 29 (2009) 4527–4538.
[217] C.M. Taniguchi, E.C. Finger, A.J. Krieg, C. Wu, A.N. Diep, et al., Cross-talk between hypoxia and insulin signaling through Phd3 regulates hepatic glucose and lipid metabolism and ameliorates diabetes, Nat. Med. 19 (2013) 1325–1330.
[218] E. Furuta, S.K. Pai, R. Zhan, S. Bandyopadhyay, M. Watabe, et al., Fatty acid synthase gene is up-regulated by hypoxia via activation of Akt and sterol regulatory element binding protein-1, Cancer Res. 68 (2008) 1003–1011.
[219] J.J. Kamphorst, J.R. Cross, J. Fan, E. de Stanchina, R. Mathew, et al., Hypoxic and Ras-transformed cells support growth by scavenging unsaturated fatty acids from lysophospholipids, Proc. Natl. Acad. Sci. USA 110 (2013) 8882–8887.
[220] A. Valli, M. Rodriguez, L. Moutsianas, R. Fischer, V. Fedele, et al., Hypoxia induces a lipogenic cancer cell phenotype via HIF1alpha-dependent and -independent pathways, Oncotarget 6 (2015) 1920–1941.
[221] T. Zhao, Y. Zhu, A. Morinibu, M. Kobayashi, K. Shinomiya, et al., HIF-1-mediated metabolic reprogramming reduces ROS levels and facilitates the metastatic colonization of cancers in lungs, Sci. Rep. 4 (2014) 3793.
[222] M. Diehn, R.W. Cho, N.A. Lobo, T. Kalisky, M.J. Dorie, et al., Association of reactive oxygen species levels and radioresistance in cancer stem cells, Nature 458 (2009) 780–783.
[223] V. Nogueira, N. Hay, Molecular pathways: reactive oxygen species homeostasis in cancer cells and implications for cancer therapy, Clin. Cancer Res. 19 (2013) 4309–4314.
[224] V.A. Rao, S.R. Klein, S.J. Bonar, J. Zielonka, N. Mizuno, et al., The antioxidant transcription factor Nrf2 negatively regulates autophagy and growth arrest induced by the anticancer redox agent mitoquinone, J. Biol. Chem. 285 (2010) 34447–34459.
[225] Y. Gonzalez, B. Aryal, L. Chehab, V.A. Rao, Atg7- and Keap1-dependent autophagy protects breast cancer cell lines against mitoquinone-induced oxidative stress, Oncotarget 5 (2014) 1526–1537.
[226] D. Gozuacik, A. Kimchi, Autophagy as a cell death and tumor suppressor mechanism, Oncogene 23 (2004) 2891–2906.
[227] Y. Chen, H. Wei, F. Liu, J.L. Guan, Hyperactivation of mammalian target of rapamycin complex 1 (mTORC1) promotes breast cancer progression through enhancing glucose starvation-induced autophagy and Akt signaling, J. Biol. Chem. 289 (2014) 1164–1173.
[228] S. Menon, B.D. Manning, Common corruption of the mTOR signaling network in human tumors, Oncogene 27 (Suppl 2) (2008) S43–S51.
[229] M. Laplante, D.M. Sabatini, mTOR signaling at a glance, J. Cell Sci. 122 (2009) 3589–3594.
[230] J.M. Mates, J.A. Segura, F.J. Alonso, J. Marquez, Oxidative stress in apoptosis and cancer: an update, Arch. Toxicol. 86 (2012) 1649–1665.
[231] G.E. Goodman, M.D. Thornquist, J. Balmes, M.R. Cullen, F.L. Meyskens Jr., et al., The Beta-Carotene and Retinol Efficacy Trial: incidence of lung cancer and cardiovascular disease mortality during 6-year follow-up after stopping beta-carotene and retinol supplements, J. Natl. Cancer Inst. 96 (2004) 1743–1750.
[232] A. Samoylenko, J.A. Hossain, D. Mennerich, S. Kellokumpu, J.K. Hiltunen, et al., Nutritional countermeasures targeting reactive oxygen species in cancer: from mechanisms to biomarkers and clinical evidence, Antioxid. Redox Signal. 19 (2013) 2157–2196.
[233] S.K. Myung, Y. Kim, W. Ju, H.J. Choi, W.K. Bae, Effects of antioxidant supplements on cancer prevention: meta-analysis of randomized controlled trials, Ann. Oncol. 21 (2010) 166–179.
[234] B. Halliwell, The antioxidant paradox, Lancet 355 (2000) 1179–1180.
[235] P.C. Hollman, A. Cassidy, B. Comte, M. Heinonen, M. Richelle, et al., The biological relevance of direct antioxidant effects of polyphenols for cardiovascular health in humans is not established, J. Nutr. 141 (2011) 989S–1009S.
[236] M. Sheikh-Ali, J.M. Chehade, A.D. Mooradian, The antioxidant paradox in diabetes mellitus, Am. J. Ther. 18 (2011) 266–278.
[237] E.R. Miller 3rd, R. Pastor-Barriuso, D. Dalal, R.A. Riemersma, L.J. Appel, et al., Meta-analysis: high-dosage vitamin E supplementation may increase all-cause mortality, Ann. Intern. Med. 142 (2005) 37–46.
[238] M.H. Hopkins, V. Fedirko, D.P. Jones, P.D. Terry, R.M. Bostick, Antioxidant micronutrients and biomarkers of oxidative stress and inflammation in colorectal adenoma patients: results from a randomized, controlled clinical trial, Cancer Epidemol. Biomarkers Prev. 19 (2010) 850–858.
[239] S.T. Mayne, G.J. Handelman, G. Beecher, Beta-Carotene and lung cancer promotion in heavy smokers–a plausible relationship? J. Natl. Cancer Inst. 88 (1996) 1513–1515.
[240] A.J. Vargas, R. Burd, Hormesis and synergy: pathways and mechanisms of quercetin in cancer prevention and management, Nutr. Rev. 68 (2010) 418–428.
[241] H.H. Schmidt, R. Stocker, C. Vollbracht, G. Paulsen, D.P. Riley, et al., Antioxidants in Translational Medicine, Antioxid. Redox Signal. (2015).
[242] A. Agudo, L. Cabrera, P. Amiano, E. Ardanaz, A. Barricarte, et al., Fruit and vegetable intakes, dietary antioxidant nutrients, and total mortality in Spanish adults: findings from the Spanish cohort of the European Prospective Investigation into Cancer and Nutrition (EPIC-Spain), Am. J. Clin. Nutr. 85 (2007) 1634–1642.
[243] V.A. Kirsh, U. Peters, S.T. Mayne, A.F. Subar, N. Chatterjee, et al., Prospective study of fruit and vegetable intake and risk of prostate cancer, J. Natl. Cancer Inst. 99 (2007) 1200–1209.
[244] C.X. Zhang, S.C. Ho, Y.M. Chen, J.H. Fu, S.Z. Cheng, et al., Greater vegetable and fruit intake is associated with a lower risk of breast cancer among Chinese women, Int. J. Cancer 125 (2009) 181–188.
[245] R.H. Liu, Potential synergy of phytochemicals in cancer prevention: mechanism of action, J. Nutr. 134 (2004) 3479S–3485S.
[246] A. Karlsen, M. Svendsen, I. Seljeflot, M.A. Sommernes, J. Sexton, et al., Compliance, tolerability and safety of two antioxidant-rich diets: a randomised controlled trial in male smokers, Br. J. Nutr. 106 (2011) 557–571.
[247] A.P. Simopoulos, The importance of the omega-6/omega-3 fatty acid ratio in cardiovascular disease and other chronic diseases, Exp. Biol. Med. (Maywood, NJ) 233 (2008) 674–688.

frontiers in Physiology

REVIEW
published: 02 August 2016
doi: 10.3389/fphys.2016.00314

"Oxygen Sensing" by Na,K-ATPase: These Miraculous Thiols

Anna Bogdanova[1], Irina Y. Petrushanko[2], Pablo Hernansanz-Agustín[3,4] and Antonio Martínez-Ruiz[3]*

[1] *Institute of Veterinary Physiology, Vetsuisse Faculty and the Zurich Center for Integrative Human Physiology (ZIHP), University of Zurich, Zurich, Switzerland,* [2] *Engelhardt Institute of Molecular Biology, Russian Academy of Sciences, Moscow, Russia,* [3] *Servicio de Inmunología, Instituto de Investigación Sanitaria Princesa (IIS-IP), Hospital Universitario de La Princesa, Madrid, Spain,* [4] *Departamento de Bioquímica, Universidad Autónoma de Madrid, Madrid, Spain*

Control over the Na,K-ATPase function plays a central role in adaptation of the organisms to hypoxic and anoxic conditions. As the enzyme itself does not possess O_2 binding sites its "oxygen-sensitivity" is mediated by a variety of redox-sensitive modifications including S-glutathionylation, S-nitrosylation, and redox-sensitive phosphorylation. This is an overview of the current knowledge on the plethora of molecular mechanisms tuning the activity of the ATP-consuming Na,K-ATPase to the cellular metabolic activity. Recent findings suggest that oxygen-derived free radicals and H_2O_2, NO, and oxidized glutathione are the signaling messengers that make the Na,K-ATPase "oxygen-sensitive." This very ancient signaling pathway targeting thiols of all three subunits of the Na,K-ATPase as well as redox-sensitive kinases sustains the enzyme activity at the "optimal" level avoiding terminal ATP depletion and maintaining the transmembrane ion gradients in cells of anoxia-tolerant species. We acknowledge the complexity of the underlying processes as we characterize the sources of reactive oxygen and nitrogen species production in hypoxic cells, and identify their targets, the reactive thiol groups which, upon modification, impact the enzyme activity. Structured accordingly, this review presents a summary on (i) the sources of free radical production in hypoxic cells, (ii) localization of regulatory thiols within the Na,K-ATPase and the role reversible thiol modifications play in responses of the enzyme to a variety of stimuli (hypoxia, receptors' activation) (iii) redox-sensitive regulatory phosphorylation, and (iv) the role of fine modulation of the Na,K-ATPase function in survival success under hypoxic conditions. The co-authors attempted to cover all the contradictions and standing hypotheses in the field and propose the possible future developments in this dynamic area of research, the importance of which is hard to overestimate. Better understanding of the processes underlying successful adaptation strategies will make it possible to harness them and use for treatment of patients with stroke and myocardial infarction, sleep apnoea and high altitude pulmonary oedema, and those undergoing surgical interventions associated with the interruption of blood perfusion.

Keywords: Sodium-Potassium-Exchanging ATPase, redox regulation, thiols, hypoxia, S-glutathionylation, S-nitrosylation

OPEN ACCESS

Edited by:
Sigrid A. Langhans, Nemours Alfred I. duPont Hospital for Children, USA

Reviewed by:
John Cuppoletti, University of Cincinnati, USA
Pablo Martín-Vasallo, University of La Laguna, Spain

****Correspondence:***
Anna Bogdanova
annab@access.uzh.ch

Specialty section:
This article was submitted to Membrane Physiology and Membrane Biophysics, a section of the journal Frontiers in Physiology

Received: *30 May 2016*
Accepted: *12 July 2016*
Published: *02 August 2016*

Citation:
Bogdanova A, Petrushanko IY, Hernansanz-Agustín P and Martínez-Ruiz A (2016) "Oxygen Sensing" by Na,K-ATPase: These Miraculous Thiols. Front. Physiol. 7:314. doi: 10.3389/fphys.2016.00314

INTRODUCTION. OXYGEN, AND OXYGEN SENSING FROM EVOLUTIONARY AND MODERN PERSPECTIVES

Oxygen, Redox State, Ions, Energy, and Na,K-ATPase

Sustaining of life is a process requiring high energy costs. Energy production in living systems utilizes transmembrane electrochemical gradients, those for ions and redox equivalents. No gradients can be sustained without a membrane, so membranes are the key elements of any living cell since the first proto-cell, the last universal common ancestor (LUCA), that existed more than 3 billion years ago on our planet (Sousa et al., 2013). As life evolved, more specialized compartments were formed within cells, each surrounded by its own membrane. Modern plasma membrane uses the energy of ATP produced by aerobic or anaerobic pathways to generate transmembrane Na^+/K^+ and Ca^{2+} gradients. One member of the P-type ATPases family, Na,K-ATPase, transforms the energy of phosphate bonds within the ATP to the energy of transmembrane Na/K gradient that is used to support the excitability of neurons and myocytes, control of intracellular Ca^{2+} levels and pH, intake of amino acids and fuel, and for sensing and signaling (Blanco and Mercer, 1998; Therien and Blostein, 2000; Blanco, 2005; Geering, 2006; Toyoshima et al., 2011; Reinhard et al., 2013; Shattock et al., 2015). It uses 1 ATP molecule to exchange 3 intracellular Na^+ ions for 2 extracellular K^+ ions per cycle. The number of cycles varies between 1500 and 10,000 per min (Liang et al., 2007) and the corresponding energy expenditure ranges between 20% of total energy consumption in non-excitable cells to 75% in excitable tissues under hypoxic conditions (Buck and Hochachka, 1993; Erecinska and Silver, 2001). Being a major sink for ATP under hypoxic conditions, Na,K-ATPase is capable of "sensing" the changes in O_2 availability and adjusting its activity to the rates of ATP production (Bogdanova et al., 2006). This review summarizes the progress in our understanding of the mechanisms utilized by the Na,K-ATPase for "O_2 sensing." Recent developments in of the field of free radical biology and medicine have provided decisive clues for dissection of these mechanisms and the role that protein thiols play in it.

Reactive Oxygen (ROS) and Nitrogen (RNS) Species As Signal Messengers

Oxygen is a key component of the cell energy production machinery driving Cambrian explosion ~500 Mio years ago. It plays a role of the final acceptor of the mitochondrial electron transport chain (ETC), which is coupled to ATP production by the H^+-dependent reversible mitochondrial ATPase in the mitochondrial oxidative phosphorylation (OXPHOS) system. Many other metabolic reactions in the cell also use oxygen as a necessary component. Thus, cells have developed systems that can sense fluctuations in oxygen concentration and perform different adaptations, and there are several links between hypoxia sensing and redox reactions that we briefly explore here.

Oxygen produces reactive oxygen species (ROS) by successive one-electron reductions (**Figure 1**). Superoxide anion ($O_2^{\bullet-}$) is the first ROS formed from O_2; its half-life is as short as 2×10^5 $M^{-1}s^{-1}$ (Kalyanaraman, 2013), what makes $O_2^{\bullet-}$ particularly difficult to detect. It is not a powerful oxidant, and its effect on protein thiols is mainly limited to disruption of iron-sulfur clusters; in this regard, mitochondrial aconitase inactivation has been a classical hallmark of mitochondrial superoxide production (Fridovich, 1995; Hausladen and Fridovich, 1996). It dismutates spontaneously or by the action of cytosolic or mitochondrial superoxide dismutases (Cu,Zn-SOD or Mn-SOD respectively), producing a reduced form, hydrogen peroxide (H_2O_2), and an oxidized form, water (H_2O). Hydrogen peroxide half-life is quite greater than that of its predecessor, 10^3–10^4 $M^{-1}s^{-1}$ (Kalyanaraman, 2013), it can cross biological membranes and oxidize thiols within Cys residues in proteins. The latter capacity has been a useful tool for nature to design molecular sensors of H_2O_2; likewise several laboratories have developed different fluorescent proteins capable of detecting H_2O_2 through reversible oxidation of critical, sensitive thiols in their structure (Hanson et al., 2004; Belousov et al., 2006; Ermakova et al., 2014). All together, these features make H_2O_2 the most easily detectable ROS and the best known. A one-electron reduction of hydrogen peroxide forms hydroxyl radical ($^{\bullet}OH$), a reaction that can be catalyzed by the oxidation of Fe^{2+} into Fe^{3+} in the so-called Fenton reaction (Kalyanaraman, 2013). $^{\bullet}OH$ is the most reactive and probably the most toxic free radical due to the initiation of radical chain reactions. It is worth mentioning the very fast reaction of superoxide with nitric oxide ($NO^{\bullet}$) to form peroxynitrite ($ONOO^-$), with a rate comparable to that of diffusion, $4–6 \times 10^9$ $M^{-1}s^{-1}$ (Kalyanaraman, 2013). Although peroxynitrite (one of the reactive nitrogen species, RNS) is well known as an inducer of tyrosine nitration, it is a peroxide and as such it is a very effective two-electron oxidant of thiols.

ROS/RNS and Hypoxia

Since ROS are chemical derivatives of O_2, hypoxia would lower the production of ROS due to the law of mass action, i.e., as there is a lower oxygen concentration, one would expect to observe a decrease in ROS production. However, cell systems are often more complicated than the basic chemical systems in a test tube with multiple players and reactions involved in production and scavenging of ROS and RNS. Apart of thermodynamic and kinetic restrains, compartmentalization within the cell and species/cell type-specific settings affect the capacity of electron donors to react with the oxygen molecules and time course of these reactions. Indeed, there has been a long-standing controversy in the field, as there are a number of observations reporting lower ROS production in hypoxia (Hagen et al., 2003; Acker et al., 2006; Chua et al., 2010; Fernandez-Aguera et al., 2015) but also the opposite (Chandel et al., 1998, 2000; Guzy and Schumacker, 2006), what has been called the paradoxical ROS increase in hypoxia (Turrens, 2003; Guzy and Schumacker, 2006). This controversy emerged from the differences in experimental design including timing of hypoxic exposure prior to ROS detection, cell type, tissue or organism, as well as from the methodological diversity in ROS detection. For example, two groups detecting $O_2^{\bullet-}$ in cells using superoxide-sensing probe (dihydroethidium) and microscopy reported the

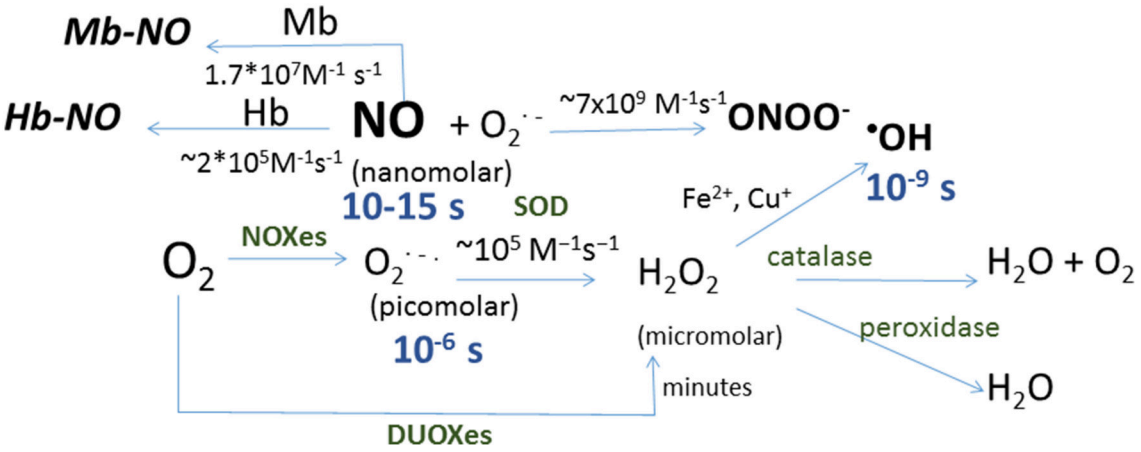

FIGURE 1 | Schematic representation of reactions in which reactive oxygen and nitrogen species are formed. Shown in blue are the half-life for each species and in brackets the concentration range for each species in biological systems, and in green the enzymes catalyzing the corresponding reactions: dual oxidizes (DOUXes), superoxide dismutases (SOD). Under the arrows are the rate constants for the reactions shown. Myoglobin (Mb) and hemoglobin (Hb) are shown as sinks for NO.

opposing findings (Quintero et al., 2006; Chua et al., 2010). The only decisive difference was the time of hypoxic exposure. Detection of $O_2^{\bullet-}$ in cells following 3 h of hypoxia showed no changes in superoxide levels compared to the normoxic control (Chua et al., 2010), while facilitation of $O_2^{\bullet-}$ production was observed during the first hour of hypoxia (Quintero et al., 2006). A recent report reconciled this apparent controversy, as it showed that production of mitochondrial superoxide is upregulated exclusively during the first minutes of hypoxia and its production decreases afterwards, in what has been called a superoxide burst in hypoxia (Hernansanz-Agustin et al., 2014).

Several sources have been proposed to be the origin of ROS in hypoxia. One of the first enzymes implicated in ROS generation in hypoxia was NADPH oxidase, which plays a role in hypoxic pulmonary vasoconstriction (HPV) (Marshall et al., 1996). Together with this, xanthine oxidase was also shown to produce ROS in hypoxia in neurons, contributing to cell death in ischemic conditions (Abramov et al., 2007).

Last but not least, mitochondria-derived ROS have been also shown to increase in hypoxia (Chandel et al., 1998, 2000; Hernansanz-Agustin et al., 2014), are necessary for ROS production by NADPH oxidase in hypoxic pulmonary vasoconstriction (Moreno et al., 2014) and are prior to the xanthine oxidase-derived ROS (Abramov et al., 2007). The source of electron leakage giving rise to an excessive production of $O_2^{\bullet-}$ remains a matter of intensive investigation. Listed below are some considerations regarding the causes and possible mechanisms of hypoxia-inducible $O_2^{\bullet-}$ burst in the mitochondria.

ROS and RNS Production in Hypoxic Mitochondria

Mitochondrial electron transport chain (mtETC) consists of four protein complexes within the mitochondrial inner membrane. Complexes I and II oxidize electron carriers NADH and $FADH_2$, and transfer the electrons to complex III by means of ubiquinone. Complex III reduces cytochrome *c*, which transports the electrons to complex IV and reduces O_2 to H_2O. These activities of complexes I, III, and IV are coupled to the pumping of H^+ across the mitochondrial inner membrane, thus creating an electrochemical gradient. The oxidative phosphorylation system (OXPHOS) includes a fifth complex, complex V or ATP synthase that transforms the energy of proton gradient to phosphorylation of ADP to ATP (Mitchell, 1961; Mitchell and Moyle, 1967).

It is suggested that ROS generation occurs mainly at the level of complex I, but also at complex III (Turrens, 2003; Murphy, 2009; Drose and Brandt, 2012). FMN group within complex I oxidizes NADH into NAD^+ and transfers electrons to a series of Fe-S clusters which, in turn, reduce ubiquinone into ubiquinol (Berrisford and Sazanov, 2009; Hunte et al., 2010; Zickermann et al., 2015) in the so-called forward electron transport. On the other hand, at high mitochondrial transmembrane potential $\Delta\Psi$mt or in the presence of the complex II substrate succinate, complex I can accept electrons from ubiquinol and reduce NAD^+ into NADH at the level of flavin mononucleotide FMN, together with the intrusion of H^+ in a process called reverse electron transport (RET) (Vinogradov and Grivennikova, 2005, 2016; Drose and Brandt, 2012). In both forward and reverse transport there is a leakage of electrons giving rise to $O_2^{\bullet-}$ production. Inhibitors targeting the ubiquinone-binding site (e.g., rotenone; Pryde and Hirst, 2011) increase the leakage in the forward transport, but inhibit it in RET. It is also reported in the presence of high concentrations of succinate, condition associated with progression of ischemia-reperfusion injury (Drose and Brandt, 2012; Chouchani et al., 2014). RET also takes place at elevated $\Delta\Psi$mt (Korshunov et al., 1997; Drose and Brandt, 2012). $O_2^{\bullet-}$ produced by complex I will be released toward the mitochondrial matrix where it is dismutated by Mn-SOD (SOD2) to H_2O_2. The latter is further detoxified by GSH-Glutaredoxin2 system

within the matrix (Drose et al., 2014). Complex III can also give rise to $O_2^{\bullet-}$ production along with oxidation of ubiquinol to ubiquinone known as Q cycle (Boveris et al., 1976; Cadenas et al., 1977). This process includes formation of semiquinone as an intermediate step (Trumpower, 1990), and this step becomes rate-limiting at high $\Delta\Psi$mt or in the presence of the complex III-Qi site inhibitor Antimycin A. In case of electron leakage from complex III $O_2^{\bullet-}$ is accumulating within the intermembrane space. After dismutation by Cu,Zn-SOD (SOD1) the resulting H_2O_2 is extruded from the mitochondria into the cytosol through porin (Drose et al., 2014) and then detoxified by catalase and GSH/glutaredoxin 2 systems. Free radicals and H_2O_2 originating from these two complexes most likely serve as local signaling messengers.

Evidence obtained using transgenic animal models suggest different mitochondrial complexes of the mtETC are involved in generation of superoxide anion participating in redox signaling. Knocking down Rieske iron-sulfur protein (RISP) within the complex III indicates the key role of electron transport by this complex for HIF-1α stabilization under hypoxic conditions (Brunelle et al., 2005; Guzy et al., 2005; Mansfield et al., 2005). Silencing of the NDUFS2 protein expression within complex I compromised hypoxia-induced ROS production and arterial chemoreception *in vivo* (Fernandez-Aguera et al., 2015). However, none of these studies explained the paradox of ROS production in hypoxia or addressed the mechanism of their production. Our recent data point to the key roles of complex I deactivation and Na^+/Ca^{2+} exchange through the mitochondrial Na^+/Ca^{2+} exchanger in the hypoxic superoxide production (Hernansanz-Agustín et al., manuscript submitted).

CO, H_2S, and NO production are most likely supported within the mitochondria by heme oxygenase 1 (Ryter et al., 2006), mitochondrial NO synthase (Ghafourifar and Sen, 2007), and 3-mercaptopyruvate sulfurtransferase (Li et al., 2011). All gasses were shown to protect tissues from irreversible suppression of respiratory capacity of mitochondria during ischemia-reperfusion injury (Elrod et al., 2007). In addition to blocking complex III H_2S is also capable of direct binding to the heme group of complex IV (Cooper and Brown, 2008). Supplementation of H_2S has been shown to inhibit HIF-1α stabilization in hypoxic, but not in anoxic conditions, which is probably related to its capacity of inhibiting mitochondrial respiration (Kai et al., 2012). Systemic administration of sulfide was shown to sustain hibernation state (Blackstone et al., 2005). Nitrite causes inhibition of complex I by S-nitrosylation (reviewed in Martinez-Ruiz et al., 2011) and decreases free radical generation in tissues exposed to ischemia-reperfusion (Shiva et al., 2007).

Genetic adaptation to hypoxia via stabilization of the alpha subunit of hypoxia-inducible factors (HIF1α and HIF2α), has been suggested to require mitochondrial ETC $O_2^{\bullet-}$ production (Chandel et al., 1998, 2000). However, how ROS act over HIFα subunits or its degrading enzymes, the prolyl-hydroxylases (EGLNs), is still unknown (Kaelin and Ratcliffe, 2008). More recently, mitochondrial complex I and ROS production have been shown to play a key role in acute oxygen sensing by carotid body (Fernandez-Aguera et al., 2015). Such increase in ROS production depolarizes glomus cells through inhibition of K^+ channels and increase of cytosolic Ca^{2+} by extracellular Ca^{2+} influx. Both stabilization of HIF-α subunits and inhibition of K^+ channels could be influenced by ROS through oxidation of thiols. Indeed, redox balance is also modified in hypoxia since ROS reversibly oxidize thiols in the cytosolic compartment of cells which, in turn, could have a role in cell signaling and survival during hypoxia (Izquierdo-Alvarez et al., 2012). Superoxide anion generation by mitochondria upon decrease in oxygenation below "normoxic values" as well as decline in NO production by neuronal and inducible NO synthases that have low affinity for O_2 (K_d 2–5 kPa; Dweik, 2005) result in an increase in oxidized glutathione in hypoxic heart tissues of animals that are hypoxia-sensitive, but not in hypoxia-resistant ones (Petrushanko et al., 2012; Yakushev et al., 2012). Oxidized glutathione joins the reactions of non-enzymatic dithiol exchange in which S-glutathionylated adducts of thiol residues are formed in multiple proteins including the Na,K-ATPase. For mitochondrial ROS/RNS to be regulators of the Na,K-ATPase function under hypoxic conditions, the ROS generators should be co-localized with the ATPase. The existence of membrane-bound pool of mitochondria has been confirmed (Westermann, 2015). However, the role of ROS and RNS produced by the mitochondria in control of the Na,K-ATPase activity, amplifying and complementing the signals generated as NADPH oxidases, xanthine oxidase and other free radical generators, awaits further investigation.

Therefore, mitochondria-derived ROS produced in the first minutes of hypoxia (Hernansanz-Agustin et al., 2014), may be a primary and necessary event in redox signaling in hypoxia, leading to the activation of multiple redox processes. All these events converge to targeted thiol oxidation and development of acute adaptive response (Izquierdo-Alvarez et al., 2012).

Both mitochondria and Na,K-ATPase are corner-stones in control of metabolic state of hypoxic tissue. The intimate relation between them remains to be unraveled as it does not seem to be limited to the production and consumption of ATP alone.

VERSATILITY OF OXYGEN SENSING. MULTIPLE SIGNALS-MULTIPLE TARGETS—MULTIPLE RESPONSES—MULTIPLE OUTCOMES

Changes in O_2 availability occurring in the course if evolution trigger multiple responses in every cell of any living organism on this planet (Holland, 2006). These responses are species- and cell type-specific. Diversity in responses matches the oxygen levels in the tissue under normoxic conditions (Bogdanova et al., 2006) and is associated with adaptations some species developed to survive hypoxic periods (Hochachka et al., 1999). A single protein, such as the Na,K-ATPase, may demonstrate essential hypoxia-insensitivity (Yakushev et al., 2012), maintain maximal activity within a narrow window of O_2 concentrations (Petrushanko et al., 2007), or show linear dose-dependence of O_2 concentration in the environment (Bogdanova et al., 2005;

Yakushev et al., 2012) depending on the species and cell type. These responses also vary depending on the duration and severity of hypoxia (Dada et al., 2003; Fuller et al., 2003; Bogdanova et al., 2006; Petrushanko et al., 2007, 2015; Yakushev et al., 2012).

Patterns of response correlate with the changes in ROS/RNS and NO production in the cells and the corresponding shifts in redox state. Apart of the regulatory thiols within the Na,K-ATPase changes in the enzyme activity are in part mediated by its phosphorylation by multiple redox-sensitive kinases and phosphatases (Devarie-Baez et al., 2016). These versatile signaling messengers as well as the variability in free radical scavenging systems make responses to hypoxia dependent on location of free radical generators and speciation of the messengers (free radical- and gaseous-based). The mechanisms of oxygen-inducible regulation are largely restricted to the oxidative modifications of thiols (formation of mixed di-thiols with glutathione, sulfide or other protein thiols, S-nitrosylation, or proline/threonine carbonylation (Yan et al., 2013). These changes occur in multiple proteins at the same time. Fine-tuning of protein complexes is accomplished translating into the protection against hypoxia or reperfusion injury at the tissue and organism levels (Yan, 2014).

OXYGEN AND REDOX-SENSITIVITY OF THE NA,K-ATPase

Na,K-ATPase and Its Thiols

Sodium potassium pump is formed by the 100–113 kDa catalytic α subunit, the regulatory obligatory 55 kDa β subunit and the tissue-specific regulatory proteins of 7–11 kDa belonging to the FXYD family (**Figure 2A**; Blanco and Mercer, 1998; Blanco, 2005; Geering, 2006; Toyoshima et al., 2011). Furthermore, Na,K-ATPase serves as a "docking station" for multiple other proteins of those other ion transporters, receptors, cytoskeletal proteins and members of signaling proteins are known (Reinhard et al., 2013). Each Na,K-ATPase subunit type contains cysteine residues. The only reduced thiol within the beta subunit is localized at the edge to the membrane surface, diving into and out of the membrane during the pumping cycle (White et al., 2009; Bibert et al., 2011). Muscle-specific FXYD subunit pospholemman (PLM) has two thiols (Bibert et al., 2011). The catalytic α subunit is the largest of the three subunits, forms the ATP binding site and binding sites for ions and transport pore, and has 23–24 thiols depending on the isoform (Bogdanova et al., 2006). Several of these thiols are considered to be the targets of regulatory reversible thiol modifications. These modifications make the Na,K-ATPase function extremely sensitive to the changes in redox state and oxygen availability (chronic and acute hypoxia).

Irreversible Oxidation of Thiols

Oxidative stress represents an imbalance between an augmented production of pro-oxidative equivalents (mostly ROS and RNS) and/or their detoxification rate by the so-called antioxidant systems (Sies, 2015). Under these circumstances oxidants attack reduced protein thiols turning them into sulfinic or sulfonic acids. Irreversible oxidation induced in the Na,K-ATPase isolated from kidneys by its exposure to 20 mM H_2O_2 results in a decrease in V_{max} to a half and inability to form oligomeric complexes (Kurella et al., 1999). Sensitivity to oxidation varied for the Na,K-ATPase isozymes, those from the heart and the brain (astrocytes) formed by the α2 isoform of the catalytic subunit being more susceptible for oxidation than the ubiquitously expressed α1 isozyme (Xie et al., 1995). ATP was protecting the enzyme from irreversible oxidation (Xu et al., 1997). Depletion of cytoplasmic and mitochondrial GSH or exposure of cerebellar granule cells to hyperoxia also caused suppression of the enzyme activity associated with massive free radical burst (Petrushanko et al., 2006, 2007).

As reviewed below terminal irreversible oxidation of the enzyme has two more consequences. It makes the regulatory thiols inaccessible for reversible thiol modifications and therefore renders the enzyme insensitive to redox changes and alterations in oxygen levels (Petrushanko et al., 2012). Irreversible oxidation primes the proteins to degradation (Thevenod and Friedmann, 1999). In the lungs severe hypoxia (1.5 kPa) promotes ubiquitination and lysosomal degradation of the alpha1-isozyme of the Na,K-ATPase by phosphorylation of the catalytic subunit at Ser18 by PKCzeta (redox-sensitive kinase containing cysteine clusters; Dada et al., 2003, 2007; Dada and Sznajder, 2003).

S-nitrosylation of Thiols

S-nitrosylation (and S-nitrosation, for nomenclature see Heinrich et al., 2013) is a common thiol modification in biological systems (Martinez-Ruiz and Lamas, 2004; Martinez-Ruiz et al., 2013). Nitric oxide is unable to directly interact with reduced thiols. Several mechanisms have been described for nitrosothiol formation, which do not require the presence of specific enzymes that catalyze these reactions (Martinez-Ruiz et al., 2013).

Direct reaction of NO to nitrosylate a cysteine thiyl radical ($P\text{-}S^{\bullet}$) whenever the latter has been formed.

$$P\text{-}S^{\bullet} + {}^{\bullet}NO \rightarrow P\text{-}S\text{-}NO \quad (1)$$

This is a fast reaction may compete with NO binding to the heme of soluble guanylate cyclase sGC heme (Madej et al., 2008; reviewed in Smith and Marletta, 2012). However, its biological significance is limited to those proteins in which the thiyl radical could be formed when NO is being produced.

NO autooxidation can also lead to S-nitrosylation, via the formation of N_2O_3:

$$2\,NO + O_2 \rightarrow 2\,NO_2 \quad (2)$$

$$NO_2 + NO \rightarrow N_2O_3 \quad (3)$$

$$N_2O_3 + RSH \rightarrow RSNO + H^+ + NO_2^- \quad (4)$$

The rate-limiting reaction is the formation of NO_2, so it requires a very high NO concentration for producing a significant amount of S-nitrosylation. This high NO concentration can be achieved in the proximity of NO sources, mainly NOS. Indeed, the reaction is 30-fold faster in hydrophobic environments (Moller et al., 2007), suggestion that it can be favored in regions close to cell membranes, where NOS enzymes localize.

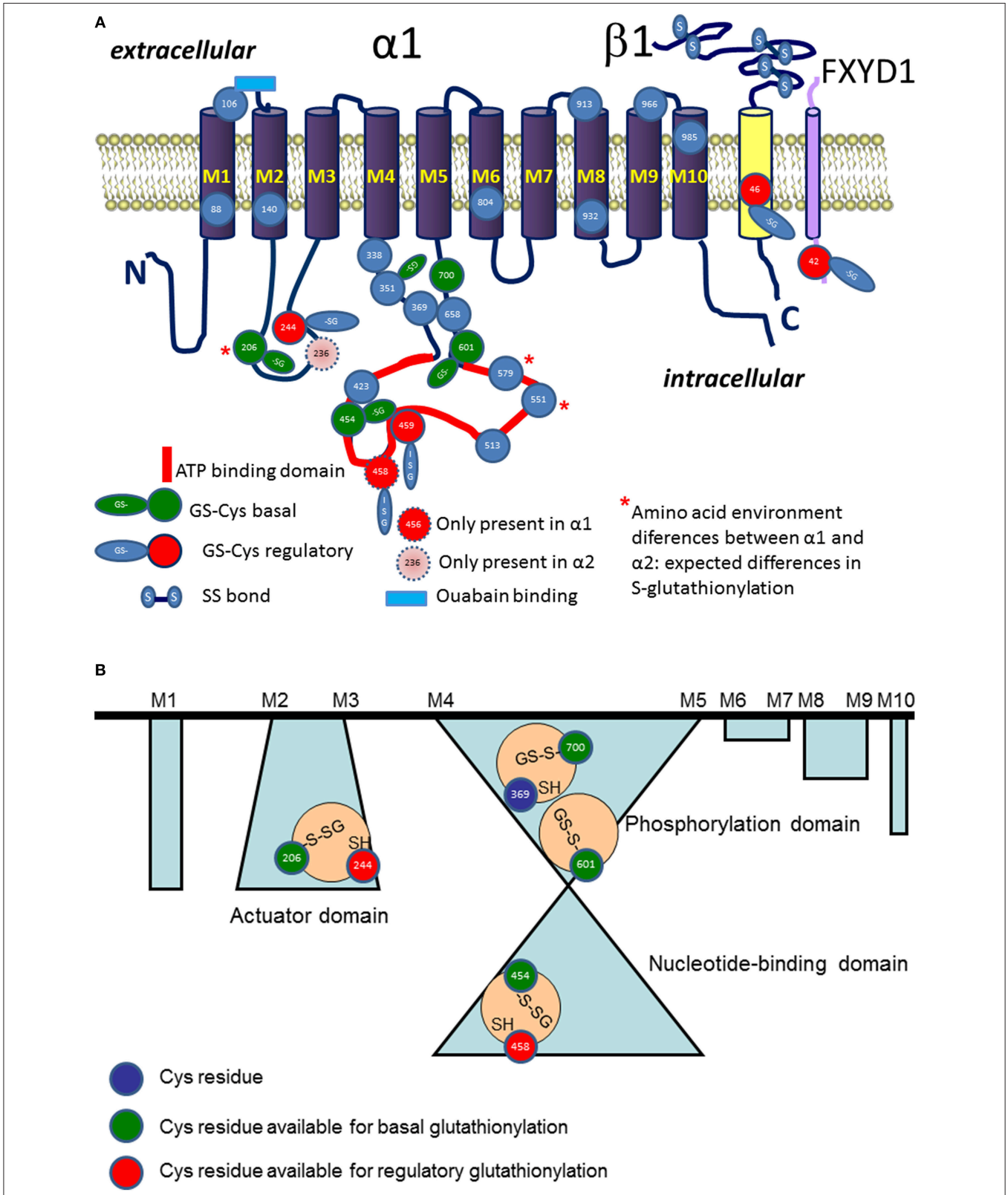

FIGURE 2 | Schematic representation of localization S-glutathionylated cysteine residues in α (in blue), β (in yellow), and phospholemman (FXYD, in cyan) subunits (A). Regulatory S-glutathionylation sites are shown in red. Basal S-glutathionylation is shown in green. ATP binding site is highlighted in red. Blue rectangle depicts ouabain binding site. Stars highlight the Cys residues with differences in pK between the α1 and α2 isoform (for details see **Table 1**). **(B)** Shows schematically the cavities with trapped S-glutathionylated Cys residues inaccessible for de-glutathionylation without detergents and representing "redox memory."

Transnitrosylation in reactions involving modified cysteine residues, including S-nitrosoglutathione, has emerged as an effective and regulated mechanism forming this modifications (Nakamura and Lipton, 2013; Kohr et al., 2014):

$$\mathrm{RSNO} + \mathrm{R'SH} \rightarrow \mathrm{RSH} + \mathrm{R'SNO}\ (\mathrm{trans-nitrosylation,\ nitrosylated\ glutathione\ may\ be\ involved}) \quad (5)$$

Interaction of peroxynitrite with cysteine thiol residues does not give S-nitrosylated products directly but causes oxidation of thiols to sulfenic acid that in turn can form mixed disulfides, in particular with glutathione (see S-glutathionylation below; Alvarez and Radi, 2003):

$$\begin{aligned} \mathrm{RS^-} + \mathrm{ONOOH} &\rightarrow \mathrm{RSOH} + \mathrm{NO_2^-} \\ \mathrm{RSO^-} + \mathrm{GSH} &\rightarrow \mathrm{RSSG} + \mathrm{OH^-} \end{aligned} \quad (6)$$

Denitrosylation mainly involves two mechanisms (Smith and Marletta, 2012). GSNO concentration is controlled by enzymatically-catalyzed NADH (for GSNO reductase (GSNOR) or NADPH-dependent (carbonyl reductase 1, CBR1) reduction to GSH. Since trans-nitrosylation of thiols involves GSNO (reaction 5), this process may be considered as rate-limiting in S-nitrosylation of proteins. This is true for the Na,K-ATPase, as increase in the levels of GSNO induces the second trans-nitrosylation step and formation of S-glutathionylated adducts of the α (Li et al., 2001; Petrushanko et al., 2015) and β (Liu et al., 2013) subunits of the enzyme. Thioredoxin catalyzes denitrosylation of multiple targets by trans-nitrosylation of its active cysteines Cys32 and 35.

Hypoxia alters the number of S-nitrosylated cysteines in numerous proteins. In endothelial cells with high levels of eNOS (NOSIII) multiple targets get S-nitrosylated under hypoxic conditions. This NO synthase has high affinity to O_2 (Kd 0.29 kPa, Dweik, 2005) and can therefore support NO production at low O_2 levels. At the same time in heart tissue, where NOSI and NOSII with low O_2 affinity are dominating (Kd 23–35 kPa, Dweik, 2005) hypoxia is associated with rapid cessation of NO production and decrease in S-nitrosylation of cysteine residues of the α subunit of the Na,K-ATPase (Yakushev et al., 2012). NO and S-nitrosylation were shown to protect thiols from irreversible oxidation and S-glutathionylation, and allow the enzyme to maintain high activity in the brain and heart (Petrushanko et al., 2007; Yakushev et al., 2012). Irreversible oxidation makes regulatory thiols inaccessible for S-nitrosylation. This may explain the fact that the sensitivity of the Na,K-ATPase to NO was lost in a mouse model of amyotrophic lateral sclerosis (Ellis et al., 2003).

S-glutathionylation of Thiols: Chemistry

S-glutathionylation (also referred to as S-glutathiolation), the formation of a mixed disulfide between a protein cysteine and that of glutathione. This thiol modification is produced in a number of chemical reactions (Klatt and Lamas, 2000; Dalle-Donne et al., 2007, 2008; Martinez-Ruiz and Lamas, 2007; Mieyal et al., 2008; Bachi et al., 2013).

Reactions resulting in formation of S-glutathionylated protein adducts include classical thiol disulfide exchange (reaction 7) that does not require any catalysis, and several mechanisms requiring prior oxidative modification of the thiol residues (either the protein thiol or cysteine residue of GSH, reactions 8–13).

$$\mathrm{P\text{-}S^-} + \mathrm{GSSG} \rightarrow \mathrm{P\text{-}SSG} + \mathrm{GS^-} \quad (7)$$

Reactions priming thiols to S-glutathionylation include prior formation of thiyl radicals with O_2 as an electron acceptor (reactions 8–9), oxidation of thiols to sulphenic acid (reaction 10–11) or to nitrosothiol (reactions 12–13)

$$\mathrm{P-S^\bullet} + \mathrm{GS^-} + \mathrm{O_2} \rightarrow \mathrm{P\text{-}SSG} + \mathrm{O_2^{\bullet -}} \quad (8)$$

$$\mathrm{P-S^-} + \mathrm{GS^\bullet} + \mathrm{O_2} \rightarrow \mathrm{P\text{-}SSG} + \mathrm{O_2^{\bullet -}}\ (\mathrm{catalyzed\ by\ glutaredoxin}) \quad (9)$$

$$\mathrm{P\text{-}SOH} + \mathrm{GSH} \rightarrow \mathrm{P\text{-}SSG} + \mathrm{H_2O} \quad (10)$$

$$\mathrm{P\text{-}SH} + \mathrm{GSOH} \rightarrow \mathrm{P\text{-}SSG} + \mathrm{H_2O} \quad (11)$$

$$\mathrm{P\text{-}SNO} + \mathrm{GSH} \rightarrow \mathrm{P\text{-}SSG} + \mathrm{HNO} \quad (12)$$

$$\mathrm{P\text{-}SH} + \mathrm{GSNO} \rightarrow \mathrm{P\text{-}SSG} + \mathrm{HNO} \quad (13)$$

S-glutathionylation of thiols in hypoxic cells is triggered by a local shift in GSSG/GSH ratio toward more GSSG (Petrushanko et al., 2012; Yakushev et al., 2012). On the other hand, oxidative stress following superoxide anion burst in hypoxic mitochondria, will promote oxidation of thiols to sulfenic acid priming them to S-glutathionylation via reaction 10.

Reversibility of S-glutathionylation is supported. Glutaredoxin1 and 2 may catalyze de-glutathionylation or glutathionylation reactions depending on the redox environment (NAD(P)H:NAD(P), GSH:GSSG, NO availability; Mieyal et al., 2008). Not all thiols in the proteins are accessible for S-glutathionylation. Whereas glutaredoxin1 is active in the cytosol and inter-membrane space, whereas glutaredoxin 2 is localized in the mitochondrial matrix, controlling the state of protein thiols in these compartments (Allen and Mieyal, 2012). Further enzymes capable to catalyze de-glutathionylation reaction include sulfiredoxin (Lei et al., 2008), glutathione transferase P (Townsend et al., 2009), and glutathione transferase omega 1 (Menon and Board, 2013).

Not all thiols are equally accessible for S-glutathionylation. Specific conditions that have to be fulfilled for the thiol to become glutathionylated are discussed below.

Localization of the Groups Favoring Glutathionylation

The likelihood for a given thiol to undergo S-glutathionylation is defined by several factors: (i) dissociation constant pKa of a thiol (ii) microenvironment (amino acid composition in vicinity to the cysteine residue), (iii) accessibility of the group and steric restrictions, and (iv) redox potential of a thiol (Nagy, 2013). Nucleophilic substitution reaction in which S-glutathionylated adduct is formed involves interaction of a thiolate anion with a GSSG molecule (Allen and Mieyal, 2012). Thiol therefore has to be deprotonated to join this reaction. The average pKa of majority of cysteine residues is 8.5. Thus, probability of deprotonation of cysteine residues under physiological conditions is relatively

low making S-glutathionylation selective (Dalle-Donne et al., 2009). Reduction in pKa of distinct thiols is supported by the positive charge of three flanking amino acids such as arginine, lysine, or histidine (Allen and Mieyal, 2012; Sun et al., 2013; Zhao et al., 2015). Proximity of negatively charged amino acids to a thiol on the contrary compromises interaction with GSSG. Protein sequence analysis for the α1 subunit of the Na,K-ATPase revealed that cysteines 204, 452, 599, and 698 (corresponding to the Cys 206, 454, 601, and 700 in **Figure 2**) are prone to S-glutathionylation (Mitkevich et al., 2016).

Steric restriction and localization of cysteine residue within the protein sequence are yet other parameters that should be taken into consideration when predicting S-glutathionylation sites (Pineda-Molina et al., 2001). Hydrophilicity of GSSG suggests that the residues should be exposed to aqueous phase as the reaction with GSSG occurs. Furthermore, the exposed surface of thiol should be sufficient for docking of GSSG to form mixed dithiols (Sun et al., 2013). "Basal S-glutathionylation" of cysteines that are buried within the protein, but are S-glutathionylated, represents a special case and is discussed below.

Further restrictions limiting the number of S-glutathionylated residues are related to the redox state of a thiol. For most proteins GSH:GSSG ratio should decrease from 100:1 to 1:1 to achieve S-glutathionylation of 50% of thiols (Allen and Mieyal, 2012). Very few proteins, such as c-Jun may be glutathionylated within physiological range of half-cell redox potential for GSH:GSSG couple (Klatt et al., 1999; Allen and Mieyal, 2012). Na,K-ATPase is one of these few proteins as interaction of the cysteine residues within its catalytic α subunit with GSSG can be observed as GSSG reaches 150 μM levels in the presence of 1.5 mM GSH (Petrushanko et al., 2012; Yakushev et al., 2012).

S-glutathionylation and Targets in the Na,K-ATPase

Alpha Subunit of the Enzyme

Cysteines of all three types of subunits forming Na,K-ATPase undergo S-glutathionylation. Catalytic α subunit contains 23 or more (depending on the isoform) cysteine residues (**Figure 2A**). Fifteen out of 23 Cys residues of the α1 isoform are localized within the cytosolic loops and are easily accessible for interaction with cytosolic GSSG. Out of seven cysteine residues of the regulatory β subunit 6 are forming S-S bonds with each other and only one remaining cysteine possesses a thiol accessible for S-glutathionylation (White et al., 2009). Tissue-specific FXYD subunits also contain 1–2 cysteines of which at least one undergoes S-glutathionylation (Bibert et al., 2011).

Regulatory S-glutathionylation Cysteine residues that were found S-glutathionylated within the α1 subunit isolated from duck salt gland were classified as targets for regulatory or basal S-glutathionylation (Petrushanko et al., 2012). Whereas basal S-glutathionylation is not associated with the changes in the enzyme hydrolytic activity, binding of glutathione to the regulatory cysteine residues causes the enzyme's complete inactivation that can be reversed upon de-glutathionylation (Petrushanko et al., 2012; Yakushev et al., 2012). Regulatory S-glutathionylation could be accomplished by incubation of the purified enzyme or membrane fraction with GSSG indicating that regulatory thiols were accessible for classical thiol disulfide exchange (reaction 5). Similar response was obtained for the α1 subunit within the broad range of tissues and cell type (cell line, salt gland, kidneys, heart tissue) and species (duck, rabbit, pig, mouse, rat, Spalax mole rat, trout, and human; Petrushanko et al., 2012, 2015; Yakushev et al., 2012; Juel, 2014; Xianyu et al., 2014; Juel et al., 2015; Mitkevich et al., 2016). Apart of α1, S-glutathionylation of the α2 isozyme was shown in heart and skeletal muscle. Moreover, α2 isozyme appeared to be more sensitive to GSSG-inducible inhibition in rat heart (Petrushanko et al., 2012; Xianyu et al., 2014; Juel, 2016). This observation is in agreement with the report of Xie on exceptionally high susceptibility of the α2 subunit to oxidation (Xie et al., 1995) and suggests that Cys residue(s) within this isoform are more accessible for oxidation (e.g., Cys 579 in **Table 1**). As can be seen from the **Table 1**, microenvironment for two cysteine residues (Cys 206 and 579) within the cytosolic loops of the α2 subunit favors S-glutathionylation as non-charged amino acids present in the α1 isoform are substituted by positively charged ones facilitating thereby deprotonation of the thiols. Furthermore, α2 subunit harbors the extra cysteine (Cys 236) in the actuator domain and lacks the Cys458 (present in the α1). Thus, although the number of cysteines does not differ between the α1 and α2 subunits, their location, pK and the ability to become S-glutathionylated show clear isoform-specificity.

Localization of the sites of regulatory S-glutathionylation was identified by means of mass spectrometry (Petrushanko et al., 2012). Three of them, Cys 454, 456, and 459 are proximal to the ATP binding site whereas Cys 244 is localized in the small cytosolic loop that may approach the ATP binding pocket in E2 conformation (Bogdanova et al., 2006). Binding of glutathione to the regulatory sites displaces adenine nucleotides from interaction with the enzyme (Petrushanko et al., 2012). In turn, GSSG cannot block the enzyme's hydrolytic activity in the presence of ATP or ADP (Petrushanko et al., 2012; Xianyu et al., 2014). ATP was showing maximal "protective effect" compared to the other nucleotides (Xianyu et al., 2014). Interaction with ATP (but not with the other nucleotides) brings the nucleotide-binding domain of the α subunit closer to the phosphorylation domain (E1-closed state) shielding thiols of the small and large cytosolic loops from attack by GSSG or oxidants (Petrushanko et al., 2014) and making them less prone to irreversible oxidation (Xie et al., 1995; Xu et al., 1997).

Increase in S-glutathionylation of the α subunit was triggered by hypoxia associated with mild oxidative stress and modest ATP depletion in rat heart and SC1 cell line derived from mouse fibroblasts (Petrushanko et al., 2012, 2015; Yakushev et al., 2012). Inhibition of the Na,K-ATPase and induction of S-glutathionylation could be mimicked by the modulation of intracellular redox state by exposure of cells to glutathione derivatives et-GSH, GSNO, GSSG, or depletion of the intracellular GSH (Petrushanko et al., 2006, 2015). S-glutathionylation of the α subunit cannot be sustained under anoxic conditions. This thiol modification is induced by 0.2% O_2

TABLE 1 | Analysis of flanking amino acids' composition of selected thiols in the α1 and α2 subunits (rat sequences).

Number of Cys	Sequence fragment	Substitutions α1-> α2	Comments
206 α1 α2	NCCKV HCCKV .****	N->H	Asp-> His (neutral to positive in α2)
236 α1 α2	NAFF NCFF **.**	A->C	Cys present in α2 and missing in α 1 isoform
458 α1 α2	EVCCGS ELSCGS *:.***	V->L C->S	Cys missing in the α2 isoform and present in α 1 Val->Leu (neutral)
513 α1 α2	DFCSS DFCST ****.	S->T	Neutral substitutions
551 α1 α2	GFCHL GFCQL ***:*	H->Q	His->Gln (positive to neutral in α2)
579 α1 α2	NLCFV KLCFV :****	N->K	Asp->Lys (neutral to positive in α2)
932 α1 α2	VICKT IICKT :****	V->I	Neutral exchange

Data shown in the table are obtained as a result of sequence alignment (Clustal O(1.2.1)) for the Na,K-ATPase α1(P06685) and α2 (P06686) subunits' sequences for rat (Rattus norvegicus), published in UniProt-Knowledgebase (Swiss-Prot collection of sequences, http://www.uniprot.org/uniprot). Included into the table are the amino acids flanking the cysteine residues for which the isoform-specific differences (substitution, omission) have been observed. Asterisks stand for the conserved amino acids whereas dots and semicolon indicate the substitutions. Cysteines are color-coded in blue and the substituted amino acids in yellow.

but less pronounced at 0.05% O_2 in mouse fibroblast-derived cell line (Petrushanko et al., 2015).

Basal S-glutationylation of the α subunit

Basal S-glutathionylation of the α subunit of the Na,K-ATPase is not associated with the changes in the enzyme function. 15 cysteine residues facing the cytosol are accessible for S-glutathionylation. Treatment of the cell lysates, membrane fractions or purified active Na,K-ATPase preparations with reducing agents (e.g., by Dithiotreitol or Tris(2-carboethyl)-phosphine, TCEP) could not completely remove glutathione bound to the α subunit's thiols (Mitkevich et al., 2016). Complete de-glutathionylation could only be achieved under conditions supporting partial denaturation of the protein (8 M urea and 8% SDS). De-glutathionylation of the cysteines inaccessible for reducing agents in the protein retaining its native structure was associated with substantial loss of the enzyme activity due to unfolding. The only chance these Cys residues shielded from GSSG and reducing agents have to acquire S-glutathionylation is before the folding was completed (**Figure 2B**). This implies that S-glutathionylation of certain Cys residues is a co-translational rather than post-translational modification and it may be required for correct protein folding. Detailed analysis of the X-ray structures of the porcine α1 subunit-containing enzyme (PBD codes: 3B8E, 3KDP, 3WGU, 3WGV, 4HYT) revealed a number of isolated cavities with unresolved electron density next to the Cys residues (numbering as in **Figure 2B**) Cys 206–Cys 244; Cys 454–Cys 458–Cys 459; Cys 700–Cys 369, Cys 601 (Mitkevich et al., 2016).

These regions of relatively high residual electron density that cannot be explained by the presence of water are sufficient in size to home glutathione. However, so far no X-ray structures of the actual catalytic subunit with S-glutathionylated cysteine adduct was reported. Detection of glutathionylated residues in crystal structures of proteins is not impossible (Srinivasan et al., 2014), but much less common that detection of these modifications by means of mass spectrometry. One of the technical approaches to use for identification of S-glutathionylated cysteine residues is tracking for glutathione localisation using analysis of unresolved density next to the cysteine residues. This approach was used for identification of glutathione bound to the ABC transporter Atm1 (Srinivasan et al., 2014). In each cavity of the α subunit only one Cys residue was reported to be S-glutathionylated (basal type of S-glutathionylation, **Figure 2B**, Mitkevich et al., 2016). These findings imply that Cys454 is located in a cavity and, hence, cannot be a regulatory thiol as suggested earlier (Petrushanko et al., 2012). Its basal S-glutathionylation will contribute to the

protein folding instead. Out of the Cys206-Cys244 couple Cys 206 is capable of basal S-glutathionylation whereas Cys 244 carries a regulatory thiol group. In contrast to regulatory S-glutathionylation observed within minutes after the drop in O_2 availability, increase in basal S-glutathionylation is only observed after 72 h of hypoxic exposure (Mitkevich et al., 2016). This kinetics correlate with the onset of *de novo* protein synthesis rather than acute alterations in thiol state.

Moreover, as this modification is retained during the life-span of a protein it represents "redox memory" that reflects the cellular redox state at the moment of synthesis of this molecule. Thus, this "redox memory" may represent the process of adaptation to the alterations in redox state occurring in particular in response to deoxygenation. The fact that basal S-glutathionylation levels differ in muscle fibers being higher in oxidative fibers compared to the glycolytic fiber type suggests that it is likely to be associated with the metabolic state of the tissue (Juel, 2014).

S-glutathionylation of Beta Subunit

A single reduced thiol group in β subunit of the Na,K-ATPase, Cys 46 (**Figure 2A**), is the one that may undergo reversible post-translational modifications. S-glutathionylation of this cysteine residue was reported for all three muscle types (skeletal, smooth, and heart muscles; Figtree et al., 2009; Liu et al., 2013; Juel et al., 2015). Since interaction of glutathione with Cys 46 results in down-regulation of the enzyme function this residue is a site of regulatory S-glutathionylation (Figtree et al., 2009). Inhibitory effect is achieved due to the weakening of the interaction between α and β subunits upon S-glutathionylation (Figtree et al., 2009). S-glutathionylation of β subunit does not inactivate the enzyme completely (Figtree et al., 2009). Unfortunately, the studies in which S-glutathionylation of the β subunit was detected were not presenting the information on the degree of S-glutathionylation of the α subunit, making it impossible to discriminate between the impacts of these two processes into the enzyme activity regulation (Liu et al., 2013).

In contrast to the regulatory cysteines of the catalytic α subunit that are readily interacting with GSSG Cys 46 does not join reaction of classical thiol disulfide exchange with GSSG (Petrushanko et al., 2012). This may be attributed to the localization of this Cys residue. According to the X-ray structure it is buried within the membrane in E2 2K+Pi conformation (Ogawa et al., 2009) and is only accessible for S-glutathionylation in E1ATP and E1Na(3) conformation (Liu et al., 2012). Furthermore, Cys 46 may become accessible or S-glutathionylation upon the loss of association between the α and β subunits (Garcia et al., 2015). Ouabain stabilizes the enzyme in E2 conformation and compromises S-glutathionylation of β subunit (Liu et al., 2012). De-glutathionylation can be achieved by treatment of the S-glutathionylated enzyme with Glutaredoxin.

Localization of the regulatory cysteine defines conditions required for its S-glutathionylation. It only occurs in the presence of peroxynitrite and hence involves reactions 12 and 13. Physiological and pathophysiological role of this form of regulatory thiol modification in the heart has been intensively investigated. Stimulation of $O_2^{\bullet-}$ production by NADPH oxidases, that co-localize and co-immunoprecipitate with the Na,K-ATPase, induces S-glutathionylation of the β subunit at Cys46 (Liu et al., 2013). The stimulation of NADPH oxidases could be triggered by their phosphorylation by PKC produced upon activation of β1/β2 adrenoceptors or treatment of the myocardium with angiotensin II. Furthermore, increase in S-glutathionylation of the β subunit was reported in the infarcted area in sheep heart (Figtree et al., 2009). Similar effect was achieved by exposure of cardiomyocytes to the activator of adenylate cyclase forskolin and the following activation of PKCε (White et al., 2010) or direct administration of ONOO- (Figtree et al., 2009). Scavenging of $O_2^{\bullet-}$ using superoxide dismutase on the contrary abolishes S-glutathionylation of the β subunit. Similar effect may be achieved by the stimulation of sGC that interfered with phosphorylation and activation of NADPH oxidases (Chia et al., 2015). Activation of β3 adrenoreceptor is a physiological stimulus decreasing S-glutathionylation of the Cys 46 (Bundgaard et al., 2010). These differential responses are easily explained based on the chemistry of S-glutathionylation of thiols. Deoxygenation is associated with suppression in production of NO by NOS1 and NOS2 as well as in reduction of activity of NADPH oxidases Kd of which for O_2 is within 2 kPa range. Thus, decrease in O_2 levels below this threshold reduces production of peroxynitrite and decreases S-glutathionylation of Cys 46 in β subunit. Uncoupling of oxidative phosphorylation and $O_2^{\bullet-}$ burst in the mitochondria on the contrary will facilitate GSSG production in the cytosol and induce S-glutathionylation of regulatory cysteines within the cytosolic loops of the catalytic α subunit.

S-glutathionylation of FXYD Subunits

Tissue-specific FXYD proteins associate with Na,K-ATPase αβ complex stabilizing it and modulating the enzyme activity (Geering, 2006). These modulatory subunits also contain 1 or 2 cysteine residues that undergo reversible thiol modifications. Most of the information on the role of these modifications in control of Na,K-ATPase function was obtained for the cardiac-specific FXYD1 subunit also known as phospholemman (PLM). It contains 2 Cys residues (C1 corresponding to Cys40 and C2 corresponding to Cys42 in human FXYD1 protein, **Figure 2A**), and S-glutathionylation of the C2 was shown to correlate reciprocally with the availability of glutathionylated form of the β subunit (Bibert et al., 2011). Localization of C2 and mechanisms of induction of S-glutathionylation of PLM are most likely shared with the β subunit of the Na,K-ATPase and involve peroxynitrite. Interaction of PLM with glutathione may be triggered by forskolin and prevented by exposure to superoxide dismutase. De-glutathionylation is also catalyzed by glutaredoxin1 or treatment with DTT. Thus, both PLM and β subunits lack cysteines that are not accessible for de-glutathionylation (redox memory). Physiological stimuli increasing the level of PLM S-glutathionylation include angiotensin II and infarction (Bibert et al., 2011).

The importance of the amino acids flanking the cysteine residue in control of accessibility of it for S-glutathionylation was emphasized as the amount of glutathionylated adducts was compared for several members of FXYD family. C2 cysteines

were found to be prone to S-glutathionylation in FXYD2 (renal) and FXYD7 (brain-derived) (Geering, 2006; Bibert et al., 2011). Phospholemman (PLM, FXYD1) interacts with both catalytic and regulatory subunits of the Na,K-ATPase. Thus, interaction between α and β subunits and the enzyme function is affected by S-glutathionylation of the FXYD1. Furthermore, the reciprocal regulation of S-glutathionylation of the β and FXYD subunits suggests that FXYD may reverse the inhibitory action mediated by binding of glutathione to the regulatory β subunit on the Na,K-ATPase. It remains unclear if glutathione is transferred from the Cys46 on to the β subunit to the C2 residue in reaction of thiol disulfide exchange of the FXYD protein or if S-glutathionylation of the FXYD protein makes Cys46 inaccessible for S-glutathionylation.

H_2S and the Na,K-ATPase

Hypoxic exposure was shown to cause a rapid increase in H_2S levels in a number of cells including chemoreceptory glomus cells (Peng et al., 2010; Olson, 2015; Yuan et al., 2015). Direct interaction of H_2S with the Na,K-ATPase has not been reported. However, exposure of renal tubular epithelial cells to H_2S causes internalization of the Na,K-ATPase in complex with other proteins. This inhibitory response of the pump is triggered by sulfhydrolation of cysteines 797 and 798 at the epidermal growth factor receptos (EGFRs) (Ge et al., 2014).

COORDINATED REGULATION OF REDOX-SENSITIVE PROTEIN NETWORKS BY REVERSIBLE THIOL MODIFICATIONS

S-glutathionylation and S-nitrosylation are altering the function of numerous proteins that form redox sensitive networks (Sun et al., 2006; Dalle-Donne et al., 2009). Protein clusters forming these networks are the ones controlling metabolism, ion transport, cell fate and cycle, adaptation, and others. This type of free radical-based signaling is of key importance in responses to hypoxia and reoxygenation mediating acute and long-term tissue-specific coordination of function of multiple proteins. S-glutathionylation of the α subunit of the Na,K-ATPase occurs among with alterations in thiol state of other proteins. The most obvious protein partners that undergo S-glutathionylation are the adjacent β and FXYD subunits. Thiol disulfide exchange in which PLM most likely acquires glutathione from the Cys 46 subunit of the β subunit is suggested to cause dissociation of the FXYD subunit of from the Na,K-ATPase as it does not co-precipitate with the α subunit (Bibert et al., 2011). As PLM is a regulatory subunit that is shared between the Na,K-ATPase and the Na/Ca exchanger, it was suggested that S-glutathionylation as well as its redox-sensitive phosphorylation of it impacts activity of both transporters (Silverman et al., 2005; Cheung et al., 2007; Zhang et al., 2011). Calcium handling in the heart is intimately linked to the Na^+ levels (Shattock et al., 2015) and, hence to the activity of the α2 isozyme of the Na,K-ATPase that is particularly prone to inhibition by GSSG (James et al., 1999; Petrushanko et al., 2012). Apart of the Na/Ca exchanger reversible thiol modifications are known to control the activity of L-type Ca^{2+} channel, RyR2 ryanodine receptors, SERCA2a Ca^{2+} pump and multiple other ion transporters (Sun et al., 2006; Bull et al., 2008; Lancel et al., 2009; Donoso et al., 2011).

These coordinated redox-driven changes in activity of multiple ion transporters may support cytoprotection and survival of the cell/tissue/organism or promote death under hypoxic conditions (see Section Regulation of the Na,K-ATPase Activity by Cardiotonic Steroids).

OXYGEN-SENSITIVE PHOSPHORYLATION

Regulatory phosphorylation is known to control the activity, sensitivity to the cardiotonic steroids, and availability of the Na,K-ATPase on the plasma membrane. Changes in phosphorylation state of the enzyme were reported in response to hypoxic challenge and for a long time believed to be the only mechanism involved in "channel arrest" response of the Na,K-ATPase in hibernating animals (MacDonald and Storey, 1999; Ramnanan and Storey, 2006; McMullen and Storey, 2008). At present "channel arrest" responses seem to be more versatile, and yet triggered by a single mechanism of regulation, in this case not only the Na,K-ATPase itself, but also the redox-sensitive kinases, namely, reversible thiol modifications of regulatory cysteine residues or action of gasotransmitters. Phosphorylation sites at the α, β and FXYD subunits are schematically presented in **Figure 3**.

Protein Kinase C (PKC)

Hypoxic exposure of alveolar epithelial cells was shown to trigger actively controlled internalization of the Na,K-ATPase in the form of clathrin-coated vesicles (Dada et al., 2003). This process was induced by phosphorylation of the α subunit of the Na,K-ATPase by at atypical PKC isozyme.

Novel and classical PKC isoforms are also capable to alter activity of the Na,K-ATPase in various cell types. Classical (conventional α, β1 and β2, and γ isoforms) and novel isoforms PKC δ, ε, η, θ, and μ may be activated diacylglycerol (DAG), phorbol esthers and phosphatidylserine and are sensitive to the changes in Ca^{2+} in the cell. Atypical PKCι and ξ retain the sensitivity to phosphatidylserine but are Ca^{2+}-insensitive (**Figure 3**; Newton, 1995; Parker and Murray-Rust, 2004).

Catalytic core of PKC contains critical cysteine-rich motifs that are conserved in all PKC isozymes making all proteins of this class redox-sensitive (Newton, 1995). This motif is duplicated in classical and novel PKC isoforms, whereas in atypical PKCs only one repeat is found. Oxidation of these cysteines causes transient activation of the enzyme but makes it unable to interact with DAG and phorbol esters making it Ca^{2+}- and DAG-insensitive (Gopalakrishna and Anderson, 1989). S-glutathionylation of these regulatory thiols is inactivating α, βI, βII, γ, δ, ε, and ζ isoforms of PKC. Formation of glutathionylated adducts occurs within physiological range of GSH concentrations (0.5–10 mM) and results in the enzyme inactivation (Ward et al., 1998, 2000; Chu et al., 2001). In addition, PKC may undergo S-nitrosylation that was shown to suppress activity of PKCα (Choi et al., 2011). Depletion of intracellular GSH by exposure to conjugating agent

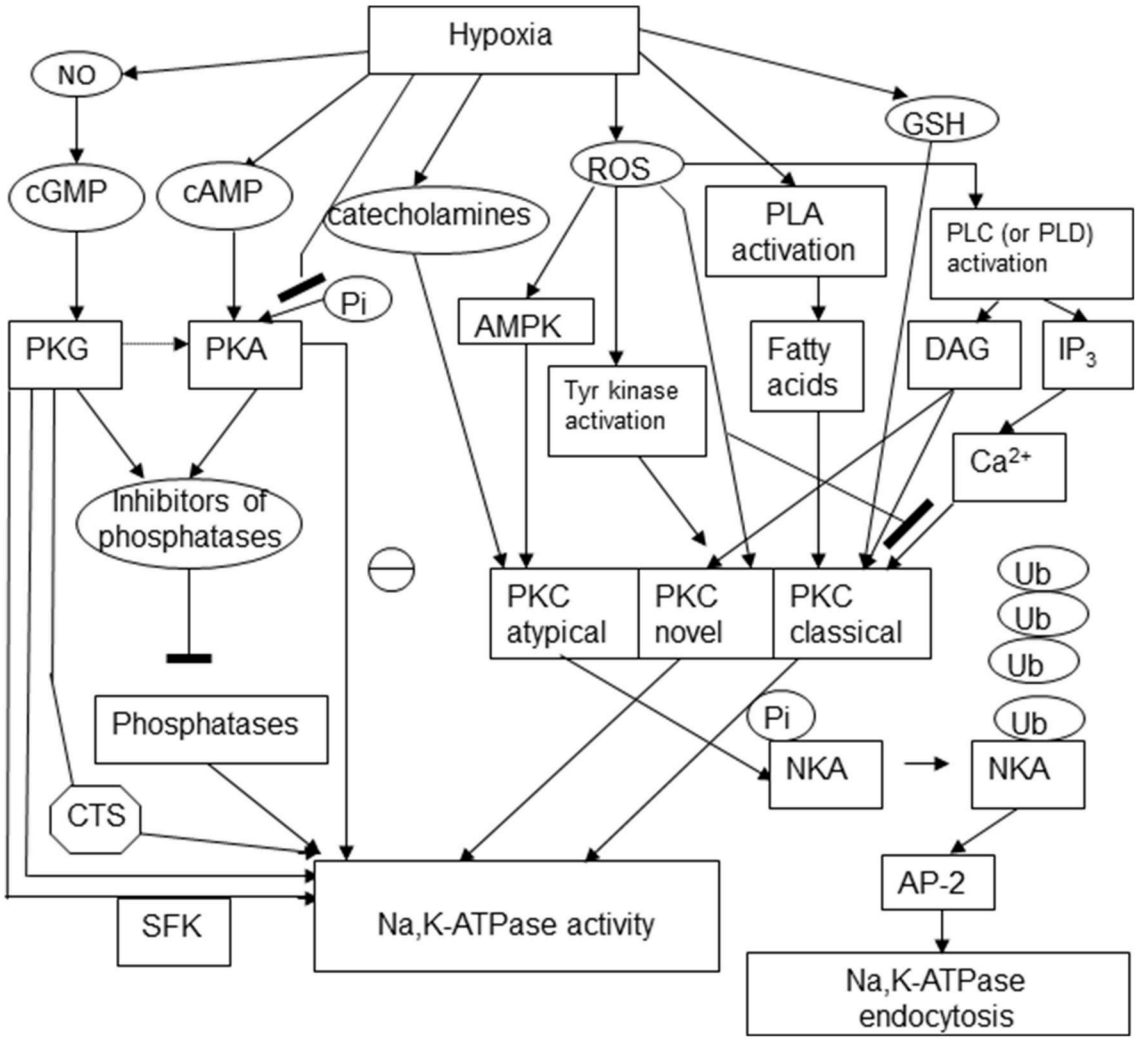

FIGURE 3 | Schematic representation of the multiple pathways involved in regulatory phosphorylation of the Na,K-ATPase under hypoxic conditions. The following abbreviations were used in the scheme: cyclic adenosine and guanosine monophosphates (cGMP and cAMP), protein kinases C, A, and G (PKC, PKA, PKG), cardiotonic steroids (CTS), Src kinase family (SFK), AMP-activated protein kinase (AMPK), phospholipase C (PLC), diacylglycerol (DAG), inositol 3-phosphate (IP3), ubiquitin (Ub), NKA (Na,K-ATPase), adaptor protein 2 (AP-2).

diethylmaleimide or inhibition of *de novo* GSH production by L-buthionine-S,R-sulfoximine results in reduction in activity of conventional PKC isoforms (α, βI, and βII) by 35–50%, along activation of the novel isoforms (δ and ε) (Domenicotti et al., 2000). This response of the PKCs to the changes in redox state will induce endocytosis of the Na,K-ATPase (**Figure 3**).

PKC phosphorylates the catalytic α1 subunit at Ser11 and 18 (rat sequence) at the N-terminus of the protein that forms the actuator domain. Ser18 that is considered as a major phosphorylation site is available for phosphorylation in the E2 conformation (Feschenko and Sweadner, 1997). In the E1 conformation the N-terminus is translocated approaching the small cytosolic loop that shields the phosphorylation site from interaction with the kinase (Feschenko et al., 1997; Segall et al., 2003). The analogs of Ser18 and Ser11 are missing in the α2 isoform of the catalytic subunit (compare sequences A24639 for α1 and B24639 for α2 subunit in PubMed protein sequence library http://www.ncbi.nlm.nih.gov) making this isozyme PKC-insensitive. Phosphorylation efficiency may also vary depending on the PKC isoform. Conventional isoforms are more efficient in phosphorylation of the α1 isoform of the pump isolated from rat retinal cells than the novel isoforms δ and ε (Kazanietz et al., 2001). Phosphorylation of the α subunit by PKC may have stimulatory of inhibitory effects on the Na,K-ATPase depending on the cell type (Therien and Blostein, 2000). It is suggested that phosphorylation modulates interaction of the enzyme with other proteins or trigger its internalization (Feschenko and Sweadner, 1997). For example, activation of the atypical isoforms of PKC ξ triggers internalization of the Na,K-ATPase in alveolar epithelial cells under hypoxic conditions (Dada and Sznajder, 2003). This effect is initiated by the free radical burst in the

mitochondria that is followed by the activation by the 5′-AMP-activated protein kinase (AMPK) that is phosphorylated at Thr172. The activated AMPK phosphorylates PKCξ at Thr410 and its translocation to the plasma membrane (Gusarova et al., 2009). Upon translocation PKC phosphorylates Na,K-ATPase at the Ser18 residue in the N-terminus of the α1 subunit. Endocytosis of the α1-containing isozyme of the ATPase is precluded by ubiquitination of the lysine residues next to the Ser18 (Dada et al., 2007; Lecuona et al., 2007). Ubiquitination makes the enzyme recognizable for the mu2 subunit of the adaptor protein that binds to the Tyr527 of the α1 subunit initiating its endocytosis in clathrin-coated vesicle is initiated with the following degradation of the Na,K-ATPase (Chen et al., 2006; Lecuona et al., 2007).

PLM is one more target of phosphorylation by PKCϵ at Ser36 and Ser 68. Phosphorylation it stimulated by Ca^{2+} and is NO-dependent (Pavlovic et al., 2013). Ischemia was associated with facilitation of phosphorylation of PLM, its de-attachment from the αβ complex and increase in the Na,K-ATPase hydrolytic activity in sarcoplasmic membrane fraction (Fuller et al., 2003, 2009).

Protein Kinase G (PKG)

Hypoxia and reoxygenation result in the alterations in NO, CO, and H_2S production (see above). All gasotransmitters are capable of activation of sGC that in turn triggers activation of cGMP-dependent protein kinase PKC (PKG) (Therien and Blostein, 2000; Chen et al., 2015). Similar to that for PKC, phosphorylation by PKG was reported to have diverse effects on the Na,K-ATPase activity (Therien and Blostein, 2000). It remains unclear if PKG can directly access the phosphorylation site within the α subunit, as it could only be phosphorylated in the presence of detergents in the purified protein preparation (Fotis et al., 1999; Beltowski et al., 2003). However, treatment of yolk-free homogenates of Xenopus oocytes with cGMP results in phosphorylation and activation of the Na,K-ATPase in the absence of detergents (Fotis et al., 1999). It may reflect the indirect action of PKG on the ATPase via the suppression of dephosphorylation. Yet one more report on the activation of the α2/3 isozymes of the Na,K-ATPase in the central nervous system involves activation of cGMP-PKG pathway following the stimulation with glutamate (Munhoz et al., 2005; Scavone et al., 2005). On the other hand, supplementation of NO donors was shown to inhibit the Na,K-ATPase in nonpigmented epithelial cells of porcine eyes that is associated with activation of PKG (Shahidullah and Delamere, 2006). This effect involves PKG-driven activation of src-family kinases (Shahidullah et al., 2014).

Apart of the alterations in the enzyme activity, stimulation of the cGMP-PKG pathway may affect binding of cardiotonic steroids to the Na,K-ATPase. Increases the sensitivity of the renotubular Na,K-ATPase to marinobufagenin triggered by atrial natriuretic peptide is mediated by the cGMP-PKG signaling cascade (Fedorova et al., 2012).

Protein Kinase A (PKA)

Cyclic AMP-sensitive protein kinase (PKA) is a redox-sensitive enzyme containing regulatory thiols (Brennan et al., 2006). In the absence of cAMP the enzyme exists in the inactive tetrameric state and the regulatory Cys199 within the C subunits is inaccessible for regulatory S-glutathionylation (Humphries et al., 2002). Binding of glutathione to this cysteine residue inactivates the kinase and enhances dephosphorylation (Humphries et al., 2005). Vector of the changes in activity of PKA in response to deoxygenation is very much dependent on the cell type and on the activity of G-protein coupled receptors signaling via cAMP-PKA transduction pathway (Jiang et al., 2011).

PKA phosphorylates the catalytic α subunit at Ser938 (rat α1 sequence) within the cytosolic M8-M9 loop. This loop may interact with the M10, C-terminus and the third Na^+ binding site. In line with that phosphorylation at Ser938 decreases affinity of this Na^+ binding site to Na^+ and thereby suppresses the enzyme function (Einholm et al., 2016).

In the purified Na,K-ATPase protein preparation this target is accessible for phosphorylation in the presence of detergent (Feschenko and Sweadner, 1994; Lutz et al., 1996). In intact COS cells phosphorylation of the α subunit at Ser943 is triggered by β-adrenergic stimulation with the following inhibition of hydrolytic and transport activity of the Na,K-ATPase (Cheng et al., 1997).

Activation of cAMP-PKA-dependent pathways in NRK-52E and L6 cell lines may suppress activity of PKC and reduce phosphorylation of the Na,K-ATPase at the PKC binding sites (Feschenko et al., 2000). This cross-talk may result from the close proximity of the PKG binding site to that of PKC (Kruger et al., 2003).

Along with PKC, PKA may catalyze phosphorylation of PLM at Ser68 (Fuller et al., 2004, 2009) in response to ischemia or β adrenergic stimulation (Despa et al., 2005) causing release of the inhibitory action of association of the FXYD1 subunit with the Na,K-ATPase.

REGULATION OF THE NA,K-ATPASE ACTIVITY BY CARDIOTONIC STEROIDS

Cardenolides and bufadienolides are the two classes of endogenous cardiotonic steroids that serve as hormones selectively interacting with Na,K-ATPase. These compounds are produced by midbrain and adrenocortical cells, and released into the circulation in sub-micromolar concentrations in response to various stimuli such as angiotensin II, acetylcholine, vasopressin, catecholamines, and hypoxic exposure (Bagrov et al., 2009). Interaction of these very low doses of endogenous inhibitors with the Na,K-ATPase does not compromise the transmembrane Na^+ gradients, but induces activation of Src kinase and formation of protein complex in which Src kinase and Na,K-ATPase associate with epidermal growth factor receptor (EGRF) and initiate several signaling cascades (Li and Xie, 2009). Signaling modalities depend on the type of cardiotonic steroid and its dose (Dvela et al., 2007). At the molecular level these differences in physiological action of cardenolide ouabain and bufadienolide marinobufagenin are reflected by the specific pattern of conformational changes unique for each steroid

upon binding to the purified Na,K-ATPase enzyme (Klimanova et al., 2015). Affinity of the Na,K-ATPase to ouabain is maximal in E2P conformation (in this conformation binding constant for ouabain exceeds that for marinobufagenin by 17-fold), whereas marinobufagenin does not discriminate between the E1 and E2 conformations when binding to the enzyme (Klimanova et al., 2015).

Notably, substitution of Cys 244 by Ala makes cells ouabain-intolerant (Shi et al., 2000). This cysteine is a target of regulatory S-glutathionylation (Petrushanko et al., 2012). Furthermore, binding of cardiotonic steroids fixes the enzyme in distinct conformation depending on the type of cardiotonic steroids (Klimanova et al., 2015). Thus, binding of cardiotonic steroids may alter susceptibility of cysteine residues to S-glutathionylation and, *vice versa*, reversible thiol modifications may possibly alter sensitivity of the enzyme to cardiotonic steroids. This hypothesis awaits further investigations.

Local (renal) or systemic reduction in oxygen availability was shown to trigger release of cardiotonic steroids (bufadienolides or endogenous ouabain) into the circulation in rodents and humans (Zhao et al., 1995; Bagrov et al., 1998; De Angelis and Haupert, 1998; Tian et al., 2010). Apart of the induction of cytoprotective signaling pathway, endocytosis of Na,K-ATPase will support reduction of ATP consumption by hypoxic tissue (De Angelis and Haupert, 1998). Protective effect of distinct cardiotonic steroids (low doses oleandrin for the brain and ouabain or the heart) was reported for the brain and heart exposed to ischemia-reperfusion (Pasdois et al., 2007; Van Kanegan et al., 2014). Binding of ouabain in low doses to the ATPase protects from toxicity of other cardiotonic steroids (Nesher et al., 2010). Whereas micormolar doses of cardiotonic steroids trigger Ca^{2+} overload and promote apoptosis (Winnicka et al., 2007), nanomolar doses of some of these compounds stimulate proliferation (Winnicka et al., 2010). This anti-apoptotic action may be reflect the changes in affinity of the Na,K-ATPase-ouabain complex to other proteins interacting with the Na,K-ATPase such as PKC, BAX, and Bcl-2 (Lauf et al., 2015). Release of them from the enzyme into the cytosol protects the cells from apoptosis.

On the other hand endogenous ouabain and marinobufagenin act as powerful vasoconstrictors actively participating in development of hypertension (Bagrov and Fedorova, 1998), and have a potential to cause Ca^{2+} overload secondary to the inhibition of the Na^+ extrusion from hypoxic tissue (Schwinger et al., 1999). At the moment, we clearly know too little about the mechanisms of cytoprotection by cardiotonic steroids to use them effectively as therapeutic agents avoiding deadly side-effects (Washam et al., 2015).

THE ROLE OF ACUTE REGULATION OF THE NA,K-ATPase IN ADAPTATION OR IRREPARABLE DAMAGE AT LOW O_2 LEVELS

As shown above, the capacity of the Na,K-ATPase to sense and respond to the changes in oxygen availability is immensely diverse with multiple signaling cascades implicated in fine-tuning of the enzyme's activity apart and before terminal ATP depletion is reached. The choice of signaling mechanism as well as the resulting vector and amplitude of the change in the Na,K-ATPase activity depends on the cell type, severity and duration of hypoxia, and is rather species-specific. Strictly speaking, we cannot refer to Na,K-ATPase as the "oxygen-sensitive" protein as all the processes involved in its responding to hypoxia are mediated by secondary products of O_2 transformation to either gaseous messengers or products of O_2 reduction.

Several types of response to hypoxia include (i) inhibition by thiol modifications (ii) modulation of the enzyme function/availability at the membrane due to the changes in phosphorylation, and (iii) interaction with nanomolar doses of endogenous cardiotonic steroids.

Diversity of regulatory pathways allows for fine dose-dependent regulation of the enzyme within minutes after the alteration in O_2 availability. Based on the current knowledge the following scheme of responses may be suggested (**Figure 4**). Following gradual deoxygenation NO availability in cells expressing NOS1 and NOS2 becomes limited whereas $O_2^{\bullet-}$ production by NADPH oxidases is maintained while pO_2 is above 2–3 kPa (K_d for NOXes $\sim$ 2 kPa) (Pacher et al., 2007). This is not the case for tissues in which NOS3 isoform of NO synthase with high affinity for O_2 prevails (such as vascular endothelial cells). These conditions most likely favor S-glutathionylation of β subunit that is associated with activation of superoxide production by NOXes (White et al., 2009) and α subunits of the Na,K-ATPase due to the gradual accumulation of GSSG (Petrushanko et al., 2012). Further decrease in oxygenation to 1–2 kPa supports uncoupling of electron transfer and triggers mitochondrial $O_2^{\bullet-}$ production and accumulation of H_2O_2 in the cytosol. Oxidation of GSSG becomes more pronounced and complete inactivation of the enzyme may be achieved as soon as ATP levels decrease below 50 μM (Petrushanko et al., 2012). Further decrease in O_2 to 0.2 kPa reduces S-glutathionylation and renders regulatory thiols within the α subunit oxidized to sulfinic and sulfonic acid making the enzyme insensitive to the changes in GSSG and $ONOO^-$ (Petrushanko et al., 2015). Phosphorylation may support or reduce the probability of complete reversible inactivation by S-glutathionylation of the regulatory cysteines by shifting the equilibrium between the E1 and E2 conformation of the enzyme (see Section Oxygen-Sensitive Phosphorylation).

Survival under hypoxic conditions implies that Na^+ uptake particularly high in excitable tissues is balanced with equally efficient extrusion of Na^+ by the pump (Hylland et al., 1997; Nilsson, 2001). Inhibition of the Na,K-ATPase is deadly when not synchronized with the closing of the cation channels and cessation of activity of the animal (channel arrest) (Buck and Hochachka, 1993; Hochachka et al., 1996; Hylland et al., 1997; Silver et al., 1997; Nilsson, 2001; Ross et al., 2006; Wilkie et al., 2008; Dave et al., 2009). If the Na,K-ATPase is suppressed and the channels are not "arrested," survival is limited to the time of Na^+/K^+ gradients dissipation in the brain and in the heart (Hylland et al., 1996, 1997; Silver

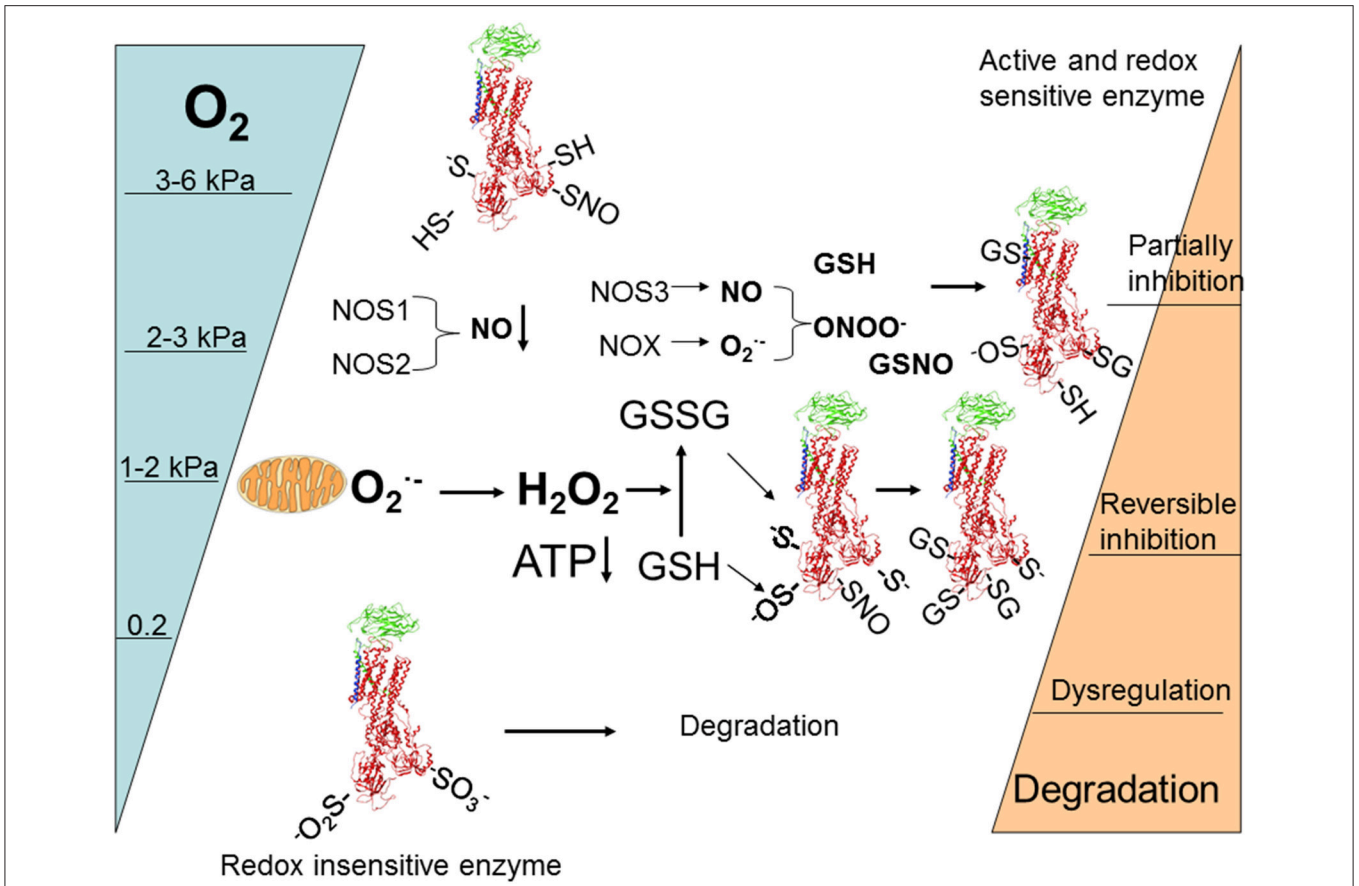

FIGURE 4 | Schematic representation of O_2-induced regulation of activity and abundance of Na,K-ATPase in majority of cells and tissues (for details see the Section The role of acute regulation of the Na,K-ATPase in adaptation or irreparable damage at low O_2 of levels of the review).

et al., 1997; Nilsson, 2001). It is tempting to assume that the alterations in free radical production and reversible thiol modifications are involved in the simultaneous regulation of multiple ion transporting systems coupling their activity to the mitochondrial function and ATP availability. However, data providing direct support for this hypothesis are currently missing.

The pilot studies suggest that preservation of redox state in hypoxic heart is sufficient to maintain the Na,K-ATPase activity in Spalax mole rate and trout supporting activity of both species under conditions of critical O_2 shortage for at least 20 min (Yakushev et al., 2012). S-nitrosylation of the regulatory cysteine residues in the α subunit may also prevent S-glutathionylation and the enzyme inactivation by GSSG in myocardial membranes (Petrushanko et al., 2012). Whether this is the case for some or all anoxia-tolerant species (e.g., Hylland et al., 1997; Nilsson, 2001; Ross et al., 2006; Dave et al., 2009), remains to be clarified.

Maintenance of the transmembrane Na^+ gradients does not only support neuronal function and heart contractility. It also regulates intracellular Ca^{2+} by controlling the activity of Na/Ca exchanger and that of voltage-gated Ca^{2+} channels. Ca^{2+} transport pathways are by themselves targets regulated by reversible thiol modifications in hypoxic cells (Lehotsky et al., 2002; Wang and Zheng, 2010).

Recent data revealed the existence of intimate link between the activity of the Na,K-ATPase and the gene expression in hypoxic cells and tissues. Two factors that were recently suggested to impact the gene expression under hypoxic conditions include the shift in transmembrane Na/K gradients (Koltsova et al., 2014) and the alteration in HIF1α levels upon binding of the nanomolar concentrations of cardiotonic steroids to their binding site within the Na,K-ATPase (Zhang et al., 2008; Cao et al., 2014). Decrease in HIF1α in hypoxic cells (1% O_2) in the presence of <50 nM ouabain is not caused by its degradation but rather by a drop in protein synthesis (Zhang et al., 2008), most likely at the level of translation (Cao et al., 2014). Alterations of HIF1α availability by cardiac glycosides contributes to the modulation of long-term hypoxic responses of the organism. For example digoxin treatment prevents remodeling of pulmonary vasculature underlying development of hypoxic pulmonary hypertension (Abud et al., 2012). It is known that signaling cascades initiated by binding of low doses of cardiotonic steroids to the Na,K-ATPase include modulation of intracellular Ca^{2+} levels and free radical production as well as activation of several kinases. Molecular mechanisms linking

these processes to the regulation of HIF1α translation remain unclear.

AUTHOR CONTRIBUTIONS

AB is the author the general schematics of review, she contributed to all the sections and assembling of the review. AM, PH were contributing to the sections Introduction. Oxygen, and Oxygen Sensing from Evolutionary and Modern Perspectives, Versatility of oxygen sensing. Multiple Signals-Multiple Targets—Multiple Responses—Multiple Outcomes, and Oxygen and Redox-Sensitivity of the Na,K-ATPase. IP contribution were the sections Oxygen and Redox-Sensitivity of the Na,K-ATPase, Coordinated Regulation of Redox-Sensitive Protein Networks by Reversible Thiol, Oxygen-Sensitive Phosphorylation, and Regulation of the Na,K-ATPase Activity by Cardiotonic Steroids. All co-authors discussed the topics and writing the review. All of them agree with the final text.

ACKNOWLEDGMENTS

The review was funded by the grants of Swiss National Science Foundation IZK0Z3_157269/1 and 310030_124970/1 to AB and Russian Science Foundation (Grant #14-14-01152) to IP Spanish Government grants (partially funded by the European Union FEDER/EDRF) PI12/00875 and PI15/00107 and a grant from the Fundación Domingo Martínez are supporting AM, PH received a travel grant from the Instituto de Investigación Sanitaria Princesa (to PH), and by COST actions TD0901 (HypoxiaNet) and CM1001. PH is recipient of a pre-doctoral FPU fellowship from the Spanish Government and AM is supported by the I3SNS programme (ISCIII, Spanish Government, partially funded by FEDER/ERDF).

REFERENCES

Abramov, A. Y., Scorziello, A., and Duchen, M. R. (2007). Three distinct mechanisms generate oxygen free radicals in neurons and contribute to cell death during anoxia and reoxygenation. *J. Neurosci.* 27, 1129–1138. doi: 10.1523/JNEUROSCI.4468-06.2007

Abud, E. M., Maylor, J., Undem, C., Punjabi, A., Zaiman, A. L., Myers, A. C., et al. (2012). Digoxin inhibits development of hypoxic pulmonary hypertension in mice. *Proc. Natl. Acad. Sci. U.S.A.* 109, 1239–1244. doi: 10.1073/pnas.1120385109

Acker, T., Fandrey, J., and Acker, H. (2006). The good, the bad and the ugly in oxygen-sensing: ROS, cytochromes and prolyl-hydroxylases. *Cardiovasc. Res.* 71, 195–207. doi: 10.1016/j.cardiores.2006.04.008

Allen, E. M., and Mieyal, J. J. (2012). Protein-thiol oxidation and cell death: regulatory role of glutaredoxins. *Antioxid. Redox Signal.* 17, 1748–1763. doi: 10.1089/ars.2012.4644

Alvarez, B., and Radi, R. (2003). Peroxynitrite reactivity with amino acids and proteins. *Amino Acids* 25, 295–311. doi: 10.1007/s00726-003-0018-8

Bachi, A., Dalle-Donne, I., and Scaloni, A. (2013). Redox proteomics: chemical principles, methodological approaches and biological/biomedical promises. *Chem. Rev.* 113, 596–698. doi: 10.1021/cr300073p

Bagrov, A. Y., and Fedorova, O. V. (1998). Effects of two putative endogenous digitalis-like factors, marinobufagenin and ouabain, on the Na+, K+-pump in human mesenteric arteries. *J. Hypertens.* 16, 1953–1958. doi: 10.1097/00004872-199816121-00015

Bagrov, A. Y., Fedorova, O. V., Dmitrieva, R. I., Howald, W. N., Hunter, A. P., Kuznetsova, E. A., et al. (1998). Characterization of a urinary bufodienolide Na+,K+-ATPase inhibitor in patients after acute myocardial infarction. *Hypertension* 31, 1097–1103. doi: 10.1161/01.HYP.31.5.1097

Bagrov, A. Y., Shapiro, J. I., and Fedorova, O. V. (2009). Endogenous cardiotonic steroids: physiology, pharmacology, and novel therapeutic targets. *Pharmacol. Rev.* 61, 9–38. doi: 10.1124/pr.108.000711

Belousov, V. V., Fradkov, A. F., Lukyanov, K. A., Staroverov, D. B., Shakhbazov, K. S., Terskikh, A. V., et al. (2006). Genetically encoded fluorescent indicator for intracellular hydrogen peroxide. *Nat. Methods* 3, 281–286. doi: 10.1038/nmeth866

Beltowski, J., Marciniak, A., Wojcicka, G., and Gorny, D. (2003). Nitric oxide decreases renal medullary Na^+, K^+-ATPase activity through cyclic GMP-protein kinase G dependent mechanism. *J. Physiol. Pharmacol.* 54, 191–210.

Berrisford, J. M., and Sazanov, L. A. (2009). Structural basis for the mechanism of respiratory complex I. *J. Biol. Chem.* 284, 29773–29783. doi: 10.1074/jbc.M109.032144

Bibert, S., Liu, C. C., Figtree, G. A., Garcia, A., Hamilton, E. J., Marassi, F. M., et al. (2011). FXYD proteins reverse inhibition of the Na+-K+ pump mediated by glutathionylation of its beta1 subunit. *J. Biol. Chem.* 286, 18562–18572. doi: 10.1074/jbc.M110.184101

Blackstone, E., Morrison, M., and Roth, M. B. (2005). H2S induces a suspended animation-like state in mice. *Science* 308, 518. doi: 10.1126/science.1108581

Blanco, G. (2005). Na,K-ATPase subunit heterogeneity as a mechanism for tissue-specific ion regulation. *Semin. Nephrol.* 25, 292–303. doi: 10.1016/j.semnephrol.2005.03.004

Blanco, G., and Mercer, R. W. (1998). Isozymes of the Na-K-ATPase: heterogeneity in structure, diversity in function. *Am. J. Physiol.* 275, F633–F650.

Bogdanova, A., Grenacher, B., Nikinmaa, M., and Gassmann, M. (2005). Hypoxic responses of Na+/K+ ATPase in trout hepatocytes. *J. Exp. Biol.* 208, 1793–1801. doi: 10.1242/jeb.01572

Bogdanova, A., Petrushanko, I., Boldyrev, A., and Gassmann, M. (2006). Oxygen- and Redox-Induced Regulation of the Na/K ATPase. *Curr. Enzyme Inhibit.* 2, 37–59. doi: 10.2174/157340806775473490

Boveris, A., Cadenas, E., and Stoppani, A. O. (1976). Role of ubiquinone in the mitochondrial generation of hydrogen peroxide. *Biochem. J.* 156, 435–444. doi: 10.1042/bj1560435

Brennan, J. P., Bardswell, S. C., Burgoyne, J. R., Fuller, W., Schroder, E., Wait, R., et al. (2006). Oxidant-induced activation of type I protein kinase A is mediated by RI subunit interprotein disulfide bond formation. *J. Biol. Chem.* 281, 21827–21836. doi: 10.1074/jbc.M603952200

Brunelle, J. K., Bell, E. L., Quesada, N. M., Vercauteren, K., Tiranti, V., Zeviani, M., et al. (2005). Oxygen sensing requires mitochondrial ROS but not oxidative phosphorylation. *Cell Metab.* 1, 409–414. doi: 10.1016/j.cmet.2005.05.002

Buck, L. T., and Hochachka, P. W. (1993). Anoxic suppression of Na(+)-K(+)-ATPase and constant membrane potential in hepatocytes: support for channel arrest. *Am. J. Physiol.* 265, R1020–R1025.

Bull, R., Finkelstein, J. P., Galvez, J., Sanchez, G., Donoso, P., Behrens, M. I., et al. (2008). Ischemia enhances activation by Ca2+ and redox modification of ryanodine receptor channels from rat brain cortex. *J. Neurosci.* 28, 9463–9472. doi: 10.1523/JNEUROSCI.2286-08.2008

Bundgaard, H., Liu, C. C., Garcia, A., Hamilton, E. J., Huang, Y., Chia, K. K., et al. (2010). beta(3) adrenergic stimulation of the cardiac Na+-K+ pump by reversal of an inhibitory oxidative modification. *Circulation* 122, 2699–2708. doi: 10.1161/CIRCULATIONAHA.110.964619

Cadenas, E., Boveris, A., Ragan, C. I., and Stoppani, A. O. (1977). Production of superoxide radicals and hydrogen peroxide by NADH-ubiquinone reductase and ubiquinol-cytochrome c reductase from beef-heart mitochondria.

Arch. Biochem. Biophys. 180, 248–257. doi: 10.1016/0003-9861(77)90035-2

Cao, J., He, L., Lin, G., Hu, C., Dong, R., Zhang, J., et al. (2014). Cap-dependent translation initiation factor, eIF4E, is the target for Ouabain-mediated inhibition of HIF-1alpha. *Biochem. Pharmacol.* 89, 20–30. doi: 10.1016/j.bcp.2013.12.002

Chandel, N. S., Maltepe, E., Goldwasser, E., Mathieu, C. E., Simon, M. C., and Schumacker, P. T. (1998). Mitochondrial reactive oxygen species trigger hypoxia-induced transcription. *Proc. Natl. Acad. Sci. U.S.A.* 95, 11715–11720. doi: 10.1073/pnas.95.20.11715

Chandel, N. S., Mcclintock, D. S., Feliciano, C. E., Wood, T. M., Melendez, J. A., Rodriguez, A. M., et al. (2000). Reactive oxygen species generated at mitochondrial complex III stabilize hypoxia-inducible factor-1alpha during hypoxia: a mechanism of O2 sensing. *J. Biol. Chem.* 275, 25130–25138. doi: 10.1074/jbc.M001914200

Chen, Y. J., Wang, L., Zhou, G. Y., Yu, X. L., Zhang, Y. H., Hu, N., et al. (2015). Scutellarin attenuates endothelium-dependent aasodilation impairment induced by hypoxia reoxygenation, through regulating the PKG signaling pathway in rat coronary artery. *Chin. J. Nat. Med.* 13, 264–273. doi: 10.1016/s1875-5364(15)30013-3

Chen, Z., Krmar, R. T., Dada, L., Efendiev, R., Leibiger, I. B., Pedemonte, C. H., et al. (2006). Phosphorylation of adaptor protein-2 mu2 is essential for Na+,K+-ATPase endocytosis in response to either G protein-coupled receptor or reactive oxygen species. *Am. J. Respir. Cell Mol. Biol.* 35, 127–132. doi: 10.1165/rcmb.2006-0044OC

Cheng, X. J., Fisone, G., Aizman, O., Aizman, R., Levenson, R., Greengard, P., et al. (1997). PKA-mediated phosphorylation and inhibition of Na(+)-K(+)-ATPase in response to beta-adrenergic hormone. *Am. J. Physiol.* 273, C893–C901.

Cheung, J. Y., Rothblum, L. I., Moorman, J. R., Tucker, A. L., Song, J., Ahlers, B. A., et al. (2007). Regulation of cardiac Na+/Ca2+ exchanger by phospholemman. *Ann. N.Y. Acad. Sci.* 1099, 119–134. doi: 10.1196/annals.1387.004

Chia, K. K., Liu, C. C., Hamilton, E. J., Garcia, A., Fry, N. A., Hannam, W., et al. (2015). Stimulation of the cardiac myocyte Na+-K+ pump due to reversal of its constitutive oxidative inhibition. *Am. J. Physiol,. Cell Physiol.* 309, C239–C250. doi: 10.1152/ajpcell.00392.2014

Choi, H., Tostes, R. C., and Webb, R. C. (2011). S-nitrosylation Inhibits protein kinase C-mediated contraction in mouse aorta. *J. Cardiovasc. Pharmacol.* 57, 65–71. doi: 10.1097/FJC.0b013e3181fef9cb

Chouchani, E. T., Pell, V. R., Gaude, E., Aksentijevic, D., Sundier, S. Y., Robb, E. L., et al. (2014). Ischaemic accumulation of succinate controls reperfusion injury through mitochondrial ROS. *Nature* 515, 431–435. doi: 10.1038/nature13909

Chu, F., Ward, N. E., and O'brian, C. A. (2001). Potent inactivation of representative members of each PKC isozyme subfamily and PKD via S-thiolation by the tumor-promotion/progression antagonist glutathione but not by its precursor cysteine. *Carcinogenesis* 22, 1221–1229. doi: 10.1093/carcin/22.8.1221

Chua, Y. L., Dufour, E., Dassa, E. P., Rustin, P., Jacobs, H. T., Taylor, C. T., et al. (2010). Stabilization of hypoxia-inducible factor-1alpha protein in hypoxia occurs independently of mitochondrial reactive oxygen species production. *J. Biol. Chem.* 285, 31277–31284. doi: 10.1074/jbc.M110.158485

Cooper, C. E., and Brown, G. C. (2008). The inhibition of mitochondrial cytochrome oxidase by the gases carbon monoxide, nitric oxide, hydrogen cyanide and hydrogen sulfide: chemical mechanism and physiological significance. *J. Bioenerg. Biomembr.* 40, 533–539. doi: 10.1007/s10863-008-9166-6

Dada, L. A., Chandel, N. S., Ridge, K. M., Pedemonte, C., Bertorello, A. M., and Sznajder, J. I. (2003). Hypoxia-induced endocytosis of Na,K-ATPase in alveolar epithelial cells is mediated by mitochondrial reactive oxygen species and PKC-zeta. *J. Clin. Invest.* 111, 1057–1064. doi: 10.1172/JCI16826

Dada, L. A., and Sznajder, J. I. (2003). Mechanisms of pulmonary edema clearance during acute hypoxemic respiratory failure: role of the Na,K-ATPase. *Crit. Care Med.* 31, S248–S252. doi: 10.1097/01.ccm.0000057895.22008.ec

Dada, L. A., Welch, L. C., Zhou, G., Ben-Saadon, R., Ciechanover, A., and Sznajder, J. I. (2007). Phosphorylation and ubiquitination are necessary for Na,K-ATPase endocytosis during hypoxia. *Cell. Signal.* 19, 1893–1898. doi: 10.1016/j.cellsig.2007.04.013

Dalle-Donne, I., Milzani, A., Gagliano, N., Colombo, R., Giustarini, D., and Rossi, R. (2008). Molecular mechanisms and potential clinical significance of S-glutathionylation. *Antioxid. Redox Signal.* 10, 445–473. doi: 10.1089/ars.2007.1716

Dalle-Donne, I., Rossi, R., Colombo, G., Giustarini, D., and Milzani, A. (2009). Protein S-glutathionylation: a regulatory device from bacteria to humans. *Trends Biochem. Sci.* 34, 85–96. doi: 10.1016/j.tibs.2008.11.002

Dalle-Donne, I., Rossi, R., Giustarini, D., Colombo, R., and Milzani, A. (2007). S-glutathionylation in protein redox regulation. *Free Radic. Biol. Med.* 43, 883–898. doi: 10.1016/j.freeradbiomed.2007.06.014

Dave, K. R., Anthony Defazio, R., Raval, A. P., Dashkin, O., Saul, I., Iceman, K. E., et al. (2009). Protein kinase C epsilon activation delays neuronal depolarization during cardiac arrest in the euthermic arctic ground squirrel. *J. Neurochem.* 110, 1170–1179. doi: 10.1111/j.1471-4159.2009.06196.x

De Angelis, C., and Haupert, G. T. Jr. (1998). Hypoxia triggers release of an endogenous inhibitor of Na(+)-K(+)-ATPase from midbrain and adrenal. *Am. J. Physiol.* 274, F182–F188.

Despa, S., Bossuyt, J., Han, F., Ginsburg, K. S., Jia, L. G., Kutchai, H., et al. (2005). Phospholemman-phosphorylation mediates the beta-adrenergic effects on Na/K pump function in cardiac myocytes. *Circ. Res.* 97, 252–259. doi: 10.1161/01.RES.0000176532.97731.e5

Devarie-Baez, N. O., Silva Lopez, E. I., and Furdui, C. M. (2016). Biological chemistry and functionality of protein sulfenic acids and related thiol modifications. *Free Radic. Res.* 50, 172–194. doi: 10.3109/10715762.2015.1090571

Domenicotti, C., Paola, D., Vitali, A., Nitti, M., D'abramo, C., Cottalasso, D., et al. (2000). Glutathione depletion induces apoptosis of rat hepatocytes through activation of protein kinase C novel isoforms and dependent increase in AP-1 nuclear binding. *Free Radic. Biol. Med.* 29, 1280–1290. doi: 10.1016/S0891-5849(00)00429-9

Donoso, P., Sanchez, G., Bull, R., and Hidalgo, C. (2011). Modulation of cardiac ryanodine receptor activity by ROS and RNS. *Front. Biosci. (Landmark Ed).* 16, 553–567. doi: 10.2741/3705

Drose, S., and Brandt, U. (2012). Molecular mechanisms of superoxide production by the mitochondrial respiratory chain. *Adv. Exp. Med. Biol.* 748, 145–169. doi: 10.1007/978-1-4614-3573-0_6

Drose, S., Brandt, U., and Wittig, I. (2014). Mitochondrial respiratory chain complexes as sources and targets of thiol-based redox-regulation. *Biochim. Biophys. Acta* 1844, 1344–1354. doi: 10.1016/j.bbapap.2014.02.006

Dvela, M., Rosen, H., Feldmann, T., Nesher, M., and Lichtstein, D. (2007). Diverse biological responses to different cardiotonic steroids. *Pathophysiology* 14, 159–166. doi: 10.1016/j.pathophys.2007.09.011

Dweik, R. A. (2005). Nitric oxide, hypoxia, and superoxide: the good, the bad, and the ugly! *Thorax* 60, 265–267. doi: 10.1136/thx.2004.038471

Einholm, A. P., Nielsen, H. N., Holm, R., Toustrup-Jensen, M. S., and Vilsen, B. (2016). Importance of a potential protein kinase A phosphorylation site of Na^+,K^+-ATPase and its interaction network for Na^+ binding. *J. Biol. Chem.* 291, 10934–10947. doi: 10.1074/jbc.M115.701201

Ellis, D. Z., Rabe, J., and Sweadner, K. J. (2003). Global loss of Na,K-ATPase and its nitric oxide-mediated regulation in a transgenic mouse model of amyotrophic lateral sclerosis. *J. Neurosci.* 23, 43–51.

Elrod, J. W., Calvert, J. W., Morrison, J., Doeller, J. E., Kraus, D. W., Tao, L., et al. (2007). Hydrogen sulfide attenuates myocardial ischemia-reperfusion injury by preservation of mitochondrial function. *Proc. Natl. Acad. Sci. U.S.A.* 104, 15560–15565. doi: 10.1073/pnas.0705891104

Erecinska, M., and Silver, I. A. (2001). Tissue oxygen tension and brain sensitivity to hypoxia. *Respir. Physiol.* 128, 263–276. doi: 10.1016/S0034-5687(01)00306-1

Ermakova, Y. G., Bilan, D. S., Matlashov, M. E., Mishina, N. M., Markvicheva, K. N., Subach, O. M., et al. (2014). Red fluorescent genetically encoded indicator for intracellular hydrogen peroxide. *Nat. Commun.* 5, 5222. doi: 10.1038/ncomms6222

Fedorova, O. V., Kashkin, V. A., Zakharova, I. O., Lakatta, E. G., and Bagrov, A. Y. (2012). Age-associated increase in salt sensitivity is accompanied by a shift in the atrial natriuretic peptide modulation of the effect of marinobufagenin on renal and vascular sodium pump. *J. Hypertens.* 30, 1817–1826. doi: 10.1097/HJH.0b013e328356399b

Fernandez-Aguera, M. C., Gao, L., Gonzalez-Rodriguez, P., Pintado, C. O., Arias-Mayenco, I., Garcia-Flores, P., et al. (2015). Oxygen sensing by arterial chemoreceptors depends on mitochondrial complex I Signaling. *Cell Metab.* 22, 825–837. doi: 10.1016/j.cmet.2015.09.004

Feschenko, M. S., Stevenson, E., and Sweadner, K. J. (2000). Interaction of protein kinase C and cAMP-dependent pathways in the phosphorylation of the Na,K-ATPase. *J. Biol. Chem.* 275, 34693–34700. doi: 10.1074/jbc.M005869200

Feschenko, M. S., and Sweadner, K. J. (1994). Conformation-dependent phosphorylation of Na,K-ATPase by protein kinase A and protein kinase C. *J. Biol. Chem.* 269, 30436–30444.

Feschenko, M. S., and Sweadner, K. J. (1997). Phosphorylation of Na,K-ATPase by protein kinase C at Ser18 occurs in intact cells but does not result in direct inhibition of ATP hydrolysis. *J. Biol. Chem.* 272, 17726–17733. doi: 10.1074/jbc.272.28.17726

Feschenko, M. S., Wetzel, R. K., and Sweadner, K. J. (1997). Phosphorylation of Na,K-ATPase by protein kinases. Sites, susceptibility, and consequences. *Ann. N.Y. Acad. Sci.* 834, 479–488. doi: 10.1111/j.1749-6632.1997.tb52306.x

Figtree, G. A., Liu, C. C., Bibert, S., Hamilton, E. J., Garcia, A., White, C. N., et al. (2009). Reversible oxidative modification: a key mechanism of Na+-K+ pump regulation. *Circ. Res.* 105, 185–193. doi: 10.1161/CIRCRESAHA.109.199547

Fotis, H., Tatjanenko, L. V., and Vasilets, L. A. (1999). Phosphorylation of the alpha-subunits of the Na+/K+-ATPase from mammalian kidneys and Xenopus oocytes by cGMP-dependent protein kinase results in stimulation of ATPase activity. *Eur. J. Biochem.* 260, 904–910. doi: 10.1046/j.1432-1327.1999.00237.x

Fridovich, I. (1995). Superoxide radical and superoxide dismutases. *Annu. Rev. Biochem.* 64, 97–112. doi: 10.1146/annurev.bi.64.070195.000525

Fuller, W., Eaton, P., Bell, J. R., and Shattock, M. J. (2004). Ischemia-induced phosphorylation of phospholemman directly activates rat cardiac Na/K-ATPase. *FASEB J.* 18, 197–199. doi: 10.1096/fj.03-0213fje

Fuller, W., Howie, J., Mclatchie, L. M., Weber, R. J., Hastie, C. J., Burness, K., et al. (2009). FXYD1 phosphorylation *in vitro* and in adult rat cardiac myocytes: threonine 69 is a novel substrate for protein kinase C. *Am. J. Physiol. Cell Physiol.* 296, C1346–C1355. doi: 10.1152/ajpcell.00523.2008

Fuller, W., Parmar, V., Eaton, P., Bell, J. R., and Shattock, M. J. (2003). Cardiac ischemia causes inhibition of the Na/K ATPase by a labile cytosolic compound whose production is linked to oxidant stress. *Cardiovasc. Res.* 57, 1044–1051. doi: 10.1016/S0008-6363(02)00810-6

Garcia, A., Eljack, N. D., Sani, M. A., Separovic, F., Rasmussen, H. H., Kopec, W., et al. (2015). Membrane accessibility of glutathione. *Biochim. Biophys. Acta* 1848, 2430–2436. doi: 10.1016/j.bbamem.2015.07.016

Ge, S. N., Zhao, M. M., Wu, D. D., Chen, Y., Wang, Y., Zhu, J. H., et al. (2014). Hydrogen sulfide targets EGFR Cys797/Cys798 residues to induce Na(+)/K(+)-ATPase endocytosis and inhibition in renal tubular epithelial cells and increase sodium excretion in chronic salt-loaded rats. *Antioxid. Redox Signal.* 21, 2061–2082. doi: 10.1089/ars.2013.5304

Geering, K. (2006). FXYD proteins: new regulators of Na-K-ATPase. *Am. J. Physiol. Renal Physiol.* 290, F241–F250. doi: 10.1152/ajprenal.00126.2005

Ghafourifar, P., and Sen, C. K. (2007). Mitochondrial nitric oxide synthase. *Front. Biosci.* 12, 1072–1078. doi: 10.2741/2127

Gopalakrishna, R., and Anderson, W. B. (1989). Ca2+- and phospholipid-independent activation of protein kinase C by selective oxidative modification of the regulatory domain. *Proc. Natl. Acad. Sci. U.S.A.* 86, 6758–6762. doi: 10.1073/pnas.86.17.6758

Gusarova, G. A., Dada, L. A., Kelly, A. M., Brodie, C., Witters, L. A., Chandel, N. S., et al. (2009). Alpha1-AMP-activated protein kinase regulates hypoxia-induced Na,K-ATPase endocytosis via direct phosphorylation of protein kinase C zeta. *Mol. Cell. Biol.* 29, 3455–3464. doi: 10.1128/MCB.00054-09

Guzy, R. D., Hoyos, B., Robin, E., Chen, H., Liu, L., Mansfield, K. D., et al. (2005). Mitochondrial complex III is required for hypoxia-induced ROS production and cellular oxygen sensing. *Cell Metab.* 1, 401–408. doi: 10.1016/j.cmet.2005.05.001

Guzy, R. D., and Schumacker, P. T. (2006). Oxygen sensing by mitochondria at complex III: the paradox of increased reactive oxygen species during hypoxia. *Exp. Physiol.* 91, 807–819. doi: 10.1113/expphysiol.2006.033506

Hagen, T., Taylor, C. T., Lam, F., and Moncada, S. (2003). Redistribution of intracellular oxygen in hypoxia by nitric oxide: effect on HIF1alpha. *Science* 302, 1975–1978. doi: 10.1126/science.1088805

Hanson, G. T., Aggeler, R., Oglesbee, D., Cannon, M., Capaldi, R. A., Tsien, R. Y., et al. (2004). Investigating mitochondrial redox potential with redox-sensitive green fluorescent protein indicators. *J. Biol. Chem.* 279, 13044–13053. doi: 10.1074/jbc.M312846200

Hausladen, A., and Fridovich, I. (1996). Measuring nitric oxide and superoxide: rate constants for aconitase reactivity. *Meth. Enzymol.* 269, 37–41. doi: 10.1016/S0076-6879(96)69007-7

Heinrich, T. A., Da Silva, R. S., Miranda, K. M., Switzer, C. H., Wink, D. A., and Fukuto, J. M. (2013). Biological nitric oxide signalling: chemistry and terminology. *Br. J. Pharmacol.* 169, 1417–1429. doi: 10.1111/bph.12217

Hernansanz-Agustin, P., Izquierdo-Alvarez, A., Sanchez-Gomez, F. J., Ramos, E., Villa-Pina, T., Lamas, S., et al. (2014). Acute hypoxia produces a superoxide burst in cells. *Free Radic. Biol. Med.* 71, 146–156. doi: 10.1016/j.freeradbiomed.2014.03.011

Hochachka, P. W., Buck, L. T., Doll, C. J., and Land, S. C. (1996). Unifying theory of hypoxia tolerance: molecular/metabolic defense and rescue mechanisms for surviving oxygen lack. *Proc. Natl. Acad. Sci. U.S.A.* 93, 9493–9498. doi: 10.1073/pnas.93.18.9493

Hochachka, P. W., Rupert, J. L., and Monge, C. (1999). Adaptation and conservation of physiological systems in the evolution of human hypoxia tolerance. *Comp. Biochem. Physiol. A Mol. Integr. Physiol.* 124, 1–17. doi: 10.1016/S1095-6433(99)00079-3

Holland, H. D. (2006). The oxygenation of the atmosphere and oceans. *Philos. Trans. R. Soc. Lond. B. Biol. Sci.* 361, 903–915. doi: 10.1098/rstb.2006.1838

Humphries, K. M., Deal, M. S., and Taylor, S. S. (2005). Enhanced dephosphorylation of cAMP-dependent protein kinase by oxidation and thiol modification. *J. Biol. Chem.* 280, 2750–2758. doi: 10.1074/jbc.M410242200

Humphries, K. M., Juliano, C., and Taylor, S. S. (2002). Regulation of cAMP-dependent protein kinase activity by glutathionylation. *J. Biol. Chem.* 277, 43505–43511. doi: 10.1074/jbc.M207088200

Hunte, C., Zickermann, V., and Brandt, U. (2010). Functional modules and structural basis of conformational coupling in mitochondrial complex I. *Science* 329, 448–451. doi: 10.1126/science.1191046

Hylland, P., Milton, S., Pek, M., Nilsson, G. E., and Lutz, P. L. (1997). Brain Na+/K+-ATPase activity in two anoxia tolerant vertebrates: crucian carp and freshwater turtle. *Neurosci. Lett.* 235, 89–92. doi: 10.1016/S0304-3940(97)00727-1

Hylland, P., Nilsson, G. E., and Lutz, P. L. (1996). Role of nitric oxide in the elevation of cerebral blood flow induced by acetylcholine and anoxia in the turtle. *J. Cereb. Blood Flow Metab.* 16, 290–295. doi: 10.1097/00004647-199603000-00014

Izquierdo-Alvarez, A., Ramos, E., Villanueva, J., Hernansanz-Agustin, P., Fernandez-Rodriguez, R., Tello, D., et al. (2012). Differential redox proteomics allows identification of proteins reversibly oxidized at cysteine residues in endothelial cells in response to acute hypoxia. *J. Proteomics* 75, 5449–5462. doi: 10.1016/j.jprot.2012.06.035

James, P. F., Grupp, I. L., Grupp, G., Woo, A. L., Askew, G. R., Croyle, M. L., et al. (1999). Identification of a specific role for the Na,K-ATPase alpha 2 isoform as a regulator of calcium in the heart. *Mol. Cell* 3, 555–563. doi: 10.1016/S1097-2765(00)80349-4

Jiang, Y. F., Tsui, K. H., Wang, P. H., Lin, C. W., Wang, J. Y., Hsu, M. C., et al. (2011). Hypoxia regulates cell proliferation and steroidogenesis through protein kinase A signaling in bovine corpus luteum. *Anim. Reprod. Sci.* 129, 152–161. doi: 10.1016/j.anireprosci.2011.12.004

Juel, C. (2014). Oxidative stress (glutathionylation) and Na,K-ATPase activity in rat skeletal muscle. *PLoS ONE* 9:e110514. doi: 10.1371/journal.pone.0110514

Juel, C. (2016). Nitric oxide and Na,K-ATPase activity in rat skeletal muscle. *Acta Physiol. (Oxf).* 216, 447–453. doi: 10.1111/apha.12617

Juel, C., Hostrup, M., and Bangsbo, J. (2015). The effect of exercise and beta2-adrenergic stimulation on glutathionylation and function of the Na,K-ATPase in human skeletal muscle. *Physiol. Rep.* 3:e12515. doi: 10.14814/phy2.12515

Kaelin, W. G. Jr., and Ratcliffe, P. J. (2008). Oxygen sensing by metazoans: the central role of the HIF hydroxylase pathway. *Mol. Cell* 30, 393–402. doi: 10.1016/j.molcel.2008.04.009

Kai, S., Tanaka, T., Daijo, H., Harada, H., Kishimoto, S., Suzuki, K., et al. (2012). Hydrogen sulfide inhibits hypoxia- but not anoxia-induced hypoxia-inducible factor 1 activation in a von hippel-lindau- and mitochondria-dependent manner. *Antioxid. Redox Signal.* 16, 203–216. doi: 10.1089/ars.2011.3882

Kalyanaraman, B. (2013). Teaching the basics of redox biology to medical and graduate students: oxidants, antioxidants and disease mechanisms. *Redox Biol.* 1, 244–257. doi: 10.1016/j.redox.2013.01.014

Kazanietz, M. G., Caloca, M. J., Aizman, O., and Nowicki, S. (2001). Phosphorylation of the catalytic subunit of rat renal Na+, K+-ATPase by classical PKC isoforms. *Arch. Biochem. Biophys.* 388, 74–80. doi: 10.1006/abbi.2000.2264

Klatt, P., and Lamas, S. (2000). Regulation of protein function by S-glutathiolation in response to oxidative and nitrosative stress. *Eur. J. Biochem.* 267, 4928–4944. doi: 10.1046/j.1432-1327.2000.01601.x

Klatt, P., Molina, E. P., De Lacoba, M. G., Padilla, C. A., Martinez-Galesteo, E., Barcena, J. A., et al. (1999). Redox regulation of c-Jun DNA binding by reversible S-glutathiolation. *FASEB J.* 13, 1481–1490.

Klimanova, E. A., Petrushanko, I. Y., Mitkevich, V. A., Anashkina, A. A., Orlov, S. N., Makarov, A. A., et al. (2015). Binding of ouabain and marinobufagenin leads to different structural changes in Na,K-ATPase and depends on the enzyme conformation. *FEBS Lett.* 589, 2668–2674. doi: 10.1016/j.febslet.2015.08.011

Kohr, M. J., Murphy, E., and Steenbergen, C. (2014). Glyceraldehyde-3-phosphate dehydrogenase acts as a mitochondrial trans-S-nitrosylase in the heart. *PLoS ONE* 9:e111448. doi: 10.1371/journal.pone.0111448

Koltsova, S. V., Shilov, B., Birulina, J. G., Akimova, O. A., Haloui, M., Kapilevich, L. V., et al. (2014). Transcriptomic changes triggered by hypoxia: evidence for HIF-1alpha-independent, [Na+]i/[K+]i-mediated, excitation-transcription coupling. *PLoS ONE* 9:e110597. doi: 10.1371/journal.pone.0110597

Korshunov, S. S., Skulachev, V. P., and Starkov, A. A. (1997). High protonic potential actuates a mechanism of production of reactive oxygen species in mitochondria. *FEBS Lett.* 416, 15–18. doi: 10.1016/S0014-5793(97)01159-9

Kruger, A., Mahmmoud, Y. A., and Cornelius, F. (2003). Protein kinase C phosphorylation directed at novel C-terminal sites in Na,K-ATPase. *Ann. N.Y. Acad. Sci.* 986, 541–542. doi: 10.1111/j.1749-6632.2003.tb07247.x

Kurella, E. G., Tyulina, O. V., and Boldyrev, A. A. (1999). Oxidative resistance of Na/K-ATPase. *Cell. Mol. Neurobiol.* 19, 133–140. doi: 10.1023/A:1006976810642

Lancel, S., Zhang, J., Evangelista, A., Trucillo, M. P., Tong, X., Siwik, D. A., et al. (2009). Nitroxyl activates SERCA in cardiac myocytes via glutathiolation of cysteine 674. *Circ. Res.* 104, 720–723. doi: 10.1161/CIRCRESAHA.108.188441

Lauf, P. K., Alqahtani, T., Flues, K., Meller, J., and Adragna, N. C. (2015). Interaction between Na-K-ATPase and Bcl-2 proteins BclXL and Bak. *Am. J. Physiol. Cell Physiol.* 308, C51–C60. doi: 10.1152/ajpcell.00287.2014

Lecuona, E., Trejo, H. E., and Sznajder, J. I. (2007). Regulation of Na,K-ATPase during acute lung injury. *J. Bioenerg. Biomembr.* 39, 391–395. doi: 10.1007/s10863-007-9102-1

Lehotsky, J., Kaplan, P., Matejovicova, M., Murin, R., Racay, P., and Raeymaekers, L. (2002). Ion transport systems as targets of free radicals during ischemia reperfusion injury. *Gen. Physiol. Biophys.* 21, 31–37.

Lei, K., Townsend, D. M., and Tew, K. D. (2008). Protein cysteine sulfinic acid reductase (sulfiredoxin) as a regulator of cell proliferation and drug response. *Oncogene* 27, 4877–4887. doi: 10.1038/onc.2008.132

Li, J., Huang, F. L., and Huang, K. P. (2001). Glutathiolation of proteins by glutathione disulfide S-oxide derived from S-nitrosoglutathione. Modifications of rat brain neurogranin/RC3 and neuromodulin/GAP-43. *J. Biol. Chem.* 276, 3098–3105. doi: 10.1074/jbc.M008260200

Li, L., Rose, P., and Moore, P. K. (2011). Hydrogen sulfide and cell signaling. *Annu. Rev. Pharmacol. Toxicol.* 51, 169–187. doi: 10.1146/annurev-pharmtox-010510-100505

Li, Z., and Xie, Z. (2009). The Na/K-ATPase/Src complex and cardiotonic steroid-activated protein kinase cascades. *Pflugers Arch.* 457, 635–644. doi: 10.1007/s00424-008-0470-0

Liang, M., Tian, J., Liu, L., Pierre, S., Liu, J., Shapiro, J., et al. (2007). Identification of a pool of non-pumping Na/K-ATPase. *J. Biol. Chem.* 282, 10585–10593. doi: 10.1074/jbc.M609181200

Liu, C. C., Garcia, A., Mahmmoud, Y. A., Hamilton, E. J., Galougahi, K. K., Fry, N. A., et al. (2012). Susceptibility of beta1 Na+-K+ pump subunit to glutathionylation and oxidative inhibition depends on conformational state of pump. *J. Biol. Chem.* 287, 12353–12364. doi: 10.1074/jbc.M112.340893

Liu, C. C., Karimi Galougahi, K., Weisbrod, R. M., Hansen, T., Ravaie, R., Nunez, A., et al. (2013). Oxidative inhibition of the vascular Na+-K+ pump via NADPH oxidase-dependent beta1-subunit glutathionylation: implications for angiotensin II-induced vascular dysfunction. *Free Radic. Biol. Med.* 65, 563–572. doi: 10.1016/j.freeradbiomed.2013.06.040

Lutz, P. L., Nilsson, G. E., and Perez-Pinzon, M. A. (1996). Anoxia tolerant animals from a neurobiological perspective. *Comp. Biochem. Physiol. B. Biochem. Mol. Biol.* 113, 3–13. doi: 10.1016/0305-0491(95)02046-2

MacDonald, J. A., and Storey, K. B. (1999). Regulation of ground squirrel Na+K+-ATPase activity by reversible phosphorylation during hibernation. *Biochem. Biophys. Res. Commun.* 254, 424–429. doi: 10.1006/bbrc.1998.9960

Madej, E., Folkes, L. K., Wardman, P., Czapski, G., and Goldstein, S. (2008). Thiyl radicals react with nitric oxide to form S-nitrosothiols with rate constants near the diffusion-controlled limit. *Free Radic. Biol. Med.* 44, 2013–2018. doi: 10.1016/j.freeradbiomed.2008.02.015

Mansfield, K. D., Guzy, R. D., Pan, Y., Young, R. M., Cash, T. P., Schumacker, P. T., et al. (2005). Mitochondrial dysfunction resulting from loss of cytochrome c impairs cellular oxygen sensing and hypoxic HIF-alpha activation. *Cell Metab.* 1, 393–399. doi: 10.1016/j.cmet.2005.05.003

Marshall, C., Mamary, A. J., Verhoeven, A. J., and Marshall, B. E. (1996). Pulmonary artery NADPH-oxidase is activated in hypoxic pulmonary vasoconstriction. *Am. J. Respir. Cell Mol. Biol.* 15, 633–644. doi: 10.1165/ajrcmb.15.5.8918370

Martinez-Ruiz, A., Araujo, I. M., Izquierdo-Alvarez, A., Hernansanz-Agustin, P., Lamas, S., and Serrador, J. M. (2013). Specificity in S-nitrosylation: a short-range mechanism for NO signaling? *Antioxid. Redox Signal.* 19, 1220–1235. doi: 10.1089/ars.2012.5066

Martinez-Ruiz, A., Cadenas, S., and Lamas, S. (2011). Nitric oxide signaling: classical, less classical, and nonclassical mechanisms. *Free Radic. Biol. Med.* 51, 17–29. doi: 10.1016/j.freeradbiomed.2011.04.010

Martinez-Ruiz, A., and Lamas, S. (2004). S-nitrosylation: a potential new paradigm in signal transduction. *Cardiovasc. Res.* 62, 43–52. doi: 10.1016/j.cardiores.2004.01.013

Martinez-Ruiz, A., and Lamas, S. (2007). Signalling by NO-induced protein S-nitrosylation and S-glutathionylation: convergences and divergences. *Cardiovasc. Res.* 75, 220–228. doi: 10.1016/j.cardiores.2007.03.016

McMullen, D. C., and Storey, K. B. (2008). Suppression of Na+K+ -ATPase activity by reversible phosphorylation over the winter in a freeze-tolerant insect. *J. Insect Physiol.* 54, 1023–1027. doi: 10.1016/j.jinsphys.2008.04.001

Menon, D., and Board, P. G. (2013). A role for glutathione transferase Omega 1 (GSTO1-1) in the glutathionylation cycle. *J. Biol. Chem.* 288, 25769–25779. doi: 10.1074/jbc.M113.487785

Mieyal, J. J., Gallogly, M. M., Qanungo, S., Sabens, E. A., and Shelton, M. D. (2008). Molecular mechanisms and clinical implications of reversible protein S-glutathionylation. *Antioxid. Redox Signal.* 10, 1941–1988. doi: 10.1089/ars.2008.2089

Mitchell, P. (1961). Coupling of phosphorylation to electron and hydrogen transfer by a chemi-osmotic type of mechanism. *Nature* 191, 144–148. doi: 10.1038/191144a0

Mitchell, P., and Moyle, J. (1967). Chemiosmotic hypothesis of oxidative phosphorylation. *Nature* 213, 137–139. doi: 10.1038/213137a0

Mitkevich, V. A., Petrushanko, I., Poluektov, Y. M., Burnasheva, K. M., Lakunina, V. A., Anashkina, A. A., et al. (2016). Basal glutathionylation of Na,K-ATPase alpha-subunit depends on redox status of cells during the enzyme biosynthesis. *Oxid. Med. Cell Longev.* 2016:9092328. doi: 10.1155/2016/9092328

Moller, M. N., Li, Q., Lancaster, J. R. Jr., and Denicola, A. (2007). Acceleration of nitric oxide autoxidation and nitrosation by membranes. *IUBMB Life* 59, 243–248. doi: 10.1080/15216540701311147

Moreno, L., Moral-Sanz, J., Morales-Cano, D., Barreira, B., Moreno, E., Ferrarini, A., et al. (2014). Ceramide mediates acute oxygen sensing in vascular tissues. *Antioxid. Redox Signal.* 20, 1–14. doi: 10.1089/ars.2012.4752

Munhoz, C. D., Kawamoto, E. M., De Sa Lima, L., Lepsch, L. B., Glezer, I., Marcourakis, T., et al. (2005). Glutamate modulates sodium-potassium-ATPase through cyclic GMP and cyclic GMP-dependent protein kinase in rat striatum. *Cell Biochem. Funct.* 23, 115–123. doi: 10.1002/cbf.1217

Murphy, M. P. (2009). How mitochondria produce reactive oxygen species. *Biochem. J.* 417, 1–13. doi: 10.1042/BJ20081386

Nagy, P. (2013). Kinetics and mechanisms of thiol-disulfide exchange covering direct substitution and thiol oxidation-mediated pathways. *Antioxid. Redox Signal.* 18, 1623–1641. doi: 10.1089/ars.2012.4973

Nakamura, T., and Lipton, S. A. (2013). Emerging role of protein-protein transnitrosylation in cell signaling pathways. *Antioxid. Redox Signal.* 18, 239–249. doi: 10.1089/ars.2012.4703

Nesher, M., Shpolansky, U., Viola, N., Dvela, M., Buzaglo, N., Cohen Ben-Ami, H., et al. (2010). Ouabain attenuates cardiotoxicity induced by other cardiac steroids. *Br. J. Pharmacol.* 160, 346–354. doi: 10.1111/j.1476-5381.2010.00701.x

Newton, A. C. (1995). Protein kinase C: structure, function, and regulation. *J. Biol. Chem.* 270, 28495–28498. doi: 10.1074/jbc.270.48.28495

Nilsson, G. E. (2001). Surviving anoxia with the brain turned on. *News Physiol. Sci.* 16, 217–221.

Ogawa, H., Shinoda, T., Cornelius, F., and Toyoshima, C. (2009). Crystal structure of the sodium-potassium pump (Na+,K+-ATPase) with bound potassium and ouabain. *Proc. Natl. Acad. Sci. U.S.A.* 106, 13742–13747. doi: 10.1073/pnas.0907054106

Olson, K. R. (2015). Hydrogen sulfide as an oxygen sensor. *Antioxid. Redox Signal.* 22, 377–397. doi: 10.1089/ars.2014.5930

Pacher, P., Beckman, J. S., and Liaudet, L. (2007). Nitric oxide and peroxynitrite in health and disease. *Physiol. Rev.* 87, 315–424. doi: 10.1152/physrev.00029.2006

Parker, P. J., and Murray-Rust, J. (2004). PKC at a glance. *J. Cell Sci.* 117, 131–132. doi: 10.1242/jcs.00982

Pasdois, P., Quinlan, C. L., Rissa, A., Tariosse, L., Vinassa, B., Costa, A. D., et al. (2007). Ouabain protects rat hearts against ischemia-reperfusion injury via pathway involving src kinase, mitoKATP, and ROS. *Am. J. Physiol. Heart Circ. Physiol.* 292, H1470–H1478. doi: 10.1152/ajpheart.00877.2006

Pavlovic, D., Hall, A. R., Kennington, E. J., Aughton, K., Boguslavskyi, A., Fuller, W., et al. (2013). Nitric oxide regulates cardiac intracellular Na(+) and Ca(2)(+) by modulating Na/K ATPase via PKCepsilon and phospholemman-dependent mechanism. *J. Mol. Cell. Cardiol.* 61, 164–171. doi: 10.1016/j.yjmcc.2013.04.013

Peng, Y. J., Nanduri, J., Raghuraman, G., Souvannakitti, D., Gadalla, M. M., Kumar, G. K., et al. (2010). H2S mediates O2 sensing in the carotid body. *Proc. Natl. Acad. Sci. U.S.A.* 107, 10719–10724. doi: 10.1073/pnas.1005866107

Petrushanko, I., Bogdanov, N., Bulygina, E., Grenacher, B., Leinsoo, T., Boldyrev, A., et al. (2006). Na-K-ATPase in rat cerebellar granule cells is redox sensitive. *Am. J. Physiol. Regul. Integr. Comp. Physiol.* 290, R916–R925. doi: 10.1152/ajpregu.00038.2005

Petrushanko, I., Simonenko, O. V., Burnysheva, K. M., Klimanova, E. A., Dergousova, E. A., Mitkevich, V. A., et al. (2015). The ability of cells to adapt to low-oxygen conditions is associated with glutathioylation of Na,K-ATPase. *Mol. Biol. (Mosk).* 49, 153–160. doi: 10.1134/S0026893315010148

Petrushanko, I. Y., Bogdanov, N. B., Lapina, N., Boldyrev, A. A., Gassmann, M., and Bogdanova, A. Y. (2007). Oxygen-induced Regulation of Na/K ATPase in cerebellar granule cells. *J. Gen. Physiol.* 130, 389–398. doi: 10.1085/jgp.200709783

Petrushanko, I. Y., Mitkevich, V. A., Anashkina, A. A., Klimanova, E. A., Dergousova, E. A., Lopina, O. D., et al. (2014). Critical role of gamma-phosphate in structural transition of Na,K-ATPase upon ATP binding. *Sci. Rep.* 4:5165. doi: 10.1038/srep05165

Petrushanko, I. Y., Yakushev, S., Mitkevich, V. A., Kamanina, Y. V., Ziganshin, R. H., Meng, X., et al. (2012). S-glutathionylation of the Na,K-ATPase catalytic alpha subunit is a determinant of the enzyme redox sensitivity. *J. Biol. Chem.* 287, 32195–32205. doi: 10.1074/jbc.M112.391094

Pineda-Molina, E., Klatt, P., Vazquez, J., Marina, A., Garcia De Lacoba, M., Perez-Sala, D., et al. (2001). Glutathionylation of the p50 subunit of NF-kappaB: a mechanism for redox-induced inhibition of DNA binding. *Biochemistry* 40, 14134–14142. doi: 10.1021/bi011459o

Pryde, K. R., and Hirst, J. (2011). Superoxide is produced by the reduced flavin in mitochondrial complex I: a single, unified mechanism that applies during both forward and reverse electron transfer. *J. Biol. Chem.* 286, 18056–18065. doi: 10.1074/jbc.M110.186841

Quintero, M., Colombo, S. L., Godfrey, A., and Moncada, S. (2006). Mitochondria as signaling organelles in the vascular endothelium. *Proc. Natl. Acad. Sci. U.S.A.* 103, 5379–5384. doi: 10.1073/pnas.0601026103

Ramnanan, C. J., and Storey, K. B. (2006). Suppression of Na+/K+-ATPase activity during estivation in the land snail Otala lactea. *J. Exp. Biol.* 209, 677–688. doi: 10.1242/jeb.02052

Reinhard, L., Tidow, H., Clausen, M. J., and Nissen, P. (2013). Na(+),K (+)-ATPase as a docking station: protein-protein complexes of the Na(+),K (+)-ATPase. *Cell. Mol. Life Sci.* 70, 205–222. doi: 10.1007/s00018-012-1039-9

Ross, A. P., Christian, S. L., Zhao, H. W., and Drew, K. L. (2006). Persistent tolerance to oxygen and nutrient deprivation and N-methyl-D-aspartate in cultured hippocampal slices from hibernating Arctic ground squirrel. *J. Cereb. Blood Flow Metab.* 26, 1148–1156. doi: 10.1038/sj.jcbfm.9600271

Ryter, S. W., Alam, J., and Choi, A. M. (2006). Heme oxygenase-1/carbon monoxide: from basic science to therapeutic applications. *Physiol. Rev.* 86, 583–650. doi: 10.1152/physrev.00011.2005

Scavone, C., Munhoz, C. D., Kawamoto, E. M., Glezer, I., De Sa Lima, L., Marcourakis, T., et al. (2005). Age-related changes in cyclic GMP and PKG-stimulated cerebellar Na,K-ATPase activity. *Neurobiol. Aging* 26, 907–916. doi: 10.1016/j.neurobiolaging.2004.08.013

Schwinger, R. H., Wang, J., Frank, K., Muller-Ehmsen, J., Brixius, K., Mcdonough, A. A., et al. (1999). Reduced sodium pump alpha1, alpha3, and beta1-isoform protein levels and Na+,K+-ATPase activity but unchanged Na+-Ca2+ exchanger protein levels in human heart failure. *Circulation* 99, 2105–2112. doi: 10.1161/01.CIR.99.16.2105

Segall, L., Lane, L. K., and Blostein, R. (2003). Insights into the structural basis for modulation of E1<–>E2 transitions by cytoplasmic domains of the Na,K-ATPase alpha subunit. *Ann. N.Y. Acad. Sci.* 986, 58–62. doi: 10.1111/j.1749-6632.2003.tb07139.x

Shahidullah, M., and Delamere, N. A. (2006). NO donors inhibit Na,K-ATPase activity by a protein kinase G-dependent mechanism in the nonpigmented ciliary epithelium of the porcine eye. *Br. J. Pharmacol.* 148, 871–880. doi: 10.1038/sj.bjp.0706795

Shahidullah, M., Mandal, A., Wei, G., and Delamere, N. A. (2014). Nitric oxide regulation of Na, K-ATPase activity in ocular ciliary epithelium involves Src family kinase. *J. Cell. Physiol.* 229, 343–352. doi: 10.1002/jcp.24454

Shattock, M. J., Ottolia, M., Bers, D. M., Blaustein, M. P., Boguslavskyi, A., Bossuyt, J., et al. (2015). Na+/Ca2+ exchange and Na+/K+-ATPase in the heart. *J. Physiol. (Lond).* 593, 1361–1382. doi: 10.1113/jphysiol.2014.282319

Shi, H. G., Mikhaylova, L., Zichittella, A. E., and Arguello, J. M. (2000). Functional role of cysteine residues in the (Na,K)-ATPase alpha subunit. *Biochim. Biophys. Acta* 1464, 177–187. doi: 10.1016/S0005-2736(99)00245-X

Shiva, S., Sack, M. N., Greer, J. J., Duranski, M., Ringwood, L. A., Burwell, L., et al. (2007). Nitrite augments tolerance to ischemia/reperfusion injury via the modulation of mitochondrial electron transfer. *J. Exp. Med.* 204, 2089–2102. doi: 10.1084/jem.20070198

Sies, H. (2015). Oxidative stress: a concept in redox biology and medicine. *Redox Biol.* 4, 180–183. doi: 10.1016/j.redox.2015.01.002

Silver, I. A., Deas, J., and Erecinska, M. (1997). Ion homeostasis in brain cells: differences in intracellular ion responses to energy limitation between cultured neurons and glial cells. *Neuroscience* 78, 589–601. doi: 10.1016/S0306-4522(96)00600-8

Silverman, B., Fuller, W., Eaton, P., Deng, J., Moorman, J. R., Cheung, J. Y., et al. (2005). Serine 68 phosphorylation of phospholemman: acute isoform-specific activation of cardiac Na/K ATPase. *Cardiovasc. Res.* 65, 93–103. doi: 10.1016/j.cardiores.2004.09.005

Smith, B. C., and Marletta, M. A. (2012). Mechanisms of S-nitrosothiol formation and selectivity in nitric oxide signaling. *Curr. Opin. Chem. Biol.* 16, 498–506. doi: 10.1016/j.cbpa.2012.10.016

Sousa, F. L., Thiergart, T., Landan, G., Nelson-Sathi, S., Pereira, I. A., Allen, J. F., et al. (2013). Early bioenergetic evolution. *Philos. Trans. R. Soc. Lond,. B,. Biol. Sci.* 368:20130088. doi: 10.1098/rstb.2013.0088

Srinivasan, V., Pierik, A. J., and Lill, R. (2014). Crystal structures of nucleotide-free and glutathione-bound mitochondrial ABC transporter Atm1. *Science* 343, 1137–1140. doi: 10.1126/science.1246729

Sun, C., Shi, Z. Z., Zhou, X., Chen, L., and Zhao, X. M. (2013). Prediction of S-glutathionylation sites based on protein sequences. *PLoS ONE* 8:e55512. doi: 10.1371/journal.pone.0055512

Sun, J., Steenbergen, C., and Murphy, E. (2006). S-nitrosylation: NO-related redox signaling to protect against oxidative stress. *Antioxid. Redox Signal.* 8, 1693–1705. doi: 10.1089/ars.2006.8.1693

Therien, A. G., and Blostein, R. (2000). Mechanisms of sodium pump regulation. *Am. J. Physiol. Cell Physiol.* 279, C541–C566.

Thevenod, F., and Friedmann, J. M. (1999). Cadmium-mediated oxidative stress in kidney proximal tubule cells induces degradation of Na+/K(+)-ATPase through proteasomal and endo-/lysosomal proteolytic pathways. *FASEB J.* 13, 1751–1761.

Tian, J., Haller, S., Periyasamy, S., Brewster, P., Zhang, H., Adlakha, S., et al. (2010). Renal ischemia regulates marinobufagenin release in humans. *Hypertension* 56, 914–919. doi: 10.1161/HYPERTENSIONAHA.110.155564

Townsend, D. M., Tew, K. D., He, L., King, J. B., and Hanigan, M. H. (2009). Role of glutathione S-transferase Pi in cisplatin-induced nephrotoxicity. *Biomed. Pharmacother.* 63, 79–85. doi: 10.1016/j.biopha.2008.08.004

Toyoshima, C., Kanai, R., and Cornelius, F. (2011). First crystal structures of Na+,K+-ATPase: new light on the oldest ion pump. *Structure* 19, 1732–1738. doi: 10.1016/j.str.2011.10.016

Trumpower, B. L. (1990). The protonmotive Q cycle. Energy transduction by coupling of proton translocation to electron transfer by the cytochrome bc1 complex. *J. Biol. Chem.* 265, 11409–11412.

Turrens, J. F. (2003). Mitochondrial formation of reactive oxygen species. *J. Physiol. (Lond).* 552, 335–344. doi: 10.1113/jphysiol.2003.049478

Van Kanegan, M. J., He, D. N., Dunn, D. E., Yang, P., Newman, R. A., West, A. E., et al. (2014). BDNF mediates neuroprotection against oxygen-glucose deprivation by the cardiac glycoside oleandrin. *J. Neurosci.* 34, 963–968. doi: 10.1523/JNEUROSCI.2700-13.2014

Vinogradov, A. D., and Grivennikova, V. G. (2005). Generation of superoxide-radical by the NADH:ubiquinone oxidoreductase of heart mitochondria. *Biochem. Mosc.* 70, 120–127. doi: 10.1007/s10541-005-0090-7

Vinogradov, A. D., and Grivennikova, V. G. (2016). Oxidation of NADH and ROS production by respiratory complex I. *Biochim. Biophys. Acta* 1857, 863–871. doi: 10.1016/j.bbabio.2015.11.004

Wang, Y. X., and Zheng, Y. M. (2010). Role of ROS signaling in differential hypoxic Ca2+ and contractile responses in pulmonary and systemic vascular smooth muscle cells. *Respir. Physiol. Neurobiol.* 174, 192–200. doi: 10.1016/j.resp.2010.08.008

Ward, N. E., Pierce, D. S., Chung, S. E., Gravitt, K. R., and O'brian, C. A. (1998). Irreversible inactivation of protein kinase C by glutathione. *J. Biol. Chem.* 273, 12558–12566. doi: 10.1074/jbc.273.20.12558

Ward, N. E., Stewart, J. R., Ioannides, C. G., and O'brian, C. A. (2000). Oxidant-induced S-glutathiolation inactivates protein kinase C-alpha (PKC-alpha): a potential mechanism of PKC isozyme regulation. *Biochemistry* 39, 10319–10329. doi: 10.1021/bi000781g

Washam, J. B., Stevens, S. R., Lokhnygina, Y., Halperin, J. L., Breithardt, G., Singer, D. E., et al. (2015). Digoxin use in patients with atrial fibrillation and adverse cardiovascular outcomes: a retrospective analysis of the Rivaroxaban Once Daily Oral Direct Factor Xa Inhibition Compared with Vitamin K Antagonism for Prevention of Stroke and Embolism Trial in Atrial Fibrillation (ROCKET AF). *Lancet* 385, 2363–2370. doi: 10.1016/S0140-6736(14)61836-5

Westermann, B. (2015). The mitochondria-plasma membrane contact site. *Curr. Opin. Cell Biol.* 35, 1–6. doi: 10.1016/j.ceb.2015.03.001

White, C. N., Figtree, G. A., Liu, C. C., Garcia, A., Hamilton, E. J., Chia, K. K., et al. (2009). Angiotensin II inhibits the Na+-K+ pump via PKC-dependent activation of NADPH oxidase. *Am. J. Physiol. Cell Physiol.* 296, C693–C700. doi: 10.1152/ajpcell.00648.2008

White, C. N., Liu, C. C., Garcia, A., Hamilton, E. J., Chia, K. K., Figtree, G. A., et al. (2010). Activation of cAMP-dependent signaling induces oxidative modification of the cardiac Na+-K+ pump and inhibits its activity. *J. Biol. Chem.* 285, 13712–13720. doi: 10.1074/jbc.M109.090225

Wilkie, M. P., Pamenter, M. E., Alkabie, S., Carapic, D., Shin, D. S., and Buck, L. T. (2008). Evidence of anoxia-induced channel arrest in the brain of the goldfish (Carassius auratus). *Comp. Biochem. Physiol. C. Toxicol. Pharmacol.* 148, 355–362. doi: 10.1016/j.cbpc.2008.06.004

Winnicka, K., Bielawski, K., Bielawska, A., and Miltyk, W. (2007). Apoptosis-mediated cytotoxicity of ouabain, digoxin and proscillaridin A in the estrogen independent MDA-MB-231 breast cancer cells. *Arch. Pharm. Res.* 30, 1216–1224. doi: 10.1007/BF02980262

Winnicka, K., Bielawski, K., Bielawska, A., and Miltyk, W. (2010). Dual effects of ouabain, digoxin and proscillaridin A on the regulation of apoptosis in human fibroblasts. *Nat. Prod. Res.* 24, 274–285. doi: 10.1080/14786410902991878

Xianyu, M., Petrushanko, I. Y., Klimanova, E. A., Dergousova, E. A., and Lopina, O. D. (2014). Glutathionylation of the alpha-subunit of Na,K-ATPase from rat heart by oxidized glutathione inhibits the enzyme. *Biochem. Mosc.* 79, 158–164. doi: 10.1134/S0006297914020096

Xie, Z., Jack-Hays, M., Wang, Y., Periyasamy, S. M., Blanco, G., Huang, W. H., et al. (1995). Different oxidant sensitivities of the alpha 1 and alpha 2 isoforms of Na+/K(+)-ATPase expressed in baculovirus-infected insect cells. *Biochem. Biophys. Res. Commun.* 207, 155–159. doi: 10.1006/bbrc.1995.1166

Xu, K. Y., Zweier, J. L., and Becker, L. C. (1997). Oxygen-free radicals directly attack the ATP binding site of the cardiac Na+,K(+)-ATPase. *Ann. N.Y. Acad. Sci.* 834, 680–683. doi: 10.1111/j.1749-6632.1997.tb52349.x

Yakushev, S., Band, M., Tissot Van Patot, M. C., Gassmann, M., Avivi, A., and Bogdanova, A. (2012). Cross talk between S-nitrosylation and S-glutathionylation in control of the Na,K-ATPase regulation in hypoxic heart. *Am. J. Physiol. Heart Circ. Physiol.* 303, H1332–H1343. doi: 10.1152/ajpheart.00145.2012

Yan, L. J. (2014). Protein redox modification as a cellular defense mechanism against tissue ischemic injury. *Oxid. Med. Cell. Longev.* 2014:343154. doi: 10.1155/2014/343154

Yan, Y., Shapiro, A. P., Haller, S., Katragadda, V., Liu, L., Tian, J., et al. (2013). Involvement of reactive oxygen species in a feed-forward mechanism of Na/K-ATPase-mediated signaling transduction. *J. Biol. Chem.* 288, 34249–34258. doi: 10.1074/jbc.M113.461020

Yuan, G., Vasavda, C., Peng, Y. J., Makarenko, V. V., Raghuraman, G., Nanduri, J., et al. (2015). Protein kinase G-regulated production of H2S governs oxygen sensing. *Sci. Signal* 8, ra37. doi: 10.1126/scisignal.2005846

Zhang, H., Qian, D. Z., Tan, Y. S., Lee, K., Gao, P., Ren, Y. R., et al. (2008). Digoxin and other cardiac glycosides inhibit HIF-1alpha synthesis and block tumor growth. *Proc. Natl. Acad. Sci. U.S.A.* 105, 19579–19586. doi: 10.1073/pnas.0809763105

Zhang, X. Q., Wang, J., Song, J., Ji, A. M., Chan, T. O., and Cheung, J. Y. (2011). Residues 248-252 and 300-304 of the cardiac Na+/Ca2+ exchanger are involved in its regulation by phospholemman. *Am. J. Physiol. Cell Physiol.* 301, C833–C840. doi: 10.1152/ajpcell.00069.2011

Zhao, N., Lo, L. C., Berova, N., Nakanishi, K., Tymiak, A. A., Ludens, J. H., et al. (1995). Na,K-ATPase inhibitors from bovine hypothalamus and human plasma are different from ouabain: nanogram scale CD structural analysis. *Biochemistry* 34, 9893–9896. doi: 10.1021/bi00031a010

Zhao, X., Ning, Q., Ai, M., Chai, H., and Yin, M. (2015). PGluS: prediction of protein S-glutathionylation sites with multiple features and analysis. *Mol. Biosyst.* 11, 923–929. doi: 10.1039/C4MB00680A

Zickermann, V., Wirth, C., Nasiri, H., Siegmund, K., Schwalbe, H., Hunte, C., et al. (2015). Structural biology. Mechanistic insight from the crystal structure of mitochondrial complex I. *Science* 347, 44–49. doi: 10.1126/science.1259859

Conflict of Interest Statement: The authors declare that the research was conducted in the absence of any commercial or financial relationships that could be construed as a potential conflict of interest.

Article

Cell Reports

Role of Mitochondrial Complex IV in Age-Dependent Obesity

Graphical Abstract

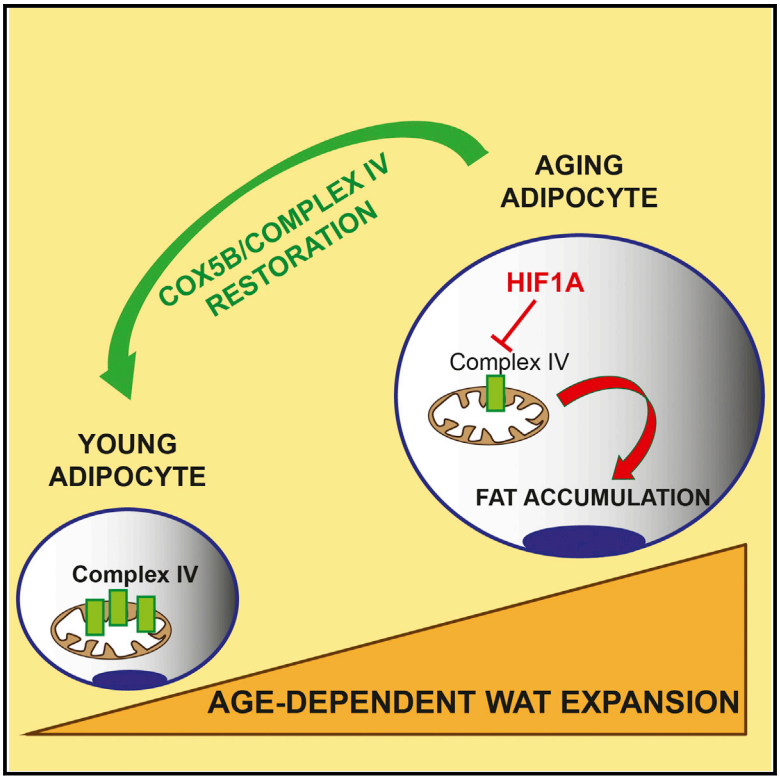

Highlights

- Mitochondrial complex IV dysfunction occurs in aging white adipocytes
- HIF1A represses complex IV subunits such as *Cox5b* in aging adipocytes
- Silencing *Cox5b* promotes WAT enlargement
- Restoration of COX5B counteracts age-dependent obesity

Authors

Ines Soro-Arnaiz, Qilong Oscar Yang Li, Mar Torres-Capelli, ..., Antonio Zorzano, Katrien De Bock, Julián Aragonés

Correspondence

jaragones.hlpr@salud.madrid.org

In Brief

Soro-Arnaiz et al. identify an age-dependent mitochondrial CIV dysfunction in white adipocytes involving HIF1A-dependent repression of CIV subunits such as *Cox5b*. Silencing *Cox5b* promotes white adipocyte enlargement in young mice, whereas its restoration prevents age-dependent obesity.

Soro-Arnaiz et al., 2016, Cell Reports *16*, 2991–3002
September 13, 2016
http://dx.doi.org/10.1016/j.celrep.2016.08.041

CellPress

Cell Reports
Article

Role of Mitochondrial Complex IV in Age-Dependent Obesity

Ines Soro-Arnaiz,[1,13] Qilong Oscar Yang Li,[1,13] Mar Torres-Capelli,[1] Florinda Meléndez-Rodríguez,[1] Sónia Veiga,[3,4,5] Koen Veys,[10,11] David Sebastian,[3,4,5] Ainara Elorza,[1] Daniel Tello,[1] Pablo Hernansanz-Agustín,[2] Sara Cogliati,[9] Jose Maria Moreno-Navarrete,[7] Eduardo Balsa,[1,12] Esther Fuertes,[1] Eduardo Romanos,[6] Antonio Martínez-Ruiz,[2] Jose Antonio Enriquez,[9] Jose Manuel Fernandez-Real,[7] Antonio Zorzano,[3,4,5] Katrien De Bock,[8] and Julián Aragonés[1,14,*]

[1]Research Unit, Hospital of Santa Cristina, Research Institute Princesa (IP), Autonomous University of Madrid, Madrid 28009, Spain
[2]Immunology Department, Hospital of La Princesa, Research Institute Princesa (IP), Autonomous University of Madrid, Madrid 28009, Spain
[3]Institute for Research in Biomedicine (IRB, Barcelona), Barcelona 08028, Spain
[4]Department of Biochemistry and Molecular Biology, University of Barcelona, Barcelona 08028, Spain
[5]CIBER of Diabetes and Metabolic Diseases (CIBERDEM), Carlos III Health Institute, Barcelona 08036, Spain
[6]Phenotyping Unit, IIS Aragón, Zaragoza 50013, Spain
[7]Department of Diabetes, Endocrinology and Nutrition, CIBEROBN Fisiopatología de la Obesidad y Nutrición, Institut d'Investigació Biomédica of Girona, Girona 17007, Spain
[8]Health Sciences and Technology Department, Laboratory of Exercise and Health, Swiss Federal Institute of Technology (ETH), Zurich 8603, Switzerland
[9]Centro Nacional de Investigaciónes Cardiovasculares (CNIC) Carlos III, Madrid 28029, Spain
[10]Laboratory of Angiogenesis and Vascular Metabolism, Vesalius Research Center, VIB, Leuven 3000, Belgium
[11]Laboratory of Angiogenesis and Vascular Metabolism, Vesalius Research Center, Department of Oncology, University of Leuven, Leuven 3000, Belgium
[12]Present address: Department of Cancer Biology, Dana-Farber Cancer Institute, Boston, MA 02115, USA
[13]Co-first author
[14]Lead Contact
*Correspondence: jaragones.hlpr@salud.madrid.org
http://dx.doi.org/10.1016/j.celrep.2016.08.041

SUMMARY

Aging is associated with progressive white adipose tissue (WAT) enlargement initiated early in life, but the molecular mechanisms involved remain unknown. Here we show that mitochondrial complex IV (CIV) activity and assembly are already repressed in white adipocytes of middle-aged mice and involve a HIF1A-dependent decline of essential CIV components such as COX5B. At the molecular level, HIF1A binds to the *Cox5b* proximal promoter and represses its expression. Silencing of *Cox5b* decreased fatty acid oxidation and promoted intracellular lipid accumulation. Moreover, local in vivo *Cox5b* silencing in WAT of young mice increased the size of adipocytes, whereas restoration of COX5B expression in aging mice counteracted adipocyte enlargement. An age-dependent reduction in *COX5B* gene expression was also found in human visceral adipose tissue. Collectively, our findings establish a pivotal role for CIV dysfunction in progressive white adipocyte enlargement during aging, which can be restored to alleviate age-dependent WAT expansion.

INTRODUCTION

With a steadily increasing incidence, obesity has become the leading medical disorder of the 21st Century. In particular, the middle-aged population appears to be prone to obesity (Ng et al., 2014; Ogden et al., 2013; van Harmelen et al., 2003). Although the reasons for this remain largely enigmatic, several factors are strongly implicated in the development of obesity, such as sedentary lifestyle and poor dietary habits. Genetic factors have also been suggested to control age-dependent obesity. For example, hypothalamic pro-opiomelanocortin neurons, which are involved in the regulation of food intake, are progressively silenced during aging (Yang et al., 2012). Most of the knowledge on fat development stems from experimental studies in which white adipose tissue (WAT) expansion occurs rapidly upon high-fat diet (HFD) feeding. The mechanisms involved in progressive WAT expansion during aging, however, remain mostly unidentified. Because obesity at a later age predisposes to life-threatening conditions such as insulin resistance, type 2 diabetes, and cardiovascular disease, understanding the causal molecular mechanisms of age-related obesity may provide a strategy for treating these disorders.

One of the hallmarks of aging is the functional dysregulation of mitochondria (López-Otín et al., 2013), which constitute the central metabolic hub in many cell types and are the gateway to aerobic metabolism. Mitochondrial oxidative phosphorylation is governed by the electron transport chain (ETC). Oxygen is the

final electron acceptor in the ETC, and cytochrome *c* oxidase (complex IV [CIV]), the terminal enzyme of the ETC, reduces it to H_2O after which energy is produced in the form of ATP by the action of ATP synthase (Saraste, 1999). In mature white adipocytes, mitochondria have a central role in many processes, such as ensuring energy generation through fatty acid β-oxidation in the mitochondrial matrix (Kusminski and Scherer, 2012; Villarroya et al., 2009). Aside from ATP production, mitochondria generate the necessary metabolic intermediates for lipid synthesis, thereby determining lipogenic potential (Kusminski and Scherer, 2012). Moreover, mitochondrial activity in WAT is associated with the release of several adipokines, including adiponectin (Kim et al., 2007; Koh et al., 2007; Kusminski and Scherer, 2012).

Aging has also been associated with increased adiposity early in the lives of mice and humans (Gargiulo et al., 2014; Kuk et al., 2009). However, it is unclear whether mitochondrial dysfunction in WAT contributes to age-related adipocyte enlargement and whether it can be restored to counteract age-dependent WAT expansion. Here we report that adipocytes of early middle-aged mice already exhibit mitochondrial dysfunction, which is largely associated with a decline of mitochondrial CIV activity and assembly. This decline in CIV activity involves a hypoxia-inducible factor 1A (HIF1A)-dependent reduction of CIV components, including cytochrome c oxidase subunit Vb (*Cox5b*). Silencing of *Cox5b* is sufficient to promote a global decline of CIV assembly, as well as decreased fat oxidation, and contributes to adipocyte enlargement during aging. Conversely, in vivo restoration of COX5B expression counteracts age-dependent white adipocyte enlargement. Collectively, our findings highlight the potential of targeting mitochondrial CIV to reverse adipocyte expansion during aging.

RESULTS

Selective Reduction of White Adipocyte Mitochondrial CIV Activity during Age-Dependent Obesity

During aging, mouse body weight progressively increased from 31.7 ± 1.2 g (in 3- to 5-month-old mice) to 43.3 ± 3.7 g (8- to 11-month-old mice), indicating that molecular mechanisms involved in age-dependent body weight gain are initiated early in life. We therefore focused the study on those initiating events of obesity in early middle-aged mice rather than in older mice. Throughout this work, 3- to 5-month-old mice are called "young" mice and 8- to 11-month-old mice are termed "aging" mice. We used the term "aging" instead of "aged" or "old" in this context to denote the process of progressively getting older. Age-dependent weight gain was accompanied by a significant increase in the size of adipocytes from epididymal WAT (eWAT) (Figures 1A, 1B, and S1), a visceral WAT depot with a remarkable expansion capacity during aging and a major risk factor for metabolic disease (Rosen and Spiegelman, 2014). To investigate the molecular mechanisms underlying age-dependent WAT enlargement, we focused on mitochondria because of their emerging fundamental role in white adipocyte biology (Bournat and Brown, 2010; Kusminski and Scherer, 2012; Rosen and Spiegelman, 2014; Villarroya et al., 2009) and in aging (López-Otín et al., 2013). Although mitochondrial content of eWAT adipocytes was similar between young and aging mice (Figure 1C), the oxygen consumption rate (OCR) and ATP turnover were significantly lower in eWAT of aging mice (Figures 1D and 1E). More detailed mitochondrial activity analysis revealed a significant decline of CIV activity in aging white adipocytes, whereas complex I, II, I+III, and II+III activities remained unchanged (Figure 1F). Furthermore, western blot analysis showed that the protein levels of representative CIV subunits, such as COX5B, NDUFA4, and mt-CO1, were significantly lower in aging than in young adipocytes (Figures 1G and 1H). By contrast, protein expression levels of NADH dehydrogenase (ubiquinone) 1 alpha subcomplex 9 (NDUFA9; complex I), succinate dehydrogenase complex, subunit A, flavoprotein (Fp) (SDHA; complex II), ubiquinol-cytochrome *c* reductase core protein 1 (UQCRC1; complex III), and mitochondrial voltage-dependent anion channel 1 (VDAC1) were not significantly changed (Figures 1G and 1H). These data show that while mitochondrial oxygen consumption is reduced in aging eWAT, not all mitochondrial complexes are equally affected during this process, and mitochondrial CIV is specifically repressed.

HIF1A Promotes Age-Dependent eWAT Expansion and a Reduction of CIV Expression

To investigate the molecular mechanisms involved in age-dependent regulation of mitochondrial CIV and adipocyte enlargement, we focused on HIF1A because previous studies have demonstrated its activation in aged tissues (Gomes et al., 2013; González-Rodríguez et al., 2012). Although these studies were performed at later stages during the lifespan of the mouse, we wondered whether HIF1A is already expressed in WAT of aging mice (8- to 11-month-old mice). Western blot analysis confirmed that the steady-state levels of HIF1A in eWAT were higher in aging than in young mice (Figure 2A), and this was not seen in other tissues, such as brown adipose tissue or liver (Figure S2A). We therefore questioned whether HIF1A could drive age-dependent white adipocyte enlargement. To do this, we generated mice with global or adipocyte-restricted *Hif1a* gene deficiency using transgenic mice expressing ubiquitin-Cre-ER^{T2} ($Hif1a^{\Delta Ubq}$) or adiponectin-Cre-ER^{T2} ($Hif1a^{\Delta Adipo}$), respectively (Figures S2B and S2F). Aging $Hif1a^{\Delta Ubq}$ and $Hif1a^{\Delta Adipo}$ mice gained significantly less body weight (Figures S2D, S2E, S2G, and S2H) and had smaller eWAT adipocytes (Figures 2B, 2C, and S2C) under normal dietary conditions than aging control mice, suggesting that adipocyte HIF1A drives age-dependent obesity.

Given that HIF1A functions as a transcription factor that can also be involved in gene repression (Eltzschig et al., 2005; Gordan et al., 2007; Krishnan et al., 2012), we next evaluated the possibility that the expression of nuclear-encoded CIV gene transcripts was repressed in aging adipocytes in a HIF1A-dependent manner. By RT-PCR analysis, we found that the levels of *Cox5b*, *Cox6a*, *Cox6c*, and *Cox8a* mRNA were all significantly lower in aging adipocytes than in young adipocytes, whereas the mRNA expression level of other CIV subunits was unaffected (Figure S2I). In addition, only *Cox5b* and *Cox8a* mRNA levels were restored in *Hif1a*-deficient adipocytes (Figure 2D). Only a few CIV genes were

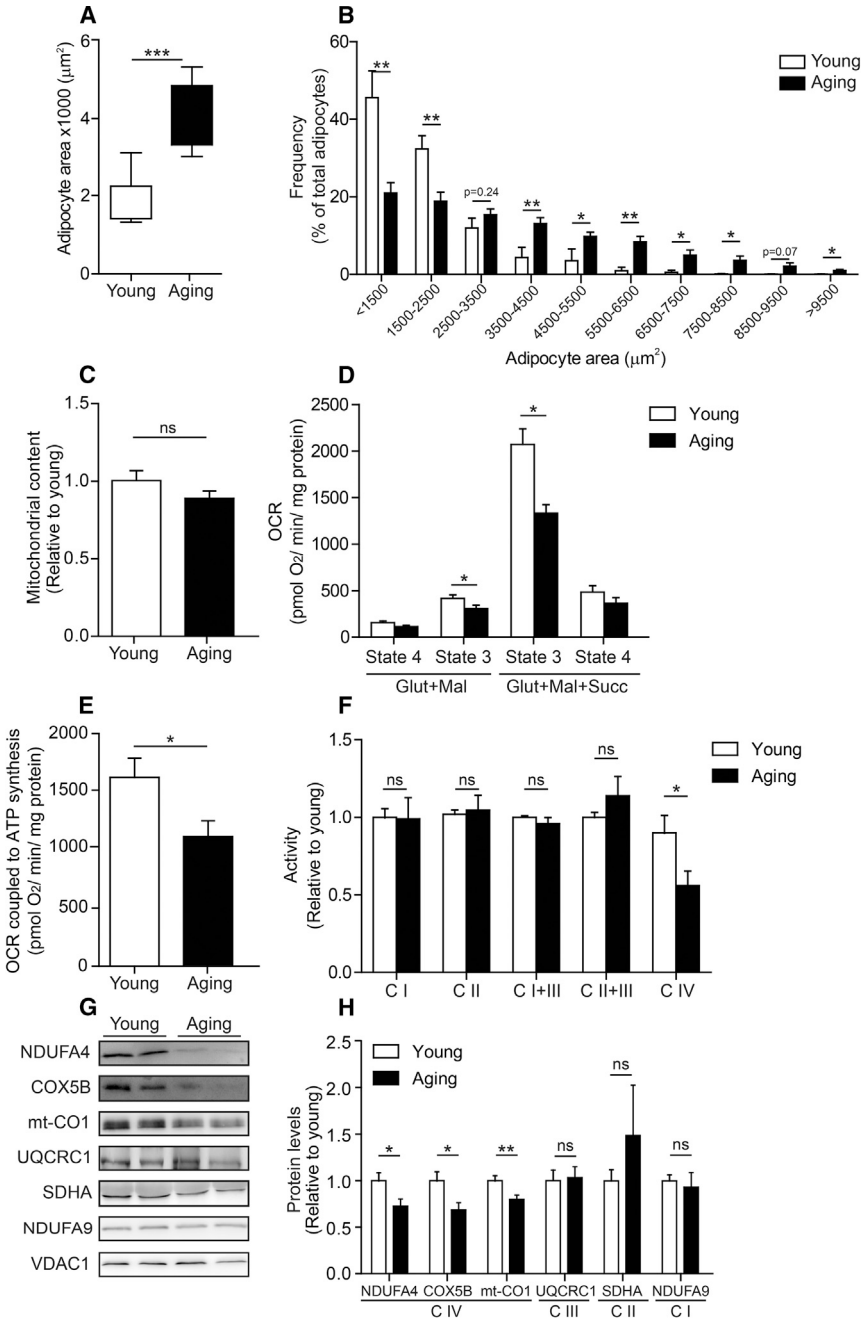

Figure 1. Mitochondrial CIV Activity Is Specifically Decreased during Age-Dependent Obesity in White Adipocytes

(A and B) Average adipocyte area (A) and adipocyte size frequency (B) distribution in young mice (n = 7) and aging mice (n = 5).

(C) Mitochondrial content in isolated white adipocytes of young mice (n = 4) and aging mice (n = 5).

(D) Mitochondrial OCR in eWAT from young mice (n = 6) and aging mice (n = 7). OCR was measured after sequential addition of glutamate and malate (Glut + Mal, State 4), ADP (Glut + Mal, State 3), succinate (Glut + Mal + Succ, State 3), and oligomycin (Glut + Mal + Succ, State 4).

(E) Mitochondrial OCR coupled to ATP synthesis (or ATP turnover) in eWAT from young mice (n = 6) and aging mice (n = 7).

(F) Activities of the indicated mitochondrial ETC complexes were measured in isolated white adipocytes of young mice (n = 6) and aging mice (n = 10).

(G and H) Western blot analysis (G) and quantification of the indicated mitochondrial subunits (H) in isolated white adipocytes of young mice (n = 12) and aging mice (n = 10). Protein expression was normalized to VDAC1.

In bar graphs, values represent mean ± SEM (error bars). In box and whiskers plots, vertical lines connect the minimum and the maximum values. Statistical significance was assessed with a two-tailed t test (*p < 0.05; **p < 0.01; ***p < 0.001; NS, not significant). See also Figure S1.

affected by aging, which was surprising because our analysis of protein content of other representative subunits, such as NDUFA4 or mt-CO1 (Figures 1G and 1H), indicated a more global repression in aging adipocytes. The protein content of NDUFA4 and mt-CO1 was restored by *Hif1a* deletion (Figure 2E), suggesting that HIF1A-dependent repression of *Cox5b* and *Cox8a* mRNAs could lead to reduced protein content of other mitochondrial CIV subunits in aging adipocytes. In this respect, it has been previously shown in a macrophage cell line that *Cox5b* silencing is sufficient to promote global CIV dysfunction by reducing the protein stability of other CIV components (Galati et al., 2009). To test whether COX5B and COX8A control CIV stability in adipocytes, we silenced both in 3T3-L1 cells (Figure 3A) and found reduced protein levels of the mitochondrial CIV subunits NDUFA4 and mt-CO1 (Figure 3B). Moreover, silencing of *Cox5b* resulted in a profound decline of both CIV activity and CIV assembly (Figures 3C and 3D). The ability of COX5B to regulate CIV stability was dose dependent, because silencing *Cox5b* by 90% (as occurred in clone #2) resulted in a stronger inhibition of CIV assembly and activity than that observed when *Cox5b* was reduced by 60%–70% (as occurred in clone #1) (Figures 3C and 3D). In addition, robust silencing of *Cox8a* mRNA (90%–95%) reduced mitochondrial CIV activity and assembly, but to a lesser extent than that observed for *Cox5b* silencing (Figures 3C and 3D). In agreement with these data, CIV assembly was also reduced in aging adipocytes (Figures 3E and 3F).

Collectively, these data show a global decline of CIV in aging white adipocytes that is characterized by repression of CIV activity and assembly. This CIV dysfunction could be initiated by repressing *Cox5b*, as well as *Cox8a*, through HIF1A stabilization during WAT expansion.

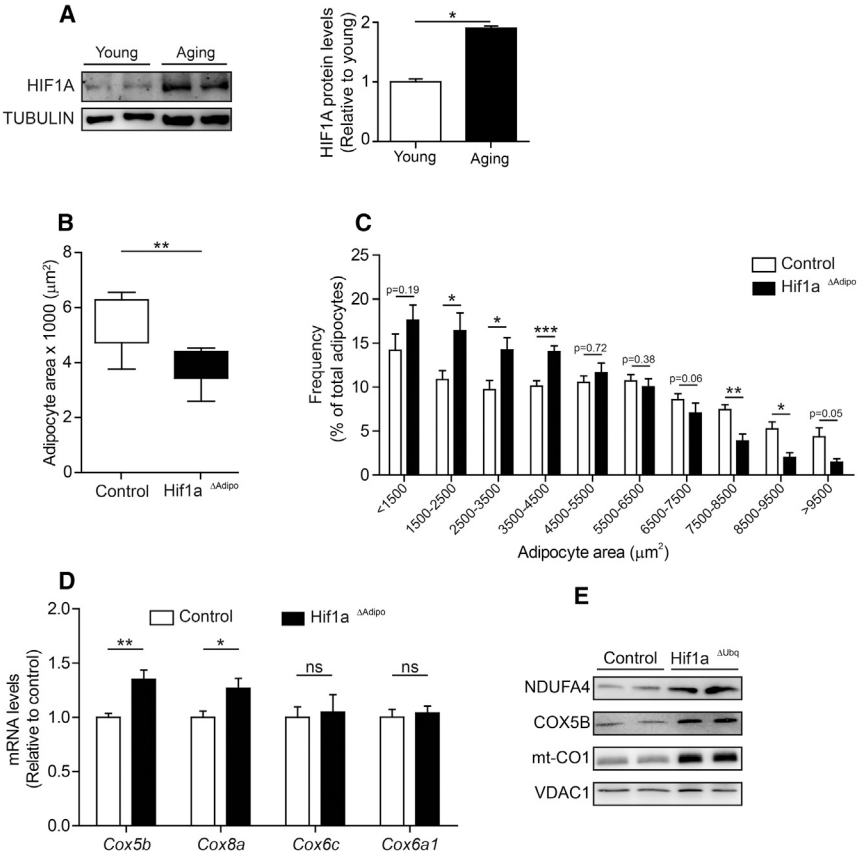

Figure 2. HIF1A Promotes Age-Dependent Complex IV Decline Associated with eWAT Expansion

(A) Representative western blot analysis and quantification of HIF1A in eWAT from young and aging mice.

(B) Average adipocyte size in Hif1a$^{\Delta Adipo}$ mice (n = 6) and *Hif1a*^{floxed} control mice (n = 8) at the age of 8–10 months.

(C) Adipocyte area frequency distribution analysis in Hif1a$^{\Delta Adipo}$ mice (n = 6) and control mice (n = 8) at the age of 8–10 months.

(D) mRNA expression levels of *Cox5b*, *Cox8a*, *Cox6c*, and *Cox6a1* in isolated adipocytes of Hif1a$^{\Delta Adipo}$ mice (n = 6) and *Hif1a*^{floxed} control mice (n = 5) at the age of 8–10 months.

(E) Western blot analysis of CIV subunits (COX5B, NDUFA4, and mt-CO1) in isolated adipocytes of Hif1a$^{\Delta Ubq}$ mice and control mice (control).

In bar graphs, values represent mean ± SEM (error bars). In box and whiskers plots, vertical lines connect the minimum and the maximum values. Statistical significance was assessed with a two-tailed t test (*p < 0.05; **p < 0.01; ***p < 0.001; NS, not significant). See also Figure S2.

HIF1A Binds the *Cox5b* Proximal Promoter

We next examined the molecular link between HIF1A and CIV gene expression, focusing our analysis on *Cox5b* and *Cox8a*. Previous studies have reported a HIF1A-dependent repression of some genes following the binding of HIF1A to their DNA regulatory regions (Eltzschig et al., 2005; Krishnan et al., 2012). We therefore first assessed the presence of HIF1A binding activity in the DNA regulatory regions of *Cox5b* and *Cox8a* (Dhar et al., 2008). Sequence analysis revealed potential HIF1A binding sites from −93 to −97 positions (Figure 4A) and from −760 to −756 positions (Figure S3A) of murine *Cox5b* and *Cox8a* DNA regulatory regions, respectively. Chromatin immunoprecipitation (ChIP) using an anti-HIF1A antibody confirmed the binding of HIF1A to the *Cox5b* proximal promoter region in 3T3-L1 cells exposed to hypoxia (Figure 4B). Moreover, binding of HIF1A was specific to this region, because it was not detected with oligonucleotides directed to amplify a distal region of the *Cox5b* promoter or the *Cox8a* proximal promoter (Figures 4A, 4B, S3A, and S3B). Consistent with HIF1A binding to this region, expression of *Cox5b* mRNA was significantly reduced in 3T3-L1 cells under hypoxia (Figure 4C), whereas the mRNA of the prolyl hydroxylase domain enzyme 3 (*Phd3*), a well-characterized HIF-inducible gene, was increased (Figure S3C). To validate the role of HIF1A in *Cox5b* gene repression, we used *Hif1a*-deficient murine embryonic fibroblasts (MEFs). We first confirmed that repression of *Cox5b* gene expression occurred in wild-type MEF exposed to hypoxia (Figure 4D), whereas *Phd3* expression was elevated (Figure S3D). Moreover, activation of the HIF pathway with dimethyloxaloylglycine (DMOG), a competitive inhibitor of prolyl hydroxylase oxygen sensors, reduced *Cox5b* gene expression in MEF (Figure 4E). As expected, *Cox5b* gene repression by hypoxia or DMOG treatment was markedly attenuated in *Hif1a*-deficient MEF (Figures 4D and 4E), strongly suggesting that HIF1A acts as a transcriptional repressor of *Cox5b*. As a positive control, the expression of *Phd3* was less evident in *Hif1a*-deficient MEF (Figures S3D and S3E).

Overall, these data indicate that *Cox5b* repression is a primary event that occurs upon HIF1A stabilization in aging adipocytes. We therefore further explored the role of CIV in the control of adipocyte size during aging by modifying white adipocyte COX5B expression.

Mitochondrial CIV Inhibition through Silencing of *Cox5b* Promotes Intracellular Lipid Accumulation and White Adipocyte Enlargement

We next determined whether COX5B-dependent mitochondrial CIV repression controls lipid accumulation and age-dependent adipocyte size enlargement. To evaluate intracellular lipid accumulation, 3T3-L1-shCOX5B (small hairpin *COX5B* RNA) cells and control cells were stained with Nile red and intracellular lipids were measured by flow cytometry. Lipid content was higher in 3T3-L1-shCOX5B cells than in control cells (Figures 5A and S4A), suggesting that a reduction in CIV activity by *Cox5b* silencing is sufficient to promote lipid storage. To confirm this finding, 3T3-L1-shSCR (small hairpin scrambled RNA) control cells were treated with sodium azide, a well-established pharmacological inhibitor of CIV. Azide treatment

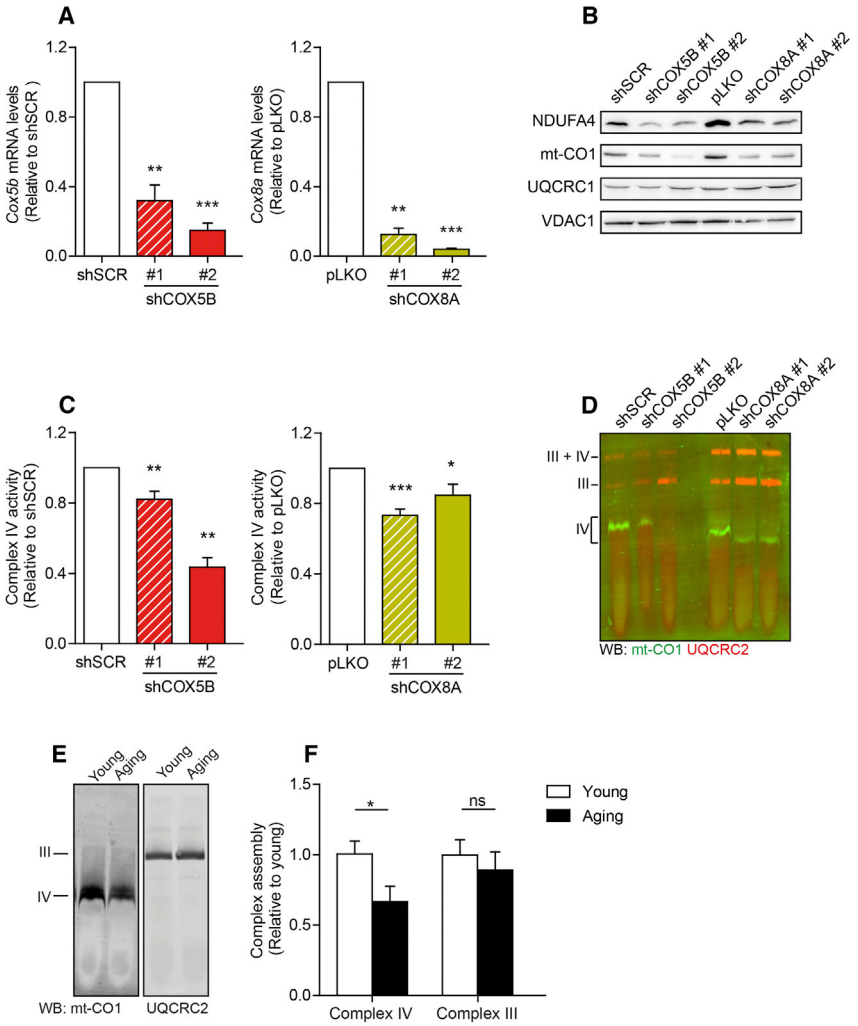

Figure 3. Comparative Analysis of *Cox5b* and *Cox8a* Silencing Effects on CIV Activity and Assembly

(A) Left panel: mRNA expression of *Cox5b* in 3T3-L1-shCOX5B cells using two shRNA sequences: clone 1 (#1) and clone 2 (#2) relative to 3T3-L1-shSCR control cells (n = 4 independent experiments). Right panel: mRNA expression of *Cox8a* in 3T3-L1-shCOX8A cells using two shRNA sequences: clone 1 (#1) and clone 2 (#2) relative to 3T3-L1-pLKO control cells (n = 3 independent experiments).

(B) Western blot analysis of the indicated mitochondrial ETC subunits in 3T3-L1-shCOX5B and 3T3-L1-shCOX8A cells and their respective controls.

(C) CIV activity in 3T3-L1-shCOX5B cells and 3T3-L1-shCOX8A cells and their respective controls.

(D) Blue native-PAGE western blot analysis showing mitochondrial complexes and super-complexes in 3T3-L1-shCOX5B and 3T3-L1-shCOX8A cells and their respective controls. UQCRC2 or mt-CO1 antibody was used to identify complex III or IV assembly.

(E and F) Representative images (E) and quantification (F) of blue native-PAGE analysis of mitochondrial complex III and IV assembly using UQCRC2 or mt-CO1, respectively, in isolated adipocytes of young mice (n = 8) and aging mice (n = 8).

In bar graphs, values represent mean ± SEM (error bars). Statistical significance was assessed with a two-tailed t test (*p < 0.05; **p < 0.01; ***p < 0.001; NS, not significant).

also increased the Nile red signal intensity in 3T3-L1-shSCR control cells (Figure 5A). Because increased fat accumulation has been associated with reduced fatty acid oxidation (Kusminski and Scherer, 2012; Vernochet et al., 2012), we also measured fatty acid oxidation in *Cox5b*-silenced cells. Both 3T3-L1-shCOX5B cells and azide-treated 3T3-L1-shSCR cells presented significantly reduced fatty acid oxidation when compared with control cells (Figure 5B). Furthermore, consistent with aging adipocytes, *Cox5b* silencing in 3T3-L1 cells reduced oxygen consumption and ATP turnover (Figures 5C, 5D, S4B, and S4C). Collectively, these data suggest that repression of *Cox5b* leads to the attenuation of mitochondrial CIV activity, which is sufficient to reduce fatty acid oxidation and promote intracellular lipid accumulation.

We next asked whether *Cox5b* silencing in young mice would promote white adipocyte enlargement in vivo. We therefore injected lentiviral shCOX5B particles into the right eWAT depot of young wild-type mice, while the left contralateral eWAT depot remained uninjected and served as an internal control (Figure 6A). An identical protocol was used for control shSCR particles (Figure 6A). Injection of shCOX5B particles significantly reduced the ratio of *Cox5b* mRNA levels in the injected to non-injected eWAT depot when compared with shSCR mice (Figure 6B), which was concomitant with a significant increase in the adipocyte size ratio (Figure 6C). Moreover, analysis of adipocyte size distribution revealed that shCOX5B-injected eWAT depots contained a greater proportion of large adipocytes and a smaller proportion of small adipocytes than shSCR-injected depots (Figure 6D). No significant differences were found in the contralateral non-injected depots (Figure S5A). Thus, the reduction of COX5B expression in the eWAT of young mice drives white adipocyte enlargement, indicating that *Cox5b* repression is an important determinant of eWAT adipocyte size.

In vivo COX5B Restoration Attenuates Adipocyte Size Enlargement in Aging Mice

These findings prompted us to evaluate whether restoration of COX5B expression could be exploited as a potential molecular target to prevent age-dependent adipocyte enlargement. To do this, we first validated that overexpression of COX5B protein is sufficient to increase mitochondrial CIV activity. Ectopic overexpression of COX5B protein in HEK293T cells (Figure S5B) increased mitochondrial CIV activity (Figure S5C). Next, lentiviral particles overexpressing COX5B were injected into the right eWAT depot of aging mice, while the left contralateral visceral

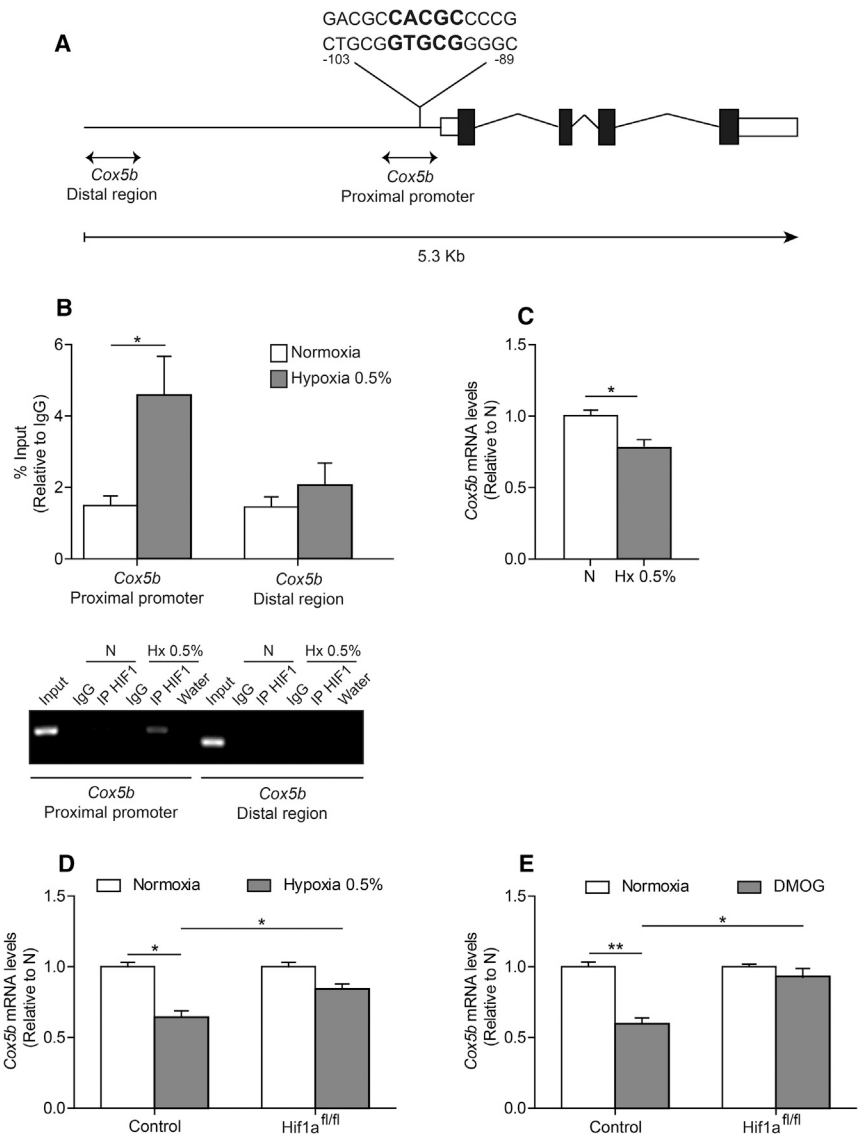

Figure 4. HIF1A Binds to the *Cox5b* Proximal Promoter

(A) Schematic representation of the mouse *Cox5b* gene and its promoter region, indicating the position of the HIF1A binding site in bold.

(B) ChIP assay to assess the relative HIF1A binding activity to the mouse *Cox5b* proximal promoter and distal region in 3T3-L1 cells exposed to normoxia or hypoxia 0.5% for 18–20 hr (n = 7 independent experiments). A representative gel showing DNA amplified in the ChIP assays is shown in the lower panel.

(C) *Cox5b* mRNA expression levels in 3T3-L1 cells exposed to normoxia or hypoxia 0.5% for 72 hr (n = 4 independent experiments).

(D) *Cox5b* mRNA expression levels in control or Hif1a$^{fl/fl}$ MEF exposed to normoxia or hypoxia 0.5% for 48 hr (n = 4 independent experiments).

(E) *Cox5b* mRNA expression levels in control or Hif1a$^{fl/fl}$ MEF under normoxia or 48 hr after 0.5 mM DMOG treatment (n = 4 independent experiments). In bar graphs, values represent mean ± SEM (error bars). Statistical significance was assessed with a two-tailed t test (*p < 0.05; **p < 0.01). See also Figure S3.

eWAT depot remained uninjected (Figure 6E). An identical protocol was used for control empty vector particles (Figure 6E). Injection of COX5B-expressing lentiviral particles significantly increased the ratio of *Cox5b* mRNA levels in the injected to non-injected eWAT depot when compared with empty vector mice (Figure 6F) and significantly decreased the adipocyte size (Figure 6G). Adipocyte size distribution analysis revealed a greater proportion of small adipocytes and a reduced proportion of large adipocytes in COX5B-injected eWAT depots when compared with the empty vector-injected eWAT depots (Figure 6H), whereas no significant differences were observed in the corresponding non-injected contralateral eWAT depots (Figure S5D).

These in vivo data demonstrate that restoring COX5B expression in visceral eWAT is sufficient to attenuate adipocyte enlargement in aging mice, underscoring the relevance of COX5B to control age-dependent adipocyte size.

Human WAT *COX5B* Expression Correlates Negatively with Age and Serves as a Prognostic Factor for Weight Loss after Bariatric Surgery

Finally, to explore the potential relevance of our findings in humans, we measured *COX5B* expression in human visceral adipose tissue (VAT) during aging in a cohort of subjects with a range of adiposity (anthropometric and clinical parameters are described in the Experimental Procedures section). We found that *COX5B* mRNA levels correlated negatively with age in this cohort (Figure 7A), which persisted after controlling for BMI in multiple linear regression analysis (Figure 7B). Expression of the mitochondrial marker *VDAC1* was not associated with age in this cohort (Figures 7C and 7D), suggesting that the decrease in *COX5B* expression was not attributable to an overall decrease in the expression of mitochondrial components. Thus, the expression of *COX5B* is highly vulnerable to visceral WAT aging, not only in mice but also in human VAT.

We also investigated the clinical value of our findings. Post-bariatric surgery weight reduction shows great disparities among individuals (Lutfi et al., 2006; Maggard et al., 2005), and age has been shown to be a prognostic factor (Scozzari et al., 2012). We therefore asked whether *COX5B* in WAT might predict long-term weight loss in humans after bariatric surgery. We found that subcutaneous white adipose tissue (SAT) *COX5B* levels negatively correlated with BMI 1 year after bariatric surgery (Figure 7E), whereas *VDAC1* showed the opposite trend (Figure 7F). Patients with higher *COX5B* levels had a lower BMI 1 year after bariatric surgery (Figure 7E), underlining the

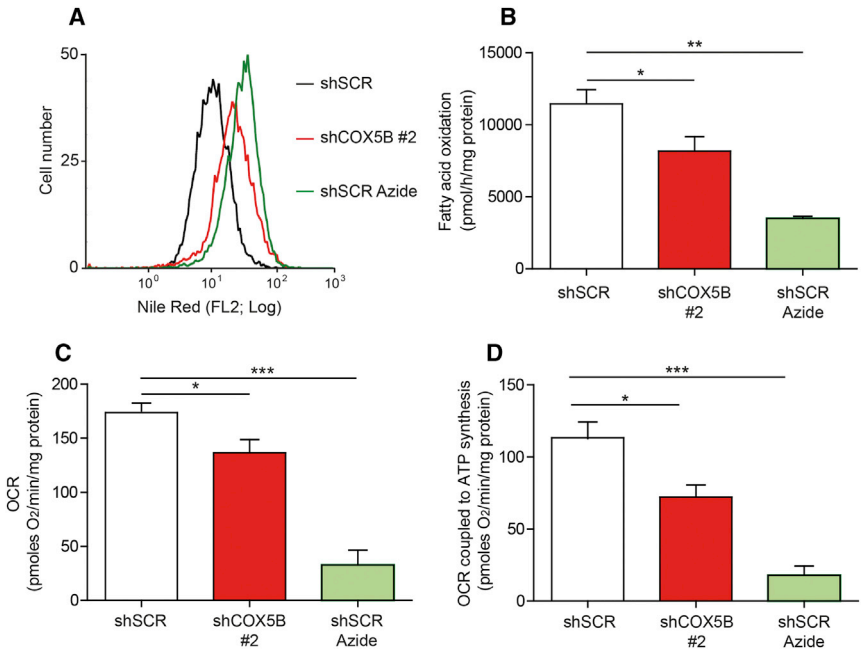

Figure 5. Mitochondrial CIV Inhibition and *Cox5b* Silencing Results in Intracellular Lipid Storage In Vitro and Decreases Mitochondrial Respiration

(A) Nile red fluorescence intensity in 3T3-L1-shCOX5B #2 cells, 3T3-L1-shSCR control cells, and 3T3-L1-shSCR control cells treated with 5 mM azide. A representative experiment out of seven independent experiments is shown.

(B) Fatty acid oxidation in 3T3-L1-shCOX5B #2 cells (n = 6), 3T3-L1-shSCR control cells (n = 5), and 3T3-L1-shSCR control cells treated with 5 mM azide (n = 6).

(C) Mitochondrial OCR in 3T3-L1-shCOX5B #2 cells, 3T3-L1-shSCR control cells, and 3T3-L1-shSCR control cells treated with 5 mM azide (n = 6).

(D) ATP turnover in 3T3-L1-shCOX5B #2 cells, 3T3-L1-shSCR control cells, and 3T3-L1-shSCR control cells treated with 5 mM azide (n = 6).

In bar graphs, values represent mean ± SEM (error bars). Statistical significance was assessed with a two-tailed t test (*$p < 0.05$; **$p < 0.01$; ***$p < 0.001$). See also Figure S4.

translational relevance and clinical value of *COX5B* measurements in SAT. Moreover, SAT samples can be gathered using a minimally invasive biopsy technique (Campbell et al., 2009), which also supports the clinical relevance of measuring *COX5B*.

Overall, our data show that repression of mitochondrial CIV activity is an early sign of age-dependent mitochondrial dysfunction in white adipocytes that drives WAT expansion during aging. Moreover, these data highlight the potential of CIV restoration to prevent increased adipocyte size enlargement during aging.

DISCUSSION

Aging is associated with increased adiposity early in life (Gargiulo et al., 2014; Kuk et al., 2009), suggesting that the molecular mechanisms underlying age-dependent WAT expansion should be initiated at an early stage of the lifetime. This is in contrast to other molecular alterations associated with aging, which are usually studied in very old mice (22- to 30-month-old mice) (Gomes et al., 2013; Houtkooper et al., 2011). Our study shows that mitochondrial CIV activity is specifically compromised in white adipocytes in early phases during aging (8- to 11-month-old mice), although the activity of other mitochondrial complexes, as well as mitochondrial content, are unaltered. Therefore, our study identifies WAT CIV dysfunction as an early sign of aging in white adipocytes that manifests in middle-aged mice, which leads to progressive age-dependent body weight gain during the lifetime.

Previous studies have demonstrated that mitochondrial activity is globally repressed in more severe models of obesity. Accordingly, mice subjected to HFD and mice with altered leptin signaling, such as *ob/ob* and *db/db* mice, show a significant decline in mitochondrial content in WAT (Choo et al., 2006; Rong et al., 2007; Sutherland et al., 2008; Valerio et al., 2006). It is possible that these settings, which are different from age-dependent obesity, have specific features that provoke global mitochondrial dysfunction in white adipocytes. The reasons for these differences are unclear, but one possible explanation is the excessive nutrient supply in HFD models. Several studies have shown that high levels of nutrients, including free fatty acids, lead to global mitochondrial dysfunction through diverse mechanisms, including oxidative stress and production of inflammatory cytokines (Gao et al., 2010; Kusminski and Scherer, 2012; Sutherland et al., 2008; Valerio et al., 2006). It is therefore conceivable that global mitochondrial dysfunction, including a decrease in mitochondrial content, is a general response to a pathological WAT scenario that is more characterized by nutrient overload. Presumably, this nutrient surplus occurs to a lesser degree, or maybe absent, during age-dependent WAT expansion. Along this line, human studies have shown that mitochondrial content is not consistently repressed in obese subjects (Kaaman et al., 2007; Lindinger et al., 2010; Yin et al., 2014). Lindinger et al. (2010) described a trend for reduced mtDNA content in diabetic obese patients but not in non-diabetic obese patients. In this regard, our present data in human VAT show that the expression of the mitochondrial marker *VDAC1* is not affected during aging, whereas the expression of *COX5B* is significantly repressed, indicating that aging can promote specific mitochondrial alterations in VAT. Furthermore, we show the prognostic potential of *COX5B* measurements in WAT, because patients with higher *COX5B* levels have lower BMI 1 year after bariatric surgery. These data are in accordance with a study showing that younger patients experienced a significantly greater and prolonged BMI decrease after surgery (Scozzari et al., 2012).

Previous studies have detected hypoxia in WAT under normal dietary conditions, based on pimonidazole staining (Hosogai et al., 2007; Lee et al., 2011; Ye et al., 2007). These data might explain the basal HIF1A expression observed in WAT of young mice (Figure 2A) (Krishnan et al., 2012; Lee et al., 2014; Yin

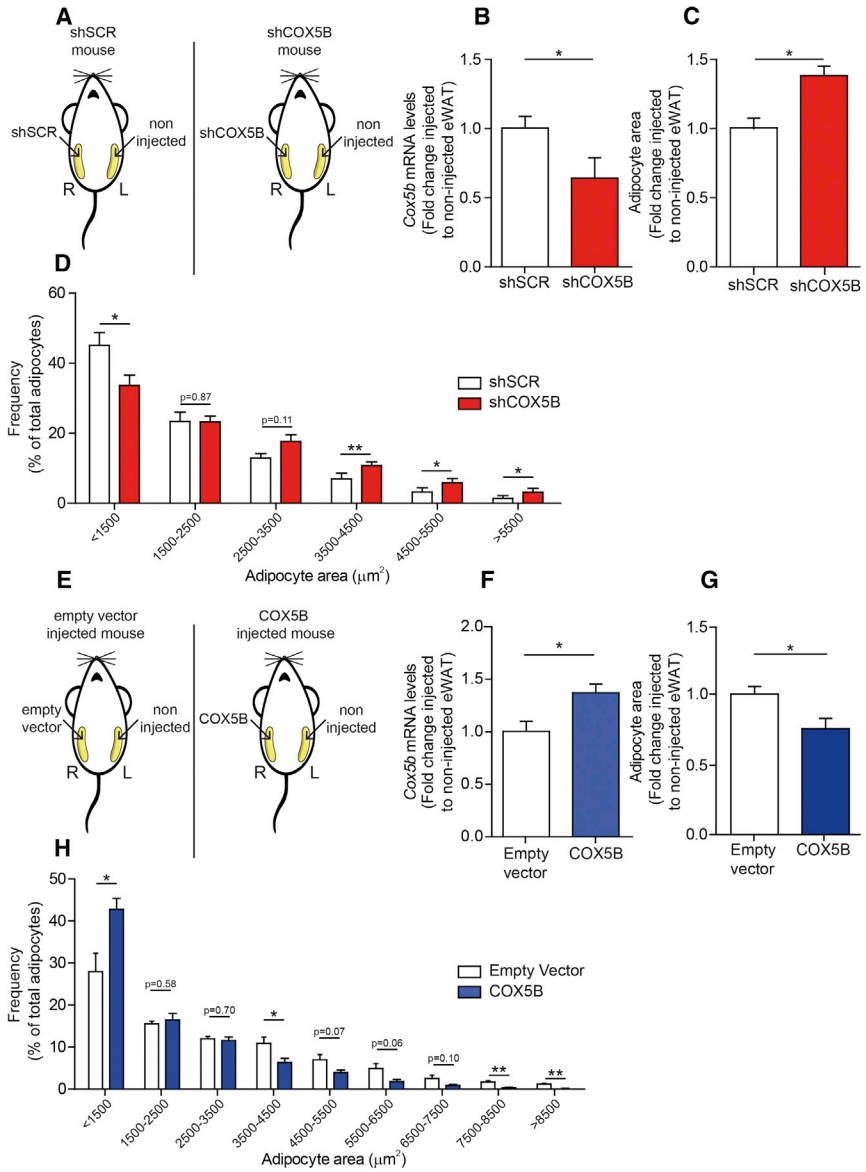

Figure 6. Opposing Effects of In Vivo Silencing and Restoration of *Cox5b* Expression in eWAT

(A) Schematic representation of eWAT injection of shSCR and shCOX5B lentiviral particles in mice.

(B) Ratio of *Cox5b* mRNA expression levels in injected to non-injected eWAT depots of shCOX5B mice (n = 4) and shSCR mice (n = 4). Fold change relative to shSCR is shown.

(C) Ratio of average adipocyte size in injected to non-injected eWAT depot of shCOX5B mice (n = 4) and shSCR mice (n = 4). Fold change relative to shSCR is shown.

(D) Adipocyte area frequency distribution analysis in shCOX5B (n = 4) and shSCR (n = 4) injected depots.

(E) Schematic representation of eWAT injection of COX5B and empty vector lentiviral particles in mice.

(F) Ratio of *Cox5b* mRNA expression in injected to non-injected eWAT depot of COX5B mice (n = 4) and empty vector mice (n = 5). Fold change relative to empty vector is shown.

(G) Ratio of average adipocyte size in injected to non-injected eWAT depots of COX5B mice (n = 4) and empty vector mice (n = 4). Fold change relative to empty vector is shown.

(H) Adipocyte area frequency distribution analysis in COX5B (n = 4) and empty vector (n = 4) injected depots.

In bar graphs, values represent mean ± SEM (error bars). Statistical significance was assessed with a two-tailed t test (*$p < 0.05$; **$p < 0.01$). See also Figure S5.

et al., 2009), which drives CIV repression and subsequent fat accumulation during aging. This latter contention is in line with a previous study showing that adipocyte-restricted inactivation of *Arnt*, a transcription factor with multiple partners, including HIF1A, counteracts age-dependent body weight gain (Lee et al., 2011). In addition, adipocyte-restricted *Hif1a* gene inactivation counteracts pathological WAT expansion in HFD-fed mice (Jiang et al., 2011; Krishnan et al., 2012; Lee et al., 2011, 2014). Regarding the molecular mechanisms executed by HIF1A leading to age-dependent white adipocyte enlargement, we found that HIF1A represses *Cox5b* and *Cox8a* gene expression. Previous studies have reported HIF1A-dependent gene repression associated with the binding of HIF1A to DNA regulatory regions of target genes (Eltzschig et al., 2005; Krishnan et al., 2012). In the present study, we found that hypoxia induces HIF1A binding to the *Cox5b* proximal promoter, which was associated with *Cox5b* repression. This promoter region has been previously shown to sustain *Cox5b* gene expression through NRF1 transcription factors (Dhar et al., 2008), suggesting that HIF1A could interfere with its basal activity. By contrast, although we acknowledge that HIF1A-dependent *Cox8a* repression can potentially cooperate with *Cox5b* to reduce CIV activity in aging adipocytes, we did not find HIF1A binding activity at the *Cox8a* proximal promoter, suggesting that HIF1A could drive *Cox8a* repression by indirect mechanisms, as described for other target genes repressed by HIF1A (Chan et al., 2009). Our analysis also shows that *Cox6a* and *Cox6c* expression in white adipocytes declined during age-dependent body weight gain but was not restored upon *Hif1a* deletion in aging adipocytes, suggesting that their regulation is executed by other hypoxia-dependent pathways (Sena and Chandel, 2012) or as a consequence of fat accumulation (Lee et al., 2014). A previous study has shown that HIF1A induces a COX4.2/COX4.1 switch to protect cells against hypoxia-induced reactive oxygen species (ROS) by optimizing respiration efficiency (Fukuda et al., 2007). However, we have not found evidence of this metabolic adaptation in aging WAT, suggesting that perhaps this switch is not operative in white adipocytes or

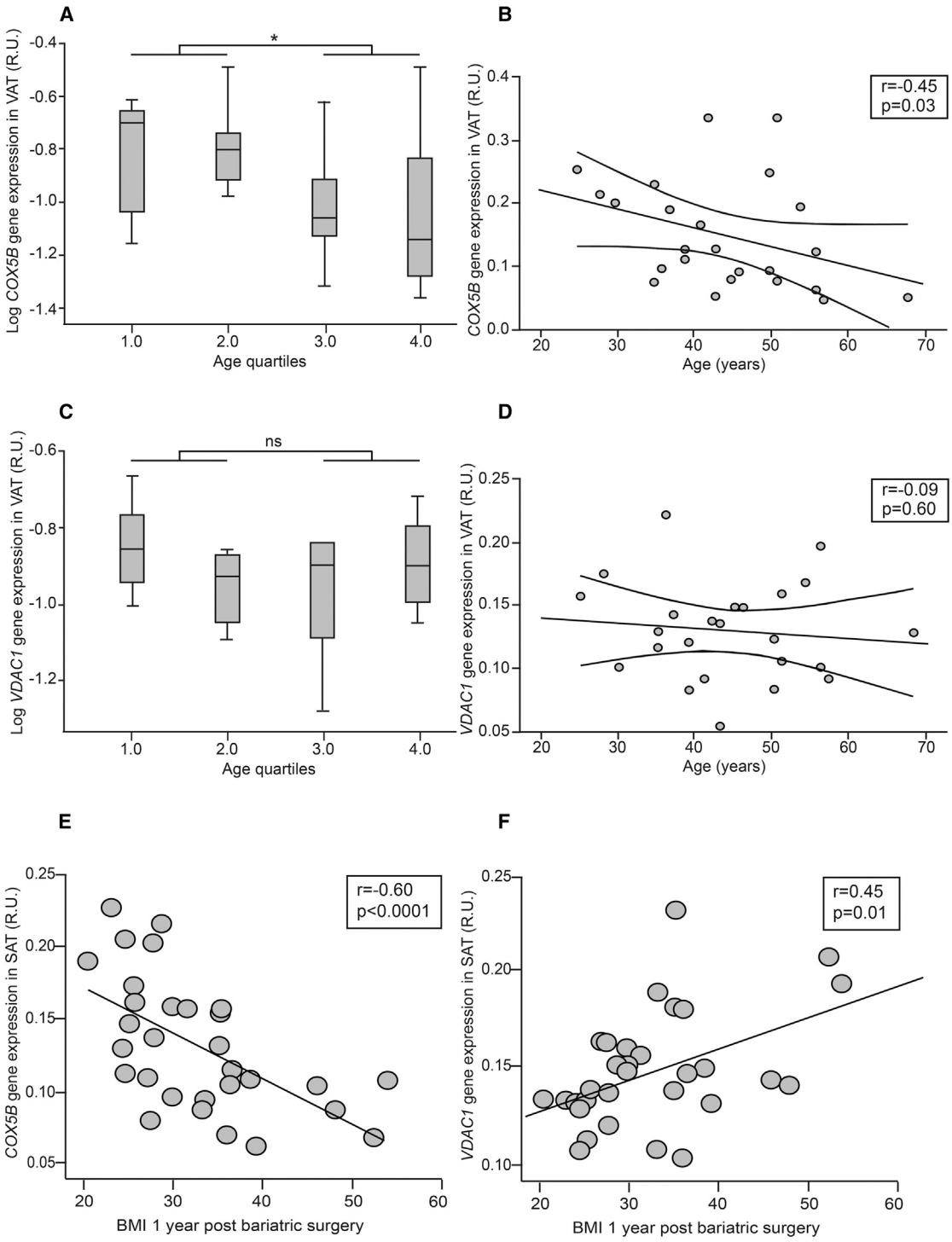

Figure 7. Age-Dependent Repression of *COX5B* Gene Expression in Human VAT and *COX5B* as a Prognostic Factor in Bariatric Surgery

(A–D) Boxplots showing log *COX5B* (A) or VDAC (C) gene expression in human VAT with increasing age quartiles (see Experimental Procedures); vertical lines connect the minimum and the maximum values (n = 24). Linear correlation analysis of the association between *COX5B* (B) or VDAC (D) gene expression in human VAT and age. Results remained significant after adjusting for Deuremberg-calculated fat mass instead of BMI.

(E and F) Linear correlation analysis of the association between *COX5B* (E) or VDAC (F) gene expression in human subcutaneous white adipose tissue (SAT) and BMI 1 year after bariatric surgery (n = 31).

Differences in human gene expression across age quartiles were evaluated with one-way ANOVA (*$p < 0.05$; NS, not significant). Linear association between gene expression and age or BMI was evaluated with Spearman's rank test.

it requires a more robust activation of HIF1A than that observed in aging adipocytes in vivo. Collectively, our data suggest that HIF1A-dependent repression of *Cox5b* expression can be considered a primary event, leading to a more global CIV decline because of the central role of COX5B in CIV stability, and further establish a molecular link between HIF1A and CIV, wherein HIF1A acts as a global repressor of CIV expression in white adipocytes.

Adipocyte-restricted inactivation and overexpression of key genes involved in mitochondrial biogenesis and activity is fundamental to better understand the role of mitochondria in adipocyte biology. It has been hypothesized that inactivation of these genes would reduce mitochondrial activity, leading to intracellular accumulation of lipids that cannot be oxidized (Kusminski et al., 2012; Vernochet et al., 2012, 2014). For example, reduced adipocyte mitochondrial activity and increased adipocyte size was detected in mice with adipose tissue-restricted overexpression of mitoNEET, an iron-sulfur protein that inhibits mitochondrial iron transport into the matrix and lowers the rate of β-oxidation (Kusminski et al., 2012). However, other studies have shown that adipocyte-restricted inactivation of the mitochondrial transcription factor A (TFAM), which is essential for maintenance of mtDNA, does not lead to increased adiposity because of an unanticipated compensatory response leading to increased mitochondrial oxygen consumption and uncoupling (Vernochet et al., 2012). Moreover, a second mouse model in which *Tfam* was inactivated in adipose tissue to a greater extent revealed a profound and global dysfunction of mitochondria, resulting in adipocyte death and subsequent lipodystrophy (Vernochet et al., 2014). In contrast to these studies, our data indicate that mitochondrial CIV dysfunction through *Cox5b* repression is sufficient to drive intracellular lipid accumulation. Our data suggest that a decline in COX5B protein content cannot be followed by compensatory mitochondrial overactivation or adipocyte death and culminates in enhanced adipocyte lipid content. Therefore, it is possible that during age-dependent body weight gain, repression of *Cox5b* guarantees enhanced lipid storage without these secondary compensatory effects on mitochondrial activity or adipocyte death.

In summary, our data establish mitochondrial CIV, and particularly COX5B, as a vulnerable mitochondrial component during visceral WAT aging in mice and humans. *Cox5b* repression is mediated by the HIF1A pathway and is sufficient to promote age-dependent white adipocyte enlargement. Moreover, our findings highlight the potential of COX5B restoration in visceral WAT to counteract age-dependent adipocyte expansion.

EXPERIMENTAL PROCEDURES

White Adipocyte Isolation

Epididymal fat pads were removed, minced, and digested using collagenase type II (Calbiochem) at 37°C for 1 hr in Krebs-Ringer-HEPES-bicarbonate (KRH) buffer supplemented with BSA (3.5%; Roche). The digested tissue was filtered through a 100 μm cell strainer (BD Falcon), and the floating adipocytes were recovered and used for RNA or protein extraction.

Mitochondrial Content

Relative concentrations of nuclear DNA and mtDNA were determined by RT-PCR. In brief, DNA was isolated from adipocytes using UltraPure phenol: chlorofom:isoamyl alcohol (25:24:1; Invitrogen) after proteinase K (Ambion) digestion at 56°C overnight. Nuclear DNA and mtDNA were measured using a Power SYBR Green PCR Master Mix kit (Applied Biosystems). The amplification data were analyzed using StepOne Software v.2.0 (Applied Biosystems). The following primer sets were used: Genomic *Hprt*: forward 5′-TGGGAGGC CATCACATTGT-3′; reverse 5′-TCCAGCAGGTCAGCAAAGAA-3′. Genomic *mt-Co1*: forward 5′-GCTAGCCGCAGGCATTACTATAC-3′; reverse 5′-GCG GGATCAAAGAAAGTTGTG-3′.

Viral Injection In Vivo

Mice were anesthetized by isoflurane (Abbott) before dissection of the skin and body wall. The lentiviral preparation ($1 \times 10^{7-8}$ plaque-forming units in a volume of 100 μl) was injected into the right eWAT depot distributed in four to six injections of 20–25 μl (each mouse was injected with 100–150 μl of lentiviral preparation). The left contralateral eWAT depot remained uninjected and served as an internal control. Separate mice were injected with different lentiviral particles. Mice injected with virus containing small hairpin RNA (shRNA) against *Cox5b* were sacrificed 2–3 weeks after surgery, and the tissues of interest were removed. Mice injected with virus containing overexpressing COX5B were sacrificed 5–6 weeks after surgery, and the tissues of interest were removed. Mice were randomly allocated to the treatment groups (shSCR group versus shCOX5B group, as well as empty vector group versus COX5B group).

Histological Analysis

Adipose tissue from eWAT depots was isolated and fixed for at least 24 hr in 4%–10% formaldehyde before embedding in paraffin. Sections (5–7 μm; Leica RM2135 microtome) were subjected to standard H&E staining and analyzed using CellD Olympus software (Olympus). At least 200 adipocytes per mouse were analyzed for adipocyte surface area measurement. For adipocyte size quantification in eWAT of injected or non-injected mice, $Hif1a^{\Delta Adipo}$ or control mice, and young or aging mice, the investigator was blinded to the group allocation.

Statistical Analysis

Data are expressed as mean ± SEM (error bars). In box and whiskers plots, vertical lines connect the minimum and the maximum values. All statistical analyses were performed using GraphPad Prism software, and differences between groups with similar variances were analyzed with a two-tailed t test. When variances of the groups were significantly different, a two-tailed t test with Welch's correction was used. Differences between variances of the groups were analyzed with the Fisher test (F-test). A p value lower than 0.05 was considered significant: $^{*}p < 0.05$, $^{**}p < 0.01$, and $^{***}p < 0.001$. Differences in human gene expression factors across age quartiles were evaluated using one-way ANOVA. Linear association between gene expression factors and age was evaluated using Spearman's rank test. A multiple linear regression analysis in a stepwise procedure was used to adjust for BMI. Deuremberg-calculated fat mass was evaluated using the following formula: percent fat mass = 1.2 × (BMI) + 0.23 × (age (years)) − 10.8 × (sex) − 5.4, where sex = 0 in women and sex = 1 in men.

Ethics Statement

All animal experimental procedures were approved by the Research Ethics Committee at the Autonomous University of Madrid (UAM). Experiments were carried out under the supervision of the head of animal welfare and health at the UAM and in accordance with Spanish and European guidelines (RD 53/2013; B.O.E, February 1, 2013). Regarding human data, all subjects gave written informed consent after the purpose of the study was explained to them, and the study was approved by the Ethics Committee of the Hospital of Girona.

SUPPLEMENTAL INFORMATION

Supplemental Information includes Supplemental Experimental Procedures and five figures and can be found with this article online at http://dx.doi.org/10.1016/j.celrep.2016.08.041.

AUTHOR CONTRIBUTIONS

I.S.-A. and Q.O.Y.L. conducted most of the experiments. I.S.-A., Q.O.Y.L., K.D.B., and J.A. were involved in the design of the experiments, data analysis, and writing the manuscript. M.T.-C. helped with histological analysis of WAT paraffin sections. A.E., D.T., and E.F. helped with western blotting and gene expression analysis. E.R. and E.B. helped with metabolic measurements. S.V. and A.Z. helped with histological analysis of WAT paraffin sections in global *Hif1a*-deficient mice. F.M.-R. helped with ChIP experiments. D.S. and A.Z. helped with in vivo oxygen consumption experiments. J.A.E., S.C., P.H.-A., and A.M.-R. helped with Blue-Native PAGE experiments. P.H.-A. and A.M.-R. helped with in vitro oxygen consumption experiments. E.F. helped with intracellular lipid accumulation experiments. K.D.B. and K.V. helped with fatty acid oxidation measurements. J.M.M.-N. and J.M.F.-R. helped with gene expression analysis in human WAT samples.

ACKNOWLEDGMENTS

The authors thank Dr. Francisco Sanchez-Madrid, Dr. Manuel O. de Landázuri, Dr. Luis del Peso, Dr. Victor Javier Sanchez-Arevalo, Dr. Barbara Acosta, and Dr. Maria Tiana for scientific advice and critical reading of the manuscript. We also thank Dr. Stefan Offermanns (Max-Planck Institute for Heart and Lung Research) and Prof. Pierre Chambon (GIE-CERB) for helping us to obtain the adipoq-CreERT2 mice. This work was supported by grants from the Ministerio de Educación y Ciencia (SAF2011-29716 and SAF2013-46058-R), Red de Cardiovascular (RD12/0042/0065), CICYT (SAF2007-60592), CAM (P2010/BMD-2542), and the European Commission (ref. 282551).

Received: June 1, 2015
Revised: September 14, 2015
Accepted: August 14, 2016
Published: September 13, 2016

REFERENCES

Bournat, J.C., and Brown, C.W. (2010). Mitochondrial dysfunction in obesity. Curr. Opin. Endocrinol. Diabetes Obes. *17*, 446–452.

Campbell, K.L., Makar, K.W., Kratz, M., Foster-Schubert, K.E., McTiernan, A., and Ulrich, C.M. (2009). A pilot study of sampling subcutaneous adipose tissue to examine biomarkers of cancer risk. Cancer Prev. Res. (Phila.) *2*, 37–42.

Chan, S.Y., Zhang, Y.Y., Hemann, C., Mahoney, C.E., Zweier, J.L., and Loscalzo, J. (2009). MicroRNA-210 controls mitochondrial metabolism during hypoxia by repressing the iron-sulfur cluster assembly proteins ISCU1/2. Cell Metab. *10*, 273–284.

Choo, H.J., Kim, J.H., Kwon, O.B., Lee, C.S., Mun, J.Y., Han, S.S., Yoon, Y.S., Yoon, G., Choi, K.M., and Ko, Y.G. (2006). Mitochondria are impaired in the adipocytes of type 2 diabetic mice. Diabetologia *49*, 784–791.

Dhar, S.S., Ongwijitwat, S., and Wong-Riley, M.T. (2008). Nuclear respiratory factor 1 regulates all ten nuclear-encoded subunits of cytochrome *c* oxidase in neurons. J. Biol. Chem. *283*, 3120–3129.

Eltzschig, H.K., Abdulla, P., Hoffman, E., Hamilton, K.E., Daniels, D., Schönfeld, C., Löffler, M., Reyes, G., Duszenko, M., Karhausen, J., et al. (2005). HIF-1-dependent repression of equilibrative nucleoside transporter (ENT) in hypoxia. J. Exp. Med. *202*, 1493–1505.

Fukuda, R., Zhang, H., Kim, J.W., Shimoda, L., Dang, C.V., and Semenza, G.L. (2007). HIF-1 regulates cytochrome oxidase subunits to optimize efficiency of respiration in hypoxic cells. Cell *129*, 111–122.

Galati, D., Srinivasan, S., Raza, H., Prabu, S.K., Hardy, M., Chandran, K., Lopez, M., Kalyanaraman, B., and Avadhani, N.G. (2009). Role of nuclear-encoded subunit Vb in the assembly and stability of cytochrome *c* oxidase complex: implications in mitochondrial dysfunction and ROS production. Biochem. J. *420*, 439–449.

Gao, C.L., Zhu, C., Zhao, Y.P., Chen, X.H., Ji, C.B., Zhang, C.M., Zhu, J.G., Xia, Z.K., Tong, M.L., and Guo, X.R. (2010). Mitochondrial dysfunction is induced by high levels of glucose and free fatty acids in 3T3-L1 adipocytes. Mol. Cell. Endocrinol. *320*, 25–33.

Gargiulo, S., Gramanzini, M., Megna, R., Greco, A., Albanese, S., Manfredi, C., and Brunetti, A. (2014). Evaluation of growth patterns and body composition in C57Bl/6J mice using dual energy X-ray absorptiometry. BioMed Res. Int. *2014*, 253067.

Gomes, A.P., Price, N.L., Ling, A.J., Moslehi, J.J., Montgomery, M.K., Rajman, L., White, J.P., Teodoro, J.S., Wrann, C.D., Hubbard, B.P., et al. (2013). Declining NAD(+) induces a pseudohypoxic state disrupting nuclear-mitochondrial communication during aging. Cell *155*, 1624–1638.

González-Rodríguez, A., Más-Gutierrez, J.A., Mirasierra, M., Fernandez-Pérez, A., Lee, Y.J., Ko, H.J., Kim, J.K., Romanos, E., Carrascosa, J.M., Ros, M., et al. (2012). Essential role of protein tyrosine phosphatase 1B in obesity-induced inflammation and peripheral insulin resistance during aging. Aging Cell *11*, 284–296.

Gordan, J.D., Bertout, J.A., Hu, C.J., Diehl, J.A., and Simon, M.C. (2007). HIF-2alpha promotes hypoxic cell proliferation by enhancing c-myc transcriptional activity. Cancer Cell *11*, 335–347.

Hosogai, N., Fukuhara, A., Oshima, K., Miyata, Y., Tanaka, S., Segawa, K., Furukawa, S., Tochino, Y., Komuro, R., Matsuda, M., and Shimomura, I. (2007). Adipose tissue hypoxia in obesity and its impact on adipocytokine dysregulation. Diabetes *56*, 901–911.

Houtkooper, R.H., Argmann, C., Houten, S.M., Cantó, C., Jeninga, E.H., Andreux, P.A., Thomas, C., Doenlen, R., Schoonjans, K., and Auwerx, J. (2011). The metabolic footprint of aging in mice. Sci. Rep. *1*, 134.

Jiang, C., Qu, A., Matsubara, T., Chanturiya, T., Jou, W., Gavrilova, O., Shah, Y.M., and Gonzalez, F.J. (2011). Disruption of hypoxia-inducible factor 1 in adipocytes improves insulin sensitivity and decreases adiposity in high-fat diet-fed mice. Diabetes *60*, 2484–2495.

Kaaman, M., Sparks, L.M., van Harmelen, V., Smith, S.R., Sjölin, E., Dahlman, I., and Arner, P. (2007). Strong association between mitochondrial DNA copy number and lipogenesis in human white adipose tissue. Diabetologia *50*, 2526–2533.

Kim, J.Y., van de Wall, E., Laplante, M., Azzara, A., Trujillo, M.E., Hofmann, S.M., Schraw, T., Durand, J.L., Li, H., Li, G., et al. (2007). Obesity-associated improvements in metabolic profile through expansion of adipose tissue. J. Clin. Invest. *117*, 2621–2637.

Koh, E.H., Park, J.Y., Park, H.S., Jeon, M.J., Ryu, J.W., Kim, M., Kim, S.Y., Kim, M.S., Kim, S.W., Park, I.S., et al. (2007). Essential role of mitochondrial function in adiponectin synthesis in adipocytes. Diabetes *56*, 2973–2981.

Krishnan, J., Danzer, C., Simka, T., Ukropec, J., Walter, K.M., Kumpf, S., Mirtschink, P., Ukropcova, B., Gasperikova, D., Pedrazzini, T., and Krek, W. (2012). Dietary obesity-associated Hif1α activation in adipocytes restricts fatty acid oxidation and energy expenditure via suppression of the Sirt2-NAD+ system. Genes Dev. *26*, 259–270.

Kuk, J.L., Saunders, T.J., Davidson, L.E., and Ross, R. (2009). Age-related changes in total and regional fat distribution. Ageing Res. Rev. *8*, 339–348.

Kusminski, C.M., and Scherer, P.E. (2012). Mitochondrial dysfunction in white adipose tissue. Trends Endocrinol. Metab. *23*, 435–443.

Kusminski, C.M., Holland, W.L., Sun, K., Park, J., Spurgin, S.B., Lin, Y., Askew, G.R., Simcox, J.A., McClain, D.A., Li, C., and Scherer, P.E. (2012). MitoNEET-driven alterations in adipocyte mitochondrial activity reveal a crucial adaptive process that preserves insulin sensitivity in obesity. Nat. Med. *18*, 1539–1549.

Lee, K.Y., Gesta, S., Boucher, J., Wang, X.L., and Kahn, C.R. (2011). The differential role of Hif1β/Arnt and the hypoxic response in adipose function, fibrosis, and inflammation. Cell Metab. *14*, 491–503.

Lee, Y.S., Kim, J.W., Osborne, O., Oh, D.Y., Sasik, R., Schenk, S., Chen, A., Chung, H., Murphy, A., Watkins, S.M., et al. (2014). Increased adipocyte O2 consumption triggers HIF-1α, causing inflammation and insulin resistance in obesity. Cell *157*, 1339–1352.

Lindinger, A., Peterli, R., Peters, T., Kern, B., von Flüe, M., Calame, M., Hoch, M., Eberle, A.N., and Lindinger, P.W. (2010). Mitochondrial DNA content in human omental adipose tissue. Obes. Surg. *20*, 84–92.

López-Otín, C., Blasco, M.A., Partridge, L., Serrano, M., and Kroemer, G. (2013). The hallmarks of aging. Cell *153*, 1194–1217.

Lutfi, R., Torquati, A., Sekhar, N., and Richards, W.O. (2006). Predictors of success after laparoscopic gastric bypass: a multivariate analysis of socioeconomic factors. Surg. Endosc. *20*, 864–867.

Maggard, M.A., Shugarman, L.R., Suttorp, M., Maglione, M., Sugerman, H.J., Livingston, E.H., Nguyen, N.T., Li, Z., Mojica, W.A., Hilton, L., et al. (2005). Meta-analysis: surgical treatment of obesity. Ann. Intern. Med. *142*, 547–559.

Ng, M., Fleming, T., Robinson, M., Thomson, B., Graetz, N., Margono, C., Mullany, E.C., Biryukov, S., Abbafati, C., Abera, S.F., et al. (2014). Global, regional, and national prevalence of overweight and obesity in children and adults during 1980–2013: a systematic analysis for the Global Burden of Disease Study 2013. Lancet *384*, 766–781.

Ogden, C.L., Carroll, M.D., Kit, B.K., and Flegal, K.M. (2013). Prevalence of obesity among adults: United States, 2011–2012. NCHS Data Brief *131*, 1–8.

Rong, J.X., Qiu, Y., Hansen, M.K., Zhu, L., Zhang, V., Xie, M., Okamoto, Y., Mattie, M.D., Higashiyama, H., Asano, S., et al. (2007). Adipose mitochondrial biogenesis is suppressed in db/db and high-fat diet-fed mice and improved by rosiglitazone. Diabetes *56*, 1751–1760.

Rosen, E.D., and Spiegelman, B.M. (2014). What we talk about when we talk about fat. Cell *156*, 20–44.

Saraste, M. (1999). Oxidative phosphorylation at the fin de siècle. Science *283*, 1488–1493.

Scozzari, G., Passera, R., Benvenga, R., Toppino, M., and Morino, M. (2012). Age as a long-term prognostic factor in bariatric surgery. Ann. Surg. *256*, 724–728, discussion 728–729.

Sena, L.A., and Chandel, N.S. (2012). Physiological roles of mitochondrial reactive oxygen species. Mol. Cell *48*, 158–167.

Sutherland, L.N., Capozzi, L.C., Turchinsky, N.J., Bell, R.C., and Wright, D.C. (2008). Time course of high-fat diet-induced reductions in adipose tissue mitochondrial proteins: potential mechanisms and the relationship to glucose intolerance. Am. J. Physiol. Endocrinol. Metab. *295*, E1076–E1083.

Valerio, A., Cardile, A., Cozzi, V., Bracale, R., Tedesco, L., Pisconti, A., Palomba, L., Cantoni, O., Clementi, E., Moncada, S., et al. (2006). TNF-alpha downregulates eNOS expression and mitochondrial biogenesis in fat and muscle of obese rodents. J. Clin. Invest. *116*, 2791–2798.

van Harmelen, V., Skurk, T., Röhrig, K., Lee, Y.M., Halbleib, M., Aprath-Husmann, I., and Hauner, H. (2003). Effect of BMI and age on adipose tissue cellularity and differentiation capacity in women. Int. J. Obes. Relat. Metab. Disord. *27*, 889–895.

Vernochet, C., Mourier, A., Bezy, O., Macotela, Y., Boucher, J., Rardin, M.J., An, D., Lee, K.Y., Ilkayeva, O.R., Zingaretti, C.M., et al. (2012). Adipose-specific deletion of TFAM increases mitochondrial oxidation and protects mice against obesity and insulin resistance. Cell Metab. *16*, 765–776.

Vernochet, C., Damilano, F., Mourier, A., Bezy, O., Mori, M.A., Smyth, G., Rosenzweig, A., Larsson, N.G., and Kahn, C.R. (2014). Adipose tissue mitochondrial dysfunction triggers a lipodystrophic syndrome with insulin resistance, hepatosteatosis, and cardiovascular complications. FASEB J. *28*, 4408–4419.

Villarroya, J., Giralt, M., and Villarroya, F. (2009). Mitochondrial DNA: an up-and-coming actor in white adipose tissue pathophysiology. Obesity (Silver Spring) *17*, 1814–1820.

Yang, S.B., Tien, A.C., Boddupalli, G., Xu, A.W., Jan, Y.N., and Jan, L.Y. (2012). Rapamycin ameliorates age-dependent obesity associated with increased mTOR signaling in hypothalamic POMC neurons. Neuron *75*, 425–436.

Ye, J., Gao, Z., Yin, J., and He, Q. (2007). Hypoxia is a potential risk factor for chronic inflammation and adiponectin reduction in adipose tissue of ob/ob and dietary obese mice. Am. J. Physiol. Endocrinol. Metab. *293*, E1118–E1128.

Yin, J., Gao, Z., He, Q., Zhou, D., Guo, Z., and Ye, J. (2009). Role of hypoxia in obesity-induced disorders of glucose and lipid metabolism in adipose tissue. Am. J. Physiol. Endocrinol. Metab. *296*, E333–E342.

Yin, X., Lanza, I.R., Swain, J.M., Sarr, M.G., Nair, K.S., and Jensen, M.D. (2014). Adipocyte mitochondrial function is reduced in human obesity independent of fat cell size. J. Clin. Endocrinol. Metab. *99*, E209–E216.

ANTIOXIDANTS & REDOX SIGNALING
Volume 18, Number 3, 2013

DOI: 10.1089/ars.2012.4765

Discoveries

FORUM REVIEW ARTICLE

Nitrosothiols in the Immune System: Signaling and Protection

Pablo Hernansanz-Agustín,[1,*] Alicia Izquierdo-Álvarez,[1,*] Almudena García-Ortiz,[2,*] Sales Ibiza,[3,‡] Juan M. Serrador,[2,†] and Antonio Martínez-Ruiz[1,†]

Abstract

Significance: In the immune system, nitric oxide (NO) has been mainly associated with antibacterial defenses exerted through oxidative, nitrosative, and nitrative stress and signal transduction through cyclic GMP-dependent mechanisms. However, S-nitrosylation is emerging as a post-translational modification (PTM) involved in NO-mediated cell signaling. ***Recent Advances:*** Precise roles for S-nitrosylation in signaling pathways have been described both for innate and adaptive immunity. Denitrosylation may protect macrophages from their own S-nitrosylation, while maintaining nitrosative stress compartmentalized in the phagosomes. Nitrosothiols have also been shown to be beneficial in experimental models of autoimmune diseases, mainly through their role in modulating T-cell differentiation and function. ***Critical Issues:*** Relationship between S-nitrosylation, other thiol redox PTMs, and other NO-signaling pathways has not been always taken into account, particularly in the context of immune responses. Methods for assaying S-nitrosylation in individual proteins and proteomic approaches to study the S-nitrosoproteome are constantly being improved, which helps to move this field forward. ***Future Directions:*** Integrated studies of signaling pathways in the immune system should consider whether S-nitrosylation/denitrosylation processes are among the PTMs influencing the activity of key signaling and adaptor proteins. Studies in pathophysiological scenarios will also be of interest to put these mechanisms into broader contexts. Interventions modulating nitrosothiol levels in autoimmune disease could be investigated with a view to developing new therapies. *Antioxid. Redox Signal*. 18, 288–308.

Introduction

SINCE THE RECOGNITION of nitric oxide (NO) as a second messenger in vertebrate cardiovascular and nervous systems, a classical signaling pathway has been established in which NO produced by nitric oxide synthase (NOS) stimulates soluble guanylate cyclase activation, cyclic GMP (cGMP) production, and cGMP-activated protein kinases (cGKs or PKGs). In addition, a less-classical pathway involves the inhibition of mitochondrial cytochrome *c* oxidase (complex IV of the electron transport chain), which has a profound influence on cell metabolism and homeostasis. Apart from these modes of action, several nonclassical mechanisms have been described, which include NO production from other sources such as nitrite anion (NO_2^-) and the covalent post-translational modification (PTM) of proteins provoked by the so-called reactive nitrogen species (RNS), a series of chemical species derived from reactions of NO with other small molecules [reviewed in Ref. (106)].

Among the PTMs induced by RNS, S-nitrosylation [also called S-nitrosation: see (42, 75, 108) for a discussion of the terminology] has emerged as an important signaling pathway related to NO production, with some particularities in terms of specificity that have been discussed elsewhere (30, 64, 90, 106, 108). It consists in the formation of a nitrosothiol (RSNO, also called thionitrite) at a protein cysteine thiol (RSH), which can potentially be achieved through several possible chemical mechanisms (41, 56, 64). Different structural motifs may confer specificity to particular cysteine residues in protein chains (32, 102), suggesting that these distinct pathways may coexist in any given biochemical environment. As NO itself is rarely a direct S-nitrosylating agent (unless it reacts with a thyil radical in the protein cysteine), most of these

[1]Servicio de Inmunología, Hospital Universitario de La Princesa, Instituto de Investigación Sanitaria Princesa (IP), Madrid, Spain.
[2]Dpto. Biología Celular e Inmunología, Centro de Biología Molecular "Severo Ochoa," CSIC-UAM, Madrid, Spain.
[3]Centro Nacional de Investigaciones Cardiovasculares (CNIC), Madrid, Spain.
*These authors contributed equally to this work amongst themselves.
†These authors contributed equally to this work amongst themselves and are both senior authors.
‡*Current affiliation:* Immunobiology Unit, Instituto de Medicina Molecular, Faculdade de Medicina de Lisboa, Lisboa, Portugal.

mechanisms proceed through formation of RNS. Other important parameters driving the specificity of S-nitrosylation signaling are subcellular compartmentalization and the proximity to or interaction with NOS, as well as the presence of denitrosylases and the recently described transnitrosylase activities (12, 30, 88, 106, 108, 124, 166, 190).

S-nitrosylation is one of several oxidative PTMs produced at cysteine thiols, such as formation of sulfenic, sulfinic, or sulfonic acid, of protein intra- or intermolecular disulfide bridges, or of mixed disulfides with low molecular mass thiols (S-thiolation, termed S-glutathionylation when formed with glutathione [GSH]). The relationships among them are complex, including shared and differential roles in cell signaling and nitroxidative stress (75, 109). In particular, S-nitrosylation has been shown to induce disulfide bridges, and especially S-glutathionylation (5, 109, 183). Indeed, this should be taken into account when studying the effect of NO donors and nitrosothiols, as they can produce different types of modifications (106, 109). For example, S-nitrosoglutathione (GSNO) is not only a nitrosylating agent but also a glutathionylating agent (106, 147, 183).

We review here several recently uncovered aspects of the role of S-nitrosylation in the mammalian immune system. One of them is the influence of S-nitrosylation in toll-like receptor (TLR) activation and signaling, through the modification of several proteins and pathways that are mainly involved in innate immunity, a good example of which is surfactant protein D (SP-D) modification in the alveolar system. Understanding the mechanisms that protect macrophages against their own unbalanced S-nitrosylation when they are activated through pathways that induce high NO and RNS production also reflects the implication of nitrosothiol in innate immunity. NF-kB activation is modulated by S-nitrosylation at many points of its pathway, which is common to innate and adaptive immunity. As such, we discuss this in a middle chapter, together with other proteins and pathways that are S-nitrosylated and that fulfill diverse roles in the immune system. In adaptive immunity, most studies dealing with the role of S-nitrosylation have been conducted on T cells. S-nitrosylation has been described to take part in specific signaling pathways during T-cell activation, while it inhibits T-cell development in the thymus. Finally, we review studies that have described a role for S-nitrosylation and NO production in the differentiation and function of the T-helper cell subsets involved in chronic inflammatory diseases of autoimmune origin, for which treatments with nitrosothiols have been shown to be beneficial in many cases.

In recent years, S-nitrosylation has been shown to play an important role in the plant immune response, sharing given mechanisms with animals [for recent references, see Refs. (100, 196)], even though the existence of NOS has yet to be confirmed in plants (47). While it would certainly be interesting to compare this response in both kingdoms, this is beyond the scope of this review. So is the effect of S-nitrosylation on the microbes that are attacked by the immune system, for example, those engulfed by phagocytic cells, which is covered in another review in this Forum (91a), and in another recent review covering several chemical mechanisms that depend on ROS and RNS (186).

Nitrosothiols in Innate Immunity

An early defense against infectious agents requires the participation of innate immune responses, a set of cellular and biochemical mechanisms representing the organism's first line of defense to pathogens. Physical and chemical barriers (*e.g.,* the respiratory epithelial mucosa and compounds with antimicrobial activity), cytokines, and phagocytic cells (*e.g.,* neutrophils and macrophages) are the main effectors of innate immunity. Among the mechanisms by which phagocytes exert their functions, recent attention has been given to TLRs, a family of transmembrane proteins that recognize microbe-derived molecules, many of which are bacterial wall constituents. TLRs increase phagocytosis and cytokine production mainly through the NF-kB signaling pathway. Ligand binding to the TLR induces the association of the adaptor MyD88 to its cytoplasmic domain, the recruitment of interleukin-1 receptor (IL-1R)-associated kinase (IRAK) and TRAF-6, and the ensuing activation of IκB-kinase (IKK), which in turn activates NF-κB by inhibiting IκB. This enhances the production of the proinflammatory cytokines tumor necrosis factor (TNF)-α, IL-1β, and IL-12 and the expression of adhesion molecules in activated endothelial cells, which favors the recruitment of leukocytes to inflammatory foci.

Role of SP-D S-nitrosylation in TLR activation

Pulmonary surfactant was initially described as a complex of lipids and proteins that reduces the surface tension at the air–liquid interface in the alveoli, thus avoiding atelectasis or collapsed lung. However, recent studies indicate that a surfactant also plays an active role in the innate immune response (89, 157, 188). Four surfactant proteins have been described that belong to the family of collagen-like lectins or collectins: surfactant protein A (SP-A), B (SP-B), C (SP-C), and D (SP-D). The N-terminal domain of the SP-D monomer contains two key Cys residues (Cys15 and Cys20), a collagen-like domain, a neck region formed by a short α-helix, and a C-type carbohydrate-recognition domain (CRD) through which it interacts with anionic phospholipids and complex carbohydrates present in pathogens in a Ca^{2+}-dependent manner (27, 136, 157). It is worth noting that the SP-D monomer does not seem to be biologically active, but rather the monomers interact through their collagen-like domains to form trimers, which can oligomerize into a dodecamer through their N-terminal domains, forming a cruciform structure (27, 136). This new structure is also able to participate in higher orders of multimerization (27).

SP-A and SP-D have a pathogen-dependent proinflammatory function (49), yet conversely, in a noninflammatory scenario, these collectins can bind to the signal inhibitory regulatory protein α (SIRP-α) *via* their CRD, leading to the activation of SHP-1 and inhibition of p38 mitogen-activated protein kinase (MAPK), and thereby suppressing the synthesis of proinflammatory mediators. However, SP-A and SP-D interact with pathogens or apoptotic cells through the CRD, allowing the collagen-like domain at the N-terminus to be presented to calreticulin/CD91, and therefore triggering a proinflammatory response through p38 activation. Thus, SP-A and SP-D can act as both anti-inflammatory and proinflammatory molecules depending on the environment within the lung (49). SP-D hides its N-terminal within the dodecamer structure, so its quaternary structure might be crucial for its immunomodulatory function. Indeed, oligomerization of SP-D (where disulfide bridges form between Cys15 and Cys20) has been demonstrated to be critical for their dual inflammatory role (17, 63, 194).

Recently, S-nitrosylation of Cys15 and Cys20 has been shown to play a pivotal role in oligomerization (7, 57), reviewed in Ref. (6). This modification disassembles the dodecamer into trimers, producing macrophage chemotaxis and triggering a proinflammatory response by activating calreticulin/CD91-dependent p38 (57). Under certain conditions, such as in the presence of pathogen or under nitrosative stress, S-nitrosylation of SP-D could drive the switch between anti- and proinflammatory activity. As mentioned above, dodecameric SP-D would act as an anti-inflammatory molecule in basal conditions. Alternatively, S-nitrosylation of SP-D disassembles the oligomer into trimers, with the N-terminal domain exposed and ready to interact with calreticulin/CD91, promoting the proinflammatory cascade (6, 57) (Fig. 1).

In models of acute lung injury, such as an 8-day exposure to bleomycin, SP-D S-nitrosylation is reduced by 80% in inducible nitric oxide synthase (iNOS) knockout mice, suggesting that this modification is mostly produced by iNOS activity (57). Thus, since iNOS is expressed in inflammatory scenarios, S-nitrosylation of SP-D would produce positive proinflammatory feedback (57).

Some questions still require further study. The oligomeric form of SP-D can bind to TLR4 (132) and inhibit the TLR4-dependent proinflammatory response (194). Thus, it would be of interest to determine whether S-nitrosylation of SP-D might allow TLR4 receptors to dimerize, activating and promoting p38-dependent synthesis of proinflammatory mediators. Likewise, it remains unknown whether S-nitrosylation of Cys15/Cys20 in SP-D is necessary for its interaction with calreticulin/CD91. Finally, it would be very interesting to assess if other oxidative modifications of these Cys residues might have a similar functional relevance.

Macrophage activation and self-protection by denitrosylases

Macrophage activation by proinflammatory cytokines (such as interferon-γ [IFN-γ], produced by other immune cells) or lipopolysaccharide (LPS) (from the bacterial walls) upregulates iNOS transcription, which produces a burst of NO. This NO acts as a part of the antimicrobial armory of these cells, and among other effects (186), it may inactivate through S-nitrosylation essential proteins of phagocytosed cells (146). A murine cell line, RAW 264.7, has frequently been used as a model of macrophage induction to study the role of S-nitrosylation. Early studies showed that when these cells were activated by LPS and IFN-γ, the amount of S-nitrosothiols in cell extracts clearly increases, mainly in the protein fraction (36), which was subsequently confirmed in the same cells (54, 199) and in the J774 macrophage cell line (37). In RAW 264.7 cells, when the intracellular levels of nitrosothiols have been measured after either the treatment of cells with exogenous transnitrosylating agents or the endogenous induction of iNOS, it seems clear that endogenous iNOS induction produces relatively lower amounts of nitrosothiols, even though considerable amounts of iNOS-derived NO are produced (nitrosothiols are estimated at about 0.02% of the nitrite generated) (199, 200). It is worth noting that in J774 cells, bacterial infection was recently reported to reduce the nitrosothiol content of activated macrophages, a process dependent on genes thought to detoxify NO in such bacteria, namely *nor*B

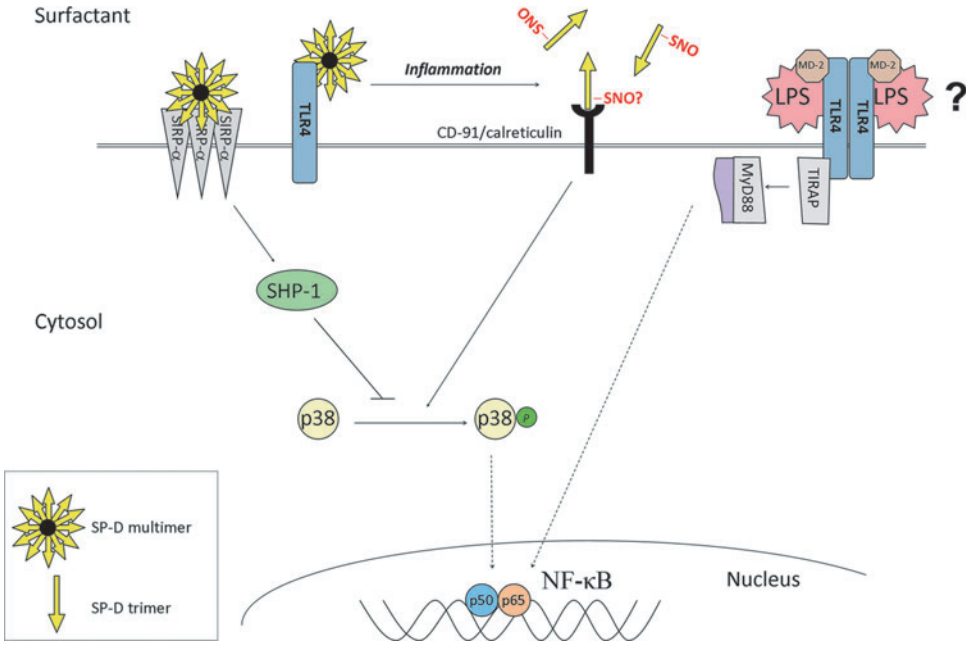

FIG. 1. S-nitrosylation modulates the quaternary structure and function of surfactant protein D (SP-D). The SP-D dodecamer binds to signal inhibitory regulatory protein α (SIRP-α) and inhibits p38 mitogen-activated protein kinase (MAPK) activation *via* SHP-1, and it also binds toll-like receptor 4 (TLR4), thereby avoiding its dimerization and subsequent activation. Upon S-nitrosylation, SP-D dodecamers disassemble into trimers, which bind to CD-91/calreticulin, a process that activates p38 MAPK and triggers a proinflammatory response. Dodecamer disassembly might allow TLR4 dimerization and downstream activation of NF-κB (To see this illustration in color, the reader is referred to the web version of this article at www.liebertpub.com/ars).

(*Neisseria meningitidis*, meningococcus) and flavohemoglobin, *Hmp* (*Salmonella enterica* and *Escherichia coli*) (92).

Despite producing large amounts of NO, activated macrophages may protect themselves against their own production of such toxic levels of NO and related RNS. It is now clear that denitrosylases may participate in this protection by acting on nitrosothiols in proteins and low-molecular-mass thiols, such as GSH. Two main denitrosylases have been described, which are related to redox pathways: GSH coupled to GSNO reductase (GSNOR) (76, 96); and thioredoxin (Trx), coupled to Trx reductase and NADPH (168) [reviewed in Ref. (12); Fig. 2].

GSNOR (also known as GSH-dependent formaldehyde dehydrogenase) breaks GSNO, and it has been shown to reduce protein S-nitrosylation levels, at least in a subset of proteins whose S-nitrosylation would be in equilibrium with GSH modification (96). Mice with a targeted deletion of GSNOR suffer increased S-nitrosylation and mortality after endotoxic shock induced by LPS, revealing a role in the regulation of innate immunity (98). In a recent report, a GSNOR inhibitor profoundly affected the expression of a number of proteins in activated macrophages (45). By using quantitative general proteomics (*i.e.*, directed at the general proteome and not identifying S-nitrosylated proteins), it has been shown that several inflammatory mediators are downregulated when GSNOR is inhibited, including iNOS, cyclooxygenase-2 (COX-2), and osteopontin, whereas targets of the Nrf2 transcription factor were upregulated, like heme oxygenase-1 and glutamate–cysteine ligase modulatory subunit. These results suggest that a feedback cycle might finely tune the presence and activity of iNOS, in which Nrf2 may also be implicated (45). Another protein susceptible of regulation by denitrosylation is histone deacetylase 2 (HDAC2). HDAC2 is inactivated through S-nitrosylation in alveolar macrophages from chronic obstructive pulmonary disease, which confers cell resistance to corticosteroid treatment. In this setting, GSH treatment and induction of Nrf2 restored HDAC2 activity and corticosteroid sensitivity, although this GSH- and Nrf2-dependent mechanism of denitrosylation was not identified (99).

The role of Trx in denitrosylating particular proteins has been studied in detail for some proteins such as caspase-3 (11, 13) as well as using proteomic approaches (see below). It is not clear if there is an increase in denitrosylation activity during macrophage activation, or if the basal denitrosylation activity is sufficient to cope with the increased RNS produced by iNOS induction. Negative feedback regulators of NOS-dependent S-nitrosylation have been postulated; for example, the Trx-interacting protein (Txnip) that inhibits Trx denitrosylation is in turn inhibited by increased NO levels. Thus, Trx denitrosylation activity is increased when NO is produced (43). In addition, Trx itself is a target of S-nitrosylation at several residues, whose specificity is different in the reduced and oxidized forms (10), and it can act also as a transnitrosylase (118, 189, 190) [reviewed in Ref. (159)]. Therefore, more detailed studies on the different roles of Trx in the regulation of S-nitrosylation in macrophages will be necessary to address this issue.

Further protection could arise through the precise subcellular localization of iNOS in the activated macrophages. Early reports showed that in primary macrophages, iNOS localizes in vesicles that could translocate to phagosomes (178). Each of the three NOS isoforms bears different structural features at the N- and C-termini that influence their subcellular location. Cysteine palmitoylation at the N-terminus of iNOS has been shown to be needed for vesicle association and correct trafficking of the protein through the Golgi apparatus to apical positions in polarized cells, which is needed for the vectorial synthesis and release of NO (125, 126). However, to our knowledge, this has not been studied in macrophages. The four C-terminal amino acids in iNOS, which become inserted

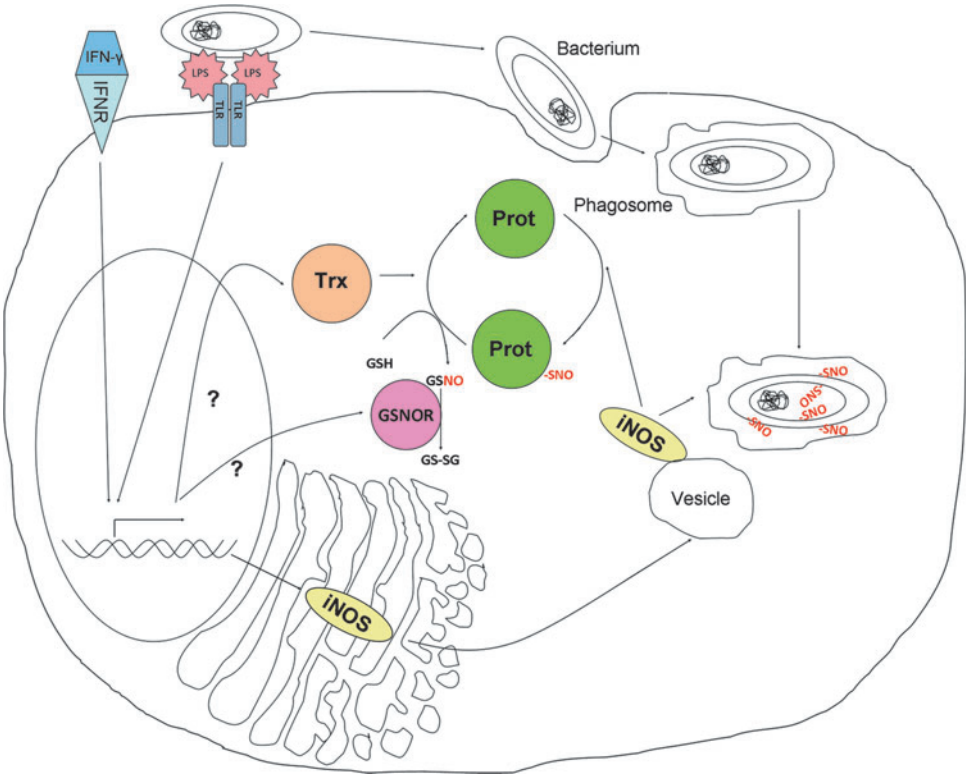

FIG. 2. Macrophages protect themselves from inducible nitric oxide synthase (iNOS)-induced S-nitrosylation. Pro-inflammatory stimuli, such as interferon-γ (IFN-γ) and lipopolysaccharide (LPS), trigger iNOS expression. This iNOS associates with vesicles through the Golgi, and it may be recruited to phagosomes where it produces large amounts of NO that can S-nitrosylate protein targets in a phagocyted cell, such as a bacterium. Thioredoxin (Trx) and glutathione (GSH)/S-nitrosoglutathione reductase (GSNOR) may denitrosylate macrophage proteins that become modified (To see this illustration in color, the reader is referred to the web version of this article at www.liebertpub.com/ars).

within PDZ domains, are also needed for its apical localization in polarized cells (51, 127). Likewise, in macrophages, the iNOS C-terminus interacts with the PDZ domains of the cytoskeleton scaffolding protein EBP50, which directs iNOS to the phagosomes (29). Interestingly, the *EBP50* gene is induced in parallel to iNOS, and its recruitment is impaired in *Mycobacterium tuberculosis*-infected phagosomes, which explains the previously observed exclusion of iNOS from these phagosomes (29, 116).

Macrophage activation, particularly in the murine cell line RAW 264.7, has been frequently used as a model for the study of the S-nitrosoproteome, illustrating the sensitivity of the proteomic methods employed to identify S-nitrosylated proteins. By 2001, more than 100 S-nitrosylated proteins had been described [see Table S1 in Ref. (167)], all studied on an individual basis. The original biotin-switch technique (BST) described by Jaffrey *et al.* (74) opened the way to study the S-nitrosoproteome, by describing a method that allowed derivatized S-nitrosylated proteins to be purified, and employing emergent proteomic techniques to identify the purified subproteome. However, one study concluded that such methodology only detected S-nitrosylated proteins when RAW 264.7 cells were treated with at least 100 μM extracellular S-nitroso-L-cysteine, which gave an intracellular S-nitrosothiol concentration of around 500 nmol/mg protein (201), well above that produced by endogenous iNOS activation by proinflammatory cytokines (around 100 pmol/mg protein) (36, 54, 199). We obtained similar results, as we were able to detect and identify S-nitrosylated proteins in endothelial cells treated with extracellular S-nitroso-L-cysteine (107, 111), but we did not detect S-nitrosylation differences in RAW 264.7 cells after cytokine-dependent induction and activation of iNOS [results published in Ref. (174), Fig. 3]. However, another study reported an increase in the S-nitrosylated protein signal using the BST, identifying up to 15 proteins modified after cytokine treatment of RAW 264.7 cells (48).

The use of fluorescent derivatization instead of biotin labeling, coupled to two-dimensional electrophoresis (2-DE), has increased the sensitivity of proteomic techniques to study the S-nitrosoproteome. Although the depth of the proteome has not been increased (*i.e.*, the number of identified proteins is not much higher), this approach implies that the starting material may be 20-fold less (174). However, when applied to RAW 264.7 cells activated with LPS/IFN-γ, we were only able to detect differentially S-nitrosylated proteins when we included auranofin, an inhibitor of the Trx pathway, thereby identifying putative targets denitrosylated by this pathway (174). A two-fluorophore scheme for derivatizing S-nitrosothiols has also been used to detect an overall increase in S-nitrosylation in cytokine-stimulated RAW 264.7 cells, mixing samples from nonactivated and activated cells in the same 2-DE (152). Compared to a one-fluorophore one-sample-per-gel scheme (174), this approach has two problems: first, each fluorophore signal has a different normalization parameter; and second, the amount of total protein in each spot from each sample is not analyzed, and thus the variations in the S-nitrosylation signal for a spot may simply be due to a change in protein abundance [reviewed in Ref. (73)].

Development of more sensitive proteomic methods will help to study the S-nitrosoproteome associated with macrophage activation and the role of the protection mechanisms. These advances may come from both general improvements in proteomic techniques, such as the use of more powerful mass spectrometers, as well as through the development of improved protocols and techniques for the specific detection of this modification. Recent advances in the application of quantitative second-generation proteomics (based on large-scale identification of peptides by tandem mass spectrometry), coupled to improved derivatization and purification of S-nitrosylated peptides, could produce advances in the field, even in the detection of S-nitrosylated proteins under basal conditions (32, 44). In the RAW 264.7 cell model of cytokine

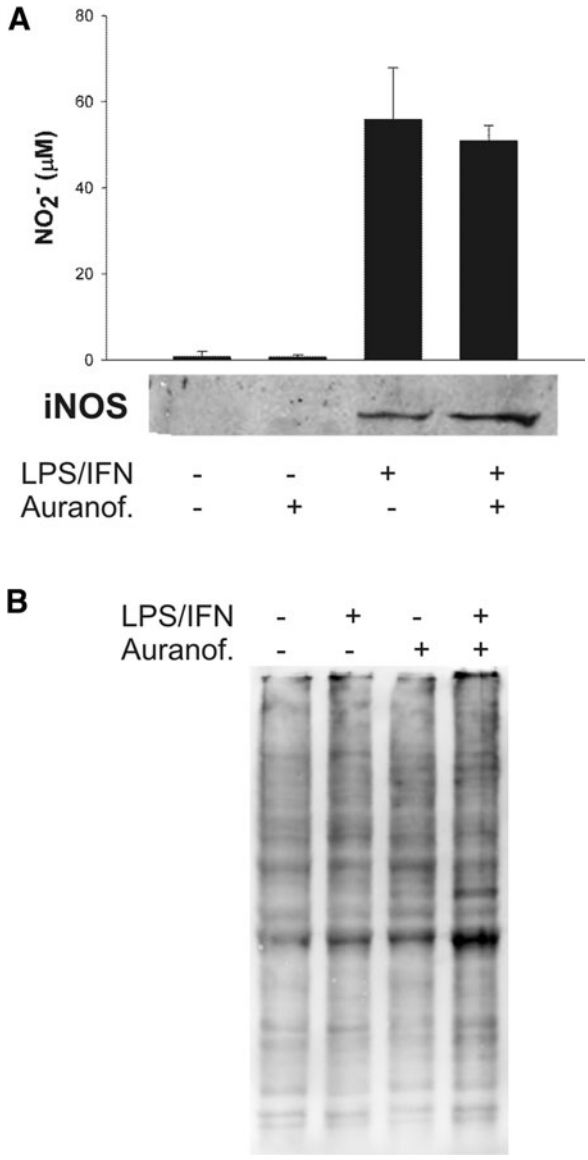

FIG. 3. The biotin-switch technique (BST) is not sensitive enough to detect endogenous S-nitrosylation produced by iNOS activation in macrophages. (A) Murine macrophage cell line RAW 264.7 was treated with LPS and IFN-γ, and with auranofin, producing iNOS that was detected in western blots and NO measured as extracellular nitrite with the Griess reagent. **(B)** Cell extracts were subjected to the BST, blotted, and detected with avidin. Although there is a clear increase in iNOS-derived NO production after LPS + IFN-γ activation, differences in S-nitrosylation are only observed when the Trx pathway is inhibited with auranofin. Reprinted by permission from Tello *et al.* (174).

activation, two methods have recently been applied that use stable isotope labeling in culture or label-free spectral counting, coupled to the purification of derivatized S-nitrosylated peptides. Through these methods, 17 or 27 proteins were described that were S-nitrosylated after cytokine activation (198, 203).

More detailed studies on the S-nitrosoproteome of macrophages during activation, combined with studies into the role of S-nitrosylation in particular proteins, could shed light on the mechanisms that could be operating in self-protection (such as denitrosylation and subcellular localization), as well as on the interaction with phagocytosed cells.

S-Nitrosylation in Innate and Adaptive Immunity

NF-κB pathway and S-nitrosylation

NF-κB is a heterodimeric transcription factor, usually comprised of a p50 and p65 subunit, which controls the expression of many genes involved in innate and adaptive immune responses, including proinflammatory cytokines and adhesion receptors. The activation of NF-κB itself is controlled by a tightly regulated protein cascade. In the basal state, the p50–p65 heterodimer is bound to the inhibitor of NF-κB (IκB), which maintains the transcription factor inactivated. IκB phosphorylation by the IKK complex (IKKα, IKKβ, and IKKγ) promotes IκB degradation by the 26S proteasome and the subsequent liberation, translocation into the nucleus, and DNA binding of NF-κB (50). Distinct stimuli trigger NF-κB activation (*e.g.*, TNF-α, IFN-γ, IL-1β, or LPS) through a series of pathways that converge on the activation of the IKK complex (66).

NO from exogenous sources or endogenous iNOS expression can modulate the promoter and DNA-binding activity of NF-κB in cells. Indeed, some elements of the activation pathway of NF-κB, including the subunits of the transcription factor itself, have been shown to be modified by S-nitrosylation (Fig. 4).

The p50 subunit of NF-κB is S-nitrosylated at a cysteine residue located in its DNA-binding domain, which inhibits its binding to DNA, and thereby decreases the proinflammatory response (104). Interestingly, S-glutathionylation of the same cysteine residue also inactivates its DNA binding (137), a modification likely to be induced by GSNO (86). Likewise, p65 can also be S-nitrosylated, producing similar consequences, and so nitrosylation of both NF-κB subunits results in its inactivation (81). IKKβ has also been shown to be S-nitrosylated at Cys179, a modification capable of modulating kinase function independently of phosphorylation, since IKKβ activity is abrogated after S-nitrosylation after TNF-α activation (145).

Other elements upstream of NF-κB activation are also S-nitrosylated. Treatment of the nonreceptor protein tyrosine kinase $p60^{Src}$ (Src) with nitrosothiol results in Src activation through autophosphorylation at Tyr416 and the formation of multimers, an action presumably exerted through S-nitrosylation at Cys498 and/or the formation of disulfide bridges between Src monomers (3, 5, 142). Furthermore, in the TLR-dependent pathway of NF-κB activation, S-nitrosylation of MyD88 disrupts its binding to the upstream Toll/IL-1R adaptor protein (TIRAP), but not to the downstream IRAK-1, which might influence the delayed development of the acute immune response (70).

CD40 is a member of the TNF receptor (TNFR) family that when stimulated by CD40L activates the NF-κB pathway (20). S-nitrosylation of the CD40 extracellular domain occurs in quiescent macrophages and monocytes, whereas denitrosylation is produced after activation by CD40L (52). This

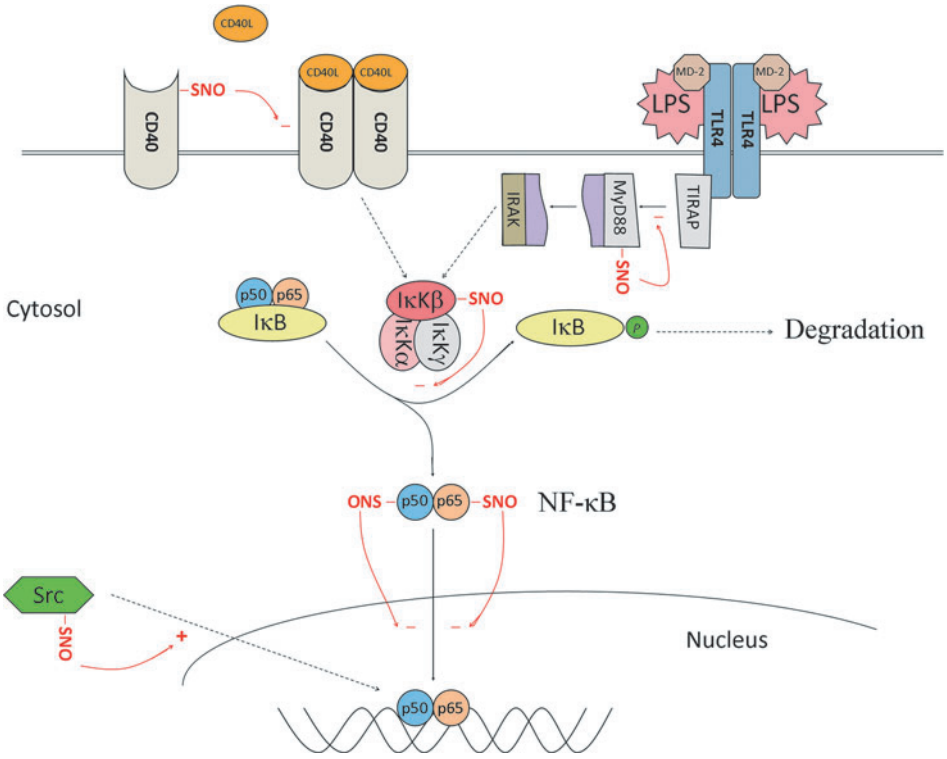

FIG. 4. The NF-κB activation pathway is regulated by S-nitrosylation. S-nitrosylation of the p50 and p65 subunits of NF-κB causes the inhibition of its binding to DNA. Upstream inhibition of the IκB-kinase (IKK) complex's kinase activity is induced by S-nitrosylation of the IKKβ subunit, abrogating NF-κB activation. S-nitrosylation of CD40 inhibits binding and activation by CD40L. MyD88 S-nitrosylation disrupts binding to its upstream partner toll/interleukin-1 receptor adaptor protein (TIRAP), which might serve to delay the development of the immune response. On the other hand, S-nitrosylation of Src may activate NF-κB (To see this illustration in color, the reader is referred to the web version of this article at www.liebertpub.com/ars).

modification blocks CD40 signal transduction, such that CD40 denitrosylation could be a prerequisite for macrophage activation *via* the CD40 pathway (52). Indeed, CD40 denitrosylation was observed in mice injected with LPS and in monocytes from patients suffering severe sepsis or septic shock (52).

It is worth noting that the *iNOS* gene promoter itself contains NF-κB response elements, and that this transcription factor is important for iNOS expression (81). Thus, it is feasible that negative feedback onto S-nitrosylation-dependent NF-κB inactivation should be taken into account. In this mechanism, inactivation of IKK/NF-κB by S-nitrosylation could downregulate iNOS expression and the associated S-nitrosylation activity, an effect reinforced by the fact that iNOS itself is susceptible to inactivation by S-nitrosylation (117, 163). As a result, NF-κB activation may be equilibrated in cells, and the levels of NF-κB-induced cytokines and endothelial adhesion molecules (vascular cell adhesion protein 1, intercellular adhesion molecule 1, and E- and P-selectins) sustained for leukocyte extravasation and function.

As shown by several groups, S-nitrosylation can affect the NF-κB activation pathway at several points, from the upstream molecules to the transcription factor itself. Although most of the described S-nitrosylation targets (MyD88, CD40, IKKβ, p50, and p65) inhibit the pathway, the modification of SP-D and Src may activate it. Hence, further studies should discriminate how these different modifications are integrated in the regulation of NF-kB.

S-nitrosylation of other relevant proteins and pathways

S100A8 expression is induced by inflammatory mediators of oxidative stress in macrophages, microvascular endothelial cells, fibroblast, and keratinocytes. It has chemotactic-, antimicrobial-, apoptosis-inducing and growth-inhibitory properties (143). S-nitrosylation of S100A8 at Cys41 could be important in the resolution of inflammation given that this modification suppresses mast cell degranulation and mast-cell-mediated inflammation in the microcirculation (95). Interactions between S100A8 and NO produced by endothelial cells may also alter endothelial cell–leukocyte interactions in the microcirculation (95).

C-Jun N-terminal kinase (JNK) belongs to the MAPK family, and it is the terminal kinase in a pathway composed by MEKK1 and MKK4/7. Phosphorylation of JNK allows it to activate target proteins such as c-Jun, a component of the AP-1 transcription factor. This pathway is involved in many different cell activities, including apoptosis, survival, and proliferation. In macrophages activated by IFN-γ, when NO is produced, the activity of JNK is inhibited by a redox mechanism compatible with S-nitrosylation and dependent on Cys116 (134). This effect is independent of its upstream partners and of antagonistic stimuli (134), and it may be mediated by the disruption of the interaction between JNK and c-Jun (135). Interestingly, this cysteine residue is only conserved among the JNK subgroup of MAPK, which suggests a specific role for this mechanism that could participate in resolving the inflammatory response (60). As in the case of the NF-κB pathway, more complex regulation could occur, as c-Jun DNA-binding activity is also inhibited by NO-dependent S-glutathionylation at a critical Cys residue (85), although we do not know of any study specifically assessing S-nitrosylation of that residue.

During the inflammatory process, COX-2, a key enzyme in prostaglandin synthesis, is activated over a similar time course to iNOS, and crosstalk between these enzymes was suspected as iNOS-derived NO had been shown to activate COX (151). In microglia and activated macrophages, iNOS has been shown to bind and S-nitrosylate COX-2, increasing its activity (83). Interestingly, COX-2 S-nitrosylation depends on direct interaction with iNOS, which provides a potential target for the pharmacological control of this pathway (83), stressing the role of S-nitrosylation as a short-range signaling mechanism (106, 110). Indeed, a similar functional interaction with neuronal NOS has been observed in the context of NMDA neurotoxicity (175). Additional synergistic regulation of the COX-2 pathway includes S-nitrosylation of cytosolic phospholipase A2α (cPLA2α), the rate-limiting enzyme upstream of COX, as COX-2 induces the iNOS-dependent cPLA2α S-nitrosylation that activates this enzyme (192).

Adaptive Immunity: Nitrosothiols in T-Cell-Mediated Immune Responses

A role for S-nitrosylation in T-cell activation

In the immune system, helper T lymphocytes orchestrate the responses to pathogenic agents, secreting cytokines whose function is to coordinate the action of leukocytes and immune-associated cells. To fulfill the multiple demands on their effector functions, T lymphocytes proliferate and differentiate in response to the action of T-cell receptor (TCR)-mediated recognition of pathogen-derived antigenic peptides on antigen-presenting cells (APCs) (162). These cognate interactions result in the phosphorylation-dependent activation of signaling pathways initiated from the TCR (112). Besides the importance of protein phosphorylation on key Tyr and Ser/Thr residues in the activation of signal transduction cascades initiated from the TCR, there is increasing evidence indicating that protein S-nitrosylation and its redox switch by denitrosylation are also PTMs able to take part in the regulation of T-cell activation.

T-cell lines and primary T lymphocytes produce NO in response to TCR engagement with CD3 antibodies, superantigens, or antigenic peptides on APCs (69, 165). Despite some controversies regarding the source of NO and the expression of NOS isoforms in immune cells of human origin (155), it has been reported that mouse and human T lymphocytes can express iNOS upon viral infection and in response to proinflammatory cytokines, or other environmental factors (25, 87, 119). Nevertheless, the rapid onset of NO production observed in T cells upon TCR engagement suggests the participation of constitutive rather than inducible NOS. In this regard, human T lymphocytes express endothelial NOS (eNOS), assessed by mRNA and protein detection (122, 144, 156), and although mouse T lymphocytes do not appear to express eNOS mRNA (46), its expression can be induced in murine T lymphocytes upon CD3 stimulation (23). Hence, species differences or conditioning by factors such as stimulation, or the origin and heterogeneity of cell samples, may distort the results of experimental studies.

We reported that eNOS-derived NO is synthesized by T lymphocytes during antigen-specific interactions with APCs (69). eNOS is rapidly activated on the Golgi complex by phosphorylation at Ser1179 due to the combined action of PI3K/AKT signaling and Ca^{2+} fluxes. As a consequence, it is

translocated toward the immune synapse (69), a specialized intercellular domain where the TCR accumulates along with signaling and cytoskeletal molecules, and adhesion receptors, which are organized to regulate the activation of T cells (34). As a result, early and late TCR-mediated signal transduction events are affected, as eNOS-derived NO increases the phosphorylation/activation of the TCR CD3ζ chain and the adaptor kinase ZAP-70. Moreover, eNOS-derived NO also activates the MAPK ERK-1 and ERK-2 through the compartmentalized S-nitrosylation of N-Ras at Cys118 on the Golgi complex, which facilitates its activation by conversion of GDP- to GTP-bound N-Ras (68) (Fig. 5). Moreover, using a specific S-nitrosocysteine antibody, we found that S-nitrosylation is mainly compartmentalized near the Golgi complex, where active eNOS localizes (68), and a similar compartmentalization of S-nitrosylation near the foci of NOS activation has been observed in other cell systems (71). This localization can be explained by the requirement of high NO concentrations to produce S-nitrosylation in comparison with other NO reactions, and it has been postulated as a mechanism for specific S-nitrosylation of proteins interacting or co-localizing with NOS isoforms, suggesting that S-nitrosylation is a short-range or proximity-based NO signaling event (30, 106, 110). We showed that although T cells express both K-Ras and N-Ras (which have the same conserved Cys residue that can be S-nitrosylated), only N-Ras

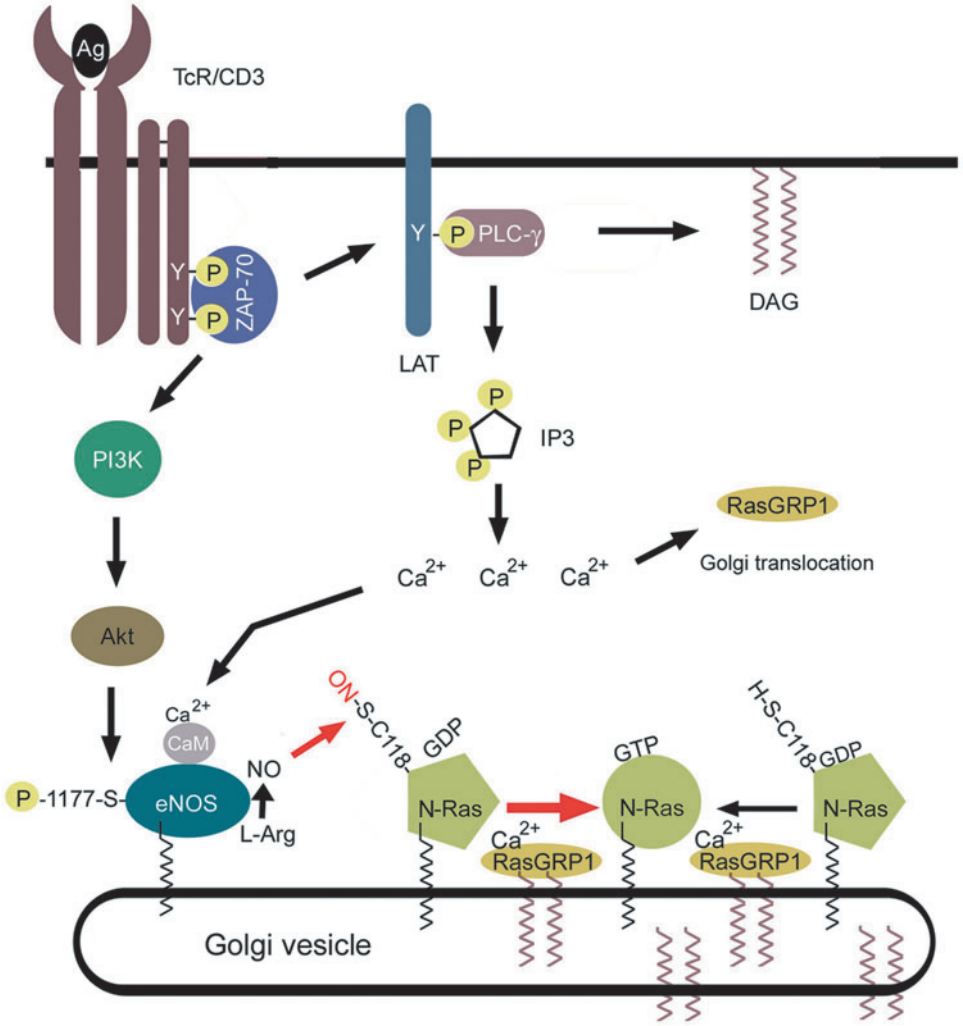

FIG. 5. Model of endothelial nitric oxide synthase (eNOS) activation of N-Ras on the Golgi complex of antigen-stimulated T cells. The figure schematically depicts the possible compartmentalized signaling through which T-cell receptor (TCR) stimulation may lead to the selective S-nitrosylation and activation of N-Ras on the Golgi complex. Engagement of the TCR by antigens results in the phosphorylation of the CD3ζ chain and the recruitment of the adapter kinase ZAP-70. This kinase in turn phosphorylates LAT and PI3K, leading to activation of PLC-γ and Akt, respectively. PLC-γ activation produces diacylglycerol (DAG) in the plasma membrane and inositol 1,4,5-triphosphate (IP3) in the cytosol. IP3 release liberates Ca^{2+} from internal stores, which binds to calmodulin-associated eNOS and induces the translocation of RasGRP1 to the Golgi, where the levels of DAG are high. Simultaneously, active Akt can phosphorylate eNOS on Ser^{1177}. As a result, eNOS might be fully activated to synthesize NO and S-nitrosylate inactive (GDP-bound) N-Ras on Cys^{118} (*small red arrow*). This would weaken its interaction with GDP, thereby facilitating RasGRP1-mediated GDP-GTP exchange on the Golgi complex (*large red arrow*) (To see this illustration in color, the reader is referred to the web version of this article at www.liebertpub.com/ars).

is S-nitrosylated due to its localization on the Golgi apparatus (68), suggesting that specific targets sensitive to regulation may be S-nitrosylated at the immune synapse.

Our findings also suggest that eNOS-dependent S-nitrosylation of N-Ras on Cys118 may foster activation-induced cell death (AICD), a protective mechanism to avoid the potentially deleterious effects of overactivated T cells (68). Similarly, other authors have found that treatment with GSNO stimulates apoptosis in the human promyelomonocytic cell line THP-1, and that mutation of Ras on Cys118 almost abrogates apoptosis, further suggesting a role of Ras S-nitrosylation in cell death (177). Events leading to apoptosis are activated in the mitochondria through the intrinsic pathway, or in the case of AICD, they are triggered by death receptors such as TNFR and CD95/Fas, a member of the TNFR family that binds to the CD95L/Fas ligand. During AICD, CD95L interacts with the Fas-associated death domain (FADD) and recruits procaspase-8, which is proteolytically activated and released to the cytosol (15).

Although the TNFR may produce antiapoptotic effects through the activation of NF-κB, binding of soluble TNF-α and the formation of dead-inducing signaling complexes associated with the cytoplasmic tail of TNFR may also represent a mechanism to sensitize T cells to AICD. In this regard, nitrosative stress confers to TNF-α the capacity to promote apoptosis in Jurkat T cells by blocking IκBα degradation and the translocation of NF-κB to the nucleus (105). However, rather than inducing apoptosis, low-to-moderate concentrations of NO have been shown to protect T cells from cell death (97).

Caspases are the best-known targets through which NO exerts its antiapoptotic effects. All caspases contain an essential Cys within their active centers that is sensitive to S-nitrosylation, and S-nitrosylation of caspase-1, 3, and 9 is correlated with their enzymatic inhibition in vitro (31, 101). However, studies carried out in Jurkat T cells suggest that rather than inhibiting caspase-3 enzymatic activity, NO attenuates its proteolysis to the active form through both the mitochondrial pathway, by interfering with the Apaf-1/caspase-9 apoptosome assembly, and the CD95 death receptor pathway, by S-nitrosylation of caspase-1 and 8 (31, 197). Another S-nitrosylation-dependent mechanism by which cells may be protected from apoptosis involves Bcl-2. In the human lung epithelial cancer cell line NCI-H460, endogenous NO produced in response to proapoptotic stimuli inhibits Bcl-2 degradation by S-nitrosylation at Cys158 and 229 (9). Nevertheless, in some cell systems, neither caspase nor Bcl-2 S-nitrosylation may be sufficient to fully rescue cells from AICD. In this regard, it has been reported that Ras/MEK/ERK activation promotes intrinsic apoptosis pathways in T cells through the phosphorylation and mitochondrial targeting of the orphan nuclear receptor Nur77. Although in cancer cells Nur77 can bind to Bcl-2 at mitochondria and convert this antiapoptotic factor into a proapoptotic mediator, in T cells, Nur77 exerts its actions through an unknown Bcl-2-independent mechanism (180). Whether eNOS-mediated N-Ras S-nitrosylation on the Golgi complex of T cells may also favor apoptosis through an AICD-independent mechanism, involving ERK-mediated Nur77 phosphorylation/activation, merits further investigation.

There is increasing evidence of a possible role for denitrosylation in T-cell activation. Initial studies on the role of redox maintenance in T cells indicated that GSH is important for proliferation and apoptosis, although it only weakly influences early activation events such as IL-2R expression (114, 153, 164). On the other hand, intracellular GSH levels enable activation of NF-kB in Molt-4 T cells (115), whereas in Jurkat T cells, NO inhibits NF-kB activation through S-nitrosylation of IKKβ at Cys179 (145). Hence, reducing environments maintained by GSH could be required to counteract the inhibitory effects exerted by NO-dependent S-nitrosylation on the proinflammatory transcription factor NF-kB. However, GSH is not the only reducing or denitrosylating agent involved in T-cell activation. Trx-maintained reducing microenvironments facilitate the proliferation of T lymphocytes during antigen-specific interactions with dendritic cells (DCs), and they buffer apoptosis in primary T lymphocytes and Jurkat T cells (4, 72). Trxs are expressed in primary T lymphocytes and T-cell lines, mainly upon mitogenic stimulation in the former (150, 169, 187), and Trx is particularly prominent in T lymphocytes of the intestinal lamina propria. These cells expressed more Trx than peripheral blood T cells (PBTs), and they produce more proinflammatory cytokines in response to activation stimuli (161). Moreover, in experimental studies, cytokine expression and endogenous Trx in activated PBTs increase after pretreatment with recombinant Trx. The importance recently attributed to Trx as a cellular enzymatic system with denitrosylase activity (11, 12, 168) suggests that its expression in T lymphocytes of the lamina propria may be important in intestinal microenvironments as a specialized first line of defense against harmful pathogens, and that this activity may be regulated by S-nitrosylation.

S-nitrosylation/denitrosylation in T-cell development

During the development of immature T cells into $CD4^+$ and $CD8^+$ subsets in the thymus, autoreactive $CD4^+CD8^+$ double-positive thymocytes must be removed by negative selection, where apoptosis is induced when the TCR strongly recognizes MHC-presented self-antigens (160). The mechanisms of apoptosis involved in negative selection in the thymus are not well characterized, although it is known that it differs from that observed in peripheral T lymphocytes, which mainly proceeds through AICD (133). High levels of NO are considered important proapoptotic stimuli that can play decisive roles in T-cell selection in the thymus: TCR-stimulated $CD4^+CD8^+$ thymocytes are highly sensitive to NO-mediated apoptosis, whereas $CD4^+CD8^-$ and $CD4^-CD8^+$ thymocytes are rather resistant (38). This possibility is supported by findings showing that increased NO synthesis by iNOS fosters negative selection of CD3-stimulated double-positive thymocytes (170).

In terms of the mechanisms by which iNOS may regulate negative selection, high levels of NO from S-nitroso-N-acetylpenicillamine have been seen to increase thymocyte apoptosis *via* caspase-1 and p53. Moreover, thymocytes from either caspase-1- or p53-null mice are more resistant to NO-induced apoptosis, supporting the hypothesis that both caspase-1 and p53 may transmit proapoptotic signals induced by NO (53, 202). In fact, it has been proposed that NO increases Bax, but reduces Bcl-2 expression through p53 (53). How the p53/Bax/Bcl-2 axis regulates caspase-1 activation in thymocytes is a subject of active research. Strikingly, recent studies indicate that S-nitrosylation/denitrosylation is required for T-cell development. In the thymus of GSNOR-

deficient mice, there is increased S-nitrosylation (with GAPDH one of the major proteins identified), apoptosis, and concomitant reduction of $CD4^+$ thymocytes, a situation that was normalized in the thymus from iNOS and GSNOR double knockout mice (195). DCs of the corticomedullary junction and medulla constitutively express iNOS in the thymus, and this expression is upregulated after their interaction with thymocytes activated with auto- or alloantigens (2, 170). Hence, NO from thymic stromal DCs may be an important secondary signal associated to TCR-mediated apoptosis, and its effects on negative selection may take place through S-nitrosylation, which can be counteracted by the denitrosylase activity of GSNOR (Fig. 6). Interestingly, recent studies carried out in macrophages and neuroblastoma cells indicate that iNOS-derived NO S-nitrosylates GAPDH, and that once S-nitrosylated, GAPDH can translocate to the nucleus after interacting with the E3-ubiquitin ligase Siah1, where it activates the acetyl transferase activity of p300/CBP and induces apoptosis by increasing p53 expression (62, 158). Further work will be required to find out whether S-nitrosylation/denitrosylation exchange on GAPDH actually regulates p53-mediated apoptosis during T-cell development.

By contrast, there is evidence that the selection of $CD8^+$ and $CD4^+$ T lymphocytes is no different in iNOS-deficient and wild-type animals (173), suggesting that the denitrosylase activity of GSNOR during T-cell development may predominate over the S-nitrosylation activity of iNOS. It remains unclear how $CD4^+$ maturation is selectively regulated by GSNOR. One possibility is that thymocytes ongoing $CD4^+$ maturation may be more sensitive to S-nitrosylation-mediated apoptosis than $CD8^+$ thymocytes. If so, MHC class II-restricted signals from DCs may upregulate GSNOR expression/activation in thymocytes undergoing $CD4^+$ maturation, preferentially counteracting the proapoptotic actions of iNOS-derived S-nitrosylation in those cells. Furthermore, iNOS-independent S-nitrosylation may also be important for T-cell development. In this regard, it has been reported that mouse

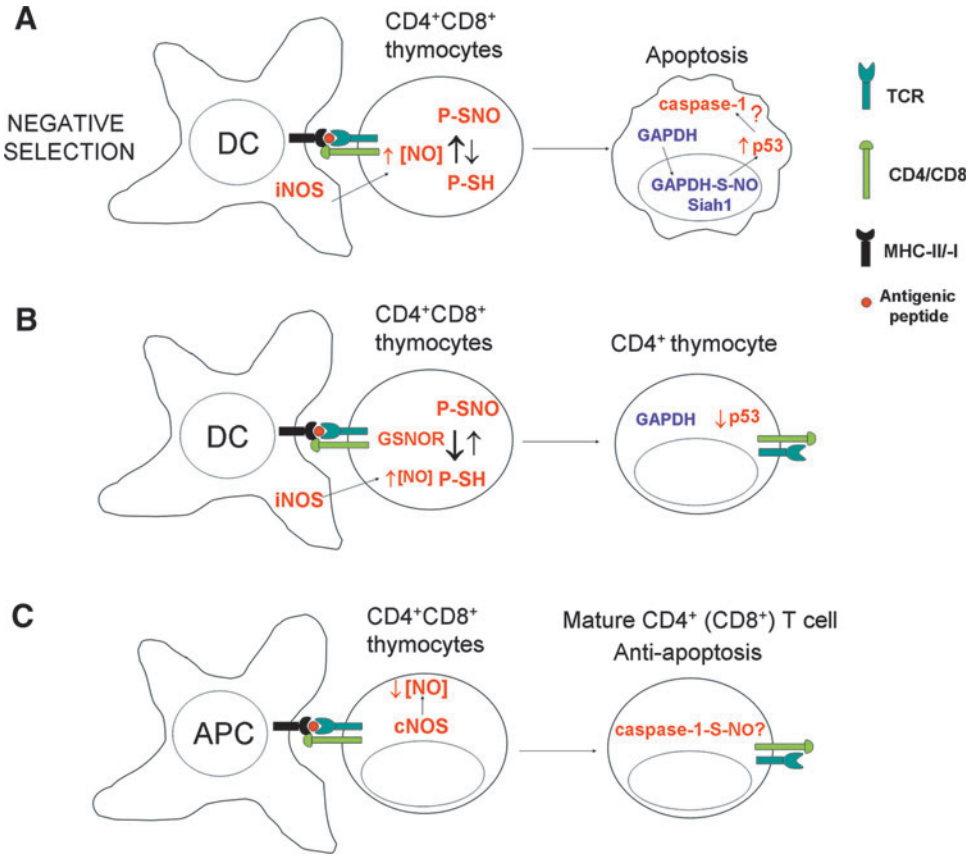

FIG. 6. Hypothetical S-nitrosylation/denitrosylation mechanisms in T-cell development. (A) Local high extracellular levels of NO produced by iNOS from corticomedullar and medullar dendritic cells (DCs) in the thymus promote S-nitrosylation in thymocytes, fostering negative selection of $CD4^+CD8^+$ double-positive thymocytes. Protein S-nitrosylation in thymocytes may induce apoptosis by increasing p53 expression. The iNOS-derived NO may promote apoptosis through the S-nitrosylation of GAPDH. S-nitrosylated GAPDH can bind to Siah1 and translocate to the nucleus, where it increases the acetyltransferase activity of p300/CBP and the ensuing synthesis of p53, which can in turn activate caspase-1 through a still-to-be determined mechanism. **(B)** Through denitrosylation, upregulated GSNOR expression or activity in thymocytes ongoing $CD4^+$ maturation may counteract the proapoptotic actions of protein S-nitrosylation mediated by iNOS-derived NO from DCs. **(C)** Low levels of NO generated in thymocytes by constitutive NOS (cNOS) during their cognate interactions with iNOS-nonexpressing DCs and macrophages (antigen-presenting cells [APC]) may protect thymocytes from cell death by S-nitrosylation of caspase-1 (To see this illustration in color, the reader is referred to the web version of this article at www.liebertpub.com/ars).

thymocytes can express constitutive NOS as well as iNOS, and produce low levels of Ca^{2+}-induced NO, even in the presence of iNOS-inducing stimuli such as LPS and proinflammatory cytokines (19, 28, 185). It is yet to be seen whether the antiapoptotic actions of caspase S-nitrosylation generated by NO from constitutive NOS might also play an important role in modulating apoptosis during thymocyte maturation.

NO and nitrosothiols in T-cell differentiation and autoimmunity

Naive $CD4^+$ T lymphocytes recognize antigens in peripheral lymphoid organs, provoking the expansion and differentiation of antigen-specific lymphocytes into subsets of effector cells that can be distinguished on the basis of the cytokines they produce. Chronic inflammatory diseases are often dominated by Th1, Th2, and Th17 cells and modulated by regulatory T cells (Tregs) (94). The most important differentiation-inducing stimuli for Th1, Th2, and Th17 cells are IL-12, IL-4, and IL-6/IL-23, respectively. The main function of Th1 and Th17 cells is to activate cellular immunity: Th1 cells produce IFN-γ and TNF-α, whereas Th17 cells produce IL-17 and IL-22. On the other hand, Th2 cells regulate humoral immune responses typically synthesizing IL-4, IL-5, IL-6, and IL-10, whereas Tregs mainly produce IL-10 and have been implicated in the generation of tolerance to exacerbated inflammatory responses (94).

The regulation of cytokines by NO has received considerable attention, because it might be relevant in the selection of adaptive immune responses and the management of autoimmune chronic inflammation (Table 1). The first solid evidence of a role for NO in T-cell differentiation came from a seminal study carried out in iNOS-deficient Balb/c mice, which generated Th1 responses upon *Leishmania major* infection instead of the characteristic Th2 polarization associated with control Balb/c mice (182). Later studies demonstrated that high NO concentrations promoted Th2 differentiation by suppressing IL-12 synthesis in activated macrophages (67). Since then, iNOS has been associated with the incidence and severity of many chronic inflammatory diseases, such as rheumatoid arthritis (113, 121), systemic lupus erythematosus (123), experimental autoimmune uveitis (EAU) (172), experimental autoimmune encephalomyelitis (EAE) (184), and asthma (58).

Th1 Differentiation. Several reports support the hypothesis that nitrosothiols may be behind the actions of NO in Th1 differentiation. In a murine model of autoimmune hepatitis induced by concanavalin-A activation of Fas-regulated apoptosis (148, 176), high levels of NO from NO-aspirin (NCX-4016) or from a NO derivative of ursodeoxycholic acid (NCX-1000) reduced Th1 responses by inhibiting the caspases involved in the processing and production of Th1 cytokines (39, 40). This effect was reverted when cell lysates were treated with DTT or $HgCl_2$, which are able to reduce oxidized cysteines (including S-nitrosothiols), suggesting that the inhibitory effect of NO on caspase activity could be achieved *via* the S-nitrosylation of essential cysteine residues within their catalytic site (39).

Moreover, Trx induction in T lymphocytes increased production of Th1 cytokines by stimulating *IFN-γ* gene expression (79). Therefore, it seems likely that high levels of NO generated by iNOS may prevent overexpansion of Th1 cells by S-nitrosylation of key transcriptional and post-transcriptional regulators of Th1 pathways. By contrast, low concentrations of NO stimulate T cells to express IL12-Rβ2 and promote Th1 differentiation *via* cGMP (130). Nevertheless, since Th1 cells are more sensitive to apoptosis induced by high concentrations of NO than Th2 cells (149), and low-to-moderate concentrations of NO can exert S-nitrosylation-mediated antiapoptotic effects, the influence of NO from constitutive NOS may improve Th1 viability and influence the Th1/Th2 balance. Indeed, it has been reported that Ras/MAPK signaling also plays an important role in T-cell differentiation: strong signals from the antigen-engaged TCR sustain ERK activation and favor Th1 differentiation, whereas weak and transient TCR-mediated activation of ERKs preferentially induces Th2 differentiation, a consequence of increased Jak-1, STAT-6, and GATA-3 activation (193). A possible role for NO in Ras/ERK-mediated Th1/Th2 differentiation is supported by eNOS and NO donors regulating ERK activity through Ras S-nitrosylation (68, 91). Nevertheless, a recent study analyzing eNOS-deficient C57BL/6 mice infected with *L. major* clearly showed that eNOS does not play any role in the selection of the Th1/Th2 immune response to infection, although it enhanced granulocyte infiltration into lesions (46). However, it remains possible that the actions of eNOS-derived NO in human and mouse T-cell differentiation could be species specific (see above).

Uveitis represents a group of sight-threatening intraocular inflammatory diseases, including Behçet's disease, birdshot retinochoroidopathy, sympathetic ophthalmia, Vogt-Koyanagi-Harada's disease, and ocular sarcoidosis, which may have an autoimmune etiology (131). EAU can be induced in susceptible rodent species by immunization with the retinal protein, interphotoreceptor retinoid-binding protein (IRBP) (181). GSNO treatment ameliorates the disease due to its ability to inhibit retinal expression of Th1 cytokines and T-cell proliferation (61). In an earlier report, administration of IL-12 to these animals protected them from disease due to apoptotic deletion of detrimental T cells, inducing IFN-γ overproduction and iNOS-derived NO (172). While not specifically assessed, these results suggest that Th1 cells could be the subset of detrimental T cells depleted. More recent work indicates that uveitis is also associated with Th17 response (24, 181), although we have not found reports of nitrosothiols participation in Th17-dependent uveitis.

Th17 Differentiation. Multiple sclerosis (MS) is a common inflammatory disease of the central nervous system (CNS) characterized by the instability and disruption of myelin, the death of oligodendrocytes and axonal damage (80). A murine EAE model of MS involves the induction of a neuroinflammatory disease by immunization with antigens derived from myelin protein. This animal model is associated with impaired integrity of the blood–brain barrier, upregulation of adhesion molecules, and the invasion of vascular inflammatory cells into the CNS.

In the recent years, increasing importance has been given to Th17 cells as mediators of EAE, and NO has emerged as a possible regulator of Th17 proliferation and function. NO inhibits the proliferation and function of polarized Th17 cells, and EAE is more severe in iNOS-deficient mice than in wild-

Table 1. Role of S-Nitrosylation in Autoimmune Diseases

Disease (model)	*T-cell response*	*Cytokines implicated*	*Endogenous NO source*	*Exogenous treatments*	*Implications for disease*	*Mechanism of action of nitrosothiol/NO*	*References*
Uveitis (EAU)	Th1* Th17*	IFN-γ TNF-α IL-10 IL-17	iNOS	GSNO	Disease improvement	Inhibition of proinflammatory cytokines and T-cell proliferation	(61, 172)
Multiple sclerosis (EAE)	Th17	IL-17 TNF-β IFN-γ IL-1β	iNOS eNOS	GSNO	Disease improvement	NO inhibits proliferation and function of polarized Th17 cells GSNO protects myelin GSNO produces differences in the S-nitrosoproteome	(139) (128) (14, 191)
Asthma	Th2		iNOS	SNAP	Disease improvement	NO suppresses proliferation of activated Th2 cells S-nitrosylated proteins reduced in asthmatic patients	(35) (140)
Autoimmune hepatitis	Th1	Th1 cytokines		NO donors (NO-aspirin, NCX-1000)	Disease improvement	Probable S-nitrosylation of caspases catalytic Cys, inhibiting Th1 response	(39, 40)
Rheumatoid arthritis		MBL			Harmful effects on disease	S-nitrosylation of MBL	(59, 65)
Crohn's disease				GSNO	Disease improvement	Reduced intestinal permeability Increases ZO-1 mRNA and protein levels	(154)

*There are not enough evidences for uveitis to be caused by a Th1 or Th17 cell response.

EAU, experimental autoimmune uveitis; eNOS, endothelial nitric oxide synthase; iNOS, inducible nitric oxide synthase; GSNO, S-nitrosoglutathione; IFN-γ, interferon-γ; SNAP, S-nitroso-N-acetylpenicillamine; MBL, mannose-binding lectin; TNF, tumor necrosis factor; IL, interleukin.

type controls (128). Moreover, GSNO attenuates EAE, protecting myelin by restricting mononuclear cell infiltration and inhibiting proinflammatory mediator expression (TNF-β, IFN-γ, and IL-1β), as well as by reducing IL-17 production through the inactivation of STAT-3 and the reduction of RORγ expression, two essential transcription factors for Th17 cell differentiation and function (139).

In EAE mice, differences in the S-nitrosoproteome have been described by comparative biotin-switch and western blot analysis, affecting cytoskeletal components (neurofilament proteins, tubulin, and β-actin), metabolic enzymes (GAPDH and neuronal-specific enolase), ion-channel-related proteins (glutamate receptor NR2A), and myelin proteins (2′,3′-cyclic nucleotide 3′-phosphodiesterase) (14). Such findings argue in favor of a neuroprotective role of iNOS-derived NO in EAE, possibly through S-nitrosylation of specific targets in Th17 cells. Nevertheless, since most of the S-nitrosylated proteins identified in the aforementioned study are abundant cellular proteins, in-depth screening with more sensitive proteomic approaches would be required in EAE-infiltrated T cells to search for key S-nitrosylation targets that may influence Th17 differentiation and function. Conversely, the participation of NO in the etiopathology of EAE is not an exclusive hallmark of iNOS. In EAE studies with eNOS-deficient mice, eNOS-derived NO appears to favor the recruitment of T lymphocytes to the CNS, whereas it attenuates EAE exacerbation. Thus, eNOS fulfills proinflammatory and neuroprotective roles during the course of the disease (191). Whether this latter effect involves protein S-nitrosylation remains to be investigated.

Th2 and Tregs. The preferential role for oxidative stress and superoxide in the differentiation toward Th2 phenotypes has recently been highlighted (23, 84). There is also evidence indicating that nitrosothiols may be important for Th2 differentiation and function. Treatment of human bronchial epithelial cells with NO reversibly suppresses proliferation of activated Th2 cells in atopic asthma (35). Moreover, S-nitrosylated proteins are substantially reduced in asthmatic patients, correlating fairly well with the increased GSNOR levels in their bronchoalveolar fluids (140). These findings are supported by studies carried out in an experimental mouse model of asthma, in which mice deficient in the expression of GSNOR were protected against hypersensitivity to the specific allergen and against hyper-reactivity to bronchoconstrictors by increasing the levels of iNOS-derived S-nitrosylated proteins in the lungs, an effect reverted by treatment with NOS inhibitors (141). Furthermore, proteomic studies of T lymphocytes have shown that Trx and other redox control proteins are increased in T cells from asthmatic patients with respect to healthy controls (77).

Several types of Tregs have been implicated in the generation of tolerance to exacerbated inflammatory responses. These include natural and adaptive $CD4^+$ $CD25^+$, $Foxp3^+$ Tregs. Natural Tregs develop in the thymus, whereas adaptive Tregs can be generated by repetitive antigen presentation to naive $CD4^+CD25^-$ T cells by immature or tolerogenic DCs (22, 78, 179). Although recent studies have clearly shown that NO can negatively regulate classical Treg differentiation by inhibiting Foxp3 expression, supposedly through a cGMP-dependent mechanism (16, 93), several lines of evidence do not exclude a role for iNOS-derived NO and S-nitrosylation in the function of Tregs. First, in response to autoantigens, Tregs secrete IFN-γ and induce iNOS-derived NO production by APCs. The APC-derived NO suppresses the proliferation of pathogenic T cells, thereby inhibiting the course of autoimmune diseases (8, 21, 171). Second, DCs expressing a kinase-defective dominant-negative form of Ikappa B kinase-2 (dnIKK2) show an impaired allostimulatory ability to upregulate MHC-II antigens and costimulatory molecules in response to either LPS or CD40 engagement (2). Naive murine T cells stimulated with antigen-loaded immature dnIKK2 DCs differentiate into $CD4^+CD25^-$ Tregs (dnIKK2-Tregs). These Tregs express iNOS, and have the ability to inhibit naive and preactivated T-cell responses in vitro (1). Finally, recent studies demonstrated the existence of a population of Tregs (NO-Treg) generated by NO in a cGMP-independent manner *via* p53-mediated expression of antiapoptotic genes and local secretion of IL-2 (129). NO-Tregs are a subset of T lymphocytes induced by NO together with TcR-mediated activation. They are $CD4^+CD25^+$, $Foxp3^-$, $GITR^+$, and $CD27^+$, and they have a Th2 phenotype that suppresses $CD4^+CD25^-$ effector T cells, exerting their activities in an IL-10-dependent manner. Nonetheless, there is still no consistent evidence that NO-involved Treg functions may take place through S-nitrosylation, beyond a recent report indicating that Tregs express high levels of Trx-1, which may confer resistance to the characteristic oxidative stress of inflammatory foci (120).

Collectively, these diverse lines of evidence suggest that NO can regulate T-cell differentiation and function through a variety of mechanisms, some of them involving the participation of S-nitrosylation, which provides benefits in the course of chronic inflammatory diseases, presumably by disturbing the differentiation and/or function of Th1, Th2, and/or Th17 cells, while the effects on Tregs remain unknown.

S-Nitrosylation as a Therapeutic Agent in Chronic Inflammatory Diseases

Crohn's disease is a chronic inflammatory disease of the gastrointestinal tract, which is probably caused by an imbalance between proinflammatory and anti-inflammatory mediators, and is associated with a permeability disorder of the mucosal barrier (26, 138) (Table 1). A murine model of the disease has been obtained by expressing the herpes simplex virus thymidine kinase (*HSV-Tk*) gene under the control of the astroglial-specific promoter for glial fibrillary acid protein (GFAP). Ganciclovir administration provokes enteric glial ablation in this model, leading to intestinal inflammation and an apparent disruption of the intestinal epithelial monolayer (18). In these mice, GSNO was implicated in promoting the function of the mucosal barrier (154). At low concentrations, and unlike GSH or GSSG, GSNO reduced the intestinal permeability caused by enteric glial cell ablation, and it protected these transgenic mice from intestinal inflammation. ZO-1 is a protein implicated in the formation of tight junctions, and its interaction with actin might directly regulate barrier integrity and permeability. ZO-1 expression increased after exposure to GSNO exposure, a possible means by which GSNO might help maintain mucosal barrier function. This protein may also be regulated by GSNO through PTMs, since ZO-1 protein has a cysteine in a transnitrosylation consensus motif situated in

the C-terminal actin-binding region (154). Future studies might elucidate the mechanisms involved.

Mannose-binding lectin (MBL) is a complement-activating protein involved in innate immune defense. MBL deficit or dysfunction is associated with autoimmune diseases such as lupus erythematosus and rheumatoid arthritis (55, 82). S-nitrosylated MBL was detected in synovial fluid of rheumatoid arthritis patients (59, 65), and there is evidence of the potential harmful effects that S-nitrosylation of MBL might provoke in such patients, including impaired function (mannan binding, complement deposition, bacterial opsonization, agglutination and phagocytosis, and induction of apoptosis) and increased anti-MBL autoantibody generation (59). Given the possible conformational changes in the MBL structure after S-nitrosylation of one or some of its cysteines, it would be of interest to further investigate these potential changes and which cysteine residues might be modified.

Inhaled NO has been used therapeutically in the treatment of acute lung injury, a poorly understood inflammatory syndrome with a significant influence on public health (33). Nevertheless, NO might be not so efficient in treating this disease, since its use may increase the formation of deleterious RNS. By studying lung inflammation in a mouse model of LPS-induced airway injury, it was recently shown that inhalation of ethyl nitrite (ENO), a gas that fosters S-nitrosylation, may decrease lung inflammation and injury in mice by inhibiting epithelial activation in the airways (103). S-nitrosylation homeostasis in the lung was disrupted on LPS treatment, which reduced S-nitrosylation levels and increased NF-κB activation, which was prevented by pretreatment with the S-nitrosylating agent ENO (103).

In conjunction, the findings that managing the levels of S-nitrosylation may be useful in treating those chronic inflammatory diseases in which S-nitrosylation homeostasis is altered considerably are promising. In this regard, S-nitrosylating/denitrosylating agents may represent therapeutic tools for the prevention and/or treatment of this group of diseases. Thus, it is reasonable to expect that in the coming years, these tools could be further developed into more efficient treatments.

Conclusions

S-nitrosylation is increasingly being considered as a signaling mechanism in many cells and systems. In the immune system, several signaling pathways are modulated by this oxidative PTM in the regulation of T-helper cell responses during adaptive immunity, as well as in the innate immunity mediated by phagocytes. Indeed, self-protection mechanisms of macrophages, specialized cells that use NO and RNS production as antimicrobial weapons, have begun to be uncovered. Further work will be required to study these issues in more detail within broader contexts, both from the molecular and pathophysiological points of view, which will benefit from methodological improvements to analyze and quantify the S-nitrosoproteome. There is accumulating evidence of the positive role for nitrosothiols and S-nitrosylation in T-cell regulation, demonstrating beneficial effects in autoimmune disease models, which certainly could be further explored and potentially translated to improve disease treatment.

Acknowledgments

We thank Dr. Ignacio Rodríguez-Crespo for helpful comments and Mark Sefton (BiomedRed) for revising the article. The research in our labs is financed by the Spanish Government grants CSD2007-00020 (RosasNet, Consolider-Ingenio 2010 programme), CP07/00143 (Miguel Servet programme), and PS09/00101 (to A.M.-R.); and PI10/02136 (to J.M.S.).

References

1. Aiello S, Cassis P, Cassis L, Tomasoni S, Benigni A, Pezzotta A, Cavinato RA, Cugini D, Azzollini N, Mister M, Longaretti L, Thomson AW, Remuzzi G, and Noris M. DnIKK2-transfected dendritic cells induce a novel population of inducible nitric oxide synthase-expressing CD4+ CD25- cells with tolerogenic properties. *Transplantation* 83: 474–484, 2007.
2. Aiello S, Noris M, Piccinini G, Tomasoni S, Casiraghi F, Bonazzola S, Mister M, Sayegh MH, and Remuzzi G. Thymic dendritic cells express inducible nitric oxide synthase and generate nitric oxide in response to self- and alloantigens. *J Immunol* 164: 4649–4658, 2000.
3. Akhand AA, Pu M, Senga T, Kato M, Suzuki H, Miyata T, Hamaguchi M, and Nakashima I. Nitric oxide controls src kinase activity through a sulfhydryl group modification-mediated Tyr-527-independent and Tyr-416-linked mechanism. *J Biol Chem* 274: 25821–25826, 1999.
4. Angelini G, Gardella S, Ardy M, Ciriolo MR, Filomeni G, Di Trapani G, Clarke F, Sitia R, and Rubartelli A. Antigen-presenting dendritic cells provide the reducing extracellular microenvironment required for T lymphocyte activation. *Proc Natl Acad Sci U S A* 99: 1491–1496, 2002.
5. Arnelle DR and Stamler JS. NO+, NO, and NO- donation by S-nitrosothiols: implications for regulation of physiological functions by S-nitrosylation and acceleration of disulfide formation. *Arch Biochem Biophys* 318: 279–285, 1995.
6. Atochina-Vasserman EN. S-nitrosylation of surfactant protein D as a modulator of pulmonary inflammation. *Biochim Biophys Acta* 1820: 763–769, 2012.
7. Atochina-Vasserman EN, Gow AJ, Abramova H, Guo CJ, Tomer Y, Preston AM, Beck JM, and Beers MF. Immune reconstitution during Pneumocystis lung infection: disruption of surfactant component expression and function by S-nitrosylation. *J Immunol* 182: 2277–2287, 2009.
8. Atochina O, Daly-Engel T, Piskorska D, McGuire E, and Harn DA. A schistosome-expressed immunomodulatory glycoconjugate expands peritoneal Gr1(+) macrophages that suppress naive CD4(+) T cell proliferation via an IFN-gamma and nitric oxide-dependent mechanism. *J Immunol* 167: 4293–4302, 2001.
9. Azad N, Vallyathan V, Wang L, Tantishaiyakul V, Stehlik C, Leonard SS, and Rojanasakul Y. S-nitrosylation of Bcl-2 inhibits its ubiquitin-proteasomal degradation. A novel antiapoptotic mechanism that suppresses apoptosis. *J Biol Chem* 281: 34124–34134, 2006.
10. Barglow KT, Knutson CG, Wishnok JS, Tannenbaum SR, and Marletta MA. Site-specific and redox-controlled S-nitrosation of thioredoxin. *Proc Natl Acad Sci U S A* 108: E600–E606, 2011.
11. Benhar M, Forrester MT, Hess DT, and Stamler JS. Regulated protein denitrosylation by cytosolic and mitochondrial thioredoxins. *Science* 320: 1050–1054, 2008.

12. Benhar M, Forrester MT, and Stamler JS. Protein denitrosylation: enzymatic mechanisms and cellular functions. *Nat Rev Mol Cell Biol* 10: 721–732, 2009.
13. Benhar M, Thompson JW, Moseley MA, and Stamler JS. Identification of S-nitrosylated targets of thioredoxin using a quantitative proteomic approach. *Biochemistry* 49: 6963–6969, 2010.
14. Bizzozero OA and Zheng J. Identification of major S-nitrosylated proteins in murine experimental autoimmune encephalomyelitis. *J Neurosci Res* 87: 2881–2889, 2009.
15. Boldin MP, Goncharov TM, Goltsev YV, and Wallach D. Involvement of MACH, a novel MORT1/FADD-interacting protease, in Fas/APO-1- and TNF receptor-induced cell death. *Cell* 85: 803–815, 1996.
16. Brahmachari S and Pahan K. Myelin basic protein priming reduces the expression of Foxp3 in T cells via nitric oxide. *J Immunol* 184: 1799–1809, 2010.
17. Brown-Augsburger P, Hartshorn K, Chang D, Rust K, Fliszar C, Welgus HG, and Crouch EC. Site-directed mutagenesis of Cys-15 and Cys-20 of pulmonary surfactant protein D. Expression of a trimeric protein with altered anti-viral properties. *J Biol Chem* 271: 13724–13730, 1996.
18. Bush TG, Savidge TC, Freeman TC, Cox HJ, Campbell EA, Mucke L, Johnson MH, and Sofroniew MV. Fulminant jejuno-ileitis following ablation of enteric glia in adult transgenic mice. *Cell* 93: 189–201, 1998.
19. Bustamante J, Bersier G, Badin RA, Cymeryng C, Parodi A, and Boveris A. Sequential NO production by mitochondria and endoplasmic reticulum during induced apoptosis. *Nitric Oxide* 6: 333–341, 2002.
20. Cerutti A, Puga I, and Cols M. Innate control of B cell responses. *Trends Immunol* 32: 202–211, 2011.
21. Chen C, Lee WH, Zhong L, and Liu CP. Regulatory T cells can mediate their function through the stimulation of APCs to produce immunosuppressive nitric oxide. *J Immunol* 176: 3449–3460, 2006.
22. Chen W, Jin W, Hardegen N, Lei KJ, Li L, Marinos N, McGrady G, and Wahl SM. Conversion of peripheral CD4+CD25- naive T cells to CD4+CD25+ regulatory T cells by TGF-beta induction of transcription factor Foxp3. *J Exp Med* 198: 1875–1886, 2003.
23. Chen W, Li L, Brod T, Saeed O, Thabet S, Jansen T, Dikalov S, Weyand C, Goronzy J, and Harrison DG. Role of increased guanosine triphosphate cyclohydrolase-1 expression and tetrahydrobiopterin levels upon T cell activation. *J Biol Chem* 286: 13846–13851, 2011.
24. Chi W, Zhu X, Yang P, Liu X, Lin X, Zhou H, Huang X, and Kijlstra A. Upregulated IL-23 and IL-17 in Behçet patients with active uveitis. *Invest Ophthalmol Vis Sci* 49: 3058–3064, 2008.
25. Choy JC, Wang Y, Tellides G, and Pober JS. Induction of inducible NO synthase in bystander human T cells increases allogeneic responses in the vasculature. *Proc Natl Acad Sci U S A* 104: 1313–1318, 2007.
26. Cottone M and Criscuoli V. Infliximab to treat Crohn's disease: an update. *Clin Exp Gastroenterol* 4: 227–238, 2011.
27. Crouch E, Persson A, Chang D, and Heuser J. Molecular structure of pulmonary surfactant protein D (SP-D). *J Biol Chem* 269: 17311–17319, 1994.
28. Cruz MT, Carmo A, Carvalho AP, and Lopes MC. Calcium-dependent nitric oxide synthase activity in rat thymocytes. *Biochem Biophys Res Commun* 248: 98–103, 1998.
29. Davis AS, Vergne I, Master SS, Kyei GB, Chua J, and Deretic V. Mechanism of inducible nitric oxide synthase exclusion from mycobacterial phagosomes. *PLoS Pathog* 3: e186, 2007.
30. Derakhshan B, Hao G, and Gross SS. Balancing reactivity against selectivity: the evolution of protein S-nitrosylation as an effector of cell signaling by nitric oxide. *Cardiovasc Res* 75: 210–219, 2007.
31. Dimmeler S, Haendeler J, Sause A, and Zeiher AM. Nitric oxide inhibits APO-1/Fas-mediated cell death. *Cell Growth Differ* 9: 415–422, 1998.
32. Doulias PT, Greene JL, Greco TM, Tenopoulou M, Seeholzer SH, Dunbrack RL, and Ischiropoulos H. Structural profiling of endogenous S-nitrosocysteine residues reveals unique features that accommodate diverse mechanisms for protein S-nitrosylation. *Proc Natl Acad Sci U S A* 107: 16958–16963, 2010.
33. Dushianthan A, Grocott MP, Postle AD, and Cusack R. Acute respiratory distress syndrome and acute lung injury. *Postgrad Med J* 87: 612–622, 2011.
34. Dustin ML, Chakraborty AK, and Shaw AS. Understanding the structure and function of the immunological synapse. *Cold Spring Harb Perspect Biol* 2: a002311, 2010.
35. Eriksson U, Egermann U, Bihl MP, Gambazzi F, Tamm M, Holt PG, and Bingisser RM. Human bronchial epithelium controls TH2 responses by TH1-induced, nitric oxide-mediated STAT5 dephosphorylation: implications for the pathogenesis of asthma. *J Immunol* 175: 2715–2720, 2005.
36. Eu JP, Liu L, Zeng M, and Stamler JS. An apoptotic model for nitrosative stress. *Biochemistry* 39: 1040–1047, 2000.
37. Feelisch M, Rassaf T, Mnaimneh S, Singh N, Bryan NS, Jourd'Heuil D, and Kelm M. Concomitant S-, N-, and heme-nitros(yl)ation in biological tissues and fluids: implications for the fate of NO *in vivo*. *FASEB J* 16: 1775–1785, 2002.
38. Fehsel K, Kroncke KD, Meyer KL, Huber H, Wahn V, and Kolb-Bachofen V. Nitric oxide induces apoptosis in mouse thymocytes. *J Immunol* 155: 2858–2865, 1995.
39. Fiorucci S, Mencarelli A, Palazzetti B, Del Soldato P, Morelli A, and Ignarro LJ. An NO derivative of ursodeoxycholic acid protects against Fas-mediated liver injury by inhibiting caspase activity. *Proc Natl Acad Sci U S A* 98: 2652–2657, 2001.
40. Fiorucci S, Santucci L, Antonelli E, Distrutti E, Del Sero G, Morelli O, Romani L, Federici B, Del Soldato P, and Morelli A. NO-aspirin protects from T cell-mediated liver injury by inhibiting caspase-dependent processing of Th1-like cytokines. *Gastroenterology* 118: 404–421, 2000.
41. Forman HJ, Fukuto JM, Miller T, Zhang H, Rinna A, and Levy S. The chemistry of cell signaling by reactive oxygen and nitrogen species and 4-hydroxynonenal. *Arch Biochem Biophys* 477: 183–195, 2008.
42. Forman HJ, Fukuto JM, and Torres M. Redox signaling: thiol chemistry defines which reactive oxygen and nitrogen species can act as second messengers. *Am J Physiol Cell Physiol* 287: C246–C256, 2004.
43. Forrester MT, Seth D, Hausladen A, Eyler CE, Foster MW, Matsumoto A, Benhar M, Marshall HE, and Stamler JS. Thioredoxin-interacting protein (Txnip) is a feedback regulator of S-nitrosylation. *J Biol Chem* 284: 36160–36166, 2009.
44. Forrester MT, Thompson JW, Foster MW, Nogueira L, Moseley MA, and Stamler JS. Proteomic analysis of S-nitrosylation and denitrosylation by resin-assisted capture. *Nat Biotech* 27: 557–559, 2009.

45. Foster MW, Yang Z, Gooden DM, Thompson JW, Ball CH, Turner ME, Hou Y, Pi J, Moseley MA, and Que LG. Proteomic characterization of the cellular response to nitrosative stress mediated by s-nitrosoglutathione reductase inhibition. *J Proteome Res* 11: 2480–2491, 2012.
46. Fritzsche C, Schleicher U, and Bogdan C. Endothelial nitric oxide synthase limits the inflammatory response in mouse cutaneous leishmaniasis. *Immunobiology* 215: 826–832, 2010.
47. Fröhlich A and Durner J. The hunt for plant nitric oxide synthase (NOS): is one really needed? *Plant Sci* 181: 401–404, 2011.
48. Gao C, Guo H, Wei J, Mi Z, Wai PY, and Kuo PC. Identification of S-nitrosylated proteins in endotoxin-stimulated RAW264.7 murine macrophages. *Nitric Oxide* 12: 121–126, 2005.
49. Gardai SJ, Xiao YQ, Dickinson M, Nick JA, Voelker DR, Greene KE, and Henson PM. By binding SIRPalpha or calreticulin/CD91, lung collectins act as dual function surveillance molecules to suppress or enhance inflammation. *Cell* 115: 13–23, 2003.
50. Ghosh S and Karin M. Missing pieces in the NF-kappaB puzzle. *Cell* 109 Suppl: S81–S96, 2002.
51. Glynne PA, Darling KE, Picot J, and Evans TJ. Epithelial inducible nitric-oxide synthase is an apical EBP50-binding protein that directs vectorial nitric oxide output. *J Biol Chem* 277: 33132–33138, 2002.
52. Godoy LC, Moretti AI, Jurado MC, Oxer D, Janiszewski M, Ckless K, Velasco IT, Laurindo FR, and Souza HP. Loss of CD40 endogenous S-nitrosylation during inflammatory response in endotoxemic mice and patients with sepsis. *Shock* 33: 626–633, 2010.
53. Gordon SA, Abou-Jaoude W, Hoffman RA, McCarthy SA, Kim YM, Zhou X, Zhang XR, Simmons RL, Chen Y, Schall L, and Ford HR. Nitric oxide induces murine thymocyte apoptosis by oxidative injury and a p53-dependent mechanism. *J Leukoc Biol* 70: 87–95, 2001.
54. Gow AJ, Chen Q, Hess DT, Day BJ, Ischiropoulos H, and Stamler JS. Basal and stimulated protein S-nitrosylation in multiple cell types and tissues. *J Biol Chem* 277: 9637–9640, 2002.
55. Graudal NA, Homann C, Madsen HO, Svejgaard A, Jurik AG, Graudal HK, and Garred P. Mannan binding lectin in rheumatoid arthritis. A longitudinal study. *J Rheumatol* 25: 629–635, 1998.
56. Guikema B, Lu Q, and Jourd'heuil D. Chemical considerations and biological selectivity of protein nitrosation: implications for NO-mediated signal transduction. *Antioxid Redox Signal* 7: 593–606, 2005.
57. Guo CJ, Atochina-Vasserman EN, Abramova E, Foley JP, Zaman A, Crouch E, Beers MF, Savani RC, and Gow AJ. S-nitrosylation of surfactant protein-D controls inflammatory function. *PLoS Biol* 6: e266, 2008.
58. Guo FH, Comhair SA, Zheng S, Dweik RA, Eissa NT, Thomassen MJ, Calhoun W, and Erzurum SC. Molecular mechanisms of increased nitric oxide (NO) in asthma: evidence for transcriptional and post-translational regulation of NO synthesis. *J Immunol* 164: 5970–5980, 2000.
59. Gupta B, Raghav SK, and Das HR. S-nitrosylation of mannose binding lectin regulates its functional activities and the formation of autoantibody in rheumatoid arthritis. *Nitric Oxide* 18: 266–273, 2008.
60. Hall JP, Merithew E, and Davis RJ. c-Jun N-terminal kinase (JNK) repression during the inflammatory response? Just say NO. *Proc Natl Acad Sci U S A* 97: 14022–14024, 2000.
61. Haq E, Rohrer B, Nath N, Crosson CE, and Singh I. S-nitrosoglutathione prevents interphotoreceptor retinoid-binding protein (IRBP(161–180))-induced experimental autoimmune uveitis. *J Ocul Pharmacol Ther* 23: 221–231, 2007.
62. Hara MR, Agrawal N, Kim SF, Cascio MB, Fujimuro M, Ozeki Y, Takahashi M, Cheah JH, Tankou SK, Hester LD, Ferris CD, Hayward SD, Snyder SH, and Sawa A. S-nitrosylated GAPDH initiates apoptotic cell death by nuclear translocation following Siah1 binding. *Nat Cell Biol* 7: 665–674, 2005.
63. Hartshorn KL, White MR, and Crouch EC. Contributions of the N- and C-terminal domains of surfactant protein d to the binding, aggregation, and phagocytic uptake of bacteria. *Infect Immun* 70: 6129–6139, 2002.
64. Hess DT, Matsumoto A, Kim S-O, Marshall HE, and Stamler JS. Protein S-nitrosylation: purview and parameters. *Nat Rev Mol Cell Biol* 6: 150–166, 2005.
65. Hilliquin P, Borderie D, Hernvann A, Menkes CJ, and Ekindjian OG. Nitric oxide as S-nitrosoproteins in rheumatoid arthritis. *Arthritis Rheum* 40: 1512–1517, 1997.
66. Hiscott J, Kwon H, and Genin P. Hostile takeovers: viral appropriation of the NF-kappaB pathway. *J Clin Invest* 107: 143–151, 2001.
67. Huang FP, Niedbala W, Wei XQ, Xu D, Feng GJ, Robinson JH, Lam C, and Liew FY. Nitric oxide regulates Th1 cell development through the inhibition of IL-12 synthesis by macrophages. *Eur J Immunol* 28: 4062–4070, 1998.
68. Ibiza S, Perez-Rodriguez A, Ortega A, Martinez-Ruiz A, Barreiro O, Garcia-Dominguez CA, Victor VM, Esplugues JV, Rojas JM, Sanchez-Madrid F, and Serrador JM. Endothelial nitric oxide synthase regulates N-Ras activation on the Golgi complex of antigen-stimulated T cells. *Proc Natl Acad Sci U S A* 105: 10507–10512, 2008.
69. Ibiza S, Victor VM, Bosca I, Ortega A, Urzainqui A, O'Connor JE, Sanchez-Madrid F, Esplugues JV, and Serrador JM. Endothelial nitric oxide synthase regulates T cell receptor signaling at the immunological synapse. *Immunity* 24: 753–765, 2006.
70. Into T, Inomata M, Nakashima M, Shibata K, Hacker H, and Matsushita K. Regulation of MyD88-dependent signaling events by S nitrosylation retards toll-like receptor signal transduction and initiation of acute-phase immune responses. *Mol Cell Biol* 28: 1338–1347, 2008.
71. Iwakiri Y, Satoh A, Chatterjee S, Toomre DK, Chalouni CM, Fulton D, Groszmann RJ, Shah VH, and Sessa WC. Nitric oxide synthase generates nitric oxide locally to regulate compartmentalized protein S-nitrosylation and protein trafficking. *Proc Natl Acad Sci U S A* 103: 19777–19782, 2006.
72. Iwata S, Hori T, Sato N, Hirota K, Sasada T, Mitsui A, Hirakawa T, and Yodoi J. Adult T cell leukemia (ATL)-derived factor/human thioredoxin prevents apoptosis of lymphoid cells induced by L-cystine and glutathione depletion: possible involvement of thiol-mediated redox regulation in apoptosis caused by pro-oxidant state. *J Immunol* 158: 3108–3117, 1997.
73. Izquierdo-Álvarez A and Martínez-Ruiz A. Thiol redox proteomics seen with fluorescent eyes: the detection of cysteine oxidative modifications by fluorescence derivatization and 2-DE. *J Proteomics* 75: 329–338, 2011.
74. Jaffrey SR, Erdjument-Bromage H, Ferris CD, Tempst P, and Snyder SH. Protein S-nitrosylation: a physiological signal for neuronal nitric oxide. *Nat Cell Biol* 3: 193–197, 2001.
75. Janssen-Heininger YM, Mossman BT, Heintz NH, Forman HJ, Kalyanaraman B, Finkel T, Stamler JS, Rhee SG, and

van der Vliet A. Redox-based regulation of signal transduction: principles, pitfalls, and promises. *Free Radic Biol Med* 45: 1–17, 2008.
76. Jensen DE, Belka GK, and Du Bois GC. S-Nitrosoglutathione is a substrate for rat alcohol dehydrogenase class III isoenzyme. *Biochem J* 33: 659–668, 1998.
77. Jeong HC, Lee SY, Lee EJ, Jung KH, Kang EH, Kim JH, Park EK, Lee SH, Uhm CS, Cho Y, Shin C, Shim JJ, Kim HK, In KH, Kang KH, and Yoo SH. Proteomic analysis of peripheral T-lymphocytes in patients with asthma. *Chest* 132: 489–496, 2007.
78. Jonuleit H, Schmitt E, Schuler G, Knop J, and Enk AH. Induction of interleukin 10-producing, nonproliferating CD4(+) T cells with regulatory properties by repetitive stimulation with allogeneic immature human dendritic cells. *J Exp Med* 192: 1213–1222, 2000.
79. Kang MW, Jang JY, Choi JY, Kim SH, Oh J, Cho BS, and Lee CE. Induction of IFN-gamma gene expression by thioredoxin: positive feed-back regulation of Th1 response by thioredoxin and IFN-gamma. *Cell Physiol Biochem* 21: 215–224, 2008.
80. Keegan BM and Noseworthy JH. Multiple sclerosis. *Annu Rev Med* 53: 285–302, 2002.
81. Kelleher ZT, Matsumoto A, Stamler JS, and Marshall HE. NOS2 regulation of NF-kappaB by S-nitrosylation of p65. *J Biol Chem* 282: 30667–30672, 2007.
82. Kilpatrick DC. Mannan-binding lectin and its role in innate immunity. *Transfus Med* 12: 335–352, 2002.
83. Kim SF, Huri DA, and Snyder SH. Inducible nitric oxide synthase binds, S-nitrosylates, and activates cyclooxygenase-2. *Science* 310: 1966–1970, 2005.
84. King MR, Ismail AS, Davis LS, and Karp DR. Oxidative stress promotes polarization of human T cell differentiation toward a T helper 2 phenotype. *J Immunol* 176: 2765–2772, 2006.
85. Klatt P, Pineda Molina E, and Lamas S. Nitric oxide inhibits c-Jun DNA binding by specifically targeted S-glutathionylation. *J Biol Chem* 274: 15857–15864, 1999.
86. Klatt P, Pineda Molina E, Pérez-Sala D, and Lamas S. Novel application of S-nitrosoglutathione-sepharose to identify proteins that are potential targets for S-nitrosoglutathione-induced mixed-disulphide formation. *Biochem J* 349: 567–578, 2000.
87. Koh KP, Wang Y, Yi T, Shiao SL, Lorber MI, Sessa WC, Tellides G, and Pober JS. T cell-mediated vascular dysfunction of human allografts results from IFN-gamma dysregulation of NO synthase. *J Clin Invest* 114: 846–856, 2004.
88. Kornberg MD, Sen N, Hara MR, Juluri KR, Nguyen JV, Snowman AM, Law L, Hester LD, and Snyder SH. GAPDH mediates nitrosylation of nuclear proteins. *Nat Cell Biol* 12: 1094–1100, 2010.
89. Kuroki Y, Takahashi M, and Nishitani C. Pulmonary collectins in innate immunity of the lung. *Cell Microbiol* 9: 1871–1879, 2007.
90. Lancaster JR, Jr., and Gaston B. NO and nitrosothiols: spatial confinement and free diffusion. *Am J Physiol Lung Cell Mol Physiol* 287: L465–L466, 2004.
91. Lander HM, Hajjar DP, Hempstead BL, Mirza UA, Chait BT, Campbell S, and Quilliam LA. A molecular redox switch on $p21^{ras}$. Structural basis for the nitric oxide-$p21^{ras}$ interaction. *J Biol Chem* 272: 4323–4326, 1997.
91a. Laver JR, McLean S, Bowman LAH, Harrison LJ, Read RC, and Poole RK. Nitrosothiols in bacterial pathogens and pathogenesis. *Antioxid Redox Signal* 2012 [Epub ahead of print]; DOI: 10.1089/ars.2012.4767.
92. Laver JR, Stevanin TM, Messenger SL, Lunn AD, Lee ME, Moir JW, Poole RK, and Read RC. Bacterial nitric oxide detoxification prevents host cell S-nitrosothiol formation: a novel mechanism of bacterial pathogenesis. *FASEB J* 24: 286–295, 2010.
93. Lee SW, Choi H, Eun SY, Fukuyama S, and Croft M. Nitric oxide modulates TGF-beta-directive signals to suppress Foxp3+ regulatory T cell differentiation and potentiate Th1 development. *J Immunol* 186: 6972–6980, 2011.
94. Lee YK, Mukasa R, Hatton RD, and Weaver CT. Developmental plasticity of Th17 and Treg cells. *Curr Opin Immunol* 21: 274–280, 2009.
95. Lim SY, Raftery M, Cai H, Hsu K, Yan WX, Hseih HL, Watts RN, Richardson D, Thomas S, Perry M, and Geczy CL. S-nitrosylated S100A8: novel anti-inflammatory properties. *J Immunol* 181: 5627–5636, 2008.
96. Liu L, Hausladen A, Zeng M, Que L, Heitman J, and Stamler JS. A metabolic enzyme for S-nitrosothiol conserved from bacteria to humans. *Nature* 410: 490–494, 2001.
97. Liu L and Stamler JS. NO: an inhibitor of cell death. *Cell Death Differ* 6: 937–942, 1999.
98. Liu L, Yan Y, Zeng M, Zhang J, Hanes MA, Ahearn G, McMahon TJ, Dickfeld T, Marshall HE, Que LG, and Stamler JS. Essential roles of S-nitrosothiols in vascular homeostasis and endotoxic shock. *Cell* 116: 617–628, 2004.
99. Malhotra D, Thimmulappa RK, Mercado N, Ito K, Kombairaju P, Kumar S, Ma J, Feller-Kopman D, Wise R, Barnes P, and Biswal S. Denitrosylation of HDAC2 by targeting Nrf2 restores glucocorticosteroid sensitivity in macrophages from COPD patients. *J Clin Invest* 121: 4289–4302, 2011.
100. Malik SI, Hussain A, Yun BW, Spoel SH, and Loake GJ. GSNOR-mediated de-nitrosylation in the plant defence response. *Plant Sci* 181: 540–544, 2011.
101. Mannick JB, Hausladen A, Liu L, Hess DT, Zeng M, Miao QX, Kane LS, Gow AJ, and Stamler JS. Fas-induced caspase denitrosylation. *Science* 284: 651–654, 1999.
102. Marino SM and Gladyshev VN. Structural analysis of cysteine S-nitrosylation: a modified acid-based motif and the emerging role of trans-nitrosylation. *J Mol Biol* 395: 844–859, 2010.
103. Marshall HE, Potts EN, Kelleher ZT, Stamler JS, Foster WM, and Auten RL. Protection from lipopolysaccharide-induced lung injury by augmentation of airway S-nitrosothiols. *Am J Respir Crit Care Med* 180: 11–18, 2009.
104. Marshall HE and Stamler JS. Inhibition of NF-kappa B by S-nitrosylation. *Biochemistry* 40: 1688–1693, 2001.
105. Marshall HE and Stamler JS. Nitrosative stress-induced apoptosis through inhibition of NF-kappaB. *J Biol Chem* 277: 34223–34228, 2002.
106. Martínez-Ruiz A, Cadenas S, and Lamas S. Nitric oxide signaling: classical, less classical, and nonclassical mechanisms. *Free Radic Biol Med* 51: 17–29, 2011.
107. Martínez-Ruiz A and Lamas S. Detection and proteomic identification of S-nitrosylated proteins in endothelial cells. *Arch Biochem Biophys* 423: 192–199, 2004.
108. Martínez-Ruiz A and Lamas S. S-nitrosylation: a potential new paradigm in signal transduction. *Cardiovasc Res* 62: 43–52, 2004.
109. Martínez-Ruiz A and Lamas S. Signalling by NO-induced protein S-nitrosylation and S-glutathionylation: convergences and divergences. *Cardiovasc Res* 75: 220–228, 2007.
110. Martínez-Ruiz A and Lamas S. Two decades of new concepts in nitric oxide signaling: From the discovery of a gas

messenger to the mediation of nonenzymatic posttranslational modifications. *IUBMB Life* 61: 91–98, 2009.
111. Martínez-Ruiz A, Villanueva L, de Orduña CG, López-Ferrer D, Higueras MÁ, Tarín C, Rodríguez-Crespo I, Vázquez J, and Lamas S. S-nitrosylation of Hsp90 promotes the inhibition of its ATPase and endothelial nitric oxide synthase regulatory activities. *Proc Natl Acad Sci U S A* 102: 8525–8530, 2005.
112. Mayya V, Lundgren DH, Hwang SI, Rezaul K, Wu L, Eng JK, Rodionov V, and Han DK. Quantitative phosphoproteomic analysis of T cell receptor signaling reveals system-wide modulation of protein-protein interactions. *Sci Signal* 2: ra46, 2009.
113. McInnes IB, Leung BP, Field M, Wei XQ, Huang FP, Sturrock RD, Kinninmonth A, Weidner J, Mumford R, and Liew FY. Production of nitric oxide in the synovial membrane of rheumatoid and osteoarthritis patients. *J Exp Med* 184: 1519–1524, 1996.
114. Messina JP and Lawrence DA. Cell cycle progression of glutathione-depleted human peripheral blood mononuclear cells is inhibited at S phase. *J Immunol* 143: 1974–1981, 1989.
115. Mihm S, Galter D, and Droge W. Modulation of transcription factor NF kappa B activity by intracellular glutathione levels and by variations of the extracellular cysteine supply. *FASEB J* 9: 246–252, 1995.
116. Miller BH, Fratti RA, Poschet JF, Timmins GS, Master SS, Burgos M, Marletta MA, and Deretic V. Mycobacteria inhibit nitric oxide synthase recruitment to phagosomes during macrophage infection. *Infect Immun* 72: 2872–2878, 2004.
117. Mitchell DA, Erwin PA, Michel T, and Marletta MA. S-Nitrosation and regulation of inducible nitric oxide synthase. *Biochemistry* 44: 4636–4647, 2005.
118. Mitchell DA, Morton SU, Fernhoff NB, and Marletta MA. Thioredoxin is required for S-nitrosation of procaspase-3 and the inhibition of apoptosis in Jurkat cells. *Proc Natl Acad Sci U S A* 104: 11609–11614, 2007.
119. Mori N, Nunokawa Y, Yamada Y, Ikeda S, Tomonaga M, and Yamamoto N. Expression of human inducible nitric oxide synthase gene in T-cell lines infected with human T-cell leukemia virus type-I and primary adult T-cell leukemia cells. *Blood* 94: 2862–2870, 1999.
120. Mougiakakos D, Johansson CC, Jitschin R, Bottcher M, and Kiessling R. Increased thioredoxin-1 production in human naturally occurring regulatory T cells confers enhanced tolerance to oxidative stress. *Blood* 117: 857–861, 2011.
121. Nagy G, Clark JM, Buzas E, Gorman C, Pasztoi M, Koncz A, Falus A, and Cope AP. Nitric oxide production of T lymphocytes is increased in rheumatoid arthritis. *Immunol Lett* 118: 55–58, 2008.
122. Nagy G, Koncz A, and Perl A. T cell activation-induced mitochondrial hyperpolarization is mediated by Ca2+ - and redox-dependent production of nitric oxide. *J Immunol* 171: 5188–5197, 2003.
123. Nagy G, Koncz A, Telarico T, Fernandez D, Ersek B, Buzas E, and Perl A. Central role of nitric oxide in the pathogenesis of rheumatoid arthritis and systemic lupus erythematosus. *Arthritis Res Ther* 12: 210, 2010.
124. Nakamura T, Wang L, Wong CC, Scott FL, Eckelman BP, Han X, Tzitzilonis C, Meng F, Gu Z, Holland EA, Clemente AT, Okamoto S, Salvesen GS, Riek R, Yates JR, 3rd, and Lipton SA. Transnitrosylation of XIAP regulates caspase-dependent neuronal cell death. *Mol Cell* 39: 184–195, 2010.
125. Navarro-Lérida I, Álvarez-Barrientos A, and Rodríguez-Crespo I. N-terminal palmitoylation within the appropriate amino acid environment conveys on NOS2 the ability to progress along the intracellular sorting pathways. *J Cell Sci* 119: 1558–1569, 2006.
126. Navarro-Lérida I, Corvi MM, Barrientos AÁ, Gavilanes F, Berthiaume LG, and Rodríguez-Crespo I. Palmitoylation of inducible nitric-oxide synthase at cys-3 is required for proper intracellular traffic and nitric oxide synthesis. *J Biol Chem* 279: 55682–55689, 2004.
127. Navarro-Lérida I, Martínez-Moreno M, Ventoso I, Álvarez-Barrientos A, and Rodríguez-Crespo I. Binding of CAP70 to inducible nitric oxide synthase and implications for the vectorial release of nitric oxide in polarized cells. *Mol Biol Cell* 18: 2768–2777, 2007.
128. Niedbala W, Alves-Filho JC, Fukada SY, Vieira SM, Mitani A, Sonego F, Mirchandani A, Nascimento DC, Cunha FQ, and Liew FY. Regulation of type 17 helper T-cell function by nitric oxide during inflammation. *Proc Natl Acad Sci U S A* 108: 9220–9225, 2011.
129. Niedbala W, Cai B, Liu H, Pitman N, Chang L, and Liew FY. Nitric oxide induces CD4+CD25+ Foxp3 regulatory T cells from CD4+CD25 T cells via p53, IL-2, and OX40. *Proc Natl Acad Sci U S A* 104: 15478–15483, 2007.
130. Niedbala W, Wei XQ, Campbell C, Thomson D, Komai-Koma M, and Liew FY. Nitric oxide preferentially induces type 1 T cell differentiation by selectively up-regulating IL-12 receptor beta 2 expression via cGMP. *Proc Natl Acad Sci U S A* 99: 16186–16191, 2002.
131. Nussenblatt RB. The natural history of uveitis. *Int Ophthalmol* 14: 303–308, 1990.
132. Ohya M, Nishitani C, Sano H, Yamada C, Mitsuzawa H, Shimizu T, Saito T, Smith K, Crouch E, and Kuroki Y. Human pulmonary surfactant protein D binds the extracellular domains of toll-like receptors 2 and 4 through the carbohydrate recognition domain by a mechanism different from its binding to phosphatidylinositol and lipopolysaccharide. *Biochemistry* 45: 8657–8664, 2006.
133. Palmer E. Negative selection—clearing out the bad apples from the T-cell repertoire. *Nat Rev Immunol* 3: 383–391, 2003.
134. Park HS, Huh SH, Kim MS, Lee SH, and Choi EJ. Nitric oxide negatively regulates c-Jun N-terminal kinase/stress-activated protein kinase by means of S-nitrosylation. *Proc Natl Acad Sci U S A* 97: 14382–14387, 2000.
135. Park HS, Mo JS, and Choi EJ. Nitric oxide inhibits an interaction between JNK1 and c-Jun through nitrosylation. *Biochem Biophys Res Commun* 351: 281–286, 2006.
136. Persson A, Chang D, Rust K, Moxley M, Longmore W, and Crouch E. Purification and biochemical characterization of CP4 (SP-D), a collagenous surfactant-associated protein. *Biochemistry* 28: 6361–6367, 1989.
137. Pineda-Molina E, Klatt P, Vázquez J, Marina A, García de Lacoba M, Pérez-Sala D, and Lamas S. Glutathionylation of the p50 subunit of NF-kappaB: a mechanism for redox-induced inhibition of DNA binding. *Biochemistry* 40: 14134–14142, 2001.
138. Podolsky DK. Inflammatory bowel disease. *N Engl J Med* 347: 417–429, 2002.
139. Prasad R, Giri S, Nath N, Singh I, and Singh AK. GSNO attenuates EAE disease by S-nitrosylation-mediated modulation of endothelial-monocyte interactions. *Glia* 55: 65–77, 2007.
140. Que LG, Liu L, Yan Y, Whitehead GS, Gavett SH, Schwartz DA, and Stamler JS. Protection from experimental asthma by an endogenous bronchodilator. *Science* 308: 1618–1621, 2005.

141. Que LG, Yang Z, Stamler JS, Lugogo NL, and Kraft M. S-nitrosoglutathione reductase: an important regulator in human asthma. *Am J Respir Crit Care Med* 180: 226–231, 2009.
142. Rahman MA, Senga T, Ito S, Hyodo T, Hasegawa H, and Hamaguchi M. S-nitrosylation at cysteine 498 of c-Src tyrosine kinase regulates nitric oxide-mediated cell invasion. *J Biol Chem* 285: 3806–3814, 2010.
143. Rammes A, Roth J, Goebeler M, Klempt M, Hartmann M, and Sorg C. Myeloid-related protein (MRP) 8 and MRP14, calcium-binding proteins of the S100 family, are secreted by activated monocytes via a novel, tubulin-dependent pathway. *J Biol Chem* 272: 9496–9502, 1997.
144. Reiling N, Kroncke R, Ulmer AJ, Gerdes J, Flad HD, and Hauschildt S. Nitric oxide synthase: expression of the endothelial, Ca2+/calmodulin-dependent isoform in human B and T lymphocytes. *Eur J Immunol* 26: 511–516, 1996.
145. Reynaert NL, Ckless K, Korn SH, Vos N, Guala AS, Wouters EF, van der Vliet A, and Janssen-Heininger YM. Nitric oxide represses inhibitory kappaB kinase through S-nitrosylation. *Proc Natl Acad Sci U S A* 101: 8945–8950, 2004.
146. Rhee KY, Erdjument-Bromage H, Tempst P, and Nathan CF. S-nitroso proteome of Mycobacterium tuberculosis: enzymes of intermediary metabolism and antioxidant defense. *Proc Natl Acad Sci U S A* 102: 467–472, 2005.
147. Rodríguez-Pascual F, Redondo-Horcajo M, Magán-Marchal N, Lagares D, Martínez-Ruiz A, Kleinert H, and Lamas S. Glyceraldehyde-3-phosphate dehydrogenase regulates endothelin-1 expression by a novel, redox-sensitive mechanism involving mRNA stability. *Mol Cell Biol* 28: 7139–7155, 2008.
148. Rodriguez I, Matsuura K, Ody C, Nagata S, and Vassalli P. Systemic injection of a tripeptide inhibits the intracellular activation of CPP32-like proteases *in vivo* and fully protects mice against Fas-mediated fulminant liver destruction and death. *J Exp Med* 184: 2067–2072, 1996.
149. Roozendaal R, Vellenga E, de Jong MA, Traanberg KF, Postma DS, de Monchy JG, and Kauffman HF. Resistance of activated human Th2 cells to NO-induced apoptosis is mediated by gamma-glutamyltranspeptidase. *Int Immunol* 13: 519–528, 2001.
150. Sahaf B, Soderberg A, Spyrou G, Barral AM, Pekkari K, Holmgren A, and Rosen A. Thioredoxin expression and localization in human cell lines: detection of full-length and truncated species. *Exp Cell Res* 236: 181–192, 1997.
151. Salvemini D, Misko TP, Masferrer JL, Seibert K, Currie MG, and Needleman P. Nitric oxide activates cyclooxygenase enzymes. *Proc Natl Acad Sci U S A* 90: 7240–7244, 1993.
152. Santhanam L, Gucek M, Brown TR, Mansharamani M, Ryoo S, Lemmon CA, Romer L, Shoukas AA, Berkowitz DE, and Cole RN. Selective fluorescent labeling of S-nitrosothiols (S-FLOS): a novel method for studying S-nitrosation. *Nitric Oxide* 19: 295–302, 2008.
153. Sato N, Iwata S, Nakamura K, Hori T, Mori K, and Yodoi J. Thiol-mediated redox regulation of apoptosis. Possible roles of cellular thiols other than glutathione in T cell apoptosis. *J Immunol* 154: 3194–3203, 1995.
154. Savidge TC, Newman P, Pothoulakis C, Ruhl A, Neunlist M, Bourreille A, Hurst R, and Sofroniew MV. Enteric glia regulate intestinal barrier function and inflammation via release of S-nitrosoglutathione. *Gastroenterology* 132: 1344–1358, 2007.
155. Schneemann M and Schoedon G. Species differences in macrophage NO production are important. *Nat Immunol* 3: 102, 2002.
156. Sciorati C, Rovere P, Ferrarini M, Heltai S, Manfredi AA, and Clementi E. Autocrine nitric oxide modulates CD95-induced apoptosis in gammadelta T lymphocytes. *J Biol Chem* 272: 23211–23215, 1997.
157. Seaton BA, Crouch EC, McCormack FX, Head JF, Hartshorn KL, and Mendelsohn R. Review: structural determinants of pattern recognition by lung collectins. *Innate Immun* 16: 143–150, 2010.
158. Sen N, Hara MR, Kornberg MD, Cascio MB, Bae BI, Shahani N, Thomas B, Dawson TM, Dawson VL, Snyder SH, and Sawa A. Nitric oxide-induced nuclear GAPDH activates p300/CBP and mediates apoptosis. *Nat Cell Biol* 10: 866–873, 2008.
159. Sengupta R and Holmgren A. The role of thioredoxin in the regulation of cellular processes by S-nitrosylation. *Biochim Biophys Acta* 1820: 689–700, 2012.
160. Shi YF, Bissonnette RP, Parfrey N, Szalay M, Kubo RT, and Green DR. *In vivo* administration of monoclonal antibodies to the CD3 T cell receptor complex induces cell death (apoptosis) in immature thymocytes. *J Immunol* 146: 3340–3346, 1991.
161. Sido B, Giese T, Autschbach F, Lasitschka F, Braunstein J, and Meuer SC. Potential role of thioredoxin in immune responses in intestinal lamina propria T lymphocytes. *Eur J Immunol* 35: 408–417, 2005.
162. Smith-Garvin JE, Koretzky GA, and Jordan MS. T cell activation. *Annu Rev Immunol* 27: 591–619, 2009.
163. Smith BC, Fernhoff NB, and Marletta MA. Mechanism and kinetics of inducible nitric oxide synthase auto-S-nitrosation and inactivation. *Biochemistry* 51: 1028–1040, 2012.
164. Smyth MJ. Glutathione modulates activation-dependent proliferation of human peripheral blood lymphocyte populations without regulating their activated function. *J Immunol* 146: 1921–1927, 1991.
165. Sriskandan S, Evans TJ, and Cohen J. Bacterial superantigen-induced human lymphocyte responses are nitric oxide dependent and mediated by IL-12 and IFN-gamma. *J Immunol* 156: 2430–2435, 1996.
166. Stamler JS and Hess DT. Nascent nitrosylases. *Nat Cell Biol* 12: 1024–1026, 2010.
167. Stamler JS, Lamas S, and Fang FC. Nitrosylation: the prototypic redox-based signaling mechanism. *Cell* 106: 675–683, 2001.
168. Stoyanovsky DA, Tyurina YY, Tyurin VA, Anand D, Mandavia DN, Gius D, Ivanova J, Pitt B, Billiar TR, and Kagan VE. Thioredoxin and lipoic acid catalyze the denitrosation of low molecular weight and protein S-nitrosothiols. *J Am Chem Soc* 127: 15815–15823, 2005.
169. Tagaya Y, Maeda Y, Mitsui A, Kondo N, Matsui H, Hamuro J, Brown N, Arai K, Yokota T, Wakasugi H, *et al.* ATL-derived factor (ADF), an IL-2 receptor/Tac inducer homologous to thioredoxin; possible involvement of dithiol-reduction in the IL-2 receptor induction. *EMBO J* 8: 757–764, 1989.
170. Tai XG, Toyo-oka K, Yamamoto N, Yashiro Y, Mu J, Hamaoka T, and Fujiwara H. Expression of an inducible type of nitric oxide (NO) synthase in the thymus and involvement of NO in deletion of TCR-stimulated double-positive thymocytes. *J Immunol* 158: 4696–4703, 1997.
171. Tang Q, Adams JY, Tooley AJ, Bi M, Fife BT, Serra P, Santamaria P, Locksley RM, Krummel MF, and Bluestone JA. Visualizing regulatory T cell control of autoimmune responses in nonobese diabetic mice. *Nat Immunol* 7: 83–92, 2006.

172. Tarrant TK, Silver PB, Wahlsten JL, Rizzo LV, Chan CC, Wiggert B, and Caspi RR. Interleukin 12 protects from a T helper type 1-mediated autoimmune disease, experimental autoimmune uveitis, through a mechanism involving interferon gamma, nitric oxide, and apoptosis. *J Exp Med* 189: 219–230, 1999.
173. Tatemichi M, Tazawa H, Masuda M, Saleem M, Wada S, Donehower LA, Ohgaki H, and Ohshima H. Suppression of thymic lymphomas and increased nonthymic lymphomagenesis in Trp53-deficient mice lacking inducible nitric oxide synthase gene. *Int J Cancer* 111: 819–828, 2004.
174. Tello D, Tarín C, Ahicart P, Bretón-Romero R, Lamas S, and Martínez-Ruiz A. A "fluorescence switch" technique increases the sensitivity of proteomic detection and identification of S-nitrosylated proteins. *Proteomics* 9: 5359–5370, 2009.
175. Tian J, Kim SF, Hester L, and Snyder SH. S-nitrosylation/activation of COX-2 mediates NMDA neurotoxicity. *Proc Natl Acad Sci U S A* 105: 10537–10540, 2008.
176. Tiegs G, Hentschel J, and Wendel A. A T cell-dependent experimental liver injury in mice inducible by concanavalin A. *J Clin Invest* 90: 196–203, 1992.
177. Tsujita M, Batista WL, Ogata FT, Stern A, Monteiro HP, and Arai RJ. The nitric oxide-sensitive p21Ras-ERK pathway mediates S-nitrosoglutathione-induced apoptosis. *Biochem Biophys Res Commun* 369: 1001–1006, 2008.
178. Vodovotz Y, Russell D, Xie QW, Bogdan C, and Nathan C. Vesicle membrane association of nitric oxide synthase in primary mouse macrophages. *J Immunol* 154: 2914–2925, 1995.
179. Walker MR, Kasprowicz DJ, Gersuk VH, Benard A, Van Landeghen M, Buckner JH, and Ziegler SF. Induction of FoxP3 and acquisition of T regulatory activity by stimulated human CD4+CD25- T cells. *J Clin Invest* 112: 1437–1443, 2003.
180. Wang A, Rud J, Olson CM, Jr., Anguita J, and Osborne BA. Phosphorylation of Nur77 by the MEK-ERK-RSK cascade induces mitochondrial translocation and apoptosis in T cells. *J Immunol* 183: 3268–3277, 2009.
181. Wang L, Yu CR, Kim HP, Liao W, Telford WG, Egwuagu CE, and Leonard WJ. Key role for IL-21 in experimental autoimmune uveitis. *Proc Natl Acad Sci U S A* 108: 9542–9547, 2011.
182. Wei XQ, Charles IG, Smith A, Ure J, Feng GJ, Huang FP, Xu D, Muller W, Moncada S, and Liew FY. Altered immune responses in mice lacking inducible nitric oxide synthase. *Nature* 375: 408–411, 1995.
183. West MB, Hill BG, Xuan YT, and Bhatnagar A. Protein glutathiolation by nitric oxide: an intracellular mechanism regulating redox protein modification. *FASEB J* 20: 1715–1717, 2006.
184. Willenborg DO, Staykova M, Fordham S, O'Brien N, and Linares D. The contribution of nitric oxide and interferon gamma to the regulation of the neuro-inflammation in experimental autoimmune encephalomyelitis. *J Neuroimmunol* 191: 16–25, 2007.
185. Williams MS, Noguchi S, Henkart PA, and Osawa Y. Nitric oxide synthase plays a signaling role in TCR-triggered apoptotic death. *J Immunol* 161: 6526–6531, 1998.
186. Wink DA, Hines HB, Cheng RY, Switzer CH, Flores-Santana W, Vitek MP, Ridnour LA, and Colton CA. Nitric oxide and redox mechanisms in the immune response. *J Leukoc Biol* 89: 873–891, 2011.
187. Wollman EE, Kahan A, and Fradelizi D. Detection of membrane associated thioredoxin on human cell lines. *Biochem Biophys Res Commun* 230: 602–606, 1997.
188. Wright JR. Immunoregulatory functions of surfactant proteins. *Nat Rev Immunol* 5: 58–68, 2005.
189. Wu C, Liu T, Chen W, Oka S, Fu C, Jain MR, Parrott AM, Baykal AT, Sadoshima J, and Li H. Redox regulatory mechanism of transnitrosylation by thioredoxin. *Mol Cell Proteomics* 9: 2262–2275, 2010.
190. Wu C, Parrott AM, Fu C, Liu T, Marino SM, Gladyshev VN, Jain MR, Baykal AT, Li Q, Oka S, Sadoshima J, Beuve A, Simmons WJ, and Li H. Thioredoxin 1-mediated post-translational modifications: reduction, transnitrosylation, denitrosylation, and related proteomics methodologies. *Antioxid Redox Signal* 15: 2565–2604, 2011.
191. Wu M and Tsirka SE. Endothelial NOS-deficient mice reveal dual roles for nitric oxide during experimental autoimmune encephalomyelitis. *Glia* 57: 1204–1215, 2009.
192. Xu L, Han C, Lim K, and Wu T. Activation of cytosolic phospholipase A2alpha through nitric oxide-induced S-nitrosylation. Involvement of inducible nitric-oxide synthase and cyclooxygenase-2. *J Biol Chem* 283: 3077–3087, 2008.
193. Yamashita M, Shinnakasu R, Asou H, Kimura M, Hasegawa A, Hashimoto K, Hatano N, Ogata M, and Nakayama T. Ras-ERK MAPK cascade regulates GATA3 stability and Th2 differentiation through ubiquitin-proteasome pathway. *J Biol Chem* 280: 29409–29419, 2005.
194. Yamazoe M, Nishitani C, Takahashi M, Katoh T, Ariki S, Shimizu T, Mitsuzawa H, Sawada K, Voelker DR, Takahashi H, and Kuroki Y. Pulmonary surfactant protein D inhibits lipopolysaccharide (LPS)-induced inflammatory cell responses by altering LPS binding to its receptors. *J Biol Chem* 283: 35878–35888, 2008.
195. Yang Z, Wang ZE, Doulias PT, Wei W, Ischiropoulos H, Locksley RM, and Liu L. Lymphocyte development requires S-nitrosoglutathione reductase. *J Immunol* 185: 6664–6669, 2010.
196. Yun BW, Feechan A, Yin M, Saidi NB, Le Bihan T, Yu M, Moore JW, Kang JG, Kwon E, Spoel SH, Pallas JA, and Loake GJ. S-nitrosylation of NADPH oxidase regulates cell death in plant immunity. *Nature* 478: 264–268, 2011.
197. Zech B, Kohl R, von Knethen A, and Brune B. Nitric oxide donors inhibit formation of the Apaf-1/caspase-9 apoptosome and activation of caspases. *Biochem J* 371: 1055–1064, 2003.
198. Zhang X, Huang B, and Chen C. SNO spectral counting (SNOSC), a label-free proteomic method for quantification of changes in levels of protein S-nitrosation. *Free Radic Res* 46: 1044–1050, 2012.
199. Zhang Y and Hogg N. Formation and stability of S-nitrosothiols in RAW 264.7 cells. *Am J Physiol Lung Cell Mol Physiol* 287: L467–L474, 2004.
200. Zhang Y and Hogg N. The mechanism of transmembrane S-nitrosothiol transport. *Proc Natl Acad Sci U S A* 101: 7891–7896, 2004.
201. Zhang Y, Keszler A, Broniowska KA, and Hogg N. Characterization and application of the biotin-switch assay for the identification of S-nitrosated proteins. *Free Radic Biol Med* 38: 874–881, 2005.
202. Zhou X, Gordon SA, Kim YM, Hoffman RA, Chen Y, Zhang XR, Simmons RL, and Ford HR. Nitric oxide induces thymocyte apoptosis via a caspase-1-dependent mechanism. *J Immunol* 165: 1252–1258, 2000.
203. Zhou X, Han P, Li J, Zhang X, Huang B, Ruan HQ, and Chen C. ESNOQ, proteomic quantification of endogenous S-nitrosation. *PLoS One* 5: e10015, 2010.

Address correspondence to:
Dr. Antonio Martínez-Ruiz
Servicio de Inmunología
Hospital Universitario de La Princesa
C/Diego de León 62
E-28006 Madrid
Spain

E-mail: amartinezr.hlpr@salud.madrid.org

Date of first submission to ARS Central, June 22, 2012; date of acceptance, July 1, 2012.

Abbreviations Used

2-DE = two-dimensional electrophoresis
AICD = activation-induced cell death
APCs = antigen-presenting cells
BST = biotin-switch technique
CNS = central nervous system
COX-2 = cyclooxygenase-2
cPLA2α = cytosolic phospholipase A2α
CRD = carbohydrate-recognition domain
DAG = diacylglycerol
DCs = dendritic cells
dnIKK2 = dominant-negative form of Ikappa B kinase-2
EAE = experimental autoimmune encephalomyelitis
EAU = experimental autoimmune uveitis
ENO = ethyl nitrite
eNOS = endothelial NOS
GFAP = glial fibrillary acid protein
GSH = glutathione
GSNO = S-nitrosoglutathione
GSNOR = S-nitrosoglutathione reductase
HDAC2 = histone deacetylase 2
HSV-Tk = herpes simplex virus thymidine kinase
IFN-γ = interferon-γ
IKK = IκB-kinase
IL-1R = interleukin-1 receptor
iNOS = inducible nitric oxide synthase
IP3 = inositol 1,4,5-triphosphate
IRAK = IL-1R-associated kinase
IRBP = interphotoreceptor retinoid-binding protein
JNK = C-Jun N-terminal kinase
LPS = lipopolysaccharide
MAPK = mitogen-activated protein kinase
MBL = mannose-binding lectin
MS = multiple sclerosis
NO = nitric oxide
PBTs = peripheral blood T cells
PTM = post-translational modification
RNS = reactive nitrogen species
SIRP-α = signal inhibitory regulatory protein α
SNAP = S-nitroso-N-acetylpenicillamine
SP-D = surfactant protein D
TCR = T-cell receptor
TIRAP = Toll/interleukin-1 receptor adaptor protein
TLR = toll-like receptor
TNF = tumor necrosis factor
TNFR = tumor necrosis factor receptor
Tregs = regulatory T cells
Trx = thioredoxin

ANTIOXIDANTS & REDOX SIGNALING
Volume 00, Number 00, 2013

DOI: 10.1089/ars.2012.5066

FORUM REVIEW ARTICLE

Specificity in S-Nitrosylation: A Short-Range Mechanism for NO Signaling?

Antonio Martínez-Ruiz,[1] Inês M. Araújo,[2,3] Alicia Izquierdo-Álvarez,[1] Pablo Hernansanz-Agustín,[1] Santiago Lamas,[4,5] and Juan M. Serrador[5]

Abstract

Significance: Nitric oxide (NO) classical and less classical signaling mechanisms (through interaction with soluble guanylate cyclase and cytochrome *c* oxidase, respectively) operate through direct binding of NO to protein metal centers, and rely on diffusibility of the NO molecule. S-Nitrosylation, a covalent post-translational modification of protein cysteines, has emerged as a paradigm of nonclassical NO signaling. ***Recent Advances:*** Several nonenzymatic mechanisms for S-nitrosylation formation and destruction have been described. Enzymatic mechanisms for transnitrosylation and denitrosylation have been also studied as regulators of the modification of specific subsets of proteins. The advancement of modification-specific proteomic methodologies has allowed progress in the study of diverse S-nitrosoproteomes, raising clues and questions about the parameters for determining the protein specificity of the modification. ***Critical Issues:*** We propose that S-nitrosylation is mainly a short-range mechanism of NO signaling, exerted in a relatively limited range of action around the NO sources, and tightly related to the very controlled regulation of subcellular localization of nitric oxide synthases. We review the nonenzymatic and enzymatic mechanisms that support this concept, as well as physiological examples of mammalian systems that illustrate well the precise compartmentalization of S-nitrosylation. ***Future Directions:*** Individual and proteomic studies of protein S-nitrosylation-based signaling should take into account the subcellular localization in order to gain further insight into the functional role of this modification in (patho)physiological settings. *Antioxid. Redox Signal.* 00, 000–000.

Introduction

Nitric oxide (NO) is clearly recognized as a signaling molecule in different pathways. A hallmark in this recognition came from the identification of NO as the endothelial-derived relaxing factor (EDRF), a factor produced by endothelial cells that induced vascular relaxation by operating on smooth muscle cells (52, 68). It was the first mammalian gas molecule discovered as a second messenger in a signaling pathway that included its production from L-arginine by a family of nitric oxide synthases (NOSs), and generation of cyclic GMP (cGMP) after the activation of soluble guanylate cyclase (sGC) by NO binding through a high-affinity metal coordination bond (26, 127). This may be considered as the "classical" mechanism of NO signaling (103, 106), and it includes a clear example of paracrine signaling, as NO produced in endothelial cells reacts with sGC located in smooth muscle cells, taking advantage of its ability to diffuse across biological membranes. In a similar way, NO produced in one neuron diffuses and acts upon surrounding neurons. Another well-established but "less classical" signaling mechanism of NO operates through the inhibition of cytochrome *c* oxidase, the complex IV of the oxidative phosphorylation system. Both signaling mechanisms rely on direct binding of NO to protein

[1]Servicio de Inmunología, Hospital Universitario de La Princesa, Instituto de Investigación Sanitaria Princesa (IP), Madrid, Spain.
[2]Regenerative Medicine Program, Department of Biomedical Sciences and Medicine, and [3]IBB-Institute for Biotechnology and Bioengineering, Centre of Molecular and Structural Biomedicine, University of Algarve, Faro, Portugal.
[4]Laboratorio Mixto Consejo Superior de Investigaciones Científicas (CSIC)/Fundación Renal "Iñigo Alvarez de Toledo" (FRIAT), Madrid, Spain.
[5]Dpto. Biología Celular e Inmunología, Centro de Biología Molecular "Severo Ochoa", CSIC-UAM, Madrid, Spain.

metal centers through coordination chemistry (reviewed in Refs. 103–106).

In addition, several "nonclassical" nitric oxide signaling mechanisms have been described, which rely mainly on covalent post-translational protein modification by a series of reactive nitrogen species (RNS) derived from the reaction of NO with other small molecules, including free radicals. Tyrosine nitration is associated with formation of peroxynitrite ($ONOO^-$) and nitrogen dioxide (NO_2), and is considered mainly as an irreversible modification that can impact on some signaling pathways (69, 124, 133, 145). Cysteine residues can be oxidized following RNS formation: $ONOO^-$ induces formation of oxygenated forms (sulfenic acid, $-SOH$; sulfinic acid, $-SO_2H$; sulfonic acid, $-SO_3H$), and S-glutathionylation and other forms of S-thiolation are induced both by $ONOO^-$ and nitrosothiol formation (3, 103, 105, 106, 111, 134, 157, 163).

S-Nitrosylation (also called S-nitrosation; see Refs. 42, 73, 104 for a discussion of the terminology) has emerged as one of the main mechanisms of nonclassical NO signaling. It implies the formation of a nitrosothiol (or thionitrite, R-S-N=O) at a cysteine residue, a subtle modification that has been shown to alter the functionality of a number of proteins. There are several reviews that highlight the particular characteristics of S-nitrosylation supporting its relevance as a mechanism of redox signaling related to NO production, as well as its implications in (patho)physiology in several species (35, 44, 61, 73, 83, 90, 104, 105, 141, 160). At least for some proteins, it has been shown that S-nitrosylation leads to disulfide formation (including S-glutathionylation), so it could be considered as an intermediate to such more stable modifications (reviewed in Refs. 73, 103, 105). For each case, detailed studies could establish if the different PTMs may have the same or different functional consequences, but it seems clear that this possibility has be integrated when studying signaling by S-nitrosylation.

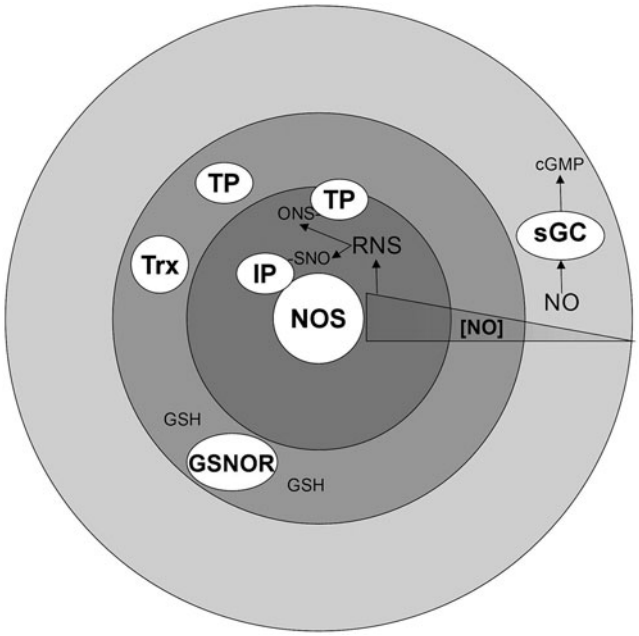

FIG. 1. Short-range and long-range NO signaling. Classical NO signaling, such as sGC activation, can be exerted at a relatively long distance from NO sources (NOS enzymes), even if NO concentration diminishes while targets are farther from the NOS. We postulate that S-nitrosylation of target proteins (TP) is essentially a short-range mechanism, limited to a tiny sphere around NOS. Among other factors described in the text, RNS formation requires higher NO concentrations, which are easier to achieve in the NOS surroundings (this is more clear in interacting proteins, IP), and denitrosylases such as Trx or GSNOR with GSH can narrow the range of action by reducing target protein S-nitrosylation.

Our aim is to review the factors that confer specificity to S-nitrosylation in order to be considered a signaling mechanism, with the proposal that its signaling function is exerted mainly in the short range, close to the NO producing sources (mainly NOS enzymes), and thus very dependent on their precise subcellular localization (Fig. 1). In addition, we provide some examples in which this short-range signaling occurs in the context of specific human and mammalian cell systems.

Biochemistry of S-Nitrosylation Specificity

Nonenzymatic biochemistry of S-nitrosylation formation

Several biochemical mechanisms have been postulated for nitrosothiol formation without requiring the presence of enzymes to catalyze it. Direct reaction of NO with cysteine residues is only relevant when the thiyl radical (P-S•) has been formed,

$$\text{P-S}\bullet + \bullet\text{NO} \rightarrow \text{P-S-NO}$$

which is relatively rare. This poses a substantial difference with classical and less classical NO signaling mechanisms, which are based on the direct reaction of NO with target proteins, and in which specificity relies on structural determinants that favor NO binding to particular metal centers. In the case of S-nitrosylation, the formation of other RNS is required, as the result of the reaction of NO with other species.

Reactions of NO with O_2 form a series of nitrogen oxides, with different oxidation states for the N atoms; among them, N_2O_3 is considered as a main nitrosating agent producing nitrite and a nitrosothiol:

$$N_2O_3 + RSH \rightarrow RSNO + H^+ + NO_2^-$$

However, the implication of N_2O_3 as a relevant nitrosating agent in biochemical environments has been challenged, mainly because its formation depends on the reaction of NO and O_2, also called NO auto-oxidation

$$2\ NO + O_2 \rightarrow 2\ NO_2$$

$$NO_2 + NO \rightarrow N_2O_3$$

and the reaction rate for its formation in water has been estimated as $\text{Rate} = k\,[NO]^2\,[O_2]$ with k being around $2–5 \times 10^6$ $M^{-2}\ s^{-1}$, consistent with the rate-limiting formation of NO_2 (11, 48, 165). Kinetic models integrating these reactions with the formation of other RNS have shown that N_2O_3 formation would not be very important at the NO concentrations estimated for biological systems (82, 87).

However, two facts can be considered that argue in favor of the relevance of this mechanism in localized cellular

environments. First, the reaction rate is very sensitive to the concentrations of the reactants, particularly NO. In a cell system where reactants concentrations are not in equilibrium, NO concentration would be much higher in a relatively small virtual sphere surrounding the NOS enzymes, allowing for faster formation of N_2O_3 and thiol S-nitrosylation. Second, it has been shown that in hydrophobic environments such as biological membranes, the same third-order rate law is observed, but the rate constant is increased up to 300 times (97, 113, 114); even with this rate acceleration, the overall NO fate would not be affected, but the reaction would be relevant enough to produce localized nitrosating species in membrane regions (114), where NOS enzymes localize due to their membrane binding structures.

An alternative mechanism for S-nitrosylation by nitrogen oxides involves the thiyl formation by NO_2 and subsequent reaction with NO (76):

$$NO_2 + RSH \rightarrow R\text{-}S\bullet + NO_2^- + H^+$$

$$NO + R\text{-}S\bullet \rightarrow RSNO$$

Again, the rate limiting step is the formation of NO_2, and it also requires an additional NO molecule, so the same considerations for the localized formation of N_2O_3 apply to this mechanism.

Metal-catalyzed formation of nitrosothiols has been described, mainly explained by a mechanism involving a one-electron oxidation of NO by oxidized transition metals, such as Fe^{3+} or Cu^{2+}; the nitrosonium (NO^+) formed could nitrosate a thiol in the proximity of such catalytic center (it is a relatively unstable species):

$$Me^{(n+1)+} + NO \rightarrow Me^n\text{-}NO^+$$

$$Me^n\text{-}NO^+ + RSH \rightarrow RSNO + Me^n + H^+$$

This mechanism has been shown to take part in specific proteins, where it can be considered as an enzymatic "nitrosylase" mechanism, such as in auto-nitrosylation of hemoglobin and other globins, and in S-nitrosoglutathione (GSNO) formation by ceruloplasmin or cytochrome *c* (reviewed in Refs. 5, 23, 53).

Recently, another pathway for S-nitrosylation formation has been described that could operate through generation of dinitrosyl-iron complexes (DNIC) from NO (20), and evidence has been found that DNIC can be a main form of NO in cells (62). This pathway will certainly deserve further investigation to assess the possible physiological role of these complexes as catalyzers of S-nitrosylation, and to test whether they are modified by subcellular localization.

Transnitrosylation

The nitroso group can be easily transferred between thiol groups, in a reversible reaction called transnitrosylation (or transnitrosation):

$$RSNO + R'SH \rightarrow RSH + R'SNO$$

Transnitrosylation among low-molecular-mass (LMM) thiols and protein thiols has been studied for a long time. LMM nitrosothiols, and especially GSNO (as the main intracellular LMM thiol is glutathione) can be considered as putative S-nitrosylation vectors in cells that could transmit the S-nitrosylation signal from the nitrosothiol-producing foci to potential protein targets. A recent study that analyzed the structural features of confirmed protein S-nitrosylation sites in the literature has postulated that a subset of proteins and residues could be specifically transnitrosylated by GSNO (101). However, the reaction of GSNO with protein thiols is more complicated, as it can also form a mixed disulfide by S-glutathionylation (reviewed in Refs. 80, 103, 105, 111), most probably with formation of nitroxyl (HNO):

$$PSH + GSNO \rightarrow PSNO + GSH$$

$$PSH + GSNO \rightarrow PSSG + HNO$$

Thus it would be interesting to compare the structural features regulating the balance between these reactions.

Several groups have recently described transnitrosylation reactions between proteins. These include protein–protein interaction determinants as specificity factors, as is the case in other enzymatic post-translational modifications used in signal transduction, such as phosphorylation. Each of the described transnitrosylases may have a restricted or broader range of target proteins and residues that can be preferentially S-nitrosylated due to their specific interactions. The nitroso group is transferred by equilibrium reactions and thus the thermodynamic comparison between both reactions (which can also be described with the redox potentials) has also to be considered. Recent reviews have thoroughly covered protein–protein transnitrosylation (5, 119), so we will just briefly describe the most relevant transnitrosylases.

Early studies on S-nitrosylated hemoglobin (SNO-Hb) reported that it was able to release NO to the blood flow causing an increase in blood pressure (50, 75, 142). Hb presents a heme group in each of its four subunits with a central iron atom, where O_2 binds. When O_2 concentration is low, NO binds to the iron; by an auto-S-nitrosylation reaction, this NO moiety is transferred to Cys93, and Hb suffers a conformational change from relaxed to tense structure. A clue for the export of the NO moiety came from the description of transnitrosylation from SNO-Hb to the most abundant protein in red blood cells, the Anion Exchanger 1 (AE1) (128). SNO-Hb interacts with AE1 in the erythrocyte membrane, promoting its transnitrosylation; subsequently the NO moiety leaves AE1 and diffuses into vessels (128). However, how this NO moiety is transferred from AE1 protein to vessels remains unclear.

Caspase-3 inactivation by S-nitrosylation of an active site Cys (Cys163) is reverted during Fas-induced signaling (100). The thioredoxin (Trx) system was described as a caspase-3 activator by denitrosylation via two different biochemical mechanisms (112). The first one implies thiol reduction in a "classical" way by means of its two active site Cys (Cys32 and Cys35) (8, 86). The second one is a transference of the NO moiety from caspase-3 to Trx by transnitrosylation of Cys32 in Trx. S-Nitrosylation of nonactive Cys has also been described, particularly Cys62, Cys69, and Cys73, in conditions where active site cysteines were oxidized (54, 59, 166). A recent study, using C32S and C35S mutants, demonstrated that Trx S-nitrosylated in Cys73 is able to transnitrosylate many cellular targets including caspase-3 (112, 166, 168). Interestingly, when Trx is S-nitrosylated in Cys73, the disulfide bond in the active site C32–C35 is not reduced by Trx reductase; both

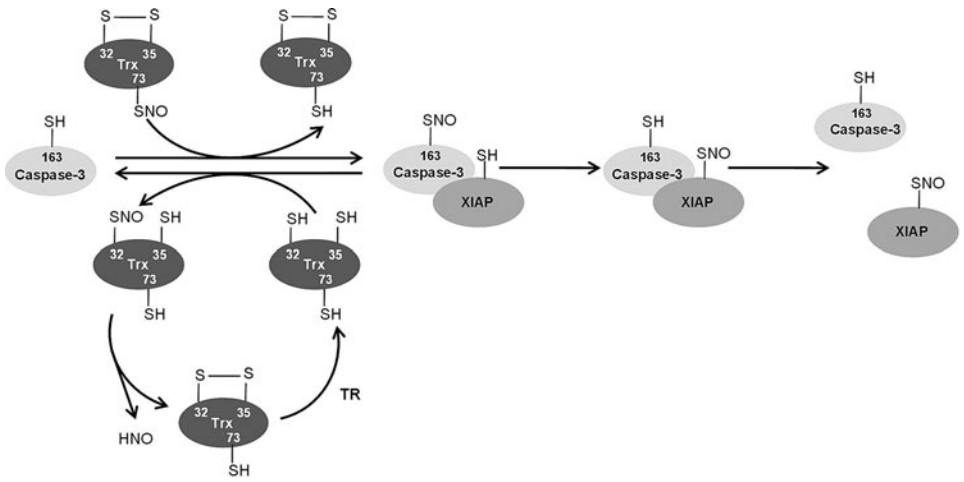

FIG. 2. Summary of transnitrosylation reactions between Trx, caspase-3, and XIAP that leads to caspase-3 activity regulation, including Cys residues that undergo S-nitrosylation. The active site of Trx denitrosylases caspase-3 in normal conditions, producing HNO and its own disulfide, which is reduced back by Trx reductase (TR). When its active site Cys is oxidized, Trx S-nitrosylated in Cys73 is able to transnitrosylate caspase-3 in Cys163. S-nitrosylated caspase-3 may also transnitrosylate its inhibitor XIAP, leading to a release of caspase-3.

enzymes are then uncoupled, which can be a mechanism to prevent the denitrosylase activity of Trx while promoting its transnitrosylase activity (59). Figure 2 summarizes the transnitrosylation and denitrosylation mechanisms involved in caspase-3 activation and inhibition in physiological and stress conditions.

Recently, S-nitrosylation of XIAP, one of the most important caspase-3/7/9 inhibitory proteins, was described in neurons (120, 155). As a consequence of this nitrosylation, the E3 ubiquitin ligase activity of XIAP is decreased and caspase degradation is inhibited, favoring apoptosis. This process is especially important in neurodegenerative diseases such as Alzheimer (AD), Parkinson (PD), and Huntington (HD) diseases, where a high content of SNO-XIAP was observed, suggesting that this reaction contributes to neuronal damage in these diseases. Interestingly, caspase-3 is able to transnitrosylate XIAP in pathophysiological situations of nitrosative stress or excitotoxicity, promoting apoptosis both by the protease activity of caspase-3 and impairing its degradation by inhibition of XIAP (120, 155).

In AD, amyloid-β peptide oligomerization provokes an increase in NO production, which leads to S-nitrosylation of Cdk5 (132). SNO-Cdk5 transnitrosylates dynamin related protein 1 (Drp1) in Cys644 (28). This reaction causes a mitochondrial fission hyperactivation as well as a compromise in mitochondrial bioenergetics which, in synaptic structures, could lead to synaptic loss (28, 159).

Glyceraldehyde-3-phosphate dehydrogenase (GAPDH) is also implicated in transnitrosylation processes. GAPDH is S-nitrosylated in its Cys150 residue; S-nitrosylated GAPDH interacts with Siah1, and it is translocated to the nucleus due to Siah1 nuclear localization signal (56). Once in the nucleus, SNO-GAPDH transnitrosylates proteins such as SIRT1, HDAC2, and DNA-PK, affecting metabolic pathways, normal aging processes, chromatin remodeling in neuronal development, or neurodegeneration (81, 121).

Transnitrosylation has been involved in the formation of pulmonary arterial hypertension (PAH). Mice chronically treated with N-acetylcysteine (NAC) or its S-nitrosylated form, S-nitroso-N-acetylcysteine (SNOAC), developed PAH, mimicking the effects of chronic hypoxia (126). This study showed that NAC needs to be converted to SNOAC and that activation of the HIF-dependent hypoxia response through transnitrosylation of particular proteins in the canonical HIF activation pathway (such as pVHL) could be among the molecular mechanisms responsible for this effect (126).

Denitrosylases

Removal of the nitroso group is another important aspect of S-nitrosylation signaling. It is generally accepted that S-nitrosylation is a labile modification, and that the levels of cellular nitrosothiols are low, due to a rapid turnover. Denitrosylation was firstly conceived as an unregulated and spontaneous process, and several nonenzymatic mechanisms of denitrosylation have been described that could potentially act *in vivo*. These include reactions mediated by nucleophilic compounds, transition metal ions, reactive oxygen species (ROS), and ascorbate (reviewed in Ref. 147).

Accumulating evidence shows that several enzymes can catalyze denitrosylation *in vitro* (14, 64, 77, 143, 154) and *in vivo* (16, 95) (reviewed in Refs. 5, 17). These enzymes may contribute to spacially limit the action of S-nitrosylation events, helping to keep their precise subcellular localization close to NO sources. They also may help to protect cells from ''excessive'' S-nitrosylation, as, for example, when inducible nitric oxide synthase (iNOS) is induced in immune cells in order to attack pathogens (reviewed in Ref. 60). In addition, they provide another mechanism of specificity and regulation since these enzymes may act over defined sets of substrate proteins. This is more important in examples of tightly regulated denitrosylation that may activate precise signals, such as the case of Fas-induced caspase-3 denitrosylation (100), which can be mediated by Trx (16), or receptor-regulated endothelial nitric oxide synthase (eNOS) activation (37).

Two main enzymatic mechanisms of denitrosylation have emerged in recent studies, GSNO reductase and the thioredoxin system. GSNO reductase (GSNOR) is an evolutionary conserved enzyme system previously known as alcohol dehydrogenase class III. GSH can react with a protein nitrosothiol leading to either transnitrosylation and subsequent generation of S-nitrosoglutathione (GSNO) or glutathionylation of the protein, in both cases with subsequent

release of the NO group from the protein thiol. This is supported by the observation that addition of GSH to SNO-proteins leads to their denitrosylation (125). GSNOR mainly catalyzes the denitrosylation of GSNO towards GSSG, utilizing NADH as an electron donor. The cycle is completed as GSSG is reduced by glutathione reductase and NADPH. Although GSNOR does not directly act on protein nitrosothiols, an equilibrium between GSNO and SNO-proteins is maintained by transnitrosylation, since *GSNOR*-knockout mice showed increased levels of both GSNO and SNO-proteins after nitrosothiol addition or lipopolysaccharide (LPS) treatment (95, 96).

GSNOR participates in signal transduction through G protein-coupled receptors (GPCRs) and, in particular, β_2-adrenergic receptor (β_2-AR). Upon agonist stimulation, GPCR kinases (GRKs) 2 and 3 are recruited to the plasma membrane by interaction with G$\beta\gamma$ subunits and phosphorylate the β_2-AR at the cytoplasmic tail (Fig. 3). This allows β-arrestin 2 to be transiently recruited by the activated receptor and driven to clathrin-coated pits where, after its dissociation, the receptor internalizes and becomes desensitized (reviewed in Ref. 135). Both GRK2 and β-arrestin 2 S-nitrosylations are controlled by GSNOR since both augment in *GSNOR*-knockout mice. S-Nitrosylation at GRK2 Cys340 decreased its kinase activity, β-arrestin 2 interaction and β_2-AR internalization and desensitization (164). On the other hand, binding of β-arrestin 2 to the clathrin pit is promoted by S-nitrosylation, which in turn increases β_2-AR internalization (123). This differential regulation of GPCR signaling by S-nitrosylation suggests that local denitrosylation of particular elements becomes important for cell signaling. GSNOR has been linked with the development and protection against several diseases. S-Nitrosylation of O6-alkylguanine-DNA alkyl transferase (AGT) in the liver of $GSNOR^{-/-}$ mice after LPS or diethylnitrosamine treatment promoted decreased capability of DNA repair, thus increasing hepatocellular carcinoma incidence (162). On the other hand, GSNOR deficiency protected against myocardial infarction (89).

The other best known denitrosylase is the thioredoxin (Trx) system. While GSNOR denitrosylates SNO-proteins indirectly through GSNO formation, Trx system has been shown to denitrosylate them directly. As mentioned above, uncoupled Trx can act as a transnitrosylase when its Cys73 is S-nitrosylated, after disulfide formation between catalytic Cys32 and Cys35; however, for its denitrosylase function it uses the catalytic center with both Cys32 and Cys35 in their reduced state (167). Trx establishes a disulfide bridge with the substrate SNO-protein allowing the release of the NO (in the form of HNO) (16). An intramolecular disulfide bond is then formed between Cys32 and Cys35, substituting the intermolecular disulfide. Thioredoxin reductase (TR) is in charge of restoring the reduced state of these Cys through a NADPH–dependent reduction of the Trx intramolecular disulfide.

Trx1 was identified as the caspase-3 constitutive and cytosolic denitrosylase since inhibition of Trx1 or TR1 produced increased amounts of SNO-caspase-3 (16). On the other hand, Trx2 was identified as a denitrosylase of mitochondrial caspase-3 upon Fas ligand stimulation, a process required for its activation and, therefore, for apoptotic cell death (16). Furthermore, the Trx-interacting protein (Txnip) has been shown to inhibit denitrosylate activity of Trx, since it increases SNO-protein levels (43).

Proteomic analyses have helped to highlight Trx as a denitrosylase. In cytokine-activated macrophages where iNOS is induced, we used a "fluorescence switch" technique to label S-nitrosylated proteins, identifying eleven proteins that were differentially S-nitrosylated when the thioredoxin reductase was inhibited with auranofin (152). Benhar *et al.* used a quantitative LC-MS/MS approach to identify proteins that were denitrosylated when they added Trx/TR to cell extracts that had been nitrosylated *in vitro* (18). Interestingly, Trx targets of transnitrosylase activity could be differentiated from those of denitrosylation, providing specificity to the search of Trx substrates in the context of S-nitrosylation (168).

Denitrosylation has emerged as a relevant mechanism by which functional relevance of S-nitrosylation is regulated.

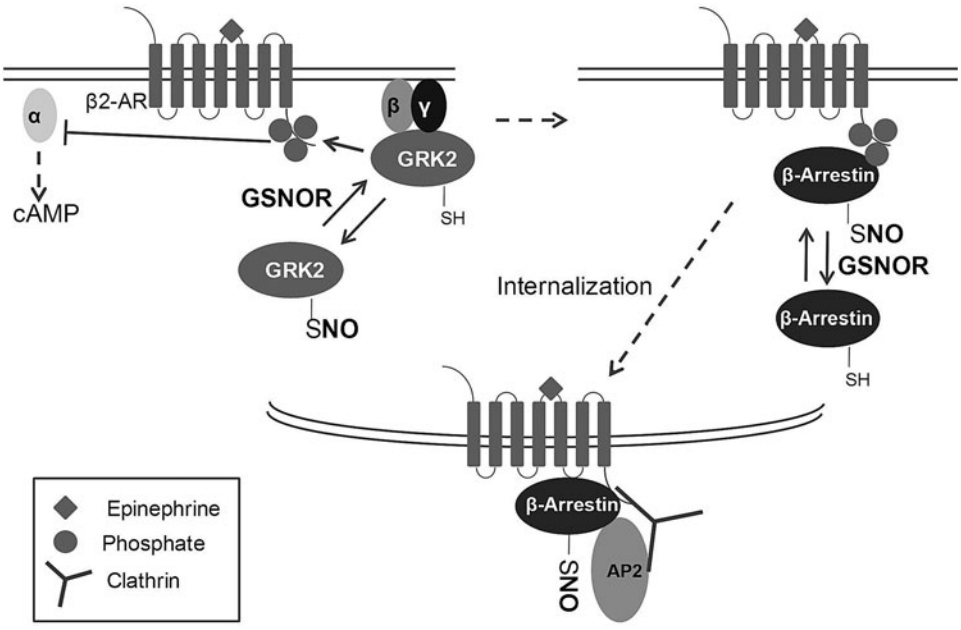

FIG. 3. Agonist-stimulated internalization of β_2-AR is regulated by S-nitrosylation. After agonist (epinephrine) stimulation, β_2-AR stimulates separation of α from β and γ subunits of the G protein. The two latter subunits bind reduced GRK2, which phosphorylates β_2-AR. S-Nitrosylation of GRK2 prevents its binding to β and γ subunits. Once phosphorylated, β_2-AR recruits β-arrestin which becomes S-nitrosylated and subsequently binds to AP2 and clathrin, thus allowing internalization. If β-arrestin is not S-nitrosylated, internalization of β_2-AR becomes attenuated.

Study of the dynamic equilibrium between nitrosothiol generation and its removal, as well as the enzymes implicated will provide more accurate knowledge of S-nitrosylation regulation *in vivo* and their connection with diseases.

Regulation of S-Nitrosylation by Subcellular Localization of eNOS

Despite some evidence indicating a possible role for the compartmentalization of iNOS and short-range actions of high levels of NO in protein S-nitrosylation—for instance, in the S-nitrosylation of matrix metalloproteinase 9 (MMP-9) at the leading edge of migrating cells, and chloride intracellular channel 4 (CLIC4) during its nuclear translocation in macrophages (58, 99)—eNOS and neuronal nitric oxide synthase (nNOS) are the prototypic NOS whose dependence between localization and S-nitrosylation has been more extensively studied (70, 151).

In cells, eNOS traffics between the plasma membrane and the cytoplasmic face of the Golgi apparatus by means of both specific interaction with proteins involved in vesicle trafficking and a cycle of palmitoylation/depalmitoylation on Cys15/Cys26, two amino acid residues whose mutations do not affect the catalytic activity of the enzyme itself but decrease NO production in cells due to alteration of eNOS localization (36, 94, 122, 146). A large body of work indicates that the confinement of eNOS in cell compartments and its proximity or binding to target proteins may lead to selective S-nitrosylation.

eNOS at the plasma membrane

Several studies have shown that preferential localization of eNOS at the plasma membrane produces higher levels of NO and S-nitrosylation in this region than in the Golgi apparatus. At the plasma membrane, eNOS is retained in its low active state associated to caveolin-1 in caveolae, and it is fully activated after dissociation from caveolin-1 by Ca^{2+}/calmodulin binding and kinase-mediated phosphorylation on key serine residues (Ser1177, Ser635, and Ser617); among them, phosphorylation of Ser1177 by Akt is particularly remarkable as the most constant sign of eNOS activation (36, 46). In contrast, the association of eNOS with the actin cytoskeleton by means of its interaction with NOS-interacting protein (NOSIP) or its trafficking towards the Golgi complex by binding to NOS traffic inducer (NOSTRIN) can reduce eNOS activity, moving the enzyme away from plasma membrane-associated signals of activation (122). eNOS activity can also be negatively regulated through auto-S-nitrosylation on Cys94 and Cys99, a negative feedback mechanism that affects NO synthesis by impairing substrate binding and/or electron transfer at the eNOS dimeric interface (36). Studies carried out with both plasma membrane-restricted eNOS and a cytoplasmic mutant deficient in myristoylation on Gly2—which alters its membrane binding and inhibits further palmitoylation—clearly show that membrane localization is required for S-nitrosylation (37, 38). Since eNOS can be reversibly S-nitrosylated, compartmentalized S-nitrosylation of eNOS might be favored, for instance, by environments devoid of denitrosylases such as thioredoxin or GSNOR. However, complementary studies carried out with compartment-targeted iNOS constructs and calcium-independent eNOS showed no differences between the activities of these mutants irrespectively of their subcellular localization (32, 72, 131), suggesting that the levels of NO produced are the most important factors for localized S-nitrosylation and that, in the case of constitutive/regulatable NOS, proximity to the upstream signaling pathways—Ca^{2+}/calmodulin and Ser/Thr kinases—may explain the differences in NO production and S-nitrosylation observed between membrane cell compartments.

In addition to auto-S-nitrosylation of eNOS, other proteins involved in what can be called the "eNOS system" are targets of S-nitrosylation, which can alter the system activity. The eNOS-binding protein caveolin-1 is constitutively S-nitrosylated in endothelial cells (117), although if this can regulate eNOS localization and activity has not been described, to our knowledge. The chaperone Hsp90 also interacts with eNOS, increasing its affinity for calmodulin and Akt, and thus its activity (51, 149). We have shown that Hsp90 can be S-nitrosylated in Cys597 (107), an amino acid residue located in the region of interaction with eNOS (40). This modification inhibits the ATPase activity of Hsp90, and its ability to activate eNOS, representing an additional S-nitrosylation-based feedback mechanism modulating eNOS activity. It is worth noting that the binding of Hsp90 to NOS is not an exclusive hallmark of eNOS since both nNOS and iNOS can also be activated by binding to Hsp90 (129, 169). Whether nNOS and/or iNOS may also S-nitrosylate Hsp90 in the context of a negative regulatory feedback loop of NOS activation, and whether their subcellular localization is actually important for Hsp90 S-nitrosylation deserves further research.

An increasing number of proteins S-nitrosylated by eNOS at the plasma membrane have been identified over the last years. eNOS can interact with the GTPase dynamin-2, increasing receptor-mediated endocytosis through S-nitrosylation of Cys607, a modification that fosters dynamin oligomerization and GTPase-dependent vesicle scission from the plasma membrane (25, 158). Interestingly, a recent report suggested a role for eNOS and dynamin-2 in the immune-escape of uropathogenic strains of *Escherichia coli* (161). The study shows that *E. coli* invasion of bladder epithelial cells in recurrent urinary tract infections is facilitated by endocytosis mediated by eNOS-dependent S-nitrosylation of dynamin-2. It would be important to address if this is a general mechanism of escape for those microorganisms infecting hosts through NO-producing specialized barriers. β-Arrestin is also regulated by eNOS-dependent S-nitrosylation; it forms a complex with eNOS that translocates to GPCRs upon agonist binding, resulting in eNOS activation and β-arrestin S-nitrosylation (123). Once β-arrestin is S-nitrosylated, eNOS dissociates from the complex, and stimulated GPCRs can internalize by association with the clathrin-β-arrestin endocytic machinery (123). β-Catenin, an essential component of adherens junctions—intercellular structures controlling permeability on epithelial and endothelial monolayers—is also a target of S-nitrosylation by eNOS. Stimulation of endothelial cells with VEGF induces eNOS-dependent S-nitrosylation of β-catenin on Cys619, an important amino acid residue for the interaction with VE-cadherin and the preservation of the permeability cell barrier (153). Up to our knowledge, it is not clear yet if there is a direct interaction between eNOS and β-catenin. H-Ras, a Ras isoform localized both at the plasma membrane and the Golgi complex, has recently been added to the list of proteins that can be activated at the plasma membrane by eNOS-dependent S-nitrosylation. In endothelial cells, bradykinin stimulation

induces preferential activation of H-Ras at the plasma membrane through a mechanism independent of Src activation which involves S-nitrosylation of H-Ras on Cys118 (15).

N-Ethylmaleimide-sensitive fusion protein (NSF), a SNARE regulator involved in vesicular trafficking and exocytosis of platelet α-granules and Weibel-Palade bodies from endothelial cells, is also S-nitrosylated by eNOS as demonstrated using NOS inhibitors and eNOS-deficient cells (109, 116). S-Nitrosylation of NSF reduces granule exocytosis by stabilizing SNARE complexes in vesicles. The possible role played by the compartmentalized activity of eNOS on NSF S-nitrosylation has been studied, trying to discriminate the effects of Golgi and plasma membrane localization. Whereas a recent study with eNOS directed to either plasma membrane or Golgi found that eNOS induces higher levels of NSF S-nitrosylation at the plasma membrane (131), imaging analysis from previous studies carried out with wild-type eNOS-transfected COS-7 cells clearly showed that in response to ATP eNOS produced NO mainly on the Golgi complex, a compartment in which most of eNOS and S-nitrosylated proteins are concentrated (71). In this regard, NSF trafficking may play an important role in a cellular model of pulmonary arterial hypertension induced with the pirrolizidine alkaloid MCTP, which induces megalocytosis of pulmonary arterial endothelial cells (117, 118). These studies show that MCTP disrupts vesicular trafficking in endothelial cells, mislocalizing eNOS in the cytoplasm accompanied by loss of NO from caveolae and reduced S-nitrosylation and localization of NSF on the Golgi. Whether reduced NSF S-nitrosylation in MCTP-induced aberrant trafficking is the consequence of eNOS dysfunction at the plasma membrane, the Golgi complex, or both remains an open question.

eNOS on the Golgi

Several studies have also shown that eNOS localization on the Golgi complex is functional and contributes to S-nitrosylation of Golgi-localized proteins (70). Although the mechanisms involved in eNOS localization on the Golgi complex are not fully understood, it is clear that palmitoylation on Cys15/Cys26 and NOSTRIN binding to eNOS play an important role. In this regard, a recent study shows that activation of the transcription factor STAT-3 by the adhesion molecule PCAM-1 induces NOSTRIN expression and the traffic of eNOS from the plasma membrane towards the Golgi complex (110). The role of subcellular localization on eNOS activation has been studied by transfecting protein versions with different localization signals. Transfection in COS-7 cells showed that cis-Golgi-targeted eNOS was less sensitive to activation by Ca^{2+}/calmodulin but more easily activated by Akt-mediated phosphorylation on Ser1179, when compared to the protein localized on the plasma membrane (45). Similar cell transfection studies performed in eNOS-deficient endothelial cells showed that on the Golgi complex eNOS may also result less sensitive to Akt activation but resistant to cholesterol and LDL inhibition, releasing lower amounts of NO than at the plasma membrane (170). Altogether, these reports suggest that compartmentalized activity of eNOS on the Golgi complex may be cell-type specific and/or that low to moderate levels of NO would be enough to S-nitrosylate Golgi resident proteins near eNOS, either due to an enhanced selectivity for S-nitrosylation, or to decreased denitrosylation.

A recent proteomic study combining biotin-switch assay and mass spectrometry has identified nine Golgi-resident proteins S-nitrosylated in Golgi membranes isolated from rat livers (136). Among those, the authors focused on the study of extracellular matrix metalloproteinase inducer (EMPRIN)—a member of the immunoglobulin superfamily involved in invasion and metastasis—and Golgi phosphoprotein 3 (GOLPH3), a potential oncogene involved in protein glycosylation and mTOR regulation. Both proteins interacted with eNOS and co-localized with it on the Golgi of endothelial cells, increasing their S-nitrosylation upon activation with the Ca^{2+} ionophore ionomycin and also in pathophysiological conditions such as cirrhosis (136).

In T cells, S-nitrosylation is mainly compartmentalized near the Golgi complex, where active eNOS localizes. In this compartment, eNOS S-nitrosylates N-Ras at Cys118, fostering the conversion of GDP- to GTP-bound N-Ras, and the consequent activation of the MAPKs ERK-1 and ERK-2 (67). Interestingly, although T cells express both K-Ras and N-Ras (which share the same conserved Cys residue sensitive to S-nitrosylation), only N-Ras becomes S-nitrosylated due to its preferential localization on the Golgi, suggesting that proximity of eNOS-derived NO to N-Ras is an important determinant of S-nitrosylation and MAPK activation (Fig. 4). MAPK phosphatase 7 (MKP7)—a negative regulator of the MAPK JNK3—is S-nitrosylated by eNOS on Cys244 in response to SDF-1, a CXC chemokine with proangiogenic properties on endothelial cells (130). S-Nitrosylation reduces the phosphatase activity of MKP7, increasing JNK3 activity, and thus endothelial cell migration. Although there is no evidence of compartmentalized S-nitrosylation of MKP7, since the Golgi complex plays an important role in the regulation of MAPK pathways (19), it would be interesting to explore whether eNOS-mediated MKP7 S-nitrosylation may take place on the Golgi.

Nitric Oxide Synthases and the Heart: Role of Localized S-Nitrosylation

Very early since the characterization of eNOS in endothelial cells, it was clear that this isoform was expressed in cardiomyocytes and that NO could play a role as a regulator of cardiac rhythm and inotropic responses (108, 139). It is now accepted that the heart expresses both eNOS and nNOS, the former in endothelial and endocardial cells, the latter in nervous tissue and autonomic ganglia, and both in cardiomyocytes. In addition, iNOS may be expressed upon exposure of endothelial cells or cardiomyocytes to cytokines or proinflammatory stimuli (9, 12). A significant discovery which shifted the view of the role of NO in the heart was related to the topological confinement of NO signaling, whereby eNOS, localized in caveolae, mainly directed its action towards the inhibition of β-adrenergic-induced inotropy. In contrast, nNOS, which is targeted to sarcoplasmic reticulum, stimulates calcium release via the ryanodine receptor (RyR) with an opposite effect on contractility (13). Both classical and nonclassical modes of signaling (103) have been demonstrated for NO within the heart. The classical cGMP-mediated pathway is responsible for several important actions of NO related to regulation of contractility and inhibition of cardiac remodeling (see Ref. 55 for review). Elevation of cGMP levels encompasses the activation of cGMP-dependent protein

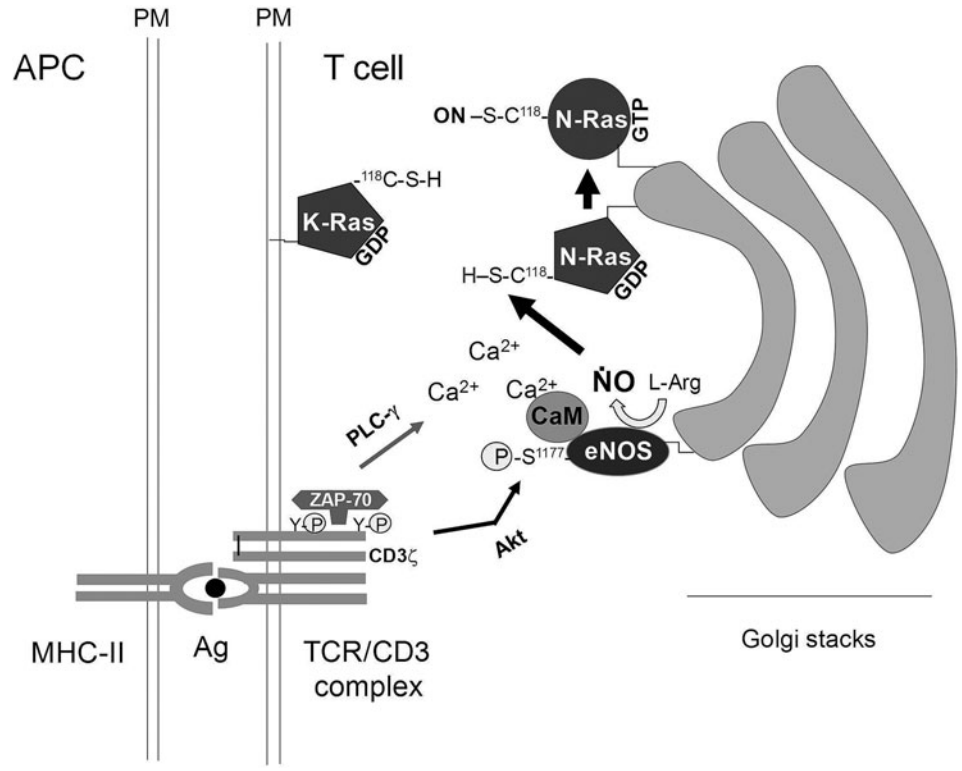

FIG. 4. Compartmentalized S-nitrosylation of N-Ras but not K-Ras in antigen-stimulated T cells. The figure represents the signaling pathways involved in the selective eNOS-dependent S-nitrosylation and activation of N-Ras on the Golgi complex. Although K- and N-Ras are both farnesylated, K-Ras is targeted to the plasma membrane (PM) by means of a basic carboxyl-terminal region of amino acids, whereas N-Ras is mainly localized on the Golgi by palmitoylation, co-localizing with eNOS. Upon TCR binding to antigen (Ag) on an antigen presenting cell (APC), the TCR complex is phosphorylated on the CD3ξ chains, which induces the activation of PLC-γ and Akt by recruitment of the tyrosine kinase ZAP-70. PLC-γ increases the cytosolic levels of inositol 1,4,5-triphosphate, releasing Ca^{2+} from internal stores, which in turn can bind calmodulin-associated eNOS. On the other hand, Akt can phosphorylate eNOS on Ser1177. As a result of the combined actions of Ca^{2+} and phosphorylation, eNOS is activated producing NO on the Golgi, fostering N-Ras activation by S-nitrosylation on Cys118, an amino acid residue shared by K-Ras but which is not S-nitrosylated in T cells due to K-Ras localization at a different cell compartment.

kinases (PKGs) that are important for the regulation of contractility through the inhibition of the L-type Ca^{2+} channel (LTCC). Noteworthy, cGMP signaling in cardiomyocytes is also compartmentalized due to specific subcellular localization of soluble and particulate guanylate cyclases and of phosphodiesterase enzymes (PDEs), thus offering another example of subcellular localization as a major means to control intracellular signaling. The nonclassical pathway is inherently related to NO-induced post-translational modifications of thiols, such as S-nitrosylation and S-glutathionylation (103, 105, 106). For a comprehensive update on the role of these PTMs in the cardiovascular system, the readers may wish to consult recent excellent reviews (102, 138).

eNOS has been shown to localize mainly within the caveolae of sarcolemma and T-tubules, which supports the idea that NO generated through this isoform exerts its action on vicinal cell surface receptors that regulate contractility, including muscarinic, β-adrenergic, and bradykinin receptors (57). The global eNOS effect is negative on chronotropy and inotropy and is counteracted by the action of nNOS, circumscribed to the sarcoplasmic reticulum. Interactions of eNOS and nNOS with other proteins sharing their subcellular localization, caveolin 3 and the RyR, respectively, are essential to understanding their action on cardiac function (156). S-Nitrosylation has been described to involve several proteins regulating contractility including LTCC, RyR, Kv1.5 channel, and sarcoplasmic/endoplasmic reticulum Ca^{2+}-activated ATPase (SERCA). The ryanodine receptor Ca^{2+} release channel (RyR2), together with SERCA2a, are critical components of the excitation–contraction coupling molecular machinery. It has been proposed that the close apposition of nNOS and RyR2 facilitates S-nitrosylation of the latter, increasing its channel opening probability (88). A similar mechanism may operate for the S-nitrosylation-induced regulation of LTCC and SERCA2a which has also been shown to become activated by NO-induced S-glutathionylation (3). A deficit of nNOS-mediated S-nitrosylation of RyR2 has been associated with pathological cardiac responses such as arrhythmia (49). Other ion channels have also been proposed to undergo S-nitrosylation: intermediate conductance potassium channel (IK1), late inward Na+ current (InaL), slowly activating delayed rectifier current (Iks), and ATP-sensitive K+ channel (see Ref. 150 for review). Finally, eNOS and vicinal scaffolding proteins are themselves potential targets for S-nitrosylation, at least in endothelial cells (37, 107), resulting in an autoinhibitory feedback mechanism. Thus, knowledge of

S-nitrosylation modification of cardiac function depicts a complex scenario which still awaits further clarification through the employment of animal models and corroboration by clinical settings where this PTM is specifically addressed.

Short-Range S-Nitrosylation Signaling in the Brain

In neurons, NO is produced essentially by neuronal NO synthase (nNOS), which can be localized in well-defined neuronal localizations, such as the presynaptic terminal or the postsynaptic density, where NO production can be coupled to synaptic transmission, either in an anterograde or retrograde manner. The best characterized signaling molecule coupled to NO production by nNOS in the brain is the neurotransmitter glutamate. Glutamate is the main excitatory neurotransmitter in the central nervous system, and is recognized by both ionotropic and metabotropic receptors. The calcium-permeable ionotropic N-methyl-D-aspartate (NMDA) receptor was shown to be associated to glutamate-induced calcium-dependent NO production by nNOS in the brain (21, 47). NMDA receptors are also central to neurodevelopment, synaptic plasticity, and neurodegeneration. Other ionotropic glutamate receptors have also been involved in these processes, such as AMPA receptors. Overactivation of glutamate receptors often results in excitotoxicity, a phenomenon caused by excitatory neurotransmitters that cause a rise in the intracellular calcium concentration induced by receptor activation, which may trigger cell death pathways (2, 41, 84).

NMDA receptor coupling to nNOS by PSD-95: Implications for neuronal survival

The participation of NMDA receptors in excitotoxic neuronal death has been extensively studied in the last 30 years, and NO has been shown to be a participant in this complex cascade of events. Glutamate release by synapses causes an increase in the intracellular calcium concentration of the postsynaptic neurons, and this rise in calcium is usually mediated by influx through voltage-dependent calcium channels, influx by calcium-permeable receptors (such as NMDA or certain types of AMPA receptors) or by reversal of the sodium–calcium exchanger (10). Activation of NMDA receptors by glutamate causes an influx of calcium through the receptor itself that was shown to be linked to the activation of nNOS and neuronal death (22). Activation of AMPA receptors was also linked to NO production by nNOS, resulting in neurotoxicity (6). NO produced by nNOS following activation of NMDA receptors was initially shown to mediate the neurotoxicity of glutamate in cultured neurons (34), and a number of studies later showed that NO produced by nNOS during a variety of brain insults is responsible, at least partially, for the neuronal damage (for review, see Refs. 2, 7, 24, 27, 78, 84).

NO is produced rapidly following stimulation of NMDA receptor, which prompted the investigation of whether a structural proximity between this glutamate receptor and nNOS existed. The PDZ domains in PSD-95 mediate a structural interaction between the NMDA receptor NR2 subunits and nNOS at the postsynaptic density (31), an area that is rich in anchoring and scaffolding proteins that help in making synaptic transmission more efficient (Fig. 5). Another study showed that uncoupling the NMDA receptor from nNOS by interfering with PSD-95 resulted in loss of the neurotoxic effect of NO (137), without loss of calcium influx through the receptor. Peptide inhibitors such as Tat-NR2B9c that disrupt the coupling of the NR2 subunits of the NMDA receptor and PSD-95 provoke a loss of NO production following NMDA receptor activation (1). Such peptide inhibitors contain a sequence similar to the C-terminal of NR2 subunits, which competes with native NMDA receptors and disrupts the interaction of NMDA receptors and PSD-95.

PSD-95 itself presents sites of competing regulation which control the targeting of PSD-95 to the postsynaptic density, on Cys3 and Cys5, which can be both regulated by S-palmitoylation (increases the localization of PSD-95 at the postsynaptic density) or by S-nitrosylation (reduces the clustering of PSD-95 on synapses), supporting a model for regulation of NMDA receptor activation coupled to NO

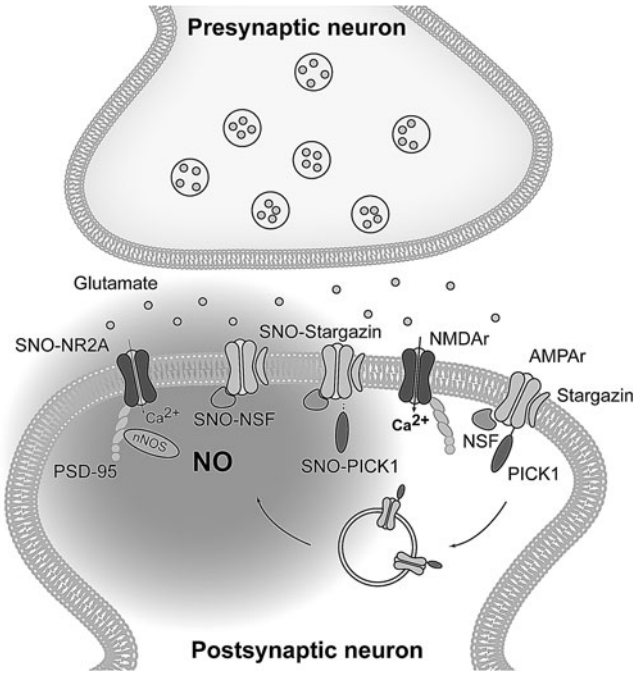

FIG. 5. Postsynaptic localization of nNOS and S-nitrosylation signaling in a glutamatergic synapse. Production of NO by nNOS following glutamate release is coupled to activation of Ca^{2+}-permeable NMDA receptors (NMDAr), which are anchored at the postsynaptic density by scaffolding proteins, including PSD-95. PSD-95 binds to NMDAr and nNOS via PDZ domains, allowing for a close proximity of permeable NMDAr and nNOS. NO produced in close proximity to NMDA receptors triggers the S-nitrosylation of NR2A subunits (SNO-NR2A), which then allow less Ca^{2+} in. Activation of NMDAr also triggers the recruitment of more AMPA receptors (AMPAr) towards the membrane surface. S-Nitrosylation of stargazin (SNO-stargazin) and NSF (SNO-NSF) contributes to increase the surface expression of AMPAr during events of synaptic plasticity following the activation of NMDAr. On the other hand, S-nitrosylation of PICK1 facilitates its release from AMPAr after membrane insertion and also facilitates surface expression of AMPAr. When these proteins are out of range of NO and are not S-nitrosylated, PICK1 interacts more strongly with the receptor while NSF interacts more weakly, allowing the binding of proteins that facilitate endocytosis of AMPAr.

production via PSD-95, by controlling the postsynaptic localization of PSD-95 as well (63).

The close proximity of nNOS and the NMDA receptor via PSD-95 in the postsynaptic density facilitates the regulatory effect of NO also on the NMDA receptor itself (29). The first reports that NO would affect redox modulatory sites of the NMDA receptor date back to the 1990s (85, 91, 93). It was then hypothesized that S-nitrosylation would decrease the permeability of the receptor, as a neuroprotective feedback mechanism (92) (Fig. 5). Site-directed mutagenesis studies later identified Cys399 in the NR2A subunit of the NMDA receptor that may undergo endogenous S-nitrosylation and thus regulate the ion channel activity, decreasing calcium influx (30, 79). S-Nitrosylation of NR1 subunits may also occur on Cys744/Cys798 pair, particularly during hypoxia or stroke conditions (148), which supports a function for S-nitrosylation of the NMDA receptor as a way to regulate calcium influx through the receptor and limit neurotoxicity.

Interestingly, it has been known for a long time that nNOS-positive neurons are relatively resistant to excitotoxic stimuli and are spared in several neurodegenerative conditions, such as Alzheimer disease (66) and Huntington disease (HD) (39). The selective resistance of nNOS-positive striatal interneurons in HD was correlated with the fact that such neurons probably have endogenous S-nitrosylation of their NMDA receptors, thus becoming less permeable to calcium influx and therefore less likely to degenerate (171). On the other hand, unlike nNOS-positive interneurons, striatal medium spiny neurons do not produce NO and are sensitive to excitotoxic damage and degenerate more easily. This may render the NMDA receptor in medium spiny neurons more permeable to calcium, and thus increase their susceptibility to injury. Furthermore, in a model of HD, it was observed that PSD-95 and nNOS are less present in association with the synaptic membrane and the NMDA receptor in striatal neurons (74), which suggests a decreased coupling between the receptor and NO production.

S-Nitrosylation and synaptic plasticity

Synaptic plasticity underlies the formation of new memories and learning processes. One form of synaptic plasticity is the insertion of synaptic AMPA receptors in postsynaptic sites following activation of NMDA receptors. The increase in AMPA receptors at the synapse makes the synapse respond with larger excitatory currents upon synaptic stimulation, thus making the synapse stronger. Several intracellular proteins are involved in the recruitment of AMPA receptors to the synaptic membrane, and some may be functionally S-nitrosylated (4, 115, 151).

Upon glutamatergic stimulation, AMPA receptors mediate the initial membrane depolarization that allows activation of NMDA receptors. Activation of NMDA receptors triggers a set of events that result in long-term changes in the number of AMPA receptors present in the synaptic membrane (98). Following activation of NMDA receptors, a number of proteins are responsible for regulating the insertion or removal of AMPA receptors to the membrane. NSF and Protein Interacting with C Kinase (PICK1) are two regulatory proteins that interact with AMPA receptors and that are sensitive to S-nitrosylation (Fig. 5). NSF is important for membrane fusion during exocytosis and was shown to be S-nitrosylated (65). In this study, the authors show that S-nitrosylation of Cys91 increases the association of NSF with GluR2-containing AMPA receptors, thus driving surface expression of AMPA receptors (65). Nitrosylation of NSF was later shown to allow unclustering of PICK1 and delivery of AMPA receptors to the membrane (144). This mechanism may be responsible for long-term potentiation dependent on activation of the NMDA receptor. Stargazin is another protein important for regulation of AMPA receptor surface expression, and physiological S-nitrosylation of stargazin at Cys302 in the C-terminal tail elicited by NMDA receptor activation was shown to increase the presence of AMPA receptors at the membrane surface (140) (Fig. 5). Interestingly, the uncoupling of NMDA-PSD-95 interaction with Tat-NR2B9c was shown to affect plasticity related to nociceptive signaling (33), but a similar approach was not yet described for synaptic plasticity. To date, of the many proteins involved in regulating AMPA receptor surface expression, only NSF, PICK1, and stargazin were shown to be functionally modified by S-nitrosylation following NMDA receptor activation and postsynaptic NO production by nNOS, but possibly other proteins may also be controlled by S-nitrosylation with implications for synaptic plasticity.

Conclusions

Protein S-nitrosylation is generally accepted as a nonclassical mechanism of NO signaling. Although the precise biochemical pathways leading to its formation are not completely understood, several of the pathways that have been so far described point out to the hypothesis that this modification is mainly localized close to the NO producing foci, which in

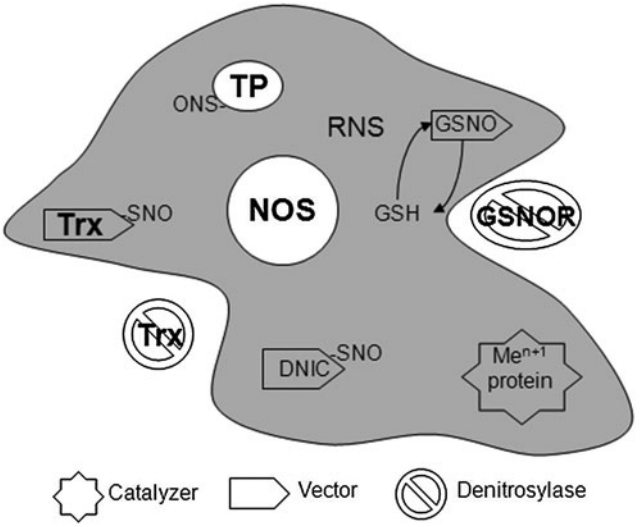

FIG. 6. Integration of several factors affecting short-range S-nitrosylation signaling. The short-range S-nitrosylation signaling range of action shadowed in gray (see also Fig. 1) becomes more complex when other factors are included. In addition to catalyzed RNS formation that could be exerted by membranes (not shown), some metal proteins are also catalyzers of S-nitrosylation formation, expanding the range of action. Transnitrosylases (including Trx) and other LMM vectors such as GSNO or DNIC can also selectively extend it to their targets. On the other hand, denitrosylases such as Trx or GSNOR, limit the influence of S-nitrosylation in certain areas and/or in certain protein targets.

mammals are mainly the NOS enzymes. Examples of subcellular compartmentalization of S-nitrosylation signaling have been described in neurons and cardiac tissue, where S-nitrosylated proteins with signaling functions co-localize with the different NOS isoforms. Similarly, in cells such as endothelial cells or T lymphocytes, eNOS-dependent S-nitrosylation is observed in proteins localized at the plasma membrane or on the Golgi, associated to regulated localization and activity of eNOS in these compartments.

A simple model of the short-range signaling exerted by S-nitrosylation in the NOS proximity is illustrated in Figure 1, where S-nitrosylation signaling is depicted in a limited spherical space around NOS. However, consideration of some of the mechanisms involved in S-nitrosothiol formation and breakage leads to a more complex picture, in which S-nitrosylation catalyzers (e.g., specific metal centers, membranes) or S-nitrosylation vectors (such as DNIC, transnitrosylases) could promote the expansion of the S-nitrosylation range of action, while the presence of denitrosylases could restrict it (Fig. 6).

Future studies will confirm, modify or even refute this hypothesis, but we consider that the subcellular localization of protein S-nitrosylation needs to be taken into account when the functional role of this modification is studied. This is important also in proteomic studies that attempt to identify the S-nitrosoproteome, even though it poses an additional challenge to current methodologies.

Acknowledgments

The research in our laboratories is financed by Spanish Government Grants CSD2007-00020 (RosasNet, Consolider-Ingenio 2010 programme; to SL and AM-R), CP07/00143 (Miguel Servet programme) and PS09/00101 (to AM-R), SAF2009-7520 (to SL) and PI10/02136 (to JMS); by Spanish-Portuguese Integrated Action Grant PRI-AIBPT-2011-1015/E-10/12 (to AM-R and IMA); by grants from the Foundation for Science and Technology (FCT, Portugal), COMPETE and FEDER (Grants PTDC/SAU-NEU/102612/2008, PTDC/SAU-NMC/112183/2009, PEst-OE/EQB/LA0023/2011; to IMA); and by the COST action BM1005 (ENOG: European Network on Gasotransmitters).

Author Disclosure Statement

No competing financial interests exist.

References

1. Aarts M, Liu Y, Liu L, Besshoh S, Arundine M, Gurd JW, Wang YT, Salter MW, and Tymianski M. Treatment of ischemic brain damage by perturbing NMDA receptor- PSD-95 protein interactions. *Science* 298: 846–850, 2002.
2. Aarts MM, and Tymianski M. Molecular mechanisms underlying specificity of excitotoxic signaling in neurons. *Curr Mol Med* 4: 137–147, 2004.
3. Adachi T, Weisbrod RM, Pimentel DR, Ying J, Sharov VS, Schoneich C, and Cohen RA. S-glutathiolation by peroxynitrite activates SERCA during arterial relaxation by nitric oxide. *Nat Med* 10: 1200–1207, 2004.
4. Ahern GP, Klyachko VA, and Jackson MB. cGMP and S-nitrosylation: Two routes for modulation of neuronal excitability by NO. *Trends Neurosci* 25: 510–517, 2002.
5. Anand P, and Stamler JS. Enzymatic mechanisms regulating protein S-nitrosylation: Implications in health and disease. *J Mol Med (Berl)* 90: 233–244, 2012.
6. Araújo IM, Ambrósio AF, Leal EC, Santos PF, Carvalho AP, and Carvalho CM. Neuronal nitric oxide synthase proteolysis limits the involvement of nitric oxide in kainate-induced neurotoxicity in hippocampal neurons. *J Neurochem* 85: 791–800, 2003.
7. Araújo IM, and Carvalho CM. Role of nitric oxide and calpain activation in neuronal death and survival. *Curr Drug Targets CNS Neurol Disord* 4: 319–324, 2005.
8. Arner ES, and Holmgren A. Physiological functions of thioredoxin and thioredoxin reductase. *Eur J Biochem* 267: 6102–6109, 2000.
9. Arstall MA, Sawyer DB, Fukazawa R, and Kelly RA. Cytokine-mediated apoptosis in cardiac myocytes: The role of inducible nitric oxide synthase induction and peroxynitrite generation. *Circ Res* 85: 829–840, 1999.
10. Arundine M, and Tymianski M. Molecular mechanisms of calcium-dependent neurodegeneration in excitotoxicity. *Cell Calcium* 34: 325–337, 2003.
11. Awad HH, and Stanbury DM. Autoxidation of NO in aqueous solution. *Intl J Chem Kinetics* 25: 375–381, 1993.
12. Balligand JL, Ungureanu-Longrois D, Simmons WW, Kobzik L, Lowenstein CJ, Lamas S, Kelly RA, Smith TW, and Michel T. Induction of NO synthase in rat cardiac microvascular endothelial cells by IL-1 beta and IFN-gamma. *Am J Physiol* 268: H1293–1303, 1995.
13. Barouch LA, Harrison RW, Skaf MW, Rosas GO, Cappola TP, Kobeissi ZA, Hobai IA, Lemmon CA, Burnett AL, O'Rourke B, Rodriguez ER, Huang PL, Lima JA, Berkowitz DE, and Hare JM. Nitric oxide regulates the heart by spatial confinement of nitric oxide synthase isoforms. *Nature* 416: 337–339, 2002.
14. Bateman RL, Rauh D, Tavshanjian B, and Shokat KM. Human carbonyl reductase 1 is an S-nitrosoglutathione reductase. *J Biol Chem* 283: 35756–35762, 2008.
15. Batista WL, Ogata FT, Curcio MF, Miguel RB, Arai RJ, Matsuo AL, Moraes MS, Stern A, and Monteiro HP. S-nitrosoglutathione and endothelial nitric oxide synthase-derived nitric oxide regulate compartmentalized Ras S-nitrosylation and stimulate cell proliferation. *Antioxid Redox Signal* 18: 221–238, 2013.
16. Benhar M, Forrester MT, Hess DT, and Stamler JS. Regulated protein denitrosylation by cytosolic and mitochondrial thioredoxins. *Science* 320: 1050–1054, 2008.
17. Benhar M, Forrester MT, and Stamler JS. Protein denitrosylation: Enzymatic mechanisms and cellular functions. *Nat Rev Mol Cell Biol* 10: 721–732, 2009.
18. Benhar M, Thompson JW, Moseley MA, and Stamler JS. Identification of S-nitrosylated targets of thioredoxin using a quantitative proteomic approach. *Biochemistry* 49: 6963–6969, 2010.
19. Berthiaume LG. Insider information: How palmitoylation of Ras makes it a signaling double agent. *Sci STKE* 2002: pe41, 2002.
20. Bosworth CA, Toledo JC, Jr., Zmijewski JW, Li Q, and Lancaster JR, Jr. Dinitrosyliron complexes and the mechanism(s) of cellular protein nitrosothiol formation from nitric oxide. *Proc Natl Acad Sci USA* 106: 4671–4676, 2009.
21. Bredt DS, and Snyder SH. Nitric oxide mediates glutamate-linked enhancement of cGMP levels in the cerebellum. *Proc Natl Acad Sci USA* 86: 9030–9033, 1989.

22. Brenman JE, and Bredt DS. Synaptic signaling by nitric oxide. *Curr Opin Neurobiol* 7: 374–378, 1997.
23. Broniowska KA, and Hogg N. The chemical biology of S-nitrosothiols. *Antioxid Redox Signal* 17: 969–980, 2012.
24. Calabrese V, Boyd-Kimball D, Scapagnini G, and Butterfield DA. Nitric oxide and cellular stress response in brain aging and neurodegenerative disorders: The role of vitagenes. *In Vivo* 18: 245–267, 2004.
25. Cao S, Yao J, McCabe TJ, Yao Q, Katusic ZS, Sessa WC, and Shah V. Direct interaction between endothelial nitric-oxide synthase and dynamin-2. Implications for nitric-oxide synthase function. *J Biol Chem* 276: 14249–14256, 2001.
26. Cary SP, Winger JA, Derbyshire ER, and Marletta MA. Nitric oxide signaling: No longer simply on or off. *Trends Biochem Sci* 31: 231–239, 2006.
27. Chabrier PE, Demerle-Pallardy C, and Auguet M. Nitric oxide synthases: Targets for therapeutic strategies in neurological diseases. *Cell Mol Life Sci* 55: 1029–1035, 1999.
28. Cho DH, Nakamura T, Fang J, Cieplak P, Godzik A, Gu Z, and Lipton SA. S-Nitrosylation of Drp1 mediates beta-amyloid-related mitochondrial fission and neuronal injury. *Science* 324: 102–105, 2009.
29. Choi YB, and Lipton SA. Redox modulation of the NMDA receptor. *Cell Mol Life Sci* 57: 1535–1541, 2000.
30. Choi YB, Tenneti L, Le DA, Ortiz J, Bai G, Chen HS, and Lipton SA. Molecular basis of NMDA receptor-coupled ion channel modulation by S-nitrosylation. *Nat Neurosci* 3: 15–21, 2000.
31. Christopherson KS, Hillier BJ, Lim WA, and Bredt DS. PSD-95 assembles a ternary complex with the N-methyl-D-aspartic acid receptor and a bivalent neuronal NO synthase PDZ domain. *J Biol Chem* 274: 27467–27473, 1999.
32. Church JE, and Fulton D. Differences in eNOS activity because of subcellular localization are dictated by phosphorylation state rather than the local calcium environment. *J Biol Chem* 281: 1477–1488, 2006.
33. D'Mello R, Marchand F, Pezet S, McMahon SB, and Dickenson AH. Perturbing PSD-95 interactions with NR2B-subtype receptors attenuates spinal nociceptive plasticity and neuropathic pain. *Mol Ther* 19: 1780–1792, 2011.
34. Dawson VL, Dawson TM, London ED, Bredt DS, and Snyder SH. Nitric oxide mediates glutamate neurotoxicity in primary cortical cultures. *Proc Natl Acad Sci USA* 88: 6368–6371, 1991.
35. Derakhshan B, Hao G, and Gross SS. Balancing reactivity against selectivity: The evolution of protein S-nitrosylation as an effector of cell signaling by nitric oxide. *Cardiovasc Res* 75: 210–219, 2007.
36. Dudzinski DM, and Michel T. Life history of eNOS: Partners and pathways. *Cardiovasc Res* 75: 247–260, 2007.
37. Erwin PA, Lin AJ, Golan DE, and Michel T. Receptor-regulated dynamic S-nitrosylation of endothelial nitric oxide synthase in vascular endothelial cells. *J Biol Chem* 280: 19888–19894, 2005.
38. Erwin PA, Mitchell DA, Sartoretto J, Marletta MA, and Michel T. Subcellular targeting and differential S-nitrosylation of endothelial nitric oxide synthase. *J Biol Chem* 281: 151–157, 2006.
39. Ferrante RJ, Kowall NW, Beal MF, Richardson EP, Jr., Bird ED, and Martin JB. Selective sparing of a class of striatal neurons in Huntington's disease. *Science* 230: 561–563, 1985.
40. Fontana J, Fulton D, Chen Y, Fairchild TA, McCabe TJ, Fujita N, Tsuruo T, and Sessa WC. Domain mapping studies reveal that the M domain of hsp90 serves as a molecular scaffold to regulate Akt-dependent phosphorylation of endothelial nitric oxide synthase and NO release. *Circ Res* 90: 866–873, 2002.
41. Forder JP, and Tymianski M. Postsynaptic mechanisms of excitotoxicity: Involvement of postsynaptic density proteins, radicals, and oxidant molecules. *Neuroscience* 158: 293–300, 2009.
42. Forman HJ, Fukuto JM, and Torres M. Redox signaling: Thiol chemistry defines which reactive oxygen and nitrogen species can act as second messengers. *Am J Physiol Cell Physiol* 287: C246–256, 2004.
43. Forrester MT, Seth D, Hausladen A, Eyler CE, Foster MW, Matsumoto A, Benhar M, Marshall HE, and Stamler JS. Thioredoxin-interacting protein (Txnip) is a feedback regulator of S-nitrosylation. *J Biol Chem* 284: 36160–36166, 2009.
44. Foster MW, Hess DT, and Stamler JS. Protein S-nitrosylation in health and disease: A current perspective. *Trends Mol Med* 15: 391–404, 2009.
45. Fulton D, Babbitt R, Zoellner S, Fontana J, Acevedo L, McCabe TJ, Iwakiri Y, and Sessa WC. Targeting of endothelial nitric-oxide synthase to the cytoplasmic face of the Golgi complex or plasma membrane regulates Akt- versus calcium-dependent mechanisms for nitric oxide release. *J Biol Chem* 279: 30349–30357, 2004.
46. Fulton D, Gratton JP, and Sessa WC. Post-translational control of endothelial nitric oxide synthase: Why isn't calcium/calmodulin enough? *J Pharmacol Exp Ther* 299: 818–824, 2001.
47. Garthwaite J, Charles SL, and Chess-Williams R. Endothelium-derived relaxing factor release on activation of NMDA receptors suggests role as intercellular messenger in the brain. *Nature* 336: 385–388, 1988.
48. Goldstein S, and Czapski G. Kinetics of nitric oxide autoxidation in aqueous solution in the absence and presence of various reductants. The nature of the oxidizing intermediates. *J Am Chem Soc* 117: 12078–12084, 1995.
49. Gonzalez DR, Beigi F, Treuer AV, and Hare JM. Deficient ryanodine receptor S-nitrosylation increases sarcoplasmic reticulum calcium leak and arrhythmogenesis in cardiomyocytes. *Proc Natl Acad Sci USA* 104: 20612–20617, 2007.
50. Gow AJ, and Stamler JS. Reactions between nitric oxide and haemoglobin under physiological conditions. *Nature* 391: 169–173, 1998.
51. Gratton JP, Fontana J, O'Connor DS, Garcia-Cardena G, McCabe TJ, and Sessa WC. Reconstitution of an endothelial nitric-oxide synthase (eNOS), hsp90, and caveolin-1 complex in vitro. Evidence that hsp90 facilitates calmodulin stimulated displacement of eNOS from caveolin-1. *J Biol Chem* 275: 22268–22272, 2000.
52. Gryglewski RJ, Palmer RM, and Moncada S. Superoxide anion is involved in the breakdown of endothelium-derived vascular relaxing factor. *Nature* 320: 454–456, 1986.
53. Guikema B, Lu Q, and Jourd'heuil D. Chemical considerations and biological selectivity of protein nitrosation: Implications for NO-mediated signal transduction. *Antioxid Redox Signal* 7: 593–606, 2005.
54. Haendeler J, Hoffmann J, Tischler V, Berk BC, Zeiher AM, and Dimmeler S. Redox regulatory and anti-apoptotic functions of thioredoxin depend on S-nitrosylation at cysteine 69. *Nat Cell Biol* 4: 743–749, 2002.
55. Hammond J, and Balligand JL. Nitric oxide synthase and cyclic GMP signaling in cardiac myocytes: From

contractility to remodeling. *J Mol Cell Cardiol* 52: 330–340, 2012.
56. Hara MR, Agrawal N, Kim SF, Cascio MB, Fujimuro M, Ozeki Y, Takahashi M, Cheah JH, Tankou SK, Hester LD, Ferris CD, Hayward SD, Snyder SH, and Sawa A. S-nitrosylated GAPDH initiates apoptotic cell death by nuclear translocation following Siah1 binding. *Nat Cell Biol* 7: 665–674, 2005.
57. Hare JM, Lofthouse RA, Juang GJ, Colman L, Ricker KM, Kim B, Senzaki H, Cao S, Tunin RS, and Kass DA. Contribution of caveolin protein abundance to augmented nitric oxide signaling in conscious dogs with pacing-induced heart failure. *Circ Res* 86: 1085–1092, 2000.
58. Harris LK, McCormick J, Cartwright JE, Whitley GS, and Dash PR. S-Nitrosylation of proteins at the leading edge of migrating trophoblasts by inducible nitric oxide synthase promotes trophoblast invasion. *Exp Cell Res* 314: 1765–1776, 2008.
59. Hashemy SI, and Holmgren A. Regulation of the catalytic activity and structure of human thioredoxin 1 via oxidation and S-nitrosylation of cysteine residues. *J Biol Chem* 283: 21890–21898, 2008.
60. Hernansanz-Agustín P, Izquierdo-Álvarez A, García-Ortiz A, Ibiza S, Serrador JM, and Martínez-Ruiz A. Nitrosothiols in the immune system: Signaling and protection. *Antioxid Redox Signal* 18: 288–308, 2013.
61. Hess DT, Matsumoto A, Kim S-O, Marshall HE, and Stamler JS. Protein S-nitrosylation: Purview and parameters. *Nat Rev Mol Cell Biol* 6: 150–166, 2005.
62. Hickok JR, Sahni S, Shen H, Arvind A, Antoniou C, Fung LW, and Thomas DD. Dinitrosyliron complexes are the most abundant nitric oxide-derived cellular adduct: Biological parameters of assembly and disappearance. *Free Radic Biol Med* 51: 1558–1566, 2011.
63. Ho GP, Selvakumar B, Mukai J, Hester LD, Wang Y, Gogos JA, and Snyder SH. S-Nitrosylation and S-palmitoylation reciprocally regulate synaptic targeting of PSD-95. *Neuron* 71: 131–141, 2011.
64. Hou Y, Guo Z, Li J, and Wang PG. Seleno compounds and glutathione peroxidase catalyzed decomposition of S-nitrosothiols. *Biochem Biophys Res Commun* 228: 88–93, 1996.
65. Huang Y, Man HY, Sekine-Aizawa Y, Han Y, Juluri K, Luo H, Cheah J, Lowenstein C, Huganir RL, and Snyder SH. S-nitrosylation of N-ethylmaleimide sensitive factor mediates surface expression of AMPA receptors. *Neuron* 46: 533–540, 2005.
66. Hyman BT, Marzloff K, Wenniger JJ, Dawson TM, Bredt DS, and Snyder SH. Relative sparing of nitric oxide synthase-containing neurons in the hippocampal formation in Alzheimer's disease. *Ann Neurol* 32: 818–820, 1992.
67. Ibiza S, Pérez-Rodríguez A, Ortega Á, Martínez-Ruiz A, Barreiro O, García-Domínguez CA, Víctor VM, Esplugues JV, Rojas JM, Sánchez-Madrid F, and Serrador JM. Endothelial nitric oxide synthase regulates N-Ras activation on the Golgi complex of antigen-stimulated T cells. *Proc Natl Acad Sci USA* 105: 10507–10512, 2008.
68. Ignarro LJ, Buga GM, Wood KS, Byrns RE, and Chaudhuri G. Endothelium-derived relaxing factor produced and released from artery and vein is nitric oxide. *Proc Natl Acad Sci USA* 84: 9265–9269, 1987.
69. Ischiropoulos H. Protein tyrosine nitration—An update. *Arch Biochem Biophys* 484: 117–121, 2009.
70. Iwakiri Y. S-Nitrosylation of proteins: A new insight into endothelial cell function regulated by eNOS-derived NO. *Nitric Oxide* 25: 95–101, 2011.
71. Iwakiri Y, Satoh A, Chatterjee S, Toomre DK, Chalouni CM, Fulton D, Groszmann RJ, Shah VH, and Sessa WC. Nitric oxide synthase generates nitric oxide locally to regulate compartmentalized protein S-nitrosylation and protein trafficking. *Proc Natl Acad Sci USA* 103: 19777–19782, 2006.
72. Jagnandan D, Sessa WC, and Fulton D. Intracellular location regulates calcium-calmodulin-dependent activation of organelle-restricted eNOS. *Am J Physiol Cell Physiol* 289: C1024–1033, 2005.
73. Janssen-Heininger YM, Mossman BT, Heintz NH, Forman HJ, Kalyanaraman B, Finkel T, Stamler JS, Rhee SG, and van der Vliet A. Redox-based regulation of signal transduction: Principles, pitfalls, and promises. *Free Radic Biol Med* 45: 1–17, 2008.
74. Jarabek BR, Yasuda RP, and Wolfe BB. Regulation of proteins affecting NMDA receptor-induced excitotoxicity in a Huntington's mouse model. *Brain* 127: 505–516, 2004.
75. Jia L, Bonaventura C, Bonaventura J, and Stamler JS. S-nitrosohaemoglobin: A dynamic activity of blood involved in vascular control. *Nature* 380: 221–226, 1996.
76. Jourd'heuil D, Jourd'heuil FL, and Feelisch M. Oxidation and nitrosation of thiols at low micromolar exposure to nitric oxide. Evidence for a free radical mechanism. *J Biol Chem* 278: 15720–15726, 2003.
77. Jourd'heuil D, Laroux FS, Miles AM, Wink DA, and Grisham MB. Effect of superoxide dismutase on the stability of S-nitrosothiols. *Arch Biochem Biophys* 361: 323–330, 1999.
78. Keynes RG, and Garthwaite J. Nitric oxide and its role in ischaemic brain injury. *Curr Mol Med* 4: 179–191, 2004.
79. Kim WK, Choi YB, Rayudu PV, Das P, Asaad W, Arnelle DR, Stamler JS, and Lipton SA. Attenuation of NMDA receptor activity and neurotoxicity by nitroxyl anion, NO. *Neuron* 24: 461–469, 1999.
80. Klatt P, and Lamas S. Regulation of protein function by S-glutathiolation in response to oxidative and nitrosative stress. *Eur J Biochem* 267: 4928–4944., 2000.
81. Kornberg MD, Sen N, Hara MR, Juluri KR, Nguyen JV, Snowman AM, Law L, Hester LD, and Snyder SH. GAPDH mediates nitrosylation of nuclear proteins. *Nat Cell Biol* 12: 1094–1100, 2010.
82. Lancaster JR, Jr. Nitroxidative, nitrosative, and nitrative stress: Kinetic predictions of reactive nitrogen species chemistry under biological conditions. *Chem Res Toxicol* 19: 1160–1174, 2006.
83. Lancaster JR Jr, and Gaston B. NO and nitrosothiols: Spatial confinement and free diffusion. *Am J Physiol Lung Cell Mol Physiol* 287: L465–466, 2004.
84. Lau A, and Tymianski M. Glutamate receptors, neurotoxicity and neurodegeneration. *Pflugers Arch* 460: 525–542, 2010.
85. Lei SZ, Pan ZH, Aggarwal SK, Chen HS, Hartman J, Sucher NJ, and Lipton SA. Effect of nitric oxide production on the redox modulatory site of the NMDA receptor–channel complex. *Neuron* 8: 1087–1099, 1992.
86. Lillig CH, and Holmgren A. Thioredoxin and related molecules—From biology to health and disease. *Antioxid Redox Signal* 9: 25–47, 2007.
87. Lim CH, Dedon PC, and Deen WM. Kinetic analysis of intracellular concentrations of reactive nitrogen species. *Chem Res Toxicol* 21: 2134–2147, 2008.
88. Lima B, Forrester MT, Hess DT, and Stamler JS. S-Nitrosylation in cardiovascular signaling. *Circ Res* 106: 633–646, 2010.

89. Lima B, Lam GKW, Xie L, Diesen DL, Villamizar N, Nienaber J, Messina E, Bowles D, Kontos CD, Hare JM, Stamler JS, and Rockman HA. Endogenous S-nitrosothiols protect against myocardial injury. *Proc Natl Acad Sci USA* 106: 6297–6302, 2009.
90. Lindermayr C, and Durner J. S-Nitrosylation in plants: Pattern and function. *J Proteomics* 73: 1–9, 2009.
91. Lipton SA, Choi YB, Pan ZH, Lei SZ, Chen HS, Sucher NJ, Loscalzo J, Singel DJ, and Stamler JS. A redox-based mechanism for the neuroprotective and neurodestructive effects of nitric oxide and related nitroso-compounds. *Nature* 364: 626–632, 1993.
92. Lipton SA, Rayudu PV, Choi YB, Sucher NJ, and Chen HS. Redox modulation of the NMDA receptor by NO-related species. *Prog Brain Res* 118: 73–82, 1998.
93. Lipton SA, and Stamler JS. Actions of redox-related congeners of nitric oxide at the NMDA receptor. *Neuropharmacology* 33: 1229–1233, 1994.
94. Liu J, García-Cardeña G, and Sessa WC. Palmitoylation of endothelial nitric oxide synthase is necessary for optimal stimulated release of nitric oxide: Implications for caveolae localization. *Biochemistry* 35: 13277–13281, 1996.
95. Liu L, Hausladen A, Zeng M, Que L, Heitman J, and Stamler JS. A metabolic enzyme for S-nitrosothiol conserved from bacteria to humans. *Nature* 410: 490–494, 2001.
96. Liu L, Yan Y, Zeng M, Zhang J, Hanes MA, Ahearn G, McMahon TJ, Dickfeld T, Marshall HE, Que LG, and Stamler JS. Essential roles of S-nitrosothiols in vascular homeostasis and endotoxic shock. *Cell* 116: 617–628, 2004.
97. Liu X, Miller MJ, Joshi MS, Thomas DD, and Lancaster JR, Jr. Accelerated reaction of nitric oxide with O_2 within the hydrophobic interior of biological membranes. *Proc Natl Acad Sci USA* 95: 2175–2179, 1998.
98. Lu W, Man H, Ju W, Trimble WS, MacDonald JF, and Wang YT. Activation of synaptic NMDA receptors induces membrane insertion of new AMPA receptors and LTP in cultured hippocampal neurons. *Neuron* 29: 243–254, 2001.
99. Malik M, Jividen K, Padmakumar VC, Cataisson C, Li L, Lee J, Howard OM, and Yuspa SH. Inducible NOS-induced chloride intracellular channel 4 (CLIC4) nuclear translocation regulates macrophage deactivation. *Proc Natl Acad Sci USA* 109: 6130–6135, 2012.
100. Mannick JB, Hausladen A, Liu L, Hess DT, Zeng M, Miao QX, Kane LS, Gow AJ, and Stamler JS. Fas-induced caspase denitrosylation. *Science* 284: 651–654, 1999.
101. Marino SM, and Gladyshev VN. Structural analysis of cysteine S-nitrosylation: A modified acid-based motif and the emerging role of trans-nitrosylation. *J Mol Biol* 395: 844–859, 2010.
102. Maron BA, Tang SS, and Loscalzo J. S-nitrosothiols and the S-nitrosoproteome of the cardiovascular system. *Antioxid Redox Signal* 18: 270–287, 2013.
103. Martínez-Ruiz A, Cadenas S, and Lamas S. Nitric oxide signaling: Classical, less classical, and nonclassical mechanisms. *Free Radic Biol Med* 51: 17–29, 2011.
104. Martínez-Ruiz A, and Lamas S. S-Nitrosylation: A potential new paradigm in signal transduction. *Cardiovasc Res* 62: 43–52, 2004.
105. Martínez-Ruiz A, and Lamas S. Signalling by NO-induced protein S-nitrosylation and S-glutathionylation: convergences and divergences. *Cardiovasc Res* 75: 220–228, 2007.
106. Martínez-Ruiz A, and Lamas S. Two decades of new concepts in nitric oxide signaling: From the discovery of a gas messenger to the mediation of nonenzymatic posttranslational modifications. *IUBMB Life* 61: 91–98, 2009.
107. Martínez-Ruiz A, Villanueva L, de Orduña CG, López-Ferrer D, Higueras MÁ, Tarín C, Rodríguez-Crespo I, Vázquez J, and Lamas S. S-Nitrosylation of Hsp90 promotes the inhibition of its ATPase and endothelial nitric oxide synthase regulatory activities. *Proc Natl Acad Sci USA* 102: 8525–8530, 2005.
108. Massion PB, Feron O, Dessy C, and Balligand J-L. Nitric oxide and cardiac function: Ten years after, and continuing. *Circ Res* 93: 388–398, 2003.
109. Matsushita K, Morrell CN, Cambien B, Yang SX, Yamakuchi M, Bao C, Hara MR, Quick RA, Cao W, O'Rourke B, Lowenstein JM, Pevsner J, Wagner DD, and Lowenstein CJ. Nitric oxide regulates exocytosis by S-nitrosylation of N-ethylmaleimide-sensitive factor. *Cell* 115: 139–150, 2003.
110. McCormick ME, Goel R, Fulton D, Oess S, Newman D, and Tzima E. Platelet-endothelial cell adhesion molecule-1 regulates endothelial NO synthase activity and localization through signal transducers and activators of transcription 3-dependent NOSTRIN expression. *Arterioscler Thromb Vasc Biol* 31: 643–649, 2011.
111. Mieyal JJ, Gallogly MM, Qanungo S, Sabens EA, and Shelton MD. Molecular mechanisms and clinical implications of reversible protein S-glutathionylation. *Antioxid Redox Signal* 10: 1941–1988, 2008.
112. Mitchell DA, and Marletta MA. Thioredoxin catalyzes the S-nitrosation of the caspase-3 active site cysteine. *Nat Chem Biol* 1: 154–158, 2005.
113. Möller MN, Li Q, Lancaster JR Jr, and Denicola A. Acceleration of nitric oxide autoxidation and nitrosation by membranes. *IUBMB Life* 59: 243–248, 2007.
114. Möller MN, Li Q, Vitturi DA, Robinson JM, Lancaster JR, Jr, and Denicola A. Membrane "lens" effect: Focusing the formation of reactive nitrogen oxides from the *NO/O2 reaction. *Chem Res Toxicol* 20: 709–714, 2007.
115. Moreno-López B, and González-Forero D. Nitric oxide and synaptic dynamics in the adult brain: Physiopathological aspects. *Rev Neurosci* 17: 309–357, 2006.
116. Morrell CN, Matsushita K, Chiles K, Scharpf RB, Yamakuchi M, Mason RJ, Bergmeier W, Mankowski JL, Baldwin WM, 3rd, Faraday N, and Lowenstein CJ. Regulation of platelet granule exocytosis by S-nitrosylation. *Proc Natl Acad Sci USA* 102: 3782–3787, 2005.
117. Mukhopadhyay S, Lee J, and Sehgal PB. Depletion of the ATPase NSF from Golgi membranes with hypo-S-nitrosylation of vasorelevant proteins in endothelial cells exposed to monocrotaline pyrrole. *Am J Physiol Heart Circ Physiol* 295: H1943–1955, 2008.
118. Mukhopadhyay S, Xu F, and Sehgal PB. Aberrant cytoplasmic sequestration of eNOS in endothelial cells after monocrotaline, hypoxia, and senescence: Live-cell caveolar and cytoplasmic NO imaging. *Am J Physiol Heart Circ Physiol* 292: H1373–1389, 2007.
119. Nakamura T, and Lipton SA. Emerging role of protein–protein transnitrosylation in cell signaling pathways. *Antioxid Redox Signal* 18: 239–249, 2013.
120. Nakamura T, Wang L, Wong CC, Scott FL, Eckelman BP, Han X, Tzitzilonis C, Meng F, Gu Z, Holland EA, Clemente AT, Okamoto S, Salvesen GS, Riek R, Yates JR, 3rd, and Lipton SA. Transnitrosylation of XIAP regulates caspase-dependent neuronal cell death. *Mol Cell* 39: 184–195, 2010.

121. Nott A, Watson PM, Robinson JD, Crepaldi L, and Riccio A. S-Nitrosylation of histone deacetylase 2 induces chromatin remodelling in neurons. *Nature* 455: 411–415, 2008.
122. Oess S, Icking A, Fulton D, Govers R, and Müller-Esterl W. Subcellular targeting and trafficking of nitric oxide synthases. *Biochem J* 396: 401–409, 2006.
123. Ozawa K, Whalen EJ, Nelson CD, Mu Y, Hess DT, Lefkowitz RJ, and Stamler JS. S-Nitrosylation of beta-arrestin regulates beta-adrenergic receptor trafficking. *Mol Cell* 31: 395–405, 2008.
124. Pacher P, Beckman JS, and Liaudet L. Nitric oxide and peroxynitrite in health and disease. *Physiol Rev* 87: 315–424, 2007.
125. Paige JS, Xu G, Stancevic B, and Jaffrey SR. Nitrosothiol reactivity profiling identifies S-nitrosylated proteins with unexpected stability. *Chem Biol* 15: 1307–1316, 2008.
126. Palmer LA, Doctor A, Chhabra P, Sheram ML, Laubach VE, Karlinsey MZ, Forbes MS, Macdonald T, and Gaston B. S-nitrosothiols signal hypoxia-mimetic vascular pathology. *J Clin Invest* 117: 2592–2601, 2007.
127. Palmer RM, Ashton DS, and Moncada S. Vascular endothelial cells synthesize nitric oxide from L-arginine. *Nature* 333: 664–666, 1988.
128. Pawloski JR, Hess DT, and Stamler JS. Export by red blood cells of nitric oxide bioactivity. *Nature* 409: 622–626, 2001.
129. Peng HM, Morishima Y, Pratt WB, and Osawa Y. Modulation of heme/substrate binding cleft of neuronal nitric-oxide synthase (nNOS) regulates binding of Hsp90 and Hsp70 proteins and nNOS ubiquitination. *J Biol Chem* 287: 1556–1565, 2012.
130. Pi X, Wu Y, Ferguson JE, 3rd, Portbury AL, and Patterson C. SDF-1alpha stimulates JNK3 activity via eNOS-dependent nitrosylation of MKP7 to enhance endothelial migration. *Proc Natl Acad Sci USA* 106: 5675–5680, 2009.
131. Qian J, Zhang Q, Church JE, Stepp DW, Rudic RD, and Fulton DJ. Role of local production of endothelium-derived nitric oxide on cGMP signaling and S-nitrosylation. *Am J Physiol Heart Circ Physiol* 298: H112–118, 2010.
132. Qu J, Nakamura T, Cao G, Holland EA, McKercher SR, and Lipton SA. S-Nitrosylation activates Cdk5 and contributes to synaptic spine loss induced by beta-amyloid peptide. *Proc Natl Acad Sci USA* 108: 14330–14335, 2011.
133. Radi R. Nitric oxide, oxidants, and protein tyrosine nitration. *Proc Natl Acad Sci USA* 101: 4003–4008, 2004.
134. Radi R, Beckman JS, Bush KM, and Freeman BA. Peroxynitrite oxidation of sulfhydryls. The cytotoxic potential of superoxide and nitric oxide. *J Biol Chem* 266: 4244–4250, 1991.
135. Reiter E, and Lefkowitz RJ. GRKs and beta-arrestins: Roles in receptor silencing, trafficking and signaling. *Trends Endocrinol Metab* 17: 159–165, 2006.
136. Sangwung P, Greco TM, Wang Y, Ischiropoulos H, Sessa WC, and Iwakiri Y. Proteomic identification of S-nitrosylated Golgi proteins: New insights into endothelial cell regulation by eNOS-derived NO. *PLoS One* 7: e31564, 2012.
137. Sattler R, Xiong Z, Lu WY, Hafner M, MacDonald JF, and Tymianski M. Specific coupling of NMDA receptor activation to nitric oxide neurotoxicity by PSD-95 protein. *Science* 284: 1845–1848, 1999.
138. Schulman IH, and Hare JM. Regulation of cardiovascular cellular processes by S-nitrosylation. *Biochim Biophys Acta* 1820: 752–762, 2012.
139. Seddon M, Shah AM, and Casadei B. Cardiomyocytes as effectors of nitric oxide signalling. *Cardiovasc Res* 75: 315–326, 2007.
140. Selvakumar B, Huganir RL, and Snyder SH. S-Nitrosylation of stargazin regulates surface expression of AMPA-glutamate neurotransmitter receptors. *Proc Natl Acad Sci USA* 106: 16440–16445, 2009.
141. Seth D, and Stamler JS. The SNO-proteome: Causation and classifications. *Curr Opin Chem Biol* 15: 129–136, 2011.
142. Singel DJ, and Stamler JS. Chemical physiology of blood flow regulation by red blood cells: The role of nitric oxide and S-nitrosohemoglobin. *Annu Rev Physiol* 67: 99–145, 2005.
143. Sliskovic I, Raturi A, and Mutus B. Characterization of the S-denitrosation activity of protein disulfide isomerase. *J Biol Chem* 280: 8733–8741, 2005.
144. Sossa KG, Beattie JB, and Carroll RC. AMPAR exocytosis through NO modulation of PICK1. *Neuropharmacology* 53: 92–100, 2007.
145. Souza JM, Peluffo G, and Radi R. Protein tyrosine nitration—Functional alteration or just a biomarker? *Free Rad Biol Med* 45: 357–366, 2008.
146. Sowa G, Liu J, Papapetropoulos A, Rex-Haffner M, Hughes TE, and Sessa WC. Trafficking of endothelial nitric-oxide synthase in living cells. Quantitative evidence supporting the role of palmitoylation as a kinetic trapping mechanism limiting membrane diffusion. *J Biol Chem* 274: 22524–22531, 1999.
147. Stamler JS, and Toone EJ. The decomposition of thionitrites. *Curr Opin Chem Biol* 6: 779–785, 2002.
148. Takahashi H, Shin Y, Cho S-J, Zago WM, Nakamura T, Gu Z, Ma Y, Furukawa H, Liddington R, Zhang D, Tong G, Chen H-SV, and Lipton SA. Hypoxia enhances S-nitrosylation-mediated NMDA receptor inhibition via a thiol oxygen sensor motif. *Neuron* 53: 53–64, 2007.
149. Takahashi S, and Mendelsohn ME. Synergistic activation of endothelial nitric-oxide synthase (eNOS) by HSP90 and Akt: calcium-independent eNOS activation involves formation of an HSP90-Akt-CaM-bound eNOS complex. *J Biol Chem* 278: 30821–30827, 2003.
150. Tamargo J, Caballero R, Gómez R, and Delpón E. Cardiac electrophysiological effects of nitric oxide. *Cardiovasc Res* 87: 593–600, 2010.
151. Tegeder I, Scheving R, Wittig I, and Geisslinger G. SNO-ing at the nociceptive synapse? *Pharmacol Rev* 63: 366–89, 2011.
152. Tello D, Tarín C, Ahicart P, Bretón-Romero R, Lamas S, and Martínez-Ruiz A. A "fluorescence switch" technique increases the sensitivity of proteomic detection and identification of S-nitrosylated proteins. *Proteomics* 9: 5359–5370, 2009.
153. Thibeault S, Rautureau Y, Oubaha M, Faubert D, Wilkes BC, Delisle C, and Gratton JP. S-Nitrosylation of beta-catenin by eNOS-derived NO promotes VEGF-induced endothelial cell permeability. *Mol Cell* 39: 468–476, 2010.
154. Trujillo M, Alvarez MN, Peluffo G, Freeman BA, and Radi R. Xanthine oxidase-mediated decomposition of S-nitrosothiols. *J Biol Chem* 273: 7828–7834, 1998.
155. Tsang AH, Lee YI, Ko HS, Savitt JM, Pletnikova O, Troncoso JC, Dawson VL, Dawson TM, and Chung KK. S-Nitrosylation of XIAP compromises neuronal survival in Parkinson's disease. *Proc Natl Acad Sci USA* 106: 4900–4905, 2009.
156. Umar S, and van der Laarse A. Nitric oxide and nitric oxide synthase isoforms in the normal, hypertrophic, and failing heart. *Mol Cell Biochem* 333: 191–201, 2010.

157. Viner RI, Williams TD, and Schöneich C. Peroxynitrite modification of protein thiols: Oxidation, nitrosylation, and S-glutathiolation of functionally important cysteine residue(s) in the sarcoplasmic reticulum Ca-ATPase. *Biochemistry* 38: 12408–12415, 1999.
158. Wang G, Moniri NH, Ozawa K, Stamler JS, and Daaka Y. Nitric oxide regulates endocytosis by S-nitrosylation of dynamin. *Proc Natl Acad Sci USA* 103: 1295–1300, 2006.
159. Wang X, Su B, Zheng L, Perry G, Smith MA, and Zhu X. The role of abnormal mitochondrial dynamics in the pathogenesis of Alzheimer's disease. *J Neurochem* 109 Suppl 1: 153–159, 2009.
160. Wang Y, Yun BW, Kwon E, Hong JK, Yoon J, and Loake GJ. S-Nitrosylation: An emerging redox-based post-translational modification in plants. *J Exp Bot* 57: 1777–1784, 2006.
161. Wang Z, Humphrey C, Frilot N, Wang G, Nie Z, Moniri NH, and Daaka Y. Dynamin2- and endothelial nitric oxide synthase-regulated invasion of bladder epithelial cells by uropathogenic *Escherichia coli*. *J Cell Biol* 192: 101–110, 2011.
162. Wei W, Li B, Hanes MA, Kakar S, Chen X, and Liu L. S-nitrosylation from GSNOR deficiency impairs DNA repair and promotes hepatocarcinogenesis. *Sci Transl Med* 2: 19ra13, 2010.
163. West MB, Hill BG, Xuan YT, and Bhatnagar A. Protein glutathiolation by nitric oxide: an intracellular mechanism regulating redox protein modification. *FASEB J* 20: 1715–1717, 2006.
164. Whalen EJ, Foster MW, Matsumoto A, Ozawa K, Violin JD, Que LG, Nelson CD, Benhar M, Keys JR, Rockman HA, Koch WJ, Daaka Y, Lefkowitz RJ, and Stamler JS. Regulation of [beta]-adrenergic receptor signaling by S-nitrosylation of G-protein-coupled receptor kinase 2. *Cell* 129: 511–522, 2007.
165. Wink DA, Darbyshire JF, Nims RW, Saavedra JE, and Ford PC. Reactions of the bioregulatory agent nitric oxide in oxygenated aqueous media: Determination of the kinetics for oxidation and nitrosation by intermediates generated in the NO/O_2 reaction. *Chem Res Toxicol* 6: 23–27, 1993.
166. Wu C, Liu T, Chen W, Oka S, Fu C, Jain MR, Parrott AM, Baykal AT, Sadoshima J, and Li H. Redox regulatory mechanism of transnitrosylation by thioredoxin. *Mol Cell Proteomics* 9: 2262–2275, 2010.
167. Wu C, Parrott AM, Fu C, Liu T, Marino SM, Gladyshev VN, Jain MR, Baykal AT, Li Q, Oka S, Sadoshima J, Beuve A, Simmons WJ, and Li H. Thioredoxin 1-mediated post-translational modifications: Reduction, transnitrosylation, denitrosylation, and related proteomics methodologies. *Antioxid Redox Signal* 15: 2565–2604, 2011.
168. Wu C, Parrott AM, Liu T, Jain MR, Yang Y, Sadoshima J, and Li H. Distinction of thioredoxin transnitrosylation and denitrosylation target proteins by the ICAT quantitative approach. *J Proteomics* 74: 2498–2509, 2011.
169. Yoshida M, and Xia Y. Heat shock protein 90 as an endogenous protein enhancer of inducible nitric-oxide synthase. *J Biol Chem* 278: 36953–36958, 2003.
170. Zhang Q, Church JE, Jagnandan D, Catravas JD, Sessa WC, and Fulton D. Functional relevance of Golgi- and plasma membrane-localized endothelial NO synthase in reconstituted endothelial cells. *Arterioscler Thromb Vasc Biol* 26: 1015–1021, 2006.
171. Zucker B, Luthi-Carter R, Kama JA, Dunah AW, Stern EA, Fox JH, Standaert DG, Young AB, and Augood SJ. Transcriptional dysregulation in striatal projection- and interneurons in a mouse model of Huntington's disease: Neuronal selectivity and potential neuroprotective role of HAP1. *Hum Mol Genet* 14: 179–189, 2005.

Address correspondence to:
Dr. Antonio Martínez-Ruiz
Servicio de Inmunología
Hospital Universitario de La Princesa
Instituto de Investigación Princesa (IP)
C/ Diego de León 62
E-28006 Madrid
Spain

E-mail: amartinezruiz@salud.madrid.org

Date of first submission to ARS Central, November 1, 2012; date of acceptance, November 18, 2012.

Abbreviations Used

AD = Alzheimer disease
β_2-AR = β_2-adrenergic receptor
eNOS = endothelial nitric oxide synthase
GAPDH = glyceraldehyde-3-phosphate dehydrogenase
GPCR = G protein-coupled receptors
GRK = GPCR kinase
GSH = reduced glutathione
GSNO = S-nitrosoglutathione
GSNOR = S-nitrosoglutathione reductase
Hb = hemoglobin
HD = Huntington disease
iNOS = inducible nitric oxide synthase
LMM = low molecular mass
LPS = lipopolysaccharide
LTCC = L-type Ca^{2+} channel
nNOS = neuronal nitric oxide synthase
NO = nitric oxide
NOS = nitric oxide synthase
$ONOO^-$ = peroxynitrite
PTM = post-translational modification
RNS = reactive nitrogen species
ROS = reactive oxygen species
RyR = ryanodine receptor
SERCA = sarcoplasmic/endoplasmic reticulum Ca^{2+}-activated ATPase
sGC = soluble guanylate cyclase
SNO-protein = S-nitrosylated protein
TR = thioredoxin reductase
Trx = thioredoxin